XXI^{ème} Colloque Louis Néel
13-16 novembre 2023
Sète

Abstract book

Contents

Scientific committee

- Vincent Baltz (SPINTEC, Grenoble)
- Nicolas Bergeard (IPCMS, Strasbourg)
- Anne Bernand-Mantel (LPCNO, Toulouse)
- David Dekadjevi (OPTIMAG, Brest)
- Anne-Lise Engelvin (INSTN, Tours)
- Aurore Finco (L2C, Montpellier)
- Joo-Von Kim (C2N, Orsay)
- Gregory Malinowski (IJL, Nancy)
- Richard Mattana (UMR CNRS/Thales, Palaiseau)
- Olena Popova (IPR, Rennes)
- Laurent Ranno (Institut Néel, Grenoble)
- Stanislas Rohart (LPS, Orsay)
- Laura Thevenard (INSP, Paris)
- Florent Tournus (ILM, Lyon)
- Bénédicte Warot-Fonrose (CEMES, Toulouse)

Local organization team (L2C, Montpellier)

- Steeve Cronenberger
- Christelle Eve
- Aurore Finco
- Vincent Jacques
- Isabelle Robert-Philip
- Denis Scalbert
- Thibault Sohier
- Masha Vladimirova

Program overview

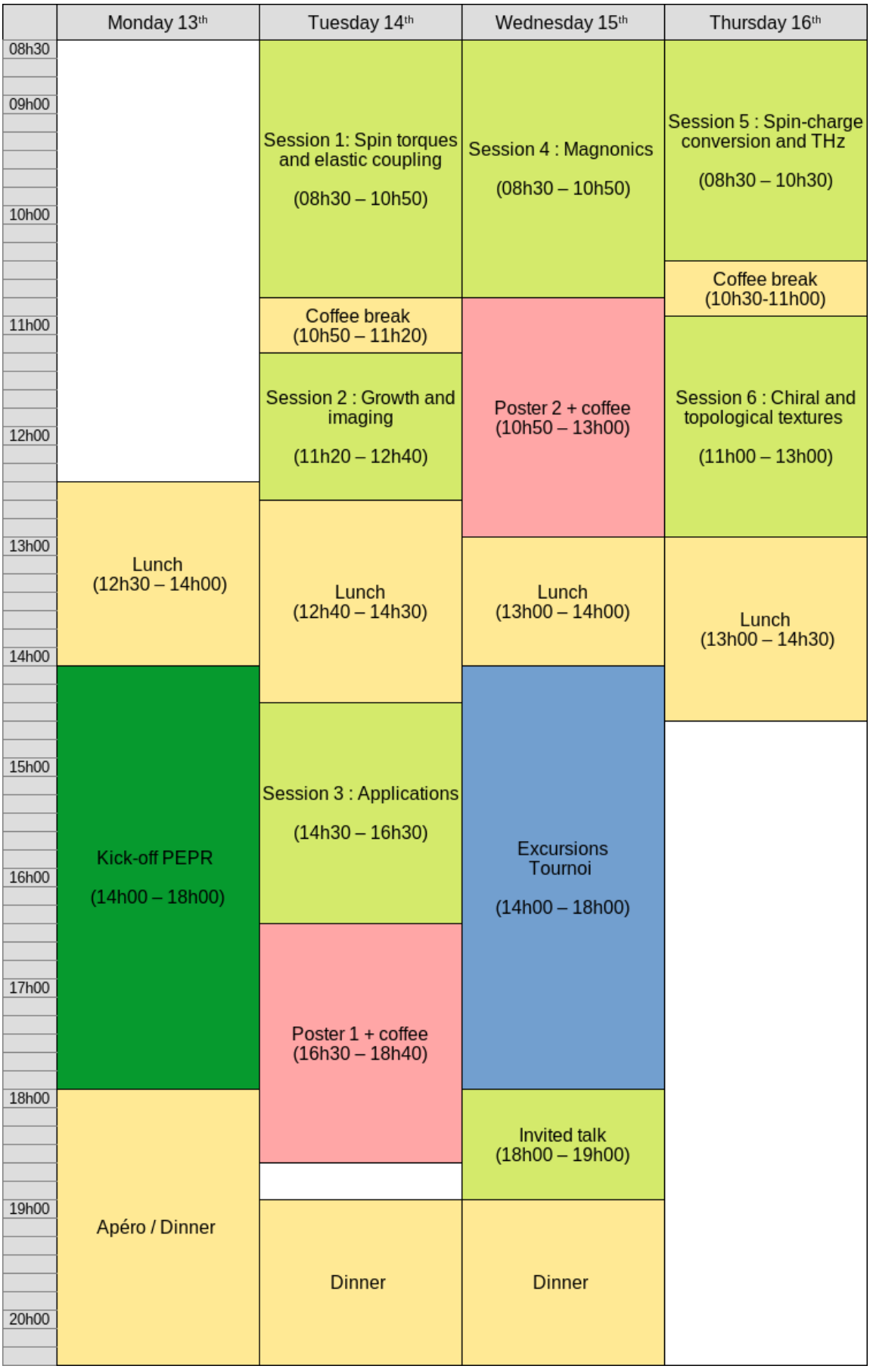

List of abstracts

Tuesday November 14th

Session 1: Control of magnetism with spin torque and elastic coupling 08h30 – 10h50 *Chair: Laura Thevenard*				
08h30 – 08h50	**Eva Diaz**	IJL	Spin-orbit torque switching in ferromagnets and ferrimagnets induced by picosecond electrical pulses	page 7
08h50 – 09h10	**Simon de Wergifosse**	UC Louvain	Capturing the full analytical dynamics of spin-torque vortex oscillators from micromagnetic simulations	page 9
09h10 – 09h30	**Diego Garcia Ovalle**	CINAM	Spin Orbit Torque for Field-Free Switching in C3v Crystals	page 11
09h30 – 09h50	**Katia Ho**	UMR CNRS/Thales	Direct STXM imaging of vortex dynamics in spin-torque nano-oscillators	page 13
09h50 – 10h10	**Benjamin Bony**	UMR CNRS/Thales	Evidence of orbital current and orbital torques in transition metals using oxidized Cu light element	page 15
10h10 – 10h30	**Stéphane Chiroli**	LSPM	Dynamique de l'aimantation dans des nanostructures soumises à des déformations élastiques : une étude expérimentale et numérique	page 17
10h30 – 10h50	**Ashwin Kavilen Vythelingum**	INSP	Temperature- and field-hysteretic magneto-acoustic interaction in FeRh	page 19

Spin-orbit torque switching in ferromagnets and ferrimagnets induced by picosecond electrical pulses

Eva Díaz[1,*], Alberto Anadón[1], Martina Morassi[2], Aristide Lemaître[2], Michel Hehn[1], and Jon Gorchon[1]

[1]*Institut Jean Lamour, CNRS, Université de Lorraine, Nancy, France*
[2]*Centre de Nanosciences et de Nanotechnologies, CNRS, Université Paris-Saclay, Palaiseau, France*
eva.diaz@univ-lorraine.fr

The development of high-speed devices with low energy consumption is currently an important challenge in the memory technology industry. In this regard, spintronic devices, which are based upon the use of the electron's spin degree of freedom, show great potential as an alternative to conventional devices. Within this realm, spin-orbit torque (SOT) switching is a largely studied mechanism which offers desirable qualities, such as high switching speed and energy efficiency. The fastest SOT switching to date has been achieved using a 6 ps electrical pulse over a sample of perpendicularly magnetized Co [1]. The electrical pulse is generated by exciting an Auston switch with a single laser pulse, and is transmitted through a coplanar waveguide (CPW) towards the magnetic sample. By measuring the switching dynamics, it was found that the zero-crossing of magnetization happens in about 70 ps [2]. Moreover, good agreement between data and a macrospin model coupled with ultrafast heating brings forth two important points: (i) the reversal is greatly assisted by Joule heating, which weakens the anisotropy field and thus decreases the energy cost of switching; and (ii) the switching process is coherent, as opposed to the expected domain nucleation and propagation that has been reported for the case of ns pulses [3, 4].

Many aspects of SOT switching remain mysterious in the ps scale. Critical current density, essential for characterizing energy efficiency, has been quantified so far only for pulse durations from the ms scale down to around 200 ps [5]. Regarding materials, SOT switching has been observed in both ferromagnets [3–5] and ferrimagnets [6–8] in the ns scale, but the ps scale has, to our knowledge, only been studied in perpendicularly magnetized Co [1, 2].

In this work we show SOT switching of both ferromagnetic and ferrimagnetic materials in the ps scale. We have prepared various samples by magnetron sputtering on a substrate of LT-GaAs. In a similar fashion to Ref. [1], we have developed a sample design including both an Auston switch and a magnetic stack embedded into a CPW. Moreover, we have established a method of characterization of electrical pulses in terms of current and energy [9]. Figure 1 shows MOKE images of a ferrimagnetic stack of Ta(3)Pt(5)Co(1)Gd(1)Ta(2)Pt(1), where the number between parentheses corresponds to thickness in nm. This sample was shaped by UV lithography into a 4×6 μm^2 film. We have found that magnetization reversal of this sample can be achieved by lower current densities as compared to previously studied Co samples, in concordance as what was reported in Ref. [6] for ns pulses.

Further details and comparison between different materials will be given during the presentation. These results can help deepen our understanding of the SOT mechanism in the ps scale and also pave the way for new SOT-based spintronics devices [10, 11].

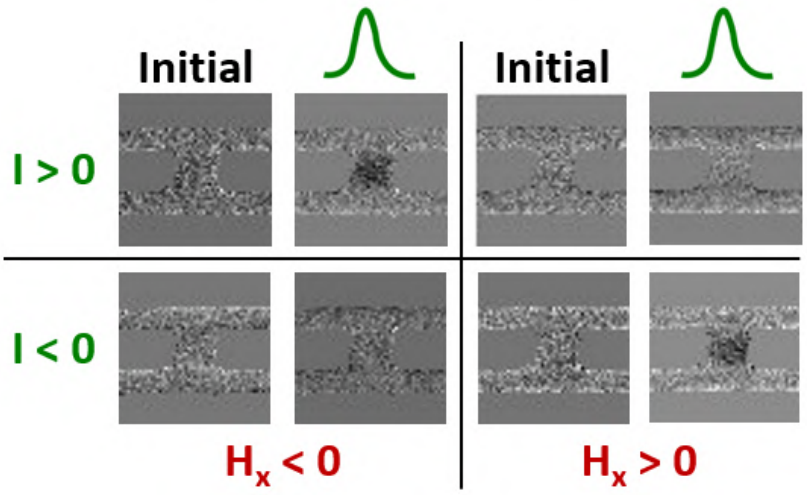

Figure 1: MOKE images of single-pulse switching of CoGd by SOT, for different configurations of current (I) and external in-plane magnetic field (H_x).

Acknowledgments

This work was supported by the ANR Project via Nos. ANR-20-CE24-0003 SPOTZ, and by the French PIA project “Lorraine Université d’Excellence”.

References

[1] Kaushalya Jhuria, Julius Hohlfeld, Akshay Pattabi, et al. Spin–orbit torque switching of a ferromagnet with picosecond electrical pulses. *Nature Electronics* 3, 680–686 (2020).

[2] Debanjan Polley, Akshay Pattabi, Ashwin Rastogi, et al. Picosecond spin-orbit torque induced coherent magnetization switching in a ferromagnet. *Submitted for publication* (2022).

[3] Eva Grimaldi, Viola Krizakova, Giacomo Sala, et al. Single-shot dynamics of spin–orbit torque and spin transfer torque switching in three-terminal magnetic tunnel junctions. *Nature Nanotechnology* 15, 111–117 (2020).

[4] Manuel Baumgartner, Kevin Garello, Johannes Mendil, et al. Spatially and time-resolved magnetization dynamics driven by spin–orbit torques. *Nature Nanotechnology* 12, 980–986 (2017).

[5] Kevin Garello, Can Onur Avci, Ioan Mihai Miron, et al. Ultrafast magnetization switching by spin-orbit torques. *Applied Physics Letters* 105, 212402 (2014). eprint: https://pubs.aip.org/aip/apl/article-pdf/doi/10.1063/1.4902443/14305507/212402_1_online.pdf.

[6] Kaiming Cai, Zhifeng Zhu, Jong Min Lee, et al. Ultrafast and energy-efficient spin–orbit torque switching in compensated ferrimagnets. *Nature Electronics* 3, 37–42 (2020).

[7] Xue Ren, Liang Liu, Bin Cheng, et al. Field-free switching of magnetization induced by spin–orbit torque in Pt/CoGd/Pt thin film. *Applied Physics Letters* 120, 252403 (2022). eprint: https://pubs.aip.org/aip/apl/article-pdf/doi/10.1063/5.0092513/16448844/252403_1_online.pdf.

[8] Giacomo Sala and Pietro Gambardella. Ferrimagnetic Dynamics Induced by Spin-Orbit Torques. *Advanced Materials Interfaces* 9, 2201622 (2022). eprint: https://onlinelibrary.wiley.com/doi/pdf/10.1002/admi.202201622.

[9] Eva Díaz, Alberto Anadón, Martina Morassi, et al. *Manuscript in preparation* (2023).

[10] Qiming Shao, Peng Li, Luqiao Liu, et al. Roadmap of Spin–Orbit Torques. *IEEE Transactions on Magnetics* 57, 1–39 (2021).

[11] Debanjan Polley, Akshay Pattabi, Jyotirmoy Chatterjee, et al. Progress toward picosecond on-chip magnetic memory. *Applied Physics Letters* 120, 140501 (2022). eprint: https://pubs.aip.org/aip/apl/article-pdf/doi/10.1063/5.0083897/16444942/140501_1_online.pdf.

Capturing the full analytical dynamics of spin-torque vortex oscillators from micromagnetic simulations

Simon de Wergifosse[1,*], Chloé Chopin[1], Anatole Moureaux[1], and Flavio Abreu Araujo[1]

[1]*Institute of Condensed Matter and Nanosciences, UCLouvain, Louvain-la-Neuve, Belgium*
*simon.dewergifosse@uclouvain.be

The theoretical description of the spin-torque vortex oscillators dynamics has become an important research topic in the nanomagnetism community, notably since their use in neuromorphic computing applications [1]. These nano-sized cylindrical heterostructures are capable of emitting microwave signals when subjected to a spin-polarized current, caused by sustained precessions of the magnetization in the free magnetic layer. In this configuration, the core of the magnetic vortex, which is the ground state at these geometries, may oscillate (see Fig. 1a) at a given orbit and frequency (depending on material parameters and the current magnitude) if the excitation is large enough. Until now, there have been two main theoretical methods for studying these devices, namely micromagnetic simulations (MMS) and an approach based on the Thiele equation [2]. However, none of these tools is both fast and accurate, which limits their relevance for any realistic large-scale study.

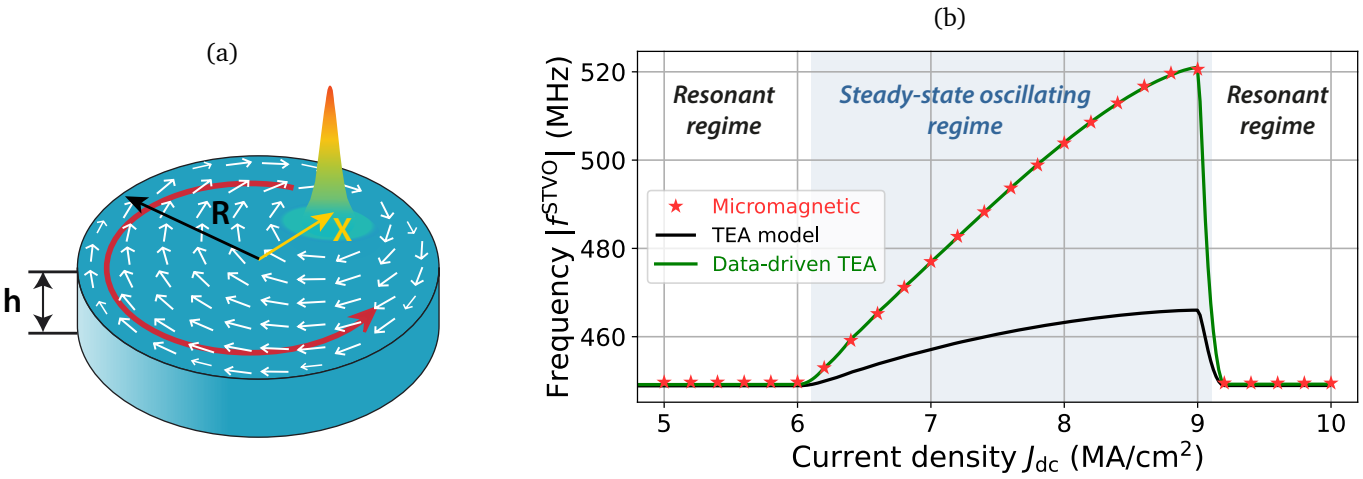

Figure 1: a) Schematic of the free magnetic layer (of radius R and thickness h) of the magnetic tunnel junction under study, presenting a vortex as magnetic ground state. The core gyration is triggered by an out-of-plane spin-polarized current. b) Comparison of the gyrotropic frequency f^{STVO} of the vortex core with respect to the imposed current density J_{dc} between micromagnetic results, a fully analytical Thiele equation approach (TEA) and our data-driven Thiele equation approach (DD-TEA, as in Ref. [3]).

Recently, we proposed an alternative to these techniques, called the data-driven Thiele equation approach (DD-TEA) [3]. Starting from a fully analytical TEA model [4], we have adjusted some of its terms based on the results of micromagnetic simulations performed with mumax3 [5]. To do so, we carried out simulations at different currents and extracted the frequency and orbital position of oscillation. The micromagnetic data enabled us to propose nonlinear corrections to the gyrotropic and damping terms of the Thiele equation, resulting in a perfect agreement between the DD-TEA model and simulations (see Fig. 1b). The major advantage of our model is that it reduces the number of equations to be solved between each time step from thousands to just two (i.e. $\mathbf{X} = (X, Y)$ coordinates of the vortex core). This achievement resulted in an acceleration factor of about six orders of magnitude between MMS and DD-TEA. However, there was remaining room for improvement, as a system of differential equations still had to be solved. In addition, around twenty simulations reaching steady state had to be performed for sufficient fitting accuracy.

Here, we have been able to transform our problem mathematically so that we do not need to solve a system of ordinary differential equation, similarly to what was obtained by Guslienko et al. [6]. Using the formalism of Bernoulli differential equations, one can show that the harmonic oscillator problem we presented in Ref. [4] may be rewritten as

$$s(t) = \frac{s_0}{\sqrt[n]{\left(1 + \frac{s_0^n}{\alpha/\beta}\right)\exp(-n\alpha t) - \frac{s_0^n}{\alpha/\beta}}}, \tag{1}$$

where $s(t) = |\mathbf{X}|/R$ and s_0 are the current and starting reduced vortex core positions, respectively, and α, β and n are parameters depending on the current density J_{dc} that can be calculated from MMS. This transformation accelerates our

method by a further three orders of magnitude, resulting in near-instantaneous solutions. Such a speed-up factor has enabled us to apply our new model to neuromorphic applications of written digit recognition (using the MNIST database), in the framework of reservoir computing, with state-of-the-art results [7].

Additionally, we propose an updated, more practical approach to calibrate our semi-analytical model. Instead of running several simulations at a fixed current value, a few simulation are used, sweeping from low currents up to the vortex stability limit. This alternative method offers a number of benefits. Firstly, it is no longer necessary to interpolate MMS results (as was done in Ref. [3]) to obtain an accurate fit, as the extracted points are virtually continuous. Furthermore, a wider range of excitation levels can be explored. Finally, from a more practical point of view, less post-processing is required as much less simulations are performed.

In this study, we propose an improvement of our data-driven Thiele equation approach. Firstly, a mathematical transformation of the dynamics helped us to jump from an accelerating factor of around 10^6 to 10^9, compared to micromagnetic simulations (for equivalent precision). Furthermore, the calibration of our model was modified to make it simpler, using a few micromagnetic simulations instead of dozens. More fundamentally, we believe that our approach could be generalized to any type of application dealing with harmonic oscillators. As long as simplified equations of the dynamics and either simulated or experimental data are available, a similar data-driven model could be developed to drastically speed up simulations and leverage applications.

Acknowledgments

Computational resources have been provided by the Consortium des Equipements de Calcul Intensif (CECI), funded by the Fonds de la Recherche Scientifique de Belgique (F.R.S.-FNRS) under Grant No. 2.5020.11 and by the Walloon Region. F.A.A. is a Research Associate and S.d.W. is a FRIA grantee, both of the F.R.S.-FNRS.

References

[1] Jacob Torrejon, Mathieu Riou, Flavio Abreu Araujo, et al. Neuromorphic computing with nanoscale spintronic oscillators. *Nature* 547, 428–431 (2017).

[2] AA Thiele. Steady-state motion of magnetic domains. *Physical Review Letters* 30, 230 (1973).

[3] Flavio Abreu Araujo, Chloé Chopin, and Simon de Wergifosse. Data-driven Thiele equation approach for solving the full nonlinear spin-torque vortex oscillator dynamics. *arXiv preprint arXiv:2206.13596* (2022).

[4] Flavio Abreu Araujo, Chloé Chopin, and Simon de Wergifosse. Ampere–Oersted field splitting of the nonlinear spin-torque vortex oscillator dynamics. *Scientific Reports* 12, 10605 (2022).

[5] Arne Vansteenkiste, Jonathan Leliaert, Mykola Dvornik, et al. The design and verification of MuMax3. *AIP advances* 4, 107133 (2014).

[6] Konstantin Y Guslienko, Oksana V Sukhostavets, and Dmitry V Berkov. Nonlinear magnetic vortex dynamics in a circular nanodot excited by spin-polarized current. *Nanoscale research letters* 9, 1–7 (2014).

[7] Anatole Moureaux, Simon de Wergifosse, Chloé Chopin, Jimmy Weber, and Flavio Abreu Araujo. Neuromorphic spintronics accelerated by an unconventional data-driven Thiele equation approach. *arXiv preprint arXiv:2301.11025* (2023).

Spin Orbit Torque for Field-Free Switching in C_{3v} Crystals

Diego García Ovalle[1,*], Armando Pezo[1], and Aurélien Manchon[1]

[1]*Aix-Marseille Université, CNRS, CINaM, Marseille, France*
**diego-fernando.garcia-ovalle@univ-amu.fr*

The manipulation of the local magnetization in a wide variety of magnetic materials is a matter of great attention, both from the theoretical and experimental standpoints. In the latter case, particularly, the interest rely on the fabrication and optimization of memory devices. Here, the magnetization switching in the absence of any external perturbation is a crucial necessity in nanoelectronic applications.

In this work [1] we are focused on trigonal crystals, which belong to the C_{3v} point group symmetry, that are able to display unconventional spin-orbit torques, i.e, beyond the common field-like and damping-like contributions. By applying the Invariant Theory [2] at the first order in electric field and up to the third order in magnetization components, we demonstrate that several nonlinear contributions to the spin-orbit torque are allowed to emerge in trigonal crystals. We have to remark the appearance of the so-called "3m" torque, which was previously identified in CuPt/CoPt heterostructures [3] and Fe_3GeTe_2 [4], and it has been indicated as the precursor of field-free magnetization switching in trigonal ferromagnetic heterostructures.

From the microscopic point of view, we also show the origin of these nonlinear contributions in the magnetization. In the frame of a trigonal crystal, we first analyze a tight binding model where linear and cubic spin-orbit coupling contributions are taken into account. We reveal that the origin of the spin-orbit torques presented here are related with the interplay between the trigonal warping of the Fermi surface and a proper band filling of the system. An illustration of the Fermi surface when the trigonal warping is active in the system is reported in Fig.1.

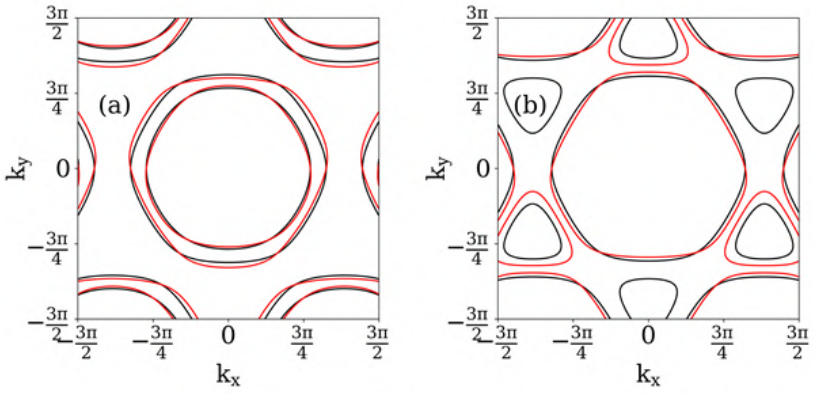

Figure 1: (Color online) Evolution of the Fermi surfaces with the band filling (lower in (a) and higher in (b)), for the cases without (black lines) and with (red lines) cubic spin-orbit coupling when the magnetization is out-of plane.

Finally, we corroborate our previous findings with realistic calculations performed in a CuPt/Co slab geometry, which exhibits a strong trigonal warping as it is depicted in Fig. 2. We notice that the "3m" contribution can be as large as the regular damping-like torque in these systems. Our article motivates further exploration of low-symmetry crystals for magnetic memory devices.

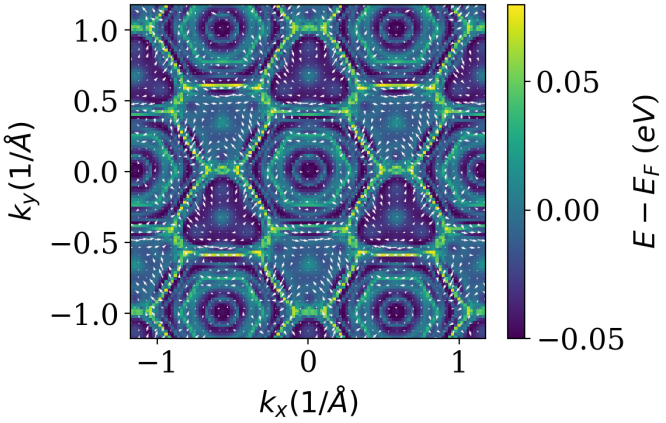

Figure 2: (Color online) Spin texture of a selected band close to the Fermi level of CuPt(111)/Co slab geometry.

Acknowledgments

This work was supported by the ANR ORION project, grant ANR-20-CE30-0022-01 of the French Agence Nationale de la Recherche. D. G.O. and A. M. acknowledge support from the Excellence Initiative of Aix-Marseille Universite - A*Midex, a French "Investissements d'Avenir" program.

References

[1] Diego García Ovalle, Armando Pezo, and Aurélien Manchon. Spin-orbit torque for field-free switching in C_{3v} crystals. *Phys. Rev. B* 107, 094422 (9 2023).

[2] Melvin J. Lax. *Symmetry Principles in Solid State and Molecular Physics*. Dover, UK: Dover Publications, 2012.

[3] Liang Liu, Chenghang Zhou, Xinyu Shu, et al. Symmetry-dependent field-free switching of perpendicular magnetization. *Nature Nanotechnology* 16, 277–282 (2021).

[4] Øyvind Johansen, Vetle Risinggård, Asle Sudbø, Jacob Linder, and Arne Brataas. Current Control of Magnetism in Two-Dimensional Fe_3GeTe_2. *Phys. Rev. Lett.* 122, 217203 (21 2019).

Direct STXM imaging of vortex dynamics in spin-torque nano-oscillators

K. Ho[1,*], S. Wittrock[2], K. Litzius[3], V. Deinhart[2], C. Klose[4], T. Sidiropoulos[4], L. Kern[4], D. Metternich[2], A. Jenkins[5], L. Benetti[5], R. Ferreira[5], S. Finizio[6], S. Wintz[2], B. Pfau[4], S. Eisebitt[4], F. Büttner[2,3], R. Lebrun[1], P. Bortolotti[1], and V. Cros[1]

[1]*Unité Mixte de Physique CNRS, Thales, Université Paris-Saclay, 91767, Palaiseau, France*
[2]*Helmholtz-Zentrum Berlin fur Materialien und Energie GmbH, Hahn-Meitner-Platz 1, 14109 Berlin, Germany*
[3]*Institut für Physik, Universität Augsburg, Universitätsstraße 1, 86159 Augsburg*
[4]*Max Born Institute For Nonlinear Optics & Short Pulse Spectroscopy, Max-Born-Str. 2A, 12489 Berlin, Germany*
[5]*International Iberian Nanotechnology Laboratory, Braga, Portugal*
[6] *Paul Scherrer Institute, Forschungsstrasse 111, 5232 Villigen PSI, Switzerland*
*katia.ho@cnrs-thales.fr

Spin torque nano-oscillators are circular-shaped MTJ devices in which radiofrequency magnetization oscillations can be generated through spin-transfer effects. Due to their nonlinearity, these devices display interesting properties such as spectral purity, frequency stability, and high tunability, opening up possibilities from wireless telecommunication to neuromorphic computing [1]. Our goal is to directly connect electrical measurements and the actual vortex core dynamics in vortex-based spin-torque nano-oscillators (STVO).

To this aim, we image the spin transfer-induced gyrotropic magnetic vortex motion in state-of-the-art TMR-based STVO devices by scanning transmission X-ray microscopy (STXM). The STXM technique allows probing volumic properties of samples of a few hundred nm depth in the soft X-ray range [2]. The experiment has been performed at the MAXYMUS beamline of the BESSY II Light Source where we focus a coherent X-ray beam down to the nanoscale range on state-of-the-art MTJs. To our knowledge, these measurements are the first direct imaging of current-induced vortex dynamics in a fully current-controlled device that is electrically characterized and in operando condition.

The studied devices are specific STVOs lithographed with very thin 50 nm thick SiO_2 membranes that allow light transmission through the device. The MTJ comprises magnetic layers separated by a crystalline magnesium oxide insulator. The 400 nm diameter nanopillar device, from bottom to top, can be summarized as the following stack: $SAF/CoFe_{30}/MgO/NiFe$, where the spin transfer vortex dynamics take place in the $NiFe$ free layer.

By shining polarized light on STVOs, we get time-resolved magnetic static and dynamic imaging which can be unambiguously attributed to the vortex dynamics. Indeed, with complete control of the soft X-ray wavelength, it is possible to access the L edges of Ni around 853.4 eV and contrast only the free layer of the MTJ. X-ray magnetic circular dichroism (XMCD) effect is used as an imaging contrast method [3]. The in-plane magnetization distribution of the vortex tail is depicted in Fig. 1 along the experimental setup schematic.

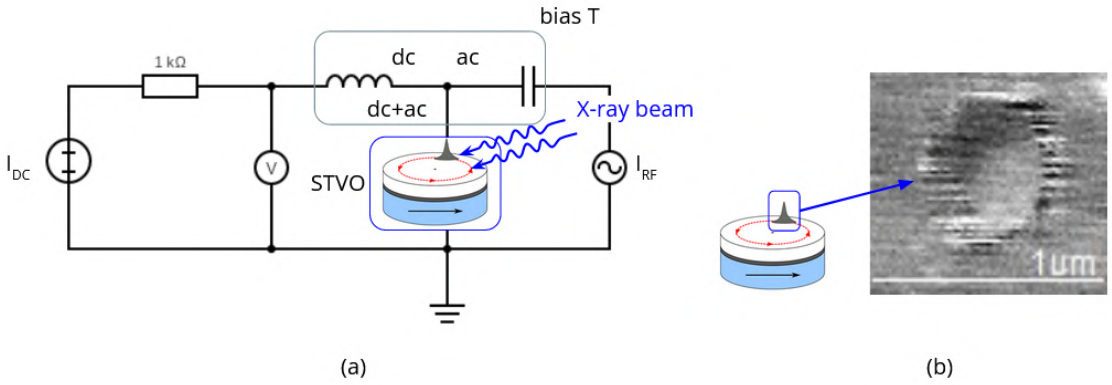

Figure 1: (a) Schematic of the experimental setup for electrical characterization of the STVO. (b) XMCD resolved vortex distribution static scan at -2 mT in-plane for a 400 nm diameter nanopillar. The in-plane magnetization is depicted by the contrast.

We could successfully resolve vortex statically and dynamically in nanopillars. The latter is done by exciting the resonance of the gyrotropic motion, the fundamental core vortex mode, with an RF signal close in frequency to the gyrotropic mode. In addition, a small DC current is also applied to compensate for the natural damping and ensure we have the right conditions for motion. This approach relates the vortex's electrical response to its trajectory in the free layer in a dynamic scan (Fig. 2). The magnetic contrast shows the vortex motion, which changes position through the 600 ms time resolution snapshots, of which we depict four frames out of thirteen.

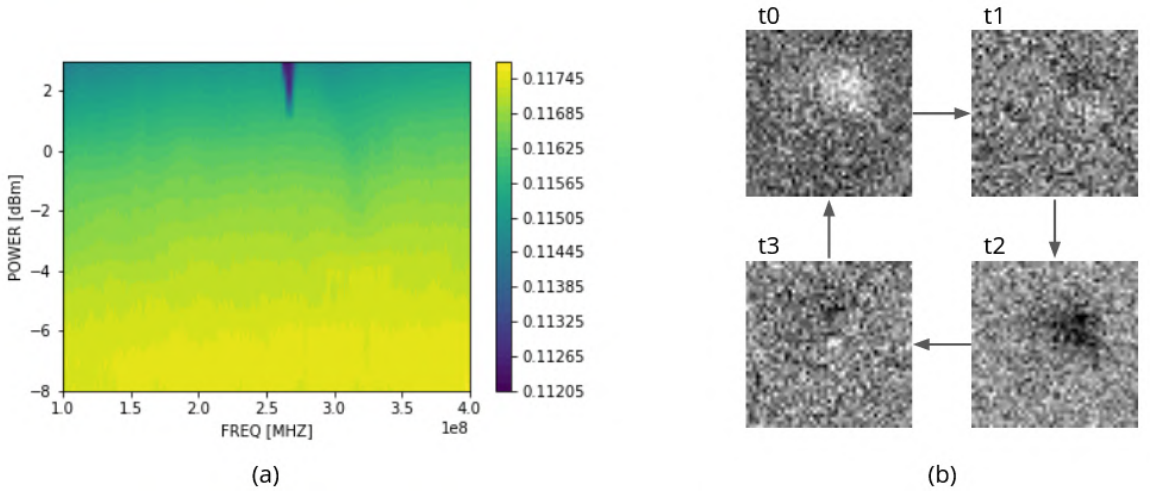

Figure 2: (a) Spindiode rectification voltage map at 254 mT and $I_{DC} = 1$mA. The gyrotropic mode is detected from $P_{rf} > 1$ dBm around 260 MHz.
(b) XMCD resolved vortex dynamic scan at +254.3 mT for four consecutive frames, with settings $I_{DC} = 1$mA, $P_{rf} = 4$ dBm and $f = 269.1$ MHz. The sample was measured with an out-of-plane field with 30 degrees tilt.

In conclusion, we can directly link electrical RF measurements and dynamics by imaging the vortex motion. This successful observation of time-resolved spin-torque-driven dynamics opens many possibilities for imaging even more complex schemes, such as synchronization [4], C-state [5], or even oscillation death [6]. Theoretical predictions and models can be directly related to images and interpreted. Moreover, observing complex dynamic states of the magnetization may be of interest for novel neuromorphic-based computing [7].

Acknowledgments

This work has received funding from the European Union's Horizon 2020 research and innovation programme under grant agreement No 101070287 (project Swan-on-chip).

References

[1] N. Locatelli, V. Cros, and J. Grollier. Spin-torque building blocks. *Nature Materials* 13, 11–20 (2013).

[2] Matti M. van Schooneveld, Jan Hilhorst, Andrei V. Petukhov, et al. Scanning Transmission X-Ray Microscopy as a Novel Tool to Probe Colloidal and Photonic Crystals. *Small* 7, 804–811 (2011). eprint: https://onlinelibrary.wiley.com/doi/pdf/10.1002/smll.201001745.

[3] Sina Mayr, Lukáš Flajšman, Simone Finizio, et al. Spin-Wave Emission from Vortex Cores under Static Magnetic Bias Fields. *Nano Letters* 21, 1584–1590 (2021).

[4] R. Lebrun, S. Tsunegi, P. Bortolotti, et al. Mutual synchronization of spin torque nano-oscillators through a long-range and tunable electrical coupling scheme. *Nature Communications* 8 (2017).

[5] Steffen Wittrock, Philippe Talatchian, Miguel Romera, et al. Beyond the gyrotropic motion: Dynamic C-state in vortex spin torque oscillators. *Applied Physics Letters* 118, 012404 (2021).

[6] Steffen Wittrock, Salvatore Perna, Romain Lebrun, et al. *Non-hermiticity in spintronics: oscillation death in coupled spintronic nano-oscillators through emerging exceptional points*. 2023. arXiv: 2108.04804 [cond-mat.mes-hall].

[7] Jacob Torrejon, Mathieu Riou, Flavio Abreu Araujo, et al. *Neuromorphic computing with nanoscale spintronic oscillators*. 2017. arXiv: 1701.07715 [cs.ET].

Evidence of orbital current and orbital torques in transition metals using oxidized Cu light element

Benjamin Bony[1,*], Sachin Krishnia[1], Sophie Collin[1], Jean-Marie George[1], Nicolas Reyren[1], Vincent Cros[1], and Henri Jaffrès[1]

[1]*Unité Mixte de Physique CNRS-Thales, Université Paris-Saclay, 91767 Palaiseau, France*
benjamin.bony@cnrs-thales.fr

The spin-orbit torque (SOT) has been widely investigated for both fundamental physics and for its industrial interest for operating on the new generations of magnetic memories. To overcome the current limitations of SOT (energy efficiency, use of heavy and scarce elements ...) a new approach has been proposed very recently [1], the orbital torque (OT) which involves the generation of polarized orbital angular momentum (OAM). Two mechanisms can be at the origin of the orbital current generation: the so-called orbital hall effect (OHE) [2] and the orbital Rashba-Edelstein effect (OREE) [3]. These effects have been shown to largely overcome their analog pure spin effects. Recent works focused on the observation of a torque enhancement due to a naturally oxidized copper layer on top of a conversion Pt layer [4] [5]. In these systems, a spin current is generated in Pt through the spin Hall effect (SHE) and an additional orbital current is generated at the interface between metallic Cu and CuOx by OREE. The orbital current is then converted into its counterpart spin-current by the large spin-orbit coupling of Pt, and hence gives rise to a large enhancement of the magnetic torque, as measured on out-of-plane insulating ferromagnet [4] together with an enhancement of spin injection detected through spin-pumping measurements driven by ferromagnetic resonance (FMR) [5]. The main objectives of this study are twofold: i) Demonstrating that a similar enhancement of magnetic torques also exists in case of transition metal ferromagnet e.g. cobalt, and ii) determining experimentally the role of the orbital contribution in this enhancement.

The studied samples are Co(t)/Pt/Cu(3)* series deposited by dc magnetron sputtering with varying Co and Pt thickness and using a 3 nm thick copper layer oxidized at ambient air to obtain Cu*. We carried out Pt thickness dependent measurements on two series of polycrystalline samples: SiOx|Co(2)|Pt(t)|Cu*(3) is the orbital based system (Cu* stands for naturally oxidized copper), and SiOx|Co(2)|Pt(t) as reference system involving only a pure spin contribution. To fully characterize our system, we investigated the oxidation properties of Cu layer through resistivity measurements and X-ray PhotoElectron Spectroscopy (XPS), that are both compatible with the presence of 1 nm of Cu and 2 nm of CuO. For torque measurements (see Fig. 1a), we have performed 1st and 2nd order harmonic Hall voltage measurements, allowing the extraction of damping-like (DL) effective field H_{DL}. In addition, we have also measured the spin (and orbital) magnetoresistances, SMR (OMR) (see Fig. 1c).

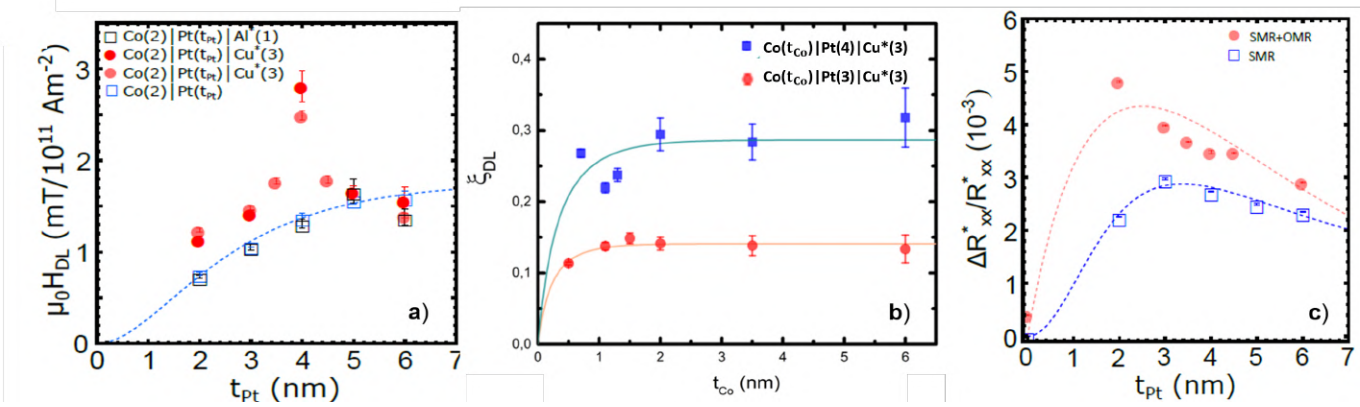

Figure 1: a) Damping-like field dependence on Pt thickness and comparison between systems with and without generation of orbital currents b) Damping-like efficiency dependence on Co thickness for 3 and 4 nm Pt c) Spin-hall magnetoresistance dependence on platinum thickness.

We present the evolution of the DL vs Pt thickness for Co/Pt/Cu* (see Fig. 1a). We find undoubtedly a torque enhancement by a factor of 2 around Pt 4 nm (see red points). In addition, we have also measured the DL torque in a series with only Pt without Cu (see blue squares) and one with a capped reference with aluminum oxide. The sharp enhancement found in the Co/Pt/Cu* samples is associated with the top Cu* layer and hence to the potential OREE at Cu/CuOx interface. The Pt

thickness for which the maximum is observed is explained by the competition in Pt between the conversion from the orbital current into spin current by spin-orbit interactions and the spin current loss in Pt. We also display the corresponding Hall magnetoresistances (SMR and OMR) and their fits using our model (see Fig. 1c), acquired on the Co/Pt reference series (blue points) together with the enhancement of the MR signal obtained on the Co/Pt/Cu* orbital series (red points). Such enhancement of MR is compatible with an additional orbital current generated at the Cu/CuO interface.

For pure spin torques, the typical length scale is given by the spin decoherence length in the ferromagnet. For orbital currents and torques, a different lengthscale might exist as recently shown for Ni [6]. Such lengthscales may then be accessed via the Co thickness (t_{Co}) dependence measurements involving the two spin and orbital additive contributions. As the DL field is known to be inversely proportional to the FM thickness, both spin and orbital decoherence length may be extracted by measuring the dependence of the integrated torque on t_{Co} as obtained from the DL efficiency (see Eq. 1):

$$\xi_{\mathrm{DL}} = \frac{2eM_s t_{Co} H_{DL}}{\hbar j_c} \tag{1}$$

with H_{DL} the DL field, M_s the saturation magnetization and J_c the charge current density. Harmonic hall voltage measurements have been carried out on Co(t)|Pt(3)|Cu(3)* and Co(t)|Pt(4)|Cu(3)* (see Fig. 1b). The values show an expected evolution from SHE scaling with a short decoherence length (about 1 nm) at low thicknesses, indicating that the orbital contribution doesn't affect the torque lenghtscale in Co. To access a potential different lenght for the orbital contribution, Co thickness dependence are currently performed on systems with only light elements : Co(t)|Cu*(3), in which we expect a pure orbital torque to arise.

Our results support the occurrence of orbital currents generated in the naturally oxidized copper layer. Further works are actually performed to disentangle the spin and orbital contribution : torque measurements on light metals-only systems Co|Cu* with both cobalt and copper thickness dependence, as well as spin and orbital-pumping measurements driven by FMR on Co/Pt/Cu* and Co/Pt series. The comparison between these measurements with the actual ones will allow us to quantify precisely the magnitude of the orbital torques and the orbital injection efficiency in these orbital systems.

Acknowledgments

We would like to thank M. Viret, J.-B. Moussy and J.-Y. Chauleau and the CEA-SPEC team for their support on this present work. We acknowledge financial support from the Agence Nationale de la Recherche, France, No. ANR-20-CE30-0022 (ORION).

References

[1] Dongjoon Lee, Dongwook Go, Hyeon-Jong Park, et al. Orbital torque in magnetic bilayers. *Nature Communications* 12, 6710 (2021).

[2] Dongwook Go, Daegeun Jo, Changyoung Kim, and Hyun-Woo Lee. Intrinsic Spin and Orbital Hall Effects from Orbital Texture. *Physical Review Letters* 121, 086602 (2018).

[3] Dongwook Go, Jan-Philipp Hanke, Patrick M. Buhl, et al. Toward surface orbitronics: giant orbital magnetism from the orbital Rashba effect at the surface of sp-metals. *Scientific Reports* 7, 46742 (2017).

[4] Shilei Ding, Andrew Ross, Dongwook Go, et al. Harnessing Orbital-to-Spin Conversion of Interfacial Orbital Currents for Efficient Spin-Orbit Torques. *Physical Review Letters* 125, 177201 (2020).

[5] E. Santos, J.E. Abrão, Dongwook Go, et al. Inverse Orbital Torque via Spin-Orbital Intertwined States. *Physical Review Applied* 19, 014069 (2023).

[6] Hiroki Hayashi, Daegeun Jo, Dongwook Go, et al. Observation of long-range orbital transport and giant orbital torque. *Communications Physics* 6, 32 (2023).

Dynamique de l'aimantation dans des nanostructures soumises à des déformations élastiques : une étude expérimentale et numérique

S. Chiroli[1,*], D.Faurie[1], M. Haboussi[1], A. O. Adeyeye[2,3], and F. Zighem[1]

[1]*LSPM-CNRS UPR3407,Université Sorbonne Paris Nord, Villetaneuse, France*
[2]*Departement of Electrical and Computer Engineering, Information Storage Materials Laboratory, National University of Singapore, Singapore*
[3]*Department of Physics, Durham University, United Kingdom*
**stephane.chiroli@univ-paris13.fr*

Les effets magnétoélastiques dans les films minces et les nanostructures sont devenus un domaine de recherche majeur en raison de leurs aspects fondamentaux et de leurs applications industrielles. Les études fondamentales et les applications liées à ces effets ont été nombreuses au cours du dernier siècle, mais elles ont été relancées ces dernières années car elles sont de plus en plus directement impliquées dans divers thèmes du nanomagnétisme tels que la straintronique, le flexomagnétisme et le magnétisme curviligne. Les effets magnétoélastiques sont essentiellement liés à la magnétostriction et ont pour effet d'une part de déformer un corps ferromagnétique sous l'application d'un champ magnétique (effet direct), et d'autre part d'induire une anisotropie magnétique (magnétoélastique) lorsqu'une contrainte est appliquée à ce corps (effet indirect). Dans notre travail, des objets ferromagnétiques soumis à des déformations élastiques ont été étudiés expérimentalement et par des simulations numériques couplants micromagnétisme et mécanique du solide [1, 2]. Nous présentons à la fois l'évolution temporelle de l'aimantation et l'analyse de fréquence modale de couches minces ferromagnétiques et de réseaux de nanostructures. À cette fin, nous avons couplé numériquement les équations du micromagnétisme (incluant l'énergie magnétoélastiques, équations 1-4) à celles de la mécanique des solides en incluant des conditions aux limites périodiques dans Comsol Multiphysics®.

$$F_{el} = \frac{1}{2}\underline{\underline{\varepsilon^{el}}} : \underline{\underline{\underline{\underline{C}}}} : \underline{\underline{\varepsilon^{el}}} \tag{1}$$

$$\underline{\underline{\varepsilon^{el}}} = \underline{\underline{\varepsilon}} - \underline{\underline{\varepsilon^{m}}} \tag{2}$$

$$\underline{\underline{\varepsilon}}(\vec{u}) = \frac{\vec{\nabla}\otimes\vec{u} + (\vec{\nabla}\otimes\vec{u})^T}{2} \tag{3}$$

$$\underline{\underline{\varepsilon^{m}}} = \frac{3}{2}\lambda\begin{pmatrix} m_x^2 - \frac{1}{3} & m_x m_y & m_x m_z \\ m_x m_y & m_y^2 - \frac{1}{3} & m_y m_z \\ m_x m_z & m_y m_z & m_z^2 - \frac{1}{3} \end{pmatrix} \tag{4}$$

avec F_{el} l'énergie magnétoélastique, $\underline{\underline{\varepsilon^{el}}}$ le tenseur des déformations élastiques, $\underline{\underline{\underline{\underline{C}}}}$ le tenseur des constantes élastiques, $\underline{\underline{\varepsilon^{el}}}$ le tenseur des contraintes totales, $\underline{\underline{\varepsilon^{el}}}$ le tenseur des contraintes d'origine magnétique, $\vec{u}$ le vecteur de déplacment, λ le coefficient de magnétostriction et m_i les composantes de l'aimantation normalisée.

Notre approche par la méthode des éléments finis a d'abord été évaluée pour une couche mince ferromagnétique magnétostrictive ($Ni_{60}Fe_{40}$) en comparant les simulations à des mesures de résonnace ferromagnétique (RFM) ainsi qu'à un modèle macrospin. Les résultats obtenus montrent à la fois une grande précision qualitative observée sur les profils spatiaux des modes simulés (modes uniforme et stationnaires) ainsi qu'un accord remarquable permettant de reproduire les évolutions des fréquences mesurées expérimentalement. La couche mince a par la suite été soumise à des déformations élastiques contrôlées induites par l'application d'un champ électrique au sein d'un substrat ferroélectrique. Parallèlement à ces simulations, une étude expérimentale (RFM *in situ*) a également été mené sur ce système, permettant de valider notre modélisation. Ces essais de déformation biaxial ont montré l'apparition d'une anisotropie induite par le champ magnétoélastique et reproduite avec beaucoup de précision par nos simulations numériques.

Nous avons par ailleurs étudié des réseaux de nanolignes modulées en largeur comme le montre l'image de microscopie électronique de la figure 1-(a). Les expériences de RFM montrent la présence de cinq modes magnétostatiques principaux dont les dépendances fréquentielles en fonction du champ sont présentées sur la figure 1-(b). Les simulations des modes propres que nous avons réalisées en l'absence de déformations appliquées montrent un excellent accord avec les expériences et les profils de modes magnétiques localisés sont comparables à des simulations réalisées par L.L. Xiong et al. [3] sur des réseaux similaires. L'application de déformations mécaniques dans ces réseaux complexes engendre un champ de contrainte hétérogène induisant des disparités significatives sur la variation des fréquences des modes magnétiques comme le montre

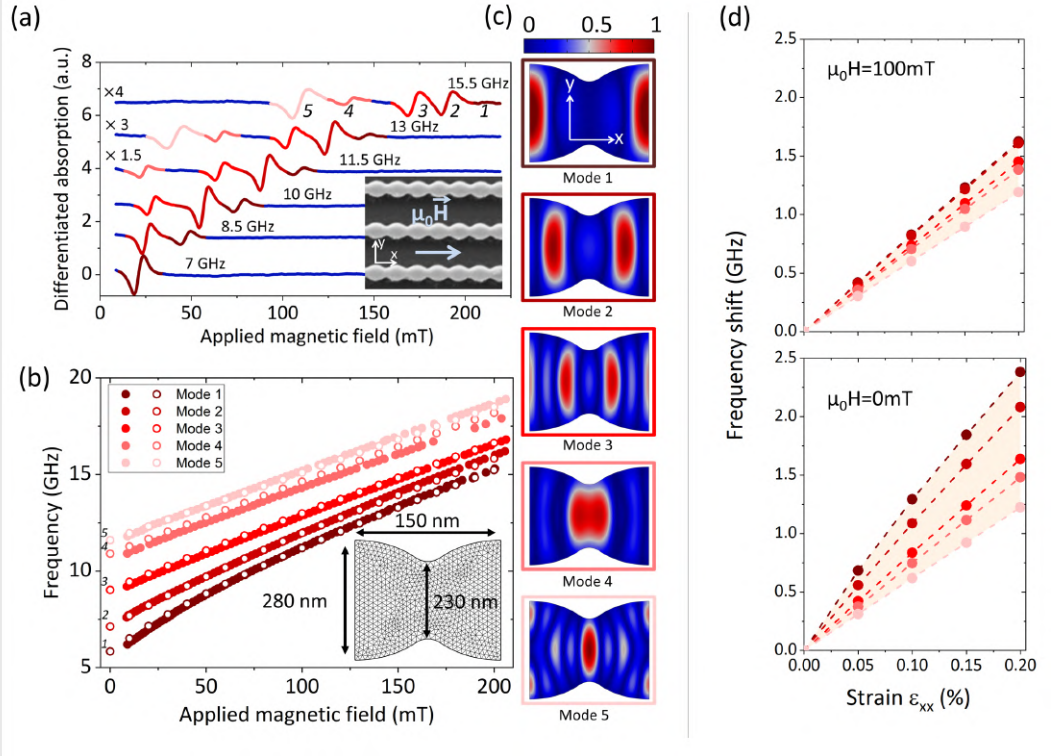

Figure 1: (a) Spectres de résonance ferromagnétique obtenus sur un réseau de nanolignes ferromagnétiques, images MEB en insert. (b) Résultats expérimentaux et simulés montrant les fréquences des modes magnétiques en fonction du champ magnétique. (c) Profils simulés des modes apparaissant sur (a) et (b). (d) Variation de la fréquence de ces modes en présence (haut) et en l'absence (bas) d'un champ appliqué.

la figure 1-(d). Ces variations des énergies des modes magnétiques en fonction de la déformation appliquée permettent de prévoir des applications où l'on pourrait contrôler de manière différenciée les énergies des ondes de spin en fonction des contraintes élastiques appliquées (voir figure 1).

Cet outil de simulation a également été étoffé avec l'implémentation de l'aspect propagatif des ondes de spin nous permettant à présent de simuler leur courbe de dispersion et leurs interactions potentielles avec les ondes acoustiques avec l'ajout de la magnétostriction directe dynamique permettant ces interactions. Ces considérations nouvelles ouvrent la voie vers l'étude de cristaux dits «magphoniques»dont les structures de bandes magnétiques sont facilement influençables par application d'un champ magnétique ou de contraintes mécaniques ayant très peu d'influence sur les bandes phononiques. Il est ainsi aisé de contrôler les bandes de fréquences interdites entre branches magnétiques et bandes phononiques.

References

[1] S. Chiroli, D. Faurie, M. Haboussi, A. O. Adeyeye, and F. Zighem. Magnetization dynamics of elastically strained nanostructures studied by coupled micromagnetic-mechanical simulations. *Physical Review B* (2023 (in press)).

[2] N. Challab, A. D. Aboumassound, F. Zighem, D. Faurie, and M. Haboussi. Micromagnetic modeling of nanostructures subject to heterogeneous strain fields. *Jounral of Physics D: Applied Physics* 52 (2019).

[3] L. L. Xiong, M. Kostylev, and A. O. Adeyeye. Magnetization dynamics of $Ni_{80}Fe_{20}$ nanowires with continuous width modulation. *Physical Review B* 95 (2017).

Temperature- and field-hysteretic magneto-acoustic interaction in FeRh

A.K. Vythelingum[1,*], G. Olivetti[1], D. Nguyen[1], E. Dandeu[1], C. Gourdon[1], and L. Thevenard[1]

[1]*Institut des Nanosciences de Paris, Sorbonne Université, Paris, France*
vythelingum@insp.jussieu.fr

Surface acoustic waves (SAWs) are an effective method to act remotely on magnetic resonance (MR) by coupling coherent phonon modes to collective magnetisation excitations called magnons (or spin-waves (SWs)) [1][2]. The physics behind this interaction springs from magneto-elastic (ME) effective fields (b_θ and b_ϕ), that are entirely dependent on the magneto-elastic constant ($\mathbf{B}_2$), the acoustic strain components (strain ϵ_{ij} and rotation ω_{ij}) and the magnetisation orientation with respect to the SAW wavevector (angle ϕ_M) as given in equation (1). While previous works on SAW-MR have focused on the resonant interaction far from the coercive field, given by the frequency and wave-vector matching: (f_{SAW}=f_{SW} and $\mathbf{k}_{SAW}$=$\mathbf{k}_{SW}$, respectively)[3][4][5], this work examines the often overlooked smaller contribution due to ubiquitous magnetic hysteresis for e.g as seen in Ni [6].

$$\left|b_{field}^{effective}\right| = \sqrt{\left[\frac{2B_2}{M_s}\cos\phi_M\,\epsilon_{xz} - \mu_0 M_s \cos\phi_M\,\omega_{xz}\right]\left[\frac{B_2}{M_s}\sin 2\phi_M\,\epsilon_{xx}\right]} \tag{1}$$

To that end we investigate FeRh, a metallic alloy which, for near equal stochiometric ratio, undergoes a first-order magneto-structural transition from the antiferromagnetic (AFM) to the ferromagnetic (FM) phase. This is accompanied by a continuously varying percentage of FM phase and consequently coercive field value with temperature during the transition. The eigen-frequencies of precession have been calculated by considering the absence/presence of the magnetic hysteresis in the FeRh sample. From figure (1) it can been seen that in the case of a hysteresis, the SW frequency goes to zero GHz at the coercive field value. The softening of the mode thus allows to study SAW-FeRh interaction near coercive fields. Field scans at different temperatures allow to investigate SAW interaction with FM domains, FM-FM domain walls (DWs) and the more exotic AFM-FM DWs.

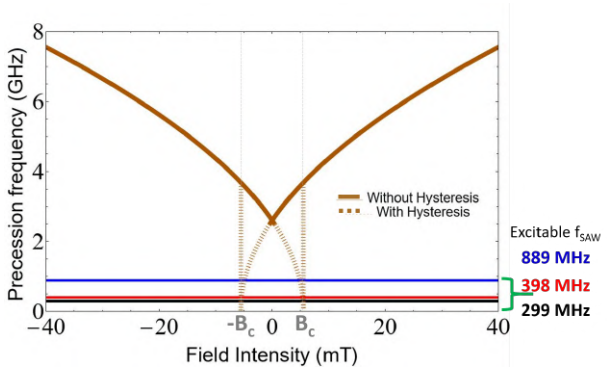

Figure 1: Numerical calculation of the eigenfrequencies at $k_{SW} = 0.654\mu m^{-1}$, in the case where the magnetic hysteresis is considered/ignored. The horizontal lines correspond to the three excitable SAW frequencies in our device.

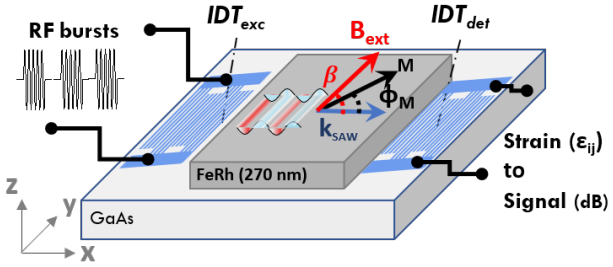

Figure 2: Schematic representation of the FeRh mesa on GaAs substrate with a pair of IDT used to respectively excite and detect the propagating SAW. k_{SAW} is emitted parallel to the crystallographic [110] direction of GaAs. Note that an external magnetic field can be applied making an angle β to the SAW wave-vector k_{SAW} and the equilibrium magnetisation angle is given as ϕ_M.

This work relies on a polycrystalline FeRh mesa of thickness (270 nm) on piezoelectric GaAs. Figure (2) is a schematic representation of the experimental setup where RF bursts are fed to the left-IDT. SAWs are thus generated by piezoelectric effect, travel across the $[110]_{GaAs}$ direction, interact with the metallic FeRh mesa and are detected by the right-IDT. The variation of the SAW amplitude and velocity with either temperature and/or magnetic-field is continuously monitored. Figure (3) gives the variation of SAW amplitude with respect to field for three excitable frequencies at 130°C, *i.e.* in the FM phase. Hysteretic amplitude variations are maximum near the coercive field value, and increase with SAW frequency up to −47 dB/cm at 889 MHz.

This is compatible with resonant ME interaction with frequency matching allowed by mode softening close to the coercive field, see Fig.(1). In order to check this interpretation, we studied the SAW transmission for varying field angle in the fully FM phase. Figure (4) shows that for field parallel and perpendicular to the SAW wavevector, the SAW transmission

is identical, in contrast to what is expected from equation (1). This will be further modelled and discussed by taking into consideration the polycrystallinity of the FeRh layer. Finally we shall present temperature-dependence results that will allow to probe the influence of (i) the coercivity, (ii) the AFM-FM phase coexistence on ME interactions.

To sum up, this work puts into new perspective the importance of hysteresis on magneto-acoustics.

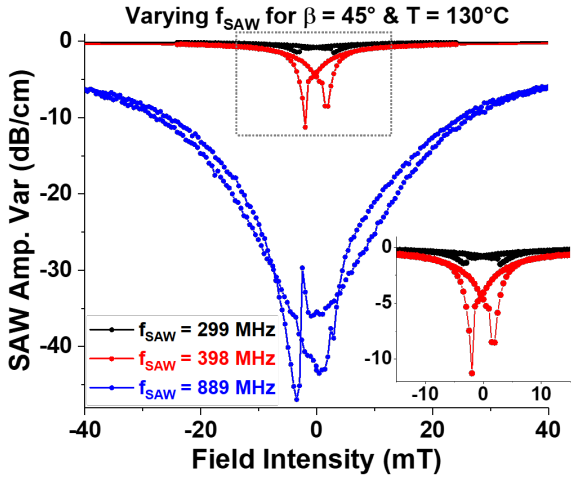

Figure 3: Magnetic field dependence of the transmitted SAW amplitude at fixed field direction for excitable f_{SAW}. Zoomed inset excluding 889MHz.

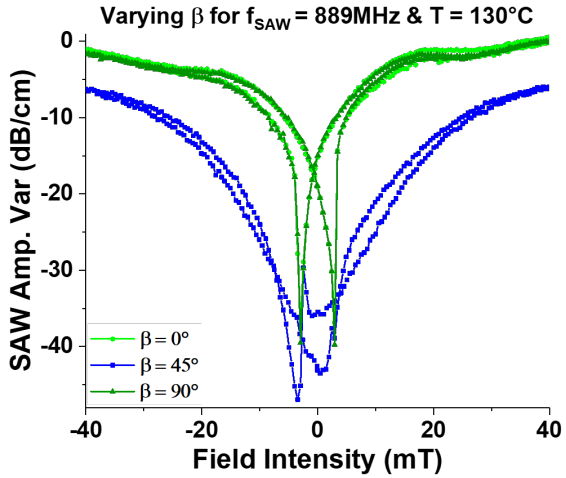

Figure 4: Magnetic field dependence of the transmitted SAW amplitude at varying orientation of the field, β, at 130°C in the fully FM phase

Acknowledgments

This work was supported in part by French MESRI Grant, N0. ANR ACAF 20-CE30-00.

References

[1] Per Delsing, Andrew N Cleland, and Martin J A Schuetz et al. The 2019 surface acoustic waves roadmap. *Journal of Physics D: Applied Physics* 52, 353001 (2019).

[2] L. Thevenard, C. Gourdon, J. Y. Prieur, et al. Surface-acoustic-wave-driven ferromagnetic resonance in (Ga, Mn)(As, P) epilayers. *Physical Review B* 90 (2014).

[3] M. Weiler, L. Dreher, C. Heeg, et al. Elastically Driven Ferromagnetic Resonance in Nickel Thin Films. *Physical Review Letters* 106 (2011).

[4] L. Thevenard, I. S. Camara, S. Majrab, et al. Precessional magnetization switching by a surface acoustic wave. *Physical Review B* 93 (2016).

[5] J.-Y. Duquesne, P. Rovillain, C. Hepburn, et al. Surface-Acoustic-Wave Induced Ferromagnetic Resonance in Fe Thin Films and Magnetic Field Sensing. *Physical Review Applied* 12 (2019).

[6] I-an Feng, M. Tachiki, Charles Krischer, and M. Levy. Mechanism for the interaction of surface waves with 200nm nickel films. *Journal of Applied Physics* 53, 177–193 (1982).

Session 2: Growth and imaging 11h20 – 12h40 *Chair: Bénédicte Warot and Florent Tournus*				
11h20 – 11h40	**Maryam Sadeghiyan Dehaghani**	IPR	Growth and multi-scale properties of hybrid magnetic tunnel junctions: towards the control of spinterfaces	page 22
11h40 – 12h00	**Corentin Pfaff**	IJL	Magnesium diboride thin films for superconducting spintronics	page 24
12h00 – 12h20	**Tristan Clua Provost**	L2C	Quantum sensing with spin defects hosted in a van der Waals material	page 26
12h20 – 12h40	**Cassandra Dailledouze**	LUMIN	Magnetic sensing with NV centers in diamond at pressures above 100 GPa	page 28

Growth and multi-scale properties of hybrid magnetic tunnel junctions: towards the control of spinterfaces

Maryam Sadeghiyan[1,*], Sophie Guézo[1], Sylvain Tricot[1], Bruno Lépine[1], Soraya Ababou-Girard,[1], Pascal Turban[1], and Francine Solal[1]

[1]*Département Matériaux-Nanosciences, Institut de Physique de Rennes, Rennes, France*
*maryam.sadeghiyan@univ-rennes1.fr

In the field of spintronics, there are many reasons to use molecular tunnel barriers in devices such as low cost, flexibility and long spin life time in organic materials [1, 2]. What happens at the interfaces in these organic-inorganic hybrid systems is so relevant to the final device properties that a word has been proposed for it: spinterface [3]. The discrete degree of hybridization at the molecular levels explains the variation of the magneto-transport properties with respect to the type of molecules and the nature of the interfaces [4]. To investigate such spinterface issues there is a need for very well-defined interfaces, which can be obtained in ultra-high vacuum conditions (UHV). The aim of this work is to realize model hybrid hetero-structures with a molecular monolayer as tunnel barrier between two ferromagnetic layers (Magnetic Tunnel Junction). Modifying the way molecules are linked to the substrate, the crystallographic orientation of the substrate and the nature of the molecules are possible ways to modify the system spinterfaces. In this study, the grafting under UHV of the molecular layer (1-hexadecanethiol molecules, noted C16MT) on epitaxial ferromagnetic Fe (001) electrodes has been studied using scanning tunneling microscopy (STM), X-ray and Ultraviolet photoelectron spectroscopy (XPS and UPS). To avoid the formation of pinholes during deposition of the Co ferromagnetic top electrode of the junction, an original soft-landing technique has been used, based on the condensation at low temperature of a Xe layer on the self-assembled monolayer before metal deposition. The electrical homogeneity of the obtained junctions has been controlled from the micro to the nanoscale by Ballistic Electron Emission Microscopy (BEEM) [5], displayed in Figure 1a, b. Investigation of the transport measurements of these model MTJs has validated the success of BLAG technique in pinhole-free molecular junctions' fabrication, shown in Figure 1c. The magnetotransport properties of the named MTJs are in progress and will be confronted to the precise analysis of the system bottom spinterface by spin-resolved IPES (Inverse PhotoEmission Spectroscopy).

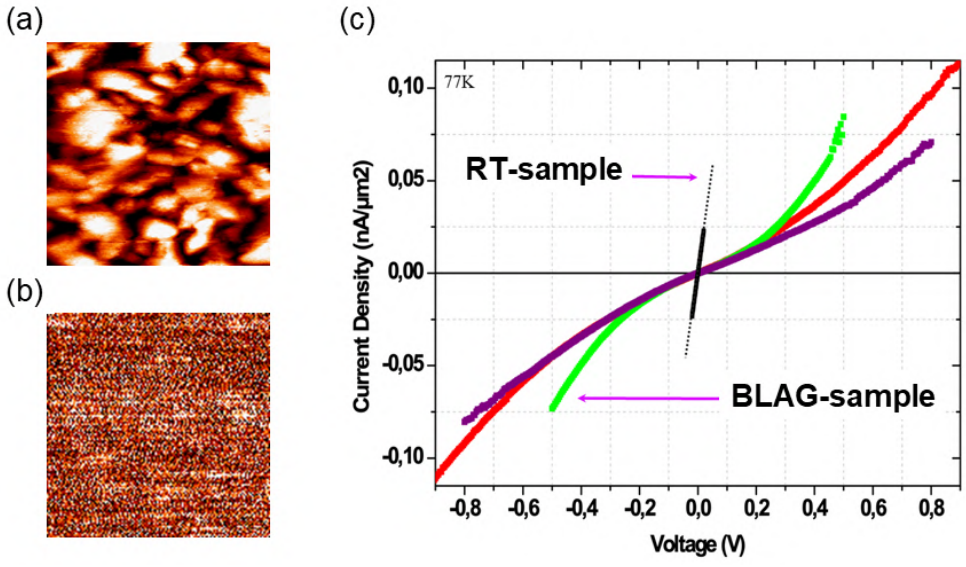

Figure 1: Study of Au/Co/C16MT/GaAs(001) molecular MTJs. (a) STM, (b) BEEM image, 100x100nm². The homogeneity of the BEEM current map demonstrates the absence of pinholes in micro-scale, (c) I-V curve from molecular MTJs of 25μm^2 surface area, top-electrode deposited by BLAG and at RT. Nonlinear I-V curve illustrates electron tunneling through SAMs, BLAG technique thus is validated for fabrication of large area pinhole-free junctions in macro-scale.

References

[1] JR Petta, SK Slater, and DC Ralph. Spin-dependent transport in molecular tunnel junctions. *Physical review letters* 93, 136601 (2004).

[2] Stefano Sanvito. Molecular spintronics. *Chemical Society Reviews* 40, 3336–3355 (2011).

[3] Stefano Sanvito. The rise of spinterface science. *Nature Physics* 6, 562–564 (2010).

[4] Marta Galbiati, Sergio Tatay, Sophie Delprat, et al. Is spin transport through molecules really occurring in organic spin valves? A combined magnetoresistance and inelastic electron tunnelling spectroscopy study. *Applied Physics Letters* 106, 082408 (2015).

[5] Alexandra Junay, Sophie Guézo, Pascal Turban, et al. Spatially resolved band alignments at Au-hexadecanethiol monolayer-GaAs (001) interfaces by ballistic electron emission microscopy. *Journal of Applied Physics* 118, 085310 (2015).

Magnesium diboride thin films for superconducting spintronics

C. Pfaff[1,*], T. Courtois[1], L. Pasquier[1], S. Andrieu[1], S. Petit-Watelot[1], S. Migot[1], J. Ghanbaja[1], M. Emo[1], M. Hehn[1], S. Mangin[1], K. Dumesnil[1], and T. Hauet[1]

[1]*Institut Jean Lamour, Université de Lorraine, Nancy, France*
corentin.pfaff@univ-lorraine.fr

The interplay between magnetism and superconductivity has been heavily studied during the past 30 years and recently led to the concept of superconducting spintronic [1]. Nevertheless, proximity effect, inverse proximity effect or injection of quasiparticles at superconductor/ferromagnet (S/F) interfaces have been essentially investigated in thick niobium or aluminium-based heterostructures grown by sputtering [2] with critical temperatures (T_c) of the order of few Kelvin. S/F stacks with a higher T_c, thinner layers and carefully tuned interfaces would enable the thorough exploration of new superconducting spintronic features, as well as the possible implementation in operating quantum devices.

We report here the growth of epitaxial MgB_2 and MgB_2/F films by Molecular Beam Epitaxy. Depending on the UHV growth conditions, we are able to control either textured polycrystalline or single crystal MgB_2 films, which are characterized by RHEED, XPS, XRD and TEM, as shown in Fig. 1(a). The critical temperature is systematically higher for single crystalline films and is measured for thicknesses as low as 5 nm (Fig. 1(b)). T_c reaches 30 K for films thicker than 15 nm, in good agreement with references [3, 4]. Using BCS model, electrical transport and magnetic measurements reveal a typical coherence length of about 5nm at the 0 K limit for the single crystalline MgB_2 films.

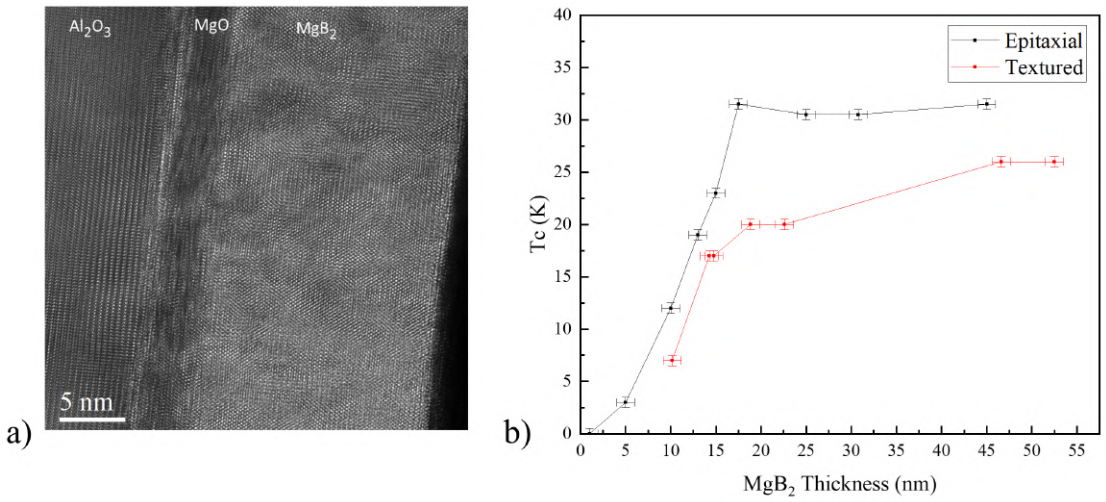

Figure 1: **a)** High resolution TEM micrograph of a Al2O3/MgO/MgB_2/Au structure. **b)** Critical temperature of single crystalline (black) and textured (red) MgB_2 thin films measured for various thicknesses.

The magnetic investigation under an external magnetic field applied perpendicular to the films has revealed an unexpected behaviour. This behaviour is characterized by an "inverted" loop (Fig. 2(a), 30K); i.e. an opposite moment compared to the usual M(H) loop described by Bean or Kim-Ji models [5, 6]. This "inverted" state is stabilized by (i) reducing the superconductor thickness and (ii) increasing the temperature. For the largest tested thickness (91nm) the "inverted" state is observed for temperatures above $0.9T_c$ but it can extend down to $0.3T_c$ for a 13nm thick film. Neither structural characteristics (textured or single crystalline) nor the chemical nature (MgB_2, Nb or V) of the film significantly affect the occurrence of this inverted loop. However, dynamical effects do have a clear influence: the measurements performed with a fast field sweeping rate (15mT/s) tend to favour a "bulk-like" behaviour that eventually relaxes towards the "inverted" one, which is itself favoured by a slow sweeping rate (0.1 mT/s). A phenomenological model based on the film geometry, will be proposed to explain these original experimental data.

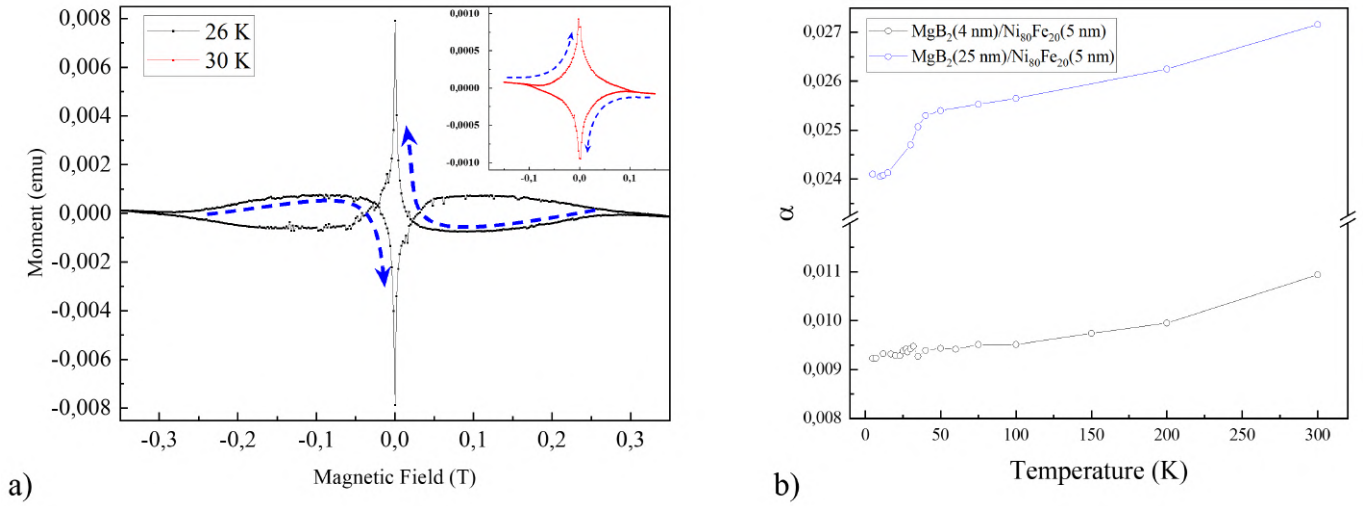

Figure 2: **a)** SQUID-VSM measurement of an epitaxial MgB_2 thin film (91nm) with a magnetic field applied along the normal. Measurements are done with a field sweeping rate of 0.1 mT/s. At 26 K (black) crosses between M(H) parts ($H_{max} \rightarrow H_{min}$ & $H_{min} \rightarrow H_{max}$) indicate the coexistence of the "inverse" state with the bulk-like one, while at 30 K (red) only the "inverse" state remains (See Inset). Blue arrows give the field sweeping direction. **b)** Temperature dependence of Gilbert damping for two MgB2/$Ni_{80}Fe_{20}$ stacks, with (blue, empty symbols) and without (black, empty symbols) superconducting transition.

Besides, MgB_2/F stacks have then been synthetized to explore their electronic properties. The growth of a Co or Permalloy layer on top of MgB_2 only reduces T_c by about 1K and allows us to investigate MgB_2/F heterostructures with critical temperature close to or above 30K. Ferromagnetic Resonance (FMR) measurements have been performed, in order to probe spin transport from F into MgB_2. The temperature dependent magnetization damping of the F layer was extracted in two stacks with different MgB_2 thicknesses (Fig. 2(b)). As expected from previous works on Nb/$Ni_{80}Fe_{20}$ [5] and NbN/$Ni_{80}Fe_{20}$ [7], the channel of momentum loss in the MgB_2 (25nm) layer is suppressed by the opening of the superconducting gap below T_c. This leads to the drop of the damping parameter below T_c in MgB_2/$Ni_{80}Fe_{20}$ bilayers (Fig. 2(b)). The drop is absent for the sample with 4nm thick MgB_2 layer that doesn't exhibit any transition towards the superconducting state.

Our results on epitaxial MgB_2-based thin films and heterostructures are promising for the investigation of superconducting spintronic physics over a large range of temperature and under temperatures larger than the H_2 liquid-gaz transition. They would also enable to study the properties related to this specific superconducting material in its single crystalline form.

References

[1] Jacob Linder and Jason W. A. Robinson. Superconducting spintronics. *Nature Physics* 11, 307–315 (2015).

[2] C. Bell, S. Milikisyants, M. Huber, and J. Aarts. Spin Dynamics in a Superconductor-Ferromagnet Proximity System. *Physical Review Letters* 100, 047002 (2008).

[3] Chen Zhang, Yue Wang, Da Wang, et al. Suppression of superconductivity in epitaxial MgB $_2$ ultrathin films. *Journal of Applied Physics* 114, 023903 (2013).

[4] Michio Naito and Kenji Ueda. MgB2 thin films for superconducting electronics. *Superconductor Science and Technology* 17, R1–R18 (2004).

[5] C. P. Bean. Magnetization of Hard Superconductors. *Physical Review Letters* 8, 250–253 (1962).

[6] D.-X. Chen and R. B. Goldfarb. Kim model for magnetization of type-II superconductors. *Journal of Applied Physics* 66, 2489–2500 (1989).

[7] Manuel Müller, Lukas Liensberger, Luis Flacke, et al. Temperature-dependent spin-transport and current-induced torques in superconductor/ferromagnet heterostructures. *Physical Review Letters* 126, 087201 (2021).

Quantum sensing with spin defects hosted in a van der Waals material

T. Clua-Provost [1], A. Durand [1], P. Kumar [1], F. Fabre [1], J. Li [2], J. H. Edgar [2], V. Ivady [3], P. Udvarhelyi [4], A. Gali [4], X. Marie [5], C. Robert [5], A. Dréau [1], B. Gil [1], I. Philip [1], A. Finco [1], G. Cassabois [1], and V. Jacques[1,*]

[1]*Laboratoire Charles Coulomb, Université de Montpellier and CNRS, 34095 Montpellier, France*
[2]*Tim Taylor Department of Chemical Engineering, Kansas State University, Manhattan, Kansas 66506, USA*
[3]*Max Planck Institute for the Physics of Complex Systems, Nothnitzer Strabe 38, 01187 Dresden, Germany*
[4]*Wigner Research Centre for Physics, P.O. Box 49, H-1525 Budapest, Hungary*
[5]*Université de Toulouse, INSA-CNRS-UPS, LPCNO, 135 Avenue Rangueil, 31077 Toulouse, France*
*vincent.jacques@umontpellier.fr

Quantum sensing technologies based on **solid-state spin defects** have already shown a huge potential to cover the growing need for high-precision sensors [1], both for fundamental research and for industrial applications. The most advanced quantum sensing platforms to date rely on optically- active spin defects embedded in three-dimensional (3D) materials. A prime example is the nitrogen- vacancy (NV) center in diamond, which has already found a wide range of applications in condensed matter physics, life sciences and geophysics [2]. Despite such success, NV-based quantum sensing technologies still face several limitations that mainly result from the 3D structure of the diamond host matrix. They include (i) a limited proximity between the quantum sensor and the target sample, which hampers its sensitivity, and (ii) the inability to engineer ultrathin and flexible diamond layers, precluding an easy transfer of the quantum sensing unit onto the samples to be probed as well as its integration into complex multifunctional devices. An emerging strategy to circumvent these limitations consists in using spin defects embedded in a **van der Waals crystal** that could be exfoliated down to the monolayer limit. Such a *2D quantum sensing foil* would offer atomic-scale proximity to the probed sample together with an increased versatility and flexibility for device integration.

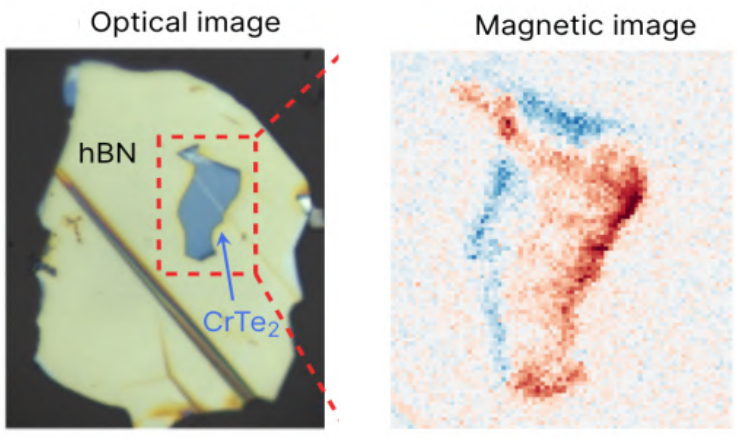

Figure 1: Magnetic field imaging using spin defects in a vdW material (hBN)

Hexagonal boron nitride (**hBN**) is currently the most promising van der Waals crystal for the design of quantum sensing foils [3]. This insulating material, which can be easily exfoliated down to few atomic layers while maintaining chemical stability, is extensively used for encapsulation of van der Waals heterostructures. Furthermore, hBN hosts a broad diversity of optically-active point defects owing to its wide bandgap [4]. In this work, we focus on the negatively-charged boron-vacancy (**VB^-**) center in hBN, which features magneto-optical properties very similar to those of the NV defect in diamond, with a spin triplet ground state whose electron spin resonance (ESR) frequencies can be measured via optically-detected magnetic resonance methods at room temperature [5] [6]. We analyze the performances of thin hBN flakes doped with VB^- centers for quantitative **magnetic field imaging in van der Waals heterostructures** [7]. As a proof-of-concept, we image the magnetic field produced by $CrTe_2$, a van der Waals ferromagnet with a Curie temperature above 300 K. Finally, we investigate how the properties of VB^- centers evolve with the hBN thickness down to the monolayer limit [8].

Acknowledgments

We wish to acknowledge the Institut Quantique Occitan for the funding of this Phd.

References

[1] C.L. Degen, F. Reinhard, and P. Cappellaro. Quantum sensing. *Rev. Mod. Phys.* 89, 035002 (25, 2017).

[2] L. Rondin, J.-P. Tetienne, T. Hingant, et al. Magnetometry with nitrogen-vacancy defects in diamond. *Rep. Prog. Phys.* 77, 056503 (2014).

[3] J.-P. Tetienne. Quantum sensors go flat. *Nat. Phys.* 17, 1074–1075 (2021).

[4] Toan Trong Tran, Kerem Bray, Michael J. Ford, Milos Toth, and Igor Aharonovich. Quantum emission from hexagonal boron nitride monolayers. *Nat Nanotechnol* 11, 37–41 (2016).

[5] Andreas Gottscholl, Mehran Kianinia, Victor Soltamov, et al. Initialization and read-out of intrinsic spin defects in a van der Waals crystal at room temperature. *Nat. Mater.* 19, 540–545 (2020).

[6] A. Haykal, R. Tanos, N. Minotto, et al. Decoherence of VB^- spin defects in monoisotopic hexagonal boron nitride. *Nat Commun* 13, 4347 (27, 2022).

[7] P. Kumar, F. Fabre, A. Durand, et al. Magnetic Imaging with Spin Defects in Hexagonal Boron Nitride. *Phys. Rev. Appl.* 18, L061002 (21, 2022).

[8] A. Durand, T. Clua-Provost, F. Fabre, et al. Optically-active spin defects in few-layer thick hexagonal boron nitride. *arXiv :2304.12071* (9, 2023).

Magnetic sensing with NV centers in diamond at pressures above 100 GPa

C. Dailledouze[1,*], A. Hilberer[1], L. Toraille[2], L. Hanlon[1], M.-P. Adam[1], G. Weck[2], M. Schmidt[1], P. Loubeyre[2], and J.-F. Roch[1]

[1]*LuMIn, ENS Paris-Saclay, 4 Avenue des sciences, 91190 Gif-sur-Yvette, France*
[2]*CEA, DAM, DIF, Chemin du Ru, 91680 Bruyères-le-Châtel, France*
*cassandra.dailledouze@ens-paris-saclay.fr

Diamond anvil cell (DAC) technology is widely used to study the electronic and magnetic properties of materials under high pressure. These materials can exhibit exotic phases of matter such as superconductivity with record critical temperatures. The main difficulty with using the DAC lies in the challenge to measure magnetic properties at high pressure (above 100 GPa) due to the minute sample size.

Here we report the implementation of high-pressure magnetometry by using diamond defects which are nitrogen-vacancy (NV) centers. These atomic like quantum systems can be implanted into the tip of diamond anvils. Due to their spin properties, NV centers are highly sensitive magnetic probes and their atomic size can allow for sub-micrometer spatial resolution. Using a customized optical microscope, we observe the spin dependent luminescence of NV centers, in order to map the magnetic field at the diamond anvil tip. The expulsion of magnetic field lines due to the Meissner effect in a superconductor results in a clear drop of the magnetic field in the close vicinity of the sample, where the NV sensors are located [1]. This detection provides an unambiguous diagnosis of superconductivity that does not rely on questionable electrical contacts or indirect probes once implemented at high pressure. This procedure can be performed on any magnetic sample and is compatible with synchrotron X-ray diffraction for structural characterization [2].

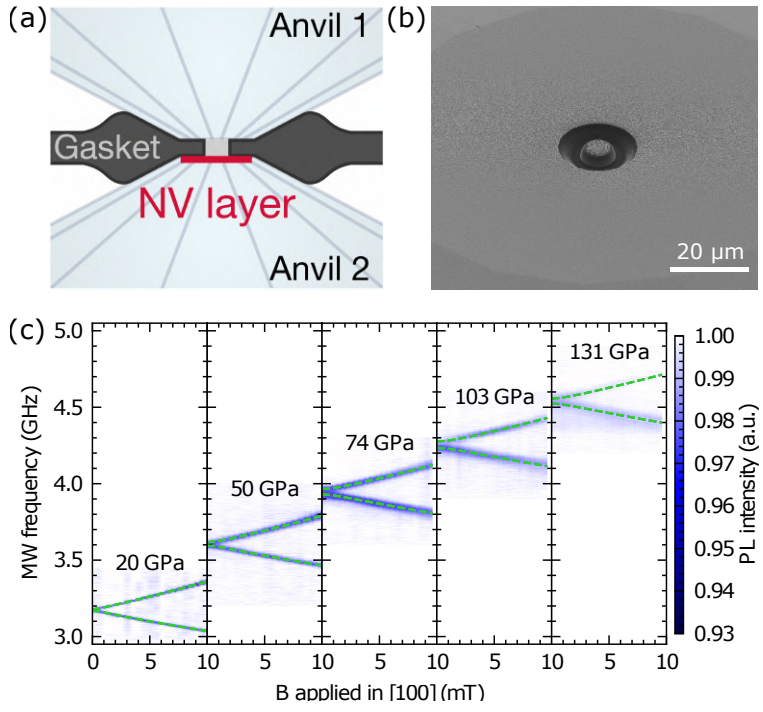

Figure 1: (a) Schematic cross-section of the location of NV centers implanted as a layer below the anvil culet surface in the DAC. (b) SEM of the diamond anvil tip with the micropillar that ensures hydrostatic compression of the NV centers. (c) ODMR spectrum of the NV centers as a function of pressure and applied magnetic field.

We demonstrate that NV magnetic micro-sensing can be implemented above 100 GPa by ensuring a quasi-hydrostatic stress environment for the NV centers [3]. This hydrostatic environment is obtained by machining a mircopillar on the tip of the anvil, as shown is Figure 1 (b). This result increases the pressure range of NV micro-sensing, with a magnetic dependence of the Zeeman effect independant of pressure. Our results enable the undisputable detection of the Meissner effect in super-hydrides that is currently under stifling debate.

References

[1] M. Lesik, T. Plisson, L. Toraille, et al. Magnetic measurements on micrometer-sized samples under high pressure using designed NV centers. *Science* 366, 1359–1362 (2019).

[2] L.Toraille, A. Hilberer, T. Plisson, et al. Combined synchrotron x-ray diffraction and NV diamond magnetic microscopy measurements at high pressure. *New Journal of Physics* 22, 103063 (2020).

[3] A. Hilberer, L. Toraille, C. Dailledouze, et al. Enabling quantum sensing under extreme pressure: Nitrogen-vacancy magnetometry up to 130 GPa. *Physical Review B* 107, L220102 (2023).

Session 3: Applications 14h30 – 16h30 *Chair: Richard Mattana and Laurent Ranno*				
14h30 – 14h50	**Mathieu Lamblin**	IPCMS	Quantum Spintronic Energy Harvester	page 31
14h50 – 15h10	**Andrea Visona**	LTM SPINTEC	Cellular Interaction with Low-Frequency -Vibrating Magnetic Nanoparticles in Bio-Mimetic Mechanical Environment	page 33
15h10 – 15h30	**Tianwen Huang**	GEEPS	Investigation of stress-induced self-biased magnetoelectric composites for powering implanted biomedical devices	page 35
15h30 – 15h50	**Erwan Plouet**	UMR CNRS/Thales	Fully Parallel Spintronic Convolutional Layer with Frequency Interconnectivity	page 37
15h50 – 16h10	**Lucile Soumah**	SPINTEC	Scalable Superparamagnetic Tunnel Junctions for Unconventional Computing	page 39
16h10 – 16h30	**Valentin Desbuis**	IJL	Low-energy spin manipulation in the molecular field of a magnetic thin film	page 41

Quantum Spintronic Energy Harvester

Mathieu Lamblin[1,*], Bhavishya Chowrira[1], Lalit Kandpal[1], Talha Zafar[1], Benoit Gobaut[1], Victor Da Costa[1], Wolfgang Weber[1], Samy Boukari[1], Michel Hehn[2], Bertrand Vileno[3], Daniel Lacour[2], and Martin Bowen[1,*]

[1]*Institut de Physique et Chimie des Matériaux de Strasbourg, UMR 7504 CNRS, Université de Strasbourg, 23 Rue du Lœss, BP 43, 67034 Strasbourg, France*
[2]*Institut Jean Lamour UMR 7198 CNRS Université de Lorraine BP 70239, Vandœuvre les Nancy 54506, France*
[3]*Institut de Chimie UMR 7177 CNRS Université de Strasbourg, 4 Rue Blaise Pascal, CS 90032, Strasbourg 67081, France*
*mathieu.lamblin@ipcms.unistra.fr, bowen@unistra.fr

Quantum heat engines have attracted extensive research as they give us a glimpse of abundant, continuous, dense, microscopic and environmentally friendly power sources [1]. Recent theory [2] and experimentation [3] have showcased how to use quantum features in order to harvest thermal energy stored as quantum heat and convert it into usable work. So far, this has required cumbersome external energy sources [4], therefore nullifying their potential standalone use cases.

Our team has proposed a spintronic implementation of such an engine that can operate autonomously by rectifying the quantum fluctuations of a spin chain trapped inside a ferromagnetic tunnel junction (see Figure. 1) [5]. We will describe additional experiments, in which the spin chain is borne by the Co paramagnetic centers of phthalocyanine molecules, and is maintained in a coherent superposition of states thanks to electron-spin selecting Fe/C_{60} interfaces [6]. This generates a spontaneous current across several molecular nanodevices.

To explain these results, we will introduce the spintronic engine and give insight towards its quantum description in terms of transport, spin, thermodynamics and quantum resources. The design of our spintronic implementation will be presented along with details showing the key structural elements that enable its quantum advantage. An overview on the magneto-transport experimental results will be shown, featuring details regarding its spintronic signatures, power output and thermal response [6]. This presentation will be followed by a brief description of the theoretical model under study, which aims at explaining the spontaneous current generation we observe in our device [7].

Two complementary approaches will be considered. A first description relies on the energy and negentropy provided by autonomous measurement back-action: the operation of the engine is split into two strokes: a thermalizing stroke that releases electrical work into the bath thanks to the relaxation of the system, followed by a measurement stroke that energizes the system by killing the entanglement present in the steady-state. The second approach models the device as a continuous engine that produces work thanks to a bosonic drive resulting from self-sustained molecular vibrations [7].

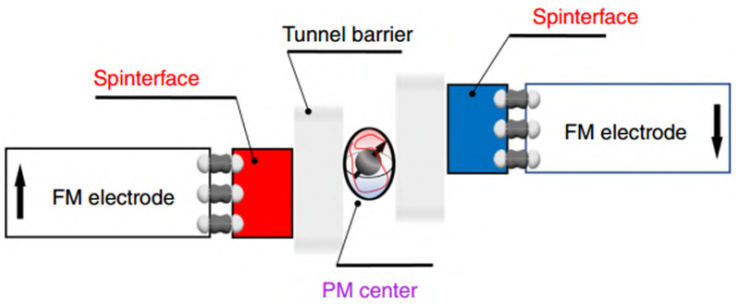

	Source	Typ. Pd (mW/cm²)	Constraint
Natural	Paramagnetic fluctuators in a MTJ	30000	R&D / Engineering...
Artificial	Solar	50	Not 24/7
	Thermoelectric	30	T gradient
	RF power	1	Distance/ Harmonics
	Vibration/PZT	0.2	Vibration frequency
	Vibration/EM	10	AC/DC conversion

Figure 1: Schematic of the spintronic engine (left) and table comparing the power densities of conventional energy harvesters with our engine (right) [5]

References

[1] Aslı Tuncer and Özgür E Müstecaplioğlu. Quantum Thermodynamics and Quantum Coherence Engines (2020).

[2] Cyril Elouard and Andrew N. Jordan. Efficient Quantum Measurement Engines. *Physical Review Letters* 120 (2018).

[3] Kensaku Chida, Samarth Desai, Katsuhiko Nishiguchi, and Akira Fujiwara. Power generator driven by Maxwell's demon. *Nature Communications* 8 (2017).

[4] James Klatzow, Jonas N. Becker, Patrick M. Ledingham, et al. Experimental Demonstration of Quantum Effects in the Operation of Microscopic Heat Engines. *Physical Review Letters* 122 (2019).

[5] K. Katcko, E. Urbain, B. Taudul, et al. Spin-driven electrical power generation at room temperature. *Communications Physics* 2 (2019).

[6] Bhavishya Chowrira, Lalit Kandpal, Mathieu Lamblin, et al. Quantum Advantage in a Molecular Spintronic Engine that Harvests Thermal Fluctuation Energy. *Advanced Materials* 34, 2206688 (2022).

[7] Mathieu Lamblin and Martin Bowen. The Quantum Measurement Spintronic Engine: Using Entanglement to Harvest Vacuum Fluctuations (2023).

Cellular Interaction with Low-Frequency-Vibrating Magnetic Nanoparticles in Bio-Mimetic Mechanical Environment

A. Visonà[1, 2, *], B. Dieny[2], R. Morel[2], H. Joisten[2], and A. Nicolas[1]

[1]*Univ. Grenoble Alpes, CNRS, LTM, 38000 Grenoble, France*
[2]*Univ. Grenoble Alpes, CEA, CNRS, Spintec, 38000 Grenoble, France*
**andrea.visona@cea.fr*

Nanotechnologies have the potential of reshaping the biomedical scene, opening the doors to novel approaches for therapies and detection techniques. Among these, magnetic nanoparticles (MNPs) have already shown to be very promising thanks to their ability of being controlled remotely through magnetic fields. Indeed, applications which space in all domains of biomedical fields have risen in the past years, such as disease treatment, imaging contrast agent, drug delivery and regenerative medicine.

In particular, vibrating MNPs can can be used to exert very local forces and transfer mechanical energy at cellular scale. They can be exploited to target mechanosensitive proteins and trigger their associated mechanotransduction processes, influencing therefore cellular life. For instance, it was shown that low frequency vibrating particles (few Hz range) can induce apoptosis in cancer cells [1], [2] or increase insulin release in pancreatic cells [3].

Indeed, in the past decades more and more knowledge has been provided about the mechano-sensitivity of cells with respect of the surrounding environment. A constant exchange of forces between the cell and the extracellular matrix (ECM) or between neighbouring cells is responsible of different cellular functions such as motility, proliferation, shape modifications and even gene and protein expression [4]. For this reason, it has become clear that studying cell behaviour on traditional culture substrate, such as plastic and glass, could mislead the preliminary *in vitro* tests, due to the huge difference in mechanical properties compared to almost all physiological environments (Stiffness of GPa instead of kPa). Very viable options to mimic mechanical properties of the ECM are Hydrogels; in particular Polyacrylamide gels (PAAG) allow different level of polymerisation for a fine tuning of the Young's modulus and easy protein coating. [5]

The Nanoparticles we use are called Vortex Micro-disks because of their magnetic and geometrical structure as shown in figure (1). They are fabricated by a "top-down approach" (lithography/metal deposition/lift-off) for a fine shape and size control. The design of the particles was optimised in order to maximise the transferable mechanical energy under vibration, their biocompatibility and dispersion [1].

We present a study of the interaction of the cells with MNPs, either static or vibrating, as a function of substrate stiffness, the cells are grown on. Two cell types have been studied: U87 Glioblastoma human cancer cells and NIH 3T3 mice fibroblast to compare the behaviour of two very standard representatives of cell types, cancer and healthy one respectively.

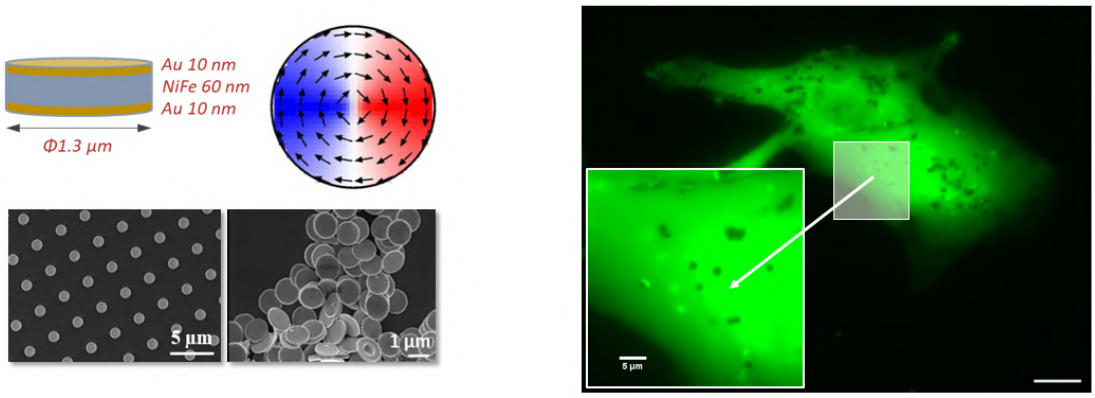

Figure 1: On the left, drawing of the Vortex micro-disks geometrical and magnetic structure and SEM images of the particles. On the right, epifluorescence image of transfected U87 (GFP) that have been incubated with MNPs. Scale bar is 25µm.

The interaction of cell with magnetic nanoparticles in absence of field was deeply studied in order to be able to decouple the effect of the simple presence of MNPs to their field-induced vibration. In particular, it was shown that cellular metabolic activity and proliferation is altered differently when exposed to MNPs depending on the mechanical properties of substrates and the cell type.

Concerning the Magneto-mechanical stimulation, based on previous studies [6], amplitude, duration and frequency of the field alongside particles concentration proved to play an important role in the cells aftermaths. The parameters of the magneto-mechanical stimulation have been therefore chosen such that both large effects (like cell death) and more subtle ones (like force rearrangement, difference in motility) could be achieved and evaluated.

Acknowledgments

We would like to acknowledge the Université de Grenoble Alpes (UGA) for funding the project, the Plateforme Technologie Amont (PTA/LTM) and CLINATEC for technical support.

References

[1] Selma Leulmi, Xavier Chauchet, Melissa Morcrette, et al. Triggering the apoptosis of targeted human renal cancer cells by the vibration of anisotropic magnetic particles attached to the cell membrane. *Nanoscale* 7, 15904–15914 (2015).

[2] Dong-Hyun Kim, Elena A. Rozhkova, Ilya V. Ulasov, et al. Biofunctionalized magnetic-vortex microdiscs for targeted cancer-cell destruction. *Nature Materials* 9, 165–171 (2009).

[3] Svetlana Ponomareva, Helene Joisten, Taina François, et al. Magnetic particles for triggering insulin release in INS-1E cells subjected to a rotating magnetic field. *Nanoscale* 14, 13274–13283 (36 2022).

[4] Fabiana Martino, Ana R. Perestrelo, Vladimir Vinarský, Stefania Pagliari, and Giancarlo Forte. Cellular Mechanotransduction: From Tension to Function. *Frontiers in Physiology* 9 (2018).

[5] Aleksandra K. Denisin and Beth L. Pruitt. Tuning the Range of Polyacrylamide Gel Stiffness for Mechanobiology Applications. *ACS Applied Materials and Interfaces* 8, 21893–21902 (2016).

[6] C. Thébault, M. Marmiesse, C. Naud, et al. Magneto-mechanical treatment of human glioblastoma cells with engineered iron oxide powder microparticles for triggering apoptosis. *Nanoscale Advances* (2021).

Investigation of stress-induced self-biased magnetoelectric composites for powering implanted biomedical devices

Tianwen HUANG[1, *], Loïc Becerra[2], Aurélie Gensbittel[1], Yunlin Zheng[2], Hakeim Talleb[1], Zhuoxiang Ren[1], and Massimiliano Marangolo[2]

[1]*Sorbonne Université, CNRS, Laboratoire de Génie Electrique et Electronique de Paris, 75252, Paris, France,*
Université Paris-Saclay, CentraleSupélec, CNRS, Laboratoire de Génie Electrique et Electronique de Paris, 91192, Gif-sur-Yvette, France
[2]*Sorbonne Université, CNRS, Institut des NanoSciences de Paris, INSP, UMR7588, F-75005 Paris, France*
**tianwen.huang@sorbonne-universite.fr*

Magnetoelectric (ME) laminate composites are notable heterostructures that interrelate magnetostrictive and piezoelectric substances via elastic strain, enabling electric polarization in response to a magnetic field or vice versa. Their unique properties make them suitable for several engineering applications including sensors, actuators, and particularly as energy transducers for wirelessly powering implanted biomedical devices [1]. Conventionally, the ME response is optimal under a small dynamic magnetic signal H_{ac} around a fixed static bias magnetic field H_{DC}. In this biomedical context, recent articles have shown the feasibility that an embedded sensor chip can be powered by a neighbouring ME resonator activated, through the human body by a weak dynamic magnetic field working in a frequency range that is transparent to the human body (hundreds of kHz), while respecting the exposure limit value (1 Oe). However, the requirement of H_{DC} (tipically hundreds of Oe) necessitates the use of permanent magnets, presenting a significant drawback for the development of implantable electronic devices. To address this issue, the self-biased ME composites that can induce a significant ME response in the absence of H_{DC} are emerging as an attractive alternative [2].

This study aims to elucidate the origin of the observed self-biased ME behavoir by comparing two distinct magnetoelectric trilayer composites Ni/(YXl)36° $LiNbO_3$/Ni (20×5×0.1 mm^3) and Ni/PZT-5H/Ni (11×5×0.22 mm^3), with approximately 10 μm thick Ni films deposited using RF sputtering. The ME performance investigation predominantly concentrates on the ME Longitudinal-Transverse (L-T) operational mode, illustrated in Fig. 1a, where longitudinal magnetic excitation is applied, consequently inducing a transversal electric voltage V, and the efficiency of the ME composites is commonly measured using the magnetoelectric coefficient expressed as $\alpha_{ME} = \delta V/(\delta H_{ac} \cdot t_p)$, where t_p is the thickness of the piezoelectric layer. As depicted in Fig. 1b, the Ni/(YXl)36° $LiNbO_3$/Ni composite demonstrates a self-biased behavior with a high remanent ME coefficient, in contrast to the Ni/PZT-5H/Ni composite.

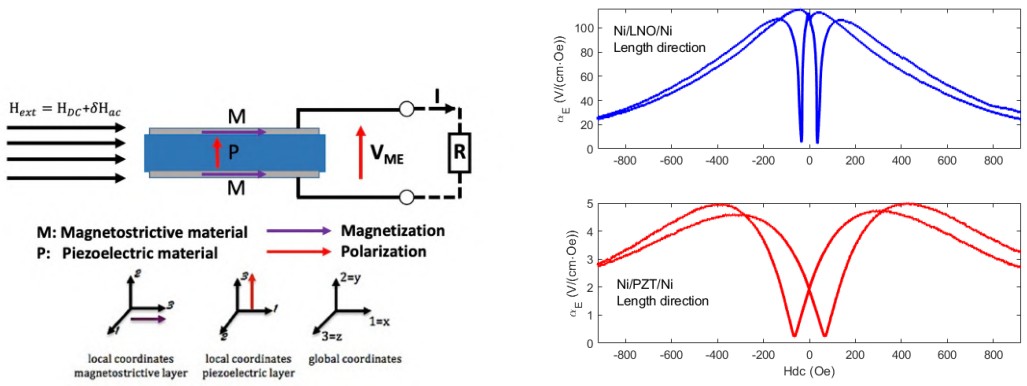

(a) (b)

Figure 1: (a) The studied ME composite is excited in L-T mode. (b) Measurements of the ME coefficient in quasi-static regime.

The ME coupling combines both piezomagnetic and piezoelectric effects, with the assumption that both effects exhibit linearity. Based on the approach presented in [3], the ME coefficient can be expressed as the multiplication of gradients corresponding to piezomagnetic and piezoelectric effects. Consequently, the magnetic field dependence of the ME coefficient can be described as $\alpha_E \propto \frac{\partial S}{\partial H} = \frac{\partial \lambda}{\partial H}$, where λ represents the strain resulting from magnetostriction. Considering that λ is

proportional to M^2, we arrive at the relation $\alpha_E \propto \frac{\partial M^2}{\partial H}$, which connects the ME response to the magnitude of magnetization. As shown in Fig. 2a, we corroborate the hypothesis that the observed variations in magnetic behavior between ME trilayer composites and the isolated Ni films can be attributed to thermal stress induced by the cooling process subsequent to the sputtering procedure [4]. These residual thermal stresses can be generally expressed as Eq. 1 [5]. This hypothesis is supported by in-plane X-ray diffraction measurements, which confirmed the measurements of changes in atomic spacing of the nickel film. In conclusion, we can attribute the self-biased ME behavior to the change in magnetic behavior of the Ni films induced by stress.

$$\sigma_{r,ii} = C_{e,iikl}(\alpha_s - \alpha_f)_{kl} \triangle T \tag{1}$$

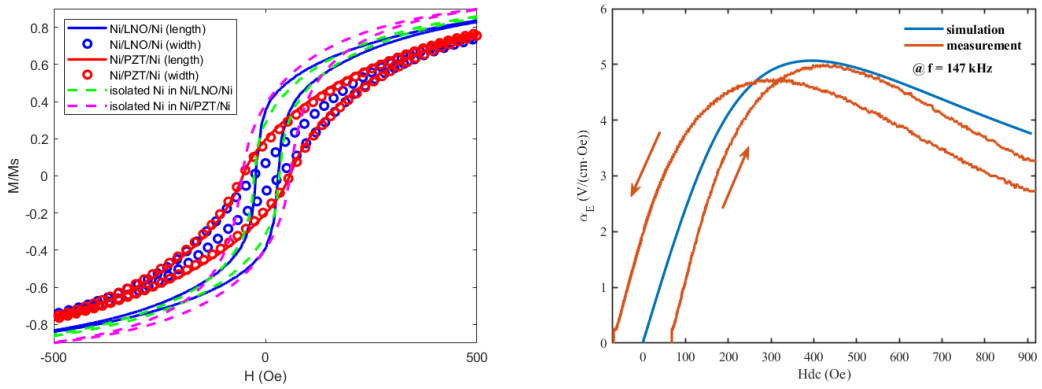

(a) (b)

Figure 2: (a) M-H curves of trilayer composites and their isolated Ni. (b) Comparison between ME measurement and simulation of Ni/PZT-5H/Ni composite in quasi-static regime

Moreover, we have developed a numerical code using the Finite Element Method (FEM) as a versatile analysis tool for multiphysics simulations. In order to accurately capture the magnetoelastic coupling of thin magnetostrictive structures, we employ the nodal shell element approach. Additionally, we enhance the FEM formulation by incorporating a simplified magnetoelastic anhysteretic model to accurately represent the nonlinear behavior of the nickel (Ni) material. An example simulation result of Ni/PZT-5H/Ni in quasi-static regime as depicted in the Fig. 2b, exhibits a good accordance with the measurements. The primary goal is to provide a valuable tool that can facilitate our ongoing research on combining Ni with different crystalline cuts of $LiNbO_3$ or diverse piezoelectric materials, with the aim of achieving improved performance in the field of self-biased ME effects

Acknowledgments

This research has received funding from the French National Research Agency under the project Biomen (Projet-ANR-18-CE19-0001).

References

[1] S Kopyl, R Surmenev, M Surmeneva, Y Fetisov, and A Kholkin. Magnetoelectric effect: principles and applications in biology and medicine–a review. *Materials Today Bio* 12, 100149 (2021).

[2] Yuan Zhou, Deepam Maurya, Yongke Yan, et al. Self-biased magnetoelectric composites: an overview and future perspectives. *Energy Harvesting and Systems* 3, 1–42 (2016).

[3] Yuan Zhou, Su Chul Yang, Daniel J Apo, Deepam Maurya, and Shashank Priya. Tunable self-biased magnetoelectric response in homogenous laminates. *Applied Physics Letters* 101, 232905 (2012).

[4] *Patent pending No.FR230315, France*.

[5] Thanh-An Truong, Tuan-Khoa Nguyen, Hangbo Zhao, et al. Engineering stress in thin films: An innovative pathway toward 3D micro and nanosystems. *Small* 18, 2105748 (2022).

Fully Parallel Spintronic Convolutional Layer with Frequency Interconnectivity

Erwan Plouet[1, *], Dédalo Sanz Hernández[1], Pankaj Sethi[1], Nathan Leroux[1], Bruno Dlubak[1], Victor Zatko[1], Alice Mizrahi[1], and Julie Grollier[1]

[1]*Unité Mixte de Physique CNRS Thales, Université Paris-Saclay, Palaiseau, France*
**erwan.plouet@cnrs-thales.fr*

Convolutional neural networks (CNNs) are state of the art algorithms for image processing. Despite a small number of synaptic weights, CNNs remain computationally costly to train in software due to the sequential application of the convolutional filter over the input. The field of neuromorphic spintronics offers the possibility of new promising parallel architectures that would perform a convolution in a single time step. Previously it has been demonstrated that the spin diode effect can be used to selectively apply a synaptic weight on a radiofrequency signal using frequency selectivity to address each device independently [1][2]. Here we go a step beyond, to show an experimental implementation of a convolutional layer able to calculate the result of a complete convolution in a single time step by exploiting the frequency domain as an additional dimension.

We design a compact architecture of 3 radio-frequency waveguides integrating each 3 spin-diodes connected in series. This architecture performs a padded convolution between a 3-pixels filter and a 5-pixels input. Inputs are represented by RF signals and are selectively processed by spin diodes at the matching frequency as represented by colors in Figure 1, the values of the filter are encoded by a small frequency detuning between the inputs and the spin-diodes resonance. Frequency selectivity enables us to produce each output with a single line geometry. Three strip lines in a crossbar configuration are implemented to write simultaneously the three weight values shared by the RF waveguides. This architecture exploits the intrinsic weight redundancy of convolutions to compute three outputs in parallel, instead of sequentially. The proposed

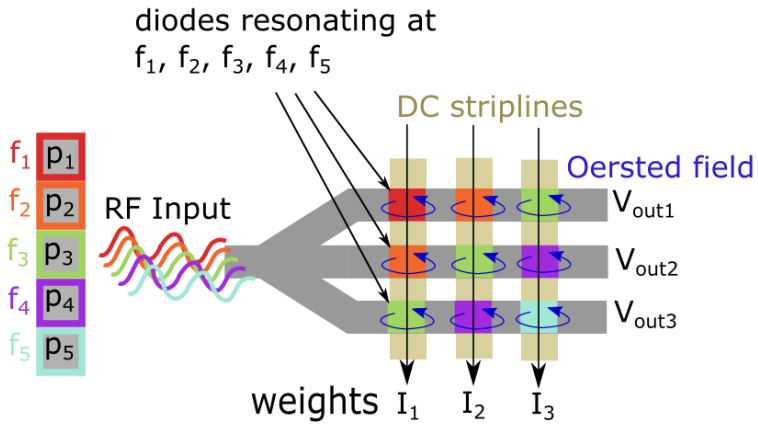

Figure 1: RF convolutional architecture

architecture enables us to both reduce the size and scaling of this hardware implementation while, at the same time, performing the convolution in one timestep contrary to previous time-multiplexed implementations. A potential decrease by one order of magnitude in energy consumption compared to current GPUs and two orders of magnitude in operating latency is envisioned upon scaling down of the technology [3]. This proof of concept of a spintronic CNN presented here, opens the path to the development of deep spintronic neural networks that can exploit the power of convolutional layers in a fully parallel, compact, and energy efficient way.

Acknowledgments

This work was supported by the European Union's grant RadioSpin No 101017098.

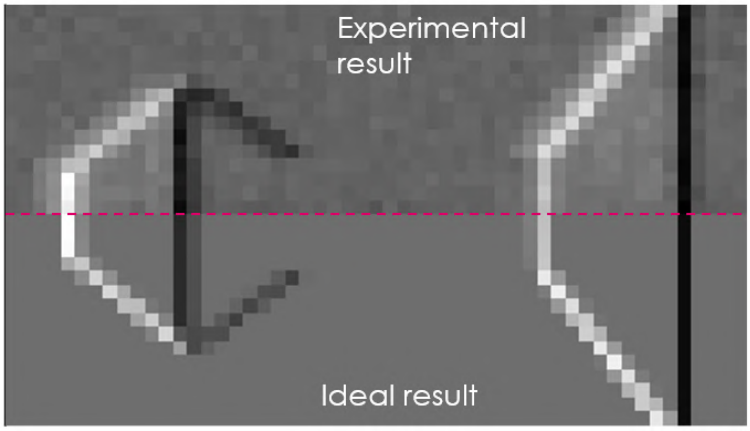

Figure 2: Convolution performed to enhance vertical edges

References

[1] Nathan Leroux, Danijela Markovi ć, Erwann Martin, et al. Radio-Frequency Multiply-and-Accumulate Operations with Spintronic Synapses. *Phys. Rev. Appl.* 15, 034067 (3 2021).

[2] Nathan Leroux, Alice Mizrahi, Danijela Marković, et al. Hardware realization of the multiply and accumulate operation on radio-frequency signals with magnetic tunnel junctions. *Neuromorphic Computing and Engineering* 1, 011001 (2021).

[3] Nathan Leroux, Arnaud De Riz, Dédalo Sanz-Hernández, et al. Convolutional neural networks with radio-frequency spintronic nano-devices. *Neuromorphic Computing and Engineering* 2, 034002 (2022).

Scalable Superparamagnetic Tunnel Junctions for Unconventional Computing

L. Soumah[1,*], N-T. Phan[1], A. Sidi El Valli[1], F. Disdier[1], R. Sousa[1], U. Ebels[1], and P. Talatchian[1]

[1]*Univ. Grenoble Alpes, CEA, CNRS, Grenoble INP, SPINTEC, 38000 Grenoble, France*
lucile.soumah@cea.fr

Magnetic tunnel junctions (MTJ), initially developed as memory storage units, have recently appeared as promising stochastic building blocks for cognitive computing [1]. An MTJ consists of two ferromagnetic layers separated by a thin oxide layer. The relative orientation of the magnetization of these two ferromagnetic layers forms two stable states corresponding to antiparallel or parallel alignment of the magnetization. Electrical reading of these two stable states is achieved thanks to the tunneling-magnetoresistive effect, leading to two binary state either 0 or 1. The energy barrier separating those two energy minimums is defined relatively to the thermal energy k_BT (where k_B is Boltzmann's constant and T=300 K is the room temperature). A significant energy barrier (>40 k_BT) between the two memory states enables to reach the required retention time (typically in the order of 10 years) for nonvolatile applications. When the energy barriers are less than 15 k_BT, thermal fluctuations at room temperature lead to random magnetization switching between the two stable configurations and the junction is called superparamagnetic tunnel junction (SMTJ). While magnetic fluctuations in SMTJs are truly random, the average time spent in each stable configuration (mean dwell time) can be tuned over a wide range of time scale (ms-ns) in a deterministic way through applied current or magnetic field. It has been shown that SMTJs with in-plane magnetic easy axis fluctuate at the nanosecond time scale when careful engineering of the energy barrier is performed [2]. However, such in-plane structures suffer from major challenges when it comes to downscaling because of their large sensitivity to small-size patterning (pillar edges) leading to important device-to-device variability's. In addition, the energy efficiency of in-plane structures still remains limited by their critical switching currents which are larger than the one observed in their perpendicular counterparts.

We tackle here the scalability and energy consumption challenges of currently developed SMTJs by engineering new magnetic structures having perpendicular magnetic easy axis and ultra low energy barriers. By careful tuning of the thicknesses within the multilayer magnetic stack, we obtained ultra-low values for the energy barrier height (<2 k_BT) and report for the first time nanosecond timescale fluctuations in perpendicular SMTJs. In order to explain the observed fast magnetic fluctuations, we develop a new analysis method based on the estimation of the free-layer magnetization energy landscape which enable us to obtain experimentally the attempt time, corresponding to the characteristic timescale constant of the fluctuation, often empirically chosen (0.1-1 ns) in most of the work on SMTJs [2, 3]. Our result doesn't only open new avenues for building low-energy, compact and fast networks of superparamagnetic tunnel junctions but also enables experimentalists to address the dynamics of SMTJs more quantitatively, which is crucial for using them as stochastic building blocks for cognitive computing.

We fabricated perpendicular SMTJs with a stack structure composed of two uniformly out-of-plane magnetized ferromagnetic (pinned and free) layers (CoFeB) separated by an oxide layer (MgO), and a perpendicular synthetic ferrimagnet composed of 2 stacks of Co/Pt multilayers antiferromagnetically coupled through RKKY interaction. The reference layer is pinned by direct exchange coupling with the synthetic ferrimagnet. The MTJ stack is then nanofabricated and patterned in 50 nm circular nanopillar with variation of resistance values from antiparallel to parallel configuration close to 70 % at room temperature and a resistance-area product of 10 $\Omega\ \mu m^2$. A wedge structure on the thickness of the CoFeB free layer is used to tune the energy barrier through the interfacial anisotropy term which is inversely proportional to the CoFeB free layer thickness. For the optimized thicknesses conditions, the free-layer magnetization of the SMTJ switches randomly between antiparallel and parallel state due to thermal fluctuations without any external current or field stimuli. For the fabricated SMTJs, we record voltage time traces corresponding to stochastic magnetization fluctuations. The analysis of the recorded voltage-time traces combined with its corresponding auto-correlation function (Fig.1(a-b)), indicates nanosecond range stochastic fluctuations which is not yet reported for perpendicular SMTJs in the literature. Interestingly, applying a larger DC current (30μA) compensates through spin transfer torque the absence of an applied magnetic field which enables zero field SMTJ operation in perpendicular structures.

In order to extract the mean dwell time of the thermally induced fluctuations with satisfactory statistical confidence, we record time traces with a sufficiently large number of transitions (>10^5). The probability density function is retrieved from the measured voltage-time trace. Assuming that the SMTJ is at thermal bath equilibrium, the extracted probability is expected to follow a Boltzmann distribution, which enables the estimation of the energy barrier height in the units of k_BT (Fig.1(c)). From our experimental voltage-time traces, we combine the estimated energy barrier and extracted mean dwell times in the modified Néel-Brown model, leading to a straightforward evaluation of the attempt time from experiments (Fig.1(c)). The proposed evaluation method offers a versatile approach for experimentalists, eliminating the need for temperature-dependent measurements often used in the literature [4]. Using different current operating points (Fig.1(d)), we evidence that, contrary to the usual assumption of a constant attempt time [3], the evaluated attempt time depends

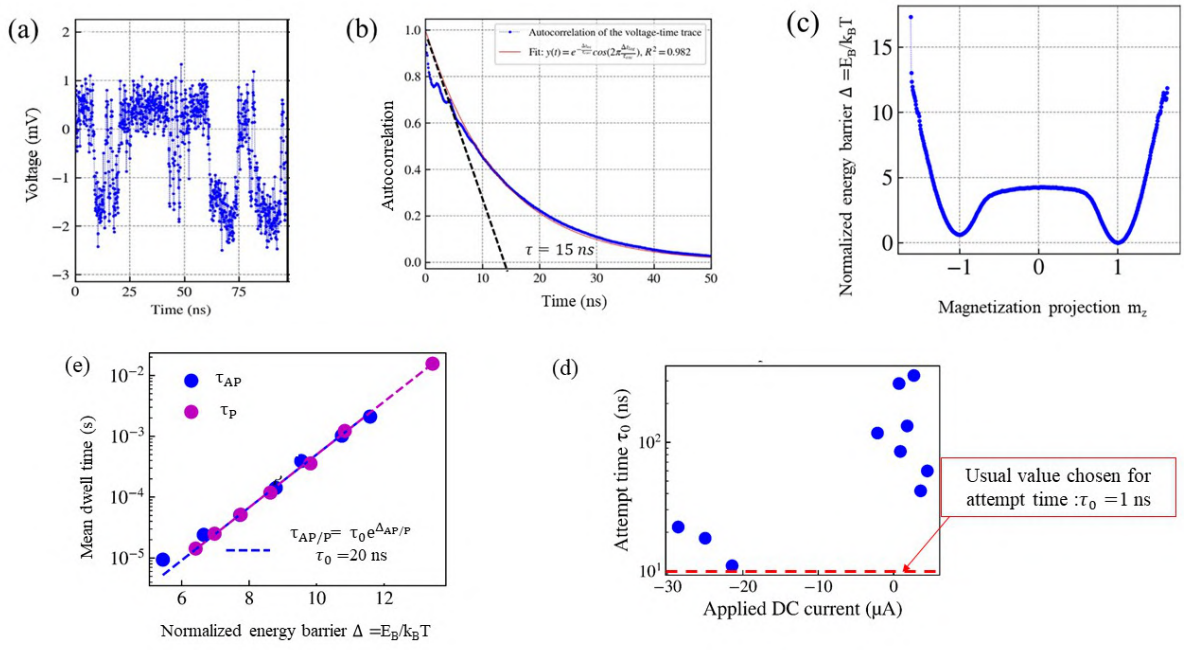

Figure 1: (a) Voltage-time trace measured at zero applied external field in a perpendicular SMTJ with ultra-low energy barrier ($< 5k_BT$) the time scale of the fluctuation : 20 ns is measured through the (b)auto-correlation function of the recorded time trace. (c)Energy landscape of a perpendicular-SMTJ obtained from the probability density function. (d) Mean dwell time τ vs normalized energy barrier Δ for a fixed applied DC current of -25 μA fitted with the modified Néel Brown's model enables to estimate the attempt time τ_0=22 ns.(e) Evolution of the evaluated attempt time with the DC applied current.

on the current, which enables reducing the time scale of the fluctuations even more. We believe that our optimization of perpendicular structures operating in the superparamagnetic regime at ultra-low applied DC current and at zero magnetic field opens a new path to integrability and scaling down of spintronic stochastic nanodevices crucial for unconventional computing schemes.

Acknowledgments

This work was supported by NSF-ANR via grant StochNet Project ANR-21-CE94-0002-01.

References

[1] Matthew W. Daniels, Advait Madhavan, Philippe Talatchian, Alice Mizrahi, and Mark D. Stiles. Energy-Efficient Stochastic Computing with Superparamagnetic Tunnel Junctions. *Phys. Rev. Appl.* 13, 034016 (3 2020).

[2] Christopher Safranski, Jan Kaiser, Philip Trouilloud, et al. Demonstration of Nanosecond Operation in Stochastic Magnetic Tunnel Junctions. *Nano Letters* 21, 2040–2045 (2021). arXiv: 2010.14393.

[3] Shun Kanai, Keisuke Hayakawa, Hideo Ohno, and Shunsuke Fukami. Theory of relaxation time of stochastic nanomagnets. *Physical Review B* 103, 1–12 (2021).

[4] William Rippard, Ranko Heindl, Matthew Pufall, Stephen Russek, and Anthony Kos. Thermal relaxation rates of magnetic nanoparticles in the presence of magnetic fields and spin-transfer effects. *Physical Review B* 84, 064439 (2011).

Low-energy spin manipulation in the molecular field of a magnetic thin film

Valentin Desbuis[1,*], Daniel Lacour[1], Coriolan Tiusan[2], Wolfgang Weber[3], and Michel Hehn[1]

[1]*Institut Jean Lamour, CNRS – Université de Lorraine, 54011 Nancy, France*
[2]*Center of Superconductivity, Spintronics and Surface Science (C4S), Technical University of Cluj-Napoca, 400114 Romania*
[3]*Institut de Physique et Chimie des Matériaux de Strasbourg, UMR 7504 CNRS, Université de Strasbourg, 23 Rue du Loess, BP 43, 67034 Strasbourg Cedex 2, France*
*valentin.desbuis@univ-lorraine.fr

The "conventional" collinear spin filtering effect demonstrated that electronic spin can support modern electronic devices, using spin valves [1, 2] or magnetic tunnel junctions [3, 4]. Yet, the spin-transfer torque effect [5], describing interactions between an electronic spin and magnetizations in such devices, induces change in the spin direction during angular momentum transfer. Therefore, control of the electron spin direction and its injection into an adjacent layer is a milestone for next-generation electronics. The presence of an electric field or a magnetic field can lead to a precession of the electronic spin. From the first spin transistor proposed by Datta and Das [6], several experiments showed that the precession effect could be triggered in different materials. The first measurement of spin precession in ferromagnets was demonstrated by D. Oberli *et al.* [7] for high energy electrons in the internal molecular field of the ferromagnetic material. This field estimated at several tens of Tesla [8] opens the door for sharp control of the electron spin direction at the nanometric scale in multilayered devices. Only a recent demonstration of spin precession could be done at low energies, compatible with applications in vertical injection geometry [9].

The lab-on-chip used for this study is based on a non-collinear magnetizations structure (Fig.1 left). A spin-polarized electron beam entering a multilayered system is affected by the ferromagnetic layer magnetization $\mathbf{M}_{AL}$. The polarization vector $\mathbf{P}$ will exhibit a precessional motion around $\mathbf{M}_{AL}$ described by the precession angle ϵ The reorientation of the polarization vector towards $\mathbf{M}_{AL}$ is given by the filtering angle θ.

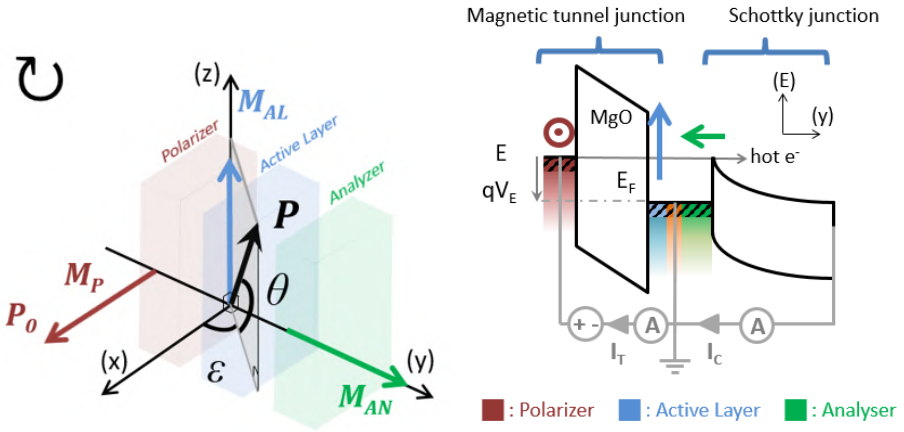

Figure 1: Left : precession and filtering angles for a beam of spin polarized electrons. Right : energy landscape experienced by the electrons. The vectors represent the polarization of the polarization layer, the active precession layer and the analyzer, from left to right.

This injection and the control of the spin energy is done by a MgO tunnel barrier [4] and by the use of crossed magnetizations geometry for an applied bias voltage [9]. Both θ and ϵ are analyzed through the GMR effect [1] occurring in the active layer / Cu / analyzer spin valve (blue / orange / green rectangles in Fig.1 - right). The use of a tunnel barrier at the injection and a Schottky diode at the collection of the spin ensure that the collected electrons in the semiconductor have always an energy higher than 0.7 eV (height of the Schottky barrier) and that collected electrons cross the Cu/Si with in an acceptance angle of roughly 4.5° (at an energy of 1 eV). As a result, the collected electrons in Si move ballistically across the spin valve with a trajectory perpendicular to the multilayer interfaces [9]. The resulting all-solid-state device is a magnetic tunnel transistor (MTT) architecture and is needed to test the precession angles (Fig.1 - right) at low energies. However, only the top magnetic tunnel junction (MTJ) is needed for the spin injection and has been shown to be integrated in all CMOS processes, compatible with applications, in vertical injection geometry to reduce the device size.

The typical stack used for this study is as follows:

$$\text{Pt(5)/IrMn (7.5)/Co(2)/Ta(0.5)/CoFeB(2)/MgO(2.5)/X(y)/Cu(3.5)/[Ni(0.6)/Co(0.2)]}_{\times 5}\text{/Ni(0.6)/Cu(5)/Ta(1)/Cu(5)//Si(100)},$$

where numbers in brackets indicate the layers thicknesses in nanometer. The multilayer is grown by sputtering on a HF cleaned Si substrate [10]. The CoFeB layer is the polarizer and X(y) is the active precession layer. The $[\text{Ni(0.6)/Co(0.2)}]_{\times 5}$/Ni(0.6) multilayer represents the analyzer and has its magnetization perpendicular to the film plane. The optimization of the three-dimensional magnetic configuration needed for the precession experiment has been done in [11]. Both material and thickness of the active precession layer can be changed as long as its magnetization lies in-plane with respect to the three-dimensional configuration of the structure (Fig.1 left). Depending on the nature of the active layer material, different parameters (thickness, temperature, energy) can be used to achieve full manipulation of the spin precession. The aim of this study is to demonstrate that engineering of the molecular field can lead to controlled spin-injection in nanometric scale devices.

The figure of merit S, function of experimentally available quantities, can be related to spin precession with the product $S = sin(\epsilon)cos(\theta)$ where ϵ and θ are the angles defined in Fig.1 right. The precession angle ϵ depends on all previously mentioned parameters. Pioneer study of C. Vautrin *et al.* [9] showed variation of the spin precession angle in CoFeB for different layer thicknesses with a fixed molecular field. Pursing this work, we designed two magnetic materials to engineer molecular fields in order to control spin-injection with temperature: CoAl and CoCu. Tuning the molecular field with temperature for both materials leads to a precession angle variation, related to the materials magnetic properties (Fig.2).

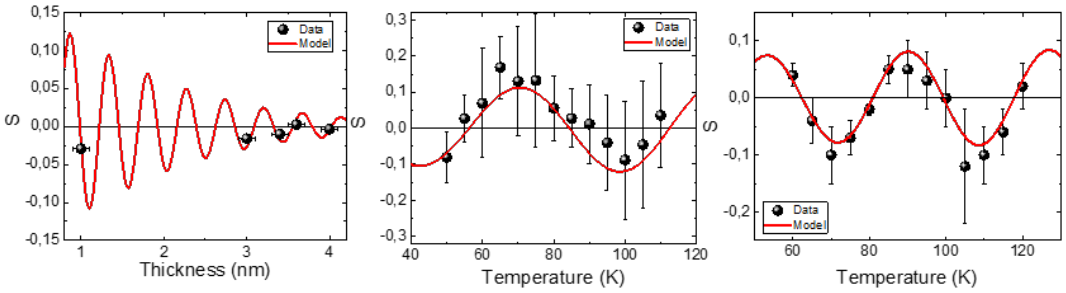

Figure 2: Spin precession signal as a function of a parameter of interest for three different active layer material (from left to right: CoFeB, CoAl, CoCu). A period of the signal corresponds to a 360° rotation of the spin.

References

[1] M.N. Baibich, J.M. Broto, A. Fert, et al. *Phys. Rev. B* 61 (1988).

[2] G. Binasch, P. Grünberg, F. Saurenbach, and W. Zinn. *Phys. Rev. B* 39 (1989).

[3] M Jullière. *Phys. Rev. Lett.* 74 (1975).

[4] J.S. Moodera, L.S. Kinder, T.M. Wong, and R. Meservey. *Phys. Rev. Lett.* 74 (1995).

[5] D. Ralph and M. Stiles. *J. Magn. Mat.* 320 (2008).

[6] S. Datta and B. Das. *Appl. Phys. Lett.* 56 (1990).

[7] D. Oberli, R. Burgermeister, and S. Riesen. *Phys. Rev. Lett.* 81 (1998).

[8] W. Weber, S. Riesen, and H.C. Siegmann. *Science* 291 (2001).

[9] C. Vautrin, D. Lacour, C. Tiusan, et al. *Ann. Phys.* 533 (2020).

[10] C. Vautrin, Y. Lu, S. Robert, et al. *J. of Phys. D* 49 (2016).

[11] C. Vautrin, D. Lacour, G. Sala, et al. *Phys. Rev. B* 96 (2017).

Session Poster 1
November 14th, 16h30 – 18h30
Applications (biology, computing, etc.)
Chiral and topological magnetic structures
Instrumentation
New materials (2D, spin ices, etc) and growth

1.01	**Nhat-Tan Phan**	SPINTEC	Bipolar Coupling of Perpendicular Superparamagnetic Tunnel Junctions for Stochastic Unconventional Computing	page 46
1.02	**Thomas Brun**	SPINTEC	High Sensitivity Amplification in Symmetric Response Magnetic Tunnel Junction with Flux Concentrator	page 48
1.03	**Massimiliano Marangolo**	INSP	A Gd based MEMS scale thermal engine	page 50
1.04	**Robert Morel**	SPINTEC	Magneto-mechanical stimulation of living cells: possible novel route towards innovative treatments of cancer and diabet	page 52
1.05	**Leandro Ferreira Martins**	SPINTEC	A non-volatile binary synapse based on a vortex nano-oscillator	page 54
1.06	**Paolo Sgarro**	SPINTEC	Spin-orbit Ferroelectric RAM, concept and study of spin-dependent transport via Finite Element Method simulations	page 56
1.07	**Hakam Abderrazak**	SPINTEC	Leveraging the phase dynamics of spin-torque nano-oscillators for unconventional computing	page 58
1.08	**Mateo Ibarra Gomez**	SPINTEC	A numerical study of Ising machines based on spin torque nano-oscillators	page 60
1.09	**Sonia Thlang**	C2N	Étude des processus non-linéaires d'ondes de spin dans des disques d'Heusler Co_2MnAl de 5 µm pour le calcul par réservoir	page 62
1.10	**Joo-Von Kim**	C2N	Pattern recognition in reciprocal space with a magnon-scattering reservoir	page 64
1.11	**Anatole Moureaux**	UCLouvain	Unveiling the potential of spintronics-based neural networks using ultrafast data-driven simulations	page 66
1.12	**Miina Leiviskä**	FZU	Dynamic imprinting of nanoscale topological phases into an antiferromagnet	page 68
1.13	**Joseba Urrestarazu**	SPINTEC	Electrical detection and nucleation of a magnetic skyrmion in a magnetic tunnel junction observed via operando magnetic microscopy	page 69
1.14	**Anne Bernand-Mantel**	LPCNO	Theory of magnetic field-stabilized compact skyrmions in thin film ferromagnets	page 71
1.15	**Titiksha Srivastava**	C2N	Resonant dynamics, spin wave generation, and spin-wave annealing in three-dimensional skyrmionic lattices	page 73
1.16	**Sougata Mallick**	UMPhy	Driving skyrmions in flow regime in synthetic ferrimagnets	page 74

1.17	**Sougata Mallick**	UMPhy	Influence of OAM light on the magnetic textures of Synthetic antiferomagnets	page 76
1.18	**William Bouckaert**	UMPhy	Evaluation of the repulsive Forces Acting on Skyrmions	page 78
1.19	**Ilaria Di Manici**	SPINTEC	Cancellation of topological charge effect on current induced skyrmion motion in Pt/Co/Ru based multilayers	page 80
1.20	**Nicolas Reyren**	UMPhy	Skyrmionic 3D cocoons in aperiodic magnetic multilayers	page 82
1.21	**Farid Fettar**	Institut Néel	Skyrmions lattice in Fe/Gd multilayers with planar magnetic anisotropy	page 84
1.22	**Aurélien Masseboeuf**	SPINTEC	Time-resolved switching of curling magnetization in nanowires	page 86
1.23	**Olivier Fruchart**	SPINTEC	Domain wall manipulation in cylindrical ferromagnetic nanotube	page 88
1.24	**Vincent Jeudy**	LPS	Domain wall and pinning disorder interaction controlled by He^+ ion irradiation in Pt/Co/AlOx ultrathin films	page 90
1.25	**Georgy Ziborov**	SPINTEC	Low PMA tuned iron garnets for the stabilization of magnetic skyrmions	page 92
1.26	**Stefania Pizzini**	Institut Néel	Improving Néel domain wall dynamics and skyrmion stability using helium ion irradiation	page 94
1.27	**Eric Clot**	SPINTEC Institut Néel	Development of a NV-center microscope for spin-wave spectroscopy	page 95
1.28	**Alexis Wartelle**	IJL	Towards hard-X-ray-based magnetic tomography: Coherent Diffraction Imaging of $Co_{1-x}Gd_x$ microbeads	page 96
1.29	**Augustin Nogier**	SPINTEC	Dynamic imaging of new MRAM devices with Electron Holography	page 98
1.30	**Aurore Finco**	L2C	Probing the chirality of magnetic textures from spin wave noise	page 100
1.31	**Alessandro Nicolaou**	SOLEIL	A unique experimental end-station for correlative RIXS and XEOL spectroscopies under electric and magnetic fields	page 102
1.32	**Christian Roubert**	LPMC	Spectroscopie de défauts paramagnétiques par transitoires de photo-courant polarisés en spin dans les nitrures dilués	page 103
1.33	**Maria Vladimirova**	L2C	Towards nuclear magnetic ordering in n-type semiconductors	page 105
1.34	**Karen Sobnath**	MPQ	Ferromagnetic resonance damping in Co/2D material heterostructures	page 106
1.35	**Tristan Riccardi**	Institut Néel	Advances in Raman scattering investigations of the room temperature van der Waals ferromagnet 1T-$CrTe_2$	page 107
1.36	**Mathieu Jamet**	SPINTEC	Proximity effects in molecular beam epitaxy grown van der Waals ferromagnet Cr_2Te_3 on two-dimensional layers	page 109

1.37	**Banan El-Kerdi**	LPS	Ferromagnetism in exfoliated Fe_xGeTe_2 flakes	page 111
1.38	**Hao Wei**	UMPhy	Spintronics with black phosphorus	page 113
1.39	**Vincent Polewczyk**	SPINTEC	Epitaxial Fe_NGeTe_2 van der Waals films: exploring heterostructure stacking for enriched magnetic properties	page 114
1.40	**Frederic Brunnett**	UMPhy	TMD Engineering of 2D-Magnetic Tunnel Junctions – From Barriers to Electrodes	page 116
1.41	**Dongzhe Li**	CEMES	Ab initio study of the Dzyaloshinskii-Moriya interaction and magnetic skyrmions in Fe_3GeTe_2 van der Waals heterostructures	page 117
1.42	**Libor Vojacek**	SPINTEC	Spin transport in CrXY monolayers: multiscale computational study	page 119
1.43	**Cyrille Barreteau**	SPEC	Spin-Crossover and Fragmentation of $Fe(neoim)_2$ on Ag and Au	page 120
1.44	**Alban Simonnot**	SCCM SPEC	The magnetic phase diagram of ternary $(Ni,Fe,Cr)_3O_4$ spinel oxides in epitaxial thin films: from the element specific magnetic behavior to magnetic modelling	page 122
1.45	**Maria Jose Vazquez Bernardez**	IPCMS	Tuning of high-frequency magnetic properties of doped $BaM_xM'_xFe_{12-2x}O_{19}$ composites	page 123
1.46	**Liza Herrera Diaz**	C2N	Oxygen Magneto-Ionics, without Oxidation	page 125
1.47	**Lamiae El Khabchi**	IPCMS	Towards spin Hall magnetoresistance with magnetically frustrated cobalt vanadate spinel CoV_2O_4 thin films	page 127
1.48	**Guillaume Bernard**	C2N	Magneto-ionics in CoFeB alloys	page 129
1.49	**Eva Choker**	GPM	Ordre magnétique dans des spinelles à propriétés thermoélectriques	page 131
1.50	**Michaela Lammel**	Univ. Konstanz	Vertical and Lateral Crystallization Dynamics of Yttrium Iron Garnet Thin Films	page 133
1.51	**Alexandre Wu-Vignolo**	MPQ	Magnetism at low symmetry surfaces	page 134
1.52	**Anne Lise Adenot Engelvin**	CEA Le Ripault	Propriétés magnétiques dynamiques de ferrites spinelles élaborés par extrusion de pâte (robocasting) en lien avec leur microstructure	page 136
1.53	**Imane Berrai**	LSPM	Graphene-based heterostructures: Effect of the intercalation of MgO and Al_2O_3 insulating barriers on structural and magnetic properties	page 138
1.54	**Julian Peiro**	UMPhy	Artificial Graphene Spin Polarized Electrode for Magnetic Tunnel Junctions	page 140
1.55	**Bohdan Kundys**	IPCMS	Photoferroelectric control of graphene magnetoresistance	page 141
1.56	**William Legrand**	ETHZ	Low-temperature epitaxial magnetic garnet thin films for quantum magnonics	page 142

Bipolar Coupling of Perpendicular Superparamagnetic Tunnel Junctions for Stochastic Unconventional Computing

Nhat-Tan Phan[1,*], Lucile Soumah[1], Ahmed Sidi El Valli[1], Lorena Anghel[1], Matthew W. Daniels[2], Ricardo Sousa[1], Juergen Langer[3], Jerzy Wrona[3], Advait Madhavan[4,5], Mark D. Stiles[2], Ursula Ebels[1], and Philippe Talatchian[1]

[1]*Univ. Grenoble Alpes, CEA, CNRS, Grenoble INP, SPINTEC, Grenoble, France*
[2]*Physical Measurement Laboratory, NIST, Gaithersburg, Maryland, USA*
[3]*Singulus Technologies AG, Kahl am Main, Germany*
[4]*Associate, Physical Measurement Laboratory, NIST, Gaithersburg, Maryland, USA*
[5]*Institute for Research in Electronics and Applied Physics, University of Maryland, Maryland, USA*
*nhat-tan.phan@cea.fr

Magnetic tunnel junctions are increasingly used in embedded non-volatile memory applications and are promising building blocks for implementing new circuits for compact and energy-efficient unconventional computing [1]. These nanoscale devices consist of two ferromagnetic layers separated by a thin insulating tunneling barrier. The relative orientations of the magnetization of the two magnetic layers form two stable configurations with parallel (P) or antiparallel (AP) magnetizations. Applying voltages to these nanojunctions results in spin-polarized tunnel currents that exert a spin transfer torque on the magnetizations. At sufficiently high voltages, the energy barrier between the two configurations is overcome, resulting in a magnetization switch and allowing the writing of the memory. Collective behavior resulting from the coupling between such SMTJs could enable hardware implementation of cognitive computing systems in which randomness is a low-cost way to encode and explore available information states.

To achieve stable storage of the information over many years, as required for non-volatile applications, the energy barrier between the two memory states must be large, i.e., greater than $40kT$, where k is Boltzmann's constant and T is the working temperature in Kelvin ($T = 300\,\mathrm{K}$). Reducing the energy barrier leads to an exponential reduction in storage time. For energy barriers lower than $\simeq 15kT$, thermal fluctuations at room temperature lead to random changes in magnetization between the two stable configurations time scales ranging from $10\,\mu\mathrm{s}$ to $100\,\mathrm{ms}$. A magnetic element whose magnetic configuration fluctuates due to a small energy barrier is called a superparamagnetic tunnel junction (SMTJ).

Most reported interaction schemes for two or more SMTJs use protocols that require additional peripheral circuitry [2, 3] or finely calibrated external stimuli [4]. This circuitry complicates the development of large generalized networks. Here we couple SMTJs using linear circuit elements. We believe such coupling can provide a more robust, less complicated, and more compact basis for future exploration of large SMTJ networks needed for deploying in hardware energy-efficient stochastic neural networks [5] as well as for Ising-model-based approaches to optimization problems [6].

We choose to work with SMTJs because of better scaling-down (below 30 nm diameter) perspectives and larger magnetoresistance effects available with the considered structure, a key parameter for enhanced coupling strength between SMTJs. More precisely, we study perpendicular SMTJs with the following composition: Si substrate / SiO_2 / TaN / $[Co(0.5)/Pt(0.2)]_6$ /Ru(0.8)/ $[Co(0.6)/Pt(0.2)]_3$ / Ta(0.2) / Co(0.9) / W(0.25) / CoFeB(1) /MgO(0.8) / CoFeB(1.4)/ W(0.3) / CoFeB(0.5) / MgO(0.75) / Ta(150) /Ru(8). Numbers in parentheses represent thicknesses in nanometers and numbers adjacent to square brackets indicate the number of bilayer repeats. The devices are nearly circular with nominal diameters of 50 nm. Their tunneling magnetoresistance (TMR) value is close to 120 % at room temperature, and they have a resistance-area product of $10\,\Omega\mu\mathrm{m}^2$.

We demonstrate bipolar coupling of superparamagnetic tunnel junctions using a straightforward electrical circuit to establish an electrical interaction between two SMTJs. Bipolar coupling implies that two interacting SMTJs can couple both preferentially ferromagnetically [favoring (P,P) and (AP,AP)] or antiferromagnetically [favoring (P,AP) and (AP,P)]. The electrical setup is shown in Fig. 1(e). Two parallel coupled SMTJs are connected in series with a resistance $R_0 = 3400\,\Omega$ and the voltage source. We monitor the shared voltage between the two SMTJs with an oscilloscope. From the measured voltage, we can determine the configuration of the two SMTJs and the time they spend in these configurations. Fig. 1(a) and (c) show time-voltage traces of the circuit. We extract the statistics of the four states corresponding to the system's four possible SMTJ resistance combinations; (AP, AP), (P, P), (AP, P), and (P, AP) from the histograms shown in Fig. 1(b) and (d). Extracting the probabilities of the four joint configuration states over a range of applied DC voltages allows us to characterize the coupling. We compute the $t = 0$ Pearson cross-correlation $C(0)$, which depends only on the probabilities that can be easily extracted from the histograms, using the analysis developed in [7]. Fig. 1(e) shows the cross-correlation evaluated as a function of the applied voltage V_{dc} in the circuit. For lower voltages, we start with negative coupling that can reach -58 % cross-correlation, for the largest value. And for bigger voltages, we observed positive coupling; that can reach

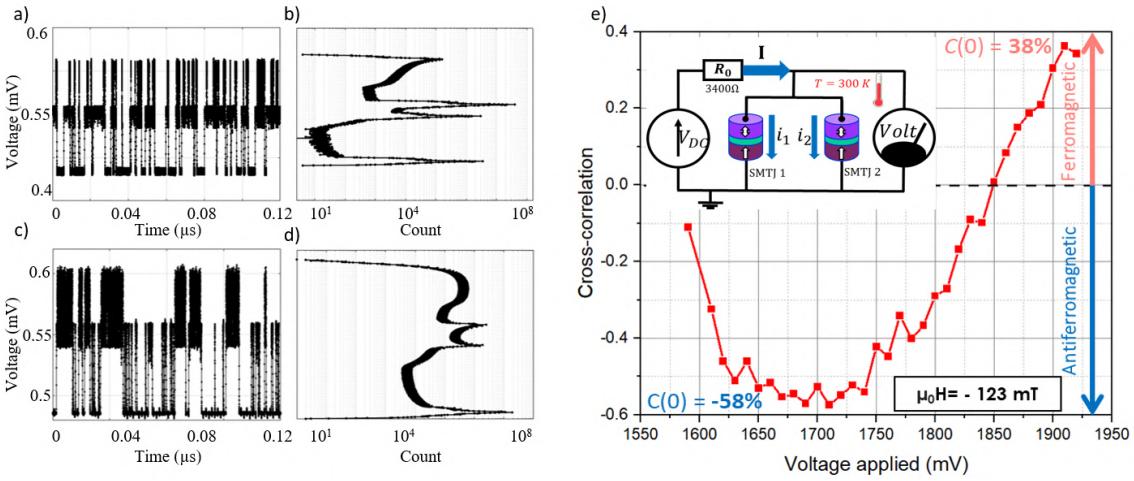

Figure 1: (a),(b),(c),(d) Time trace and histogram of the voltage of two coupled SMTJs for $V_{\mathrm{dc}} = 1710\,\mathrm{mV}$ and $V_{\mathrm{dc}} = 1910\,\mathrm{mV}$, respectively. (e) Setup of coupling 2 SMTJs and the evolution of the $t = 0$ Pearson cross-correlation $C(0)$ extracted for the coupled SMTJ system as a function of the applied DC voltage.

38 % cross-correlation. This is almost two times larger than the coupling demonstrated previously in the literature [3, 7]. This evolution as a function of voltage can be seen as a transition from antiferromagnetic to ferromagnetic coupling.

Obtaining a bipolar coupling that can be tuned externally between SMTJs is a crucial feature for many probabilistic computing schemes opening a path towards the hardware implementation of energy-based models such as Boltzmann machines, invertible logic networks [2], or stochastic neural network schemes [5].

Acknowledgments

This work was supported by NSF-ANR via grant StochNet Project ANR-21-CE94-0002-01, Grenoble INP Bourse Présidence, and MIAI institute.

References

[1] Julie Grollier, Damien Querlioz, K Y Camsari, et al. Neuromorphic spintronics. *Nat. electron.* 3, 360–370 (2020).

[2] Kerem Yunus Camsari, Rafatul Faria, Brian M Sutton, and Supriyo Datta. Stochastic p-bits for invertible logic. *Physical Review X* 7, 031014 (2017).

[3] Punyashloka Debashis, Rafatul Faria, Kerem Y Camsari, Supriyo Datta, and Zhihong Chen. Correlated fluctuations in spin orbit torque coupled perpendicular nanomagnets. *Physical Review B* 101, 094405 (2020).

[4] A Mizrahi, N Locatelli, J Grollier, and D Querlioz. Synchronization of electrically coupled stochastic magnetic oscillators induced by thermal and electrical noise. *Physical Review B* 94, 054419 (2016).

[5] Matthew W Daniels, Advait Madhavan, Philippe Talatchian, Alice Mizrahi, and Mark D Stiles. Energy-efficient stochastic computing with superparamagnetic tunnel junctions. *Phys. Rev. Appl.* 13, 034016 (2020).

[6] William A Borders, Ahmed Z Pervaiz, Shunsuke Fukami, et al. Integer factorization using stochastic magnetic tunnel junctions. *Nature* 573, 390–393 (2019).

[7] Philippe Talatchian, Matthew W Daniels, Advait Madhavan, et al. Mutual control of stochastic switching for two electrically coupled superparamagnetic tunnel junctions. *Physical Review B* 104, 054427 (2021).

High Sensitivity Amplification in Symmetric Response Magnetic Tunnel Junction with Flux Concentrator

T. Brun[1, 2, *], S. Manceau[1, 2], C. Ducruet[3], P. Sabon[1], L. Prejbeanu[1], C. Cavoit[2], G. Jannet[2], M. Kretzschmar[2], and C. Baraduc[1]

[1]*SPINTEC, Univ. Grenoble Alpes, CNRS, CEA, 17 avenue des Martyrs, Grenoble, France*
[2]*LPC2E, CNRS & Université d'Orléans, 3a avenue de la recherche scientifique, Orléans, France*
[3]*Crocus Technology, 3 Av Doyen Louis Weill, Grenoble, France*
**thomas.brun@cea.fr*

Magnetic Tunnel junctions (MTJs) are often used as magnetic sensors due to their high sensitivities but are limited by their 1/f noise. Detecting sub-nanoTesla magnetic fields is therefore challenging. A possible route to achieve this goal is to amplify the sensor sensitivity by using a high gain flux concentrator. Here we demonstrate a gain of 440 with the addition of Flux Concentrators (FCs) on Symmetric Response MTJs (SR-MTJs).

The challenge in increasing the sensitivity of the MTJ itself lies in the compromise between the ability of the free layer magnetization to rotate freely and the need to keep the magnetization uniform without domain formation. This is a key point as reducing the noise of the sensor requires increasing the magnetic volume and thus using micron-size junctions. The solution we developed for our symmetric response MTJ is to use a soft-pinned free layer [1]. We precisely control the exchange coupling strength between the free layer and an IrMn layer by inserting a thin Ru spacer layer. The corresponding exchange field value is measured with a vibrating sample magnetometer.

With a soft-pinned free layer, we obtained SR-MTJs with a sensitivity 3.6 %/mT. Our experimental results are well described by an analytical model based on Stoner-Wohlfarth model considering exchange, Zeeman and shape anisotropy energies. We also included in the model any possible misalignment due to the process (orientation of the junction, direction of the magnetic field during annealing) or to the measurement.

To further control the free layer stabilization, we patterned our junctions in different shapes and aspect ratio, ranging from a 0.8*4 µm ellipse to a 4*25 µm rectangle. Shapes elongated along the magnetization at rest (y axis) will increase the overall pinning: it leads to a decrease of sensitivity as can be seen in Fig. 1 for positive shape anisotropy fields ($\mu_0 H_{k,shape} > 0$). In our convention, negative shape anisotropy fields correspond to junctions whose shape is elongated along the applied field axis (x axis). In this case the sensitivity increases as a result of lowering the free layer stabilization at the eventual cost of loosing the uniform magnetization. Thus we expect that a fine tuning of the shape anisotropy should increase the sensitivity by compensating for the magnetocrystalline anisotropy.

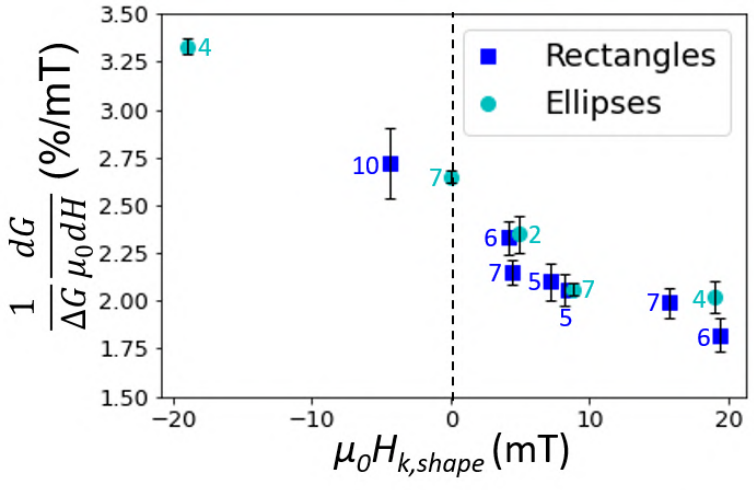

Figure 1: Average normalized sensitivity measured on nominally identical junctions of different shapes with $\mu_0 H_{ex} = 4.75mT$ as a function of the shape anisotropy field. Squares and circles represent rectangular and elliptical junctions respectively. The number of samples measured for calculating the average sensitivity is indicated close to each data point. The error bar corresponds to the standard deviation. Shapes elongated along y (x) correspond to $\mu_0 H_{k,shape} > 0$ (< 0) and disks correspond to $\mu_0 H_{k,shape} = 0$.

Finally, to strongly increase the sensitivity, 6µm-thick NiFe flux concentrators were electrodeposited around the MTJs. Their elongated shape and narrow air-gap of 10 µm are the key points to obtain the highest amplification by contrast to previously published studies [2]. We have measured a gain of 440 for our most recent fabrication. The effect of the flux concentrators is shown in Fig. 2 with the response of the SR-MTJ without FC in inset. The FC very high gain results in a drastic increase of sensitivity on small fields range.

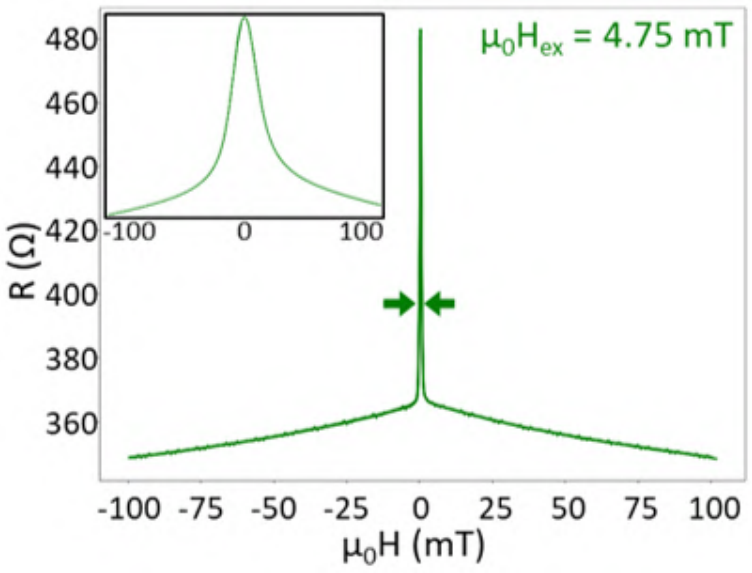

Figure 2: Symmetric response of a soft-pinned junction with flux concentrators aligned with the hard axis. The high gain result in a strong increase of the sensitivity at low magnetic field. Inset: same junction without flux concentrators. The exchange soft-pinning field is 4.75 mT.

To conclude, using the high gain flux concentrators we achieve a sensitivity of 1580 %/mT. This result paves the way towards the detection of very small fields with an integrated sensor. For space missions, such a miniature sensor could advantageously replace currently used magnetometers with a significant reduction of mass [3].

Acknowledgments

This work has been supported by CNES R&T and ANR-22-CE42-0020 project MAROT.

References

[1] R. Ferreira, E. Paz, P. P. Freitas, J. Wang, and S. Xue. Large Area and Low Aspect Ratio Linear Magnetic Tunnel Junctions With a Soft-Pinned Sensing Layer. *IEEE Transactions on Magnetics* 48, 3719–3722 (2012).

[2] S. Cardoso, D. C. Leitao, L. Gameiro, et al. Magnetic tunnel junction sensors with pTesla sensitivity. *Microsystem Technologies* 20, 793–802 (2014).

[3] Amandine Bocheux, Claude Cavoit, Myckael Mouchel, et al. “High sensitivity magnetic field sensor for spatial applications”. *2016 IEEE Sensors Applications Symposium (SAS)*. 2016, 1–5.

A Gd based MEMS scale thermal engine

Massimiliano Marangolo[1,*], Morgan Almanza[2], Nesrine Belkadi[3], Jean-Eudes Duvauchelle[1], Erika Fontana[4], Doan Nguyen Ba[1,2], Loïc Becerra[1], Thibaud Devilliers[4], Nora M. Dempsey[4], Fabien Parrain[3], and Martino LoBue[2]

[1]*Sorbonne Université, CNRS, Institut des NanoSciences de Paris, UMR7588, 75252 Paris, France*
[2]*Université Paris-Saclay, ENS Paris-Saclay, CNRS, SATIE, F-91190 Gif-sur-Yvette, France*
[3]*Université Paris-Saclay, CNRS, Centre de Nanosciences et de Nanotechnologies, 91120, Palaiseau, France*
[4]*Université Grenoble Alpes, CNRS, Grenoble INP, Institut Néel, 38000 Grenoble, France*
*massimiliano.marangolo@insp.upmc.fr

Novel technologies for thermal energy harvesting at the small scale (i.e. harnessing small temperature gradients over distances of a few millimeters) represent a growing research field due to the need for supplying low-power wireless sensor nodes, wearable devices, implants, and other autonomous micro-devices. Indeed, the rise of IoT, and the global sustainability challenges (i.e. smart-buildings, smart-cities) bring new focus on the recovery of ultralow waste heat (i.e. in a temperature range from 25 °C to 80 °C) [1], definitely the cheapest, and most ubiquitous energy source in anthropized environments. This makes efficient low-grade heat recovery an almost obvious, and essential technological goal.

In spite of their extreme design simplicity, Seebeck effect based devices fall short of the efficiency needs, particularly when working over small temperature gradients [2]. Nowadays, caloric materials, originally studied for cooling applications [3] have been identified as a possible alternative to thermoelectrics with some very promising results reported on pyroelectrics [4].

Besides, self-actuating thermomagnetic generators (TMG), have been demonstrated as another alternative to thermoelectrics [5]. Recently, a device using a 40 μm Gd film bounded on a cantilever as active substance, has been reported [6].

Here we present a self-oscillating, autonomous TMG prototype, based on the so called linear-design [7], working over a 20 °C temperature difference between the hot, and cold reservoirs. The device size, and weight have been reduced, keeping a high power output thanks to an improved thermal management, and to the use of an optimized field source. This makes the prototype presented here the smallest and lightest TMG device reported so far.

The active material, a flexible, freestanding, 17 μm Gd film [8], shown in Fig.1.b, oscillates between the hot, and cold ends, as shown in Fig.1.a, over a gap of 40 μm. Heat exchange between the active substance and the reservoirs take place through direct solid-solid contact thanks to the excellent surface smoothness of the film, and to its flexibility. This is a key issue of the proposed design as it allows getting rid of heat exchange fluids, and of their energy consuming management.

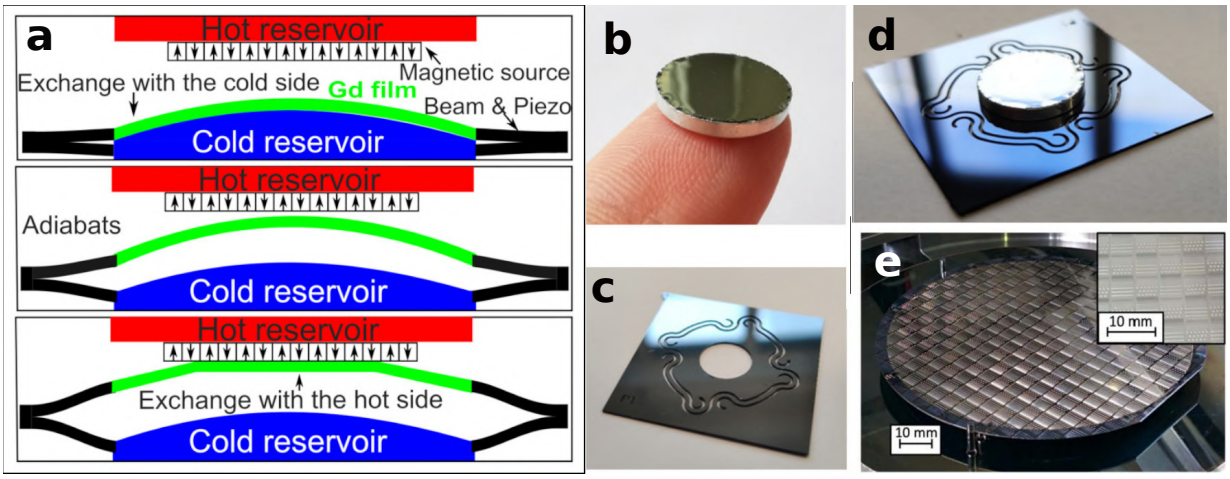

Figure 1: a) schematic representation of the linear device design. b) Gd film. c) laser cut piezoelectric spring. d) the Gd film mounted over the spring. e) the patterned NdFeB hard-magnet film.

The field source is a patterned NdFeB hard-magnet film [9], shown in Fig.1.e. The resulting magnetic field is highly confined, and shows strong gradients, over displacements of tens of micrometers. In this way, the field is used to switch the caloric effect, and at the same time to move the film against the elastic force of the spring. On the other hand, a laser-cut piezoelectric spring, shown in Fig.1.b, allows achieving a self-oscillating bistable regime converting the mechanical energy into electrical energy. Experiments show that a frequency of 100 Hz is achievable working over a small temperature difference, with the hot side at 30 °C and heat sink at 10 °C. This result is a key step towards higher output power. We shall present the main characteristics of the device with a particular focus on its self-actuating dynamics, and on the prospects to achieve further improvements of its throughput.

Acknowledgments

This research has received funding from the French National Research Agency under the project HiPerTher-Mag (ANR-18-CE05-0019), and from the financial support of the LabEx LaSIPS (ANR-10-LABX-0032-LaSIPS) under the "Investissements d'avenir" program (ANR-11-IDEX-0003).

References

[1] Mauro Luberti, Robert Gowans, Patrick Finn, and Giulio Santori. An estimate of the ultralow waste heat available in the European Union. *Energy* 238, 121967 (2022).

[2] Morgan Almanza, Alexandre Pasko, A Bartok, Frédéric Mazaleyrat, and Martino Lobue. "Thermal energy harvesting: thermomagnetic versus thermoelectric generator". *7th International Conference on Magnetic Refrigeration at Room Temperature (Thermag VII)*. 2016.

[3] X. Moya and N. D. Mathur. Caloric materials for cooling and heating. *Science* 370, 797–803 (2020). eprint: https://science.sciencemag.org/content/370/6518/797.full.pdf.

[4] Shishir Pandya, Joshua Wilbur, Jieun Kim, et al. Pyroelectric energy conversion with large energy and power density in relaxor ferroelectric thin films. *Nat. Mater.* 17, 432 (2018).

[5] Marcel Gueltig, Frank Wendler, Hinnerk Ossmer, et al. High-Performance Thermomagnetic Generators Based on Heusler Alloy Films. *Adv. Energy Mater.* 7, 1601879–n/a (2017).

[6] Joel Joseph, Erika Fontana, Thibaut Devillers, Nora M Dempsey, and Manfred Kohl. A Gd-Film Thermomagnetic Generator in Resonant Self-Actuation Mode. *Advanced Functional Materials*, 2301250 (2023).

[7] Andrej Kitanovski. Energy Applications of Magnetocaloric Materials. *Advanced Energy Materials* 10, 1903741 (2020).

[8] Doan Nguyen Ba, Yunlin Zheng, Loic Becerra, et al. Magnetocaloric Effect in Flexible, Free-Standing Gadolinium Thick Films for Energy Conversion Applications. *Physical Review Applied* 15 (2021).

[9] Frederico O. Keller, Richard Haettel, Thibaut Devillers, and Nora M. Dempsey. Batch Fabrication of 50 μm-Thick Anisotropic Nd–Fe–B Micro-Magnets. *IEEE Transactions on Magnetics* 58, 1–5 (2022).

Magneto-mechanical stimulation of living cells: possible novel route towards innovative treatments of cancer and diabet

R. Morel[1,*], A. Visonà[1,3], C. Naud[1,2], C. Thébault[1], S. Ponomareva[1], H. Joisten[1], F. Berger[2], M. Carrière[4], Y. Hou[4], A. Nicolas[3], and B. Dieny[1]

[1]*Univ. Grenoble Alpes, CEA, CNRS, Spintec, 38000 Grenoble, France*
[2]*BrainTech Lab, U1205, INSERM, Univ. Grenoble Alpes, CHU-Grenoble, France*
[3]*Univ. Grenoble Alpes, CNRS, LTM, 38000 Grenoble, France*
[4]*Univ. Grenoble Alpes, CEA, CNRS, IRIG-SyMMES, 38000 Grenoble, France*
robert.morel@cea.fr

Mechanobiology is the study of mechanisms by which cells sense and respond to mechanical signals. This field relates to both the intrinsic mechanical properties of the cell constituents and the way the cell reacts to the stiffness and stress from the environment. In this context, the use of magnetic nanoparticles provides a unique and very effective way to exert remote forces and torques at the nanoscale, on living cells. A great advantage of using magnetism in this field of mechanobiology is that the induced stress can be easily tuned remotely by playing on a number of parameters such as external magnetic field amplitude, direction, frequency. Magnetically induced mechanical stimulation is also much easier to implement, not only for in vitro testing with cells, but also for in vivo experiment. It has been for instance demonstrated that the mechanical stimulation of cancer cells can trigger cells death, thanks to the low frequency vibrations of nanoparticles [1–4], which allows to envision the development of medical treatment at a later stage. At a lower level of mechanical stress the magneto-mechanical stimulation has a strong influence on the cells cytoskeleton, which triggers a variety of signaling pathways and, consequently, of physiological reactions (Fig.1).

The magnetic nanoparticles used for biomedical applications are often functionalized superparamagnetic iron oxide particles with size in the 5 to 20 nm range. However, because the force and torque resulting from an applied magnetic field depend on their volume, they are too small to induce a sizeable mechanical effect at the cell scale: To get forces in the nano-newton range, magnetic particles with size closer to 1 micron are required. One challenge is then to design magnetic particles in this size range with good biocompatibility, easy to disperse in liquid without agglomerating, and easy to functionalize with surface chemistry. Two example of magnetic nanoparticles that we have developed are gold-covered permalloy ($Ni_{80}Fe_{20}$) thin disks with diameter 1.3 μm. Due to their aspect ratio and low magnetocrystalline anisotropy they show a vortex magnetic structure in the absence of applied field, providing them with good dispersion properties [5]. A second type of particles that we have developed, which are easier process, is a magnetite powder obtained from ball-milling [3] (Fig.1).

The magneto-mechanical stimulation of cells was tested with different types of cells. For instance, using U87 glioma brain cancer cells, we observed that a weak stimulation induces already a severe disturbance of the cell actin cytoskeleton, resulting in a cell contraction, a loss of mobility and a pause in cell division. A stronger stimulation can induce the spontaneous death of the cell through apoptosis [1–3]. Thanks to a stimulation with a moderate alternating field of 20 mT at 20 Hz for 30 minutes, the death of 80% of the cancer cells can be induced, in particular via apoptosis (Fig.1). Remarkably, the cells that survive the mechanical stress do not proliferate any more during several days. The magneto-mechanical treatment can be repeated until the cancer cells are fully destroyed. This approach can lead to a new approach towards cancer treatment, either alone or in conjunction with chemotherapy. An even stronger stimulation can result in a disruption of the cell membrane and thereby cell necrosis, accompanied with inflammatory reactions potentially inducing metastasis.

Similar experiments of magneto-mechanical cancer cells destruction has been made with mice (to which human glioblastoma brain cancer cells were implanted). Contrary to expectations following the in vitro tests, the magneto-mechanical treatment did not induce significant difference in the survival time for the mice. Subsequent analyzes however showed two major differences between in vitro and in vivo studies: on the one hand, under in vivo conditions, the nanoparticles do not penetrate the cell membrane and, on the other hand, the nanoparticles injected in the tumor stay close to the injection site so that only the center area of the tumor was affected by the magnetic treatment.

Experiments were also conducted with insulin-producing INS1 pancreatic cells [4]. We demonstrated that the magnetically induced mechanical stimulation these cells allows enhancing insulin secretion (Fig.1). The experiments were conducted both by culturing pancreatic cells on vibrating magnetic membranes as well as by dispersing vibrating magnetic particles among the pancreatic cells. This observation can also open a new route towards innovative diabetes-2 treatment whereby the insulin level of a diabetic patient would be increased, not by injection of insulin with a syringe, but by an external magnetic field with magnetic particles being permanently dispersed in the pancreas.

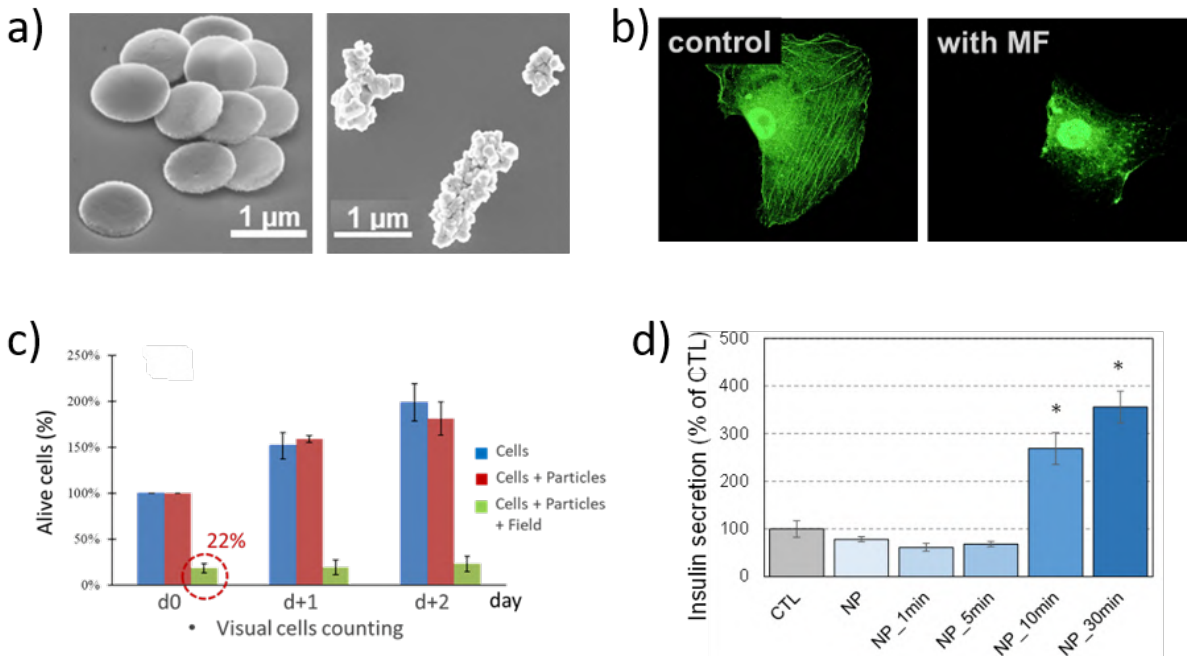

Figure 1: a) Two types of superparamagnetic-like particles used for the magneto-mechanical stimulation of cells: Au coated magnetic NiFe vortex nanoparticles (left) and magnetite nanopowder (right). b) Cytoskeleton disruption: U87 cancer control cell with stained actin cytoskeleton (left); cell with damaged cytoskeleton after NP magneto-mechanical vibration (right). c) In vitro results of magneto-mechanical stimulation of U87 glioma cancer cells. Blue and red bars: control cells (cells without particles and cells with particles but no oscillating field), green bar: cells with particles, submitted to oscillating magnetic field. Right after field application 80% of the cancer cells are dead (d0). Interestingly, the remaining alive cells do not proliferate for the next two days (d1 and d2). d) Insulin production of INS1 pancreatic cells under mechanical stimulation. A significant increase in insulin secretion is observed after 10 minutes.

References

[1] S. Leulmi et al. *Nanoscale* 7, 1594 (2015).

[2] C. Naud et al. *Nanoscale Adv.* 2, 3632 (2020).

[3] C. Thébault et al. *Nanoscale Adv.* 3, 6213 (2021).

[4] S. Ponomareva et al. *Nanoscale* 14, 13274 (2022).

[5] H. Joisten et al. *Appl. Phys. Lett.* 97, 253112 (2010).

A non-volatile binary synapse based on a vortex nano-oscillator

Leandro Martins[1,*], Alex Jenkins[1], Jérôme Borme[1], Lara San Emeterio Alvarez[1], and Ricardo Ferreira[1]

[1]*International Iberian Nanotechnology Laboratory (INL), Braga, Portugal*
leandro.ferreiramartins@cea.fr

In recent years, spin torque nano-oscillators (STNOs) have been intensively studied as spintronic devices for use in artificial neural networks (ANNs) [1]. Non-trivial tasks such as vowel recognition were achieved in a computing system, where four STNOs represent a chain of four artificial neurons [2]. More recently, STNOs have also been proposed to work as synapses in ANNs where, based on the spin diode effect [3], the synaptic weight depends on the frequency difference between the input RF signal and the resonator [4].

In this work, a new mechanism to combine a non-volatile behaviour with the spin diode detection of a vortex-based STNO is presented [5]. Experimentally, it is observed that the spin diode response (i.e. synaptic weight) of the oscillator depends on the binary vortex chirality (clockwise or counterclockwise sense of the in-plane magnetic moments). Consequently, as shown in Fig. 1, fixing the frequency of the incoming signal and switching the vortex chirality results in a different rectified voltage (V^+ and V^-) and, consequently, different synaptic weights (slopes W^+ and W^-). The chirality is stable at remanence, leading to a non-volatile control of the output voltage for a given input frequency. Micromagnetic simulations corroborate the experimental results and show the main contribution of the Oersted field created by the input RF current density in defining two distinct spin diode detections for different chiralities. This work opens new perspectives for the integration of spintronic devices in neuromorphic hardware.

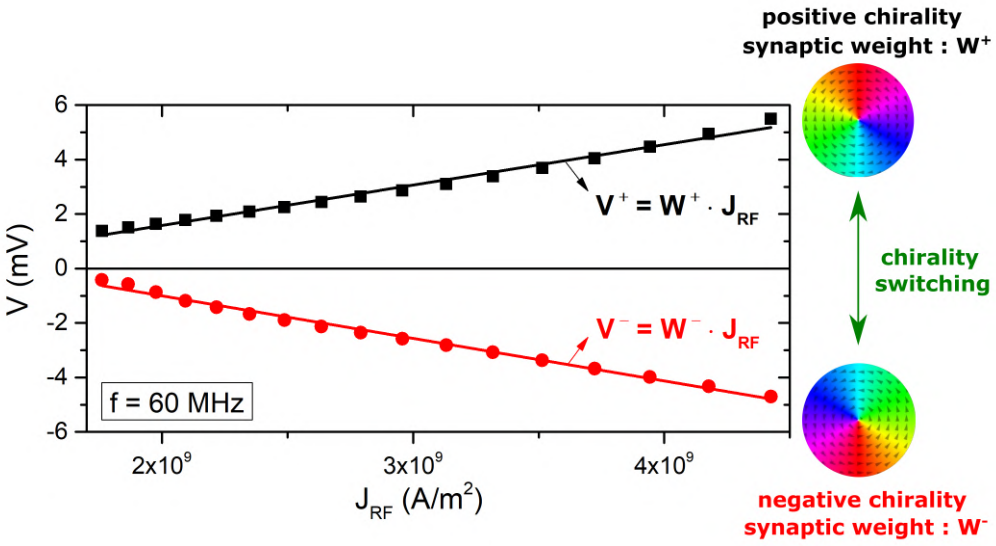

Figure 1: Rectified voltage measured at a fixed frequency of 60 MHz and presented as a function of the input RF current density. A linear fit is also calculated for each set of experimental data. Different chiralities lead to different slopes, corresponding to two distinct synaptic weights, W^+ and W^-. On the right, from micromagnetic simulations, two illustrations show the magnetic vortex state for each chirality.

Acknowledgments

Leandro Martins would like to thank FCT — Fundação para a Ciência e a Tecnologia — for support concerning his PhD grant SFRH/BD/128833/2017. This work has received funding from the European Union's Horizon 2020 research and innovation programme under grant agreement No. 101017098 (project RadioSpin) and grant agreement No. 899559 (project SpinAge).

References

[1] J. Grollier, D. Querlioz, K. Y. Camsari, et al. Neuromorphic spintronics. *Nature Electronics* 3, 360–370 (2020).

[2] Miguel Romera, Philippe Talatchian, Sumito Tsunegi, et al. Vowel recognition with four coupled spin-torque nano-oscillators. *Nature* 563, 230–234 (2018).

[3] A. A. Tulapurkar, Y. Suzuki, A. Fukushima, et al. Spin-torque diode effect in magnetic tunnel junctions. *Nature* 438, 339–342 (2005).

[4] Nathan Leroux, Alice Mizrahi, Danijela Marković, et al. Hardware realization of the multiply and accumulate operation on radio-frequency signals with magnetic tunnel junctions. *Neuromorphic Computing and Engineering* 1, 011001 (2021).

[5] Leandro Martins, Alex S. Jenkins, Lara San Emeterio Alvarez, et al. Non-volatile artificial synapse based on a vortex nano-oscillator. *Scientific Reports* 11, 16094 (2021).

Spin-orbit Ferroelectric RAM, concept and study of spin-dependent transport via Finite Element Method simulations

Paolo Sgarro[1,*], Theo Frottier[1], Aurélie Kandazoglou[1], Salvatore Teresi[1], Maxime Culot[1], Maxen Cosset-Chéneau[1], Filip Osana[1], Lorena Anghel[1], Alain Marty[1], Laurent Vila[1], Guillaume Prenat[1], and Jean-Philippe Attané[1]

[1]*Spintec, IRIG, DEFI, Univ. Grenoble Alpes, CEA, CNRS, F-38000 Grenoble, France*
paolo.sgarro@cea.fr

Spin-related phenomena are attracting increasing interest from information technology, due to the possibility to bring together the advantages of non-volatile devices and low energy state switching. Physical effects like spin-orbit torque and spin-transfer torque have found application for fast non-volatile memories, and recently, the MagnetoElectric Spin-Orbit (MESO) device, proposed by INTEL, is expected to bring a dramatic improvement with respect to CMOS in terms of power consumption and logic density [1].

In a previous work [2], a novel device featuring the interplay of ferromagnetism and ferroelectricity has been proposed; in which the data is stored in a ferroelectric layer, and can be read by injecting a spin-polarized current and exploiting the ferroelectric control of spin-to-charge interconversion. This phenomenon can be observed in several materials, ranging from oxide-based two dimensional electron gases [2], to Ferroelectric Rashba semiconductors [3]. We expect this device to be interesting for applications in logic, memories and non-conventional computing. In this work, we want to propose a novel technology called Spin-orbit Ferroelectric RAM (SoFRAM), in which the pheonomenon described above is exploited for a non volatile memory with a lower writing energy with respect to magnetic memories, and with a non destructive reading of the ferroelectric state.

We show the development of the compact model of the device, which is later tested by means of Finite Element Method (FEM) simulations for spin-dependent transport. Later, these simulations are also used to optimize the performances of the device, with a particular focus on the output signal, and materials choice is also discussed. In the last part, we propose a few architectures, with reading and writing strategies, in which the SoFRAM can be implemented for a large-scale memory array.

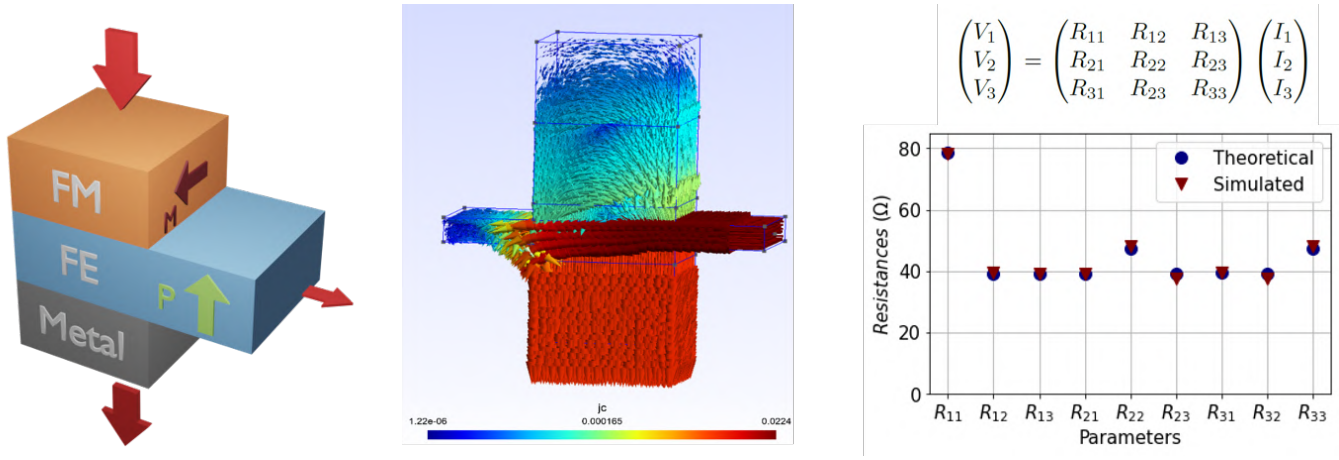

Figure 1: (left) Sketch of the sofRAM, (middle) representation of the current lines computed via FEM, and (right) comparison of the compact model parameters computed analytically with the results of simulations.

Acknowledgments

This project has received funding from the European Union's Horizon 2020 research and innovation program under the Marie Skłodowska-Curie grant agreement N°955671. We acknowledge support from the Institut Universitaire de France, the French Research Agency (ANR) as part of the project CONTRABASS (ANR–20–CE24–0023) and in the framework of the "Investissements d'avenir" program (ANR–15–IDEX–02).

References

[1] Sasikanth Manipatruni, Dmitri E Nikonov, Chia-Ching Lin, et al. Scalable energy-efficient magnetoelectric spin–orbit logic. *Nature* 565, 35–42 (2019).

[2] Paul Noël, Felix Trier, Luis M Vicente Arche, et al. Non-volatile electric control of spin–charge conversion in a SrTiO3 Rashba system. *Nature* 580, 483–486 (2020).

[3] Sara Varotto, Luca Nessi, Stefano Cecchi, et al. Room-temperature ferroelectric switching of spin-to-charge conversion in germanium telluride. *Nature Electronics* 4, 740–747 (2021).

Leveraging the phase dynamics of spin-torque nano-oscillators for unconventional computing

Abderrazak Hakam[1, *], Nhat-Tan Phan[1], Leandro Martins[1], Louis Hutin[2], Franck Badets[2], Luana Benetti[3], Alex Jenkins[3], Ricardo Ferreira[3], Philippe Talatchian[1], and Ursula Ebels[1]

[1]*Univ. Grenoble Alpes, CEA, CNRS, Grenoble INP, SPINTEC, 38000 Grenoble, France*
[2]*CEA-Leti Minatec, Grenoble, France*
[3]*International Iberian Nanotechnology Laboratory (INL), 4715-31 Braga, Portugal*
*abderrazak.hakam@cea.fr

Solving computational problems of ever-increasing complexity and size, in response to the needs of the modern information and computation society, poses major challenges for the development of future technologies. A main concern is the increase in the energy consumption of computing systems, related to the computing architecture that imposes a constant data transfer between memory and processing units. In addition, energy consumption continues to increase with the complexity of the problems. Therefore, novel hardware approaches are needed to remedy the issue of energy consumption, while improving at the same time crucial parameters such as high speed, compactness and integrability. In this context, spin-torque nano-oscillators (STNOs) have been explored recently to develop innovative cognitive computing schemes, demonstrating vowel recognition via the synchronization of an array of STNOs [1]. STNOs thus provide an important avenue to develop novel computing approaches, making a detailed analysis of their amplitude, frequency, and phase dynamics essential, particularly when implementing arrays of coupled STNOs.

In this contribution, the phase dynamics is explored for vortex-based STNOs, for which a magnetic vortex is stabilized in the free layer and whose dynamics is excited by spin-transfer torque using an applied electrical DC current. While the free-running STNO has an arbitrary phase, subject to large phase fluctuations, the phase takes discrete values with bounded noise, when the STNO is synchronized to an external RF signal [2, 3]. This synchronization operation is called injection-locking. Besides locking the frequency to the external source frequency, see Figure 1(a), injection-locking provides a stable phase reference and allows discretization of the phase values. A particular case is the second harmonic injection-locking (SHIL) where the external signal has two times the STNO's frequency. This enables the phase to take binary π shifted values. Thermal fluctuations lead to small, bounded oscillations around the stable phase state and can in addition induce stochastic phase jumps between the two discrete phase values. Those phase jumps are illustrated in Figure 1(b). Their occurrence and rate will depend on the properties of the STNO, the frequency mismatch with the external RF source as well as on the experimental conditions.

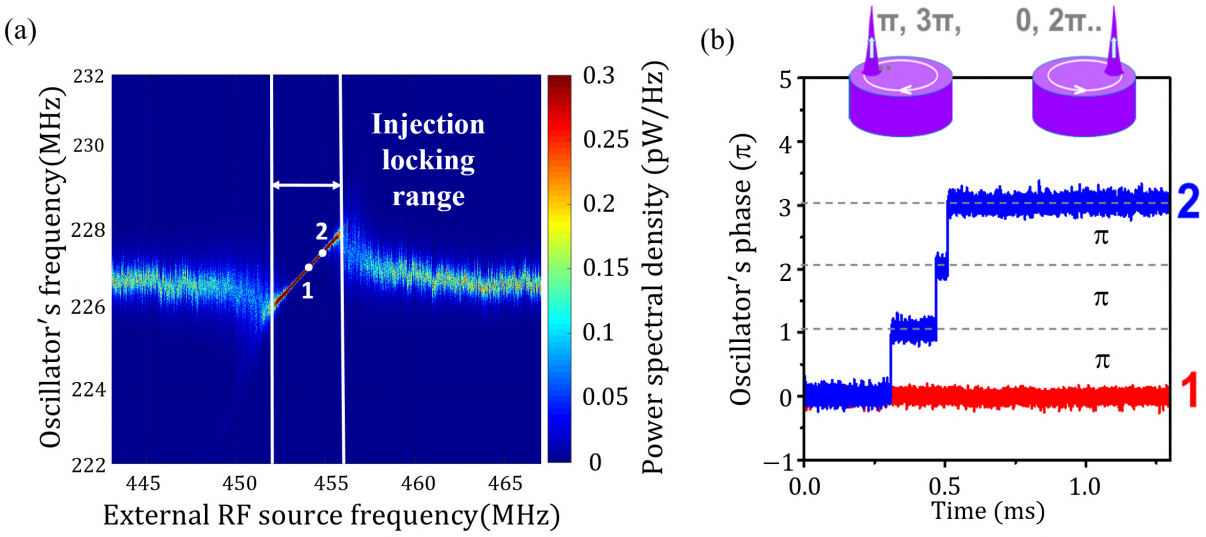

Figure 1: (a) Color map of the power spectral density for a vortex STNO under second harmonic injection-locking. (b) The instantaneous phase difference between STNO and RF source, for two values (red and blue curves) of the locking signal frequency. The phase was extracted by applying the Hilbert transform to the voltage time trace of the STNO's output signal.

While stochastic phase jumps will be detrimental for applications such as phase-shift-keying [3], they can be exploited for cryptography applications to generate true random numbers or for unconventional computing schemes such as Ising

machines. The Ising machine is a hardware implementation of the Ising model of a 2D binary spin-lattice, built to solve optimization problems. It relies on the convergence of the system's energy towards its global minimum to find the solution to a given optimization problem that is mapped to the Ising model through the coupling between spins. Reference [4] proposes to build such an Ising machine using the binary phase states of SHIL oscillators. In this study, we leverage the stochastic phase jumps of a SHIL vortex-based STNOs, to converge to the energy minimum and to provide a proof of concept of an oscillator-based Ising machine.

To achieve this ambitious goal, it is fundamental to understand experimentally the phase dynamics of an injection-locked STNO which are subject to phase fluctuations as well as to additional signals either from an RF source or from coupling to other STNOs. Results will be presented to illustrate how the stochastic phase jumps can be controlled by the operating point (DC current, applied magnetic field), the ratio and mismatch between the STNO and external RF source frequencies, the RF excitation type (via current or field), and an additional weak RF signal provided by a signal generator or the coupling to one or more STNOs. We discuss how this phase dynamics can be exploited to develop an oscillator-based Ising machine or Hopfied networks [5].

Acknowledgments

This research was funded in part by l'Agence Nationale de la Recherche (ANR), projects SpinIM ANR-22-CE24-0004 and StochNET ANR-21-CE94-0002 as well as by the CEA projects PTC-MINOS and Carnot AE SIGMA.

References

[1] Miguel Romera and Philippe Talatchian et al. Vowel recognition with four coupled spin-torque nano-oscillators. *Nature* 563, 230–234 (2018).

[2] R. Lebrun and A. Jenkins et al. Understanding of Phase Noise Squeezing Under Fractional Synchronization of a Nonlinear Spin Transfer Vortex Oscillator. *Physical Review Letters* 115, 017201 (2015).

[3] A. Litvinenko et al. Analog and Digital Phase Modulation and Signal Transmission with Spin-Torque Nano-Oscillators. *Physical Review Applied* 16, 024048 (2021).

[4] Tianshi Wang and Jaijeet Roychowdhury. OIM: Oscillator-Based Ising Machines for Solving Combinatorial Optimisation Problems. *Unconventional Computation and Natural Computation*, 232–256 (2019).

[5] Nitin Prasad, Prashansa Mukim, Advait Madhavan, and Mark D Stiles. Associative memories using complex-valued Hopfield networks based on spin-torque oscillator arrays. *Neuromorphic Computing and Engineering* 2, 034003 (2022).

A numerical study of Ising machines based on spin torque nano-oscillators

Mateo Ibarra Gomez[1,*], Philippe Talatchian[1], Liliana D. Buda-Prejbeanu[1], and Ursula Ebels[1]

[1]*Univ. Grenoble Alpes, CEA, CNRS, Grenoble INP, SPINTEC, 38000 Grenoble, France*
mateo.ibarragomez@cea.fr

Spin torque nano-oscillators (STNO) are nanoscale devices based on magnetic tunnel junctions. Such STNOs generate microwave voltage signals upon injection of a DC current. The phase dynamics of weakly coupled arrays of STNOs and/or coupling of STNOs to an external RF signal (injection locking), can be harnessed to develop novel hardware approaches for unconventional computing [1]. When injection locked to a signal with two times the natural frequency of the oscillator (2f injection locking), the phase difference between the STNO and the external signal can take two discrete stable values, i.e. it becomes binary. In this case, such phase difference, that we call ψ, can be exploited to represent the binary spins of an Ising Hamiltonian, given in Eq. 1. Here $\sigma_{i,j}$ represent the binary spins, $J_{i,j}$ is the coupling between spins i and j and the Hamiltonian gives the energy of the coupled Ising spin system.

$$\mathscr{H}(\sigma) = \sum_{i,j} J_{i,j}\sigma_i\sigma_j - \mu\sum_j h_j\sigma_j \tag{1}$$

Interestingly, many combinatorial optimization problems (COP) can be mapped to such an Ising Hamiltonian. The minimization of it or, in other words, the inherent convergence towards the global energy minimum of the Ising system can then be used as an algorithm to determine the solution of a COP. Specific hardware implementations of such an Ising system are called Ising machine (IM). Here, we address in a numerical study the implementation of an Oscillator based Ising Machine (OIM) [2] using STNOs.

For the extraction of the dynamic properties of STNOs, we resort to solving numerically the Landau-Lifshitz-Gilbert-Slonczewski equation including thermal fluctuations, in combination with the non-linear auto-oscillator model [3].

The possibility of implementing an STNO based IM has been studied in [4] for a particular set of parameters. Nevertheless, since the dynamics of STNOs described by the Lifshitz-Gilbert-Slonczewski (LLGS) equation is quite complex, it is crucial to explore a wider set of conditions analyzing how the phase difference ψ and the coupling of the oscillators evolve. With this in mind we simulate systems of multiple STNOs that are electrically coupled and 2f injection locked. Figure 1 illustrates one of such systems for 2 STNOs.

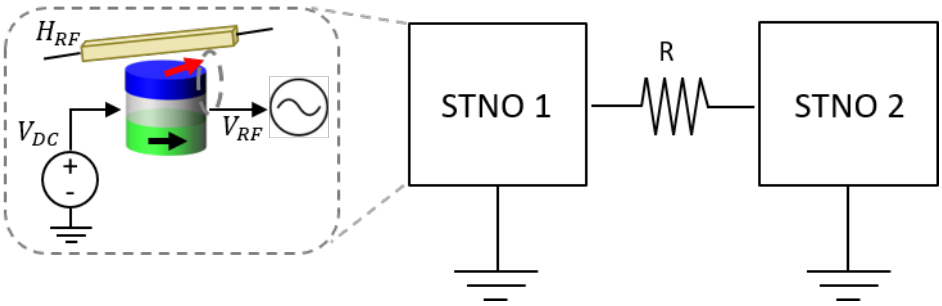

Figure 1: Schematics showing the STNO operation and the electrical coupling of two STNOs via a resistance R. H_{RF} is the RF field that injection locks the oscillators and V_{DC} is the DC voltage applied to the STNO device.

For every simulation, we investigate the stochastic phase dynamics induced by thermal fluctuations. In each simulation the phase ψ_i of each oscillator i is extracted. In figure 2 one can notice the binary nature of ψ which undergoes π transitions stochastically. Then, we compute the correlation between the phases of the oscillators and the probabilities of the system to be in each one of the possible phase configurations. One example of the possible configuration for 2 STNOs is shown in figure 3.

This study is performed as a function of the operating point, the temperature, the strength and sign of the coupling between the STNOs as well as the frequency mismatch to the external locking signal. The results will provide a guide for the practical implementation of an OIM based on STNOs, considering the specific non-linear dynamic properties of STNOS.

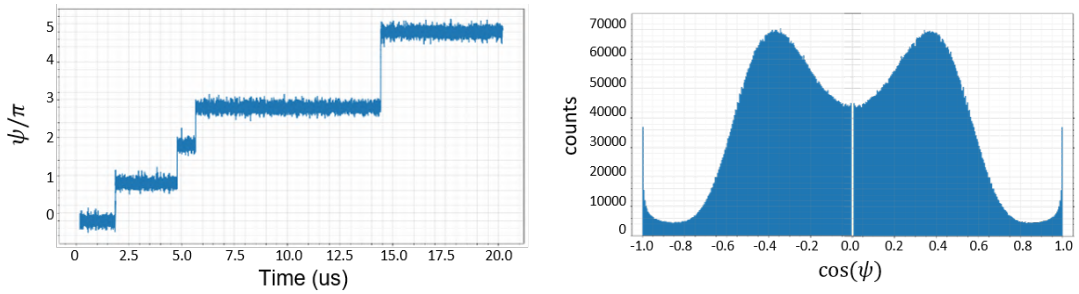

(a) Time evolution of ψ/π

(b) Histogram of $cos(\psi)$

Figure 2: Phase difference ψ for a 2f injection locked STNO with $V_{DC} = 1.4V$, $\mu_0 H_{DC} = 0.04T$, $\mu_0 H_{RF} = 0.25mT$. The cosine in (b) was used to limit ψ between two values.

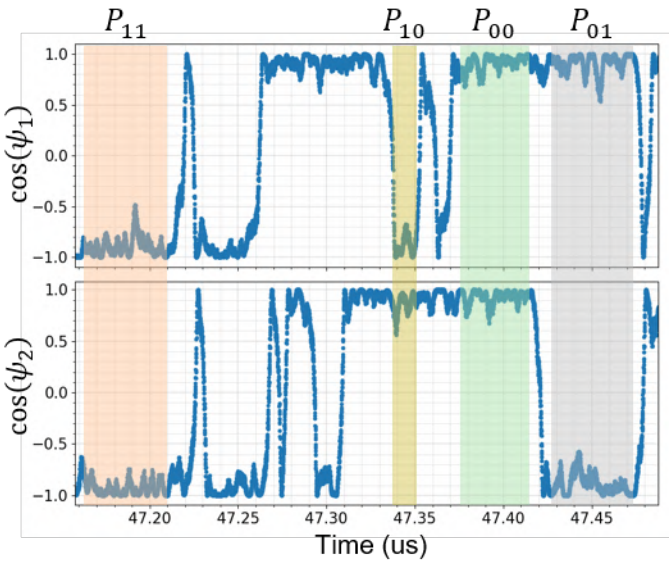

Figure 3: $Cos(\psi_i)$ with i=1,2 corresponding to two electrically coupled STNOs that are 2f injection locked. P_{jk} with j,k=0,1 represent each possible phase configuration of the two oscillators where $\psi = 0$ corresponds to j,k=0 and $\psi = \pi$ to j,k=1.

Acknowledgments

This research was funded in part by l'Agence Nationale de la Recherche (ANR), project SpinIM ANR-22-CE24-0004 and the CEA projects PTC-MINOS and Carnot AE SIGMA. MIG acknowledges financial support from the French Space Agency (CNES) and the European Union's Horizon 2020 research and innovation programme under grant agreement No 800945 — NUMERICS — H2020-MSCA-COFUND-2017.

References

[1] J. Grollier, D. Querlioz, K. Y. Camsari, et al. Neuromorphic spintronics. *Nature Electronics* 3, 360–370 (2020).

[2] Tianshi Wang and Jaijeet Roychowdhury. OIM: Oscillator-Based Ising Machines for Solving Combinatorial Optimisation Problems. *Unconventional Computation and Natural Computation*, 232–256 (2019).

[3] A. Slavin and V. Tiberkevich. Nonlinear Auto-Oscillator Theory of Microwave Generation by Spin-Polarized Current. *IEEE Transactions on Magnetics* 45, 1875–1918 (2009).

[4] Dagur Ingi Albertsson, Mohammad Zahedinejad, Afshin Houshang, et al. Ultrafast Ising Machines using spin torque nano-oscillators. *Applied Physics Letters* 118, 112404 (2021).

Poster 1.09, November 14th, 16h30–18h30

Étude des processus non-linéaires d'ondes de spin dans des disques d'Heusler Co_2MnAl de 5 µm pour le calcul par réservoir

S. Thlang[1,*], A.-M. Friedel[2], S. Petit-Watelot[2], S. Andrieu [2], J.-P. Adam[1], and J.-V. Kim[1]

[1]*Centre de Nanosciences et de Nanotechnologies, CNRS, Université Paris-Saclay, 91120 Palaiseau, France*
[2]*Institut Jean Lamour, CNRS, Université de Lorraine, 54011, Nancy, France*
*sonia.thlang@universite-paris-saclay.fr

Le calcul par réservoir est une méthode de machine learning récemment proposée dans les années 2000. Elle s'inscrit dans la famille des réseaux de neurones artificiels [1]. Son principe de fonctionnement se calque sur celui du cerveau avec des connections faites entre des neurones par le biais de synapses. Le réservoir est un système physique dont la dynamique et la non-linéarité peuvent être exploitées pour l'analyse de données telles que la reconnaissance vocale. Une série de signaux est injectée à l'entrée du réservoir, et une nouvelle série de données est lue en sortie. En passant dans le réservoir les signaux sont modifiés de manière non-linéaire. Cette transformation permet de projeter les signaux d'entrées sur des dimensionalités de calcul supérieures.
Du fait de la richesse de la dynamique qu'offrent les ondes de spin, nous nous proposons d'exploiter leurs propriétés afin d'élaborer un tel réservoir physique. Ces excitations élémentaires et collectives de l'aimantation possèdent une gamme de fréquence de l'ordre des GHz (idéale pour les applications télécoms et pour un traitement de données rapide). Les modes propres d'un état magnétique (par exemple un vortex) peuvent jouer le rôle de signaux d'entrée et de sortie d'un réservoir. En activant le régime non-linéaire, par application d'un champ rf au-dessus d'un certain seuil, des interactions complexes - telles que la *diffusion à trois ou quatre magnons* - sont engendrées [2]. Ces processus permettent ainsi aux modes propres de l'état magnétique de se coupler entre eux, et procure la non-linéarité nécessaire au calcul neuro-morphique.

Dans ce projet nous avons alors exploité les processus non-linéaires d'ondes de spin d'un état de vortex au sein d'un disque d'Heusler Co_2MnAl de 5 µm pour le calcul neuro-inspiré. Les simulations micromagnétiques ont été réalisées sous le programme Mumax3. Le faible facteur d'amortissement $\alpha \approx 10^4$ qu'offre les Heuslers permet la prolongation des états non-linéaires. L'état magnétique de vortex facilite la *diffusion à trois magnons* et ses

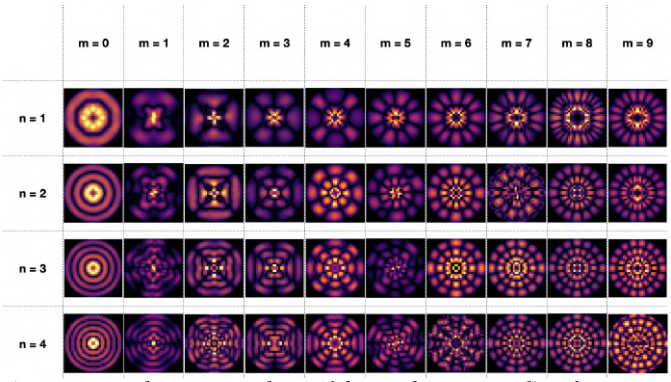

Figure 1: *Catalogue non exhaustif des modes propres d'un état de vortex dans un disque de Co_2MnAl de 5 µm.*

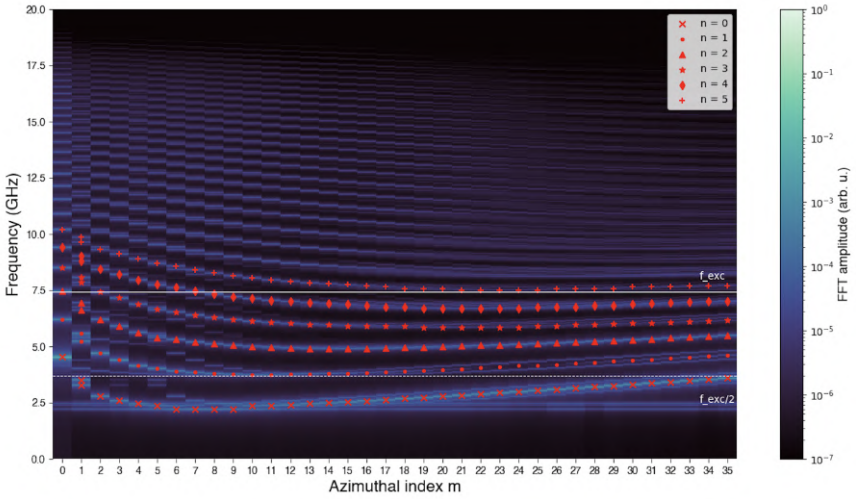

Figure 2: *Spectre des ondes de spin pour un disque Co_2MnAl de 5 µm dans un état de vortex*

modes propres ont déjà étudiés pour des disques de 5 µm dans d'autres matériaux [3]. Les modes propres d'un état de vortex au sein d'un disque sont plus facilement définissables que dans d'autres états magnétiques. La géométrie circulaire donne lieu à une symétrie spatiale pour les profils de modes. Chaque mode propre est caractérisé par des indices (n, m). Ces indices recensent le nombre de noeuds dans la direction radiale et azimutale du disque. Chacun des modes résonne à une fréquence déterminée par le matériau et les dimensions du système.
Nous avons étudié les modes propres d'un disque de Co_2MnAl de 5 µm hébergeant un vortex. Un champ extérieur B_{ext} a été appliqué hors du plan (selon z) dépendant du temps et de l'espace - en raison de la symétrie donnée par (n, m). La dépendance en temps se présente sous la forme d'un sinus cardinal à une fréquence de coupure de 50 GHz, afin d'exciter tous les modes propres. La dépendance en espace se base de la fonction de Bessel - dû à la géométrie circulaire de notre système - englobant la direction radiale n et azimutal m du disque. Le champ extérieur appliqué devient :

$B_{ext} = sinc(\pi \times freq \times t) \times J1\left[\frac{k_n}{\rho}\sqrt{x^2+y^2} \times cos(m\phi)\right]$, où J1 est le premier ordre de la fonction de Bessel, k_n est le n-ième zéro de la fonction de Bessel et est associé au mode n, ρ est le rayon du disque et ϕ est l'angle azimutal. Sur la figure 1 nous avons représenté la composante z de l'aimantation. Les amplitudes sont plus importantes au centre du disque. Les fréquences de résonance sont typiquement comprises entre 2 GHz et 20 GHz, et augmentent avec le mode n (voir figure 2). La relation de dispersion démontre un caractère $backward - volume$ des ondes de spin.
La géométrie et l'état magnétique du système donnent lieu à des *règles de sélection* [4] pour lesquelles un magnon initial se sépare spontanément en deux autres magnons, c'est la *diffusion à trois magnons*. L'énergie initiale et le moment angulaire sont conservés durant le processus. Si le magnon initial est un mode $m = 0$, il se sépare en deux magnons, de modes $\pm m$ et des modes radiaux n différents. À l'inverse si le magnon initial est un mode m$\neq$ 0, les magnons produits ont des modes azimutaux |m| différents, sans restriction sur n. Les fréquences des modes secondaires sont symétriquement réparties autour de $\frac{f_{exc}}{2} \pm \Delta f$. Ainsi sur la figure 2, la fréquence d'excitation a été choisie à 7.5 GHz, les modes secondaires éligibles à la *diffusion à trois magnons* doivent se trouvés à une fréquence de $3.75 - \Delta f$ et $3.75 + \Delta f$.
La *diffusion à trois magnons* émane de la dynamique non-linéaire de notre système. Sur la figure 3 nous activons le régime non-linéaire avec l'application d'un champ rf de 2 mT (seuil pour lequel des modes diffusés apparaissent). La composante z de l'aimantation est représentée sous une échelle logarithmique. Des modes diffusés/secondaires sont distinguables pour des fréquences d'excitation comprises entre 6.3 GHz et 7.8 GHz. Ces modes sont la signature de la *diffusion à trois magnons*. Les canaux verticaux peuvent correspondre à des modes n et à des processus non-linéaires supplémentaires. Les lignes horizontales en arrière-plan représentent les ondes de spin thermiques.

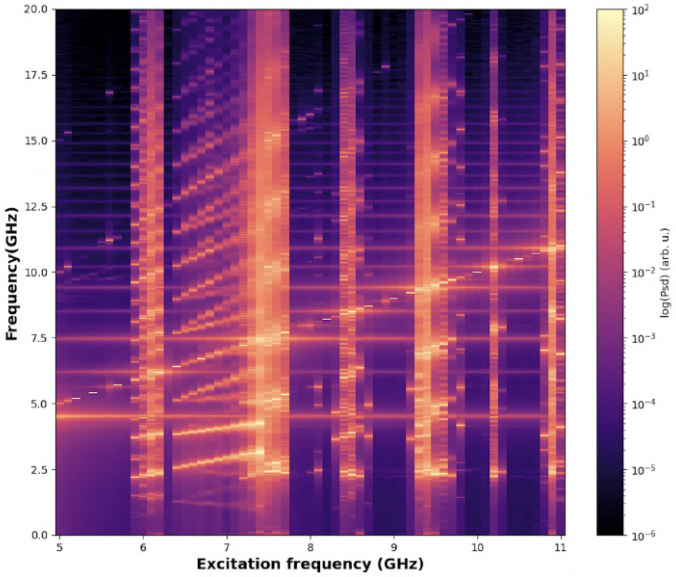

Figure 3: *Carte de densité spectrale de puissance d'ondes de de spin dans un état de vortex sous l'application d'un champ rf de 2 mT*

Les résultats présentés démontrent le caractère non-linéaire de notre état de vortex d'un disque d'Heusler Co_2MnAl de 5 µm. L'identification des canaux de résonance permettent d'implémenter des fréquences d'entrée - d'un magnon initial - au sein du réservoir et prédire les fréquences de sortie -des magnons secondaires- afin d'entraîner le système à la classification de séries de données. Des expériences par spectroscopie Brillouin permettront d'observer la *diffusion à trois magnons* et cartographier les ondes de spin au sein d'une couche mince de Co_2MnAl. La couche magnétique a été déposé sur un substrat de MgO à l'Insitut Jean Lamour - (001)[110] Co_2MnAl (20nm)/(001)[100] MgO (250 µm) - par croissance épitaxiale. Elle est tournée de 45 degrés par rapport au plan (001) du MgO. Les disques ont été patternés au C2N au moyen des processus de nanofabrication conventionnels. Ils sont encapsulés par un isolant $SiO_2(100nm)$. Des antennes Au encadrent les disques et sont connectés à des ground-signal pads.

References

[1] Gouhei Tanaka, Toshiyuki Yamane, Jean Benoit Héroux, et al. Recent advances in physical reservoir computing: A review. *Neural Networks* 115, 100–123 (2019).

[2] K. Schultheiss, R. Verba, F. Wehrmann, et al. Excitation of Whispering Gallery Magnons in a Magnetic Vortex. *Physical Review Letters* 122 (2019).

[3] Lukas Körber, Katrin Schultheiss, Tobias Hula, et al. "Theory and simulation on nonlinear spin-wave dynamics in magnetic vortices". PhD thesis. Technische Universität Dresden, 2020.

[4] Roman Verba, Lukas Körber, Katrin Schultheiss, et al. Theory of three-magnon interaction in a vortex-state magnetic nanodot. *Physical Review B* 103 (2021).

Pattern recognition in reciprocal space with a magnon-scattering reservoir

Lukas Körber[1,2], Christopher Heins[1,2], Tobias Hula[1,3], Joo-Von Kim[4,*], Sonia Thlang[4], Helmut Schultheiss[1,2], Jürgen Fassbender[1,2], and Katrin Schultheiss[1]

[1]*Institut für Ionenstrahlphysik und Materialforschung, Helmholtz-Zentrum Dresden-Rossendorf, 01328 Dresden, Germany*
[2]*Fakultät Physik, Technische Universität Dresden, 01062 Dresden, Germany*
[3]*Institut für Physik, Technische Universität Chemnitz, 09107 Chemnitz, Germany*
[4]*Centre de Nanosciences et de Nanotechnologies, CNRS, Université Paris-Saclay, 91120 Palaiseau, France*
joo-von.kim@c2n.upsaclay.fr

Magnons, the fundamental excitations in magnetic materials, can undergo complex multimode scattering processes when subjected to high input power. Within confined geometries such as vortex states in thin film disks, previous work has demonstrated that three-magnon scattering can induce a conversion of radial modes into azimuthal modes [1], a process that can also involve nonlocal stimulation [2]. In this presentation, we detail a recent investigation that leveraged such nonlinear magnon scattering events within a magnetic vortex, confined in a 5 μm-diameter permalloy disk, for the purpose of pattern recognition [3].

Our findings illustrate how the magnetic response to signal inputs composed of sine-wave pulses with varying frequencies can result in the excitation of distinct azimuthal modes. Importantly, the power spectrum of these scattered modes exhibits a significant dependence on the input sequences. Time-resolved micro-focus Brillouin light scattering spectroscopy measurements reveal that the temporal overlaps of different input symbols promote cross-stimulation, resulting in a large number of scattering channels and consequently leading to richer transient dynamics within the scattered mode populations.

Furthermore, micromagnetic simulations demonstrate that recognition rates of up to 99.4% can be achieved for four-symbol sequences utilizing these scattered modes. This high level of performance persists even in the presence of amplitude noise within the input signals. Our work introduces a novel approach to reservoir computing – termed modal multiplexing – which hinges on the transport of information in reciprocal space, as opposed to the spatial or temporal domains that are typically used.

Acknowledgments

This study was supported by the Deutsche Forschungsgemeinschaft within programmes SCHU 2922/1-1, KA 5069/1-1 and KA 5069/3-1, the Agence Nationale de la Recherche under contract No. ANR-20-CE24-0012 (MARIN), and the Horizon Europe Framework Programme of the European Commission under contract no. 101070290 (NIMFEIA). Support by the Nanofabrication Facilities Rossendorf (NanoFaRo) at the IBC is gratefully acknowledged.

References

[1] K. Schultheiss, R. Verba, F. Wehrmann, et al. Excitation of Whispering Gallery Magnons in a Magnetic Vortex. *Physical Review Letters* 122, 097202 (2019).

[2] L. Körber, K. Schultheiss, T. Hula, et al. Nonlocal Stimulation of Three-Magnon Splitting in a Magnetic Vortex. *Physical Review Letters* 125, 207203 (2020).

[3] L. Körber, C. Heins, T. Hula, et al. *Pattern recognition in reciprocal space with a magnon-scattering reservoir*. arXiv:2211.02328.

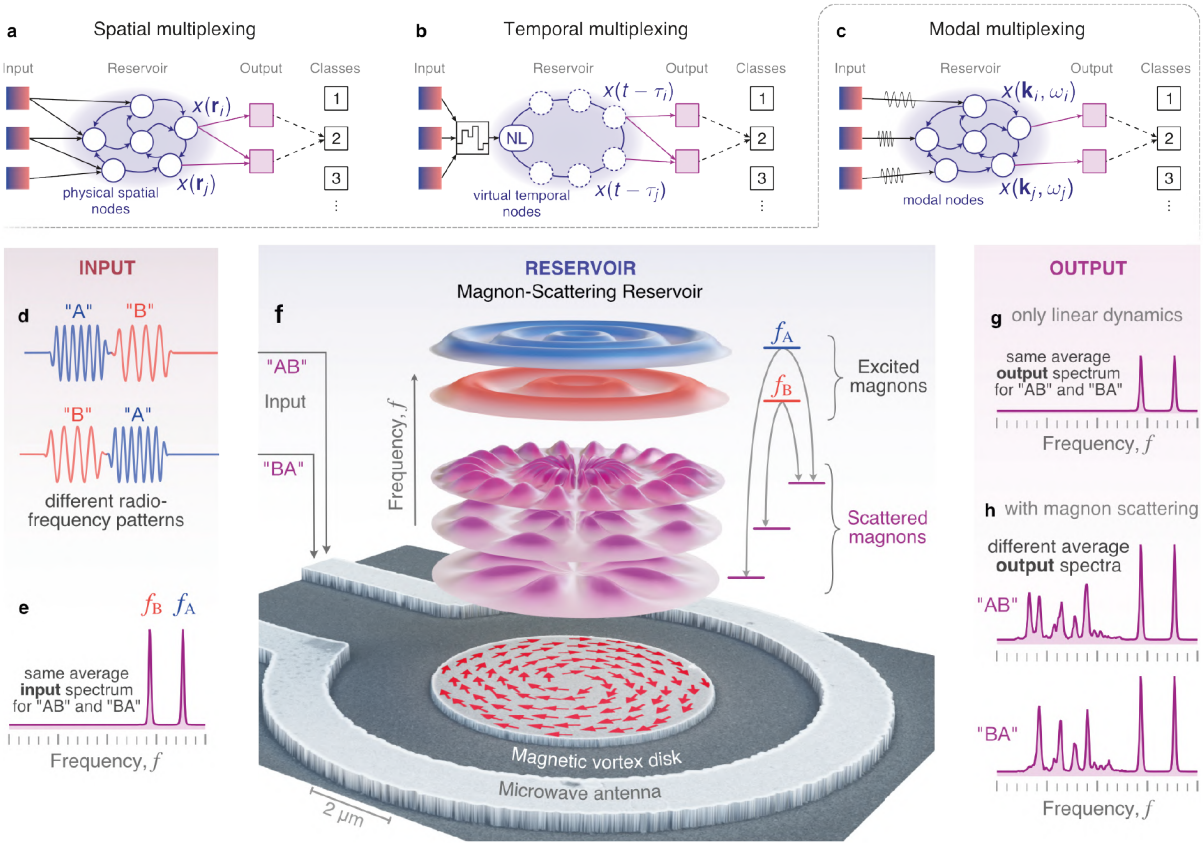

Figure 1: Working principle of a magnon-scattering reservoir (MSR). Sketches of different reservoirs based on (a) spatial, (b) temporal and (c) modal multiplexing, the concept behind the MSR. (d) Radiofrequency pulses with different temporal order but (e) the same average frequency content are used to trigger (f) nonlinear scattering between the magnon eigenmodes in a magnetic vortex disk. The dynamic response is experimentally detected using Brillouin-light-scattering microscopy. In contrast to a linear system (g), the MSR produces different outputs depending on the temporal order of the input (h).

Unveiling the potential of spintronics-based neural networks using ultrafast data-driven simulations

Anatole Moureaux[1, *], Simon de Wergifosse[1], Chloé Chopin[1], and Flavio Abreu Araujo[1]

[1]*Institute of Condensed Matter and Nanosciences, UCLouvain, Louvain-la-Neuve, Belgium*
anatole.moureaux@uclouvain.be

As artificial intelligence continues to rapidly develop worldwide, the increasing energy demands of traditional computing approaches have sparked the need for more energy-efficient alternatives. A promising solution lies in the development of neuromorphic computing systems drawing their inspiration from the human brain features *i.e.*, high energy efficiency and parallel processing capabilities [1, 2]. In particular, vortex-based spin-torque oscillators (STVOs) are promising candidates for the realization of hardware neural networks. These nanoscale DC to AC converters have been successfully used to perform automatic data classification thanks to their highly nonlinear dynamics, stability and CMOS-compatibility (see Fig. 1) [3–5]. To facilitate the development of such STVO-based neuromorphic systems, simulations provide a valuable strategy for overcoming the challenges associated with manipulating such nanostructures.

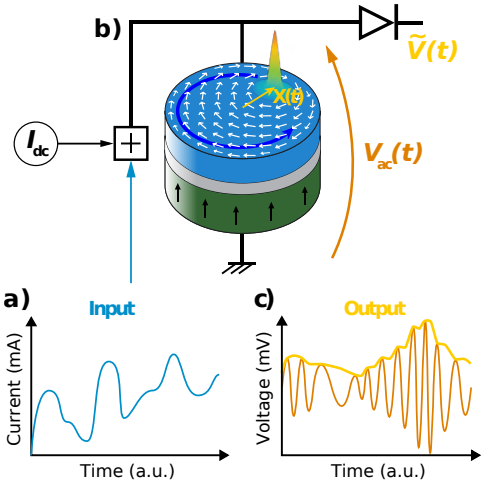

Figure 1: The complex STVO dynamics can be used to process information nonlinearly. **a)** An input signal modulated in amplitude is added to a DC bias current I_{dc} and injected into a magnetic tunnel junction (MTJ). **b)** The spin transfer torque leads to sustained oscillations of the vortex core in the plane of the MTJ. **c)** The amplitude of the voltage across the STVO depends nonlinearly on the intensity of the input signal.

Recently, Abreu Araujo *et al.* developed an ultrafast STVO simulation framework based on the Thiele equation approach [6]. The so-called data-driven Thiele equation approach (DD-TEA) combines the theoretical background of the Thiele equation with numerical results extracted from micromagnetic simulations (MMS). This technique effectively models the nonlinear STVO dynamics through an analytical description of the time-dependent reduced position of the vortex core $s(t)$ (see Eq. 1). The resulting relation is described in Eq. 2, with $\mathbf{X}(t)$ the position of the vortex core shown in Fig. 1, R the radius of the STVO, D_t the sampling interval of the input signal, and $\alpha(t)$, $\beta(t)$ and $n(t)$ dynamical parameters extracted from MMS, depending on t through the time-varying input signal. While the results are as accurate as MMS, they can be obtained about 2.4 billion times faster [7].

$$s(t) = \frac{||\mathbf{X}(t)||}{R} \tag{1}$$

$$s(t) = \frac{s(t - D_t)}{\sqrt[n(t)]{\left(1 + \frac{s(t-D_t)^{n(t)}}{\alpha(t)/\beta(t)}\right)\exp(-n(t)\alpha(t)D_t) - \frac{s(t-D_t)^{n(t)}}{\alpha(t)/\beta(t)}}} \tag{2}$$

DD-TEA offers a valuable means to optimize the operating conditions of an experimental STVO-based neural network. Parametric studies, which were previously impractical to conduct due to the time-intensive nature of MMS, have been executed efficiently. The influence of the input signal amplitude and the level of noise in the system was assessed during the classification of sine and square waveforms (see Fig. 2a). Furthermore, DD-TEA performs well at simulating the classification of higher-dimensional data like images. The simulations speed allowed making quantitative comparisons between our

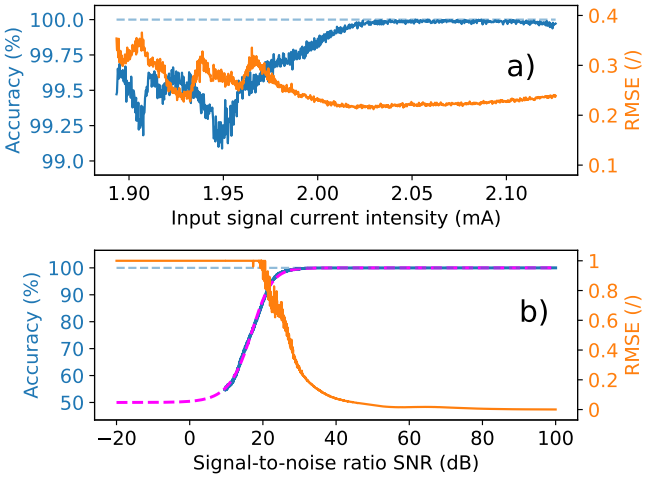

(a) Accuracy and RMSE for waveforms recognition depending on (**top**) the input signal amplitude and (**bottom**) the level of noise in the system.

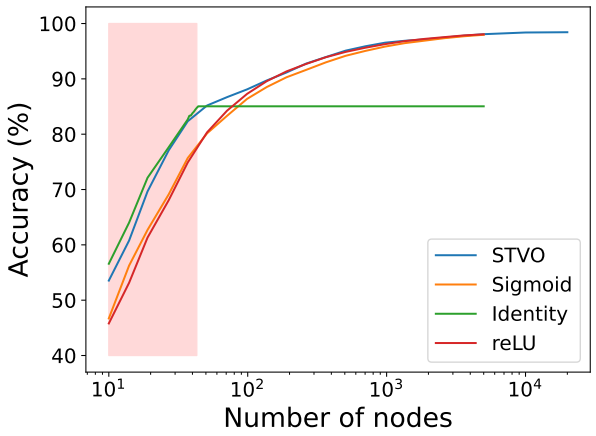

(b) Comparison between STVO-based neural networks and implementations based on conventional activations functions, for a varying number of nodes (MNIST). The red area corresponds to networks with insufficient numbers of parameters.

Figure 2: Parametric studies of STVO-based neural networks performances conducted using the DD-TEA framework.

STVO-based neural networks and conventional software implementations on the MNIST handwritten digits recognition task, also confirming the STVO dynamics efficacy for data classification (Fig. 2b).

DD-TEA is a technique that effectively simulates the complex dynamics of STVOs. It was used to conduct extensive studies on the performances of STVO-based neural networks, allowing to observe the influence of operating parameters on the quality of the classification for two different tasks. These results are highly valuable to optimize the fabrication of an experimental setup efficiently. Furthermore, it will lead to the testing of more complex architectures to tackle sophisticated machine learning tasks. To conclude, we expect that Eq. 2 will soon provide a path for enhancing our mathematical understanding of the data processing mechanisms that take place inside STVO-based neural networks.

References

[1] Danijela Marković, Alice Mizrahi, Damien Querlioz, and Julie Grollier. Physics for neuromorphic computing. *Nature Reviews Physics* 2, 499–510 (2020).

[2] Laurent Larger, Miguel C Soriano, Daniel Brunner, et al. Photonic information processing beyond Turing: an optoelectronic implementation of reservoir computing. *Optics express* 20, 3241–3249 (2012).

[3] Julie Grollier, Damien Querlioz, KY Camsari, et al. Neuromorphic spintronics. *Nature electronics* 3, 360–370 (2020).

[4] Flavio Abreu Araujo, Mathieu Riou, Jacob Torrejon, et al. Role of non-linear data processing on speech recognition task in the framework of reservoir computing. *Scientific reports* 10, 328 (2020).

[5] Jacob Torrejon, Mathieu Riou, Flavio Abreu Araujo, et al. Neuromorphic computing with nanoscale spintronic oscillators. *Nature* 547, 428–431 (2017).

[6] Flavio Abreu Araujo, Chloé Chopin, and Simon de Wergifosse. Data-driven Thiele equation approach for solving the full nonlinear spin-torque vortex oscillator dynamics. *arXiv preprint arXiv:2206.13596* (2022).

[7] Anatole Moureaux, Simon de Wergifosse, Chloé Chopin, Jimmy Weber, and Flavio Abreu Araujo. Neuromorphic spintronics accelerated by an unconventional data-driven Thiele equation approach. *arXiv preprint arXiv:2301.11025* (2023).

Dynamic imprinting of nanoscale topological phases into an antiferromagnet

Miina Leiviskä[1,*], Sarah Jenkins[2], Richard F. L. Evans[2], Daria Gusakova[1], and Vincent Baltz[1]

[1]*Univ. Grenoble Alpes, CNRS, CEA, Grenoble INP, IRIG-Spintec, F-38000 Grenoble, France*
[2]*School of Physics, Engineering and Technology, University of York, York YO10 5DD, United Kingdom*
*miina.leiviska@cea.fr

Controlling the magnetic order of antiferromagnets is challenging due to the vanishing net magnetisation. For this reason, the study of topologically protected real-space states of antiferromagnets is restricted by the difficulty in nucleating these states.

Here, using atomistic simulations we demonstrate how to overcome the challenge of nucleating an antiferromagnetic skyrmion in a thin film antiferromagnet, γ-$IrMn_3$ (see Fig. 1). Utilising the exchange bias coupling between a ferromagnet and an antiferromagnet, we imprint the spin structure of the former through the latter by means of a thermal cycling procedure. The imprinted textures are shown to be stable against field perturbations. We discuss how various parameters affect the efficiency of this imprinting and the characteristics of the imprinted textures.

This work paves way for further studies on topologically protected real-space phases in antiferromagnets and promotes the development of denser and faster spintronic devices [1], [2].

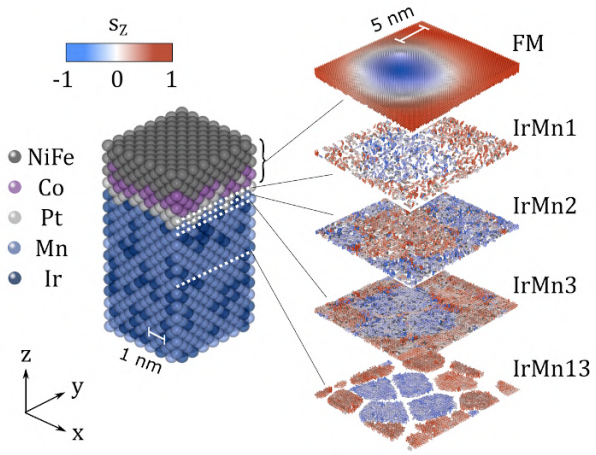

Figure 1: (Left) Atomic structure of a slice of the simulation system consisting of a hybrid NiFe/Co/Pt ferromagnetic single crystal coupled to a granular γ-$IrMn_3$ antiferromagnet, across an atomically intermixed interface. The full size of the simulation system is $100\times100\times6.67$ nm. (Right) Cross-section of the spin texture obtained in the ferromagnet and at several depths in the antiferromagnet, following a thermal cycling. The numbers indicate the relative position of the monolayers away from the interface.

Acknowledgments

This study was partially supported by the France-UK Alliance Hubert Curien programme (PHC) (Grant No. 46298XC) and the UK EPSRC programme (Grant No. EP/V007211/1). This work used the ARCHER2 UK National Supercomputing Service.

References

[1] M. Leiviskä, S. Jenkins, R. F. L. Evans, D. Gusakova, and V. Baltz. Dynamic imprinting of nanoscale topological phases into an antiferromagnet. *arXiv:2302.08842* (2023).

[2] K. G. Rana, R. L. Seeger, S. Ruiz-Gómez, et al. Imprint from ferromagnetic skyrmions in an antiferromagnet via exchange bias. *Applied Physics Letters* 119, 192407 (2021).

Electrical detection and nucleation of a magnetic skyrmion in a magnetic tunnel junction observed via *operando* magnetic microscopy

Joseba Urrestarazu Larrañaga[1,*], Naveen Sisodia[1], Van Tuong Pham[2], Aurélien Masseboeuf[1], Florian Disdier[1], Bruno Fernandez[2], Sebastian Wintz[3], Markus Weigand[4], Mohamed Belmeguenai[5], Stefania Pizzini[2], Ricardo Sousa[1], Liliana Buda-Prejbeanu[1], Gilles Gaudin[1], and Olivier Boulle[1]

[1]*Univ. Grenoble Alpes, CNRS, CEA, Grenoble INP, SPINTEC, Grenoble, France*
[2]*Univ. Grenoble Alpes, CNRS, Institut Néel, Grenoble, France*
[3]*Helmholtz-Zentrum Berlin für Materialien und Energie, Berlin, Germany*
[4]*Max Planck Institute for Intelligent Systems, Stuttgart, Germany*
[5]*LSPM, CNRS, Villetaneuse, France*
joseba.urrestarazularranaga@cea.fr

Magnetic skyrmions have recently attracted a large interest owing to their rich physics at the frontier of topology and magnetism and promising applications for non-volatile technological memory and logic devices. Skyrmions are local chiral whirlings of the magnetization texture with particle like properties, owing to their small lateral dimensions (down to the nanometer scale) and topological stability. They were recently demonstrated at room temperature in ultrathin heavy metal/ferromagnetic films as well as their fast manipulation by electrical current [1]. Those were first important steps toward technological applications where skyrmions in tracks are the information carriers. However, important challenges still need to be faced regarding the electrical detection and the low power nucleation of the skyrmions, which are required for the read and write operation in devices.

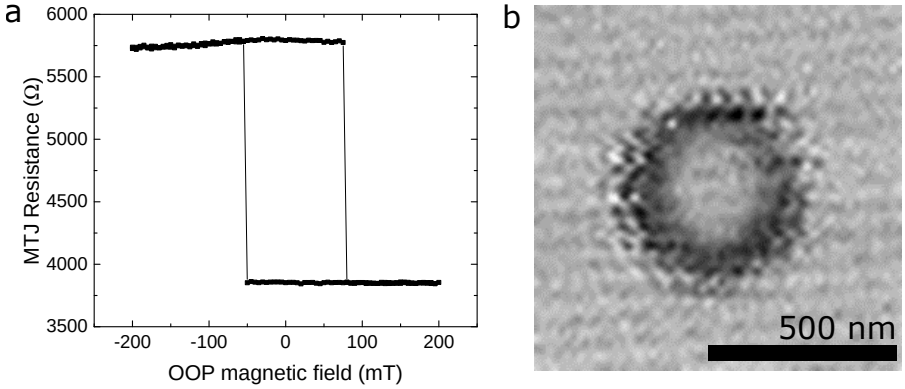

Figure 1: (a) Resistance vs out of plane magnetic field hysteresis loop of the device. (b) XMCD-STXM image of a magnetic skyrmion in a MTJ pillar of 500nm.

Here we demonstrate the nucleation by gate voltage and the electrical detection of a magnetic skyrmion in a magnetic tunnel junction (MTJ) using tunnelling magnetoresistance (TMR). To demonstrate this result, we combined scanning tunnelling magnetic microscopy (STXM) and operando magneto-transport measurements of a MTJ fabricated on top of an ultrathin SiN membrane. This allowed us to perform simultaneously high spatial resolution magnetic imaging of the spin texture within the MTJ and transport measurements to enable an unambiguous electrical detection of the magnetic skyrmion. Fig. 1a shows the hysteresis loop of a 500 nm diameter MTJ showing a TMR of 53% with sharp reversal and a resistance area product around 700 $\Omega\cdot\mu m^2$. Starting from the parallel magnetization resistance state with a uniform magnetization, the application of a voltage pulse (10 ns) leads to a jump of the resistance (470 Ω) to a stable intermediate resistance state. XMCD-STXM imaging shows that this new resistance state is associated with the nucleation of a skyrmion in the free layer of the MTJ (see Fig. 1b). Micromagnetic simulations using experimental parameters show that the nucleation can be explained by the transient nucleation of a vortex state, via voltage-induced decrease of the magnetic anisotropy, which eventually relaxes towards a skyrmionic state. These results demonstrate the read and write operations of a skyrmion based device and are an important milestone for low power applications based on the manipulation of magnetic skyrmions.

Acknowledgments

We acknowledge the support of the French Agence Nationale de la Recherche (SKYLOGIC project) and the DARPA TEE program. We would like to thank Martien den Hertog for her help in the preparation of the SiN membranes and the Helmholtz-Zentrum Berlin für Materialien und Energie for the allocation of synchrotron radiation beamtime.

References

[1] Albert Fert, Nicolas Reyren, and Vincent Cros. Magnetic skyrmions: advances in physics and potential applications. *Nature Reviews Materials* 2 (2017).

Theory of magnetic field-stabilized compact skyrmions in thin film ferromagnets

Anne Bernard-Mantel[1, 2, *], Anaïs Fondet[1, 2], Cyrill B. Muratov[3,4], Theresa M. Simon[5], and Valery Slastikov [6]

[1]*Université de Toulouse, Laboratoire de Physique et Chimie des Nano-Objets, UMR 5215 INSA, CNRS, UPS, 135 Avenue de Rangueil, F-31077 Toulouse Cedex 4, France*
[4]*Department of Mathematical Sciences, New Jersey Institute of Technology, Newark, NJ 07102, USA*
[3]*Departimento di Matematica, Universitá di Pisa, L. Bruno Pontecorvo, 5, 56127 Pisa, Italy*
[5]*Institut für Analysis und Numerik, Westfälische Wilhelms-Universität Münster, Einsteinstr. 62, 48149 Münster, Germany*
[6]*School of Mathematics, University of Bristol, Bristol BS8 1TW, United Kingdom*
[2]*Centre d'Elaboration de Matériaux et d'Etudes Structurales, CEMES-CNRS, 29 rue Jeanne Marvig, 31055 Toulouse, France*
**anne.bernand-mantel@cnrs.fr*

Compact magnetic skyrmions are potential bit-encoding states for spintronic memory and logic applications that have been the subject of a rapidly growing number of studies in recent years. Nevertheless, despite numerous attempts, a satisfactory theoretical description of these objects is still lacking today due to the highly non-trivial character of the magnetostatic interaction that plays a major role in determining the nature of magnetization patterns in ferromagnetic materials. The orthodox theory of skyrmions in ultrathin ferromagnetic layers with interfacial DMI relies on a model that accounts for the dipolar interaction through an effective anisotropy term, neglecting long-range effects. At the same time, in single ferromagnetic layers with interfacial DMI, large chiral skyrmions, also called skyrmionic bubbles have been observed, suggesting a non-trivial interplay between DMI and long-range dipolar effects [1]. We will present our work where we used rigorous mathematical analysis to develop a skyrmion theory that takes into account the full dipolar energy in the thin film regime and provides analytical formulas for compact skyrmion radius, rotation angle and energy [2]. Our theory reveals the existence of a new regime at low DMI were skyrmions are stabilized by a combination of non-local dipolar interaction and a magnetic field applied parallel to their core . This predictions are confirmed by our numerical simulations[3]. Finally, we will discuss the theory of skyrmion lifetime in a continuum field theory where we interpret skyrmion collapse events as capture by an absorber at microscale. This yields to an explicit Arrhenius collapse rate for skyrmions with both the barrier height and the prefactor as functions of all the material parameters [4]. Or work provides a guide in material system design in view of optimizing the skyrmion lifetime for applications.

References

[1] Anne Bernand-Mantel, Lorenzo Camosi, Alexis Wartelle, et al. The skyrmion-bubble transition in a ferromagnetic thin film. *SciPost Physics* 4, 027 (2018).

[2] Anne Bernand-Mantel, Cyrill B. Muratov, and Thilo M. Simon. Unraveling the role of dipolar versus Dzyaloshinskii-Moriya interactions in stabilizing compact magnetic skyrmions. *Physical Review B* 101, 045416 (2020).

[3] Anne Bernand-Mantel, Sarah Barnova, Anaïs Fondet, Cyrill B. Muratov, and Theresa M. Simon. Theory of magnetic field-stabilized compact skyrmions in thin film ferromagnets. *arXiv:2306.01413* (2023).

[4] Anne Bernand-Mantel, Cyrill B. Muratov, and Valeriy V. Slastikov. A micromagnetic theory of skyrmion lifetime in ultrathin ferromagnetic films. *Proceedings of the National Academy of Sciences* 119, e2122237119 (2022).

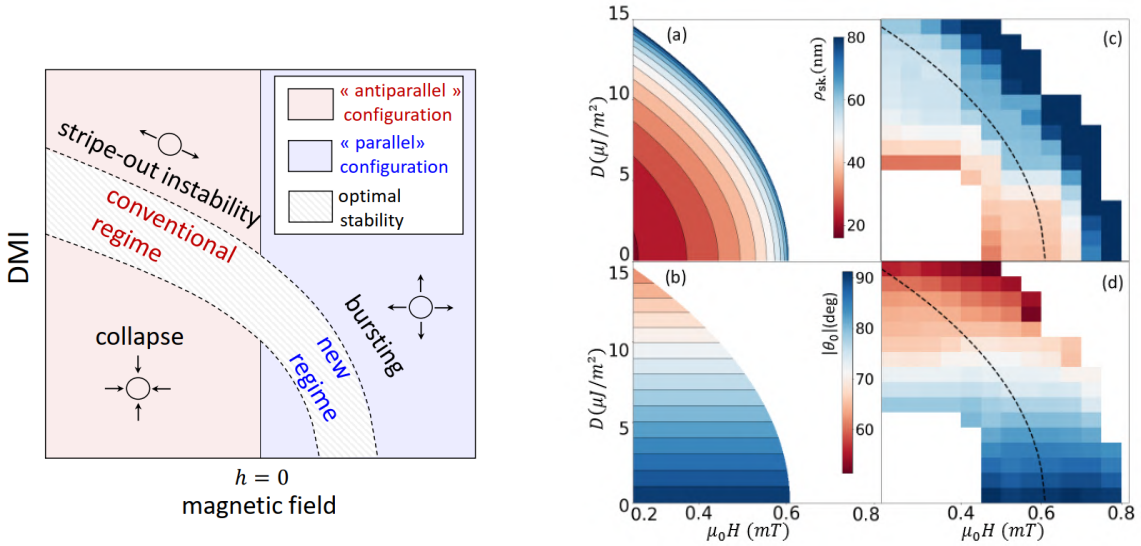

Figure 1: Left side: Schematic representation of the skyrmion phase diagram as a function of DMI and applied magnetic field where positive field is applied in the direction along with the magnetization in the skyrmion core (parallel configuration). We represent 3 types of skyrmion instabilities, stripe out, collapse and bursting as well as the optimal skyrmion stability zone.The new regime of field stabilized skyrmions is indicated. Right side: Analytical predictions of the skyrmion characteristics in the low DMI regime for $d = 5$ nm, $A = 20$ pJ/m, $M_s = 10^5$ A/m, and $K_u = 6346$ J/m^3 corresponding to $Q = 1.01$: (a) Skyrmion radius r_{sky} and (b) skyrmion rotation angle. (c) skyrmion radius and (d) skyrmion rotation angle from MuMax3 simulations on a 2048×2048 nm^2 square box with mesh size $2 \times 2 \times 5$ nm. The dashed line is the line of zero bursting barrier.

Resonant dynamics, spin wave generation, and spin-wave annealing in three-dimensional skyrmionic lattices

Titiksha Srivastava[1,2,3 *], Yanis Sassi[2], Fernando Ajejas[2], Aymeric Vecchiola[2], Igor Ngouagnia[3], Hervé Hurdequint[3], Karim Bouzehouane[2], Nicolas Reyren[2], Vincent Cros[2], Thibaut Devolder[1], Joo-Von Kim[1 **], and Grégoire de Loubens[3]

[1]*Centre de Nanosciences et de Nanotechnologies, CNRS, Université Paris-Saclay, 91120, Palaiseau, France*
[2]*Unité Mixte de Physique, CNRS, Thales, Université Paris-Saclay, 91767, Palaiseau, France*
[3]*SPEC, CEA, CNRS, Université Paris-Saclay, 91191, Gif-sur-Yvette, France*
*titiksha.srivastava@c2n.upsaclay.fr,
**joo-von.kim@c2n.upsaclay.fr

Skyrmions in magnetic materials are nanoscale, chiral topological solitons which exhibit several dynamical phenomena that have garnered much interest for fundamental reasons and technological applications alike [1]. While most studies until now have focused on their motion as rigid particles under different stimuli like spin currents or thermal fluctuations, only a few experimental reports [2, 3] exist on their internal mode dynamics owing to large damping coefficients.

Here we present the resonant dynamics of ultrathin film $[Pt/CoFeB/AlOx] \times 20$ multilayers hosting stable skyrmion lattices under ambient conditions while exhibiting low Gilbert damping $\alpha = 0.02$ [4]. We identify distinct spin wave modes associated with skyrmions by combining magnetic force microscopy (MFM) and ferromagnetic resonance (FMR) experiments with micromagnetic simulations. At low frequencies (<2 GHz), we observe several modes related to the precession of the uniform background state of individual layers close to or at the surfaces of the stack, along with eigenmodes localized to the skyrmion edges. At intermediate frequencies (2 −8 GHz), the precession of the uniform background near the centre of the stack dominates the response. We report the experimental observation of a new dynamical mode at high frequency (>12 GHz), which is most visible in the skyrmion lattice phase. FMR spectroscopy reveals clear peaks in the susceptibility above 12 GHz over a range of applied magnetic fields, which we find through micromagnetics simulations to correspond to a coherent precession of the skyrmion core. The skyrmions here have a distinct three-dimensional structure due to the competition between all the existing magnetic interactions in these multilayers. Moreover, the simulations show that this core precession generates spin waves, with wavelengths in the range of 50 to 80 nm, that flow into the ferromagnetic background, illustrating the potential of skyrmions to convert uniform radiofrequency waves into nanoscale excitations.

Using micromagnetic simulations we also examine the role of spin wave interactions with the skyrmion cores. As the applied field increases and skyrmions begin to annihilate, leaving vacancies in the hexagonal lattice, the excitation of the high-frequency mode can "anneal" the lattice, resulting in a glassy state. These results also shed new light on how dynamical excitations can influence phase transitions associated with the melting of skyrmion lattices [5].

Acknowledgments

This work was partially supported by the Agence Nationale de la Recherche (ANR) under grant no. ANR-17-CE24-0025 (TOPSKY) and the Horizon2020 Research Framework Program of the European Commission under contract numbers 824123 (SKYTOP) and 899646 (k-NET). It was also supported by a public grant overseen by the ANR as part of the "Investissements d'Avenir" program (Labex NanoSaclay, reference: ANR-10-LABX-0035).

References

[1] A. Fert, N. Reyren, and V. Cros. Magnetic skyrmions: advances in physics and potential applications. *Nat Rev Mat* 2, 17031 (2017).

[2] L. Flacke, V. Ahrens, S. Mendisch, et al. Robust formation of nanoscale magnetic skyrmions in easy-plane anisotropy thin film multilayers with low damping. *Phys. Rev. B* 104, L100417 (2021).

[3] B. Satywali, Kravchuk V.P., L. Pan, et al. Microwave resonances of magnetic skyrmions in thin film multilayers. *Nat Commun* 12, 1909 (2021).

[4] T. Srivastava, Y. Sassi, F. Ajejas, et al. Resonant dynamics of three-dimensional skyrmionic textures in thin film multilayers. *APL Materials* 6, 061110 (2023).

[5] P. Huang, T. Schönenberger, M. Cantoni, and Heinen L. et al. Melting of a skyrmion lattice to a skyrmion liquid via a hexatic phase. *Nat. Nanotechnol.* 15, 761–767 (2020).

Driving skyrmions in flow regime in synthetic ferrimagnets

Sougata Mallick[1,*], Yanis Sassi[1], Nicholas Figueiredo Prestes[1], Sachin Krishnia[1], Fernando Gallego[1], Thibaud Denneulin[2], Sophie Collin[1], Karim Bouzehouane[1], André Thiaville[3], Rafal E. Dunin-Borkowski[2], Vincent Jeudy[3], Albert Fert[1], Nicolas Reyren[1], and Vincent Cros[1]

[1]*Unité Mixte de Physique, CNRS, Thales, Université Paris-Saclay, 91767 Palaiseau, France*
[2]*Forschungszentrum Jülich, ER-C for Microscopy and Spectroscopy with Electrons, Jülich, Germany*
[3]*Laboratoire de Physique des Solides, CNRS, Université Paris-Saclay, 91400 Orsay, France*
sougata.mallick@cnrs-thales.fr

Magnetic skyrmions, spin swirling particle like entities, have been in the focal point of many researches in condensed matter physics due to their solitonic nature combined with their chiral and topological properties. To increase their thermal stability up to room temperature, one of the strategies has been to increase individual layer thickness or the number of repetitions in multilayers. However, this is at the cost of an enhanced impact of dipolar interaction, resulting in an enlargement of the skyrmion size and a reduction of the stability for smallest skyrmion. A solution to these issues that has been proposed is to rely on materials with reduced or cancelled magnetization i.e., ferrimagnets[1] or synthetic antiferromagnets[2]. Besides the gain in static properties, another advantage of skyrmions in ferrimagnets (or antiferromagnets) is that the so-called skyrmion Hall angle, a transversal motion due to their topological charge, is reduced or even cancelled. For most of the skyrmionic systems, an important issue is the presence of a finite pinning landscape that impedes them to reach their flow regime of motion. There are predominantly two reasons for this limitation. First, as mentioned before, the impact of skyrmion Hall angle can lead to skyrmion annihilation on the device edges before they can reach very large velocities. The second is that the driving force i.e., the amplitude of SOT is not large enough. Hence, in spite of several works reporting high DW velocity in ferrimagnets, there are not many reports on the motion of fast skyrmions (>>100 ms^{-1}).
In this study, we investigate the SOT driven motion of small skyrmions in magnetic-multilayers based on a ferrimagnetic system with the aim of achieving high mobility together with reduced skyrmion Hall effect. To achieve these goals, we consider Pt|Co|Tb multilayers of various thicknesses with antiferromagnetic coupling between the Co and Tb magnetization, hence forming a synthetic ferrimagnet. In order to increase the velocity of ferrimagnetic skyrmions, there are two important levers that can be activated. The first one is the amplitude of SOT that can be increased by enhancing the charge-to-spin conversion either in the bulk through the choice of nonmagnetic materials in contact with ferromagnet or at the interfaces. The second parameter is the energy dissipation rate, that can be efficiently reduced by increasing the antiferromagnetic (AFM) coupling between the Co and Tb layers. Through the tuning of these two parameters, we succeed to reach the flow regime for skyrmion motion at the largest current densities, with velocities up to 400 ms^{-1} for current densities around 8×10^{11} A/m^2.

The sputtering deposited multi-layered samples have the following structure: Si/SiO_2(280 nm)/Ta (5 nm)/Pt (5 nm)/[Pt (3 nm)/Co (t_{Co})/Tb (t_{Tb})/Al (3 nm)]$_N$/Pt (2 nm), where t_{Co}=1.0-1.5 nm, t_{Tb}=0.25-1.0 nm, and N=1 and 5. HAADF STEM images along with EDX mapping reveals that beyond t_{Tb}=0.5 nm, there is distinct EDX peaks associated to Tb confirming the formation of well defined Tb layer. However, since the thickness of Tb has been varied continuously from 0.25 – 1.0 nm, we expect to transit from less than a monolayer to continuous layers of Tb albeit with limited accuracy on exact thicknesses. We find a decrease in magnetization and an enhancement of PMA with increasing Tb thickness, both being associated to the enhancement of the AFM coupling between the Co and Tb layers. This increase of coupling between Co and Tb films has been confirmed by XMCD measurements both at Co and Tb edges. The presence of rather large interfacial DMI ($D_s = -1.62 \pm 0.20$ pJ/m, measured using BLS) together with the interlayer dipolar coupling results in the stabilization of skyrmions in the multilayer samples up to t_{Tb}= 0.6 nm. However, for thicker Tb (upto 1 nm), the anisotropy energy arising from the AFM coupling between Co and Tb becomes too large, impeding the formation of any skyrmionic phase.

Skyrmions under an external out-of-plane field of ~41 mT is illustrated by a sequence of MFM images in Fig. 1(a) – (d). First, we observe that the position of the skyrmions after a series of pulses remain in the central part of the 1 µm wide track, with no clear transverse displacement due to skyrmion Hall effect. This relative straight motion is due to the combination of the reduced skyrmion Hall angle expected in ferrimagnet and the finite repulsion from the track edges. This explanation is further confirmed by the observation of a transverse skyrmion motion in a wider track (3 μm), in which skyrmions are found to move with an angle of $\sim 29^o$, in good agreement to the calculated value of 27.5^o. In Fig. 1(e), we display the experimental skyrmion velocity vs. current density for different samples with varying Tb thickness, namely 0.25 nm, 0.4 nm and 0.6 nm. Each velocity is obtained by the measuring the displacements for all the skyrmions (typically between 5 and 10) present in the 10-20 µm long track. From the comparison between field induced DW and current induced skyrmion motion, different dynamical regimes can be clearly identified. Above the depinning transition, the skyrmion motion is predicted to reach the flow regime which is independent of pinning and controlled by dissipation. As observed in Fig. 1(e), the flow

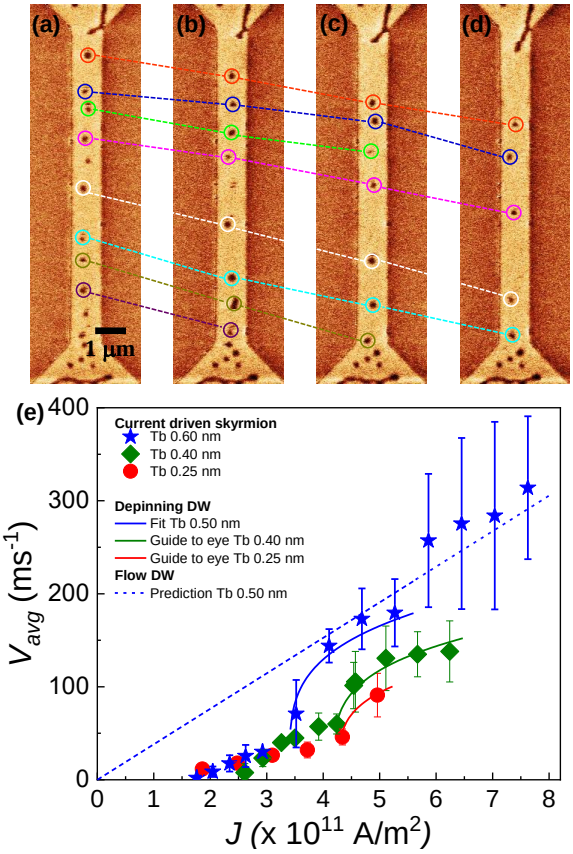

Figure 1: (a) – (d) Current induced skyrmion motion in [Pt (3 nm)/Co (1.3 nm)/Tb (0.6 nm)/Al (3 nm)]×5 multilayers after application of two successive 10 ns wide current pulses in between two images with $J = 3.5 \times 10^{11}\ A/m^2$ under an external perpendicular field 41 mT. The circles and the dashed lines are guide to eye to track the motion of individual skyrmions. (e) Average skyrmion velocity (filled symbols) vs current density for different samples with varying Tb thickness in the multilayers. Error bars corresponding to each data points represent the standard deviation of the skyrmion velocity inside the tracks. The blue straight and dashed lines correspond to the fit of depinning law and the prediction for the flow regime, respectively. The green and red lines are guides to eye underlying the depinning law.

regime is only reached for t_{Tb}=0.6 nm. Note that the maximum velocity ∼400 m/s (specifically for skyrmions with radius $<$ 100 nm) is among the largest ones for dynamics of ferrimagnetic skyrmions. We confirm that the enhanced skyrmion velocity in our system is a consequence of the systematic engineering of the efficient damping-like torque (spin Hall angle ∼ 8.6%) as well as the AFM coupling between the Co-Tb layers.

Acknowledgments

We acknowledge ANR 2022 CE42 "STORM" for providing the research funding.

References

[1] Se Kwon Kim, Geoffrey S. D. Beach, Kyung-Jin Lee, et al. Ferrimagnetic spintronics. *Nature Materials* 21, 24–34 (2021).

[2] William Legrand, Davide Maccariello, Fernando Ajejas, et al. Room-temperature stabilization of antiferromagnetic skyrmions in synthetic antiferromagnets. *Nature Materials* 19, 34–42 (2019).

Influence of OAM light on the magnetic textures of Synthetic antiferomagnets

Sougata Mallick[1,*], Peng Ye[2], Yanis Sassi[1], Karim Bouzehouane[1], Sergey Babenkov[2], David Gauthier[2], Willem Boutu[2], Marie Froidevaux[3], Hamed Merdji[3], Jean-Yves Chauleau[2], Manuel Bibes[1], Nicolas Reyren[1], Michel Viret[2], and Vincent Cros[1]

[1]*Unité Mixte de Physique, CNRS, Thales, Université Paris-Saclay, 91767 Palaiseau, France*
[2]*SPEC, CEA, CNRS, Université Paris-Saclay, Gif-sur-Yvette, France*
[3]*LOA, CNRS, Ecole Polytechnique, ENSTA Paris, Institut Polytechnique de Paris, Palaiseau, France*
sougata.mallick@cnrs-thales.fr

Skyrmions in metallic multilayers qualify as ultrasmall bits of magnetic information, and have been proposed for mass data storage and logic operations, although their application is hindered by the significant power required for their manipulation. An approach to circumvent this limitation with possible advantages in terms of operation speed, detectability, and power has been to use ferrimagnetic or even antiferromagnetic systems. A crucial advantage of skyrmions in antiferromagnetic systems is that the so-called skyrmion Hall angle, a transversal motion due to their topological charge, is reduced or even cancelled. Moreover, as intrinsic dynamics in AFMs is dominated by the strength of the exchange energy, AFM solitons benefit from increased velocities.

Multilayers are adequate systems to produce synthetic antiferromagnets (SAFs), where two ferromagnetic layers are coupled antiferromagnetically through a normal metal carrying the so-called RKKY interaction [1]. However, it should be noted that, due to compensation of the magnetization, SAFs remain nearly unaffected by moderate magnetic fields. Hence, a bias layer with uniform magnetization (**m**=**z**) is required to couple ferromagnetically with one of the magnetic layers to promote the spin spirals along **z** and expand in the expense of the parts with **m**=-**z**. However, the use of such a bias layer has been proven to be detrimental for efficient optimization of the spin torques to drive the skyrmions in SAFs. In this regard, optical vortex beams (Fig. 1(a)) offer an opportunity to overcome these difficulties by transferring their orbital angular momentum (OAM) [as well as spin angular momentum (SAM)] to magnetic materials. The coupling between photon magnetic fields and local magnetic moments operates via a coherent Zeeman or magneto-electric interaction, potentially also being helped by induced local temperature gradients. The potential flexibility of the technique to nucleate skyrmions at well-defined positions is already attractive in itself, but OAM light also offers a new handle to move the created skyrmions. In this work, we focus on exploring the possibilities to nucleated and stabilize skyrmionic spin textures in the non-biased SAFs at remanence by shooting them with OAM laser pulses.

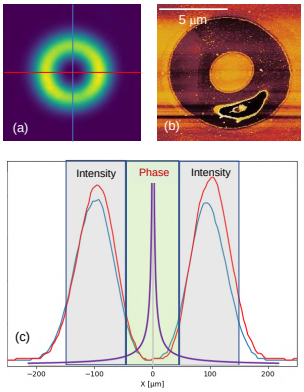

Figure 1: (a) Shape of an OAM laser beam. (b) Consequence of an OAM beam in modifying the topography of a sample. (c) Energy and phase gradient distribution of an OAM beam.

Typical shape of an OAM laser beam is shown in Fig. 1(a). Most of the energy is distributed over the ring, whereas the central part of the beam consists of lowest energy and highest OAM. The consequence of such a beam on the topography of the sample can be observed in Fig. 1(b), where the ring area is significantly perturbed due to the high energy of the beam whereas the central part is intact. The distribution of the energy and the phase gradient of the OAM beam is shown in Fig. 1(c).

In order to image the resultant configuration after shooting with laser pulses, we have performed the magnetic force microscopy (MFM) imaging in vacuum to obtain the required sensitivity to prove AFM spin textures using home-built magnetic tips. The MFM phase signal of the exposed area after shooting a Gaussian pulse (OAM=0) is depicted in Fig. 2(a).

It can be observed that due to transfer of energy from the Gaussian beam, some textures are formed at the centre of the beam with the phase contrast of $\sim 2^o$ (similar to the expected range for AFM textures). Further, Fig. 2(b) and (c) represent the same areas after applying an external perpendicular field of 100 mT and at remanence, respectively. It can be observed that, skyrmions (small white dots) can be stabilized at finite applied field as previously reported in literature. However, upon releasing the external field, the system goes back to the initial state and does not retain the skyrmionic textures.

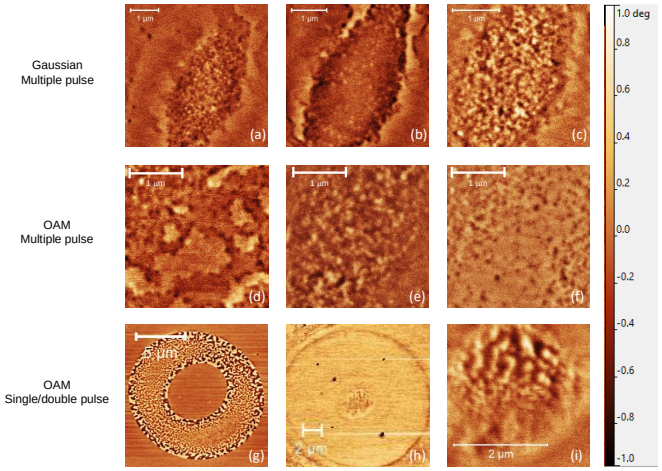

Figure 2: (a)-(c) Magnetic states of the samples in areas exposed to Gaussian laser pulses. The MFM phase signal of the exposed area after the laser pulse is depicted in (a), whereas (b) and (c) represents the same areas at 100 mT and remanence, respectively. Similarly, the MFM phase of the exposed area shoot with linear OAM laser pulse is shown in (d), whereas (e) and (f) represent the same area at 90 mT and remanence, respectively. MFM image of the samples exposed to either (g) single shot, or (h-i) two-shots OAM pulses.

Similarly, the MFM image of the exposed area after shooting a linear OAM pulse (SAM=0) is depicted in Fig. 2(d). We see a co-existence of white big patches (domains) as well as skyrmion like textures (small black dots). Fig. 2(e) and (f) represent the same areas after applying an external field of 90 mT and at remanence, respectively. In contrary to the gaussian pulse, we observe that the skyrmionic textures are retained at magnetic remanence (Fig. 2(f)) when the sample is exposed to the linear OAM laser pulse. We further verify that the size and density of the skyrmionic textures at remanence can be modified by the strength of the applied magnetic fields. It should be noted that the sample has been exposed to multiple shots (>100) of laser pulses in the MFM images shown in Fig. 2(a)-(f). In order to understand the role of OAM more properly, we have performed the same experiments for either single shot (Fig. 2(g)) or two-shots (Fig. 2(h)-(i)) OAM pulses. Due to unavailability of sufficient energy (as discussed in Fig. 1) in the center for the single shot pulse, the magnetic state remains unperturbed at the centre of the OAM pulse (Fig. 2(g)) whereas due to high energy in the ring area, the phase signal increases to more than 2^o indicating partial break of the AFM coupling between the two magnetic layers. Nevertheless, with careful tuning of the number of pulses and the energy, we show that skyrmionic textures can be stabilized in the central high OAM area of the laser pulse as demonstrated in Fig. 2 (h) and (i). The perspective will be to identify how the skyrmion properties and/or their density are depending the OAM characteristics.

Acknowledgments

We acknowledge ANR 2022 CE42 "STORM" and the European Union's Horizon 2020 research and innovation programme under the Grant No. 964931 (TSAR) for providing the research funding.

References

[1] William Legrand, Davide Maccariello, Fernando Ajejas, et al. Room-temperature stabilization of antiferromagnetic skyrmions in synthetic antiferromagnets. *Nature Materials* 19, 34–42 (2019).

Evaluation of the repulsive Forces Acting on Skyrmions

W. Bouckaert[1, *], Y. Sassi[1], D. Sanz-Hernández[1], S. Krishnia[1], N. Reyren[1], and V. Cros[1]

[1]*Unité Mixte de Physique, CNRS, Thales, Université Paris-Saclay, 1 av. Augustin-Fresnel, Palaiseau, France*
*william.bouckaert@cnrs-thales.fr

Often the study of skyrmions is motivated by technological applications where the skyrmion acts as a bit of information in a circuit made of magnetic materials [1, 2]. The skyrmions are interesting in such applications, because, having a soliton behaviour, they can move around corners or even edge defects, keeping their shape and properties [3]. Moreover, skyrmions will not easily merge with each others, so their number is conserved. All these desirable properties result from repulsive forces from any type of "walls", notably track edges, magnetic domain walls, and other skyrmions. Despite the prime importance of these repulsion forces, reports about their experimental measurements are scarce [4].

In this study, we present results obtained on (Pt|Co|Al) based multilayers, with typically ten repetitions. This structure has been chosen because it allows a high thermal stability of the skyrmions as well as an optimized SOT generated both from the Pt layers and from the Co|Al interface [5]. We have been able to perform current-induced motion of skyrmion, with diameters close to 200 nm, at speeds exceeding 20 m s^{-1} with a skyrmion Hall angle $\theta_{Sk} = 45°$ (see Fig. 1a). From those experiments, we have found a threshold below which the skyrmions are not annihilated when they reach the opposite edge of the device, permitting the measurement of the skyrmion-edge repulsion force (≈ 0.4 pN.). This repulsion enables the straight motion of skyrmions over more than 30 µm (Fig. 1b) which is accompanied by an increase of their velocity.

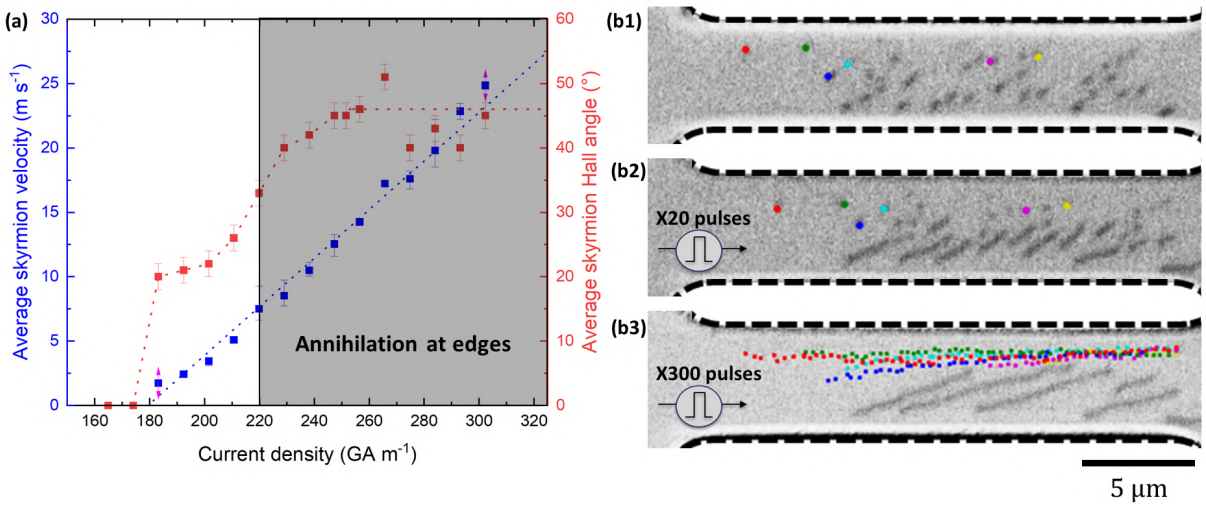

Figure 1: Example of skyrmion-edge interaction. (a) Evolution of skyrmion velocity and skyrmion Hall angle as a function of J. (b) Current-induced motion of skyrmions over micrometres distances due to the repulsion from the top edge of the track.

We have also investigated the skyrmion-skyrmion interaction which is of importance to perform, for example, skyrmion logic operations [6]. We have found that this repulsion is strong enough to permit the depinning of a skyrmion (see Fig. 2a) and to quantify its amplitude we have analysed the phenomena happening at the exit of a device, namely repulsion and merging. With COMSOL calculations we have estimated this force to be ≈ 0.02 pN.

The last interaction that we have investigated is the skyrmion-domain one. We have observed in various experiments that the presence of domains within a track can alter the current-induced motion of the skyrmions for example by modifying their trajectory. To take advantage of this behaviour, we have stabilized a long magnetic domain within a track, joining both exit of the device to fix its position. Thanks to the presence of a notch at one of the edge of the device, we have been able to precisely nucleate skyrmions and to drive them close to the domain (see Fig. 3). We have evaluated the amplitude of this force and found ≈ 0.3 pN.

Acknowledgments

This work has been supported by DARPA TEE program grant (MIPRHR - 0011831554), ANR grant TOPSKY (ANR-17-CE24-0025), the FLAG - ERA Sograph MEM (ANR-15-GRFL-0005) and the Horizon2020 Framework Program of the European Commision, under FETProactive Grant agreement No. 824123 (SKYTOP) (H2020 FET proactive 824123).

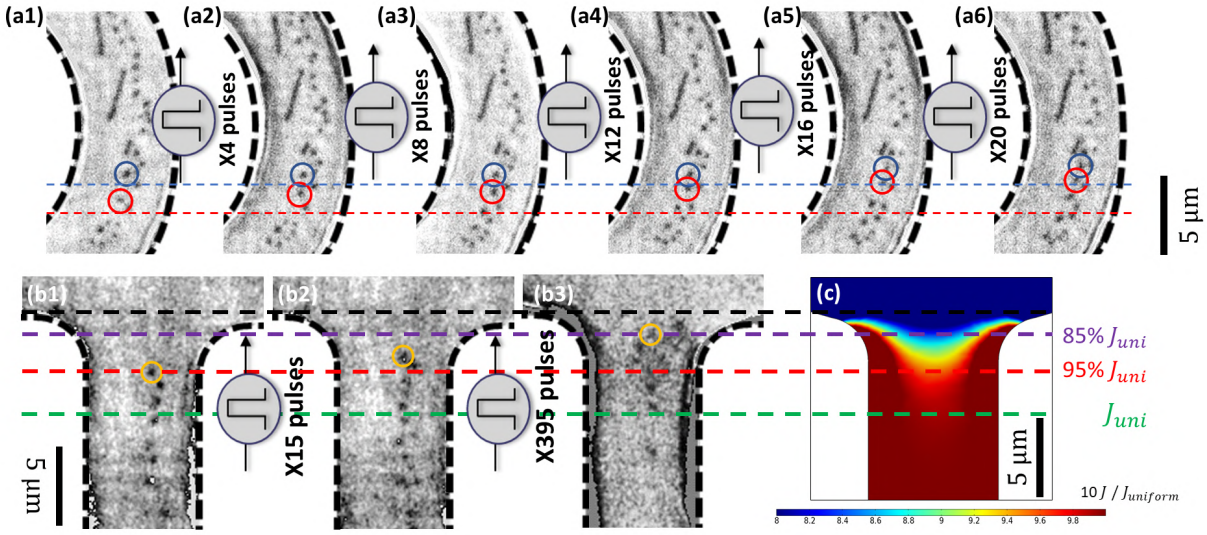

Figure 2: Examples of skyrmion-skyrmion interaction. (a) Depinning of a skyrmion (circle in blue) due to the repulsion, which add to the driving force from the SOT, from the new coming skyrmion (circle in red). (b) Measurement of the repulsion force between skyrmions, interacting (repulsion and/or merging) at the exit of a track, (c) through COMSOL calculations which permit to plot the current density profile.

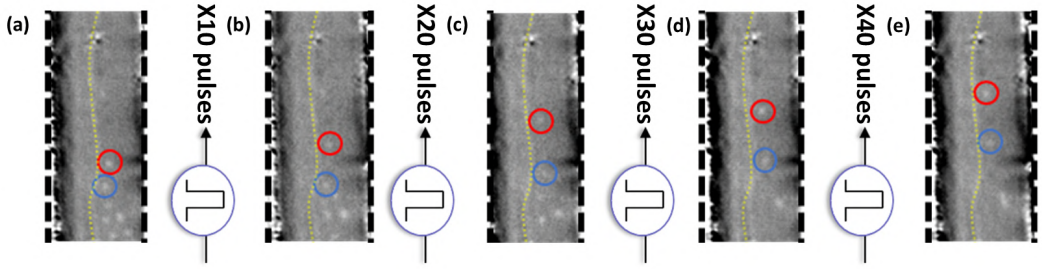

Figure 3: Example of skyrmion-domain wall interaction. (a-e) Sequence of Kerr images exhibiting the current-induced motion of a skyrmion along a domain of parallel magnetization (with respect to the direction of the magnetization in the core of the skyrmion). The motion is exempt from skyrmion Hall angle.

References

[1] A. Fert, N. Reyren, and V. Cros. Magnetic skyrmions: Advances in physics and potential applications. *Nature Reviews Materials* 2, 17031 (2017).

[2] J. Zázvorka, F. Jakobs, D. Heinze, et al. Thermal skyrmion diffusion used in a reshuffler device. *Nature Nanotechnology* 14, 658–661 (2019).

[3] J. Sampaio, V. Cros, S. Rohart, A. Thiaville, and A. Fert. Nucleation, stability and current-induced motion of isolated magnetic skyrmions in nanostructures. *Nature Nanotechnology* 8, 839–844 (2013).

[4] S. Yang, K. Wu, Y. Zhao, et al. Inhibition of Skyrmion Hall effect by a stripe domain wall. *Physical Review Applied* 18 (2022).

[5] S. Krishnia, Y. Sassi, F. Ajejas, et al. Large interfacial Rashba interaction and giant spin-orbit torques in atomically thin metallic heterostructures (2022). arXiv: 2205.08486 [cond-mat.mes-hall].

[6] N. Sisodia, J. Pelloux-Prayer, L. D. Buda-Prejbeanu, et al. Programmable skyrmion logic gates based on skyrmion tunneling. *Physical Review Applied* 17, 064035 (2022).

Cancellation of topological charge effect on current induced skyrmion motion in Pt/Co/Ru based multilayers

Ilaria Di Manici[1,*], Van Tuong Pham[1], Naveen Sisodia[1], Joseba Urrestarazu Larrañaga[1], Kaushik Bairagi[1], Johan Pelloux-Prayer[1], Liliana D. Buda-Prejbeanu[1], Rodrigo Guedas Garcia[1], Stéphane Auffret[1], Andrea Locatelli[2], Tevfik Onur Mentes[2], Stefania Pizzini[3], Pawan Kumar[4], Aurore Finco[4], Vincent Jacques[4], Gilles Gaudin[1], and Olivier Boulle[1]

[1]*Univ. Grenoble Alpes, CNRS, CEA, SPINTEC, 38054 Grenoble, France*
[2]*Elettra-Sincrotrone Trieste S.C.p.A, 34149 Basovizza, Trieste, Italy*
[3]*Univ. Grenoble Alpes, CNRS, Institut Néel, 38042 Grenoble, France*
[4]*Laboratoire Charles Coulomb, CNRS, Unviersité de Montpellier, 34095 Montpellier, France*
**ilaria.dimanici@cea.fr*

Skyrmions have been capturing scientific interest in the last years for their promising applications as nanoscale bits of information for memories and logic devices [1]. Magnetic skyrmions are local chiral whirling of the magnetization presenting topological stability with a particle-like behaviour. Magnetic skyrmions at room temperature and their current induced motion in multilayers have been demonstrated recently [2, 3] in ultrathin heavy metal/ferromagnetic films. However, ferromagnetic skyrmions suffer from several limitations for applications: their maximum velocity hardly reaches 100 m/s and their motion deviates from the current direction, a phenomenon named skyrmion Hall effect. The latter is a direct consequence of the skyrmion topological charge which leads to an additional gyrotropic force perpendicular to the skyrmion velocity [4]. A possible solution to address these obstacles is the use of Synthetic Antiferromagnets (SAF). SAF consists of two ferromagnetic layers antiferromagnetically coupled through a non magnetic layer via RKKY interaction. Skyrmions in the two FM layers present an opposite topological charge that leads to a net gyrotropic vector equal to zero and hence a cancellation of the skyrmion Hall effect [5]. This cancellation also leads to the enhancement of the skyrmion velocity.

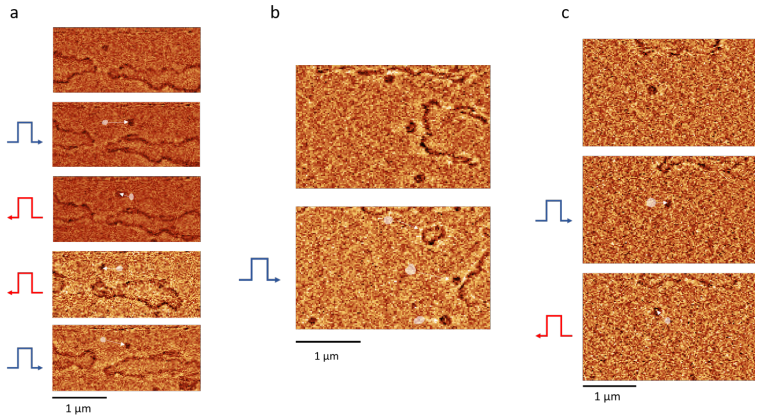

Figure 1: Current induced motion of SAF skyrmions observed by magnetic force microscopy (MFM). a. Sequence of images acquired after injection of subsequent pulses of 1.24 ns, 1.28 ns, 1.19 ns 1.17 ns with respectively current density $J = 6.39 \times 10^{11} A/m^2, -5.81 \times 10^{11} A/m^2, -7.15 \times 10^{11} A/m^2, 7.24 \times 10^{11} A/m^2$. b. Sequence of images acquired before and after the injection of a pulse of 0.88 ns with current density of $J = 8,09 \times 10^{11} A/m^2$. c. Sequence of images acquired before and after the injection of two subsequent pulses of 0.54 ns and 0.53 ns with current density respectively of $J = 7.71 \times 10^{11} A/m^2$ and $-8.02 \times 10^{11} A/m^2$.

In this presentation, we show that in optimized compensated SAF the cancellation of the topological charge allows skyrmions to be driven by spin orbit torque very fast, up to 885 m/s along the current direction. The SAF stack considered is composed of two Pt/Co layers AF coupled via a Ru interlayer. The Pt/Co interface provides the PMA and DMI required for skyrmion stabilization at room temperature and the Ru interlayer thickness is tuned to provide the maximum AF coupling via RKKY interaction. 3 μm wide tracks were patterned on the device to study the current induced dynamics. A single pulse of current is injected in the track and the magnetic contrast is recorded with a magnetic force microscopy (MFM) before and after the pulse. By measuring the displacement of skyrmion in subsequent images and dividing it by the applied

pulse width we obtained the velocity and the angle of deviation from the current trajectory. Figure 1 shows examples of MFM images after successive injection of current pulses. The skyrmions are moving with small deviations from the current direction. The dynamics is found to be irregular due to the effect of pinning by inhomogeneities in the material, nonetheless events of motion with velocity higher than 1000 m/s are observed. By performing systematic measurements, the average skyrmion velocity and skyrmion Hall angle were measured as a function of the current density (Figure 2). We observe that the skyrmion velocity increases with the current density (Figure 2a). A maximal velocity of around 885 m/s is measured for a current density of $8.9 \times 10^{11} A/m^2$. The skyrmion Hall angle is found to depend little on the skyrmion velocity with an average deviation from the current trajectory around 6° (Figure 2b). These results demonstrate the fast current induced skyrmion motion in SAF with a cancellation of the skyrmion Hall effect.

To study the impact of the cancellation of the topological charge provided by the AF coupling, we also investigated a synthetic ferromagnetic (SF) stack and the ferromagnetic Pt/Co/Ru trilayer. The former is obtained by coupling ferromagnetically the two Co layers via RKKY using a thicker Ru interlayer, while the thickness of all the other layers is the same as in the SAF stack. The two samples showed similar dynamics with skyrmion velocity that reached a maximum of around 80 m/s for the SF and 120 m/s for the single layer with respectively a maximum deflection angle of 87.9° and 61.7°. These values are consistent with what was previously obtained by inducing current motion in ferromagnetic ultra thin films. This demonstrates that the cancellation of topological charge increases by about one order of magnitude the velocity of the skyrmions in ultrathin ferromagnetic/heavy metal layers while maintaining the skyrmions trajectory along the current direction.

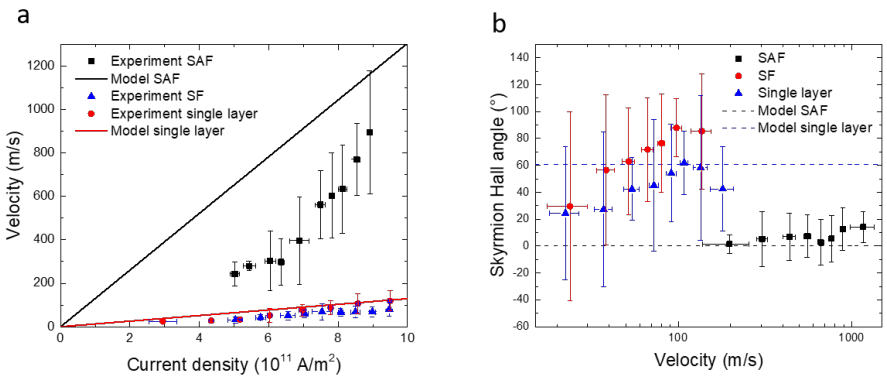

Figure 2: a. Average skyrmion velocity as a function of the current density measured experimentally (black squares). The black line correspond to the skyrmion velocity obtained Thiele equation model using experimental parameters. The blue triangles are the velocities measured for the synthetic ferromagnetic (SF) skyrmions while the red squares are the velocities for the single layer Pt/Co/Ru. The red line correspond to the skyrmion velocity obtained from the Thiele equation b. Skyrmion Hall angle as a function of the skyrmion velocity of the SAF skyrmions (black squares), SF skyrmions (red dots) and single layer Pt/Co/Ru (blue triangles).

References

[1] Albert Fert, Vincent Cros, and João Sampaio. Skyrmions on the track. *Nature Nanotechnology* 8, 152–156 (2013).

[2] Olivier Boulle, Jan Vogel, Hongxin Yang, et al. Room temperature chiral magnetic skyrmion in ultrathin magnetic nanostructures. *Nature Nanotechnology* 11, 449–454 (2016).

[3] Roméo Juge, Soong-Geun Je, Dayane de Souza Chaves, et al. Current-Driven Skyrmion Dynamics and Drive-Dependent Skyrmion Hall Effect in an Ultrathin Film. *Physical Review Applied* 12, 044007 (2019).

[4] Felix Büttner, Ivan Lemesh, and Geoffrey S. D. Beach. Theory of isolated magnetic skyrmions: From fundamentals to room temperature applications. *Scientific Reports* 8, 4464 (2018).

[5] Xichao Zhang, Yan Zhou, and Motohiko Ezawa. Magnetic bilayer-skyrmions without skyrmion Hall effect. *Nature Communications* 7, 10293 (2016).

Skyrmionic 3D cocoons in aperiodic magnetic multilayers

M. Grelier[1], R. Battistelli[2], C. Léveillé[3], S. Collin[1], A. Vecchiola[1], F. Godel[1], K. Bouzehouane[1], A. Fert[1], S. Finizio[4], F. Büttner[5], H. Popescu[2], N. Jaouen[2], V. Cros[1], and N. Reyren[1,*]

[1]*Unite Mixte de Physique, CNRS, Thales, Universite Paris-Saclay, 91767, Palaiseau, France*
[2]*Synchrotron SOLEIL, L'Orme des Merisiers, Gif-sur-Yvette, 91192, France*
[3]*Helmholtz-Zentrum Berlin, 14109 Berlin, Germany*
[4]*Paul Scherrer Institut, 5232 Villigen PSI, Switzerland*
[5]*Institüt für Physik, Universität Augsburg, 86159 Augsburg, Germany*
*nicolas.reyren@cnrs-thales.fr

Topological magnetic textures have been under close scrutiny in recent years as they could represent an original asset for the development of next-generation spintronics devices, especially in terms of stability and energy consumption. Chiral magnets and magnetic multilayers allow for the stabilization of two-dimensional (2D) textures that have been extensively investigated, like the magnetic skyrmion. Beyond these 2D textures, a new interest has surged for more complex quasi-particles that display variations over the thickness, i.e., three-dimensional (3D) objects, leading to the discovery of new categories of topological textures. To cite a few, truncated skyrmion have been reported [1], as well as bobbers [2] or even hopfions [3] in magnetic multilayers. In this work, we show how by engineering Pt/Co/Al based multilayers with variable Co thickness, we observe the signature of new textures, called skyrmionic cocoons [4] that are only present in a fraction of the magnetic layers. Interestingly, these cocoons can coexist with more standard 'tubular' skyrmions going through all the multilayer as evidenced by the existence of two very different contrasts in the magnetic force microscopy (MFM) images recorded at room temperature that can be easily correlated with the corresponding micromagnetic simulations (Fig. 1).

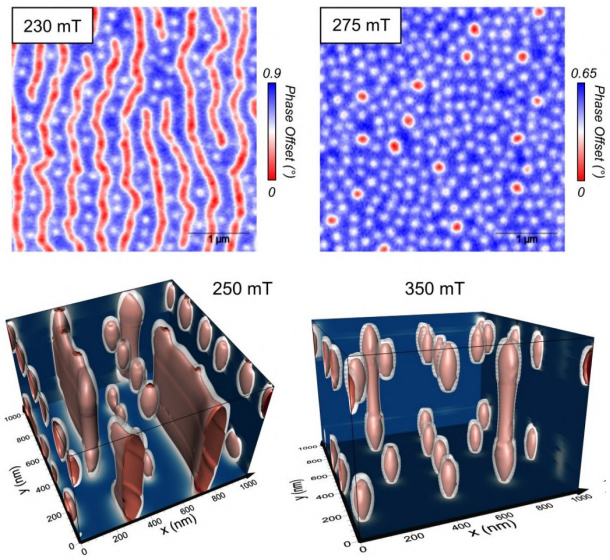

Figure 1: Cocoons and skyrmion tubes. Top: experimental MFM phase maps displaying two types of textures (two different contrasts). Bottom: corresponding micromagnetic simulations, evidencing the 3D nature of the cocoons and the skyrmion tubes (iso surfaces at $m_z = -0.8$ are displayed in red).

One major shortcoming of studying 3D textures is the difficulty to access information about the bulk magnetization. To this end, we also performed magneto-transport measurements as well as X-ray measurements at various synchrotrons. In Fig. 2a, an image acquired by holography, a transmission technique, clearly shows different contrasts that thus corresponds to objects with various vertical extension [5]. Moreover, in Fig. 2b, a reconstruction of the magnetization, measured with X-ray laminography, is shown, evidencing the different magnetic textures in our aperiodic multilayers. Their coexistence and the discovery of a novel magnetic texture are particularly interesting as they can open new paths for three-dimensional spintronics.

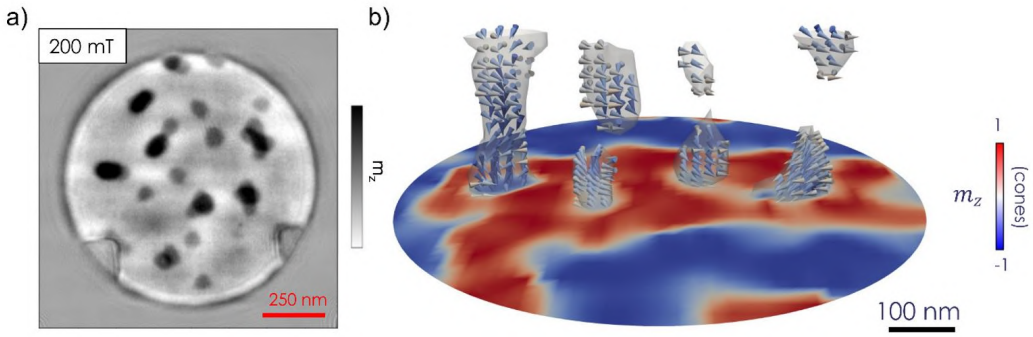

Figure 2: Synchrotron characterization. a) X-ray Fourier transform holography, a transmission technique, showing isolated cocoons (gray dots) and paired ones (black dots). b) Experimental 3D magnetization distribution obtained with X-ray laminography measurements (iso surface at $m_z = 0$ is displayed in white).

Acknowledgments

Financial supports from FLAG-ERA Sograph MEM (ANR-15-GRFL-0005), from ANR under the grant ANR-17- CE24-0025 (TOPSKY) and ANR-20-CE42-0012-01(MEDYNA) and as part of the “Investissements d’Avenir" pro- gram SPiCY (ANR-10-LABX-0035).

References

[1] Andrada-Oana Mandru, Oğuz Yıldırım, Riccardo Tomasello, et al. Coexistence of distinct skyrmion phases observed in hybrid ferromagnetic/ferrimagnetic multilayers. *Nature Communications* 11, 6365 (2020).

[2] Fengshan Zheng, Filipp N Rybakov, Aleksandr B Borisov, et al. Experimental observation of chiral magnetic bobbers in B20-type FeGe. *Nature Nanotechnology* 13, 451–455 (2018).

[3] Noah Kent, Neal Reynolds, David Raftrey, et al. Creation and observation of Hopfions in magnetic multilayer systems. *Nature Communications* 12, 1562 (2021).

[4] Matthieu Grelier, Florian Godel, Aymeric Vecchiola, et al. Three-dimensional skyrmionic cocoons in magnetic multilayers. *Nature Communications* 13, 6843 (2022).

[5] M Grelier, F Godel, A Vecchiola, et al. X-ray holography of skyrmionic cocoons in aperiodic magnetic multilayers. *Physical Review B* 107, L220405 (2023).

Skyrmions lattice in Fe/Gd multilayers with planar magnetic anisotropy

Farid Fettar[1,*], Aurélien Massboeuf[2], Intan Kusumaningrum[1], Jean Marc Tonnerre[1], Dann Mannix[1], Florent Blondelle[1], Frédéric Gay[1], David Barral[1], Eric Mossang[1], Philippe David[1], Guillaume Beutier[3], Alexis Wartelle[3], Marisel Di Pietro Martınez[3], Luc Ortega[4], and Valberto Pedruzzi Nascimento[5]

[1]*Institut Néel, Grenoble, 38042 France*
[2]*SPINTEC, Grenoble, 38042 France*
[3]*Université Grenoble Alpes, CNRS, Grenoble INP, SIMaP, 38000 Grenoble, France*
[4]*Université Paris-Saclay, CNRS, Laboratoire de Physique des Solides, 91405, Orsay, France.*
[5]*Physics Department, Federal University of Espírito Santo, 29075-910 Vitoria, Espírito Santo, Brazil*
*farid.fettar@neel.cnrs.fr

Magnetic skyrmions, localized and topologically non-trivial entities, are extensively investigated due to their solitonic nature. They may be created in appropriated conditions in terms of temperature (close to RT) and operating magnetic fields (from a few hundreds of mT down to zero field). In most experimental studies reported in the literature for thin multilayers, the observation of skyrmions requires an easy axis of magnetization perpendicular to the plane of the layers (namely PMA, Perpendicular Magnetic Anisotropy), as well as the Dzyaloshinskii-Moriya Interaction (DMI), as for instance [1, 2]. Unfortunately, these latter studies often imply low material thicknesses [(4-15)Å, for strong surface anisotropies] and high Gilbert damping factor (0.3) as in Ref.[2] leading to low thermal stability of skyrmions and large current densities ($3\,10^{11}$A/m^2 [1]) for their motion. These characteristics are serious obstacles for applications in spintronics. An alternative is to use ferrimagnets [3, 4] leading to the fabrication of skyrmions with higher magnetic thickness as 19Å [4], lower current density as $1.1\,10^9$A/m^2 [2], and lower damping value as 0.07 [3], with in particular the use of multilayers [3, 4].

The case of Fe(t_{Fe})/Gd(t_{Gd}) multilayers, where t designate the thicknesses in the sub-nanometric range, is interesting to explore when the thicknesses of layers, and consequently the Gd rate (namely τ_{Gd}), are modified. In particular, this system changes from perpendicular to in-plane magnetic anisotropy (IMA) at RT by enhancing τ_{Gd} in the (20-32)% range (rare earth rich composition regime) [5]. The critical τ_{Gd} value, revealing the crossover from PMA to IMA, is close to 29.5% for $[Fe(5.1)/Gd(5.9)]_{77}$ (leading to a period λ=t_{Fe}+t_{Gd} equals to 11.0Å), as seen in the previous reference. Moreover, dipole-stabilized skyrmions are formed at RT in similar stack with lower thicknesses, $[Gd(4Å)/Fe(3.4Å)]_{80}$ where λ=7.4Å and similar τ_{Gd} (≈29%) behaving PMA [6]. The reason is lying on the competition of dipolar field and exchange energy for such a sample, PMA being favoured for these thin thicknesses, and DMI interactions are assumed to be negligible. By comparing the references [5, 6], a diminishing of λ seems to favor PMA. The composition of the sample (thicknesses and number of repeats), as well as the operating temperature, appears to be important for tuning the magnetic anisotropy in Fe/Gd [5, 7].

For the case of nanostructures behaving planar magnetic anisotropy, skyrmions can be also created, but for nevertheless a few reported studies as in Ref.[8]. IMA is obtained for a magnetic thickness slightly higher than the cross-over from PMA to IMA. In parallel, some recent theoretical works as [9] reveal the possibility of generating skyrmions by taking account an in-plane-magnetization system. For our part, a $[Fe(3.4Å)/Gd(7.2Å)]_{60}$ multilayer where λ=10.6Å and τ_{Gd}=43.0% presents a robust planar magnetic anisotropy [see Fig.1(b)]. The thicknesses are derived from fitted X-Ray Reflectivity measurements. The effective magnetic anisotropy constant (K_{eff}) and the saturation magnetization (M_{sat}) reach -7.640 10^5 erg/cm^3 and 411.9 emu/cm^3 respectively (leading to K_u=-1.230 10^5 erg/cm^3 consistent with the strongest τ_{Gd} value). Nevertheless, 46% as remanence is measured, and a particular double magnetic jump is observed in the (-500/500) Oe range for planar magnetic fields data as shown in inset of Fig.1(b). This feature is useful when both planar and perpendicular magnetic fields are applied during the Lorentz Transmission Electron Microscopy (LTEM) measurements.

From LTEM data [Fig.1(a)] at RT, different magnetic objects are firstly formed (such as in plane domain walls, concentric circular lines, stripes, ripple contrast). Then, skyrmionic/bubbles entities, by a appropriate procedure of both planar and perpendicular magnetic fields, are observed. An organized network of 110 nm broad skyrmion-like objects is observed. Here, domains with magnetization parallel/antiparallel [respectively ↑/ ↓ as displayed in Fig.1(a)] to the perpendicular direction appear as white/dark textures respectively. It appears a near equal population of these 2 opposite spins. We will detail the protocol of measurements, and give some possible explanations to the remarkable picture in Fig.1(a) during the presentation of results.

Moreover, additional Ferromagnetic Magnetic Resonance investigations at RT for perpendicular and planar magnetic fields at RT will be also included.

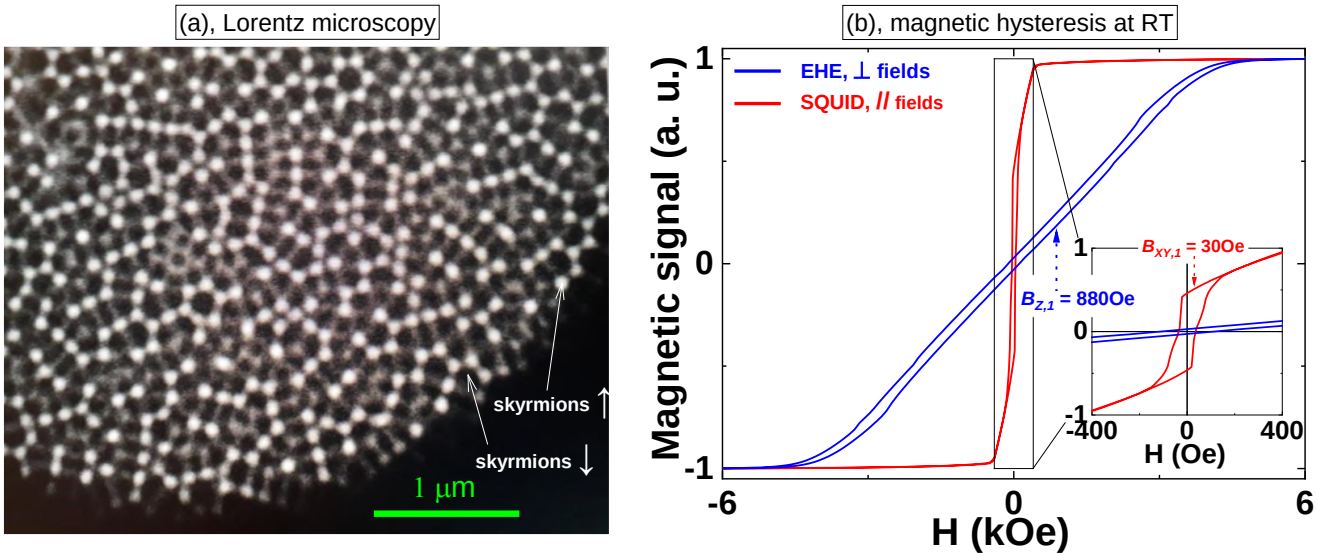

Figure 1: (a) : Lorentz Transmission Electron Microscopy (LTEM) at RT for a $[Fe(3.5Å)/Gd(7.3Å)]_{N=60}$ multilayer when a perpendicular magnetic field ($B_{Z,1}$=880 Oe) and a planar magnetic field ($B_{XY,1}$=30 Oe) are applied. See the equal distribution of circular ↑ and ↓ magnetic domains. (b) : Magnetic loops at RT of the same stack for planar (B_{XY}, red curve obtained from SQUID data) and perpendicular (B_Z, blue curve obtained from EHE, Extraordinary hall effects) variable magnetic fields. The EHE signal has been multiplied by (-1) for clarity of presentation, revealing a rare earth rich film. Here, $B_{Z,1}$ and $+B_{XY,1}$ are indicated in (b).

References

[1] A. Hrabec, J. Sampaio, M. Belmeguenai, et al. Current-induced skyrmion generation and dynamics in symmetric bilayers. *Nature Communications* 8 (2017).

[2] Ruyi Chen, Yang Gao, Xichao Zhang, et al. Realization of Isolated and High-Density Skyrmions at Room Temperature in Uncompensated Synthetic Antiferromagnets. *Nano Letters* 20, 3299–3305 (2020).

[3] Katharina Zeissler, Simone Finizio, Craig Barton, et al. Diameter-independent skyrmion Hall angle observed in chiral magnetic multilayers. *Nature Communications* 11 (2020).

[4] Andrada-Oana Mandru, Oğuz Yıldırım, Riccardo Tomasello, et al. Coexistence of distinct skyrmion phases observed in hybrid ferromagnetic/ferrimagnetic multilayers. *Nature Communications* 11 (2020).

[5] E. Stavrou and K. Röll. Magnetic anisotropy in Gd/(FeCo) and Gd/Fe multilayers for high density magneto-optical recording. *Journal of Applied Physics* 85, 5971–5973 (1999).

[6] S. A. Montoya, S. Couture, J. J. Chess, et al. Tailoring magnetic energies to form dipole skyrmions and skyrmion lattices. *Physical Review B* 95 (2017).

[7] E. Stavrou, R. Sbiaa, T. Suzuki, S. Knappmann, and K. Röll. Magnetic anisotropy and spin reorientation effects in Gd/Fe and Gd/(FeCo) multilayers for high density magneto-optical recording. *Journal of Applied Physics* 87, 6899–6901 (2000).

[8] Luis Flacke, Valentin Ahrens, Simon Mendisch, et al. Robust formation of nanoscale magnetic skyrmions in easy-plane anisotropy thin film multilayers with low damping. *Physical Review B* 104 (2021).

[9] Satoru Hayami. In-plane magnetic field-induced skyrmion crystal in frustrated magnets with easy-plane anisotropy. *Physical Review B* 103 (2021).

Time-resolved switching of curling magnetization in nanowires

A. Masseboeuf[1], D. Gusakova[1], L. Alvaro-Gomez[1,3], C. Thirion[2], J.C. Toussaint[2], L. Perez[3], M. Weigand[4], S. Wintz[4], and O. Fruchart[1]

[1]*Spintec (CNRS, CEA, UGA) Grenoble, France*
[2]*Institut Néel (CNRS, Grenoble INP) Grenoble, France*
[3]*IMDEA Nanociencia, Madrid, Spain*
[4]*Helmholz Zentrum (Bessy), Berlin, Germany*
*aurelien.masseboeuf@cnrs.fr

Motion of domain wall depending on their structure in cylindrical magnetic nanowires in an intense topic of research [1] to achieve racetrack-memory. The Bloch Point Wall (BPW) consists of a Bloch point surrounded by azimuthal curling of magnetization at the wire periphery. Velocity of such wall is predicted to be above 1 $km.s^{-1}$. On the experimetal side intense efforts are made to overcome unwanted pinning of walls in such system to promote fast and controlled motion. Geometrical and chemical modulations or tubular and core-shell structure are many aspect that are currently under investigation. In a recent experiment, we considered Permalloy $Fe_{20}Ni_{80}$ nanowires with micrometers-long segments chemicaly modulated by the insertion of $Fe_{80}Ni_{20}$ sections of few tens of nanometers. We reported BPW velocity above 600 $m.s^{-1}$ under a ns pulse of spin-transfer-torque[2], dynamically stabilised by the Œrsted field during motion. Simulations suggest an interplay between volume topological objects (Bloch points) and surface objects (vortex-antivortex pairs) during the motion. Two curling magnetization segments may be found in such conduits. Aside the BPW that are easy to nucleate with large current pulses, magnetostatic energy induces the occurrence of curling magnetization at the modulations. Such circulation has been shown to be switchable using 1-10 ns electrical current pulses, driven by the associated Œrsted field [3].

We will present time-resolved (TR) magnetic imaging using Scanning Transmission X-ray Microscopy (STXM) (see Fig. **??**) , that reveals the reproducible switching mechanism of both of these elements with a 50 ps time resolution. The threshold current for switching is around 5.10^{11} $A.m^2$. Above typically 7.10^{11} $A.m^2$ the circulation switching occurs in less than 200 ps. This points at an ultrafast swiching mechanism, which we explain by the strength of Œrsted field and dynamic dipolar field in nanowires. When approaching the current threshold the switching time tends to diverge, consistent with expectations from theory and simulations. A comparison with micromagnetic simulations and analytical simulations will be shown, with a view to provide a comprehensive picture of this ultrafast phenomenon, which we believe should be common to other curvilinear systems.

Acknowledgments

French RENATECH network, The team of the Nanofab platform (CNRS Institut Néel).

References

[1] Michal Staňo and Olivier Fruchart. “Chapter 3 - Magnetic Nanowires and Nanotubes”. *Handbook of Magnetic Materials*. Ed. by Ekkes Brück. Vol. 27. Elsevier, 2018, 155–267.

[2] Michael Schöbitz, Ondrej Novotný, Beatrix Trapp, et al. A Material View on Extrinsic Magnetic Domain Wall Pinning in Cylindrical CoNi Nanowires. *The Journal of Physical Chemistry C* 127, 2387–2397 (2023).

[3] L. Álvaro-Gómez, S. Ruiz-Gómez, C. Fernández-González, et al. Micromagnetics of magnetic chemical modulations in soft-magnetic cylindrical nanowires. *Physical Review B* 106, 054433 (2022).

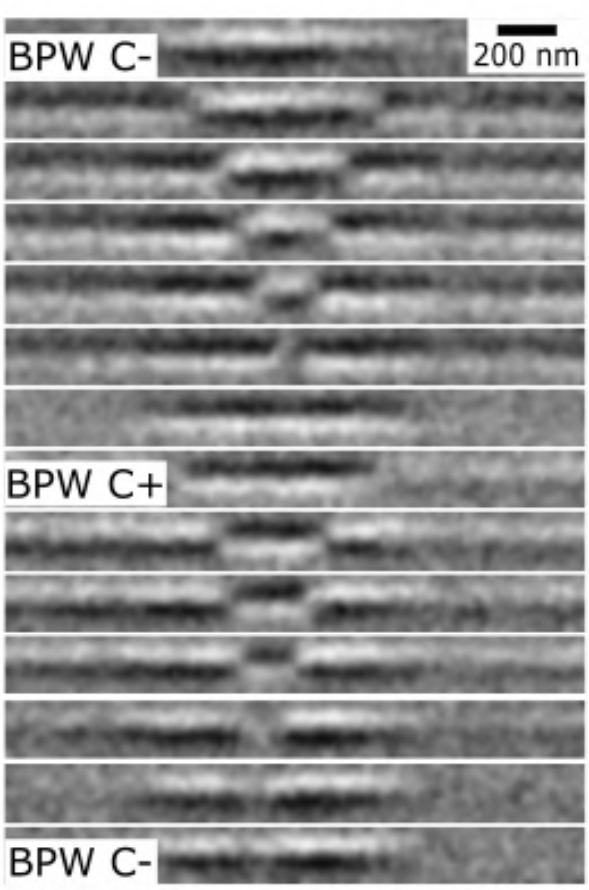

Figure 1: Time-resolved STXM imaging of BPW circulation switching. Images are separated of 100ps.

Domain wall manipulation in cylindrical ferromagnetic nanotubes

M. Scheuerlein[1], L. M. Kandpal[2,*], D. Tiwari[2], M. Jaber[2], W. Ensinger[1], E. Pereiro[3], S. Finizio[4], C. Thirion[5], L. Cagnon[5], D. Gusakova[2], A. Masseboeuf[2], and O. Fruchart[2]

[1]*Technical Univeristy of Darmstadt, Darmstadt, Germany*
[2]*SPINTEC (CNRS, CEA, UGA), Grenoble, France*
[3]*ALBA Synchrotron, Barcelona, Spain*
[4]*Swiss Light Source (SLS) Synchrotron, Villigen, Switzerland*
[5]*Institut Néel (CNRS), Grenoble, France*
lalit-mohan.kandpal@cea.fr

Magnetic domains walls (DWs)[1] are one of the key spin-texture elements bearing the ability to move along the flow of an externally applied electrical current, e.g. through spin-transfer torque (STT)[2] or Oersted (Oe)-field. This makes them interesting entities for information encoding or electrically controlled memory applications. Until now, such studies on magnetic DWs have generally been performed in two-dimensional (2D) strips, however for their 3D integration in race tracks[3] nanowires/tubes have been proposed.

As compared to 2D strips, the curved 3D topology[4] induces the existence of specific DWs called Bloch-point walls (BPW). The BPW exhibits azimuthal curling of magnetic moments around a Bloch point, a local singularity of the magnetization vector[5]. Potential advantages of the BPW is that they tend to be stabilized under Oe-field[6] and have been predicted to retain a steady-state motion without undergoing the Walker breakdown[5]. Recent experiments have shown that these BPW can attain DW velocities $> 600\,\mathrm{m\,s^{-1}}$ under current densities $\sim 2.4 \times 10^{11}\mathrm{Am^{-2}}$[5]. The case of magnetic nanotubes is at first sight very similar, except that the core is missing. However, using specific materials such as NiCoB it is possible to stabilize domains with azimuthal magnetization. This makes them very suitable to be addressed by the application of Oe-fields, not STT.

Here we report Oe-field driven DW motion experiments using transmission X-ray microscopy (TXM) on ferromagnetic nanotubes. These tubes have been grown by electro-less deposition of CoNi in a porous polycarbonate membrane, then filled with copper (Cu) by electrodeposition and finally contacted over X-ray transparent windows (see Fig. 1). We selected tubes of diameter 250 nm made of soft ferromagnetic alloys NiCoB with expected composition of 60 % of Co and 40 % of Ni. This system display azimuthal magnetization with several magnetic domains separated by narrow DWs. Experiments have been conducted at the Pollux SLS beamline and the ALBA Mistral beamline with home-made design electronics allowing to send electric pulses as narrow as 1 ns. Fig. 2 shows a static images taken during a series of current pulses that allowed us to move the DWs under Oe-field. Consecutive pulses of same width and height let us move the walls in a quite reproducible fashion. This led us to a first estimation of $100\,\mathrm{m\,s^{-1}}$ for the domain wall speed.

A complete study of these DWs will be presented including domain wall structure analysis using micromagnetic simulations combined with electron holography.

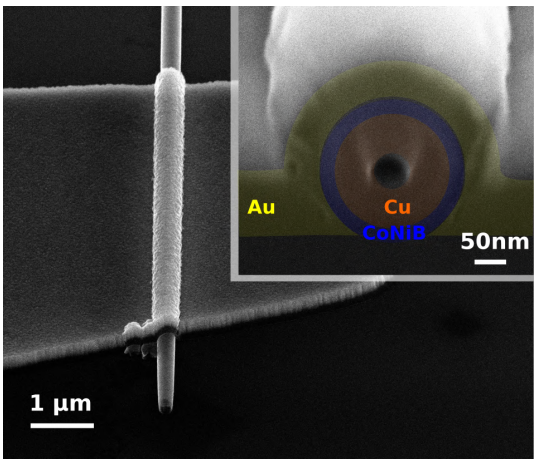

Figure 1: NiCo tubes with 250 nm diameter and wall thickness of $\sim$ 30 nm, filled by Cu and contacted electrically. The inset is a cross section (using FIB) showing the conformation of the metal contact onto the tube.

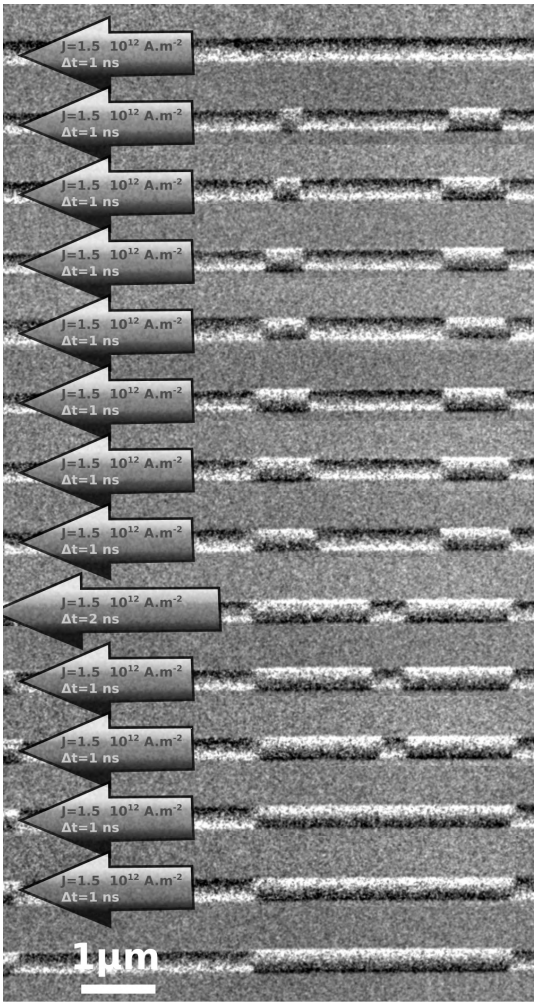

Figure 2: XMCD contrast obtained with TXM microscopy of a contacted tube. A pulse of current is sent between each image (see details on the left side of the image).

Acknowledgments

This project received financial support from the ANR-DFG C3DS project (ANR-18-CE92-0045, DFG-406700532). The authors acknowledge CNRS-RENATECH clean room facility and Nanofab plateform of Institut Néel for the nano/micro fabrication.

References

[1] Alex Hubert and Rudolf Schäfer. *Magnetic domains: the analysis of magnetic microstructures*. Springer Science & Business Media, 2008.

[2] John C Slonczewski. Current-driven excitation of magnetic multilayers. *Journal of Magnetism and Magnetic Materials* 159, L1–L7 (1996).

[3] Stuart SP Parkin, Masamitsu Hayashi, and Luc Thomas. Magnetic domain-wall racetrack memory. *Science* 320, 190–194 (2008).

[4] Amalio Fernández-Pacheco, Robert Streubel, Olivier Fruchart, et al. Three-dimensional nanomagnetism. *Nature communications* 8, 15756 (2017).

[5] M Schöbitz, A De Riz, S Martin, et al. Fast domain wall motion governed by topology and Œrsted fields in cylindrical magnetic nanowires. *Physical Review Letters* 123, 217201 (2019).

[6] M Schöbitz, S Finizio, A De Riz, et al. Time-resolved imaging of Œrsted field induced magnetization dynamics in cylindrical magnetic nanowires. *Applied Physics Letters* 118, 172411 (2021).

Domain wall and pinning disorder interaction controlled by He^+ ion irradiation in Pt/Co/AlOx ultrathin films

V. Jeudy[1, *], C. Balan[2], J. W. van der Jagt[3, 4], J. Peña Garcia[2], J. Vogel[2], L. Ranno[2], M. Bonfim[5], D. Ravelosona[3,4], and S. Pizzini[2]

[1]*Laboratoire de Physique des Solides, Université Paris-Saclay, CNRS, 91405 Orsay, France*
[2]*Univ. Grenoble Alpes, CNRS, Institut Néel, 38042 Grenoble, France*
[3]*Spin-Ion Technologies, 10 Boulevard Thomas Gobert, 91120 Palaiseau, France*
[4]*Centre de Nanosciences et de Nanotechnologies, CNRS, Université Paris-Saclay, 10 boulevard Thomas Gobert, 91120 Palaiseau, France*
[5]*Dep. de Engenharia Elétrica, Universidade Federal do Parana, Curitiba, Brasil*
vincent.jeudy@universite-paris-saclay.fr

We have studied the effect of He^+ irradiation on the dynamics of chiral domain-walls (DWs) in ultra-thin Pt/Co/AlOx trilayers [1]. Through a self-consistent description of the creep and depinning dynamics [2] completed by a scaling model of DW depinning [3] (relating microscopic DW pinning properties to DW dynamics and micromagnetic parameters), we reveal an excellent scaling between the variations of the DW pinning length scale ξ and the DW width parameter. This scaling strongly suggests that the modification of the DW pinning by irradiation is essentially dominated by the variations of DW magnetic texture (via the variation of the magnetic anisotropy), while short range atomic displacement produced by irradiation have a weak impact on the pinning disorder [4].

The DW velocity versus applied perpendicular magnetic field is reported in the Figure 1(a) for increasing He^+ fluence. As it can be observed, the irradiation leads to a strong decrease of the depinning field and an enhancement of DW velocity. The velocity curves present a good agreement with the self-consistent description of the creep (solid lines) and depinning (dashed lines) dynamics, which allows extracting the values of the pinning parameters [3] (depinning field, temperature and velocity (not shown)). Complementary characterizations of the trilayers (determination of the saturation magnetization, anisotropy, and Dzyaloshinskii-Moriya interaction (DMI)) reveal that irradiation essentially reduces the anisotropy, which increases the DW width, while the other micromagnetic parameters remain only weakly affected. Using the scaling model of DW depinning [2], we deduce the pinning length ξ (see Fig. 1(b)) and the pinning strength f_{pin} (see Fig. 1(c)). Their variations with He^+ fluence are found to present a perfect scaling with those of the DW width Δ and DW energy per unit length σt, respectively.

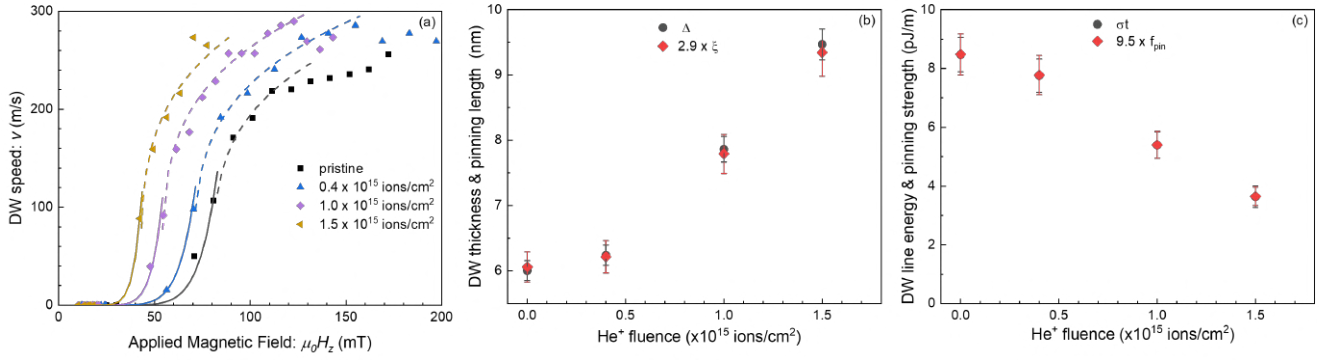

Figure 1: Effect of He^+ ion irradiation on DW dynamics and DW-disorder interaction: (a) domain wall velocity versus out-of plane field $\mu_0 H_z$ for increasing irradiation fluence; comparison between (b) DW-disorder characteristic length scale ξ and DW parameter Δ , (c) pinning strength f_{pin} and DW energy per unit length σt.

References

[1] Cristina Balan, Johannes W van der Jagt, Jose Peña Garcia, et al. Control of the interaction between pinning disorder and domain walls in Pt/Co/AlOx ultrathin films by He+ ion irradiation. *Applied Physics Letters* 122 (2023).

[2] Vincent Jeudy, R Díaz Pardo, W Savero Torres, Sebastian Bustingorry, and Alejandro Benedykt Kolton. Pinning of domain walls in thin ferromagnetic films. *Physical Review B* 98, 054406 (2018).

[3] P Géhanne, S Rohart, A Thiaville, and Vincent Jeudy. Strength and length scale of the interaction between domain walls and pinning disorder in thin ferromagnetic films. *Physical Review Research* 2, 043134 (2020).

[4] T Devolder. Light ion irradiation of Co/Pt systems: Structural origin of the decrease in magnetic anisotropy. *Physical Review B* 62, 5794 (2000).

Low PMA tuned iron garnets for the stabilization of magnetic skyrmions

Georgy Ziborov[1, 2, *], Laurent Ranno[1], Olivier Boulle[2], Éric Mossang[1], and Stéphane Grenier[1]

[1]*Institut Néel, CNRS/UGA UPR 2940, Grenoble, France*
[2]*Spintec, IRIG, CNRS/CEA/UGA UMR 8191, Grenoble, France*
*georgy.ziborov@neel.cnrs.fr

Magnetic skyrmions are local whirling of the magnetization found in certain magnetic films. Their properties including topological stability, sizes down to nm-scale and the possibility of manipulation by electrical current, leading to the proposal of novel memory and logic technologies where skyrmions in racetrack are information carriers. These applications require high data throughput and computing speed. Room temperature skyrmions and their current induced manipulation were recently demonstrated in ultrathin ferromagnetic/heavy metal multilayers, which was an important step toward their use in devices [1]. The heterostructures composed of ferrimagnetic oxides (FMOx) based on rare-earth iron garnets in contact with high spin-orbit materials (SOM) have recently attracted a large attention grace to their assets for the current induced skyrmion manipulation. Their advantages include electrical insulation which allows to minimize the energy loss due to current shunting, small saturation magnetization M_s, small magnetic damping α, leading to large domain wall mobility, significant DMI interaction at the FMOx/SOM interface [2–4]. In addition to this, FMOx are thermally and chemically more stable than metals and their the magnetic properties can be tuned by playing on the strain, composition, annealing conditions or interfaces [5–7].

The Thulium Iron Garnet (TmIG - $Tm_3Fe_5O_{12}$) and Yttrium Iron Garnet (YIG - $Y_3Fe_5O_{12}$) samples with thicknesses varying from 6 to 100 nm were deposited on Gadolinium Gallium Garnet (GGG - $Gd_3Ga_5O_{12}$) (111) substrate using radio frequency sputtering technique, and were annealed in air after the deposition. The structural properties of the deposited films were studied after using X-ray reflectivity (XRR) and X-ray diffraction (XRD) techniques, which demonstrated a good quality of the samples and the presence of $0,8\%$ strain in the TmIG layer, causing magnetoelastically induced perpendicular magnetic anisotropy (PMA). The YIG samples are not strained and have in-plane easy magnetization axis.

TmIG/GGG samples exhibit perpendicular magnetization for all thicknesses ranging between 6 and 40 nm with square hysteresis loop and sharp reversal (see Fig. 1) associated with large magnetic domains. 5 nm Pt layer was deposited on the TmIG(12 nm)/GGG sample in order to study Spin Hall effect, which demonstrated the injection of spin-current into the TmIG layer with the Hall resistance $R_H = 1$ mΩ. However, the quite large PMA in the stacks did not allow the nucleation of magnetic skyrmions.

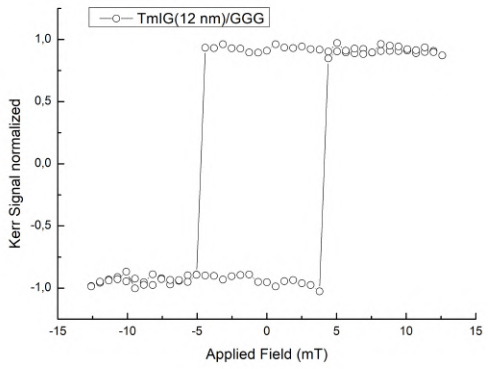

Figure 1: The hysteresis loop of the TmIG(12 nm)/GGG sample measured in the MOKE microscope under out-of-plane magnetic field.

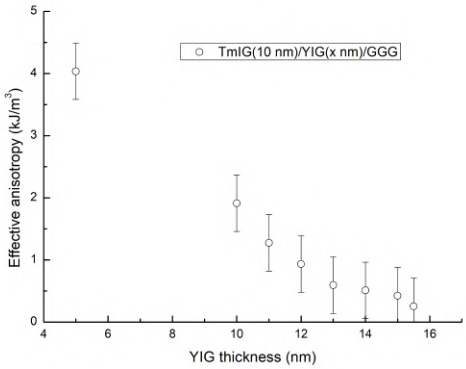

Figure 2: K_{eff} dependence on YIG layer thickness in TmIG(10 nm)/YIG(x nm)/GGG bilayers.

With the purpose to significantly reduce the anisotropy of the films, bilayers TmIG/YIG/GGG with fixed TmIG layer thickness $t_{TmIG} = 10$ nm and different t_{YIG} were fabricated. These samples have only one easy axis magnetization, depending on the proportions of the layers, since both layers have the same iron network. With the increase of YIG layer the effective anisotropy can be reduced to a value down to $K_{eff} = 0,2 \pm 0,5$ kJ/m^3 for TmIG(10 nm)/YIG(15,5 nm)/GGG, as shown in the Fig. 2. The PMA bilayer samples with $K_{eff} < 1$ kJ/m^3 have butterfly-type hysteresis loop with reduced remanence (see Fig. 3), exhibiting magnetic bubbles (see Fig. 4).

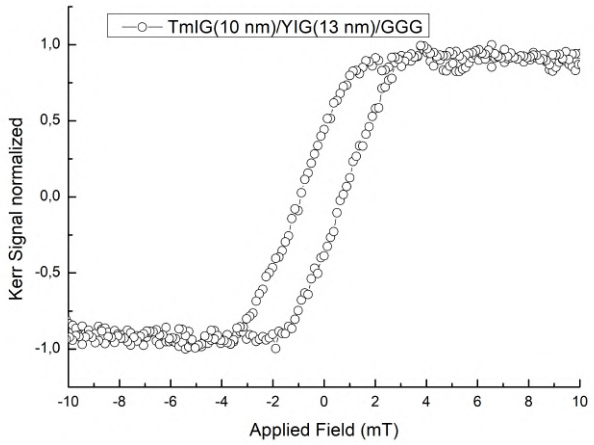

Figure 3: The hysteresis loop of the TmIG(10 nm)/YIG(13 nm)/GGG sample measured in the MOKE microscope in the out-of-plane magnetic field.

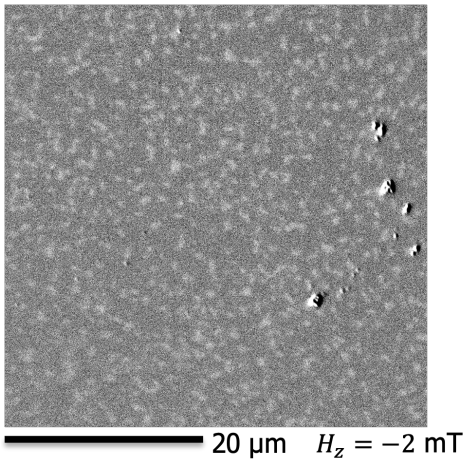

Figure 4: The polar-MOKE image of the TmIG(10 nm)/YIG(13 nm)/GGG sample measured in the applied out-of-plane magnetic field $B_z = -2$ mT.

Brillouin Light Scattering (BLS) experiments and current-induced experiments are currently in progress to study the dynamics of these magnetic bubbles driven by spin orbit torque and identify the nature of their chirality and topology. In addition, domain propagation by applying short magnetic pulses experiments are planned to check the presence of DMI.

Acknowledgments

The authors would like to thank the LabEx LANEF and Nanosciences Foundation for financial support of this work.

References

[1] Olivier Boulle, Jan Vogel, Hongxin Yang, et al. Room-temperature chiral magnetic skyrmions in ultrathin magnetic nanostructures. *Nature Nanotechnology* 11, 449–454 (2016).

[2] Can Onur Avci, Ethan Rosenberg, Lucas Caretta, et al. Interface-driven chiral magnetism and current-driven domain walls in insulating magnetic garnets. *Nature Nanotechnology* 14, 561–566 (2019).

[3] Lucas Caretta, Ethan Rosenberg, Felix Büttner, et al. Interfacial Dzyaloshinskii-Moriya interaction arising from rare-earth orbital magnetism in insulating magnetic oxides. *Nature Communications* 11 (2020).

[4] Saül Vélez, Jakob Schaab, Martin S. Wörnle, et al. High-speed domain wall racetracks in a magnetic insulator. *Nature Communications* 10 (2019).

[5] C. N. Wu, C. C. Tseng, Y. T. Fanchiang, et al. High-quality thulium iron garnet films with tunable perpendicular magnetic anisotropy by off-axis sputtering – correlation between magnetic properties and film strain. *Scientific Reports* 8 (2018).

[6] C. N. Wu, C. C. Tseng, K. Y. Lin, et al. High-quality single-crystal thulium iron garnet films with perpendicular magnetic anisotropy by off-axis sputtering. *AIP Advances* 8, 055904 (2018).

[7] Gilvânia Vilela, Hang Chi, Gregory Stephen, et al. Strain-tuned magnetic anisotropy in sputtered thulium iron garnet ultrathin films and TIG/Au/TIG valve structures. *Journal of Applied Physics* 127, 115302 (2020).

Improving Néel domain wall dynamics and skyrmion stability using helium ion irradiation

Cristina Balan[1], Johannes. W. van der Jagt[2], Vincent Jeudy[3], André Thiaville[3], Aymen Fassatoui[1], Laurent Ranno[1], Jan Vogel[1], Dafiné Ravelosona[2], and Stefania Pizzini[1,*]

[1]*Univ. Grenoble Alpes, CNRS, Institut Néel, 38042 Grenoble, France*
[2]*Spin-Ion Technologies; 10 Boulevard Thomas Gobert, 91120 Palaiseau, France*
[3]*Laboratoire de Physique des Solides, Université Paris-Saclay, CNRS, 91405 Orsay, France*
*stefania.pizzini@neel.cnrs.fr

Ion irradiation with light ions is an appealing way to finely tune the magnetic properties of thin magnetic films and in particular the perpendicular magnetic anisotropy (PMA) [1]. In this work [2] we illustrate the effect of He^+ irradiation on the magnetization reversal and the domain wall dynamics in Pt/Co/AlOx trilayers. Fluences up to 1.5×10^{15} ions/cm^2 strongly decrease the PMA, without affecting neither the spontaneous magnetization nor the strength of the interfacial Dzyaloshinskii-Moriya interaction (DMI). This confirms experimentally the robustness of the DMI interaction against interfacial chemical intermixing, already predicted by theory [3]. In parallel with the decrease of the PMA, a strong decrease of the domain wall depinning field is observed after irradiation. This allows the domain walls to reach large maximum velocities with a lower magnetic field compared to that needed for the pristine films. Decoupling PMA from DMI can therefore be beneficial for the design of low energy devices based on domain wall dynamics. When the samples are irradiated with larger He^+ fluences ($\approx 3\times10^{15}$ ions/cm^2), the magnetization gets close to the out-of-plane/in-plane reorientation transition, where ≈100nm size magnetic skyrmions are stabilized. We observe that as the He^+ fluence increases, the skyrmion size decreases while these magnetic textures become more stable against the application of an external magnetic field, as predicted by theoretical models developed for ultrathin films with labyrinthine domains.

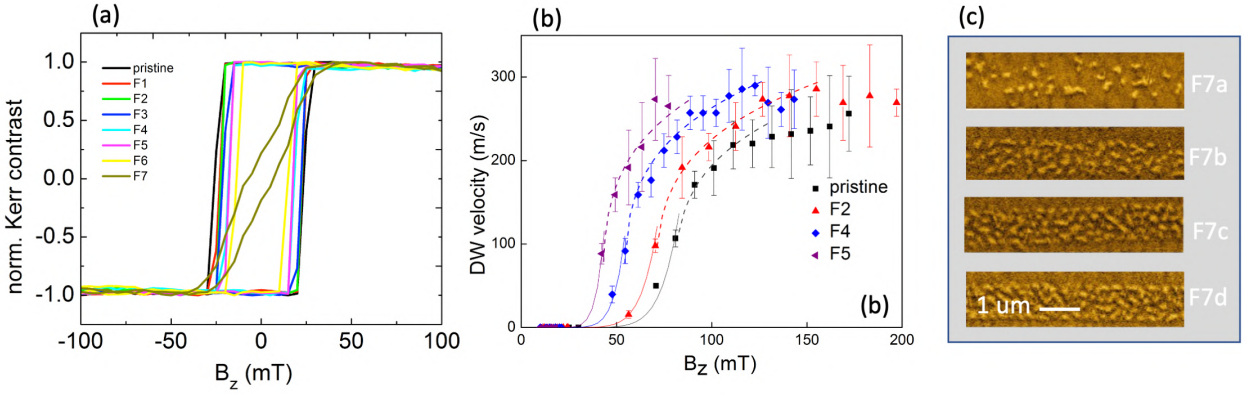

Figure 1: (a,b) variation of coercive field (a) and domain wall velocity (b) with increasing He^+ fluence; (c) stripe domains and skyrmion bubbles stabilised for the highest He^+ fluences, from 2.5 (top) to 3.2 (bottom) $\times10^{15}$ ions/cm^2.

References

[1] T. Devolder. Light ion irradiation of Co/Pt systems: Structural origin of the decrease in magnetic anisotropy. *Phys. Rev. B* 62, 5794 (2000).

[2] C. Balan, J. W. van der Jagt, A. Fassatoui, et al. Improving Néel Domain Walls Dynamics and Skyrmion Stability Using He Ion Irradiation. *Small*, 2302039 (2023).

[3] B. Zimmermann, W. Legrand, D. Maccariello, et al. Dzyaloshinskii-Moriya interaction at disordered interfaces from ab initio theory: Robustness against intermixing and tunability through dusting. *Applied Physics Letters* 113, 232403 (2018).

Development of a NV-center microscope for spin-wave spectroscopy

Eric Clot[1, 2, *], Vladimir Naletov[1], Isabelle Joumard[1], Benjamin Pigeau[2], and Olivier Klein[1]

[1]*SPINTEC, CEA/CNRS/UGA, Grenoble, France*
[2]*Institut Néel, CNRS, Grenoble, France*
*Eric.clot@cea.fr

Collective spin excitations, or spin-waves, inside a magnet provide a unique spectroscopic signature on the nature of the magnetic material as well as the magnetic texture present inside. The magnetic texture can be either a heterogeneity in the equilibrium configuration (point defect, skyrmion, magnetic bubble, vortex, Bloch point ect...) or the dynamical one (non-linear soliton, bullet mode, or spin-wave droplet). So far, the spectral signature is still mostly incomplete because most of the spin-wave eigen-modes remain undetected due to the difficulties to couple them with spatially averaged quantities. To circumvent this difficulty requires to use a local probe.

To achieve precisely this, we are currently developing a home-made NV-center microscope, whose purpose is to image with nanometer precision the spatio-temporal profile of spin-wave eigen-modes inside a magnetic object [1, 2]. The technical originality of our development is that the NV centre microscope seats between the poles of a 1.4 T electromagnet, as shown in Figure. 1. In addition the originality of our setup is that the field of the electromagnet is defined and stabilised at ppm resolution in order to study ultra narrow spectral features. As a first goal, we want to use this instrument to study the influence of the dynamical pattern on the relaxation process. In magnetic system, the processes of dissipation are generally poorly known, while they are key to several functions exploiting the very long relaxation time of magnetic resonance.

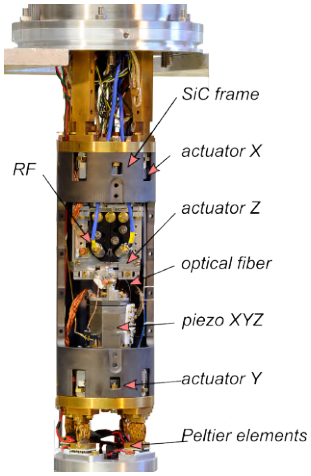

Figure 1: Picture of the NV center microscope developed at Spintec. A SiC frame supports XYZ actuators covering a field of ±2.5mm with a precision of about 10 pm. The non-magnetic assembly is inserted in a 1.4 T electromagnet. This preliminary version operates at room temperature..

Acknowledgments

This work is supported by the LANEF foundation.

References

[1] Gruber.A, Dräbenstedt.A, Tietz.C, et al. Scanning Confocal Optical Microscopy and Magnetic Resonance on Single Defect Centers. *Science* 276, 2012–2014 (1997).

[2] Gross.I, Akhtar.W, Garcia.V, et al. Real-space imaging of non-collinear antiferromagnetic order with a single-spin magnetomete. *Nature* 549, 252–256 (2017).

Towards hard-X-ray-based magnetic tomography: Coherent Diffraction Imaging of $Co_{1-x}Gd_x$ microbeads

Alexis Wartelle[1,2,*], Yuriy Chushkin[2], Vincent Favre-Nicolin[2,3], Philippe David[4], Frédéric Charlot[5], Jean-François Motte[4], Nora Dempsey[4], Marisel Di Pietro Martínez[6], Federico Zontone[2], Marco Cammarata[2], Steven Leake[2], Carsten Detlefs[2], and Guillaume Beutier[7]

[1]*Université de Lorraine, CNRS, IJL, F-54000 Nancy, France*
[2]*European Synchrotron Radiation Facility, F-38043 Grenoble, France*
[3]*Université Grenoble Alpes, 38400 Grenoble, France*
[4]*Université Grenoble Alpes, CNRS, Grenoble INP, Institut Néel, 38042 Grenoble, France*
[5]*Consortium des Moyens Techniques Communs, Grenoble INP, 38402 Saint Martin d'Hères, France*
[6]*Max Planck Institute for Chemical Physics of Solids, Noethnitzer Str. 40, 01187 Dresden, Germany*
[7]*Université Grenoble Alpes, CNRS, Grenoble INP, SIMaP, 38000 Grenoble, France*
*alexis.wartelle@esrf.fr

A wealth of novel 3D magnetic architectures have been enabled by recent advances in micro-/nanofabrication [1, 2]. In order to tackle the complexity of such systems, it is often necessary to resolve their magnetic configurations in their finest details, which in turn implies the use of magnetization-sensitive vector tomographic approaches [3, 4]. Above a few 100's of nm in sample size, hard X-rays are the probe of choice. Notably, hard-X-ray imaging has been successfully applied to rare-earth/transition metal alloy or multilayer samples with dimensions of a few microns [5–7]. These investigations have used techniques relying on focused X-ray beams, namely ptychography and laminography; in practice, the presence of optical elements close to the sample severely impedes upgrades to the sample environment. By contrast, plane-wave Coherent Diffraction Imaging (CDI) [8, 9] with hard X-rays poses much less stringent requirements in terms of setup. This technique allows to solve the phase problem in the case of far-field diffraction by an isolated object, provided that its dimensions are small enough for the phase retrieval to succeed. With this in mind, we intend to augment the outstanding tomographic capabilities of CDI [10] with vector magnetic imaging, in a dual-axis tomography approach [3].

First of all, sensitivity to magnetism is achieved through X-ray Resonant Magnetic Scattering (XRMS) [11], using circularly polarized light. The contrast is then proportional to the magnetization component along the beam, integrated along the path through the object. We use a diamond single crystal as quarter-wavelength plate [12] to obtain a high enough degree of circular polarization at the energies of interest, typically at the L_3 or L_2 absorption edge of a magnetic rare earth present in the sample (*e.g.* 7243 eV for the Gd L_3 edge).

In terms of system to be imaged, we take advantage of high-fluence Pulsed Laser Deposition (PLD) to create 3D objects. The latter are frozen droplets of target material with predominantly round shapes and a broad size distribution. We can thus obtain beads with a size suitable for CDI ($\lesssim$5 µm in our case) and a composition close to that of our target, $Co_{80}Gd_{20}$. Beads that do not adhere too much to the initial substrate can be micromanipulated onto SiN or SiC membranes for synchrotron experiments, as shown in Fig. 1.a). The CDI measurements are performed on the ID10 beamline at ESRF. At the photon energy of interest, here 7244 eV, scattering patterns I_+, I_- can be acquired with opposite circular polarizations (+/-). An exemplary scattering pattern I_+ and the corresponding difference $\Delta I = (I_+ - I_-)$ between opposite-polarization patterns are displayed in Fig. 1.b-c).

We are currently tackling the "inversion" of our reciprocal-space data. As a first step, we succeeded in obtaining 3D structural reconstructions with conventional CDI phase retrieval algorithms, which recover the sample's electronic density. Two views of the reconstruction of the bead from Fig. 1.a) are included in Fig. 1.c-d). However, the reconstruction accuracy is questionable since our strongly-scattering sample violates the hypotheses underlying the CDI algorithms. Magnetism, which only produces a small modulation of the scattered intensities, is therefore not straightforwardly recovered. Moreover, this modulation is an interference between structure and magnetism *i.e.* not a case for which the CDI algorithms have been developed.

Our goal is to overcome this post-processing challenge and apply plane-wave CDI to magnetic imaging for the very first time. The acquired data does suggest that vector magnetic tomography is possible with this technique, which can be better-suited than *e.g.* ptychography or laminography for imaging under magnetic fields.

Acknowledgements

We acknowledge the Agence Nationale de la Recherche for funding under project number ANR-19-CE42-0013-05, and the European Synchrotron Radiation Facility (ESRF) for provision of synchrotron beamtime.

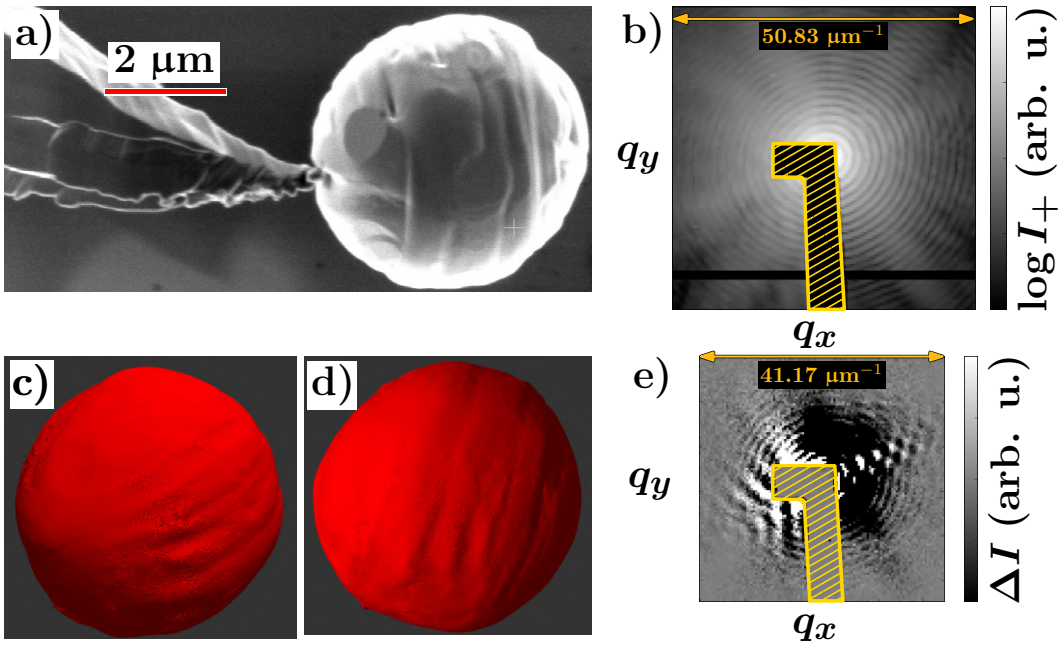

Figure 1: a) A $Co_{1-x}Gd_x$ bead during micromanipulation onto a SiC membrane (not visible here). b) Scattering pattern at the Gd L_3 edge obtained with circular polarization. c-d) CDI structural reconstructions of the sample shown in a). e) Difference between scattering patterns acquired with opposite circular polarizations. The intensity differences typically correspond to <1% contrast. The yellow hatched area corresponds to the beamstop.

References

[1] Amalio Fernández-Pacheco, Robert Streubel, Olivier Fruchart, et al. Three-dimensional nanomagnetism. *Nature Communications* 8, 15756 (2017).

[2] Luka Skoric, Dédalo Sanz-Hernández, Fanfan Meng, et al. Layer-by-Layer Growth of Complex-Shaped Three-Dimensional Nanostructures with Focused Electron Beams. *Nano Letters* 20, 184–191 (2019).

[3] Claire Donnelly and Valerio Scagnoli. Imaging three-dimensional magnetic systems with X-rays. *Journal of Physics: Condensed Matter* 32, 213001 (2020).

[4] Marisel Di Pietro Martínez, Alexis Wartelle, Carlos Herrero Martínez, et al. Three-dimensional tomographic imaging of the magnetization vector field using Fourier transform holography. *Physical Review B* 107, 094425 (2023).

[5] Claire Donnelly, Valerio Scagnoli, Manuel Guizar-Sicairos, et al. High-resolution hard x-ray magnetic imaging with dichroic ptychography. *Physical Review B* 94, 064421 (6 2016).

[6] Claire Donnelly, Manuel Guizar-Sicairos, Valerio Scagnoli, et al. Three-dimensional magnetization structures revealed with X-ray vector nanotomography. *Nature* 547, 328–331 (2017).

[7] Claire Donnelly, Simone Finizio, Sebastian Gliga, et al. Time-resolved imaging of three-dimensional nanoscale magnetization dynamics. *Nature Nanotechnology* 15, 356–360 (2020).

[8] Henry N. Chapman, Anton Barty, Stefano Marchesini, et al. High-resolution ab initio three-dimensional x-ray diffraction microscopy. *Journal of the Optical Society of America A* 23, 1179 (2005).

[9] Y. Chushkin, F. Zontone, E. Lima, et al. Three-dimensional coherent diffractive imaging on non-periodic specimens at the ESRF beamline ID10. *Journal of Synchrotron Radiation* 21, 594–599 (2014).

[10] Y. Chushkin, F. Zontone, O. Cherkas, and A. Gibaud. Quantitative nanotomography of amorphous and polycrystalline samples using coherent X-ray diffraction. *Journal of Applied Crystallography* 52, 571–578 (2019).

[11] Stöhr, J. and Siegmann, H. C. *Magnetism: From Fundamentals to Nanoscale Dynamics*. Springer Berlin Heidelberg, 2006.

[12] Motohiro Suzuki, Yuichi Inubushi, Makina Yabashi, and Tetsuya Ishikawa. Polarization control of an X-ray free-electron laser with a diamond phase retarder. *Journal of Synchrotron Radiation* 21, 466–472 (2014).

Dynamic imaging of new MRAM devices with electron holography

Augustin Nogier[1,*], Corentin Bouchard[2], Louis Hutin[2], Eric Gautier[1], Kévin Garello[1], and Aurélien Masseboeuf[1]

[1]*CEA, IRIG, SPINTEC, Grenoble, France*
[2]*CEA, LETI, Grenoble, France*
**augustin.nogier@cea.fr*

Recent improvements in spintronics led to generations of non-volatile Magnetoresistive Random-Access Memories (MRAM) devices that enable short switching time of few ns and low power consumption, such as the emerging current-induced Spin-Orbit Torque (SOT) [1].

So far, studies of such devices mostly rely on the measurement of their electrical and magnetic characteristics using all electrical methods [2, 3]. Meanwhile, direct observation can help understanding more finely the processes of reversal and transport, which is becoming increasingly important in order to control and optimize these objects. However, these components have small dimensions (typically <60 nm lateral, <1 nm in thickness), and observing magnetization textures and reversal in these devices during their activation remains challenging and requires the use of large scale instruments [4].

On the other hand, transmission electron microscopy (TEM) is a unique tool offering the combination of nm-scale spatial resolution and magnetic sensitivity and enabling detailed studies of said systems (see Fig. 1). Indeed, static magnetic field-free Electron Holography (EH) can be performed on unbiased samples to give quantitative 2D projected electric field and magnetic induction maps [5] with a magnetic sensitivity in the nmT range and details down to the nm scale. In order to improve further the understanding of the magnetic reversal processes taking place inside these devices upon writing and reading data, this work aims for an *operando* analysis (*e.g.* the quantitative dynamic imaging of their inner magnetic structure) by performing EH with a controlled external bias applied on adequately prepared samples [6, 7].

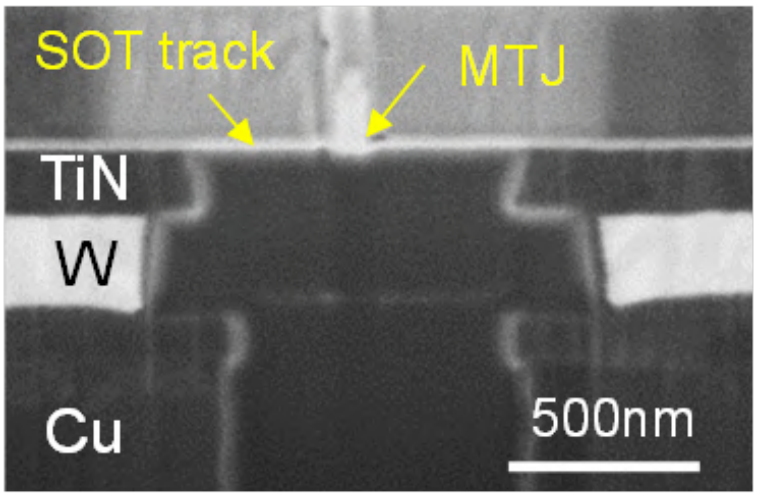

Figure 1: TEM dark-field imaging of the inner structure in a SOT-MRAM device

The structures of interest that we will present are SOT Magnetic Tunnel Junctions (SOT-MTJ) with ferromagnetic layers less than 1 nm thick. Weak internal fields close to the magnetic detection limit [8] makes the quality of the measurements of particular importance. In addition, the device under observation has to be sufficiently thinned to allow the electron beam to pass through heavy materials while remaining intact and without any behavior alteration, which requires a highly controlled preparation process [9]. Finally, the injection of an electrical current, voltage or external field on the device inside the electron microscope chamber is a technological challenge in and on itself [10], which also implies a specific preparation protocol.

We will present a study that applies these concepts to SOT-MTJ devices in a pseudo-static regime, where *in-situ* Electron Holography is performed with a constant applied bias on the device. Comparison of electrical characterizations will provide an insight about the effect of the sample preparation process on their integrity. An exhaustive in-depth review of the drawbacks of the method as well as the necessary precautions for a successful experiment will be presented, keeping in mind the study of domain wall motion in such devices as the next step to build a deeper understanding of the SOT mechanisms.

Acknowledgments

We thank the *Université Grenoble Alpes* and *IRGA* for funding this project.

References

[1] Qiming Shao, Peng Li, Luqiao Liu, et al. Roadmap of Spin–Orbit Torques. *IEEE Transactions on Magnetics* 57, 1–39 (2021).

[2] Cheng Song, Ruiqi Zhang, Liyang Liao, et al. Spin-orbit torques: Materials, mechanisms, performances, and potential applications. *Progress in Materials Science* 118, 100761 (2021).

[3] Eva Grimaldi, Viola Krizakova, Giacomo Sala, et al. Single-shot dynamics of spin–orbit torque and spin transfer torque switching in three-terminal magnetic tunnel junctions. *Nature Nanotechnology* 15, 111–117 (2020).

[4] Manuel Baumgartner, Kevin Garello, Johannes Mendil, et al. Spatially and time-resolved magnetization dynamics driven by spin–orbit torques. *Nature Nanotechnology* 12, 980–986 (2017).

[5] E. Javon, C. Gatel, A. Masseboeuf, and E. Snoeck. Electron holography study of the local magnetic switching process in magnetic tunnel junctions. *Journal of Applied Physics* 107, 09D310 (2010).

[6] Joshua F. Einsle, Christophe Gatel, Aurélien Masseboeuf, et al. In situ electron holography of the dynamic magnetic field emanating from a hard-disk drive writer. *Nano Research* 8, 1241–1249 (2014).

[7] Maria Brodovoi, Kilian Gruel, Aurélien Masseboeuf, et al. Mapping electric fields in real nanodevices by operando electron holography. *Applied Physics Letters* 120, 233501 (2022).

[8] Victor Boureau, Michal Staňo, Jean-Luc Rouvière, et al. High-sensitivity mapping of magnetic induction fields with nanometer-scale resolution: comparison of off-axis electron holography and pixelated differential phase contrast. *Journal of Physics D: Applied Physics* 54, 085001 (2020).

[9] Petr Formanek and Eberhard Bugiel. Specimen preparation for electron holography of semiconductor devices. *Ultramicroscopy* 106, 365–375 (2006).

[10] M. Mecklenburg, M. Brodie, W. Hubbard, et al. Fabrication of a Lift-Out Grid with Electrical Contacts for Focused Ion Beam Preparation of Lamella for In Situ Transmission Electron Microscopy. *Microscopy and Microanalysis* 19, 458–459 (2013).

Probing the chirality of magnetic textures from spin wave noise

Aurore Finco[1,*], Pawan Kumar[1], Van-Tuong Pham[2], Joseba Urrestarazu[2], Olivier Boulle[2], Joo-Von Kim[3], and Vincent Jacques[1]

[1]*Laboratoire Charles Coulomb, Université de Montpellier, CNRS, Montpellier, France*
[2]*Université Grenoble Alpes, CEA, CNRS, Grenoble INP, IRIG-SPINTEC, Grenoble, France*
[3]*Centre de Nanosciences et de Nanotechnologies, CNRS, Université Paris-Saclay, Palaiseau, France*
*aurore.finco@umontpellier.fr

NV centers are defects in diamond which can be used as quantum sensors to probe magnetism at the nanoscale when integrated in an atomic force microscope. Such a measurement relies on the spin S = 1 of the NV center: the static stray field produced by a magnetic state induces a Zeeman shift on the spin sublevels, which can be detected optically. In addition, NV centers are also sensitive to spin waves, as the magnetic noise originating from thermally activated spin waves accelerates their spin relaxation. In this case, the enhanced relaxation leads to a decrease of the photoluminescence emitted by the NV center [1], which allows an easy localization of spin waves interacting with magnetic textures. We applied this approach to the study of Co-based perfectly compensated synthetic antiferromagnetic layers [2], in which we were able to detect spin waves channeled inside the domain walls [3].

We report here on a more detailed investigation of domain walls and skyrmions in synthetic antiferromagnetic layers using this approach. Our measurements reveal that the spatial distribution of the detected magnetic noise and its amplitude are related to the chirality of the magnetic texture. We looked at Néel domain walls from both sides of the stack, after growing it on a membrane, and we found a stronger noise signal for counter-clockwise rotating walls than for clockwise rotating ones (see figure), in agreement with calculations.

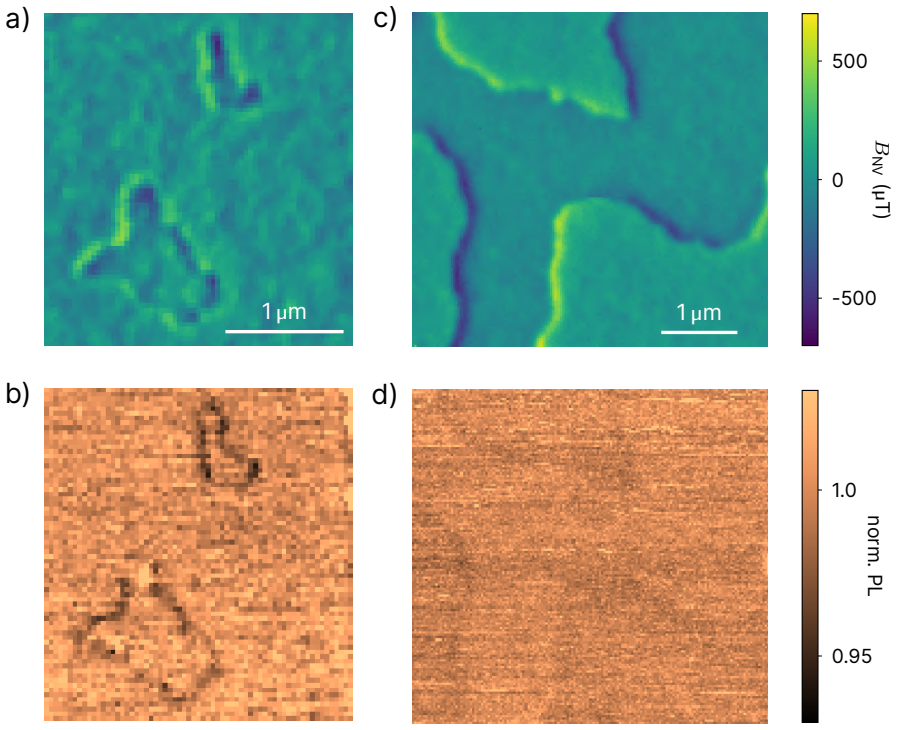

Figure 1: a) Magnetic stray field map measured above the synthetic antiferromagnet stack, showing counter-clockwise rotating Néel walls. b) Simultaneously recorded NV center photoluminescence map, showing the presence of magnetic noise coming from the walls. c) Magnetic stray field map measured from the other side of the stack, showing clockwise rotating Néel walls. d) Simultaneously recorded NV center photoluminescence map, where the magnetic noise from the walls is hardly visible.

Furthermore, we also extracted the magnetic noise pattern around the boundary of skyrmions and found that it is linked to their internal texture. Our experimental data allows us to exclude Bloch skyrmions and is in agreement with the expected noise distribution coming from Néel skyrmions.

References

[1] Maxime Rollo, Aurore Finco, Rana Tanos, et al. Quantitative Study of the Response of a Single NV Defect in Diamond to Magnetic Noise. *Physical Review B* 103, 235418 (2021).

[2] William Legrand, Davide Maccariello, Fernando Ajejas, et al. Room-Temperature Stabilization of Antiferromagnetic Skyrmions in Synthetic Antiferromagnets. *Nature Materials* 19, 34–42 (2020).

[3] Aurore Finco, Angela Haykal, Rana Tanos, et al. Imaging Non-Collinear Antiferromagnetic Textures via Single Spin Relaxometry. *Nature Communications* 12, 767 (2021).

A unique experimental end-station for correlative RIXS and XEOL spectroscopies under electric and magnetic fields

Alessandro Nicolaou[1,*], Victor Porée[1], Željko Rapljenović[2], Alberto Zobelli[3], Laura Susana[3], Jean-Denis Blazit[3], Mathieu Kociak[3], Victor Pinty[1], Fabrice Marteau[1], Eric Dupuy[1], Patrick Rommeluere[1], Francois Bouvet[1], Dubuisson Jean-Michel[1], and Christian Herbeaux[1]

[1]*Synchrotron SOLEIL, L'Orme des Merisiers, Saint-Aubin, BP 48, F-91192 Gif-sur-Yvette, France*
[2]*Institute of Physics, Bijenička c. 46, HR-10000 Zagreb, Croatia*
[3]*Laboratoire de Physique des Solides, Universite Paris-Saclay, CNRS UMR 8502, F-91405, Orsay, France*
**alessandro.nicolaou@synchrotron-soleil.fr*

Since beginning 2020 the inelastic branch of the SEXTANTS beamline offers to the users a novel sample environment for performing resonant inelastic X-ray scattering (RIXS) experiments under electric and magnetic fields, MAGELEC. It consists of a sample holder equipped with 12 electrical contacts, which is combined with a compact quadrupolar magnet delivering a rotatable magnetic field with a maximum strength of 0.45 T. Thanks to its particular design the whole scattering plane is available for magnetic dichroism RIXS (RIXS-MD) experiments in a temperature range from 400 K down to 18 K. Compatible with MAGELEC, we have recently installed an optical system allowing to correlate RIXS(-MD) measurements with X-ray excited optical luminescence spectroscopy (XEOL). I will start by presenting the layout of this unique sample environment. I will show the results obtained on ferromagnetic transition metal compounds, where RIXS spectra show an important magnetic dichroic contrast in the energy loss and/or fluorescence channel. I will conclude by showing one of the very first study of correlated RIXS and XEOL measurements performed under magentic field. I will discuss how these novel perspectives offered by inelastic branch the SEXTANTS beamline will promote fundamental research on magnetic materials through the possibility of tackling several kinds of open questions in the field of transition metal compounds beyond the accuracy obtained by the widely used X-ray magnetic circular and/or linear magnetic dichroism.

Acknowledgments

Part of this work has been supported by the Labex Palm (Grant No.ANR-10-LABX-0039-PALM).

Spectroscopie de défauts paramagnétiques par transitoires de photo-courant polarisés en spin dans les nitrures dilués

A. C. Ulibarri[1,*], C. J. J. Roubert[1], C. T. K. Lew[2], B. C. Johnson[3], M. Morassi[4], J. C. Harmand[4], J. Peretti[1], and A. C. H. Rowe[1]

[1]*LPMC, CNRS, Palaiseau, France*
[2]*University of Melbourne, Melbourne, Australia*
[3]*RMIT University, Melbourne, Australia*
[4]*C2N, CNRS, Palaiseau, France*
agatha.ulibarri@polytechnique.edu

La recombinaison dépendante du spin est un processus de type Shockley-Read-Hall (SRH) qui a lieu dans un centre paramagnétique [1]. Avec une polarisation en spin des électrons de conduction induite par pompage optique, les centres s'aimantent hors équilibre par un processus de polarisation dynamique.

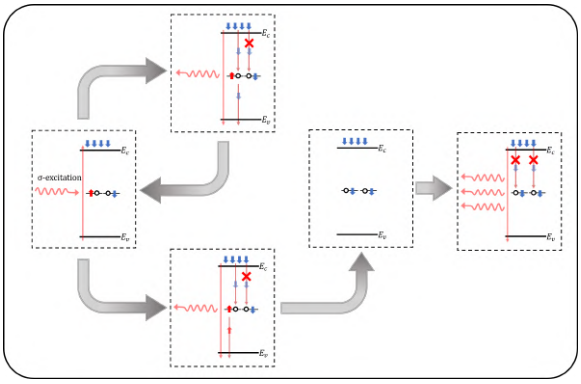

Figure 1: Schéma de la recombinaison dépendante du spin

Dans les matériaux nitrures dilués de type $GaAs_{1-x}N_x$ avec $0.007 < x < 0.04$, cette polarisation dynamique des centres bloque la recombinaison SRH via un effet d'échange sur le centre polarisé. Ceci se manifeste par une augmentation spectaculaire du temps de vie des porteurs et en conséquence l'intensité de la photoluminescence et du photo-courant.

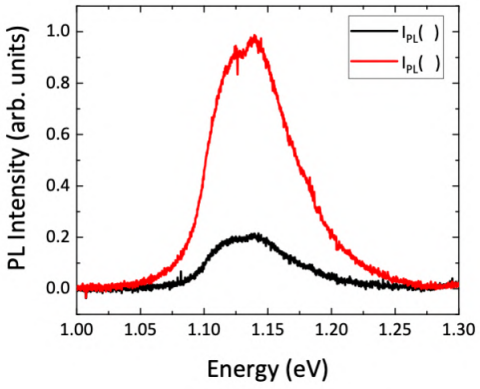

Figure 2: Courbe montrant la différence entre l'intensité de photoluminescence de la recombinaison dépendante du spin en rouge et sans spin en noir

Bien que la nature de ce centre soit connue (Ga^{2+} interstitiel [2]) grâce aux mesures de résonance de spin détectés optiquement, les détails électroniques (énergie d'activation dans le gap) pourtant primordial pour la caractérisation de tout défaut, restent inconnus. Ici, on utilise une modification originale de la technique dite «photo-induced current transient

spectroscopy» ou PICTS en anglais [3], où le photo-courant est polarisé en spin en conditions de pompage optique. On identifie des transitoires dépendant du spin, liées donc au piégeage d'électrons polarisés, et des transitoires non-polarisés en spin, liées donc aux trous. Les énergies d'activation sont de 0,3 eV par rapport à la bande de conduction et 0,8 eV par rapport à la bande de valence respectivement. La somme vaut le gap du matériau, 1,1 eV pour le $GaAs_{0.978}N_{0.022}$ [4], ce qui donne confiance sur cette première mesure de l'énergie des centres associés avec l'interstitiel Ga^{2+}.

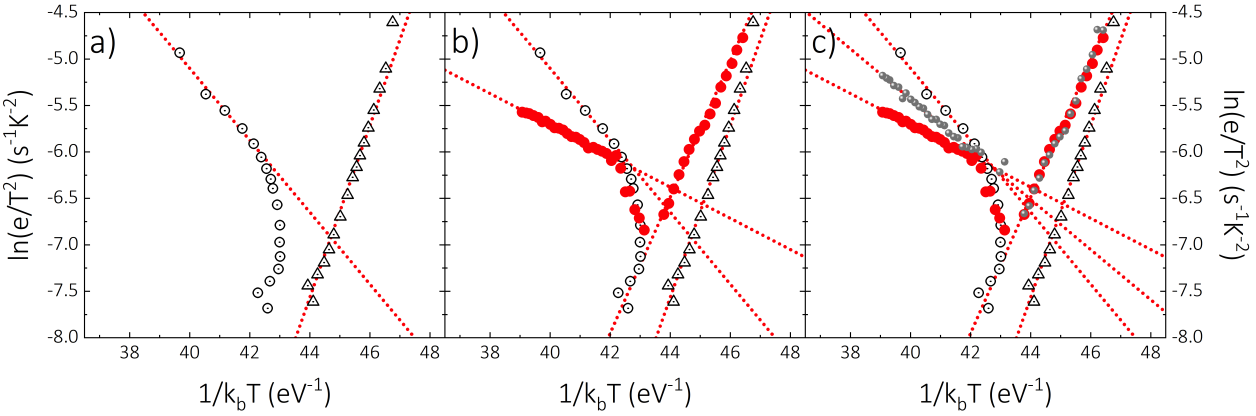

Figure 3: Courbe montrant les pentes des différentes méthodes pour déterminer l'énergie d'activation du centre ((a) Boxcar (b) Laplace (c)exponentielles)

References

[1] E.L. Ivchenko, V.K. Kalevich, A.Yu Shiryaev, M.M. Afanasiev, and Y. Masumoto. Optical orientation and spin-dependent recombination in GaAsN alloys under continuous-wave pumping. *Journal of Physics: Condensed Matter* 22 (2010).

[2] X.J. Wang, I.A. Buyanova, F. Zhao, et al. Room-temperature defect-engineered spin filter based on a non-magnetic semiconductor. *Nature materials* 8, 198–202 (2009).

[3] Ch. Hurtes, M. Boulou, A. Mitonneau, and D. Bois. Deep-level spectroscopy in high-resistivity materials. *Applied Physics Letters* 32, 821–823 (2008). eprint: https://pubs.aip.org/aip/apl/article-pdf/32/12/821/7739722/821_1_online.pdf.

[4] Agatha C. Ulibarri, Rishabh Kothari, Alejandro Garcia, et al. A Systematic Study of Spin-Dependent Recombination in $GaAs_{1-x}N_x$ as a Function of Nitrogen Content. *physica status solidi (b)* 260, 2200361 (2023). eprint: https://onlinelibrary.wiley.com/doi/pdf/10.1002/pssb.202200361.

Towards nuclear magnetic ordering in n-type semiconductors

Maria Vladimirova[1,*], Denis Scalbert[1], Steeve Cronenberger[1], and Kirill Kavokin[2]

[1]*Laboratoire Charles Coulomb, UMR 5221 CNRS/Univ Montpellier, Montpellier, France*
[2]*Spin Optics Laboratory, St. Petersburg State University, St. Petersburg, Russia*
*maria.vladimirova@umontpellier.fr

Critical temperatures for nuclear spin ordering in solids are generally less than 1 μK, because interactions between nuclear spins are much weaker than electronic spin interactions. On the other hand, nuclear spin system (NSS) can be cooled down to temperatures much lower than the lattice temperature because NSS reaches an internal equilibrium within a time much shorter than the spin-lattice relaxation time. This offers an opportunity to explore the magnetic phase diagram at negative temperatures. In metals and dielectrics NSS cooling and ordering has been reached using complex and unique purpose-built setups. We have shown that in semiconductor structures (i) spin temperatures of the order of 1 μK can be reached using commercial cryostats and table-top electromagnets [**vladimirova_spin_2018**]; (ii) Two kinds of nuclear magnetic ordering can be induced by resident electrons in a deeply cooled nuclear spin system, depending on the sign of the NSS temperature [**vladimirova_electron-induced_2021**].

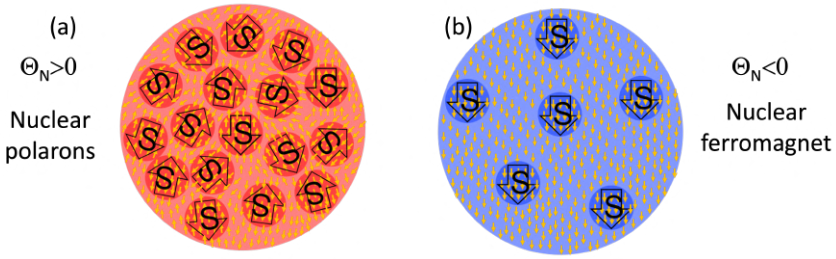

Figure 1: Two kinds of nuclear magnetic ordering expected in n-doped semiconductors: (a) randomly oriented nuclear spin polarons at positive nuclear spin temperature and (b) ferromagnetic state maintained by dynamic spin transfer between electron and nuclear spin systems at negative nuclear spin temperature. The large arrows labelled S represent the localized electron spins, while the small yellow arrows represent the nuclear spins.

Nuclear spin ordering in semiconductors remains theoretical until now. The potential experimental detection of the electron-induced nuclear correlations and ordering rely on our ability to efficiently cool the NSS and detect its magnetisation non-destructively. The lifetime of the ordered states is limited by the inevitable heating of the system, typically several seconds. We discuss how the nuclear spin ordering can be detected within this time by off-resonant Faraday rotation or by spin noise spectroscopy, eventually combined with radio- frequency absorption [**vladimirova_electron-induced_2021**, **litvyak_warm-up_2021**, **vladimirova_simultaneous_2022**].

Acknowledgments

Financial support from French national research agency is gratefully acknowledged (ANR-21-CE30-0049).

Ferromagnetic resonance damping in Co/2D material heterostructures

Karen Sobnath[1,*], Mehrdad Rahimi[1], Maria Luisa Della Rocca[1], Philippe Lafarge[1], Clément Barraud[1], and François Mallet[1,2]

[1]*Laboratoire Matériaux et Phénomènes Quantiques - Université Paris Cité, Paris, France*
[2]*Sorbonne Université, Paris, France*
*karen.sobnath@u-paris.fr

One of the key challenges in spintronics is the efficient generation and detection of spin currents, paving the way for ultra-fast and low power consumption devices for data storage and data processing. While many of the first proposed approaches are suffering from conductance mismatch and power dissipation issues [1], spin pumping provides a powerful route to inject and control dissipationless spin currents without charge current. This phenomena relies on the magnetization dynamic of a ferromagnetic material (FM), brought to its ferromagnetic resonance (FMR) with an external magnetic field, leading to the transfer of spin angular momentum at the interface between the FM and a non magnetic material (NM) [2]. The understanding of the importance of interface effects in these systems, accelerated by the huge progress in nanofabrication techniques, has oriented spintronics towards bidimensional (2D) materials. Indeed, 2D materials can be combined with potentially defect-less interfaces, they cover nowadays all condensed matter phases (from metallic, to semiconducting, insulating, superconducting and even recently magnetic) and present a large sensitivity to external parameters such as proximity effect, electrostatic gating, strain, light, stacking and superlattice effects [3].

In our group, we aim to investigate spin pumping through different FM/2D material interfaces. For this purpose, I performed broadband (4 GHz to 14 GHz) FMR measurements at room temperature in Co/graphene/hBN and Co/WSe_2/hBN samples compared to reference samples of Co and Co/Pd, deposited on a 6x10 µm² area on a on-chip microstrip RF antenna (see Fig. 1). I will present the effect of these different interfaces on the magnetic damping of Co and discuss about their origin.

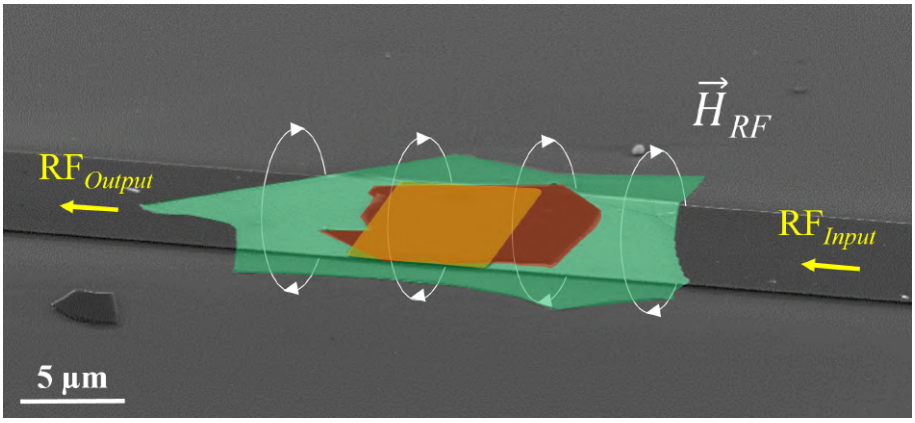

Figure 1: SEM image of a heterostructure of Co (orange)/WSe_2 (red)/hBN (green) deposited on a on-chip Au microstrip (from top to bottom) for FMR measurements.

References

[1] Nikolaos Tombros, Csaba Jozsa, Mihaita Popinciuc, Harry T. Jonkman, and Bart J. van Wees. Electronic spin transport and spin precession in single graphene layers at room temperature. *Nature* 448, 571–574 (2007).

[2] Yaroslav Tserkovnyak, Arne Brataas, and Gerrit E. W. Bauer. Enhanced Gilbert Damping in Thin Ferromagnetic Films. *Physical Review Letters* 88 (2002).

[3] Ethan C. Ahn. 2D materials for spintronic devices. *npj 2D Materials and Applications* 4 (2020).

Poster 1.35, November 14th, 16h30–18h30

Advances in Raman scattering investigations of the room temperature van der Waals ferromagnet 1T-$CrTe2_2$

Tristan Riccardi[1,2,*], Johann Coraux[1], Nicolas Rougemaille[1], Jan Vogel[1], Amit Pawbake[2], Dipankar Jana[2], and Clément Faugeras[2]

[1]*QUEST, Institut Néel, Grenoble, France*
[2]*LNCMI-CNRS, Univ. Grenoble Alpes, Grenoble, France*
*tristan.riccardi@neel.cnrs.fr

$CrTe_2$ is known in its bulk form to be a room temperature ferromagnet. Its layered nature makes it a particularly promising material in the search for a 2D magnet at room temperature. Over the last few years, several works have started to explore its properties, including magnetic one, for more-or-less thin layers, in some cases down to the 2D limit. Layer-dependent changes in the magnetic properties have been reported [1–6], but several contradicting results have appeared [7]. The current understanding [7] is that the unambiguous characterization of the material's composition and structure is hard to achieve, while several possible Cr-Te polymorphs are (meta)stable; additionally the material can transform into different phases depending on various factors, especially related to temperature and to long-term exposure to air. Recent experimental works showed that exfoliated $CrTe_2$ has an in-plane spontaneous magnetization above room temperature, low coercivity, and hosts Neel-type domain walls [2]. we have now explored such exfoliated thin flakes deposited on different substrates, with inelastic light scattering techniques. Our first purpose is to track phonon vibrations and how they evolve with temperature, from about 4 K to 500 K, in a temperature range where the material is expected to remain in its 1T phase. We observe a characteristic, almost linear variation of the phonon's energy with temperature, with no characteristic saturation of the energy changes when reaching the lowest temperatures, in contrast to most van der Waals materials [8]. Above 500 K, we find that the CrTe2 phonon peaks progressively loose intensity, and in the meantime other peaks appear, indicative of a structural/compositional change of the material (which relates to changes of the magnetic properties). Finally, we also sought for another kind of inelastic light scattering process, namely the excitation of magnons that are essentially unexplored in this material. So far, our low energy (E_{cutoff} ~1 meV) magneto-Raman scattering experiments could not detect such excitations down to low temperature (4 K) or under intense magnetic fields.

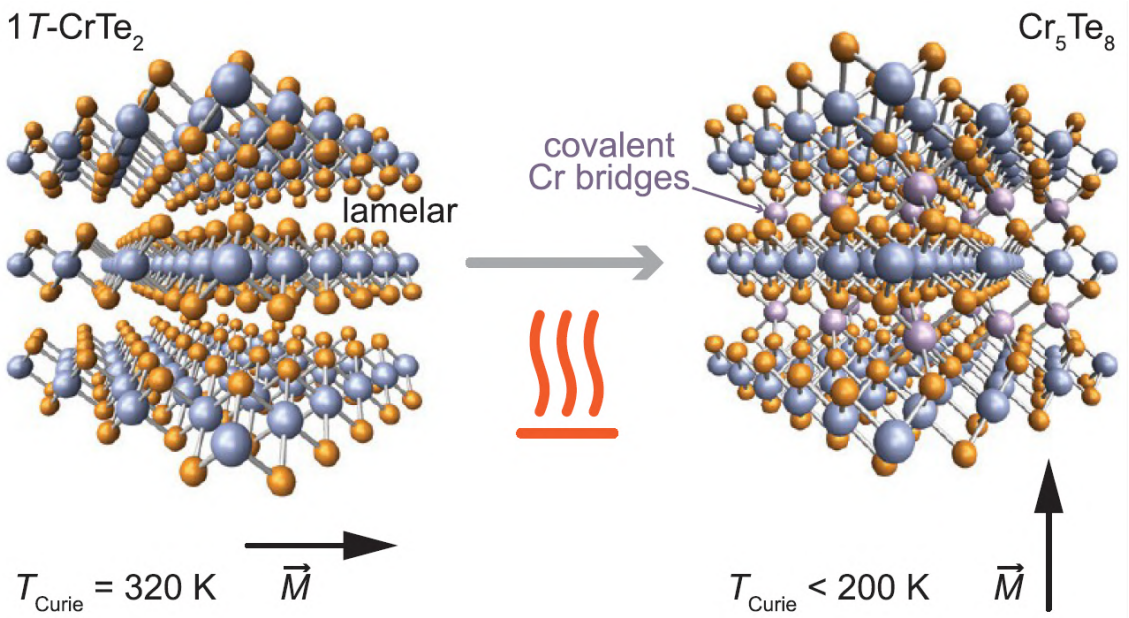

Figure 1: Transformation of $CrTe_2$ into Cr5Te8 by heating [7].

References

[1] Xingdan Sun, Wanying Li, Xiao Wang, et al. Room temperature ferromagnetism in ultra-thin van der Waals crystals of 1T-CrTe2. *Nano Research* 13, 3358–3363 (2020).

[2] Anike Purbawati, Johann Coraux, Jan Vogel, et al. In-Plane Magnetic Domains and Néel-like Domain Walls in Thin Flakes of the Room Temperature CrTe2 Van der Waals Ferromagnet. *ACS Applied Materials & Interfaces* 12, 30702–30710 (2020).

[3] Lingjia Meng, Zhang Zhou, Mingquan Xu, et al. Anomalous thickness dependence of Curie temperature in air-stable two-dimensional ferromagnetic 1T-CrTe2 grown by chemical vapor deposition. *Nature Communications* 12 (2021).

[4] Yizhe Sun, Pengfei Yan, Jiai Ning, et al. Ferromagnetism in two-dimensional CrTe2 epitaxial films down to a few atomic layers. *AIP Advances* 11, 035138 (2021).

[5] Xiaoqian Zhang, Qiangsheng Lu, Wenqing Liu, et al. Room-temperature intrinsic ferromagnetism in epitaxial CrTe2 ultrathin films. *Nature Communications* 12 (2021).

[6] Jing-Jing Xian, Cong Wang, Jin-Hua Nie, et al. Spin mapping of intralayer antiferromagnetism and field-induced spin reorientation in monolayer CrTe2. *Nature Communications* 13 (2022).

[7] Anike Purbawati, Suman Sarkar, Sébastien Pairis, et al. Stability of the In-Plane Room Temperature van der Waals Ferromagnet Chromium Ditelluride and Its Conversion to Chromium-Interleaved CrTe2 Compounds. *ACS Applied Electronic Materials* 5, 764–774 (2023).

[8] Siqi Zhu and Wei Zheng. Temperature-Dependent Phonon Shifts in van der Waals Crystals. *The Journal of Physical Chemistry Letters* 12, 5261–5270 (2021).

Poster 1.36, November 14th, 16h30–18h30

Proximity effects in molecular beam epitaxy grown van der Waals ferromagnet Cr_2Te_3 on two-dimensional layers

Quentin Guillet[1], Hervé Boukari[2], Libor Vojacek[1], Djordje Dosenovic[3], Hanako Okuno[3], Fatima Ibrahim[1], Jing Li[4], Céline Vergnaud[1], Alain Marty[1,*], Frédéric Bonell[1], Mairbek Chshiev[1], and Matthieu Jamet[1]

[1]*Univ. Grenoble Alpes, CEA, CNRS, IRIG-SPINTEC 38000 Grenoble, France*
[2]*Univ. Grenoble Alpes, CNRS, Institut Neel, 38000 Grenoble, France*
[3]*Univ. Grenoble Alpes, CEA, CNRS, IRIG-MEM 38000 Grenoble, France*
[4]*CEA, LETI, Univ. Grenoble Alpes, 38000 Grenoble, France*
*alain.marty@cea.fr

Achieving the large-scale growth of 2D ferromagnetic materials with high Curie temperature and perpendicular magnetic anisotropy is highly desirable for the development of future ultra-compact magnetic sensors or magnetic memories. In this context, van der Waals (vdW) Cr_2Te_3 appears as a promising candidate. It exhibits strong perpendicular magnetic anisotropy and a Curie temperature in bulk of 180 K. In this work, we will demonstrate the growth of quasi-freestanding few layers of Cr_2Te_3 on various 2D, which exhibit strong variation in terms of magnetic anisotropy with the crystal structure and exotic magnetotransport properties with of charge transfer from the 2D substrates.

The newly discovered class of two-dimensional (2D) ferromagnetic materials like CrI_3 [1] and $Cr_2Ge_2Te_6$ [2] has raised a great interest in the scientific community. 2D ferromagnets with Curie temperatures (T_c) higher than room temperature and perpendicular magnetic anisotropy (PMA) are required for future applications in the field of spintronics [3]-[4]. We report here the successful epitaxial growth of 5 layers of van der Waals (vdW) Cr_2Te_3 layers achieved by molecular beam epitaxy (MBE) on various vdW substrates such as monolayer (ML) graphene/SiC(001), monolayer WSe_2/GaAs(111) and few layers of Bi_2Te_3/Al_2O_3 [5]. This material was reported to have varying T_c up to 350 K and magnetic anisotropy depending on its the stoichiometry [6].

We obtain single crystalline Cr_2Te_3 layers on a cm scale, as shown by reflection high-energy electron diffraction (RHEED) (Fig. 1A). We also perform post-growth imaging of the heterostructure (Fig. 1B) using Transmission electron microscopy (TEM). We clearly observe a vdW gap at the interface suggesting that the ferromagnet is in a quasi-freestanding state. We also resolve a difference between full and partially filled planes of chromium (see Fig. 1B for the crystal structure). A full structural analysis is performed as well using x-ray diffraction. The quality of the 2D layers is studied by Raman spectroscopy and the Cr_2Te_3 stoichiometry is verified using Rutherford back scattering (RBS) measurements. We find contraction in-plane, which is mostly vanishing after annealing.

SQUID magnetometry shows perpendicular magnetic anisotropy and long-range ferromagnetic order for all vdW heterostructures studied here (Fig. 1C). X-ray magnetic circular dichroism (XMCD) is also performed to verify the origin of the magnetic signal. We also find a distribution of coercive field and magnetic anisotropy of the various layers, that we attribute to structural deviations. To support our experimental observations we performed first principle calculations that confirm a good correlation between the magnetic anisotropy and the out-of-plane lattice parameter of Cr_2Te_3 (Fig. 1D). All our samples have a Curie temperature close to 180 K, and we conclude that the stoichiometry 2:3 of the layers measured by RBS is the driving factor that determines the Curie temperature of theses systems as reported in [6].

We report Hall resistivity measurement using Hall bars. We have access in our measurements to temperatures down to 2 K and magnetic fields up to 7 T and we measured longitudinal magnetoresistance as well as Hall signal. Spin textures such as skyrmions have been reported in heterostructures of Cr_2Te_3/Bi_2Te_3 due to interface Dzyaloshinskii-Moriya interaction [7]. We find non trivial phenomena including a change of sign of the anomalous Hall contribution with temperature (Fig. E), which we correlate to a charge transfer between the 2D substrate layers and the vdW ferromagnet. The origin of the effect is related to the Berry phase of Cr_2Te_3. When the Fermi level of the system is changed by proximity of a 2D material or disorder, the temperature dependence of the anomalous Hall effect is tuned (Fig. E). We also report a "bump" in the Hall resistivity at the coercive field and we attribute these observations as possible topological effects or as two Hall contributions with opposite signs. Finally, we estimate the spin-orbit torques electrically generated in the 2D layers and acting on the vdW Cr_2Te_3 ferromagnet.

References

[1] Cheng Gong, Lin Li, Zhenglu Li, et al. Discovery of intrinsic ferromagnetism in two-dimensional van der Waals crystals. *Nature* 546, 265–269 (2017).

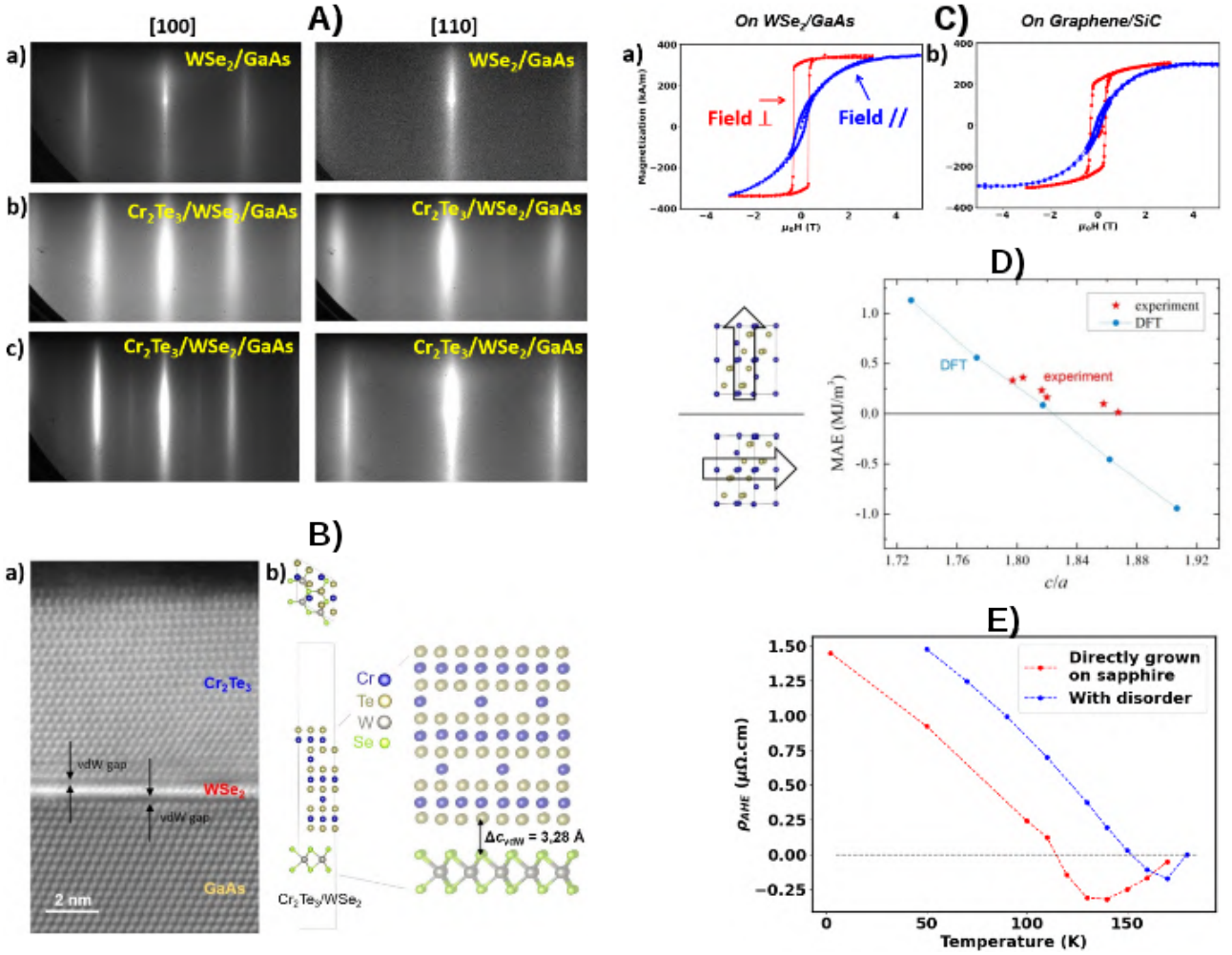

Figure 1: A) RHEED images during growth along two main crystal axis of the substrate. a) on grown WSe_2 b) After the growth of the ferromagnet at 300C. c) After annealing at 400C B) TEM image with the presence of a vdW gap at the interface and Supercells and slabs used for ab initio calculation C) Magnetization curves of 5 ML Cr_2Te_3 measured at 5 K. D) Magnetic anisotropy energy as a function of out-of-plane strain. DFT calculations confirm the experimental trend. E) Anomalous Hall contribution of five layers Cr_2Te_3 as function of temperature for 2 samples on sapphire.

[2] Bevin Huang, Genevieve Clark, Efrén Navarro-Moratalla, et al. Layer-dependent ferromagnetism in a van der Waals crystal down to the monolayer limit. *Nature* 546, 270 (2017).

[3] Qing Hua Wang, Amilcar Bedoya-Pinto, Mark Blei, et al. The Magnetic Genome of Two-Dimensional van der Waals Materials. *ACS Nano* 16, 6960–7079 (2022).

[4] Hyunsoo Yang, Sergio O Valenzuela, Mairbek Chshiev, et al. Two-dimensional materials prospects for non-volatile spintronic memories. *Nature* 606, 663 (2022).

[5] Quentin Guillet, Libor Vojáček, Djordje Dosenovic, et al. Epitaxial van der Waals heterostructures of Cr 2 Te 3 on two-dimensional materials. *Phys. Rev. Mater.* 7, 054005 (2023).

[6] Y. Fujisawa, M. Pardo-Almanza, J. Garland, et al. Tailoring magnetism in self-intercalated $Cr_{1+\delta}Te_2$ epitaxial films. *Physical Review Materials* 4, 114001 (2020).

[7] Junshu Chen, Linjing Wang, Meng Zhang, et al. Evidence for Magnetic Skyrmions at the Interface of Ferromagnet/Topological-Insulator Heterostructures. *Nano Letters* 19, 6144 (2019).

Ferromagnetism in exfoliated Fe_xGeTe_2 flakes

Banan El-Kerdi[1,*], Louis Lerey[1], João Sampaio[1], and Alexandra Mougin[1]

[1]*Université Paris-Saclay, CNRS, Laboratoire de Physique des Solides, 91405 Orsay, France*
*Banan.Kerdi@universite-paris-saclay.fr

Recently, long-range magnetism was reported in 2D dimensional materials [1, 2]. This has triggered immense research on exploring new phenomena [3, 4]. In particular, vdW magnets containing heavy elements like Fe_xGeTe_2 (FGT) [4–7] compounds – hence with potentially a sizable spin-orbit coupling (SOC) – are strong candidates for hosting perpendicular magnetic anisotropy (PMA) and Dzyaloshinskii–Moriya interaction (DMI). In FGT compounds, the Fe content largely determines the magnetic anisotropy (strong PMA in Fe_3GeTe_2, often easy plane magnetization in Fe_5GeTe_2) and the T_C (230 K in Fe_3GeTe_2, 300 K in Fe_5GeTe_2). A variety of magnetic behaviors was observed in FGT, with reports of ferrimagnetism/ferromagnetism, the occurrence of metastable magnetic configurations dependent on the thermal history, and a significant influence of Fe vacancies [**albarakati2019antisymmetric**, 4–8].

These observations call for the development of new strategies to engineer and understand the magnetism in a controlled way. One approach would rely on epitaxially grown continuous films with high crystallinity and PMA down to the single monolayer. This requires a refine expertise and provides impressive results as demonstrated in [9, 10] for example. We started recently another approach based on exfoliation, as developed in [11], with the aim to perform a complete investigation of the magnetic properties of the FGT flakes in temperature : hysteresis loops, magnetic imaging by magneto-optical Kerr microscopy and direct DMI measurements by Brillouin Light Scattering. Optical microscopy and AFM experiments can be also performed to identify details and measure the thickness of suitable flakes.

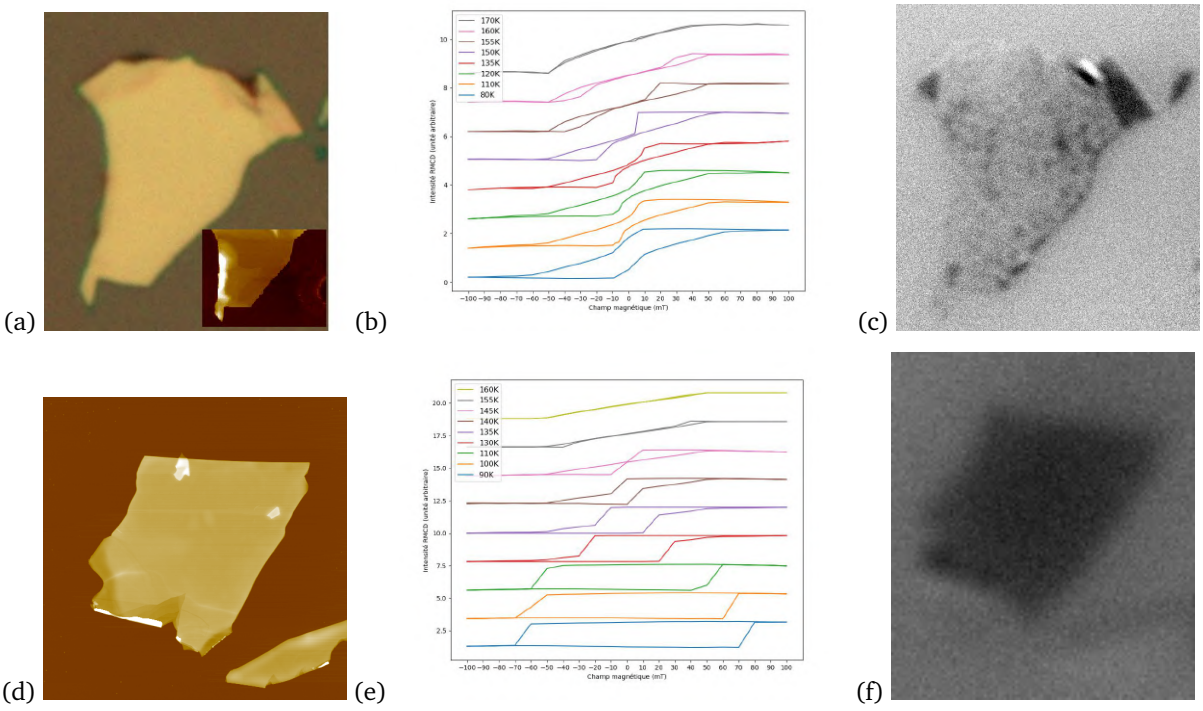

Figure 1: Exfoliated Fe_3GeTe_2 flakes : (a) Optical image of a F_3GT flake of thickness ≈38 nm in its center (From AFM -insert) and 15 μmm maximum in width. (b) Hysteresis loops measured by PMOKE versus temperature. (c) Magnetic domains without applied field at 110 K. (d) AFM image (15x15μm^2) of a F_3GT flake of thickness ≈50 nm in its center. (e) Hysteresis loops measured by PMOKE versus temperature. (f) No magnetic domains without applied field at 110 K.

We fabricated FGT flakes by exfoliating commercial bulk crystals onto Si/SiO_x substrate. Different exfoliation protocols (scotch tapes, PDMS, temperature) have been used to obtain large and as thin as possible FGT flakes. Once the FGT flakes have been deposited on the substrate, the samples were put in an oxygen plasma for a few minutes to remove any residual traces of tape. This cleaning method most likely causes oxidation of the FGT flakes but all other chemical cleaning methods gave unsatisfactory results. We could prepare both F_3GT and F_5GT flakes, with a large panel of thicknesses and lateral sizes. Both families exhibit ferromagnetic behavior. As expected from literature, we observe a decrease of T_C with

the thickness. F_5GT flakes exhibit a larger T_C than F_3GT ones. Regardless of the Fe content, most flakes are out-of-plane magnetized. Depending on the thickness, square and remnant hysteresis or domains are observed without magnetic field. Investigations are ongoing (including EHE and contacting experiments to inject currents) and we will discuss these and the following results during the colloquium.

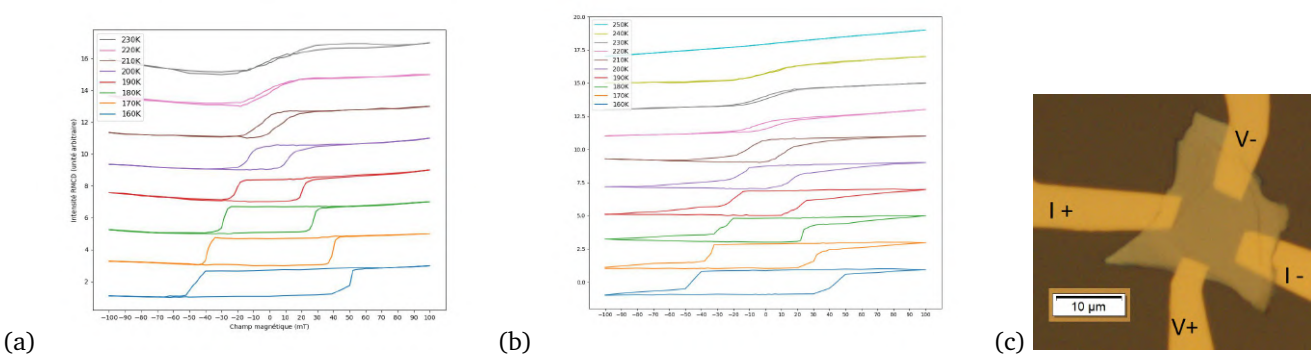

Figure 2: Exfoliated Fe_5GeTe_2 flakes (a) Hysteresis loops measured by PMOKE versus temperature in a 120 nm thick (a) and 45 nm thick (b) flake. (c) Optical image of a Hall cross of Fe_5GeTe_2 with 3 μm wide contacts for EHE.

This work was supported by the Agence Nationale de la Recherche (ANR) through the project ACAF (ANR-20-CE30-0027), and by the public grant overseen by the ANR as part of the 'Investissement d'Avenir' programme (LABEX NanoSaclay, ANR-10-LABX-0035 CHIVAWAA).

References

[1] Cheng Gong, Lin Li, Zhenglu Li, et al. Discovery of intrinsic ferromagnetism in two-dimensional van der Waals crystals. *Nature 2017 546:7657* 546, 265–269 (7657 2017).

[2] Yujun Deng, Yijun Yu, Yichen Song, et al. Gate-tunable room-temperature ferromagnetism in two-dimensional Fe3GeTe2. *Nature 2018 563:7729* 563, 94–99 (7729 2018).

[3] Yun Zhang, Haiyan Lu, Xiegang Zhu, et al. Emergence of kondo lattice behavior in a van der waals itinerant ferromagnet, Fe3GeTe2. *Science Advances* 4 (1 2018).

[4] Hongrui Zhang, David Raftrey, Ying Ting Chan, et al. Room-temperature skyrmion lattice in a layered magnet (Fe0.5Co0.5)5GeTe2. *Science Advances* 8, 7103 (12 2022).

[5] Bei Ding, Zefang Li, Guizhou Xu, et al. Observation of Magnetic Skyrmion Bubbles in a van der Waals Ferromagnet Fe3GeTe2. *Nano Letters* 20, 868–873 (2020).

[6] Yingying Wu, Senfu Zhang, Junwei Zhang, et al. Néel-type skyrmion in WTe2/Fe3GeTe2 van der Waals heterostructure. *Nature Communications 2020 11:1* 11, 1–6 (1 2020).

[7] Tae Eon Park, Licong Peng, Jinghua Liang, et al. Néel-type skyrmions and their current-induced motion in van der Waals ferromagnet-based heterostructures. *Physical Review B* 103, 104410 (10 2021).

[8] Andrew F. May, Craig A. Bridges, and Michael A. McGuire. Physical properties and thermal stability of Fe5-x GeTe2 single crystals. *Physical Review Materials* 3, 104401 (10 2019).

[9] Thomas Guillet, Regina V. Galcera, Juan F. Sierra, et al. *Spin-orbit torque switching in 2D ferromagnet / topological insulator heterostructure grown by molecular beam epitaxy*. 2023. arXiv: 2302.01101 [cond-mat.mes-hall].

[10] Mário Ribeiro, Giulio Gentile, Alain Marty, et al. Large-scale epitaxy of two-dimensional van der Waals room-temperature ferromagnet Fe5GeTe2. *npj 2D Materials and Applications 2022 6:1* 6, 1–9 (1 2022).

[11] Banan El-Kerdi, André Thiaville, Stanislas Rohart, et al. Evidence of large Dzyaloshinskii Moriya interaction at the cobalt/hexagonal boron nitride interface. *Nano Letters* 12, 21 (2022).

Spintronics with black phosphorus

H. Wei[1,*], M. Galbiati[1], J. Peiro[1], SMM Dubois[3], F. Brunnett[1], V. Zatko[1], R.Galceran[1], P.Brus[2], F.Godel[1], D.Perconte[1], F.Bouamrane[1], E. Gaufrès[4], A. Loiseau[4], O.Bezencenet[2], B.Servet[2], F.Petroff[1], JC Charlier[3], M.-B.Martin[1], B.Dlubak[1], and P.Seneor[1]

[1]*Unité Mixte de Physique, CNRS, Thales, Université Paris-Saclay, 91767 Palaiseau, France*
[2]*Thales Research and Technology, Palaiseau, France*
[3]*Institute of Condensed Matter and Nanosciences (IMCN), Université Catholique de Louvain, B-1348 Louvain-la- Neuve, Belgium*
[4]*Laboratoire d'Étude des Microstructures (LEM), CNRS, ONERA, Université Paris-Saclay, 92322 Châtillon, France*
*hao.wei@cnrs-thales.fr

Spintronics is a paradigm focusing on spin as the information vector in fast and ultra-low-power non- volatile devices such as the new spin-transfer-torque Magnetic Radom Access Memory (MRAM). Beyond its widely distributed applications, spintronics aims at providing more complex architectures and a powerful beyond CMOS solution from storage to quantum information. The recent discovery of graphene, and other 2D materials such as hexagonal boron nitride (h-BN) or dichalcogenides (WS_2...), has opened novel exciting opportunities in terms of functionalities and performances for spintronics devices[1]. Typically, graphene has shown a strong versatility by providing both highly efficient spin information transport properties[2, 3] and potential for strong spin filtering in 2D- MTJs[1]. However, the lack of a gap has led to extensive research to find a semiconducting sibling of graphene that would display its good properties in addition to a gap.

In this direction, Black phosphorus (BP) has attracted an explosive interest since 2014 as it displays major properties for (opto-)electronic devices: (a) high hole and electron mobilities in thin layers exfoliated BP (about 3000 cm^2/Vs) and (b) high ON/OFF current ratio (about 10^5) in a transistor configuration with ambipolar characteristics. Additionally, the bandgap of BP is predicted to be widely tunable in relation to the number of stacked layers and remains direct from the bulk to the monolayer. Thanks to the natural low spin-orbit coupling of phosphorus, BP is expected to present highly efficient spin information transport, similarly to graphene [2, 3] but with the addition of a band gap. This difference with graphene is fundamental for the implementation of spin manipulation schemes and the experimental realization of a spin gate.

However, the key issue for BP devices has been the handling of its degradation under atmospheric conditions. While the mechanism has been well understood[4] this still remains a clear problem for applications. We will present a recently developed in-situ approach to circumvent the issue of degradation under atmospheric conditions [5, 6]. By passivating the BP without exposing it to air we achieve protection down to the monolayer with 1 nm Al_2O_3. We will further discuss how this passivation layer can play the role of the tunnel barrier required for efficient spin injection [2, 3, 6] and provide a high potential path for spintronics applications from vertical to lateral devices. In addition, we will talk about the demonstration of BP integration into Co/BP/Co spin valves showing large spin signals. We will discuss a novel selective spin-splitted transport mechanism as supported by first-principle theoretical investigation. This illustrate the potential of BP for spin injection/detection, strongly supporting BP's vision as an outstanding platform for spintronics.

References

[1] Maëlis Piquemal-Banci, Regina Galceran, Marie-Blandine Martin, et al. 2D-MTJs: introducing 2D materials in magnetic tunnel junctions. *Journal of Physics D: Applied Physics* 50, 203002 (2017).

[2] Bruno Dlubak, Marie-Blandine Martin, Cyrile Deranlot, et al. Highly efficient spin transport in epitaxial graphene on SiC. *Nature Physics* 8, 557–561 (2012).

[3] P. Seneor, B. Dlubak, M.-B. Martin, et al. Spintronics with graphene. *MRS Bulletin* 37, 1245–1254 (2012).

[4] Alexandre Favron, Etienne Gaufrès, Frédéric Fossard, et al. Photooxidation and quantum confinement effects in exfoliated black phosphorus. *Nature Materials* 14, 826–832 (2015).

[5] R. Galceran, E. Gaufres, A. Loiseau, et al. Stabilizing ultra-thin black phosphorus with in-situ-grown 1 nm-Al_2O_3 barrier. *Applied Physics Letters* 111, 243101 (2017).

[6] L.-M. Kern, R. Galceran, V. Zatko, et al. Atomic layer deposition of a MgO barrier for a passivated black phosphorus spintronics platform. *Applied Physics Letters* 114, 053107 (2019).

Epitaxial Fe_NGeTe_2 van der Waals films: exploring heterostructure stacking for enriched magnetic properties

V. Polewczyk[1,*], J. Courtin[1], C. Jego[1], I. De Moraes[1], C. Vergnaud[1], A. Marty[1], M. Jamet[1], and F. Bonell[1]

[1]*University Grenoble Alpes, CNRS, CEA, IRIG-Spintec, F-38000 Grenoble, France*
vincent.polewczyk@cea.fr

The replacement of bulk materials with two-dimensional (2D) ones based on van der Waals (vdW) layered structures holds promises for overcoming the approaching quantum limit in electronic device scaling. Among these 2D compounds, magnetic materials, initially discovered in 2017 with exfoliated flakes of $Cr_2Ge_2Te_6$ [1] and CrI_3 [2], are of utmost interest. Their discovery opened up a rich avenue for using the electron spin as an additional degree of freedom in 2D materials, but also leading to the identification of other 2D vdW magnets, especially the metallic ones. Among these, the Fe_NGeTe_2 (FGT) ternary compounds have attracted significant attention due to their ferromagnetism with strong magnetic anisotropy near room temperature: perpendicular magnetic anisotropy (PMA) up to 230 K and easy plane magnetic anisotropy up to 290 K for Fe_3GeTe_2 (F3GT) [3] and Fe_5GeTe_2 (F5GT) [4], respectively. Notably, the Curie temperature (Tc) and magnetic anisotropy of FGT materials can be easily tailored, making them highly desirable for specific applications. To achieve this, various methods are employed such as ionic gating, ion implantation, patterning methods, and doping/substitution with Co for instance [5]. An alternative approach is through interface engineering, especially in full vdW heterostructures that offer interface abruptness and cleanliness beyond what is achievable with traditional metals or oxides [6]. However, limited studies have been conducted on these magnetic systems, mostly due to the complexity of the film growth process. The most accurate technique for film growth is molecular beam epitaxy (MBE), which allows for reliable and fully controlled deposition of high-quality films over large areas.

In this context, our focus is on the all-epitaxial F5GT/F3GT heterostructures, with a particular emphasis on varying the stacking order and layer thicknesses down to their 2D limits.

We performed MBE growth of highly-crystalline F3GT and F5GT vdW magnets, both in single and bilayer forms, and closely investigated their structural and magnetic properties using *in situ* reflection high-energy electron diffraction (RHEED) and *ex situ* x-ray diffraction (XRD), as well as magneto-optical Kerr effect (MOKE) techniques, respectively. To explore and fully master the growth conditions, we varied several deposition parameters, including deposition flux, deposition temperature, and annealing conditions. We discovered more restricted conditions for F5GT growth compared to F3GT, probably reflecting its thermodynamic instability. This is a crucial observation since the film growth quality significantly affects the magnetic properties. While a standard deposition process typically results in the expected magnetic properties for bulk materials with thicknesses above a few monolayers (ML), such as PMA with a large magnetic coercive field for F3GT and easy-plane magnetic anisotropy with a small coercive field for F5GT, we also observed an increase in their Tc up to 400 K after optimization. This was accomplished by deliberately and carefully varying the growth conditions. When combining two FGT compounds in a vdW heterostructure, numerous properties were observed varying the stacking, including a decoupled behavior for thick layers for instance, and revealing the simultaneous presence of both robust easy-plane and PMA at their respective ordering temperatures. In specific conditions, we also detected a ferromagnetic behavior above room temperature, retaining strong PMA. A typical example of this highly crystalline heterostructure is shown in the Fig. 1 with distinct and continuous RHEED diffraction streaks in (a), intense diffracting peaks of the (000l) planes of the vdW layers in (b), and the magnetic behavior in (c).

The successful stacking of FGT films opens up opportunities for the design and fabrication of ultra-compact advanced spintronic devices with enhanced functionality and performance thanks to the tunability of magnetic properties. These findings not only highlight the potential of FGT but also serve as a prototypical example that can be extended to other 2D systems.

Acknowledgments

This work has been performed in the framework of the ANR ELMAX project (ANR-20-CE24-0015) and MNEMOSYN FLAG-ERA graphene basic research project (ANR-21-GRF1-0005-01). The French National Research Agency (ANR) is acknowledged for its support through the ESR/EQUIPEX+ ANR-21- ESRE-0025 2D MAG projects. The LANEF framework (No. ANR-10-LABX-0051) is acknowledged for its support with mutualized infrastructure.

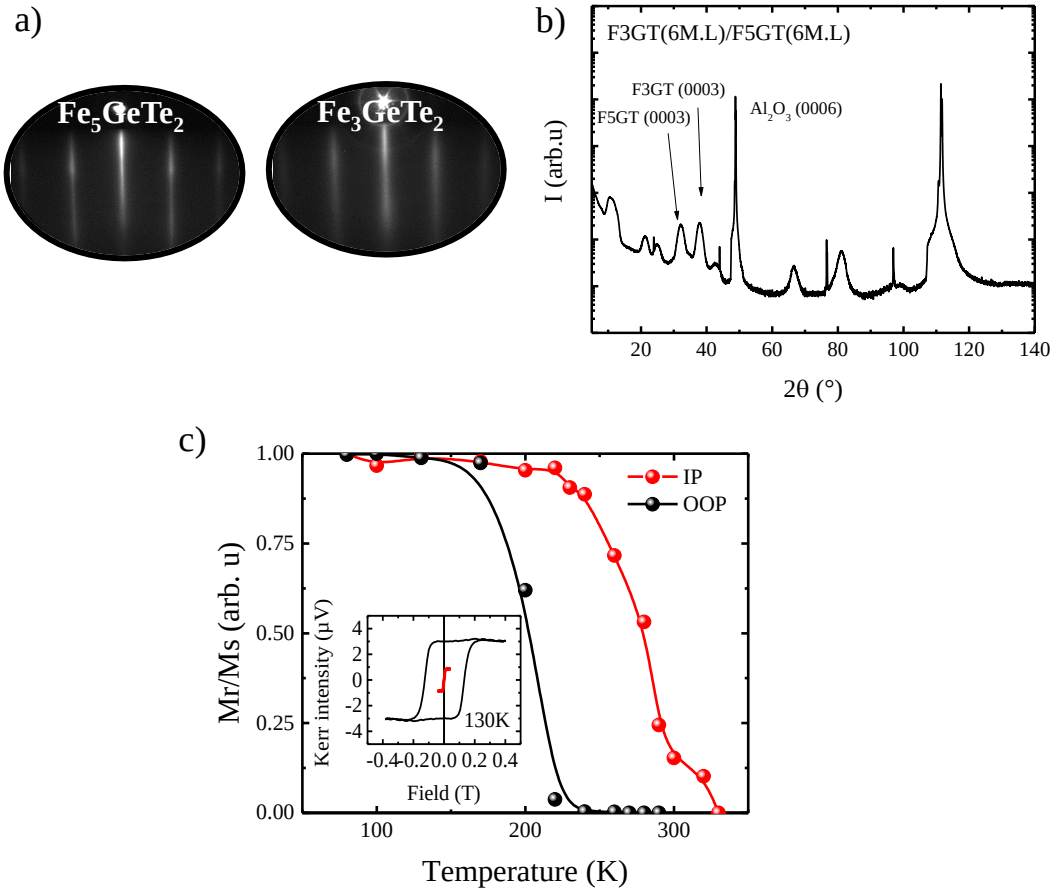

Figure 1: Structural and magnetic properties of an epitaxial Al_2O_3(0001)//F5GT(6ML)/F3GT(6ML) heterostructure. (a) RHEED patterns collected at the growth temperature (650 K) along the [11-20] azimuth, (b) specular X-ray diffraction scan and (c) in-plane (IP) and out-of-plane (OOP) remanence magnetization (Mr) over saturation magnetization (Ms) recorded with MOKE. Inset: corresponding magnetic hysteresis loops at 130K.

References

[1] Cheng Gong, Lin Li, Zhenglu Li, et al. Discovery of intrinsic ferromagnetism in two-dimensional van der Waals crystals. *Nature* 546, 265–269 (2017).

[2] Bevin Huang, Genevieve Clark, Efrén Navarro-Moratalla, et al. Layer-dependent ferromagnetism in a van der Waals crystal down to the monolayer limit. *Nature* 546, 270–273 (2017).

[3] Zaiyao Fei, Bevin Huang, Paul Malinowski, et al. Two-dimensional itinerant ferromagnetism in atomically thin Fe3GeTe2. *Nature materials* 17, 778–782 (2018).

[4] Mario Ribeiro, Giulio Gentile, Alain Marty, et al. Large-scale epitaxy of two-dimensional van der Waals room-temperature ferromagnet Fe5GeTe2. *npj 2D Materials and Applications* 6, 10 (2022).

[5] Andrew F May, Mao-Hua Du, Valentino R Cooper, and Michael A McGuire. Tuning magnetic order in the van der Waals metal Fe5GeTe2 by cobalt substitution. *Physical Review Materials* 4, 074008 (2020).

[6] K S Novoselov, Artem Mishchenko, o A Carvalho, and AH Castro Neto. 2D materials and van der Waals heterostructures. *Science* 353, aac9439 (2016).

Poster 1.40, November 14th, 16h30–18h30

TMD Engineering of 2D-Magnetic Tunnel Junctions – From Barriers to Electrodes

Frederic Brunnett[1,*], H. Wei[1], J. Peiro[1], V. Zatko[1], S. M.-M. Dubois[2], M. Galbiati[1], O. Bezencenet[3], B. Servet[3], M. Och[4], C. Mattevi[4], F. Godel[1], J.-C. Charlier[2], M.-B. Martin[1], B. Dlubak[1], and P. Seneor[1]

[1]*Unité Mixte de Physique CNRS/Thales-Université Paris-Saclay, Palaiseau, France*
[2]*Institute of Condensed Matter and Nanosciences (IMCN), Université Catholique de Louvain, Louvain-la-Neuve, Belgium*
[3]*Thales Research and Technology, Palaiseau, France*
[4]*Department of Materials, Imperial College, London, UK*
Frederic.Brunnett@cnrs-thales.fr

Spin-based electronics has already revolutionized data storage and readout technologies. Nowadays it targets a variety of new architectures like embedded MRAMs, spin logics or neuromorphic computing, which makes it one of the most promising post-CMOS approaches. Meanwhile, 2D materials and their combination in heterostructures have opened novel exciting opportunities in terms of functionalities and performances for spintronics devices. The broad family of 2D materials offers many possibilities to engineer the properties of layered stacks and devices in particular via interfacial exchange and proximity effects. One very attractive topic is the field of MTJs based on 2D materials (2D-MTJs).[1]

Indeed, graphene has proved its strong potential for MTJs with evidence for spin-filtering through band structure or strong hybridization effects (i.e. spinterface) achieving a record spin polarization of up to -98% . In parallel, advances within the broad Transition Metal Dichalcogenides family of 2D semiconductors and recent 2D ferromagnets have opened new possibilities to tailor spintronics properties further. As an example, we will show how TMDs could be integrated into a hybrid spin-valves 2D-MTJs and show layer-dependent spin filtering effects. We can show that the spin polarisation can be reversed depending on the number of layers. The layer thickness largely influences the band structure and thus allows control over the open spin channels for vertical electron transport. We will also discuss how to reach one step further with the large scale integration of these materials into tailored 2D heterostructures. For this we developed 2D ferromagnets based on $Fe_{3+x}GeTe_2$. We will show that they can be grown in large scale using Pulsed laser deposition (PLD) and reach curie Temperatures (T_C) above room temperature (RT) while being integrated with other TMDs. Thus, allowing the design of in-situ fabricated devices with artificial properties. We will highlight how these PLD grown ferromagnetic 2D layers could further reinforce the 2D materials family's potential for 2D-MTJs.[2–5]

References

[1] Maëlis Piquemal-Banci, Regina Galceran, Marie-Blandine Martin, et al. 2D-MTJs: introducing 2D materials in magnetic tunnel junctions. *Journal of Physics D: Applied Physics* 50, 203002 (2017).

[2] Victor Zatko, Marta Galbiati, Simon Mutien-Marie Dubois, et al. Band-Structure Spin-Filtering in Vertical Spin Valves Based on Chemical Vapor Deposited WS_2. *ACS Nano* 13, 14468–14476 (2019).

[3] Victor Zatko, Simon Mutien-Marie Dubois, Florian Godel, et al. Band-Gap Landscape Engineering in Large-Scale 2D Semiconductor van der Waals Heterostructures. *ACS Nano* 15, 7279–7289 (2021).

[4] Victor Zatko, Simon M.-M. Dubois, Florian Godel, et al. Almost Perfect Spin Filtering in Graphene-Based Magnetic Tunnel Junctions. *ACS Nano* 16, 14007–14016 (2022).

[5] F. Brunnett et al. In preparation ().

Ab initio study of the Dzyaloshinskii-Moriya interaction and magnetic skyrmions in Fe_3GeTe_2 van der Waals heterostructures

Dongzhe Li[1,*], Soumyajyoti Haldar[2], and Stefan Heinze[2,3]

[1]*CEMES, Université de Toulouse, CNRS, 29 rue Jeanne Marvig, F-31055 Toulouse, France*
[2]*Institute of Theoretical Physics and Astrophysics, University of Kiel, Leibnizstrasse 15, 24098 Kiel, Germany*
[3]*Kiel Nano, Surface, and Interface Science (KiNSIS), University of Kiel, Germany*
**dongzhe.li@cemes.fr*

Magnetic skyrmions – topologically protected chiral spin structures with particle-like properties – show great promise for spintronic applications. The recent discovery of two-dimensional (2D) magnets opened new opportunities for topological spin structures in atomically thin van der Waals (vdW) materials [1–4]. In this talk, using first-principles and atomistic spin simulations, I will present how external stimuli can efficiently tune different magnetic interactions in Fe_3GeTe_2 (FGT) vdW heterostructures [5]. In particular, the Dzyaloshinskii-Moriya interaction (DMI) is highly tunable by strain, leading to a very large DMI. After that, I will further show that the efficient control of the DMI, the exchange coupling, and the magnetic anisotropy energy by strain allows stabilizing zero-field skyrmions in FGT vdW heterostructures with diameters close to 10 nm, becoming technologically competitive [6]. Finally, if time allows, I will propose a vdW tunnel junction with nonmagnetic electrodes as an ideal sub-5nm skyrmion platform with easy implementation into device architectures (i.e., skyrmion racetrack memories). I will further demonstrate that the proposed tunnel junctions exhibit a reliable all-electrical detection scheme for magnetic skyrmions due to extremely large noncollinear magnetoresistance.

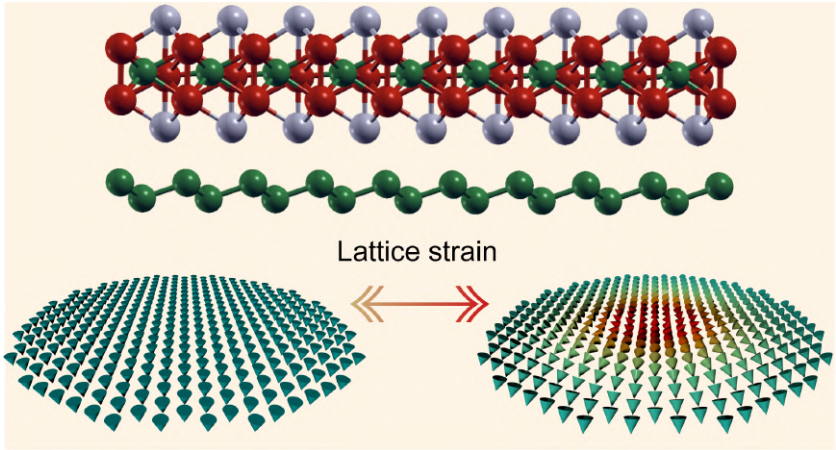

Figure 1: The emergence of magnetic skyrmions in Fe_3GeTe_2/gemanene by strain.

Acknowledgments

This study has been supported through the ANR Grant No. ANR-22-CE24-0019. This work has been (partially) supported through the grant NanoX no. ANR-17-EURE-0009 in the framework of the “Programme des Investissements d’Avenir". S. Haldar and S. Heinze. gratefully acknowledge financial support from the Deutsche Forschungsgemeinschaft (DFG, German Research Foundation) through SPP2137 “Skyrmionics" (project no. 462602351). This work was performed using HPC resources from CALMIP.

References

[1] B. Ding, Z. Li, G. Xu, et al. Observation of Magnetic Skyrmion Bubbles in a van der Waals Ferromagnet Fe_3GeTe_2. *Nano Lett.* 20, 868–873 (2020).

[2] Y. Wu, S. Zhang, J. Zhang, et al. Néel-type skyrmion in WTe_2/Fe_3GeTe_2 van der Waals heterostructure. *Nat. Commun.* 11, 3860 (2020).

[3] T.E. Park, L. Peng, J. Liang, et al. Néel-type skyrmions and their current-induced motion in van der Waals ferromagnet-based heterostructures. *Phys. Rev. B* 103, 104410 (2021).

[4] Y. Wu, B. Francisco, Z. Chen, et al. A Van der Waals Interface Hosting Two Groups of Magnetic Skyrmions. *Adv. Mater.* 34, 2110583 (2022).

[5] D. Li, S. Haldar, T. Drevelow, and S. Heinze. Tuning the magnetic interactions in van der Waals Fe_3GeTe_2 heterostructures: A comparative study of ab initio methods. *Phys. Rev. B* 107, 104428 (10 2023).

[6] D. Li, S. Haldar, and S. Heinze. Strain-Driven Zero-Field Near-10 nm Skyrmions in Two-Dimensional van der Waals Heterostructures. *Nano Lett.* 22, 7706–7713 (2022).

Poster 1.42, November 14th, 16h30–18h30

Spin transport in CrXY monolayers: multiscale computational study

Libor Vojáček[1,*], Joaquín Medina Dueñas[2], Jing Li[3], Fatima Ibrahim[1], Stephan Roche[2,4], Mairbek Chshiev[1,5], and José H. Garcia[2]

[1]*Univ. Grenoble Alpes, CEA, CNRS, SPINTEC, 38054 Grenoble, France*
[2]*Catalan Institute of Nanoscience and Nanotechnology (ICN2), CSIC and BIST, Campus UAB, Bellaterra, 08193 Barcelona, Spain*
[3]*Univ. Grenoble Alpes, CEA, Leti, F-38054, Grenoble, France*
[4]*ICREA–Institució Catalana de Recerca i Estudis Avançats, 08010 Barcelona, Spain*
[5]*Institut Universitaire de France, Paris 75231, France*
libor.vojacek@cea.fr

For applications in spintronics, spin-orbit torque (SOT) is an efficient mechanism to switch a magnetic layer electrically. By its nature, SOT is limited to controlling in-plane magnetization. An additional external magnetic field is often used to switch an out-of-plane magnetization, which is more relevant for applications. Recently, it has been shown that systems with a trigonal 3*m* (C_{3v}) symmetry group and Fermi surface warping can replace an external magnetic field to facilitate field-free spin-orbit-torque switching [1]. Based on *ab initio* calculations, we show that CrXY dichalcogenide Janus monolayers [Fig. 1(a)] have all three ingredients necessary for field-free SOT switching: the 3*m* symmetry, Fermi-surface warping, and a prominent Rashba splitting [Fig. 1(b)].

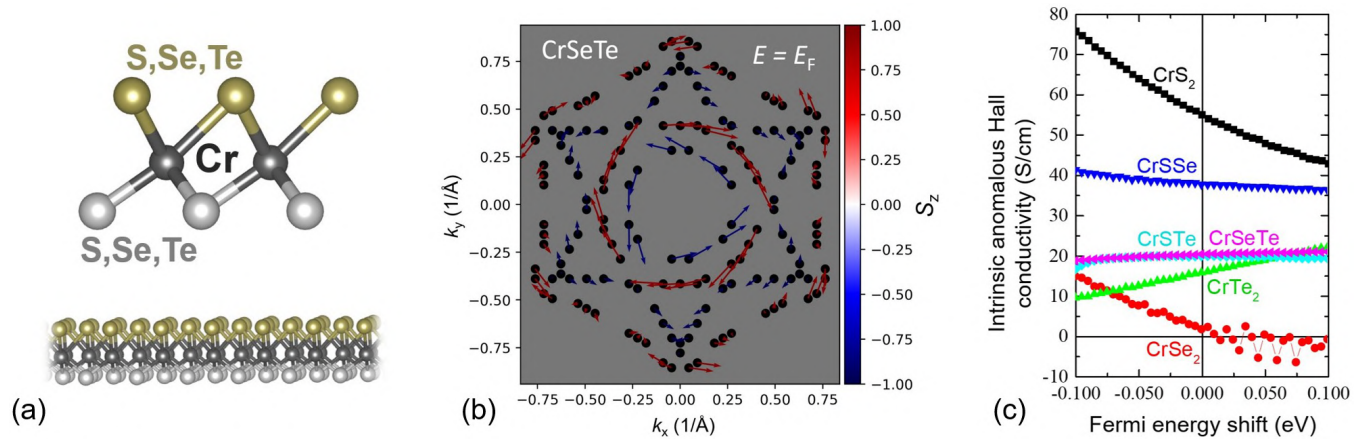

Figure 1: (a) The structure of 1T-CrXY monolayers. (b) The Fermi-level spin texture of CrSeTe showing prominent Rashba effect, hexagonal warping and second-order spin-orbit coupling terms. (c) Intrinsic anomalous Hall conductivity calculated from the Wannier tight-binding models.

The reciprocal-space spin textures exhibit complex forms which are shown to originate from higher-order terms in the in-plane momentum expansion of the spin-orbit Hamiltonian. With Wannier tight-binding models derived from the *ab initio* ground state, we calculate the resulting transport properties, including the different types of spin-orbit torques and the intrinsic anomalous Hall conductivity [Fig. 1(c)].

Acknowledgments

This project has received funding from the *European Union's Horizon 2020 research and innovation programme* under grant agreement No *800945* — NUMERICS — H2020-MSCA-COFUND-2017 and grant agreement 881603 (Graphene Flagship). We also acknowledge the French National Research Agency through the MAGICVALLEY project (ANR-18-CE24-0007).

References

[1] Diego García Ovalle, Armando Pezo, and Aurélien Manchon. Spin-orbit torque for field-free switching in C3v crystals. *Physical Review B* 107, 094422 (2023).

Poster 1.43, November 14th, 16h30–18h30

Spin-Crossover and Fragmentation of $Fe(neoim)_2$ on Ag and Au

Cyrille Barreteau[1,*], Sven Johannsen[2], Richard Berndt[2], Manuel Gruber[3], Troels Markussen[4], José Antonio Real[5], and Maksym Seredyuk[5,6]

[1]*Université Paris-Saclay, CEA, CNRS, SPEC, 91191 Gif-sur-Yvette, France*
[2]*Institut für Experimentelle und Angewandte Physik, Christian-Albrechts-Universität, 24098 Kiel, Germany*
[3]*Faculty of Physics and CENIDE, University of Duisburg-Essen, 47057 Duisburg, Germany*
[4]*Synopsys Denmark, Fruebjergvej 3, DK-2100 Copenhagen, Denmark*
[5]*Instituto de Ciencia Molecular (ICMol)/Departamento de Química Inorgánica, Universidad de Valencia, 46980 Paterna, Valencia, Spain*
[6]*Department of Chemistry, Taras Shevchenko National University of Kyiv, 64/13, Volodymyrska Street, 01601 Kyiv, Ukraine*
*cyrille.barreteau@cea.fr

Spin-crossover (SCO) molecules are metal-organic complexes that can be switched between a low-spin (LS) and high-spin (HS) state under the application of various stimuli such as pressure, temperature, light etc.[1] Deposition on a substrate can greatly affect the SCO properties.[2, 3]

A new neutral spin crossover complex $Fe(neoim)_2$has been synthesized and successfully evaporated and deposited intact on Ag(111). In addition the $Fe(neoim)_2$molecule exhibits a spin crossover switch when a sufficient voltage is applied between an STM tip and the metallic surface while the $Ni(neoim)_2$does not show such transition. Surprisingly the molecule fragments on a gold surface which is usually considered as the most "noble" metallic surface due to its inertness.

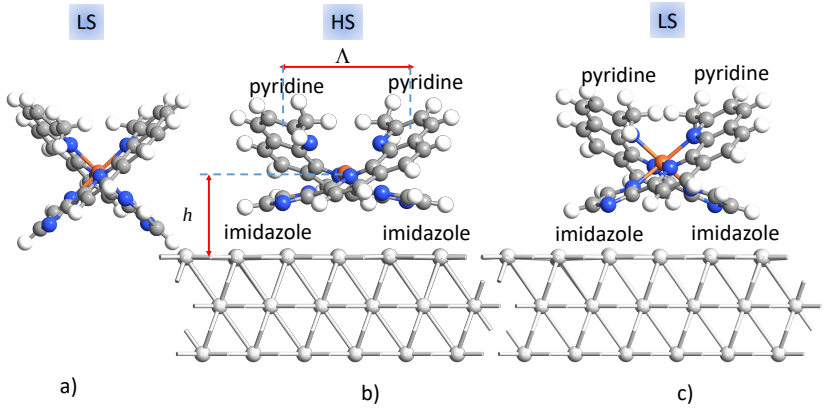

Figure 1: Sideview of a) an isolated $Fe(neoim)_2$ molecule and deposited on Ag(111) for both b) HS and c) LS states as obtained from DFT optimization. The flatteining of the molecule is clearly visible when adsorbed on the metallic substrate.

A very extensive Density Functional Theory (DFT) study using hybrid functional and van der Waals (vdW) correction will be presented to explain these results. The adjustment of the hybrid functional to reproduce correctly the LS-HS energy balance will first be discussed. Then we will show that the $Fe(neoim)_2$is drastically distorted by the interaction with the substrate (see Fig. 1) in particular by vdW forces that play an essential role in the energetic of this system. In particular dispersion interaction is decisive in the relative stability between HS and LS, favoring HS due to the largest flexibility of the HS configuration. In contrast $Ni(neoim)_2$does not exhibit any spin state switching. A detailed analysis to trace back the fragmentation mechanism of $Fe(neoim)_2$on gold will be provided. Interestingly the fragmentation originates from the combination of vdW interaction, which is often believed to be of secondary importance, and the specific electronic structure of Au (compared to Ag) due to scalar relativistic effects[4]. More specifically, the iron-gold interaction (significantly stronger than iron-silver) is at the origin of the fragmentation. These findings align seamlessly with the experimental results.[5]

Acknowledgments

We acknowledge financial support from the European Union's Horizon 2020 program, grant number 766726. JAR thanks Spanish Ministerio de Ciencia e Innovación (Grant PID2019-106147GB-I00 funded by MCIN/AEI/10.13039/501100011033). RB thanks Felix Tuczek and Alexandre Tkatchenko for discussions.

References

[1] Malcolm A. Halcrow, ed. *Spin-Crossover Materials: Properties and Applications*. Wiley, 2023.

[2] Kaushik Bairagi, Olga Iasco, Amandine Bellec, et al. Molecular-scale dynamics of light-induced spin cross-over in a two-dimensional layer. *Nature Communications* 7, 12212 (2016).

[3] Manuel Gruber and Richard Berndt. Spin-Crossover Complexes in Direct Contact with Surfaces. *Magnetochemistry* 6, 35 (2020).

[4] Neil Bartlett. Relativistic effects and the chemistry of gold. *Gold Bulletin* 31, 22–25 (1998).

[5] Sven Johannsen, Manuel Gruber, Cyrille Barreteau, et al. Spin-Crossover and Fragmentation of Fe(neoim)$_2$ on Ag and Au. *Submitted to ACS Nano* (2023).

The magnetic phase diagram of ternary $(Ni,Fe,Cr)_3O_4$ spinel oxides in epitaxial thin films: from the element specific magnetic behavior to magnetic modelling

Alban Simonnot[1, 2, *], Patrick Schoeffmann[3], Pâmella Vasconcelos Borges Pinho[4], Antoine Barbier[2], Alain Chartier[1], Frédéric Miserque[1], and Jean-Baptiste Moussy[2]

[1]*Université Paris-Saclay, CEA, Service de recherche en Corrosion et Comportement des Matériaux, 91191 Gif Sur Yvette, France*
[2]*Université Paris-Saclay, CEA/CNRS, Service de Physice de l'Etat Condensé, 91191 Gif sur Yvette, France*
[3]*Synchrotron Soleil, DEIMOS, L'orme des merisiers, 91190 Saint Aubin*
[4]*European Synchrotron Radiation Facility, 38000 Grenoble*
**alban.simonnot@cea.fr*

Due to the strong interactions among the spin, orbital, and lattice degrees of freedom, the transition metal oxides with the spinel-type structure, AB_2O_4 (with A, B= Fe, Cr, Ni...), exhibit complicated magnetic and structural phase transitions and have attracted extensive attention in past years [**buschow2003handbook**, **lee2002emergent**]. In this structure, the cations (e.g. Fe^{2+}/Fe^{3+}, Ni^{2+}, Cr^{3+}) occupy either the tetrahedrally coordinated (Td) sites or the octahedrally coordinated (Oh) sites with ferro- or antiferromagnetic interactions. The chromites, $Fe_{3-x}Cr_xO_4$ (with the parent compounds: $FeCr_2O_4$, Fe_2CrO_4, $NiCr_2O_4$), or the ferrites (Fe_3O_4, $NiFe_2O_4$) are considered significant due to their potential applications over a broad spectrum (ferrimagnetic, ferroelectric, multiferroic, or photoconductive behavior) [**wang2003situ**, **chambers2017electronic**, **ma2014magnetic**, **hoppe2015enhanced**, **pinho2023stoichiometry**].

In addition, the corrosion of Fe-Cr-Ni alloys at high temperature in an aqueous medium leads to complex phenomena: mixing passivation, dissolution and precipitation. It gives rise to a multiphase oxide layer for which several studies have emphasized the presence of a spinel-type structure [**sennour2010detailed**, **marchetti2015xps**]. This spinel oxide phase forms a continuous corrosion layer. It therefore plays a major role in corrosion processes because it governs the transport between the alloy and the aqueous medium. Surprisingly, the physical properties of $(Ni,Fe,Cr)_3O_4$ oxide layers are poorly documented because of its variable composition, complex microstructure and low thickness. Their magnetic properties critically depend on the site occupation and composition changes which enables the use of the magnetic response as a fine marker for understanding these materials.

To tackle the issue of complex microstructure and variable composition, we grow, above Al_2O_3 (111), model Fe-rich $Fe_{3-x-y}Cr_xNi_yO_4$ (111) and Cr-rich $Cr_{2-x}Fe_{x+y}Ni_{1-y}O_4$ (111) spinel layers by oxygen assisted molecular beam epitaxy (O-MBE). These layers are characterized both in-situ and ex-situ. The epitaxy and structure of layers are checked through in-situ diffraction, which shown nice streaks. This is characteristics of 2D growth mode. Then, the composition is checked by spectroscopy, both in-situ and ex-situ. And finally, the film thickness, structure and magnetic properties are verified through respectively reflectivity, diffraction and magnetometry. To determine the site occupation and charge of cations, XAS/XMCD measurements has been realized (Soleil Synchrotron). These experiments has been simulated with Crystal Field multiplet calculations to have the occupation and charge of each element with the Quanty code [**lu2014efficient**].

Our results indicate an occupation of the Oh sites for Ni in the Fe-rich region, as opposite in Cr rich region were Ni occupy Td sites. More surprisingly, Fe is found in the form Fe^{2+} in the Td site only if the sum of Ni and Cr in the ternary composition percentage rise above 33 %. Below this limit, Fe is shared between Oh and Td sites, with the Td site occupied only by Fe^{3+} and Oh site shared by Fe^{2+} and Fe^{3+} .

Tuning of high-frequency magnetic properties of doped $BaM_xM'_xFe_{12-2x}O_{19}$ composites

Maria Jose Vazquez Bernardez[1,*], Daniel Stoeffler[1], Christophe Lefevre[1], and Nicolas Vukadinovic[2]

[1]*Institut de Physique et Chimie des Matériaux, CNRS-Université de Strasbourg, 67034 Strasbourg, France*
[2]*Dassault Aviation, 92552 St-Cloud, France*
mariajose.vazquez@ipcms.unistra.fr

The development of frequency-adaptable electromagnetic wave absorbents has become a subject of increasing interest for microwave applications. Composites made up of chemically substituted M-type hexaferrite particles dispersed into a polymer matrix are promising absorbents with frequencies operating at Ku, K and Ka bands (from 12 GHz to 40 GHz). In order to serve as performant materials, these are required to present a strong absorption in a broad frequency band. In the context of this work, chemical substitution is presented as a tool allowing to modify the shape, the band width, and the frequency of the absorption spectra of $BaM_xM'_xFe_{12-2x}O_{19}$ composites.

Previous studies have demonstrated that the resonance frequency of $BaM_xM'_xFe_{12-2x}O_{19}$ ferrites can be modified via substitution of Fe^{3+} ions by other transition metal cations [1] like Mn^{2+} and Ti^{4+}. The substitution of Fe^{3+} by these ions allows to modify the anisotropy field $2K_1/M_s$, where K_1 is the first-order uniaxial anisotropy constant and M_s the saturation magnetization. Consequently, the resonance frequency of the magnetic particles is shifted through Kittel's relationship for the natural ferromagnetic resonance (FMR) [2]. Although existing numerous evidence of this phenomena, no explanation of the role of each substituent has been provided in literature, and there are many questions that have not been answered yet. The extraction of micromagnetic parameters from polycrystalline samples remains also a challenging task.

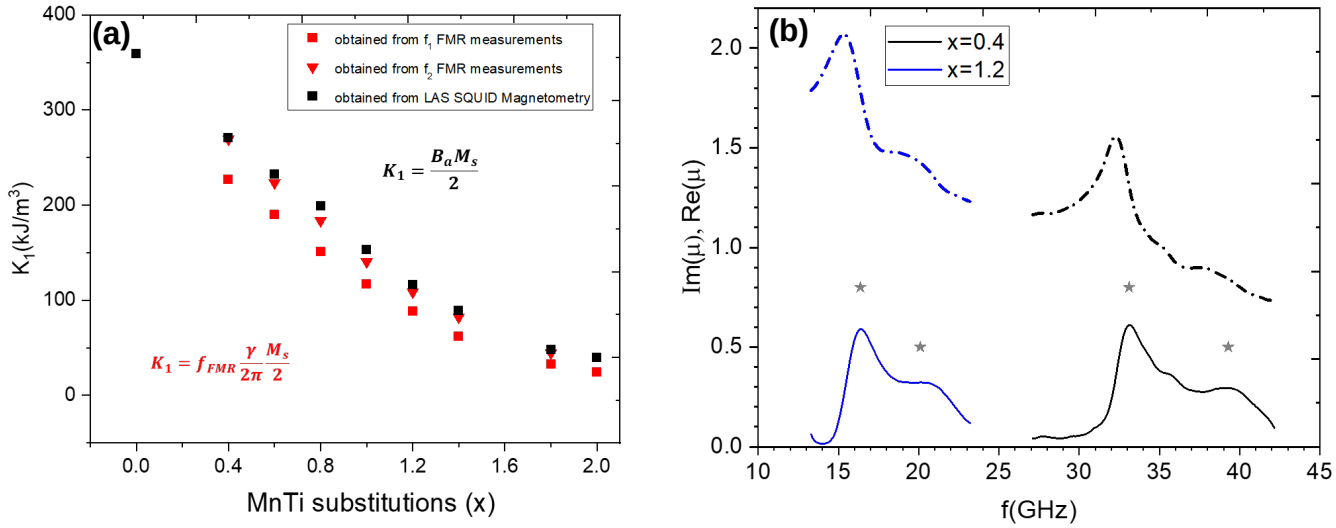

Figure 1: (a) Evolution of first order magnetic anisotropy with chemical substitution of $BaTi_xMn_xFe_{12-2x}O_{19}$ ferrite obtained from FMR and from the Law of Approach to Saturation (LAS) Analysis (b) Real (above) and Imaginary (below) experimental magnetic permeability spectra for $BaTi_xMn_xFe_{12-2x}O_{19}$ composites with x=0.4 and x=1.2.

For instance, for most ferrites belonging to this family a spin reorientation transition is expected over a certain degree of chemical substitution [3]. This transition is mainly due to a chemically induced change in the state of the magnetocrystalline anisotropy (from c-axis to c-plane) accompanied by a gradual increase of the second-order anisotropy constant K_2. However, such transition has not been identified for $BaTi_xMn_xFe_{12-2x}O_{19}$ ferrites. In addition, scarce results have been reported for extracting K_1 and K_2 values from measurements on polycrystalline powder or composite samples.

Similarly, previous authors have reported that the magnetic resonance spectra of $BaTi_xMn_xFe_{12-2x}O_{19}$ composites possesses two different resonance frequencies separated by 6 GHz in the K-band [2]. No clear explanation of the origin of the second peak is provided. This peak could be due to the presence of a second resonance mode related to the magnetic texture supported by the particles or to a distribution of different magnetocrystalline anisotropies within the polycrystalline sample due to chemical inhomogeneities and concentration gradients.

This work aims to combine micromagnetic simulations with experimental magnetic and structural characterizations to provide an explanation of the phenomena involved in the resonance spectra of chemically substituted $BaTi_xMn_xFe_{12-2x}O_{19}$ composites.

Powder samples of $BaTi_xMn_xFe_{12-2x}O_{19}$ with $x \in [0.0, 2.0]$, were synthesized by a conventional ceramic technique and were incorporated into a polymer matrix. The magnetic permeability spectra were measured by a zero-field microwave reflection-transmission method using an Anritsu vector network analyzer operating from 1 MHz to 43.5 GHz. The micromagnetic parameters (M_s, K_1) were extracted from SQUID MPMS 3 Magnetometer measurements applying the Law of Approach to Saturation (LAS) for the last two parameters (see figure 1 (a)) [4]. The values of the phenomenological damping constant and the gyromagnetic ratio for different degrees of substitution were estimated from broad-band FMR measurements. In parallel, micromagnetic simulations were performed for $BaM_xM'_xFe_{12-2x}O_{19}$ assuming different morphologies: hexagonal column, core-shell and uniform and bi-domain spherical particles to explore the different configurations of the particles that could give rise to more than one resonance mode (see Figure 2).

It has been demonstrated that there are two aspects that drive the tuning of the permeability spectra of $BaTi_xMn_xFe_{12-2x}O_{19}$ composites: (i) chemical substitution is responsible for the modification of the frequency of the main FMR mode (see Figure 1 (b)), and (ii) particle morphology, size and composition, modify the shape of the absorption spectra and induce additional modes (see Figure 2). The current work explores this hypothesis for a range of x comprised between 0.0 and 2.0 where a large variation of K_1 is observed Figure 1 (a).

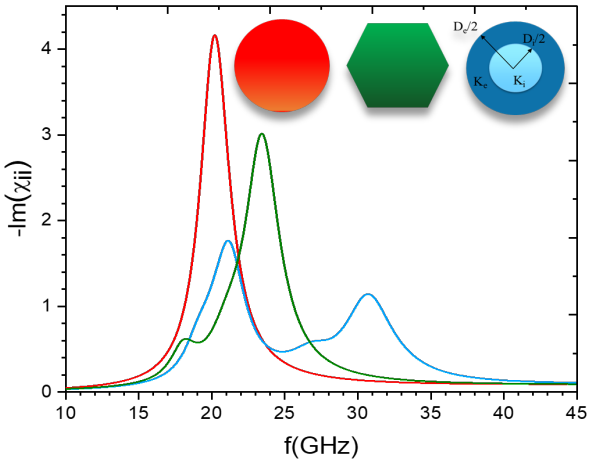

Figure 2: Simulated magnetic susceptibility spectra of isolated $BaM_xM'_xFe_{12-2x}O_{19}$ particles having different morphologies

Acknowledgments

The authors acknowledge the joint research laboratory MOLIERE for supporting this work.

References

[1] Robert C. Pullar. Hexagonal ferrites: A review of the synthesis, properties and applications of hexaferrite ceramics. *Progress in Materials Science* 57, 1191–1334 (2012).

[2] Z.W. Li, Z.H. Yang, L.B. Kong, and Y.J. Zhang. High-frequency magnetic properties at K and Ka bands for barium-ferrite/silicone composites. *Journal of Magnetism and Magnetic Materials* 325, 82–86 (2013).

[3] J. Kreisel, Hou Vincent, Francis Tasset, Muhammad Pate, and Jean-Pierre Ganne. An Investigation of the Magnetic Anisotropy Change in BaFe12-2xTixCoxO19 Single Crystals. *Journal of Magnetism and Magnetic Materials* 224, 17–29 (2001).

[4] R. Grössinger. Correlation between the inhomogeneity and the magnetic anisotropy in polycrystalline ferromagnetic materials. *Journal of Magnetism and Magnetic Materials* 28, 137–142 (1982).

Poster 1.46, November 14th, 16h30–18h30

Oxygen Magneto-Ionics, without Oxidation

T. Bhatnagar-Schöffmann[1,*], P. Schöffmann[2], A. Lampert[3], A. Kovàcs[4], D. Ourdani[5], M.-A. Syskaki[6], Y. Roussigné[3], S.Ono[7], J. Langer[5], R. E. Dunin-Borkowski[4], D. Ravelosona[1], M. Belmeguenai[3], A. Solignac[8], and L. Herrera Diez[1,*]

[1]*Centre de Nanosciences et de Nanotechnologies, CNRS-Université Paris-Saclay, Palaiseau, France*
[2]*Synchrotron SOLEIL, L'Orme des Merisiers, 91190 Saint-Aubin, France*
[3]*CNR-IMM, Agrate Unit, Via C. Olivetti 2, 20864 Agrate Brianza (MB), Italy*
[4]*Forschungszentrum Jülich GmbH, Ernst Ruska-Centre for Microscopy and Spectroscopy with Electrons and Peter Grünberg Institute (PGI-5), 52425 Jülich, Germany*
[5]*Laboratoire des Sciences des Procédés et des Matériaux, CNRS-UPR 3407, Université Sorbonne Paris Nord, 93430 Villetaneuse, France*
[6]*Singulus Technologies AG, Hanauer Landstrasse 103, 63796 Kahl am Main, Germany*
[7]*Central Research Institute of Electric Power Industry, Yokosuka, Kanagawa 240-0196, Japan*
[8]*SPEC, CEA, CNRS, Université Paris-Saclay, CEA Saclay, 91191 Gif-sur-Yvette Cedex, France*
*tanvi.bhatnagarschoeffmann@universite-paris-saclay.fr
liza.herrera-diez@c2n.upsaclay.fr

In this study we show that a Pt dusting layer of a nominal thickness of 0.09 nm inserted at the interface between CoFeB and MgO in a Ta/CoFeB/MgO/HfO_2 induces in-plane magnetic anisotropy in the stack, which can be switched to perpendicular magnetic anisotropy (PMA) through magneto-ionic gating (see figure). The polycristalline structure of the MgO layer observed by transmission electron microscopy in the as-grown state is preserved after gating [1], indicating a potential magneto-ionic mechanism mediated by oxygen motion through grain boundaries.

Interestingly, this system does not show evidence of the typical oxidation involved in magneto-ionics relying on voltage-induced migration of oxygen species [2]. XAS measurements show a strong and reversible change in the oxygen edge upon gate voltage exposure, showing that the magneto-ionic process is mediated by the incorporation and release of oxygen species. However, XMCD measurements show that the voltage-gate induced spin-reorientation transition in the CoFeB/Pt/MgO stacks is not accompanied by any significant reduction in the magnetic moment of neither Fe nor Co.

This magneto-ionic mechanism is attributed on the one hand to the crystallinity of the MgO barrier, and on a likely change in the oxidation potential of the Co and Fe atoms at the oxide interface through the interaction with the Pt atoms in the dusting layer. This shows that the fine-tuning of the chemistry at the interfaces of magneto-ionic stacks is important for the design of magneto-ionics materials and devices.

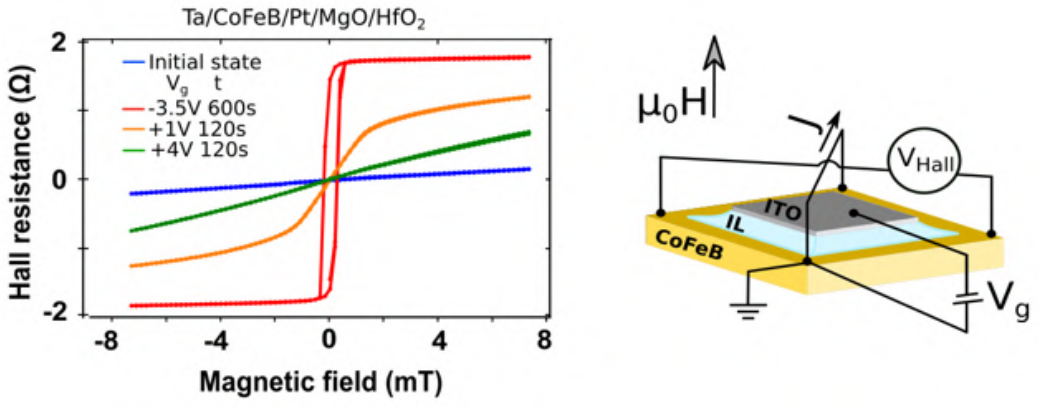

Figure 1: Anomalous Hall effect signal at different ionic-liquid gate voltages in Ta/CoFeB/Pt/MgO/HfO_2 (left), and a cartoon of the device geometry (right).

Acknowledgments

We acknowledge financial support from the European Union H2020 Program: grant MSCA ITN 860060 and Grant No. 823717, project "ESTEEM3" for access to TEM experiments. We also thank the French National Research Agency (JCJC SplaSy and Labex NanoSaclay, reference: ANR-10-LABX-0035).

References

[1] T. Bhatnagar-Schöffmann, A. Kovàcs, R. Pachat, et al. Controlling interface anisotropy in CoFeB/MgO/HfO2 using dusting layers and magneto-ionic gating. *Applied Physics Letters* 122, 042402 (2023). eprint: https://doi.org/10.1063/5.0132870.

[2] L. Herrera Diez, Y.T. Liu, D.A. Gilbert, et al. Nonvolatile Ionic Modification of the Dzyaloshinskii-Moriya Interaction. *Phys. Rev. Applied* 12, 034005 (3 2019).

Towards spin Hall magnetoresistance with magnetically frustrated cobalt vanadate spinel CoV_2O_4 thin films

Lamiae El Khabchi[1,*], Antonio Peña Corredor[1], Laurent Schlur[1], Marc Lenertz[1], Jérôme Robert[1], Cédric Leuvrey[1], Gilles Versini[1], François Roulland[1], Daniele Preziosi[1], Christophe Lefevre[1], and Nathalie Viart[1]

[1]*Department of Inorganic Materials Chemistry, Institut de Physique et Chimie des Matériaux de Strasbourg - IPCMS UMR 7504 Université de Strasbourg-CNRS, , 67000 Strasbourg, France*
**lamiae.elkhabchi@ipcms.unistra.fr*

Transition metal oxides constitute an intriguing playground within the strongly correlated materials thanks to their diverse degrees of freedom that are charge, spin, orbital and lattice. Spinel vanadates, of general formula AV_2O_4 (A = transition metal), captured the attention in the condensed matter community because thanks toof their versatile magnetic and electrical properties. Their structure consists of a diamond sublattice of tetrahedrally coordinated A2+ ions combined with a geometrically frustrated pyrochlore sublattice formed by the octahedrally coordinated V3+ (3d2, S=1) ions. Among all spinel vanadates, CoV_2O_4 (CVO) is a unique spinel oxide. It is a normal spinel having a cubic structure with Fd3 $\bar{m}$ symmetry and a lattice parameter of a = 8.407 Å [1] . The reason why the spinel CoV_2O_4 grabbed special attention is because not only does it have a pyrochlore sublattice formed by the magnetically active V3+ atoms which are geometrically frustrated, but it also has the shortest V-V distance among all spinel vanadates and stands at the crossover from between insulating to and itinerant behaviours which makes it very close to a Metal-Insulator Transition (MIT) compound. These two main assets make CVO a potential candidate for several low power electronic devices, such as the Spin-Orbit Torque Magnetic Random Access Memories (SOT-MRAM) or the Mott-transition based Resistive Random Access Memories (RRAM).

Unlike the bulk form, CVO thin films have been very scarcely studied, with only four publications and non-converging results concerning the crystallographic system in which the film crystallizes, which is reported to be either orthorhombic [2] or tetragonal [1] . Beside the fact that all films were grown in a compressive state, either on $SrTiO_3$ (STO) or on $(La_{0.3}Sr_{0.7})(Al_{0.65}Ta_{0.35})O_3$ (LSAT) [1] ,[2] substrates, which rather pushes the system into the insulating state, the films were surprisingly not grown from a CoV_2O_4 target, but from a CoV_2O_6 one, probably due to the fact that CoV_2O_4 is difficult to synthesize. The originality of our approach, relies both on the choice of the target from which the deposition is made, as well as on the choice of the substrates.

Our target is a CoV_2O_4 spinel single-phased target which we successfully elaborated through a solid state chemistry optimized method. Our aim is to control and manipulate the spins orientation and frustration as well as the V-V distances by growth engineering. We use the pulsed laser deposition (PLD) technique to grow CVO thin films onto well-chosen substrates that will exert different kinds of strain (compressive/tensile) in order to see their effect in terms of structural, magnetic and electrical properties of the CVO thin films.

Some depositions were thus performed on MgO substrates, in addition to the STO ones, in order to probe the new strain state (tensile) such a deposition allows. We showed that for both systems, CVO//MgO as well as CVO//STO, the elaborated CVO thin films adopt a tetragonal structure but with different in plane (IP) and out-of-plane (OOP) distortions and show different magnetic anisotropies. For instance, with the CVO//MgO system, the similarity of the hysteresis loops measured at 50 K in both IP and OOP configurations indicates the absence of anisotropy with very close coercivities and almost the same saturation magnetizations (See Fig. 1). On the other hand, the hysteresis loops of the system CVO//STO also performed at 50 K, clearly present an important anisotropy between the IP and OOP signals (See Fig. 2). It seems that there are two decoupled magnetic phases, as indicated by the wasp-waisted OOP hysteresis loop and the fact that the IP magnetization does not reach as high a value as the OOP one, even at the highest reachable field of 7 T. A part of the layer seems to be very hard to saturate IP. The CVO//STO system thus shows a clear perpendicular magnetic anisotropy (PMA), its c-axis direction being easier than the IP ones. This result goes well with our ambition to further elaborate heterostructures Pt/CVO//STO and study their magneto-transport properties with the hope of chasing a strong spin Hall magnetoresistance. Further studies must be conducted to confirm the existence of multiple magnetic phases and better characterize them.

Acknowledgments

This work was partly supported by the Interdisciplinary Thematic Institute QMat, which as part of the ITI 2021 2028 program of the University of Strasbourg, CNRS and Inserm, was supported by IdEx Unistra (ANR 10 IDEX 0002), and by SFRI STRAT'US project (ANR 20 SFRI 0012) and ANR-11-LABX-0058-NIE and ANR-17-EURE-0024 under the framework of the French Investments for the Future Program.

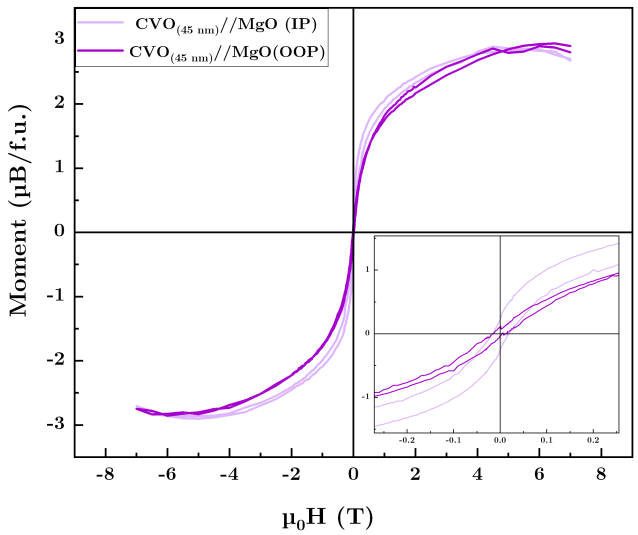

Figure 1: M vs. H hysteresis loops for the system CVO//MgO in both IP and OOP configurations.

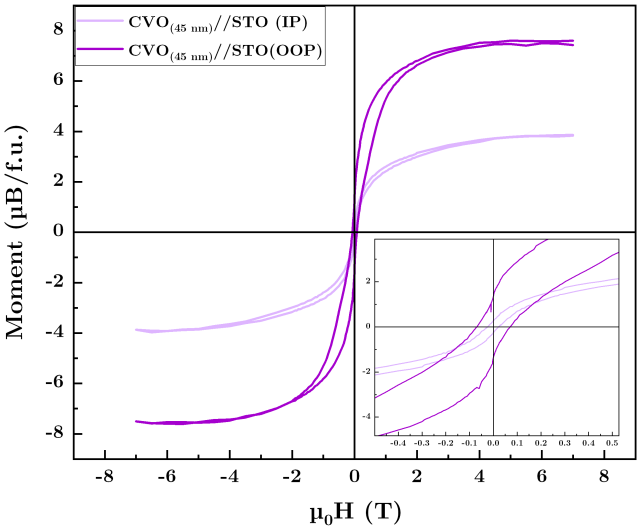

Figure 2: M vs. H hysteresis loops for the system CVO//STO in both IP and OOP configurations.

References

[1] BC Behera, G Sabat, Shwetha G Bhat, et al. Tailoring magnetism in spinel vanadate CoV2O4 epitaxial thin films. *Journal of Physics: Condensed Matter* 33, 365801 (2021).

[2] Christie J Thompson, Dalmau Reig-i-Plessis, Lazar Kish, et al. Spin canting and orbital order in spinel vanadate thin films. *Physical Review Materials* 2, 104411 (2018).

Magneto-ionics in CoFeB alloys

G. Bernard[1,*], R. Pachat[1], T. Bhatnagar-Schoeffmann[1], M.-A. Syskaki[4], S. Ono[3], J. Langer[4], D. Ravelosona[1], D. Querlioz[1], A. Solignac[2], and L. Herrera Diez[1]

[1]*Centre de Nanosciences et de Nanotechnologies, CNRS, Université Paris-Saclay, 91120 Palaiseau, France*
[4]*Singulus Technology AG, Hanauer Landstrasse 103, 63796 Kahl am Main, Germany*
[3]*Central Research Institute of Electric Power Industry, Yokosuka,Kanagawa 240-0196, Japan*
[2]*SPEC, CEA, CNRS, Université Paris-Saclay, CEA Saclay, 91191 Gif-sur-Yvette Cedex, France*
guillaume.bernard@c2n.upsaclay.fr

Magneto-ionics is a rapidly growing field in spintronics that offers great promise for the development of high-performance devices for information storage and processing. The ability to manipulate magnetic properties through ionic motion in materials in a non-volatile way, rather than the volatile purely electronic means, presents exciting opportunities for the development of non-volatile and low-energy memory devices. CoFeB alloys are among the most technologically relevant materials for spintronics, therefore, the integration of magneto-ionics into CoFeB-based devices can rapidly lead to new functionalities and enhanced performance.

In Ta/CoFeB/HfO_2, ionic gating induces migration of oxygen-rich species within the stack, leading to different magneto-ionic regimes and spin-reorientation transitions. Our previous studies [1] show that an irreversible regime I exists when going from an under-oxidised to an optimally oxidised CoFeB/HfO_2 interface, where perpendicular magnetic anisotropy (PMA) is observed, while a highly reversible and cyclable regime II is present when going from PMA to over-oxidised. This behaviour is attributed to a non-equivalent distribution and binding of the mobile oxygen species at the surface of the magnetic layer in the different magneto-ionic regimes.

Hall-bar devices containing a solid state gate were fabricated using the same Ta/CoFeB/HfO_2 wafer as in [1] by adding an HfO_2 layer grown by atomic layer deposition (ALD), as a replacement for the ionic liquid gate. Interestingly, in these devices the irreversible regime I is completely absent in solid state devices most likely due to the impact of ALD growth and/or fabrication on surface chemistry, and in turn, on the magneto-ionic performance. The devices show PMA in the as-fabricated state, in contrast to the in-plane anisotropy observed in the as-fabricated ionic liquid gate device, and the underoxidised present in the as-grown wafer can not be accessed with the available range of gate voltages, which is compatible with our previous studies. Nevertheless, the regime II in solid state devices can be accessed and is fully reversible, as found in the ionic-liquid gating experiments (see Figure 1). The solid state devices show faster dynamics compared to ionic liquid gating, due to the elimination of the slow ionic migration inside the ionic liquid, revealing the kinetics of only the ionic motion inside the oxyde/ferromagnetic stack.

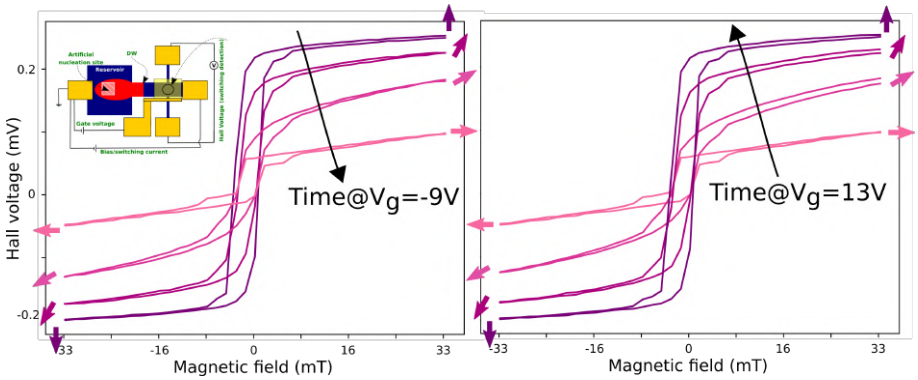

Figure 1: A series of Hall measurements were conducted after sequentially applying a gate voltage, with negative values showcased on the left and positive ones on the right. The steps of intermediate oxidation exhibit remarkable similarity in both directions, the regime II is fully reversible. A schematic of the device in represented in the inset.

This highlights the importance of characterising the differences between the ionic-liquid and solid-state gating methods for disentangling potential effects linked to the device design and fabrication from the intrinsic magneto-ionic mechanisms.

Acknowledgments

We gratefully acknowledge financial support from the European Union H2020 Program (MSCA ITN 860060), the French National Research Agency (Splasy), and by Labex NanoSaclay, (ANR-10-LABX-0035). This work was also partly supported by the French RENATECH network.

References

[1] R. Pachat, D. Ourdani, J.W. van der Jagt, et al. Multiple Magnetoionic Regimes in Ta/$Co_{20}Fe_{60}B_{20}$/HfO_2. *Phys. Rev. Appl.* 15, 064055 (6 2021).

Ordre magnétique dans des spinelles à propriétés thermoélectriques

E. Choker[1,*], S. Haber[2], D. Pelloquin[2], R. Daou[2], A. Maignan[2], S. Hébert[2], F. Richomme[1], A. Fnidiki[1], and J. Juraszek[1]

[1]*Groupe de Physique des Matériaux, Université de Rouen Normandie, Rouen, France*
[2]*Laboratoire de Cristallographie et Sciences des Matériaux, Université de Caen Normandie, Caen, France*
**eva.choker@univ-rouen.fr*

Parmi les familles de matériaux considérées pour les applications thermoélectriques, les chalcogénures occupent une place de choix, avec l'exemple emblématique de Bi_2Te_3, meilleur matériau utilisé et commercialisé à ce jour pour ces applications. De nouvelles familles sont étudiées à l'échelle internationale et parmi elles la structure spinelle apparaît très intéressante car elle présente des ZT pouvant atteindre 0.5 – 0.6 à 700K, et des comportements magnétiques et électroniques très variés peuvent être obtenus selon la composition chimique AM_2X_4 (A = Cu, Fe, ... ; M = Cr, V,... ; X = O, S, Se,..). Les propriétés thermoélectriques des spinelles peuvent être modifiées par dopage, mais le magnétisme peut également jouer un rôle important, notamment sur le coefficient Seebeck.

Cette contribution porte sur l'étude magnétique des matériaux chalcogénures aux propriétés thermoélectriques, et plus précisément des matériaux thiospinels à base de fer tel que le composé $FeCr_2S_4$. Il repose sur une approche combinant des mesures thermoélectriques et magnétiques macroscopiques couplées à la détermination du magnétisme à l'échelle locale par spectrométrie Mössbauer du ^{57}Fe, dans le but de comprendre les couplages entre spins, magnétisme et propriétés thermoélectriques.

Le composé $FeCr_2S_4$ cristallise dans une structure cubique, où les ions Fe^{2+} et Cr^{3+} occupent des sites tétraédriques et octaédriques, respectivement [1]. Ce composé est un semi-conducteur ferrimagnétique avec une température de transition magnétique T_c = 170 K [2]. Dans l'état paramagnétique au-dessus de T_c, le spectre Mössbauer se compose d'une raie Lorentzienne (voir Fig. 1), indiquant un environnement symétrique pour les ions Fe^{2+} en accord avec la structure cubique du composé. En-dessous de T_c, la mise en ordre magnétique progressive se traduit par des interactions hyperfines magnétiques et quadripolaires combinées, liées à un gradient de champ électrique induit par effet de spin, et une phase magnétique hélicoïdale apparaît en dessous de 60 K [3]. L'influence de la substitution de Fe par Cu sur les propriétés magnétiques seront étudiées en fonction de la température par magnétométrie SQUID et spectrométrie Mössbauer du ^{57}Fe.

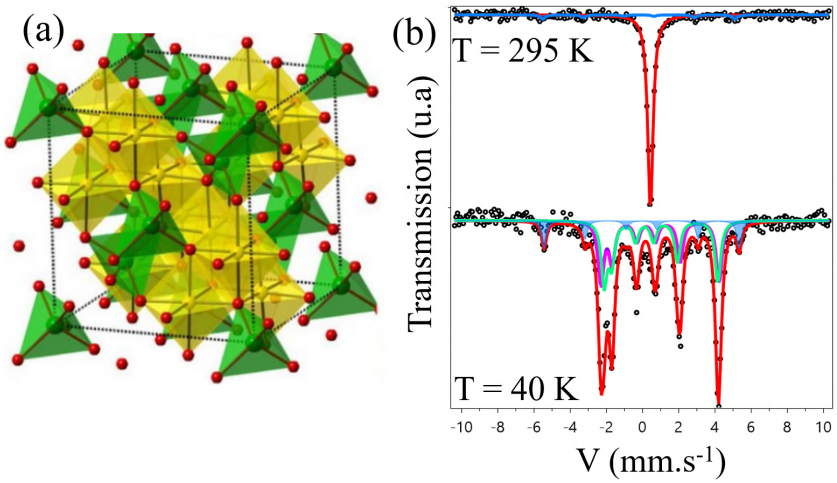

Figure 1: (a) Structure cristallographique de la spinelle AM_2X_4 montrant les sites octaédriques MX_6 et tétraédriques AX_4, (b) Spectres Mössbauer de $FeCr_2S_4$ mesurés à T=295 K et à T=40 K.

Remerciements

Ce travail est soutenu par l'Agence Nationale de la Recherche française (ANR), dans le cadre de projet SPINTEP à travers le programme Labex EMC3.

References

[1] Amar Nath, Zoltán Klencsár, Erno Kuzmann, et al. Nanoscale magnetism in the chalcogenide spinel (formula presented) Common origin of colossal magnetoresistivity. *Physical Review B-Condensed Matter and Materials Physics* 66, 1–4 (2002).

[2] AP Ramirez, Robert Joseph Cava, and J Krajewski. Colossal magnetoresistance in Cr-based chalcogenide spinels. *Nature* 386, 156–159 (1997).

[3] J Engelke, FJ Litterst, Alexander Krimmel, et al. Spin re-orientation in FeCr 2 S 4. *Hyperfine Interactions* 202, 57–61 (2011).

Vertical and Lateral Crystallization Dynamics of Yttrium Iron Garnet Thin Films

Sebastian Sailler[1], Gregor Skobjin[1], Heike Schlörb[2], Andy Thomas[2,3], Sebastian T. B. Goennenwein[1], and Michaela Lammel[1,*]

[1]*Universität Konstanz, Germany*
[2]*IFW Dresden, Germany*
[3]*Technische Universität Dresden, Germany*
*michaela.lammel@uni-konstanz.de

Yttrium iron garnet ($Y_3Fe_5O_{12}$, YIG) is a prototypical material in spintronics due to its exceptional magnetic properties. To exploit these properties high quality thin films are needed. Multiple deposition techniques are known for the fabrication of YIG. Whereas techniques like liquid phase epitaxy or high temperature pulsed laser deposition lead directly to single crystalline YIG thin films, deposition techniques like low temperature pulsed laser deposition and sputter deposition produce amorphous films, which need a post annealing step to induce crystallization. However, not much is known about the exact dynamics of the formation of crystalline YIG out of the amorphous phase.

First, we conduct an extensive time and temperature series to study the crystallization behavior of sputtered amorphous YIG thin films on different substrates and extract the corresponding crystallization velocities as well as the activation energies needed to promote vertical crystallization (cp. Fig. 1, **(a)**). We find vertical crystallization velocities of 0.84 nm min^{-1} at 600 °C for YIG on GGG, 0.27 nm min^{-1} at 600 °C for YIG on YAG and 16.7 nm min^{-1} at 700 °C for YIG on SiO_x, respectively. Together with the activation energies these can be used to generally describe the crystallization process of YIG on GGG, YAG and arbitrary substrates like SiO_x. Therewith, we are able to extrapolate the time needed for a fully crystalline film at any temperature and for any film thickness.

Taking the knowledge of these crystallization regimes then allows us to determine a temperature window where solid phase epitaxy from a lattice matched substrate is possible, while nucleation is still kinetically hindered. Within this window the formation of single crystalline YIG on an amorphous SiO_x layer by lateral crystallization with a rate of 0.17 nm min^{-1} at 600 °C is possible, while simultaneously avoiding the formation of any polycrystalline grains (cp. Fig. 1, **(b)**). Understanding these dynamics allows for a controlled and precise manufacturing of single crystalline YIG thin films on arbitrary substrates across large length scales and therefore pave the way for engineering more complicated non planar structures.

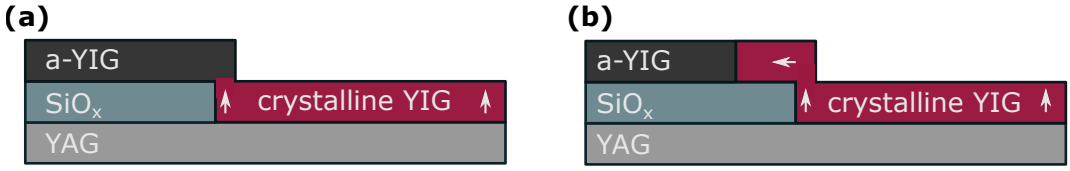

Figure 1: From the lattice matched substrate, the amorphous YIG layer (a-YIG) first crystallizes vertically as shown in panel **(a)**. Subsequently a laterally growing front is expected, which is depicted in panel **(b)**.

Poster 1.51, November 14th, 16h30–18h30

Magnetism at low symmetry interfaces

Alexande Wu-Vignolo[1,*], Yves Roussigné[2], Mourad Cherif[2], Alexandra Mougin[3], Shishun Zhao[4], Hyunsoo Yang[4], Yuan He[1], Amandine Bellec[1], and Vincent Repain[1]

[1]*Laboratoire des Matériaux et Phénomènes Quantiques, Université Paris-Cité, Paris, France*
[2]*Laboratoire des Sciences des Procédés et des Matériaux, Univ. Paris 13 Nord, 93430 Villetaneuse, France*
[3]*Laboratoire de Physique des Solides, Univ. Paris-Sud, CNRS UMR 8502 - 91405 Orsay Cedex, France*
[4]*Spin and Energy Lab, Department of Electrical and Computer Engineering, National University of Singapore, Singapore*
*alexandre.wu-vignolo@u-paris.fr

Crystal symmetries, as stated by the Curie's law, are a key ingredient to tailor physical properties at will. In magnetism, such symmetries are particularly important to define the easy axis of magnetization and the values of the coercive and saturation fields[1]. Controlling those parameters is crucial for the development of magnetic memories or spintronic devices [2]. In this work, I explore the impact of very low symmetry interfaces on the magnetic properties of ferromagnetic ultrathin films. More particularly, I investigate substrates with no mirror planes, that can be therefore called 'chiral' surfaces.

I will present results on Co films deposited on a Au(643) surface which is composed of a nanometric array of step edges and atomic kinks with a point group symmetry 2 (no mirrors, 1 rotation axis). The 'chirality' of this surface has been characterized by Low Energy Electron Diffraction, ellipsometry and Sum Frequency Generation.

A sandwich of Pt(1.5nm)/Co(0.7nm)/Pt(2nm) was deposited by sputtering, resulting in an out-of-plane magnetization of the substrate. A reference sample was prepared in the same batch, on a silicon oxyde substrate. The most striking result is that it is possible to reverse out-of-plane magnetization with a rather low in-plane magnetic field. Furthermore, this switching field is found to be very anisotropic in the plane of the sample (cf figure1a). We have also observed the magnetic domains which are very elongated, showing again a strong magnetic anisotropy (cf figure1b). Finally, we have probed magnon modes by Brillouin Light Spectroscopy, and an azimuthal angular dependence of the asymmetry between the Stokes and the anti-Stokes frequencies was observed, in contrary to what has been measured on the reference sample. I will also show that it is possible to obtain those low symmetry magnetic interfaces on intrinsic silicon wafers, opening the study of their spintronic properties.

The interpretation of those results is still under study. First complex magneto-optical effects can occur on such low-symmetry samples due to a coupling between structural anisotropy and standard magneto-optical terms. Models taking into account a possible tilted anisotropy will also be discussed in the light of experimental results. Finally, a non-collinearity of the magnetic texture is a possible driving force for such unusual behaviors.

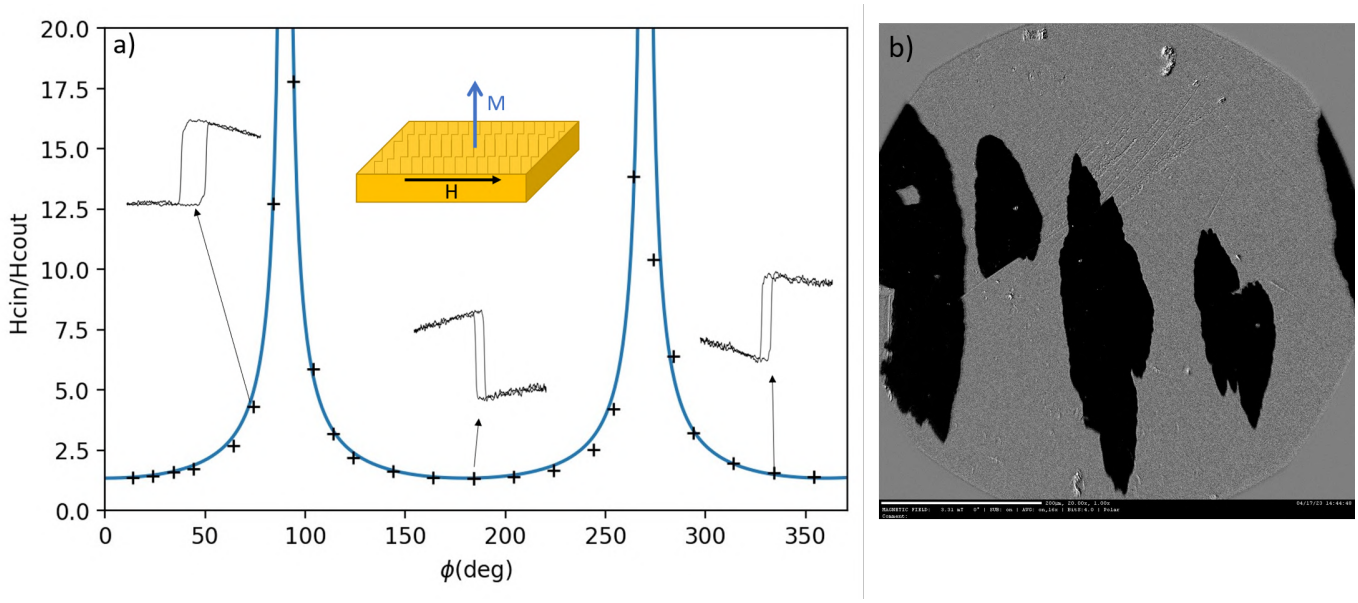

Figure 1: a) Plot of the in-plane switching field of out-of-plane magnetization normalized by value of the out-of-plane switching field (polar MOKE configuration) versus the azimuthal angle between the field an the step edges direction ($\phi = 0° : H_{in} \parallel$ steps; $\phi = 90° : H_{in} \perp$ steps. The blue line is the Kondorsky law Hc(0)/cos(ϕ). In inset, a sketch of the experiment configuration and three typical MOKE cycles. b) Magnetic Domains imaged in Kerr polar configuration

Acknowledgments

Thesis co-funded by the French National Quantum Plan and the Labex SEAM. BLS measurements were done at LSPM, Université Paris 13. MOKE measurements were done at the LPS, Université Paris Saclay. Film deposition was done at the SEL, National University of Singapore.

References

[1] M Dąbrowski, M Cinal, AK Schmid, Jürgen Kirschner, and M Przybylski. Fine-tuning of canted magnetization in stepped Fe films through thickness variation, Au capping, and quantum confinement. *Physical Review B* 99, 184420 (2019).

[2] Aurelien Manchon, Jakub Železnỳ, Ioan M Miron, et al. Current-induced spin-orbit torques in ferromagnetic and antiferromagnetic systems. *Reviews of Modern Physics* 91, 035004 (2019).

Propriétés magnétiques dynamiques de ferrites spinelles élaborés par extrusion de pâte (robocasting) en lien avec leur microstructure

Aziz Zekhnini[1,3,*], Gérard Delette[1], Anne-Lise Adenot-Engelvin[2], and Olivier Isnard [3]

[1]*LITEN, Université Grenoble Alpes, CEA, Grenoble, France*
[2]*CEA-DAM, Le Ripault, Tours, France*
[3]*Institut Néel, Université Grenoble Alpes et CNRS, Grenoble, France*
*aziz.zekhnini@cea.fr

Les ferrites (Mn,Zn)Fe_2O_4 et (Ni,Zn,Cu)Fe_2O_4 sont largement utilisés pour élaborer à l'échelle industrielle des composants fonctionnant dans des gammes de fréquence de 1-10 MHz en électronique de puissance et de 0.1-10 GHz pour les applications RF (absorbants, substrats d'antenne, composants...). Ces matériaux élaborés avec une structure spinelle présentent des propriétés magnétiques et électriques qui permettent de les utiliser à haute fréquence[1][2], avec une limitation liée aux échauffements des composants. Leur mise en forme par pressage et frittage restreignait jusqu'ici les géométries accessibles, mais l'émergence des procédés de fabrication additive ouvre des opportunités nouvelles pour concevoir des composants architecturés afin de réduire les volumes, notamment grâce à une meilleure gestion thermique. Cependant, l'utilisation de ces nouveaux procédés conduit à des microstructures différentes (porosités, taille de grains, compositions des joints de grains,). Cette étude porte sur l'influence d'un procédé de FA sur les propriétés magnétiques dynamiques de ferrites.

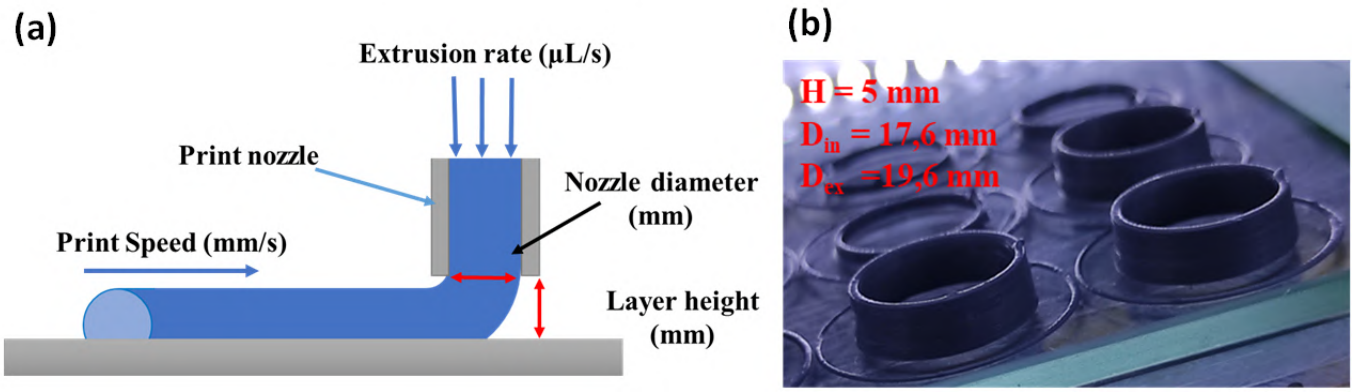

Figure 1: (a)Procédé d'impression par robocasting, et (b) tores imprimés à base de ferrite (Mn,Zn)Fe_2O_4.

Dans ce travail, nous avons décidé de fabriquer des pièces par un procédé innovant d'impression 3D par extrusion de pâte, également appelée robocasting ou DIW (Direct Ink Writing). [3] Ce procédé, illustré dans la figure 1(a), consiste à extruder une pâte organique chargée par une suspension céramique de (Ni,Zn,Cu)Fe_2O_4 ou (Mn,Zn)Fe_2O_4. Les pâtes préparées présentent des comportements rhéofluidiants pour permettre l'extrusion sous cisaillement au travers de buses métalliques puis la tenue de l'ébauche après le dépôt. L'utilisation de buses métalliques permet d'extruder des formulations très chargées en poudres afin d'obtenir des pièces denses avec moins de retrait de géométrie lors du déliantage et du frittage.Les pièces imprimées sont présentées dans la figure 1(b). Ces tores ont été imprimés avec une pâte chargée avec 84 % en masse de poudre de ferrite MnZn. Les premières pièces imprimées étaient des tores destinés aux mesures des propriétés magnétiques. Elles subissent une étape de déliantage et de frittage thermique pour éliminer les éléments organiques et densifier la pièce.

Afin de pouvoir valider le procédé utilisé pour fabriquer ces tores à base de (Mn,Zn)Fe_2O_4, des tores par compression uniaxiale ont été préparés à partir du même feedstock utilisé pour l'impression robocasting. La figure 2(a) montre le comportement dynamique d'un tore de référence élaboré par compression uniaxiale (CU) et un tore par robocasting (Robo) mesuré par une technique d'impédance-métrie entre 0.01 MHz et 100 MHz. Au premier ordre, les niveaux de perméabilité sont liés à la masse volumique des tores : le tore imprimé présente une densité relative de 91 % et une porosité ouverte d'environ 3 %, alors que la pièce de référence (CU) présente une densité relative de 96 % avec une faible porosité ouverte.

De plus, les mécanismes de résonance et de relaxation des domaines magnétiques des tores imprimés semblent différents de ceux des tores de référence : la courbe de perméabilité imaginaire µ" d'un tore imprimé est plus étalée en fréquence, avec un décalage en fréquence de résonance vers les hautes fréquences. Cet écart pourrait être interprété par des différences de

dispersion de taille de grains entre les deux matériaux. Une mesure de la taille moyenne des grains sur l'image présentée dans la figure 2(b) montre des valeurs de 3,52 ± 1,50 µm. Cette taille moyenne peut refléter une dispersion des grains monodomaines et bidomaines magnétiques, puisque d'après [4], des grains monodomaines ont été observés lorsque la taille est inférieure à 4 µm dans un (Mn,Zn)Fe_2O_4. Des caractérisations quantitatives de dispersion de taille de grains (figure 2(b)) sont en cours pour confirmer cette hypothèse.

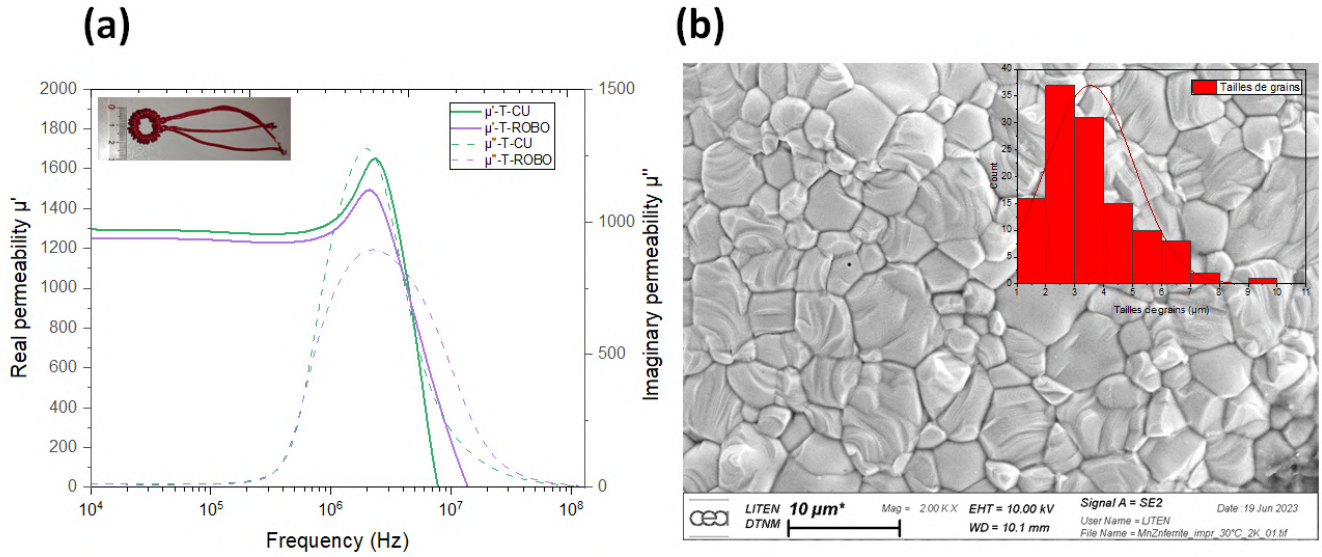

Figure 2: (a) Perméabilité réelle µ' et imaginaire µ" pour un tore imprimé par robocasting et un tore obtenu par compression uniaxiale, et (b) microstructure d'un tore ferrite (Mn,Zn)Fe_2O_4 imprimé et fritté à 1160°C sous atmosphère contrôlée.

References

[1] H. P. J. Wijn, J. Smit, and J.-F. MarchandSmit. Les ferrites: Les propriétés physiques des oxydes ferrimagnétiques en relation avec leurs applications techniques Traduit du néerlandais par Jean-François Marchand.Dunod (1961).

[2] R. Lebourgeois. Ferrites doux pour l'électronique de puissance. *Tech. Ing.,* (2005).

[3] M. Yetna N'Jock, E. Camposilvan, L. Gremillard, et al. Characterization of 100Cr6 lattice structures produced by robocasting. *Mater. Des.* vol. 121, p. 345–354 (mai 2017).

[4] J. Aarts, I. Shiekah, and P. J. van der Zaag. Domain structure in polycrystalline MnZn ferrite imaged by magnetic force microscopy. *J. Appl. Phys.* vol. 85, p. 7302–7309 (mai 1999).

Graphene-based Heterostructures: Effect of the Intercalation of MgO and Al_2O_3 Insulating Barriers on Structural and Magnetic Properties

I. Berrai1[1,*], M. Belmeguenai[1], Y. Roussigné[1], W. Alimi[1], P.A. Dainone[2], Y. Lu[2], S. Farhat[1], and S.M. Chérif[1]

[1]*Université Sorbonne Paris Nord, Laboratoire des Sciences des Procédés et des Matériaux, CNRS, LSPM-LPR 3407, F-93430 Villetaneuse, France*
[2]*Institut Jean Lamour, Université de Lorraine, CNRS UMR 7198, Campus ARTEM, 2 Allée André Guinier, BP 50840, 54011 Nancy, France*
imane.berrai@lspm.cnrs.fr

Due to its unique physical properties and ultimate thickness, monolayer graphene (Gr) has been widely used in nano-electronics. The importance of this material for both fundamental spintronics and future applications was quickly realized after the first unambiguous demonstration of spin transport in graphene at room temperature [1]. Thanks to its weak spin-orbit coupling and large spin diffusion length, the Gr has been the subject of research in a number of applications, such as magnetic junctions with or without a tunnel barrier. However, in addition to the wavy surface of the Gr, the deposition of a metallic layer on it causes defects or even amorphisation of the Gr layer [2]. Controlling the quality of the Gr/ferromagnetic material (FM) interface, which directly affects the magnetic properties of the basic units of spintronic devices, is a major challenge, and few works in the literature have been reported on the effect of intercalating an insulating barrier between the Gr and the FM on the dynamic magnetic properties of these Gr/FM-based heterostructures. Here we report on the effects of two different barriers, namely MgO and Al_2O_3 on the structural and magnetic properties of SiO_2/Gr/Barrier/CoFeB (CFB)/Ta structures (Figure 1.a), which are compared with those of control samples without Gr layer (Figure 1.b). In our work, a monolayer of high-quality Gr was synthesized by inductive heating chemical vapor deposition (CVD), while MgO and Al_2O_3 were deposited by molecular beam epitaxy (MBE) and atomic layer deposition (ALD), respectively. The CFB and Ta films were deposited by means of the physical vapor deposition (PVD) technique. Raman characterizations showed that Gr exhibits more defects with MgO barrier than when it is associated with Al_2O_3. This is confirmed by the increase of the intensity of the defect peak (D) of the Gr/MgO/CFB Raman spectrum (Figure 1.c) in regard of the Gr/Al_2O_3/CFB one (Figure 1.d), but without reaching the amorphization stage. Our results are consistent with those reported in the literature [2] and with our Magneto-Optical Kerr effect (MOKE) results that showed that the Gr/MgO/CFB system exhibits higher coercivity compared to Gr/Al_2O_3/CFB one (Figure 1.f) while the reference samples have a same coercivity (Figure 1.e).

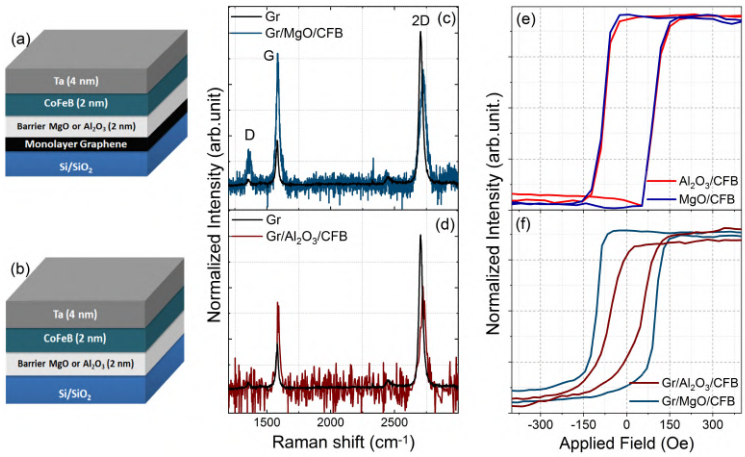

Figure 1: (a) samples structure; (b) controls structure; (c) Raman spectra of Gr and Gr/MgO/CFB; (d) Raman spectra of Gr and Gr/Al_2O_3/CFB; (e) MOKE cycles of controls; (f) MOKE cycles of samples.

Dynamic magnetic properties were also investigated. Micro-Stripe Ferromagnetic Resonance (MS-FMR) results showed that the Gr/MgO/CFB heterostructure exhibits various resonance modes, which is not the case for the Al_2O_3 based one (Figure 2.a). This result could also be an indication of the heterogeneity of the MgO-based system, in agreement with Raman and MOKE characterizations. Brillouin light scattering (BLS) measurements showed that the presence of graphene in both systems reduces the measured BLS frequencies (Figure 2.b). This could be attributed to an increase in the perpendicular

magnetic anisotropy (PMA). This effect is more pronounced in the case of Gr/Al_2O_3/CFB. It is worth noting that PMA enhancement has been reported in the literature at Gr/FM interfaces [3, 4]. This effect was attributed to direct hybridization between the metal 3d and graphene π orbitals. In our work, we observe a similar effect while Gr and CFB are decoupled by the insulating barrier. We are making progress toward understanding this behavior and highlighting the role of insulating barriers in monitoring the magnetic response of such heterostructures.

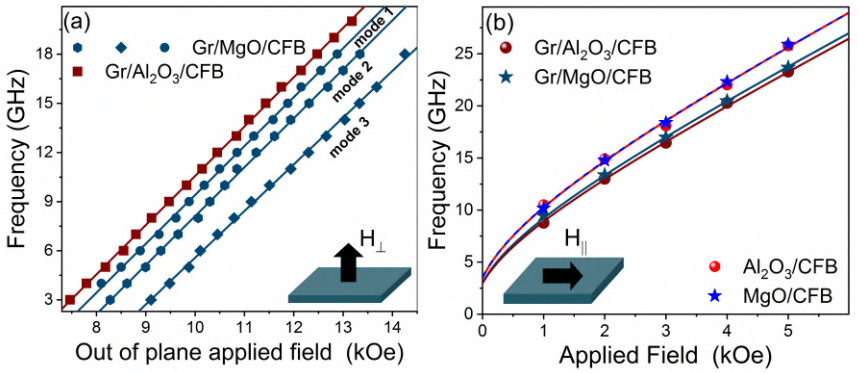

Figure 2: MS-FMR measurements on Gr/MgO/CFB or Gr/Al_2O_3/CFB heterostructures; (b) BLS measurements on Gr-based heterostructures and reference films (without Gr).

References

[1] Nikolaos Tombros, Csaba Jozsa, Mihaita Popinciuc, Harry T Jonkman, and Bart J Van Wees. Electronic spin transport and spin precession in single graphene layers at room temperature. *nature* 448, 571–574 (2007).

[2] B Dlubak, P Seneor, A Anane, et al. Are Al_2O_3 and MgO tunnel barriers suitable for spin injection in graphene? *Applied Physics Letters* 97, 092502 (2010).

[3] F Donati, L Gragnaniello, A Cavallin, et al. Tailoring the magnetism of Co atoms on graphene through substrate hybridization. *Physical review letters* 113, 177201 (2014).

[4] Hongxin Yang, Anh Duc Vu, Ali Hallal, et al. Anatomy and Giant Enhancement of the Perpendicular Magnetic Anisotropy of Cobalt–Graphene Heterostructures. *Nano Letters* 16, 145–151 (2016).

Poster 1.54, November 14th, 16h30–18h30

Artificial Graphene Spin Polarized Electrode for Magnetic Tunnel Junctions

Julian Peiro[1,*], F. Brunnett[1], R. Galceran[1], M. Galbiati[1], F. Godel[1], L. M. Kern[1], D. Perconte[1], F. Ibrahim[2], A. Hallal[2], M. Chshiev[2], B. Martinez[3], C. Frontera[3], L. Balcells[3], P. R. Kidambi[4], J. Robertson[5], S. Hoffman[5], S. Collin[1], F. Petroff[1], M-B. Martin[1], B. Dlubak[1], and P. Seneor[1]

[1]*Unité Mixte de Physique CNRS/Thales, 91767 Palaiseau, FRANCE*
[2]*Université Grenoble Alpes, CEA, CNRS, Spintec, 38000 Grenoble, FRANCE*
[3]*Institut de Ciencia de Materials de Barcelona, ICMAB-CSIC, Campus UAB, 08193 Bellaterra, SPAIN*
[4]*Department of Chemical and Biomolecular Engineering, Vanderbilt University, Nashville, Tennessee 37212, UNITED STATES*
[5]*Department of Engineering, University of Cambridge, Cambridge CB3 0FA, UNITED KINGDOM*
**julian.peiro@cnrs-thales.fr*

2D materials offer the ability to expose their electronic structure to manipulations by a proximity effect. This could be harnessed to craft properties of 2D interfaces and van der Waals heterostructures in devices and quantum materials.[1, 2] We explore the possibility to create an artificial spin polarized electrode from graphene through proximity interaction with a ferromagnetic insulator to be used in a magnetic tunnel junction (MTJ). Ferromagnetic insulator/graphene artificial electrodes were fabricated and integrated in MTJs based on spin analyzers.[3] Evidence of the emergence of spin polarization in proximitized graphene layers was observed through the occurrence of tunnel magnetoresistance. We deduced a spin dependent splitting of graphene's Dirac band structure (≈15 meV) induced by the proximity effect, potentially leading to full spin polarization and opening the way to gating.[4] The extracted spin signals illustrate the potential of 2D quantum materials based on proximity effects to craft spintronics functionalities, from vertical MTJs memory cells to logic circuits.

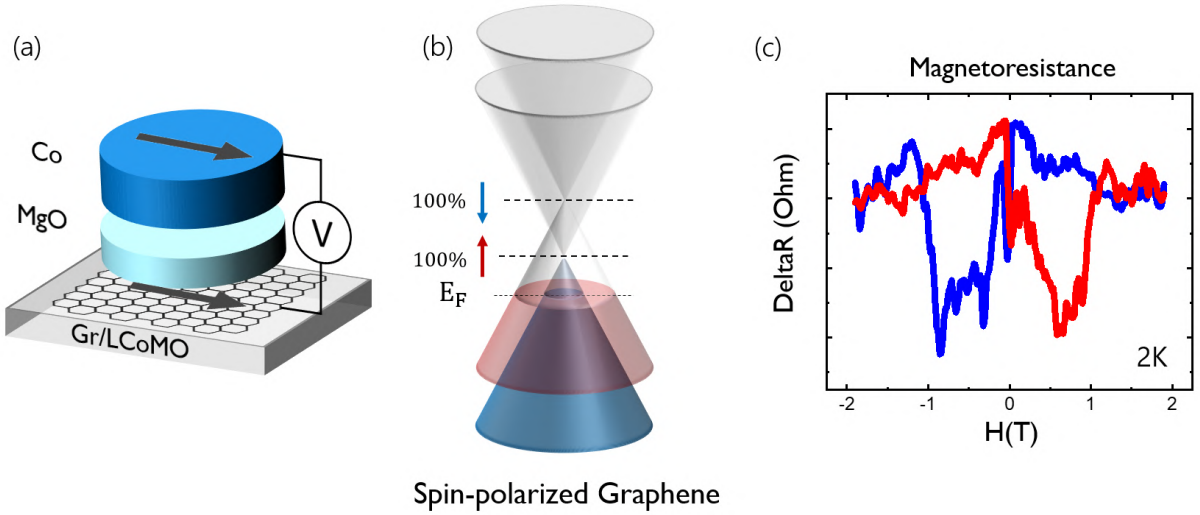

Figure 1: (Left) Device concept of magnetic tunnel junction with magnetized graphene as spin polarizer. (Center) Exchange-induced spin splitting of the graphene Dirac cones by proximity effect. (Right) Typical spin signal recorder on one of our devices.

References

[1] Victor Zatko, Marta Galbiati, Simon Mutien-Marie Dubois, et al. Band-Structure Spin-Filtering in Vertical Spin Valves Based on Chemical Vapor Deposited WS_2. *ACS Nano* 13, 14468–14476 (2019).

[2] Maëlis Piquemal-Banci, Regina Galceran, Simon M.-M. Dubois, et al. Spin filtering by proximity effects at hybridized interfaces in spin-valves with 2D graphene barriers. *Nature Communications* 11, 5670 (2020).

[3] R. Galceran, C. Frontera, Ll. Balcells, et al. Engineering the microstructure and magnetism of La2CoMnO6-δ thin films by tailoring oxygen stoichiometry. *Applied Physics Letters* 105, 242401 (2014). eprint: 1407.2072.

[4] Victor Zatko, Regina Galceran, Marta Galbiati, et al. Artificial Graphene Spin Polarized Electrode for Magnetic Tunnel Junctions. *Nano Letters* 23, 34–41 (2023).

Photoferroelectric control of graphene magnetoresistance

Krishna Maity[1], Jean-François Dayen[1], Bernard Doudin[1], Roman Gumeniuk[2], and Bohdan Kundys[1,*]

[1]*Université de Strasbourg, CNRS, Institut de Physique et Chimie des Matériaux de Strasbourg, UMR 7504, 23 rue du Loess, Strasbourg, F-67000, France.*
[2]*Institut für Experimentelle Physik, TU Bergakademie Freiberg, Leipziger Str. 23, Freiberg 09596, Germany.*
*kundys@ipcms.fr

Due to their atomic-scale dimensionality, 2D materials are ultrasensitive to adjacent charges, enabling even post-processing electric control. However, the task of adding functionality to 2D layers continues to pose a significant challenge for on-demand device-property exploitation. Here we report that electrical and even fully optical way to control and write modifications to magnetoresistive (MR) response of CVD-deposited graphene is achievable through the electrostatics of the photoferroelectric substrate (see Fig.1). For electrical control the ferroelectric (FE) switch of polarization modifies magnetoresistance by 67 percents due to graphene Fermi level shift with related modification in charge mobility. Similar function is also attained entirely by light due to substrate photovoltaic (PV) effect. Moreover, the all-optical way to imprint and recover graphene magnetoresistance by light will be reported as well as magnetic control of graphene transconductance.

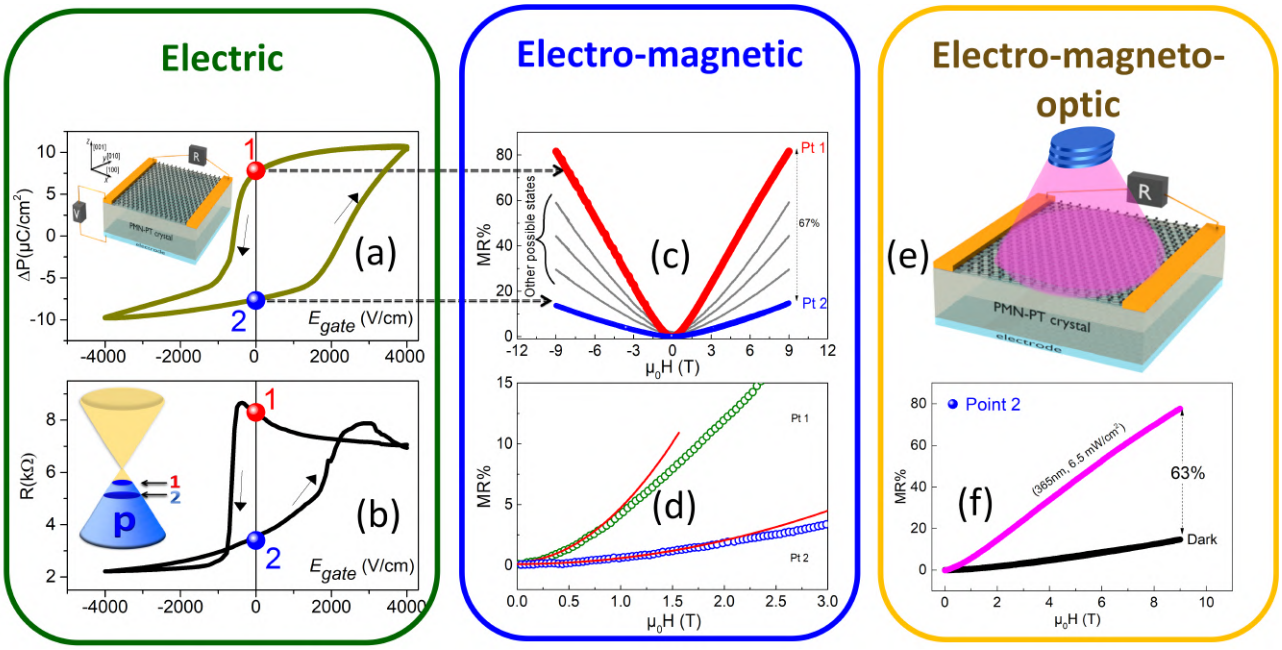

Figure 1: The FE loop (a) induces graphene transconductance (b) with remanent states "1" and "2" manifesting different magnetoresistance (c,d). The MR effect in state "2" can be also controlled by PV effect (e,f).

These findings extend recently reported new type of all-optical and re-writable memory concept [1] to a new magnetic dimension and advance wireless operation for sensors and field-effect transistors.

Acknowledgments

Partial support from IdEx 2022 - AAP Recherche Exploratoire program from UdS is acknowledged.

References

[1] D. Kundys, A. Cascales, A. S. Makhort, et al. Optically Rewritable Memory in a Graphene–Ferroelectric-Photovoltaic Heterostructure. *Phys. Rev. Applied* 13, 1488–1495 (2020).

Low-temperature epitaxial magnetic garnet thin films for quantum magnonics

William Legrand[1,*], Hanchen Wang[1], Yana Kemna[1], Francesca Zanichelli[1], Richard Schlitz[1], Michaela Lammel[2], Myriam H. Aguirre[3,4,5], and Pietro Gambardella[1]

[1]*Department of Materials, ETH Zürich, Switzerland*
[2]*Department of Physics, University of Konstanz, Germany*
[3]*Dpto. Física de la Materia Condensada, Universidad de Zaragoza, Spain*
[4]*Instituto de Nanociencia y Materiales de Aragón, INMA-CSIC, Spain*
[5]*Laboratorio de Microscopias Avanzadas, Universidad de Zaragoza, Spain*
*william.legrand@mat.ethz.ch

Magnetically ordered systems sustain collective dynamical states, quantized into magnons, in which magnetic moments precess at adjustable frequencies. Magnons are prime candidates for encoding quantum information that can be processed, propagated and converted in other types of signals [1]. Yttrium Iron Garnet (YIG) is the magnetic material known to feature the lowest magnon losses when shaped in the form of bulk single-crystal spheres, and has been the most studied platform in this context. The use of epitaxial thin films of magnetic garnets for on-chip integration has, by contrast, remained a major difficulty.

Extrinsic magnetic losses are commonly observed in epitaxial thin film garnets at cryogenic temperatures, due to the presence of a paramagnetic substrate at the interface with the magnetic film. Besides, variations in the composition of the garnet have been explored, by doping or even by full substitution of Y with ions spanning nearly all the $4f$ rare-earths from Ce to Lu. Many of them tune the perpendicular magnetic anisotropy in epitaxially-strained films. Thin films of LuIG [2], YIG [3] and Bi-doped YIG (BiYIG) [4, 5] represent the only compositions that enable a Gilbert damping parameter α in the 10^{-4} range or lower, required for the coherent manipulation of magnons. This calls for a rethinking of the epitaxial garnets system combinations.

We cover in this contribution our recent progress in the growth, using magnetron sputtering, of ultrathin garnet films with tunable magnetic anisotropy and low damping. The thickness of the epitaxial films ranges within 3-30 nm. We study their degree of crystalline perfection, strain, elemental composition and magnetic properties including damping, using X-ray diffraction, TEM imaging, ferromagnetic resonance and non-local magnon transport measurements.

The other aspect of our work concerns the integration of these magnetic systems within smaller microwave resonators. We will show how to use lumped-element cavity resonators for this aim. At the micron scale, the next step lies in nano-lithographed superconducting resonators, aiming to achieve strong couplings and to obtain systems displaying a high value of the cooperativity [6, 7]. By redesign of the resonators, we can significantly improve their magnetic coupling to our ferromagnetic ensembles of spins.

In a context where results on single-spin electron resonance have never been so promising [8], we can be confident overall that an integrated platform operated at few K and coupling superconducting elements with garnet nanomagnets would constitute a precious resource for different classes of magnonic experiments. We will briefly cover the perspectives offered by such hybrid magnon-photon systems.

Acknowledgments

W.L. acknowledges the support of the ETH Zurich Postdoctoral Fellowship Programme (grant 21-1 FEL-48).

References

[1] Yutaka Tabuchi, Seiichiro Ishino, Atsushi Noguchi, et al. Coherent coupling between a ferromagnetic magnon and a superconducting qubit. *Science* 349, 405–408 (2015).

[2] Colin L. Jermain, Hanjong Paik, Sriharsha V. Aradhya, et al. Low-damping sub-10-nm thin films of lutetium iron garnet grown by molecular-beam epitaxy. *Appl. Phys. Lett.* 109, 192408 (2016).

[3] Jinjun Ding, Chuanpu Liu, Yuejie Zhang, et al. Nanometer-Thick Yttrium Iron Garnet Films with Perpendicular Anisotropy and Low Damping. *Phys. Rev. Appl.* 14, 014017 (2020).

[4] Lucile Soumah, Nathan Beaulieu, Lilia Qassym, et al. Ultra-low damping insulating magnetic thin films get perpendicular. *Nat. Commun.* 9, 3355 (2018).

[5] Diane Gouéré, Hugo Merbouche, Aya El Kanj, et al. Temperature-independent ferromagnetic resonance shift in Bi-doped YIG garnets through magnetic anisotropy tuning. *Phys. Rev. Mater.* 6, 114402 (2022).

[6] Justin T. Hou and Luqiao Liu. Strong Coupling between Microwave Photons and Nanomagnet Magnons. *Phys. Rev. Lett.* 123, 107702 (2019).

[7] Yi Li, Tomas Polakovic, Yong-Lei Wang, et al. Strong Coupling between Magnons and Microwave Photons in On-Chip Ferromagnet-Superconductor Thin-Film Devices. *Phys. Rev. Lett.* 123, 107701 (2019).

[8] Zhiren Wang, Léo Balembois, Milos Rančić, et al. Single electron-spin-resonance detection by microwave photon counting. *arXiv:2301.02653* (2023).

Wednesday November 15th

Session 4: Magnonics 08h30 – 10h50 *Chair: Joo-Von Kim*				
08h30 – 08h50	**Konstantinos Sourounis**	CINAM	Impact of Interactions on Topological Magnonic Transport	page 145
08h50 – 09h10	**Sarah Mantion**	CEMES	Reconfigurable Co_2MnSi Heusler-based magnonic crystals	page 147
09h10 – 09h30	**Aya El Kanj**	UMR CNRS/Thales	Unraveling non-reciprocal and non-degenerated ultra-fast spin-waves in the canted antiferromagnet α-Fe_2O_3	page 149
09h30 – 09h50	**Loic Temdie**	IMT Atlantique STICC	Chiral excitation of exchange spin waves using gold nanowire grating	page 151
09h50 – 10h10	**Louis Christienne**	INSP	Resonant coupling between Surface Acoustic Waves and Spin Waves : propagation and non reciprocity	page 153
10h10 – 10h30	**Florian Millo**	C2N	Evidence of unidirectional spin waves in synthetic antiferromagnets	page 155
10h30 – 10h50	**Asma Mouhoub**	C2N	All-inductive observation of nonlinear spin wave processes in synthetic antiferromagnet microstripes	page 157

Impact of Interactions on Topological Magnonic Transport

Konstantinos Sourounis[1,*] and Aurelien Manchon[1]

[1]*Aix-Marseille Université, CNRS, CINaM, Marseille, France*
*konstantinos.sourounis@univ-amu.fr

The transport of magnons is a popular alternative to electrons for low power spintronic applications due to the absence of Joule heating and the long relaxation length of magnon carriers. Transport effects in magnetic insulators usually appear under the application of a temperature gradient which makes the processes inherently temperature-dependent and, thereby, highly sensitive to magnon interactions. In fact, the widely used Linear Spin Wave Theory (LSWT) employed to describe magnonic transport neglects such interactions and consequently results in an improper account of thermal effects. This theory is formally valid only as long as the fluctuations of S^z are neglected, i.e., close to T=0. In other words, at non-zero temperature, the independent magnon picture fails and interactions must be taken into account. The importance of magnon interactions has been pointed out rather early in antiferromagnets e.g., [1] as well as in nontrivial ferromagnets [2], suggesting that such interactions are in fact ubiquitous. Recent theories suggest that magnon interactions can trigger topological phase transitions [3, 4].

To assess the impact of magnon interactions on topological transport, we focus on a collinear honeycomb antiferromagnet with out-of-plane Dzyaloshinskii-Moriya interaction (DMI), a system that is known to display magnonic spin Nernst effect in the absence of interactions [5, 6]. The system is described by the following spin Hamiltonian

$$H = J_l \sum_{\langle ij \rangle} S_i \cdot S_j + K \sum_i (S_i^z)^2 + D_z \sum_{\langle\langle ij \rangle\rangle} \hat{z} \cdot (S_i \times S_j) + D_{||} \sum_{\langle ij \rangle} \eta_{ij} \cdot (S_{A,i} \times S_{B,j}) \tag{1}$$

where J are the Heisenberg interactions, K is the easy-axis anisotropy, D_z is the out-of-plane DMI and $D_{||}$ is the intefacial DMI. We consider two cases of interactions: the four magnon interactions (order $O(S^0)$) due to higher order of the Holstein-Primakoff transformation that should appear naturally in higher temperatures and the three magnon interactions (order $O(S^{1/2})$) that appear in the case of the interfacial DMI introduced in Eq. (1). We will consider an interacting Hamiltonian

$$H_{int} = H_k^{(2)} + H_k^{(4)}(T) + \Sigma_k^{(3)}(\epsilon, T), \tag{2}$$

where $H_k^{(2)}$ is the LSWT Hamiltonian, the four-magnon Hamiltonian $H_k^{(4)}(T)$ will be treated by a Mean Field Theory (MFT) and $\Sigma_k^{(3)}(\epsilon, T)$ is the self-energy correction caused by the three-magnon interaction of the $D_{||}$. In Fig. 1, we plot the energy renormalization of the magnon spectrum due to the four-magnon term treated in MFT. This correction to the Hamiltonian is temperature dependent and it influences both the band structure and the Berry curvature.

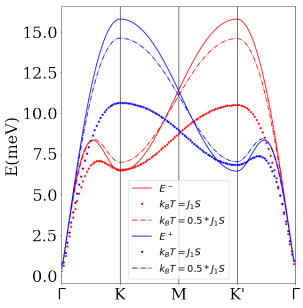

Figure 1: The energy spectrum along the high symmetry path of the Brillouin Zone for both the non-interacting model (straight line) and interacting model at higher temperatures (dash-dot line, point line).

In Fig. 2, we plot the Spin Nernst conductivity for the non-interacting case and the conductivity corrected by the MFT temperature-dependent theory. In the non-interacting case, two different values of the out-of-plane DMI, D_z and $D_z/4$, is plotted. We can see that the interacting conductivity matches the original value at low temperatures but it approaches the smaller value at higher temperatures.

In conclusion, we can see that the interactions affect the topological transport of magnons in multiple non-trivial ways and should be considered to properly describe the anomalous magnonic transport.

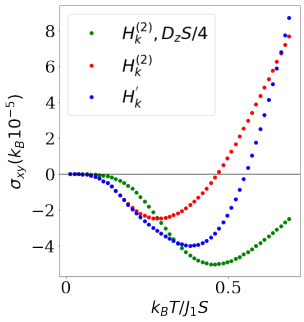

Figure 2: The magnon Spin Nernst conductivity is plotted along the temperature for the non-interacting model for two different values of out-of-plane DMI (green and red line) and the interacting model (blue line). The interacting conductivity matches the non-interacting one for low temperatures but as the temperature increases it approaches the negative values for a lower DMI.

Acknowledgments

K.S. and A.M acknowledge support from the Excellence Initiative of Aix-Marseille Universite - A*Midex, a French "Investissements d'Avenir" program.

References

[1] A.B Harris et al. Dynamics of an antiferromagnet at low temperatures: spin-wave damping and hydrodynamics. *Phys. Rev. B* 3, 961 (1971).

[2] A.L. Chernyshev and P.A. Maksimov. Damped Topological Magnons in the Kagome-Lattice Ferromagnets. *Phys. Rev. Lett.* 117, 187203 (2016).

[3] A. Mook et al. Interaction-Stabilized Topological Magnon Insulator in Ferromagnets. *Phys. Rev. X* 11, 021061 (2021).

[4] Y.-S. Lu et al. Topological Phase Transitions of Dirac Magnons in Honeycomb Ferromagnets. *Phys. Rev. Lett.* 127, 217202 (2021).

[5] R. Cheng et al. Spin Nernst effect of magnons in collinear antiferromagnets. *Phys. Rev. Lett.* 117, 217202 (2016).

[6] V.A. Zyuzin and A.A. Kovalev. Magnon Spin Nernst Effect in Antiferromagnets. *Phys. Rev. Lett.* 117, 217203 (2016).

Reconfigurable Co_2MnSi Heusler-based magnonic crystals

S. Mantion [*1,*], M. Madami[2], S. Tacchi[3], and N. Biziere[1]

[1]*CEMES, Université de Toulouse, CNRS, UPS, Toulouse, France*
[2]*Dipartimento di Fisica e Geologia, Università di Perugia, Perugia, Italy*
[3]*Istituto Officina dei Materiali del CNR (CNR-IOM), Università di Perugia, Perugia, Italy*
*nicolas.biziere@cemes.fr

Magnonic crystals are magnetic materials whose magnetic properties are periodically and artificially modified, which generates specific frequency band gaps in the spin waves dispersion. These micro/nanostructured systems can be used for passive microwave devices, such as filters, waveguides, sensors, and for logic components, such as transistors [1]. Currently, the majority of the magnonic devices present in the literature have to operate with saturated magnetization states stabilized with the application of a saturation field. This requires the use of permanent magnets, which limits their on-chip integration. Studies are then conducted to develop magnonic devices that can be reconfigurable at zero bias field, i.e. at remanence. In the magnonic context, a reconfigurable device is a system that can offer different microwave responses that can be modified on purpose. In this context, Heusler based Co_2MnSi (CMS) thin films are promising candidates for magnonic applications owing to their relatively high saturation magnetization ($\approx$ 1.2 T [2]), low damping coefficient (2.10^{-3} down to 7.10^{-4} [2, 3]) and strong magneto-crystalline anisotropy ($\approx$ 30 mT [2]).

In particular, we first demonstrated with micromagnetic simulations that its strong cubic anisotropy allows the stabilization of different quasi-uniform remanent states depending on the direction of an applied initialization field in a magnonic crystal model system: a square magnetic antidot lattice with antidot sizes in the range $300-50$ nm and for an aspect ratio lower than 1/3 [4]. When a microwave signal is applied, these different remanent states offer different microwave responses, in particular one where the spin wave modes are well excited ("ON" state) and one where the latter are strongly attenuated ("OFF" state). We also showed that the transition between the different remanent states can be achieved with low amplitudes of field pulses of a few mT and switching times in the order of 1 ns. CMS magnonic crystals with antidot size 200 nm and spacing $600-800$ nm were then fabricated with a combination of e-beam lithography (EBL) and ion beam etching (IBE) (see Fig. 1 a)). Ferromagnetic resonance (FMR) experiments were performed to firstly study the excited quantized and confined spin wave modes in these magnonic crystals. Their microwave response was measured via a deposited micro-antenna. Well-resolved standing spin wave modes were observed, resulting in the measurement of a reconfigurable property at remanence numerically predicted (see Fig. 1 c) and d)). Micromagnetic simulations in the case of ideal geometries and magnetic properties quantitatively fit the experimental results. Micro-Brillouin Light Scattering (BLS) measurements performed on another sample but processed by the same technique further confirm the good agreement between the simulations and the FMR experiments (see Fig. 1 b)).

Acknowledgments

This work was performed using HPC resources from CALMIP (Grant No. 2022-p1554).

References

[1] A V Chumak, A A Serga, and B Hillebrands. Magnonic crystals for data processing. *Journal of Physics D: Applied Physics* 50, 244001 (2017).

[2] I Abdallah, B Pradines, N Ratel-Ramond, et al. Evolution of magnetic properties and damping coefficient of Co2MnSi Heusler alloy with Mn/Si and Co/Mn atomic disorder. *Journal of Physics D: Applied Physics* 50, 035003 (2016).

[3] C. Guillemard, S. Petit-Watelot, L. Pasquier, et al. Ultralow Magnetic Damping in Co_2Mn-Based Heusler Compounds: Promising Materials for Spintronics. *Phys. Rev. Appl.* 11, 064009 (6 2019).

[4] S. Mantion and N. Biziere. Cubic Anisotropy for a Reconfigurable Magnonic Crystal Based on Co_2MnSi Heusler Alloy. *Phys. Rev. Appl.* 17, 044054 (4 2022).

*now working at Unité Mixte de Physique CNRS, Thales, Université Paris-Saclay, Palaiseau, France

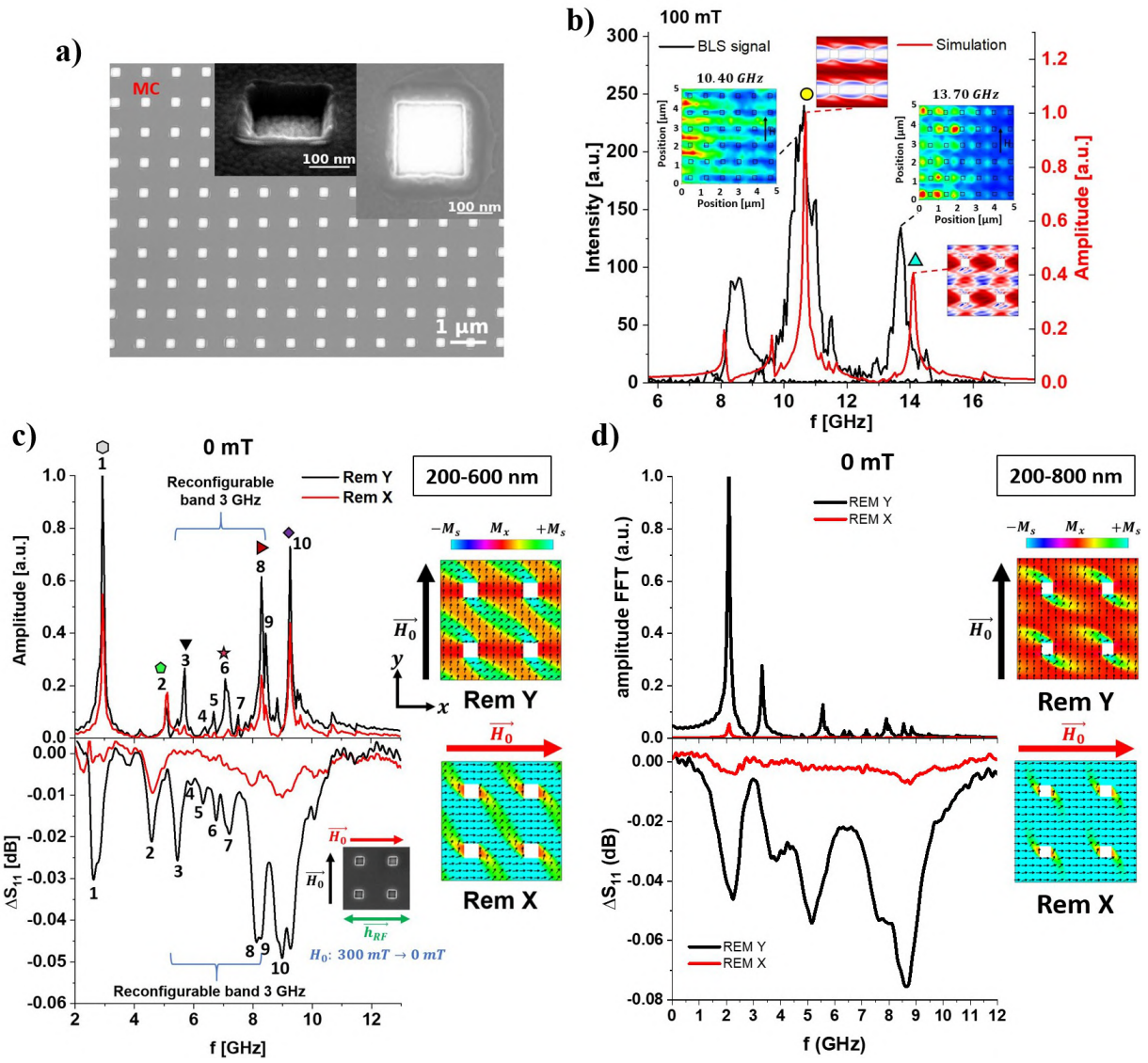

Figure 1: a) SEM image of the CMS magnonic crystal (2D antidot lattice) with square antidot size of 200 nm and spacing 600 nm (as insets, zoomed SEM images of a CMS antidot at a 52° tilted view (left) and top view (right)). b) Micro-BLS intensity (black curve) and FFT (red curve) spectra at $\mu_0 H_0 = 100$ mT measured on a CMS magnonic crystal. Insets of the 2D spatial mapping of the amplitude of two main propagating spin wave modes, extended (indexed with yellow circle) and localized (cyan triangle). c), d) (Right) Calculated remanent magnetic states when an initialization field is applied along y (Rem Y) or along x (Rem X), (Left) plots of the FFT spectra (upper graph) and the measured ΔS_{11} parameters (lower graph) in the Rem Y (black line) and Rem X (red line) states for a CMS magnonic crystal with antidot size 200 nm and c) spacing 600 nm, d) spacing 800 nm.

Unraveling non-reciprocal and non-degenerated ultra-fast spin-waves in the canted antiferromagnet α-Fe_2O_3

Aya El Kanj[1,*], Olena Gomonay[2], Isabella Boventer[1], Paolo Bortolotti[1], Vincent Cros[1], Abdelmadjid Anane[1], and Romain Lebrun[1]

[1]*Unité Mixte de Physique, CNRS, Thales, Université Paris-Saclay, 91767 Palaiseau, France*
[2]*Institute of Physics, Johannes Gutenberg-University Mainz, 55128 Mainz, Germany*
*aya.elkanj@cnrs-thales.fr

Magnonics, the study of spin-Waves (SW) and their quanta magnons, has emerged as an attractive field of research and has been studied extensively in ferromagnetic materials (FM) in the last few decades. One attractive property of these spin-waves is their existence on nanometer wavelengths at GHz frequencies, making them promising candidates for information processing applications. Additionally, thanks to the presence of uncompensated dipolar fields in FM, many important properties were revealed, including non-reciprocity, magneto-static spin waves [1], and Bose-Einstein condensation [2]. These properties play a crucial role in developing integrated magnonic devices for beyond CMOS technologies.

Whereas the other family displaying magnetic order, namely the antiferromagnetic materials (AFM), has for many years been scarcely studied [3]. It is only recently that there is a renewal of interest in canted antiferromagnetic materials, with the presence of bulk Dzyaloshinskii-Moriya interaction or standard collinear antiferromagnets under applied magnetic fields as they exhibit a dipole-exchange regime of their antiferromagnetic spin-waves making them accessible to inductive excitation and detection schemes which of most relevance for applications. The associated dipolar interaction holds the promise of a rich landscape of properties and tunability equivalent to that of FM spin-waves such as anisotropy, non-reciprocity and Bose-Einstein Condensation.

Here we highlight the existence of ultra-fast magneto-static SWs in the canted antiferromagnetic phase of (α-Fe_2O_3) [4], known as Hematite, using propagating spin wave spectroscopy between two inductive k-selective antennas (**Figure 1 (a)**). We study the propagation in two configurations, one where the propagation vector **k** is perpendicular to the Néel vector **n** (bulk magnons) and the other where the propagation vector **k** is parallel to the Néel vector **n** (surface magnons). As a result, we find a lifted non-degeneracy between the two magnon dispersion modes of up to 1 GHz [5] (see **Figure 1 (b-c)**). To go further, we use time of flight spin-wave spectroscopy [6] to determine the spin-wave velocity, ranging from 10 to 20 km/s, and demonstrate the presence of both non-reciprocal and reciprocal antiferromagnetic surface magnon modes.

Lastly, we achieve an efficient electrical detection of propagating non-reciprocal antiferromagnetic spin-wave using non-local inverse spin-Hall effects measurements via spintronic (platinum) transducers [7]. We believe that our experimental results demonstrate all the potentials of such antiferromagnets for establishing a new research field in magnonics based on canted antiferromagnets, which can also possess altermagnets behavior, and hold a lot of opportunities for high-frequency magnonics.

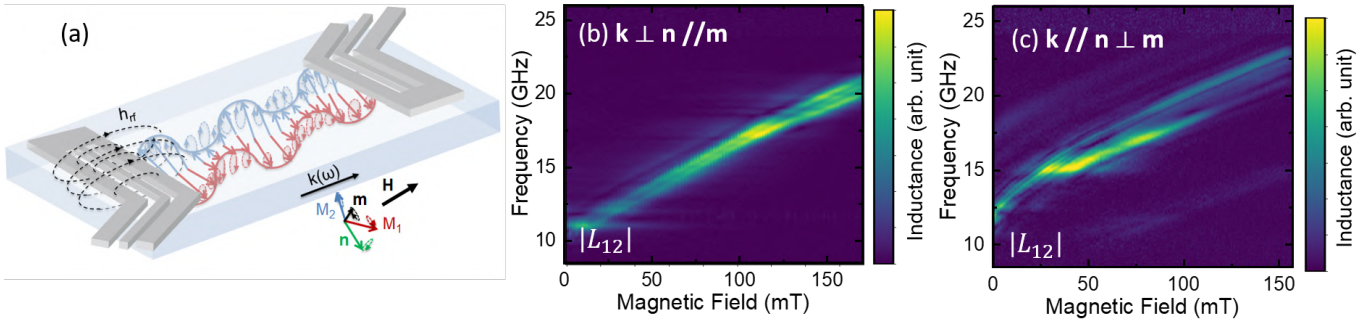

Figure 1: (a) Schematic of the set-up, (b-c) Spin wave transmission measurement showing the transmitted amplitude $|L_{12}|$ at k ≈ 0.6 rad/μm for k ⊥ n (//m) for panel (b) and k //n (⊥ m) for panel (c).

Acknowledgments

Financial supports from the Horizon 2020 Framework Programme of the European Commission under FET-Open grant agreement No. 863155 (s-Nebula), under FET-Open grant agreement No. 964931 (TSAR) and under the ITN Grant agreement ID: 861300 (COMRAD) are acknowledged. The authors also acknowledge support from the ANR TRAPIST (ANR-21-CE24-0011).

References

[1] B A Kalinikos and A N Slavin. Theory of dipole-exchange spin wave spectrum for ferromagnetic films with mixed exchange boundary conditions. *Journal of Physics C: Solid State Physics* 19, 7013–7033 (20, 1986).

[2] B. Divinskiy, H. Merbouche, V. E. Demidov, et al. Evidence for spin current driven Bose-Einstein condensation of magnons. *Nature Communications* 12, 6541 (11, 2021).

[3] R. E. Camley. Long-Wavelength Surface Spin Waves on Antiferromagnets. *Physical Review Letters* 45, 283–286 (28, 1980).

[4] R. Lebrun, A. Ross, O. Gomonay, et al. Long-distance spin-transport across the Morin phase transition up to room temperature in ultra-low damping single crystals of the antiferromagnet α-Fe_2O_3. *Nature Communications* 11, 6332 (10, 2020).

[5] A. El Kanj, O. Gomonay, I. Boventer, et al. Evidence of non-degenerated, non-reciprocal and ultra-fast spin-waves in the canted antiferromagnet α-Fe_2O_3 (2023). arXiv: 2301.06329 [cond-mat.mes-hall].

[6] T. Devolder, G. Talmelli, S. M. Ngom, et al. Measuring the dispersion relations of spin wave bands using time-of-flight spectroscopy. *Physical Review B* 103, 214431 (21, 2021). arXiv: 2104.04262[cond-mat,physics:physics].

[7] A. V. Chumak, A. A. Serga, M. B. Jungfleisch, et al. Direct detection of magnon spin transport by the inverse spin Hall effect. *Applied Physics Letters* 100, 082405 (20, 2012).

Chiral excitation of exchange spin waves using gold nanowire grating

Loic Temdie[1,2 *], Vincent Castel[1,2], Carsten Dubs[3], Gyandeep Pradan[4], Jose Solano[4], Romain Bernard[4], Hicham Majjad[4], Yves Henry[4], Matthieu Bailleul[4], and Vincent Vlaminck[1,2]

[1]*IMT- Atlantique, Dpt. MO, Technopole Brest-Iroise CS83818, 29238 Brest Cedex 03, France*
[2]*2Lab-STICC - UMR 6285 CNRS, Technopole Brest-Iroise CS83818, 29238 Brest Cedex 03, France*
[3]*INNOVENT e.V. Technologieentwicklung, Pruessingstrasse 27B, 07745 Jena, Germany*
[4]*IPCMS - UMR 7504 CNRS Institut de Physique et Chimie des Matériaux de Strasbourg, France*
**loic.temdie-kom@imt-atlantique.fr*

Magnonics is a promising scientific field in which spin waves, or their quanta, magnons, are used for their potential applications for the development of non-reciprocal components [1, 2]. The ability to stir and shaped spin wave beams at the submicron scale [3–5] opens up significant opportunities for advancing the miniaturization of interferometric devices. Recent advances have demonstrated the successful unidirectional transmission of exchange spin waves by taking advantage of the chiral coupling between resonant ferromagnetic nanowires and the high wave-vector spin wave modes in a thin YIG film. [6, 7].

In this work, we propose a new approach to study the unidirectional excitation of exchange spin waves. Taking advantage of the chiral coupling of the magnetization precession with the microwave field of a nanowire, we designed two nanowire arrays distant each other by D=20 µm, directly fabricated onto a 55 nm-thin YIG film (see Fig.1(a)). We show in Fig.1(b),(c) mapping (H_{ext},f) of the transmission spectra ΔL_{12} and ΔL_{21} respectively measured from -192 to 192 mT. We observe up to 6 well-resolved branches, which display complete non-reciprocity at higher frequency, that is reversed when switching the polarity of the applied static field. Fig.1(d)-(g) shows a zoom of the spectra at 65 mT for the four peaks corresponding to the uniform thickness mode $m = 0$. We notice a partial chirality for the two first peak $k_0^{m=0}$ and $k_1^{m=0}$ (see Fig.1(d) and (e)) , while the spectra for higher wave vectors $k_2^{m=0}$ and $k_3^{m=0}$ (see Fig.1(f) and (g)) show perfect unidirectional transmission. With such a geometry of excitation, where all the nanowires microwave fields are in phase, we obtain very well-resolved peaks, whose wavevectors are multiples of the inverse of the grating periodicity (a), namely $k_n = n\frac{2\pi}{a}$. Although the amplitude of the higher frequency peak decays rapidly, we are able to sense with this particular device (e.g. 100 nm-wide bars spaced by a=400 nm) exchange spin-waves up to 50 $rad.\mu m^{-1}$. It is make possible to excite the highest wave vectors with this geometry, simply by reducing the periodicity between the Au nanowires. Taking advantage of the sharp spectral definition of this technique, we present a complete study of the spin wave propagation properties, including in particular the wavevector dependence of the relaxation time. Therefore, this robust technique constitutes a method of choice for spin wave spectroscopy characterization of high wave vector in any orientation of external field. Furthermore, we show how the multimodes bandwidth can be engineered by adjusting the dimensions and spacing of the nanowire grating, with achiveable range up to 100 $rad.\mu m^{-1}$. Our findings have important implications for the development of non-reciprocal magnonic devices.

Acknowledgments

The authors acknowledge the financial support from the French National research agency (ANR) under the project MagFunc, the Region Bretagne with the CPER-Hypermag project, and the Département du Finistère through the project SOSMAG.

References

[1] A. V. Chumak, P. Kabos, M. Wu, et al. Advances in Magnetics Roadmap on Spin-Wave Computing. *IEEE Transactions on Magnetics* 58, 1–72 (2022).

[2] Anjan Barman, Gianluca Gubbiotti, S Ladak, et al. The 2021 Magnonics Roadmap. *Journal of Physics: Condensed Matter* 33, 413001 (2021).

[3] N. Loayza, M. B. Jungfleisch, A. Hoffmann, M. Bailleul, and V. Vlaminck. Fresnel diffraction of spin waves. *Physical Review B* 98 (2018).

[4] Joachim Gräfe, Pawel Gruszecki, Mateusz Zelent, et al. Direct observation of spin-wave focusing by a Fresnel lens. *Physical Review B* 102 (2020).

[5] V. Vlaminck, L. Temdie, V. Castel, et al. Spin wave diffraction model for perpendicularly magnetized films. *Journal of Applied Physics* 133, 053903 (2023).

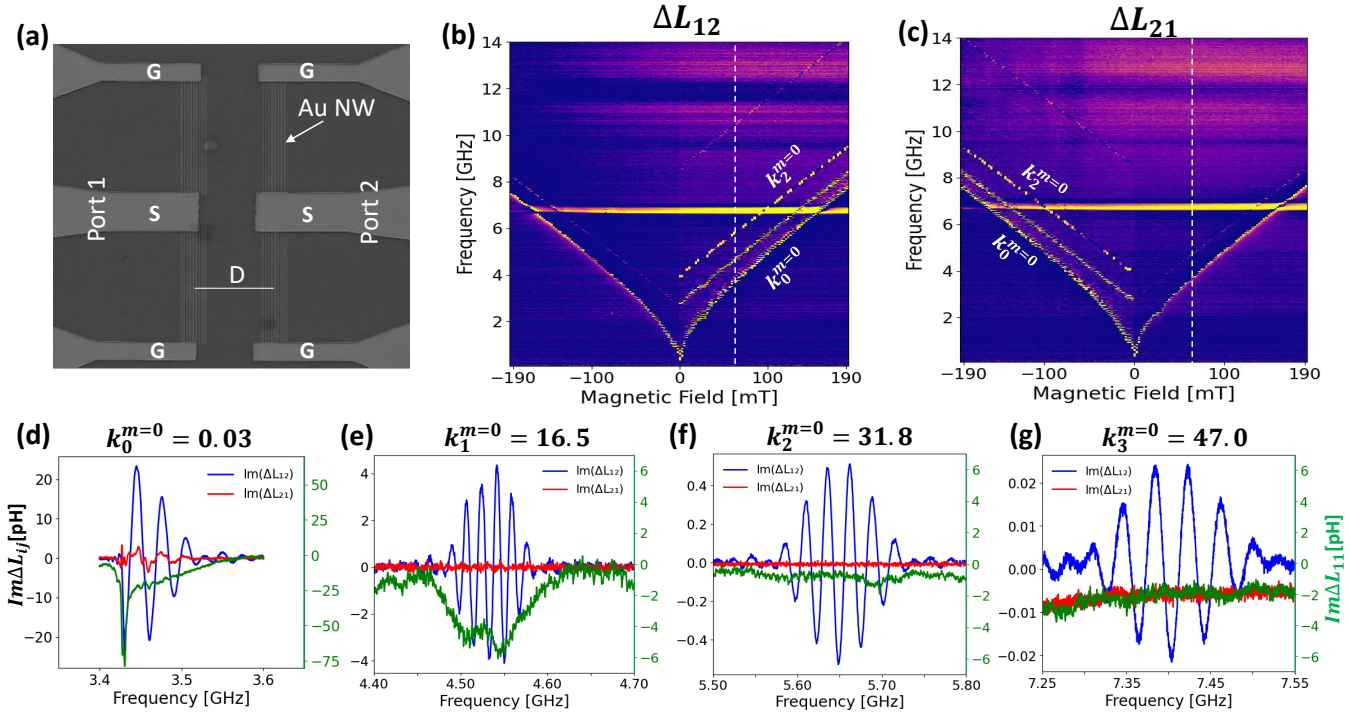

Figure 1: (a) SEM image of the Au nanowire-grating sample. (b) and (c) mapping (H_{ext},f) of the transmission spectra measured from -192 to 192 mT applied field. Spectra obtained at $\mu_0 H_{\text{ext}}$=65 mT for (d)-(g) the first four spin wave modes corresponding to the uniform thickness mode $m = 0$.

[6] Jilei Chen, Tao Yu, Chuanpu Liu, et al. Excitation of unidirectional exchange spin waves by a nanoscale magnetic grating. *Physical Review B* 100 (2019).

[7] L. Temdie, V. Castel, C. Dubs, et al. High wave vector non-reciprocal spin wave beams. *AIP Advances* 13, 025207 (2023).

Resonant coupling between Surface Acoustic Waves and Spin Waves : propagation and non reciprocity

Louis Christienne[1,*], Pauline Rovillain[1], Silvia Tacchi[2], Marco Madami[3], Jean-Yves Duquesne[1], Mahmoud Eddrief[1], Abdelmadjid Anane[4], and Massimiliano Marangolo[1]

[1]*INSP, Sorbonne Université, CNRS, Paris, France*
[2]*Istituto Officina dei Materiali del CNR, Sede secondaria di Perugia c/o Dipartimento di Fisica e Geologia, Università di Perugia, Italy*
[3]*Università di Perugia, Dipartimento di Fisica e Geologia, Perugia, Italy*
[4]*Unité Mixte De Physique, CNRS, Thales, Université Paris-Saclay, Palaiseau, France*
*louis.christienne@insp.upmc.fr

Lord Raleigh's principle, established in 1873, states that the signal received by a receiver remains unchanged when the positions of the vibration source and receiver are interchanged, highlighting the concept of reciprocity in wave propagation. This principle poses a fundamental limitation, as under reciprocity, it is impossible to tune transmission to different levels in opposite directions, thereby impeding the creation of acoustic and elastic wave devices that exploit unidirectional transmission, such as acoustic diodes.[1] However, it is well-known that breaking time symmetry in ferromagnetic materials can lead to non-reciprocal sound propagation. In 1958, Kittel provided a field-theoretical treatment of the magnetoelastic coupling of magnons and phonons in ferromagnetic crystals, emphasizing the substantial effects when the wavelengths and frequencies of the two fields coincide, suggesting the possibility of creating non-reciprocal acoustic elements, including acoustic gyrators. [2] In this context, acoustics takes benefit of the 'natural' non reciprocity of Spin Waves (SWs). Building upon this theoretical foundation, our study focuses on Surface Acoustic Waves (SAWs) propagation in epitaxial iron thin films on GaAs in the GHz regime completed by Brillouin Light Scattering experiments to probe SWs dispersion and SWs non reciprocity. To interpret the experimental data, we employ a phenomenological approach that considers LLG equations and magnetoelastic interaction to describe the observed relative changes in SAW velocity and attenuation as a function of the direction and the intensity of the applied magnetic field. [3], [4] Remarkably, our findings demonstrate that the observed velocity variation and the non-reciprocity of SAWs can be effectively described by incorporating into the usual elastic magnetoelastic calculations the spin-wave dispersion and the so-called rotation tensor ω (XZ component defined in eq.1, represented in Fig. 1) [5], an additional dynamical component that survives in the thin-film limit.

$$\varepsilon_{XX} = \frac{\partial u_X}{\partial X},\ \varepsilon_{XZ} = \frac{1}{2}\left(\frac{\partial u_X}{\partial Z} + \frac{\partial u_Z}{\partial X}\right),\ \omega_{XZ} = \frac{1}{2}\left(\frac{\partial u_X}{\partial Z} - \frac{\partial u_Z}{\partial X}\right) \tag{1}$$

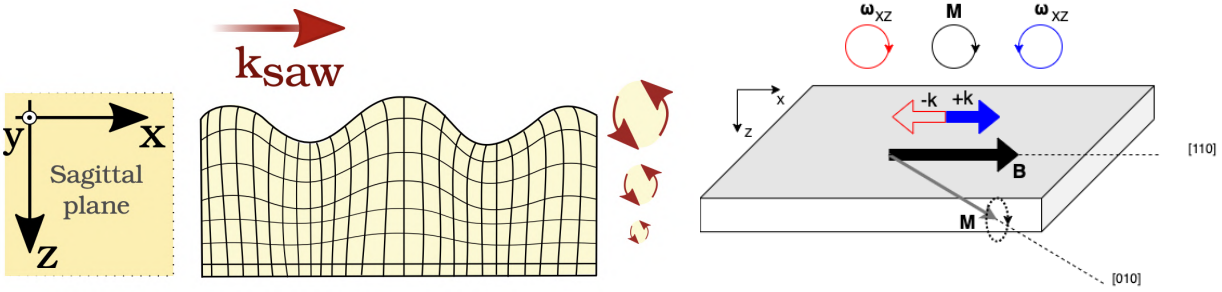

Figure 1: Rayleigh-type Surface Acoustic Wave described as its surface displacement and rotation. The lattice rotates in opposite direction when the SAW direction is reversed. Hence, the SAW-SWs coupling depends on the SAW propagation direction leading to non reciprocity.

By accounting for the influence of spin waves, our analysis provides a comprehensive understanding of the experimental phenomena observed in SAW propagation (attenuation and velocity change in the wave, see Fig.2). These results highlight the significance of considering spin-wave effects in achieving non-reciprocal sound propagation and emphasize the potential for developing advanced acoustic devices. Our study represents a significant contribution to the field of non-reciprocal acoustics, showcasing successful SAW propagation in epitaxial iron on GaAs and providing a solid interpretation framework through the incorporation of spin-wave dispersion.

Furthermore, the observed non-reciprocity in surface acoustic wave propagation holds crucial implications for magnonic devices, where surface acoustic waves not only act as triggers for magnetization dynamics but also promote preferential spin waves propagation in a specific direction. This interplay between non-reciprocal acoustic behavior and magnetization dynamics highlights the potential for developing novel magnonic devices controlled by remote SAW transducers.

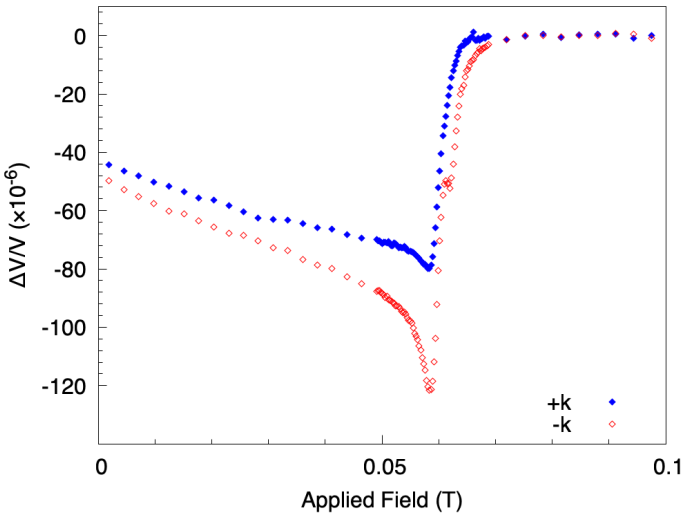

Figure 2: Non reciprocity in the velocity variation at resonance between positive (blue) and negative (red) SAW wave vector

Acknowledgments

The authors acknowledge support from the Agence National de la Recherche Française Grant No. ANR-22-CE24-0015 SACOUMAD and from the European Union within the HORIZON-CL4- 2021-DIGITAL-EMERGING-01 Grant No. 101070536 MandMEMS.

References

[1] Hussein Nassar, Behrooz Yousefzadeh, Romain Fleury, et al. Nonreciprocity in acoustic and elastic materials. *NATURE REVIEWS MATERIALS* 5, 667–685 (2020).

[2] C KITTEL. INTERACTION OF SPIN WAVES AND ULTRASONIC WAVES IN FERROMAGNETIC CRYSTALS. *PHYSICAL REVIEW* 110, 836–841 (1958).

[3] Pauline Rovillain, Jean-Yves Duquesne, Louis Christienne, et al. Impact of Spin-Wave Dispersion on Surface-Acoustic-Wave Velocity. *PHYSICAL REVIEW APPLIED* 18 (2022).

[4] J-Y Duquesne, P. Rovillain, C. Hepburn, et al. Surface-Acoustic-Wave Induced Ferromagnetic Resonance in Fe Thin Films and Magnetic Field Sensing. *PHYSICAL REVIEW APPLIED* 12 (2019).

[5] Mingran Xu, Kei Yamamoto, Jorge Puebla, et al. Nonreciprocal surface acoustic wave propagation via magneto-rotation coupling. *SCIENCE ADVANCES* 6 (2020).

Evidence of unidirectional spin waves in synthetic antiferromagnetic

Florian Millo[1, *], Jean-Paul Adam[1], Claude Chappert[1], Joo-Von Kim[1], Asma Mouhoub[1], Aurelie Solignac[2], and Thibaut Devolder[1]

[1]*C2N - Université Paris-Saclay, Palaiseau 91120, France*
[2]*SPEC, CEA, Gif-sur-Yvette 91190, France*
**florian.millo@university-paris-saclay.fr*

Spin waves (SWs) are elementary magnetic excitation exhibiting nonreciprocity (NR) and nonlinear behaviour. NR is the situation where the frequency $\omega(\vec{k})$ of a SW changes upon reversing the direction of phase propagation[1]. During the last decades, NR SWs have grown in interest for many applications such as magnonic diodes, directional spin wave emitters, and passive non-reciprocal filters.

In this work we study the NR behaviour of SWs in (CoFeB / Ru / CoFeB) [see Fig. 1(a) and Fig. 2(a)] synthetic antiferromagnet (SAF) i. e. two ferromagnetic layers separated by a spacer layer that mediates an effective interlayer coupling energy $J < 0$ favoring an antiparallel state. SWs in SAF have two precession modes[2], acoustical (in-phase) and optical (out-of-phase).

In layer-to-layer dipolar dominated SAF system a large NR of SWs can lead to unidirectional flow of energy for acoustical mode. To evidence it, we use two experimental techniques where an in-plane static field is applied; 1) Brillouin Light Scattering (BLS) [see Fig. 1(b)] to measure the dispersion relation [see Fig. 1(c)] of SWs in Si / SiO_x/ SAF. We observed non-reciprocity for the two modes. The interesting case is the large NR of acoustical mode which leads to the "unidirectional" flow of energy of acoustical SWs.

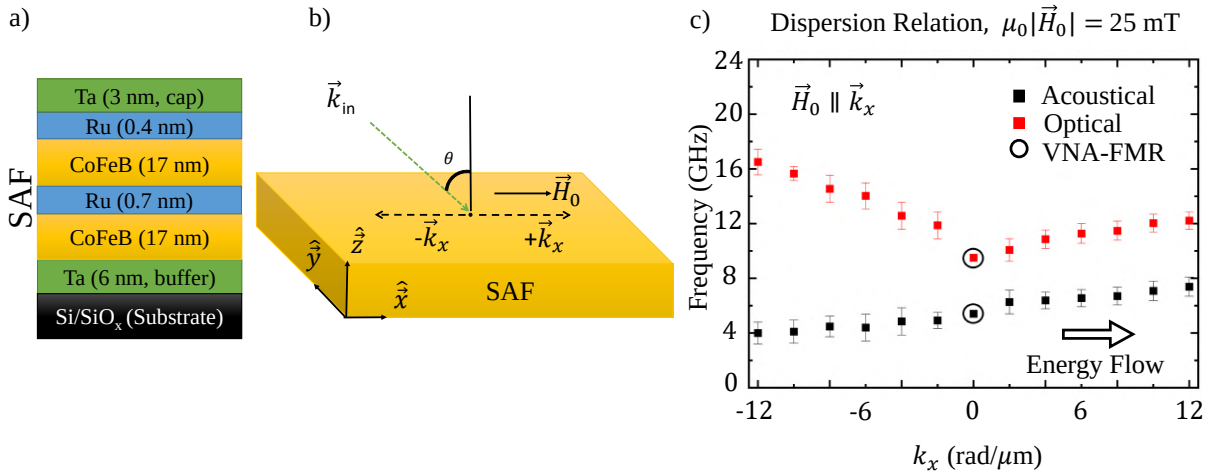

Figure 1: a) Stack of the synthetic antiferromagnet used for the BLS experiments. b) BLS geometry: the applied field $\vec{H}_0$ is parallel to the $\hat{x}$ axis, plane of incidence (xz), wavelength of laser beam $\lambda = 532$ nm. c) Dispersion relations are measured by BLS for $\vec{H}_0 \parallel \vec{k}_x$. The uniform resonances (k=0) were measured by VNA-FMR. The error bars are the linewidths (full width at half maximum). The black arrow recalls that the group velocity of the acoustical SWs always points toward the positive side, irrespective of the sign of the wavevector.

2) Propagating spin wave spectroscopy [see Fig. 2(c,d,e,f)] to electrically demonstrate that acoustical SWs travel in a one way manner "unidirectional" which was not demonstrated before. A similar electrical experiment was performed in Ishibashi *et al*[3] to electrically switch the non-reciprocity sign of optical SWs in SAF but not being able to demonstrate the unidirectional propagation of acoustical SWs.

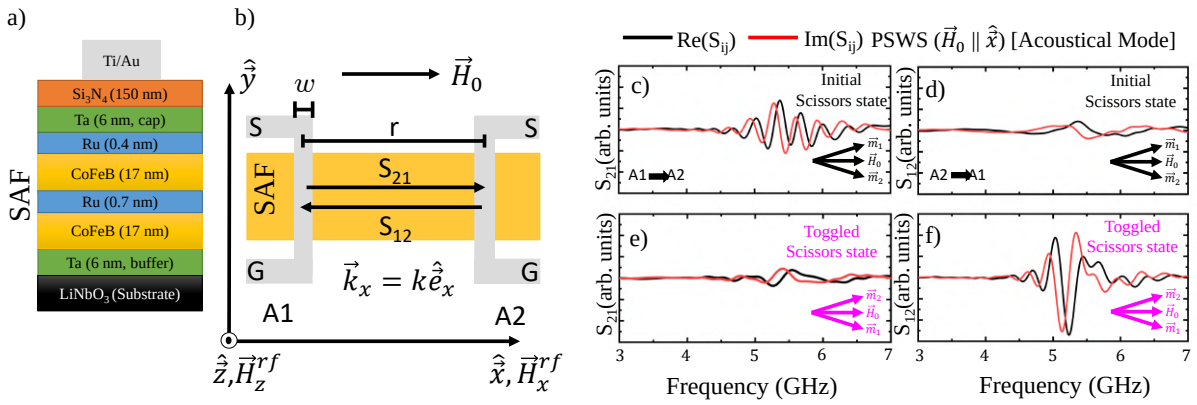

Figure 2: a) Stack of synthetic antiferromagnetic film patterned into devices for propagating spin wave spectroscopy experiments. b) Geometry of the device. Gray: single-wire antennas with $r = 6$ μm and $w = 1.8$ μm. Antenna 1 (A1) and Antenna 2 (A2) are connected to a VNA to collect transmission $[S_{12}, S_{21}]$ parameters. c) and d) Forward and backward transmission parameter measured for wave propagating from A1-to-A2, A2-to-A1 respectively and at one of two possible degenerate scissors state. e) and f) Forward and backward transmission parameter measured for propagating SWs after toggling the scissors state.

To make a complete investigation, we compare experimental measurements with micromagnetic simulations[4] and analytical framework based on Dynamic Matrix Theory[1, 5]. Different situations are taken into account; $\vec{H}_0 \parallel \vec{k}_x$, $\vec{H}_0 \perp \vec{k}_x$ and angle-resolved dispersion relations. Two first situations are compared with Ishibashi's analytical model[3] whereas angle-resolved dispersion relations are first introduced by us.

Our formalism predicts the unidirectional acoustical SWs and provides a simple to use equation to calculate the NR of SWs:

$$\delta f_{op},\ -\delta f_{ac} = \gamma_0 M_s k\, t_{\text{mag}} \sqrt{1-\left(\frac{H_0}{H_j}\right)^2}\ \cos\varphi \tag{1}$$

Overall, we perform a comparison between different experimental techniques, micromagnetic simulations, and existing analytical frameworks where we find a good qualitative and quantitave agreement allowing us to better understand the system.

Acknowledgments

The authors acknowledge the French National Research Agency (ANR) under contract N^o ANR-20-CE24-0025 (MAXSAW). This work was supported by a public grant overseen by the French National Research Agency (ANR) as part of the "Investissements d'Avenir" program (Labex NanoSaclay, reference: ANR-10-LABX-0035, project SPICY). This work was done within the C2N micro nanotechnologies platforms and partly supported by the RENATECH network and the General Council of Essonne.

References

[1] F. C. Nörtemann, R. L. Stamps, and R. E. Camley. Microscopic calculation of spin waves in antiferromagnetically coupled multilayers: Nonreciprocity and finite-size effects. *Physical Review B* 47, 11910–11923 (1993).

[2] R. L. Stamps. Spin configurations and spin-wave excitations in exchange-coupled bilayers. *Physical Review B* 49, 339–347 (1994).

[3] Mio Ishibashi, Yoichi Shiota, Tian Li, et al. Switchable giant nonreciprocal frequency shift of propagating spin waves in synthetic antiferromagnets. *Science Advances* 6 (2020).

[4] Arne Vansteenkiste, Jonathan Leliaert, Mykola Dvornik, et al. The design and verification of MuMax3. *AIP Advances* 4, 107133 (2014).

[5] Yves Henry, Olga Gladii, and Matthieu Bailleul. *Propagating spin-wave normal modes: A dynamic matrix approach using plane-wave demagnetizating tensors*. 2016.

All-inductive observation of nonlinear spin wave processes in synthetic antiferromagnet microstripes

A. Mouhoub[1, *], C. Chappert[1], J.-V. Kim[1], A. Solignac[2], and T. Devolder[1]

[1]*Université Paris-Saclay, CNRS, Centre de Nanosciences et de Nanotechnologies, 91120 Palaiseau, France*
[2]*SPEC, CEA, CNRS, Université Paris-Saclay, 91191 Gif-sur-Yvette, France*
**asma.mouhoub@u-psud.fr*

Spin waves (SW) are the eigen-excitations of magnetic order parameters. The transport of information by spin is one of the important domains in condensed matter physics and of fundamental importance for the further development of spintronic devices due to their specific properties such as: GHz frequency, nanoscale wavelength, anisotropic propagation, non-linearity [1, 2], and non-reciprocal character. Synthetic antiferromagnet (SAF) which consists of two magnetic layers separated by a thin nonmagnetic spacing is adequate to study the nonlinearity of spin waves. Here we report on an all-inductive study of nonlinear processes in microstripes of SAF. Such films exhibit two types of SW modes, known as acoustical and optical modes. The frequencies of these modes vary with the applied magnetic field. For specific configurations of the applied static magnetic field H_{DC}, the frequency of the acoustical magnon mode (f_{ac}) becomes half that of the optical magnon mode (f_{op}), a favorable condition to investigate nonlinear phenomena in SAF [1].

We used the experimental configuration shown in Fig.1.a to measure the nonlinear SW processes in a SAF inductively. An RF stimulus is sent through an inductive antenna using a synthesizer to excite spin waves in an optimized $Co_{40}Fe_{40}B_{20}$/Ru/CoFeB stripe [3] acting as spin wave conduit. The response is then recorded on a spectrum analyzer using a second antenna. To investigate nonlinear effects, three parameters are varied: i) the static field H_{DC} chosen for each sample to ensure f_{op}=2 f_{ac}, ii) the microwave power arriving at the sample (-15<P_{in}<11 dBm), and iii) the pump frequency to excite the optical mode (10<f_{pump}<15 GHz). To evidence the nonlinear behaviors, an excess power spectral density is determined by subtracting values recorded on the same sample but for a slightly different value of H_{DC}. A typical spectra is shown in Fig.1.b. The doublets near $f_{pump}/2$ evidence a three-magnon process where one optical magnon at f_{pump} splits into two acoustical magnons at $f_{pump}/2$-δ and $f_{pump}/2$+δ. 2). The second harmonics of the doublet around the f_{pump} indicates that we are deep in the nonlinear regime and the strong halo around f_{pump} corresponds to a four-magnon scattering process, in which two optical magnons excited at f_{pump} annihilate and create two new optical magnons [1, 4].

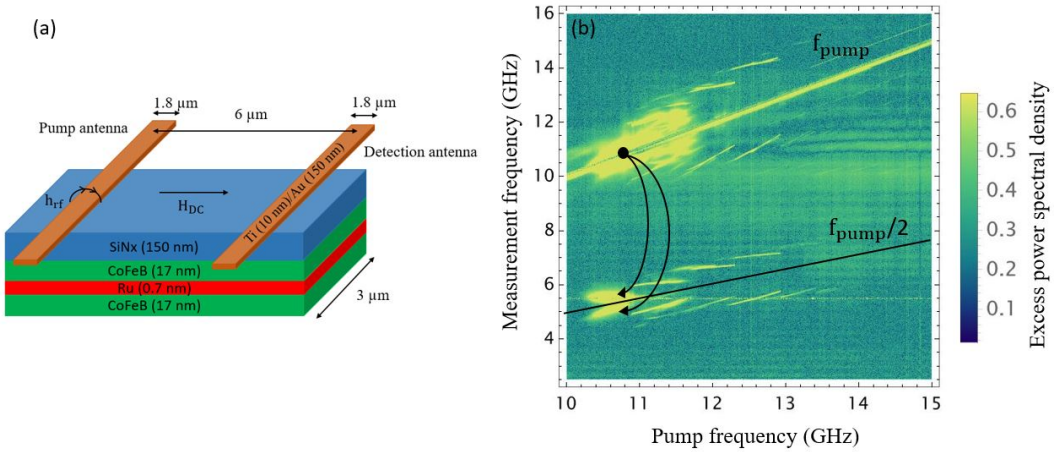

Figure 1: a) Scheme of the experimental configuration. In practice, 4 well separated $Co_{40}Fe_{40}B_{20}$ microstripes are positioned under the antennas to improve the signal-to-noise ratio. b) Spectra of excess power spectral density versus pump frequency at excitation power arriving at the sample 11 dBm and H_{DC}=20 mT, for a SAF with 2x17 nm of CoFeB.

For the three-magnon scattering process, we observe that the frequency of the split magnons is directly related to the input frequency and the power level applied. To further investigate the threshold behavior, we performed a detailed study on the power dependence of the magnon amplitude at various input frequencies. Figure 2.b demonstrates the threshold character of the splitting process.

Furthermore, we are developing a methodology to investigate a time-resolved measurement of nonlinear SW where we use a pulsed RF excitation instead of a continuous wave. The mechanisms of splitting are closely related to the timescales of magnetization dynamics. Magnon lifetimes are on the order of a few nanoseconds, so it is important to ensure that the duration of the pulsed excitation is sufficient to induce nonlinear interactions. To achieve this, we varied the duration of RF pulses from 500 ns to 5 ns. By systematically varying the pulse duration and analyzing the measurements, we can determine the time of the magnons creation and gain insight into their dynamics.

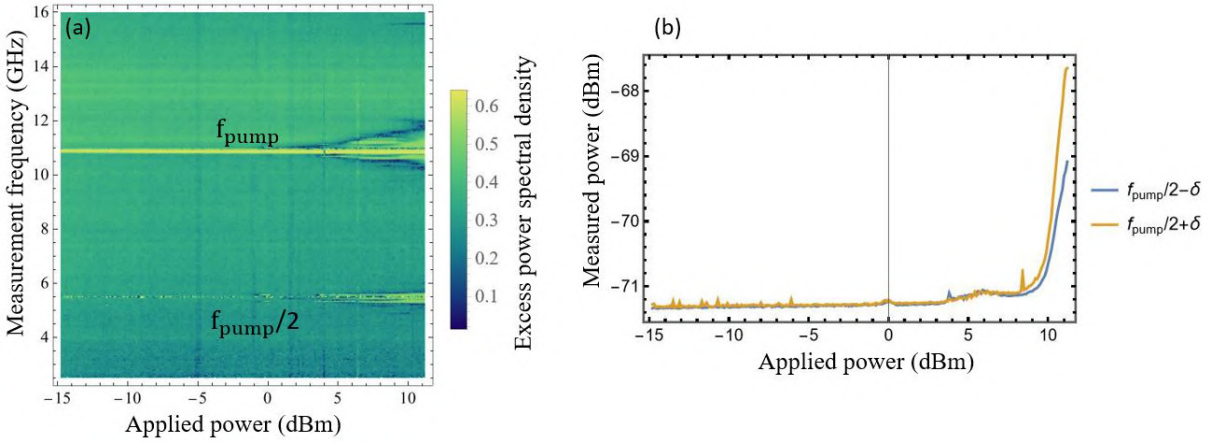

Figure 2: a) The power dependence of the non-linear effects at f_{pump}=10.8 GHz. b) The power threshold of the three-magnon splitting process around the frequencies $f_{pump}/2$-δ=5.4 GHz and $f_{pump}/2$+δ=5.6 GHz as a function of the microwave power arriving at the sample.

Acknowledgments

We acknowledge financial support from the EOBE doctoral school of Paris-Saclay University. This work was done within the C2N micro nanotechnologies platforms and partly supported by the RENATECH network and the General Council of Essonne.

References

[1] A Kamimaki, S Iihama, KZ Suzuki, Natsuhiko Yoshinaga, and S Mizukami. Parametric amplification of magnons in synthetic antiferromagnets. *Physical Review Applied* 13, 044036 (2020).

[2] Roman Verba, Lukas Körber, Katrin Schultheiss, et al. Theory of three-magnon interaction in a vortex-state magnetic nanodot. *Physical Review B* 103, 014413 (2021).

[3] A. Mouhoub, F. Millo, C. Chappert, et al. Exchange energies in CoFeB/Ru/CoFeB synthetic antiferromagnets. *Phys. Rev. Mater.* 7, 044404 (4 2023).

[4] H Schultheiss, K Vogt, and B Hillebrands. Direct observation of nonlinear four-magnon scattering in spin-wave microconduits. *Physical Review B* 86, 054414 (2012).

Session Poster 2 10h50 – 13h00 *Interactions of magnetism with light and photons* *Spin dynamics* *Spintronics* *Strain effects and coupling to phonons*				
2.01	**Maxen Cosset-Chéneau**	Univ. Gronigen	Directional spin Seebeck effect controlled by magnon dipolar stray field chirality	page 162
2.02	**Hugo Merbouche**	SPEC	Non-degenerate parametric excitation in YIG nanostructures	page 163
2.03	**Amel Kolli**	SPEC	Nonlinear interactions between spin-wave modes in YIG microdisks	page 165
2.04	**Gabriel Soares**	SPEC	Damping in garnet microdisks coupled to microwave antennas	page 167
2.05	**Gaël Thiancourt**	C2N	Measurement of the dispersion relation of spin waves using an electrical method	page 169
2.06	**Nessrine Benaziz**	C2N	Spin wave dynamics in antiferromagnetically coupled multilayers	page 171
2.07	**Pauline Rovillain**	INSP	Spin Waves engineering by N-atoms implantation in a Fe film	page 173
2.08	**Paul Noël**	ETHZ	Nonlinear longitudinal and transverse magnetoresistances due to current-induced magnon creation-annihilation processes	page 175
2.09	**Yann Le Guen**	IJL	Study of the manipulation of magnetisation at nano-metric scale by plasmonic systems	page 177
2.10	**Gyandeep Pradhan**	IPCMS	Spin-wave dynamics in curved magnets	page 179
2.11	**Tristan Da Câmara Santa Clara Gomes**	UCLouvain	Interplay between diffusion and magnon-drag thermopower in iron-based nanowire networks	page 181
2.12	**David Schmool**	GeMAC	Spin dynamics in $NdCo_x$/Al/YIG trilayer systems	page 183
2.13	**Pascal Thibaudeau**	CEA Le Ripault	Physics-Informed Neural Networks for nutating anti-ferromagnetic moments	page 185
2.14	**Gauthier Philippe**	C2N	Émission unidirectionnelle d'onde de spin par effet Tcherenkov	page 186
2.15	**Giovanni Olivetti**	SPINTEC	Inversion of the polarity of angular velocity inside a precessing magnet	page 187
2.16	**Sali Salama**	C2N	Micromagnetic simulations of magnon non-linear interactions in YIG disk magnetic vortex	page 188
2.17	**Vincent Vlaminck**	Lab-STICC	Spin-wave near-field diffraction model for in-plane magnetized films	page 190
2.18	**Maryam Massouras**	C2N	Time-resolved Noncommutativity of Parametric Excitations in YIG disks	page 191
2.19	**Nicolas Sebe**	UMPhy	Rashba Edelstein Effect enhancement induced by insertion of a light metallic layer	page 193

2.43	**Richard Schlitz**	Univ. Konstanz	Magnetization dynamics affected by phonon pumping	page 237
2.44	**Valentin Cherruault**	IPR	Investigation of ultrafast magneto-acoustic interactions in ferromagnetic cobalt/nickel multilayers	page 238
2.45	**Igor Ngouagnia**	IPCMS	Spin waves propagation in an FeN guide induced by the excitation of an inserted Fe pad	page 239
2.46	**Maya Khelif**	LSPM	Effets de courbure et de déformation mécanique sur la distribution de l'aimantation de nano-objets	page 241
2.47	**Fatih Zighem**	LSPM	Propriétés magnéto-mécaniques de couches minces sur substrats flexibles mesurées par MOKE in situ	page 242
2.48	**Vincent Castel**	Lab-STICC	Generation of circulating cavity magnon polaritons in a compact geometry resonator	page 244
2.49	**Guillaume Bourcin**	Lab-STICC	Spincavitronics System: Engineering Level Attraction in Multimode System	page 245
2.50	**Guillaume Bourcin**	Lab-STICC	Spincavitronics System: Approaching Deep-Strong Coupling	page 247
2.51	**Alan Gardin**	Lab-STICC	Manifestation of the coupling phase in microwave cavity magnonics	page 249
2.52	**Hervé Hurdequint**	SPEC	Cavity-FMR studies of LPE epitaxial YIG films	page 251
2.53	**Maxime Ardisson**	Lab-STICC	Observation of Antiferromagnetic Cavity Magnon Polariton in Cr_2O_3	page 253
2.54	**Harjinder Singh**	IJL	THz generation dependence of Co_xFe_{1-x} alloy composition	page 255
2.55	**Artem Levchuk**	SPEC	Inverse Rashba-Edelstein effect in CoFeB/MgO magnetic bilayers revealed with THz emission spectroscopy	page 256
2.56	**Boyu Zhang**	Beihang Univ.	All-optical Helicity-Independent Switching State Diagram in Gd-Fe-Co Alloys	page 258
2.57	**Boyu Zhang**	Beihang Univ.	Manipulating exchange bias with a single femtosecond laser pulse	page 260
2.58	**Juliette Dubois**	LCPMR	Ultrafast magnetization dynamics in nanostructured thin layers	page 262
2.59	**Marcel Hennes**	INSP	Co-Tb alloy thin films: from static magnetic properties to laser-induced ultrafast demagnetization and domain wall broadening	page 264
2.60	**Fausto Sirotti**	LPMC	Electronic structure drives the game: subpicosecond magnetic phase transition in FeRh	page 266
2.61	**Anda Elena Stanciu**	SPINTEC	Dynamics of vortex state generation in laser demagnetized permalloy packman dots	page 268
2.62	**Sanjay René**	SPEC	Ultrafast pure spin current transport through antiferromagnetic insulators	page 270

Directional spin Seebeck effect controlled by magnon dipolar stray field chirality

M. Cosset-Chéneau[1,*], S.H. Tirion[1], X. Wei[1], and B.J. van Wees[1]

[1]*Physics of Nanodevices, Zernike Institute for Advanced Materials, University of Groningen, 9747 AG Groningen, The Netherlands*

*m.n.c.g.cosset-cheneau@rug.nl

The spin Seebeck effect is one of the most fundamental phenomena in the field of spin caloritronics [1], as it allows the generation of a magnon spin current from a temperature gradient in ferromagnetic insulators in the absence of charge carriers. A wide variety of phenomena can be probed using this effect, and it is to this day the subject of continuous investigations.

One important feature of magnon transport is that their spin angular momentum is not their only degree of freedom. The propagating spin wave nature of these quasi-particles gives them a chiral character which provides an additional knob to control their propagation. This has been exploited since the beginning of the field of magnonics as it, for instance, controls the propagation direction of dipolar spin waves in the Damon-Eschbach configuration.

More recently, the importance of the rotating dipolar stray fields generated by these chiral particles for the control of their motion has been recognized. These dipolar stray fields possess a handedness, or chirality, that depends on the magnon propagation direction. This allows to selectively couple propagating magnons to a neighboring magnon reservoir in a way which is controllable by the reservoir magnetization direction.

This selective coupling has recently been used to induce the non-reciprocal transport of coherent [2] and diffusive [3] dipolar-exchange spin waves controlled by the magnetization direction of a ferromagnetic gate placed on top of YIG. However, the demonstration of such a control has been lacking for thermally-generated magnons. In addition, it has been predicted that this magnon dipolar stray field chirality can be used to generate a directional magnon flow [4]. While such a directional generation of a spin current has been demonstrated for coherent magnons [5], it has never been observed so far in the incoherent case.

Here, we demonstrate the control of a thermally-generated flow of magnon in the non-local spin Seebeck geometry by a ferromagnetic gate in YIG. We show that the symmetries of this effect are consistent with a coupling of the magnons to the ferromagnetic gate controlled by the chirality of the magnon-dipolar stray field. Finally, we show that a directional generation of thermal magnon can be achieved in the non-local spin Seebeck geometry using a ferromagnetic wire. This directionality is tunable by the wire magnetization direction, and it displays symmetries consistent with a dipolar stray field chirality-controlled generation of thermal magnons.

References

[1] E. Saitoh G. Bauer and B. van Wees. Spin caloritronics. *Nature Mater.* 11, 391 (2012).

[2] J. Chen et al. Excitation of unidirectional exchange spin waves by a nanoscale magnetic grating. *Phys. Rev. B* 100, 104427 (2019).

[3] J. Han et al. Nonreciprocal transmission of incoherent magnons with asymmetric diffusion length. *Nano Lett.* 21, 7037–7043 (2021).

[4] Tao Yu, Yaroslav M Blanter, and Gerrit EW Bauer. Chiral pumping of spin waves. *Phys. Rev. Lett.* 123, 247202 (2019).

[5] B.G. Simon. Directional excitation of a high-density magnon gas using coherently driven spin waves. *Nano Lett.* 21, 8213–8219 (2021).

Poster 2.02, November 15th, 10h50–13h00

Non-degenerate parametric excitation in YIG nanostructures

H. Merbouche[1,*], P. Che[2], T. Srivastava[3], N. Beaulieu[4], J. Ben Youssef[4], M. Muñoz[5], M. d'Aquino[6], C. Serpico[6], P. Bortolotti[2], G. de Loubens[3], A. Anane[2], S.O. Demokritov[1], and V.E. Demidov[1]

[1]*Institute for Applied Physics, University of Muenster, Germany*
[2]*Unité Mixte de Physique CNRS-Thales, Palaiseau*
[3]*SPEC, CEA, CNRS, Université Paris-Saclay, Gif-sur-Yvette, France*
[4]*Lab-STICC, UMR 6285 CNRS, Brest, France*
[5]*Instituto de Tecnologías Físicas y de la Información (CSIC), Madrid, Spain*
[6]*Department of Electrical Engineering and ICT, University of Naples Federico II, Italy*
*hugo.merbouche@gmail.com

Spin-waves represent a promising alternative to charge carriers for new information technology due to their low energy, small wavelength, large degree of freedom (frequency and phase), and their easily attainable non-linear dynamics. These characteristics make them particularly suited for neuromorphic computing schemes that take advantage of the massive parallelization of operations in the frequency space and of the non-linear properties of spin-waves. Such schemes require the excitation of many modes in small magnetic structures. This task can be fulfilled by parametric processes, where a photon or a magnon at frequency $2f$ splits in two magnons at frequencies $f-\delta f$ and $f+\delta f$ [1]. The splitting can be degenerate ($\delta f = 0$) or non-degenerate ($\delta f \neq 0$). Recently, the non-degeneracy was shown to open the possibility to cross-stimulate a mode using multiple parametric excitations, effectively implementing an interconnected recurrent neural network capable of classifying rf signals [2]. While exciting degenerate magnon pairs is simple, the observation of non-degenerate pairs has been limited to µm-thick YIG films [3] and metallic microstructures with a vortex ground state [2].
In this study, we demonstrate that by varying the direction of the parametric excitation field one can efficiently excite degenerate or non-degenerate magnon-pairs in a 500nm diameter YIG disk. When the rf field is applied parallel to the static magnetization, a photon splits into a degenerate magnon-pair at half the pump frequency as expected (Fig. 1a). However, when the rf field is applied transversely, it non-resonantly excites a magnon which splits into a magnon-pair that is typically non-degenerate (Fig. 1b). This non-resonant transverse parametric pumping in YIG is flexible in terms of external field and sample shape. These findings greatly facilitate the implementation of promising k-space computing schemes in the most attractive magnonic material that is YIG.

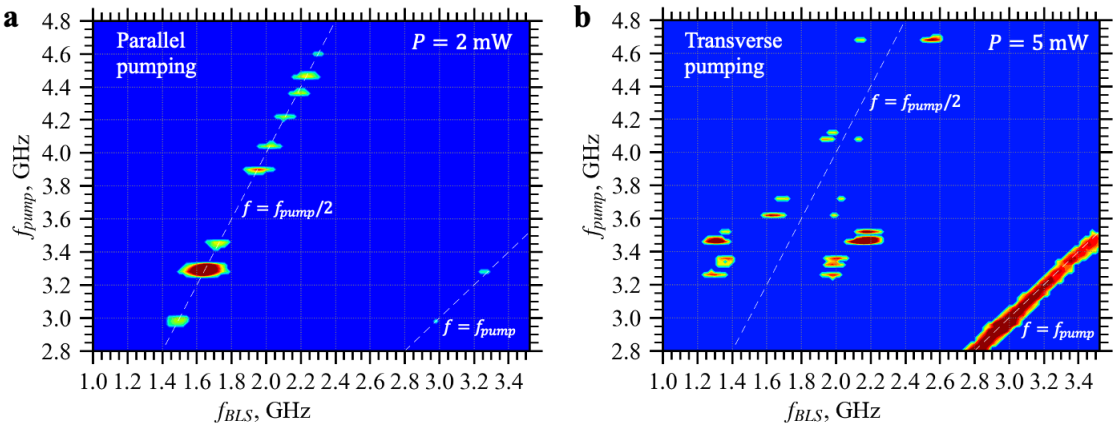

Figure 1: µ-BLS spectra as a function of the pump frequency for a pumping field parallel (a) and transverse (b) to the static magnetic field. In the parallel case, there is no excitation at $f = f_{pump}$ and a degenerate magnon-pair can be excited at $f_{pump}/2$ when it coincides with a mode frequency. In the transverse case, non-resonant excitation is observed at $f = f_{pump}$ and non-degenerate magnon-pairs are excited at $f_{pump}/2 \pm \delta f$

Acknowledgments

This work was supported by the Horizon2020 Research Framework Programme of the European Commission under grant no. 899646 (k-NET).

References

[1] G A Melkov and A.G. Gurevich. *Magnetization Oscillations and Waves*. CRC Press. New York, 1996.

[2] Lukas Körber et al. *Pattern recognition with a magnon-scattering reservoir*. 2022.

[3] A Melkov and S V Sholom. Parametric excitation of spin waves by a surface magnetostatic wave. *Journal of Experimental and Theoretical Physics* 96, 712–719 (1989).

Nonlinear interactions between spin-wave modes in YIG microdisks

Amel Kolli[1,*], Gabriel Soares[1], Rafael L. Seeger[1], Igor Ngouagnia[1], Titiksha Srivastava[1,2], Maryam Massouras[2], Joo-Von Kim[2], Hugo Merbouche[3], Sergej Demokritov[3], Vladislav Demidov[3], Nathan Beaulieu[4], Jamal Ben Youssef[4], Manuel Muñoz[5], Salvatore Perna[6], Massimiliano d'Aquino[6], Claudio Serpico[6], Abdelmadjid Anane[7], and Grégoire de Loubens[1]

[1]*SPEC, CEA, CNRS, Université Paris-Saclay, Gif-sur-Yvette, France*
[2]*Université Paris-Saclay, CNRS, Centre de Nanosciences et de Nanotechnologies, France*
[3]*Institute for Applied Physics, University of Muenster, Germany*
[4]*LabSTICC, CNRS, Université de Bretagne Occidentale, Brest, France*
[5]*Instituto de Tecnologías Físicas y de la Información (CSIC), Madrid, Spain*
[6]*Department of Electrical Engineering and ICT, University of Naples Federico II, Italy*
[7]*Unité Mixte de Physique, CNRS, Thales, Université Paris-Saclay, France*
*amel.kolli@universite-paris-saclay.fr

Leveraging on nonlinear magnetization dynamics is promising for neuromorphic computing [1]. Recently, pattern recognition has been demonstrated using a magnon-scattering reservoir [2]. To proceed further from this stage, one should be able to train the neural network. In magnetic microstructures, spin-wave eigenmodes – neurons – are defined in the k-space. Mutual nonlinear couplings between these modes – synaptic weights – are predominantly determined by their amplitudes. We have previously demonstrated that parametric pumping allows the selective excitation of a large number of eigenmodes in YIG microdisks [3].

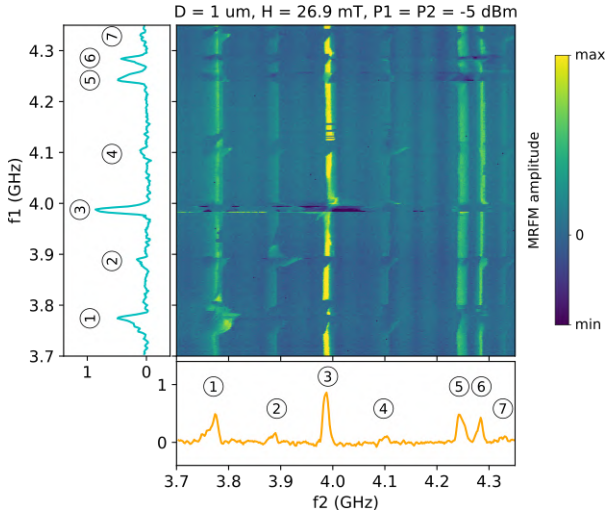

Figure 1: Two-tone parametric spectroscopy in a 1 µm diameter YIG disk.

Here, we simultaneously excite pairs of modes by this mean to study their mutual nonlinear interactions. Two-tone MRFM spectroscopy demonstrates that each mode is coupled to all other modes, with enhanced or suppressed peaks, and the appearance of additional peaks in the spectrum (Fig. 1). Full micromagnetic simulations and a description of the nonlinear magnetization dynamics in terms of normal modes [4] provide some insights into these nonlinear processes.

Acknowledgments

This work has received financial support from the Horizon 2020 Framework Programme of the European Commission under FET-Open grant agreement no. 899646 (k-NET).

References

[1] Ádám Papp, Wolfgang Porod, and Gyorgy Csaba. Nanoscale neural network using non-linear spin-wave interference. *Nature Commun.* 12, 1–8 (2021).

[2] L. Körber, et al. Pattern recognition with a magnon-scattering reservoir ().

[3] T. Srivastava, et al. Complete identification of spin-wave eigenmodes excited by parametric pumping in YIG microdisks ().

[4] S. Perna et al. Computational micromagnetics based on normal modes: Bridging the gap between macrospin and full spatial discretization. *J. Magn. Magn. Mater.* 546, 168683 (2022).

Damping in garnet microdisks coupled to microwave antennas

Gabriel Soares[1, *], Rafael Lopes Seeger[1], Amel Kolli[1], Igor Ngouagnia[1], Titiksha Srivastava[1], Nathan Beaulieu[2], Jamal Ben Youssef[2], Manuel Muñoz[3], Vladimir Naletov[4], Olivier Klein[4], Ping Che[5], Diane Gouéré[5], Hugo Merbouche[5], Abdelmadjid Anane[5], and Grégoire de Loubens[1]

[1]*SPEC, CEA, CNRS, Université Paris-Saclay, France*
[2]*LabSTICC, CNRS, Université de Bretagne Occidentale, Brest, France*
[3]*Instituto de Tecnologías Físicas y de la Información (CSIC), Madrid, Spain*
[4]*Université Grenoble Alpes, CEA, CNRS, Grenoble INP, Spintec, France*
[5]*Unité Mixte de Physique, CNRS, Thales, Université Paris-Saclay, France*
gabriel.soares@cea.fr

Magnetic garnet thin films, with thicknesses of 10 to 100 nm, damping parameters in the 10^{-4} range, and tunable anisotropy can now be routinely grown by liquid phase epitaxy (LPE) [1] and pulsed laser deposition (PLD) [2]. For magnonic applications, these films often have to be patterned at the (sub)micron-scale and coupled to microwave antennas. As such, it is important to monitor the damping after these stages [3]. In this work, we use MRFM to study the evolution of the damping as a function of the diameter of microdisks patterned from 30 nm thick PLD BiYIG and 52 nm thick LPE YIG films. Narrow microwave antennas made of Ti/Au are integrated either on top of or beside the disks. When the antenna is directly patterned on top of the disks (keeping the e-beam resist mask), we observe an increased damping as the diameter decreases, due to spin pumping at the disk periphery between the YIG and Ti/Au. Inserting an insulating layer between the YIG microdisks and the metallic antenna leads to the opposite behavior: a reduced damping as the diameter goes down (Fig. 1b). We ascribe it to radiation damping [4], which scales up with the volume of the magnetic sample. We also verify that the microdisks beside the antenna have smaller inductive coupling, and therefore a smaller damping.

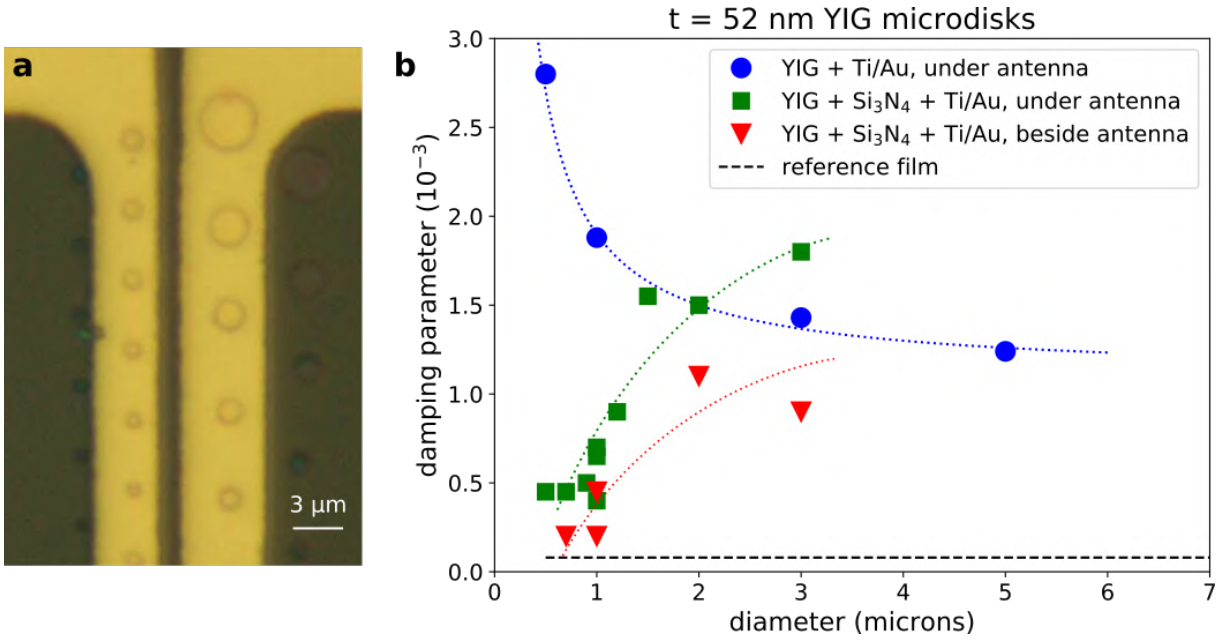

Figure 1: Optical image of the 52 nm thick YIG microdisks and integrated antennas. (b) Dependence of the damping parameter on diameter in different configurations. Dotted lines are guides to the eye.

Acknowledgments

This work has received financial support from the Horizon 2020 Framework Programme of the European Com- mission under FET-Open grant agreement no. 899646 (k-NET).

References

[1] Nathan Beaulieu, Nelly Kervarec, Nicolas Thiery, et al. Temperature Dependence of Magnetic Properties of a Ultrathin Yttrium-Iron Garnet Film Grown by Liquid Phase Epitaxy: Effect of a Pt Overlayer. *IEEE Magnetics Letters* 9, 1–5 (2018).

[2] Lucile Soumah, Nathan Beaulieu, Lilia Qassym, et al. Ultra-low damping insulating magnetic thin films get perpendicular. *Nature Communications* 9 (2018).

[3] C. Hahn, V. V. Naletov, G. de Loubens, et al. Measurement of the intrinsic damping constant in individual nanodisks of $Y_3Fe_5O_{12}$ and $Y_3Fe_5O_{12}$|Pt. *Applied Physics Letters* 104 (2014).

[4] Martin A. W. Schoen, Justin M. Shaw, Hans T. Nembach, Mathias Weiler, and T. J. Silva. Radiative damping in waveguide-based ferromagnetic resonance measured via analysis of perpendicular standing spin waves in sputtered permalloy films. *Physical Review B* 92 (2015).

Measurement of spin waves dispersion relation using an electrical method

G. Thiancourt[1,*], S.M. Ngom[1], A. Solignac[2], and T. Devolder[1]

[1]*Université Paris-Saclay, CNRS, Centre de Nanosciences et de Nanotechnologies, 91120, Palaiseau, France*
[2]*SPEC, CEA, CNRS, Université Paris-Saclay, 91191 Gif-sur-Yvette, France*
*gael-yann.thiancourt@universite-paris-saclay.fr

Magnonics is a field that has been attracting increasing interest from the research community in recent years. Spin waves potentially offer high-frequency applications and have a possibility to couple with other physical degrees of freedom. The dispersion relation is a primordial prerequisite information for most applications. Laser spectroscopy such as Brillouin Light scattering (BLS) is one of the most popular methods to determine spin wave's band structure. Inductive methods have become more and more popular to characterize magnons. Using a Vector Network Analyzer (VNA) and the fabrication of nano-antenna, a high-resolution propagation spin wave spectroscopy (PSWS) is achievable [1]. The use of an antenna at micrometer size allows to excite a wide range of wavevectors. Using a formalism developed in a previous work [2] and the PSWS method, we attempt to determine spin wave's dispersion relation of a synthetic antiferromagnetic stack (SAF) in the scissors state, for which we anticipate a monotonous character [3].

Our SAF is a composite material made of two layers of CoFeB (17 nm-CoFeB) separated by a spacer layer of non-magnetic material (0.7 nm-Ru). In the remanent state the two layers have anti-parallel magnetizations. SAF has generally two kinds of spin wave modes: the acoustical mode and the optical mode that differ due to the in-phase and out-of-phase precession of the magnetizations of the two layer. We focus on the acoustical mode characterized by a line-shaped dispersion relation[3]. Antennas are made of gold and present different geometries [4]. Two devices are used in our experiments:
(i) a microscopic stripe-shaped antenna with many circular SAF 4 μm dots [Fig. 1.a] underneath. The antenna generated an almost uniform RF field, and hence it can be used to determine the acoustical spin waves frequency at $k_x = 0$. This is similar to a VNA-FMR experiment.
(ii) a unique disk of SAF with a diameter of 13 μm diameter with 1 μm nominal width simple antennas [4] is used to excite spin waves at different wavevectors [see Fig. 1.a].

We excite spin waves using inductive antennas under an external field. The VNA expresses the measured propagation through scattering matrix elements (S_{11}, S_{21}...). The VNA signal contains several contributions: a small one due to the propagation of spin waves and parasitic contributions related to the electromagnetic cross-talk between antennas [5]. Most of this parasitic signal is removed by an adequate reference measurement but there remains a small baseline [Fig. 1.d] that needs to be corrected. This can be done in two ways: (i) either by differentiating S_{21} over the field and/or (ii) by using a time gating approach [Fig. 1.c] to remove the signals transmitted in travel times incompatible with spinwave velocities (note that spinwaves are much slower than the electromagnetic waves responsible for the cross-talk).

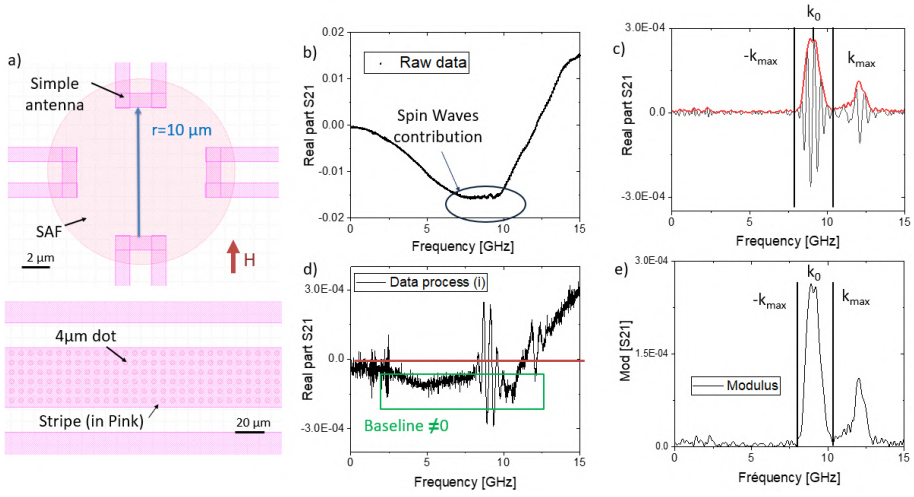

Figure 1: *Scattering parameter S_{21} for an applied field equals to 59 mT before and after data processes. Devices(a). VNA raw data(b) and data after process[iii](c) and process[ii](d). Modulus of time gated data(e)*

As presented in [Fig. 1.c], the spin wave signal has a shape of a damped sine. By respecting some conditions, such as having an antenna width smaller than the spin wave attenuation length, we can describe S_{21} through our formalism [see Eq. 1]. In our case we simplify the formula by taking L_{att} larger than the propagation distance r.

$$S_{21} \approx i e^{-ik_x|r|}\, e^{-\frac{|r|}{L_{\text{att}}}}\, [h_x(k_x)]^2 \tag{1}$$

The envelope $[h_x(k_x)]^2$ corresponds to the efficiency of the antenna versus wavevector, which for our geometry is proportional to a the square of a cardinal sine [4]. The frequency at $k_x = 0$ should correspond to the maximum of the modulus [Fig. 1.e]. To verify this assumption, we did a VNA-FMR experiment on the stripe to measure independently the $k_x = 0$ frequency for each applied field. After applying a correction due to the difference of demagnetizing fields between the two systems, we compare the VNA-FMR data with the maximum of the envelope of PSWS data that go through different types of processes [Fig. 2 a]. This agreement between the two methods providing the resonant frequency at $k_x = 0$ validates the procedure. The dispersion relation was estimated by noticing that k_x is related to the argument of the S_{21} parameter [see Eq. 2]. The $2n\pi$ uncertainty can be solved by knowing the position of the $k_x = 0$ frequency and by unwrapping the phase.

$$\frac{S_{21}}{||S_{21}||} = e^{-ik_x r} \longrightarrow k_x(\omega) = -\frac{1}{r}\Big(\arg(S_{21}) + 2n\pi\Big) \tag{2}$$

Finally by applying the formula, we are able to uncover the dispersion relation from data that go through different types of data processing methods. The different data processing methods give us dispersion relations that differs beyond a certain range of wavevectors. We compare the different data and we keep the values that are in agreement [Fig. 2 b]. By doing so we isolate the most probable values that describe magnon dispersion relation. In this work, we demonstrate that PSWS experiment using micrometer size antenna are a promising method to probe monotonous relation dispersion of magnons. To verify our formalism we have to compare dispersion relations obtain through the presented process with theoretical equation and simulation.

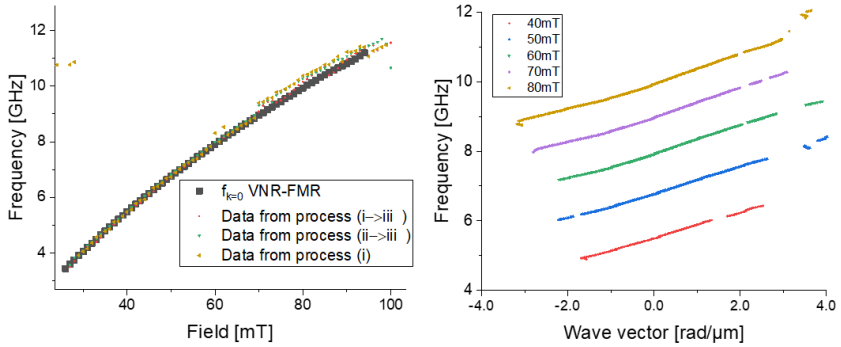

Figure 2: *Results from experiments to get magnon's dispersion relation. Comparison of the frequency at $k_x = 0$ from different data processing (a). Spin wave's dispersion relation on time gated data for different applied fields(b)*

References

[1] M Bailleul, D Olligs, and C Fermon. Propagating spin wave spectroscopy in a permalloy film: A quantitative analysis. *Applied Physics Letters* 83, 972–974 (2003).

[2] T Devolder, G Talmelli, SM Ngom, et al. Measuring the dispersion relations of spin wave bands using time-of-flight spectroscopy. *Physical Review B* 103, 214431 (2021).

[3] F Millo, J-P Adam, C Chappert, et al. Unidirectionality of spin waves in Synthetic Antiferromagnets. *arXiv preprint arXiv:2306.05259* (2023).

[4] M Sushruth, M Grassi, K Ait-Oukaci, et al. Electrical spectroscopy of forward volume spin waves in perpendicularly magnetized materials. *Physical Review Research* 2, 043203 (2020).

[5] J Greil, M Golibrzuch, M Kiechle, et al. Secondary Excitation of Spin-Waves: How Electromagnetic Cross-Talk Impacts on Magnonic Devices. *arXiv preprint arXiv:2303.11303* (2023).

Spin wave dynamics in antiferromagnetically coupled multilayers

N. Benaziz[1,*], T. Devolder[1], J-P. Adam[1], and A. Solignac[2]

[1]*Centre des Nanosciences et des Nanotechnologies, Université Paris-Saclay, CNRS,91120 Palaiseau, France*
[2]*CEA SPEC,CNRS,Université Paris Saclay, 91191 Gif-sur-Yvette, France*
nessrine.benaziz@u-psud.fr

Spin Waves (SW) are collective oscillations of a spin system in a magnetic material and present non-linear properties [1]. We study SW dynamics in Synthetic antiferromagnet (SAF) which allow to better control the SW propagation [2]. It consists of two ferromagnetic layers coupled by a metal layer that induces an anti-parallel configuration of the magnetizations at equilibrium [3]. Due to the coupling between these layers, two uniform resonance modes appear: the acoustic mode, where magnetization precess in phase, and the optical mode, where magnetization are in phase opposition [4]. Adding more layers leads to more resonance modes [5] and here we present experimental measurements of these modes. Our sample is drawn Fig. 1(a). It has been grown by sputtering deposition in UHV and it is composed of 4 layers of 8.5 nm CoFeB and 3 layers of 0.7 nm Ru on a Si/SiO_2 substrate. We carried out dynamic measurements of the Ferromagnetic Resonance using a Vector Network Analyzer (VNA-FMR). In this experiment, we excite the SW of the sample with a RF field generated by a co-planar wave guide as a function of the in-plane applied magnetic field. We measured the real and imaginary parts of the permeability as a function of frequency. An example of the signal measured for a applied field of 15 mT is represented Fig. 1 (b). Four different modes of different amplitude were detected at low field. The amplitude of the signal depends on the sensibility of the measurement and on the susceptibility of the material.

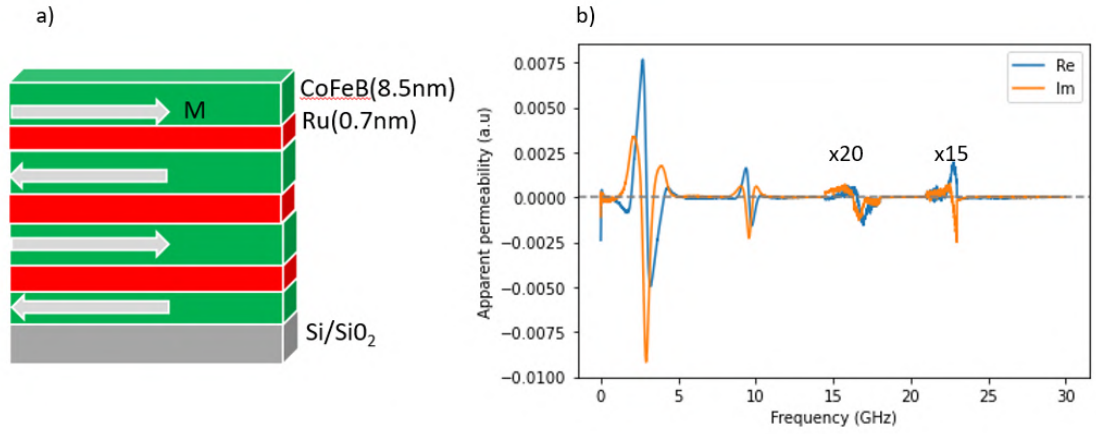

Figure 1: a) Sketch of the double SAF b) Apparent permeability for an applied field of 15 mT as function of the frequency. The two signals at high frequency were amplified by a factor of ×20 and ×15 in order to discern them.

We extracted the resonance frequency for each field by taking the maximum of the modulus of the apparent permeability. The results are plotted in Fig. 2(a). At low field, we detected four modes, in agreement with the theoretical calculation described in the literature [5]. However, from a field of 50 mT, we observe a splitting of the fundamental mode. We hypothesize this to originate from structural defects between layers. These defects lead to a gradient of the magnetic properties along the stack. To get a deeper understanding of our results, we will perform material characterisation, in addition to the analytical calculation and simulation that we are currently performing. The micromagnetic simulation are running using Tetrax [6, 7]. The parameters values were taken from experimental results in literature [4]. We see for the fundamental mode a difference between experiment Fig. 2(a). and simulation Fig. 2(b). This originates from presence of an anisotropy in our system that we didn't implement in our simulation. In addition, in our experimental result, we get a positive slope for the highest mode, whereas in our simulations, we get a negative one. To correct this, we have to optimize our parameters of the micromagnetic modeling.

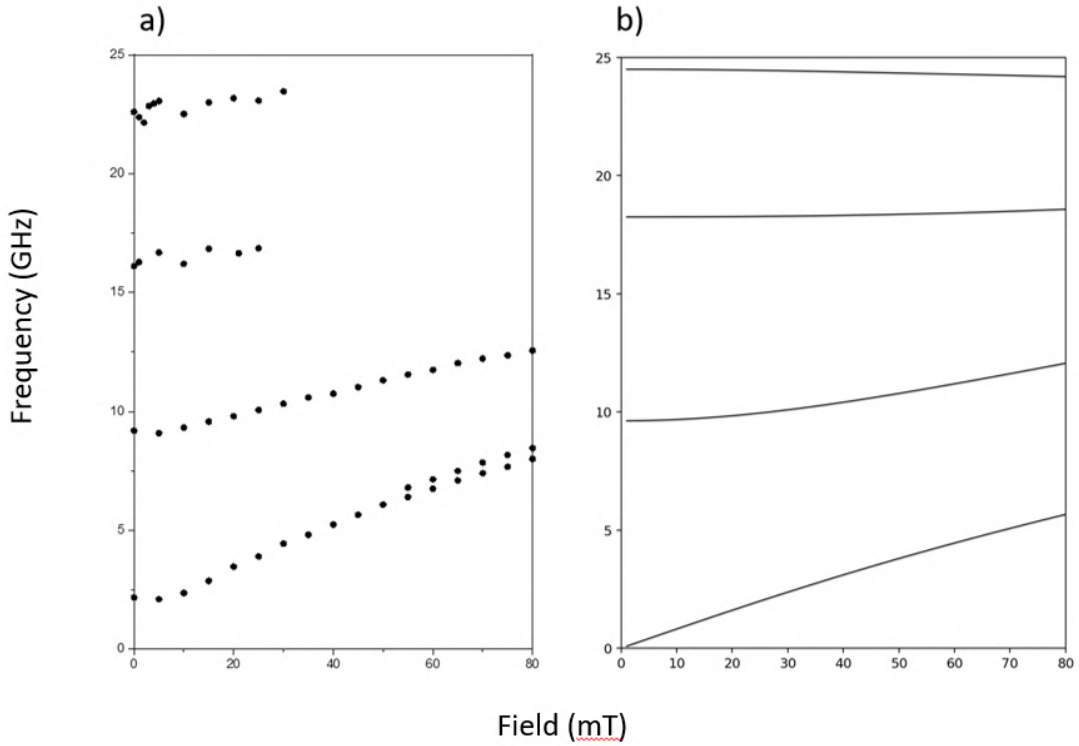

Figure 2: Field dependence of the mode frequencies a) Experimental result b) micromagnetic modeling. The micromagnetic modeling is implemented with a magnteric stiffness $t_{mag} = 8.5nm$, a saturation magnetization Ms $= 1.350 \times 10^6 A/m$, a interlayer exchange coupling $J_{ex} = -1.85mJ/m^2$, and a exchange stiffness $A_{\text{ex}} = 13.4$ pJ/m

Acknowledgments

This work was supported by ANR MAXSAW n°ANR-20-CE24-0025.

References

[1] A.V. Chumak, V.I. Vasyuchka, A.A. Serga, and B. Hillebrands. Magnon spintronics. *Nature physics* 11, 453–461 (2015).

[2] R.A. Gallardo, P. Alvarado-Seguel, A. Kákay, J. Lindner, and P. Landeros. Spin-wave focusing induced by dipole-dipole interaction in synthetic antiferromagnets. *Physical Review B* 104, 174417 (2021).

[3] P. Grünberg, R Schreiber, Y Pang, M.B. Brodsky, and H Sowers. Layered magnetic structures: evidence for antiferromagnetic coupling of Fe layers across Cr interlayers. *Physical review letters* 57, 2442 (1986).

[4] A. Mouhoub, F. Millo, C. Chappert, et al. Exchange energies in CoFeB/Ru/CoFeB synthetic antiferromagnets. *Physical Review Materials* 7, 044404 (2023).

[5] F. C. Nörtemann, R.L Stamps, and R.E Camley. Microscopic calculation of spin waves in antiferromagnetically coupled multilayers: Nonreciprocity and finite-size effects. *Physical Review B* 47, 11910 (1993).

[6] L. Körber, G. Quasebarth, A. Hempel, et al. *TetraX: Finite-Element Micromagnetic-Modeling Package*. 2022.

[7] L. Körber, G. Quasebarth, A. Otto, and A. Kákay. Finite-element dynamic-matrix approach for spin-wave dispersions in magnonic waveguides with arbitrary cross section. *AIP Advances* 11, 095006 (2021).

Spin Waves engineering by N-atoms implantation in a Fe film

Louis Christienne[1], Silvia Tacchi[2], Marco Madami[3], Pauline Rovillain[1,*], Mahmoud Eddrief[1], Igor Ngouagnia[4], Yves Henri[4], Daniel Stoeffler[4], Franck Fortuna[6], Madjid Anane[5], and Massimiliano Marangolo[1]

[1]*INSP, Sorbonne Université, CNRS, Paris, France*
[2]*Istituto Officina dei Materiali del CNR, Sede secondaria di Perugia c/o Dipartimento di Fisica e Geologia, Università di Perugia, Italy*
[3]*Università di Perugia, Dipartimento di Fisica e Geologia, Perugia, Italy*
[4]*IPCMS, Université de Strasbourg, CNRS, Strasbourg, France*
[5]*Unité Mixte De Physique, CNRS, Thales, Université Paris-Saclay, Palaiseau, France*
[6]*ISMO, CNRS, Université Paris-Saclay, Orsay, France*
**pauline.rovillain@insp.upmc.fr*

In magnonic devices, the engineering of spin wave (SW) spectra plays a crucial role in manipulating local propagation modes, enabling the control of SW propagation or remote field-induced SW excitation. One promising method for modifying the local spin wave propagation is through ion implantation, utilizing a focused ion beam (FIB). In this study, we present a combined VSM and Brillouin light scattering (BLS) investigation that demonstrates the impact of N atoms implantation on the in-plane and out-of-plane magnetic anisotropy in a Fe thin film.

The focus of our research lies in low-dose implantation, where the out-of-plane anisotropy remains low enough to prevent the stabilization of the well-known weak magnetic domains structure.[1], [2] Through systematic analysis, we uncover how ion implantation with N atoms alters the magnetic anisotropy properties in the Fe thin film. By precisely controlling the implantation parameters, we manipulate the spin wave spectra, achieving desired modifications in the propagation modes, as shown in Fig. 1.

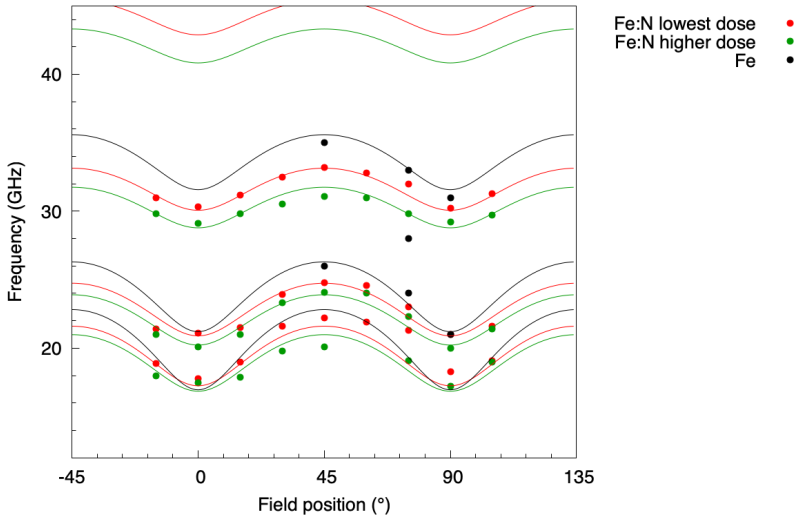

Figure 1: BLS measurements changing the angle of applied in-plane magnetic field and calculated (lines) using dipole-exchange SW theory

By combining experimental measurements with computational simulations, we gain a comprehensive understanding of the impact of N atoms implantation on the local spin wave propagation and magnetic anisotropy. The simulation results provide valuable insights into the underlying mechanisms governing the observed experimental phenomena, validating the effectiveness of our ion implantation approach in modifying the SW spectra.

The ability to tailor spin wave propagation and magnetic anisotropy through ion implantation offers new avenues for developing advanced magnonic devices with enhanced functionalities. This research paves the way for the design and optimization of future magnonic systems capable of efficient SW manipulation and remote field-driven SW excitation.

Acknowledgments

The authors acknowledge support from the Agence Nationale de la Recherche Grant No. ANR-22-CE24-0015 SACOUMAD.

References

[1] I. S. Camara, S. Tacchi, L-C Garnier, et al. Magnetization dynamics of weak stripe domains in Fe-N thin films: a multitechnique complementary approach. *JOURNAL OF PHYSICS-CONDENSED MATTER* 29 (2017).

[2] Louis-Charles Garnier, Massimiliano Marangolo, Mahmoud Eddrief, et al. Stripe domains reorientation in ferromagnetic films with perpendicular magnetic anisotropy. *JOURNAL OF PHYSICS-MATERIALS* 3 (2020).

Nonlinear longitudinal and transverse magnetoresistances due to current-induced magnon creation-annihilation processes

Paul Noël[1,*], Richard Schlitz[1], Emir Karadza[1], Charles-Henri Lambert[1], Luca Nessi[1,2], Federico Binda[1], and Pietro Gambardella[1]

[1]*Department of Materials, ETH Zurich, CH-8093 Zurich, Switzerland*
[2]*Dipartimento di Fisica, Politecnico di Milano, Via G. Colombo 81, 20133 Milano, Italy*
*paul.noel@mat.ethz.ch

At finite temperatures, the magnetization vector is not a fixed quantity. Quantized spin waves – magnons –excited by thermal fluctuations reduce the magnetization from the full alignment of all spins. These magnons can carry or excite spin currents and reciprocally can be excited by a spin current. The charge-spin conversion phenomena such as the spin Hall effect allow for the excitation of magnons in a magnetic layer by passing an electric current in an adjacent nonmagnetic conductor [1]. The total magnon population, and thus total magnetization can be modified by spin currents in ferromagnet (FM)/normal metal (NM) bilayers [2, 3]. The excitation of magnons by an interfacial spin accumulation depends on the relative direction of the accumulated spins and the magnetization. Spin-flip scattering leads to the creation (annihilation) of magnons when the magnetization is parallel (antiparallel) to the spin accumulation, as depicted in Fig. 1. In turn, the modification of the magnon population with spin current leads to a change of the magnetization M.

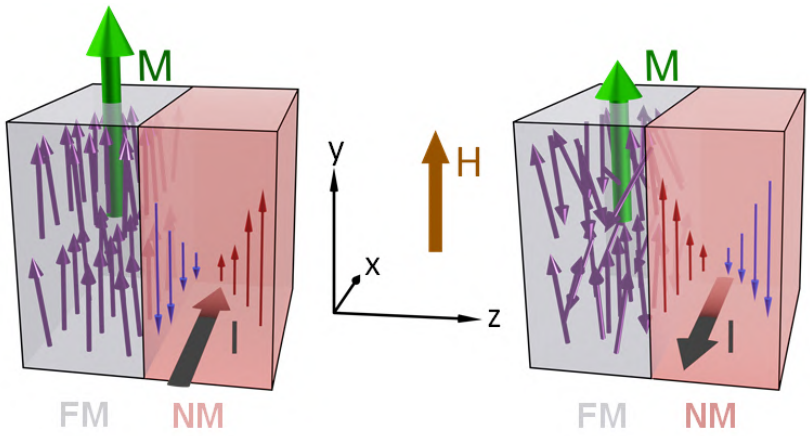

Figure 1: Schematic of the annihilation and creation of magnons in a FM due to current-induced spin accumulation in the NM. The local magnetic moments are shown as purple arrows, the spin moments are shown as thin red and blue arrows. The spin magnetic moment is opposite to the spin moment.

We demonstrate that this current-induced modification of the magnetization generates an additional nonlinear longitudinal and transverse magnetoresistance for every magnetoresistance that depends on the magnetization. In particular, we evidence the existence of the nonlinear anisotropic magnetoresistance, the nonlinear spin Hall magnetoresistance, the nonlinear magnon magnetoresistance and the nonlinear planar Hall effect. We term this set of nonlinear effects the magnon creation-annihilation magnetoresistances ($m^{\dagger}m$MRs) [4]. Interestingly, these effects have angular dependencies similar to the ones associated with the spin orbit torque contributions [5] and can strongly affect the estimation of the spin orbit torques if not properly accounted [6].

Our results apply to both insulating and metallic magnetic layers, elucidating the dependence of the magnetoresistance on applied current and magnetic field for a broad variety of systems excited by spin currents. We evidence that these magnon creation-annihilation magnetoresistances dominate the second harmonic longitudinal and transverse resistance of thin $Y_3Fe_5O_{12}$/Pt bilayers. As seen in Fig. 2 the second harmonic signal is similar to the expected angular dependence of the nonlinear spin Hall magnetoresistance (SMR) and nonlinear planar Hall effect (PHE).

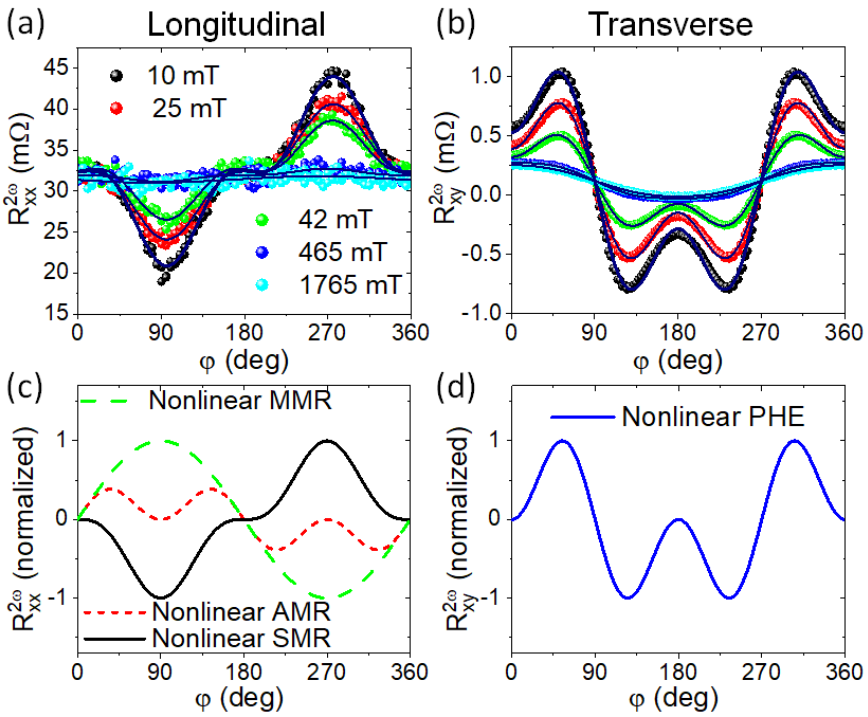

Figure 2: Angular dependence of the second harmonic (a) longitudinal and (b) transverse resistance of YIG/Pt for different values of the applied field at a current of 4 mA. (c, d) Expected angular dependence of the longitudinal and transverse second harmonic resistance due to the nonlinear SMR, MMR, AMR and PHE.

Acknowledgments

This work was supported by the Swiss National Science Foundation (Grant No. 200020_200465). P.N. acknowledges the support of the ETH Zurich Postdoctoral Fellowship Program 19-2 FEL-61.

References

[1] L. J. Cornelissen, J. Liu, R. A. Duine, J. Ben Youssef, and B. J. van Wees. Long-distance transport of magnon spin information in a magnetic insulator at room temperature. *Nature Physics* 11, 1022–1026 (2015).

[2] V. E. Demidov, S. Urazhdin, E. R. J. Edwards, et al. Control of Magnetic Fluctuations by Spin Current. *Physical Review Letters* 107, 107204 (2011).

[3] I. V. Borisenko, V. E. Demidov, S. Urazhdin, A. B. Rinkevich, and S. O. Demokritov. Relation between unidirectional spin Hall magnetoresistance and spin current-driven magnon generation. *Applied Physics Letters* 113, 062403 (2018).

[4] P. Noel, E. Karadza, R. Schlitz, et al. Nonlinear longitudinal and transverse magnetoresistances due to current-induced magnon creation-annihilation processes (In preparation).

[5] Can Onur Avci, Kevin Garello, Mihai Gabureac, et al. Interplay of spin-orbit torque and thermoelectric effects in ferromagnet/normal-metal bilayers. *Physical Review B* 90, 224427 (2014).

[6] P. Noel, E. Karadza, R. Schlitz, et al. Spin orbit torques estimation accounting for magnon creation-annihilation (In preparation).

Study of the manipulation of magnetisation at nano-metric scale by plasmonic systems

Y. Le Guen[1,2,*], S. Mangin[1], S. van Dijken[2], M. Hehn[1], and J. Hohlfeld[1]

[1]*Université de Lorraine, CNRS, Institut Jean Lamour, F-54000 Nancy, France*
[2]*NanoSpin, Department of Applied Physics, Aalto University School of Science, Aalto FI-00076, Finland*
yann.le-guen@univ-lorraine.fr

All Optical Switching (AOS) has been an active research area in the past years as it has a great potential for applications. It has been shown that it is possible to switch magnetisation in ferromagnetic films with circular polarised femtosecond laser pulses [1]. This phenomenon, named All Optical Helicity Dependent Switching (AO-HDS), and its underling mechanism are not yet fully understood. Multiple origins for this effect have been proposed such as the Inverse Faraday Effect (IFE) [2] and magnetic circular dichroism (MCD) [3]. The IFE describe the emergence of a static field like magnetisation in magnetic materials when excited with a circular polarised light. While MCD describe a difference of absorption of circular polarised light based on the direction of the magnetisation.

Plasmonics is another domain of great interest as it has been shown that plasmonic systems can confine and enhance electromagnetic fields at the nano-metric scale [4]. Surface Plasmon Polaritons (SPP) can confine fields near the interface between a metal and a dialectic. Furthermore, due its nature as propagating surface wave, SPP are intrinsically circularly polarised, and its direction of polarisation is locked in the plane perpendicular to its propagation direction.[5].

Given their properties, SPP are prime candidates for efficient in plane magnetic manipulation and the study of the IFE. They can easily be coupled to magnetic waveguide through grating coupling. And the resulting effect on the waveguide can be measured with Magneto-optical Kerr Effect (MOKE).

$Co_{40}Fe_{40}B_{20}$ thin film have been characterised before being pattern into gratings and waveguides. Optical transmission measurements were performed to allow the study of the SPP coupling in the visible wavelength range. In parallel, optical simulations were run using the Finite Element Method (FEM) with in COMSOL. This allowed to fit the resulting spectrum and investigate the origin of observed structures in the spectrum. MOKE imaging was done to look into the impact of laser coupled SPP on magnetic domain walls in the waveguide as illustrated in Fig.1b. Finally Time Resolved MOKE (TR-MOKE) was carried out to measure SPP induced magnetic precession. To do so a pump prob system was used : a magnetic field was applied along the waveguide, the pump was positioned on the grating while the probe was shifted onto the waveguide as illustrated in Fig.1a.

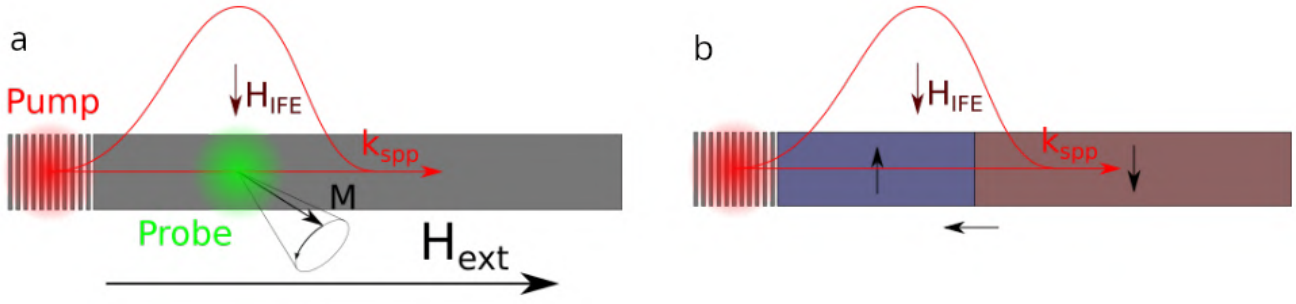

Figure 1: (a) TR-MOKE experiment. (b) MOKE imaging experiment.

Transmission measurements show a resonance dip at the wavelength were SPP coupling should occur and shifts with the periodicity of the grating. This way, coupling wavelength can be tailored and the coupling efficiency maximised. MOKE images indicate some magnetic domain wall motion after a large number of pulses at high incident power. However, the SPP origin of this effect could not be demonstrated. TR-MOKE measurements have shown some precession but its origin and the impact of the coupled SPP is still unclear as the precession remains even if the incoming light polarisation is parallel to the grating and therefore shouldn't couple to the SPP. This precession could come from the magnetic grating shape anisotropy

resulting in an unknown magnetic state a the interface with the waveguide.

Further measurements are needed to get an overview of the impact of SPP on magnetisation. Other materials could be used to get stronger effects. Overall, this study will provide a better understanding of the interaction between light, matter and magnetisation.

References

[1] C. D. Stanciu, F. Hansteen, A. V. Kimel, et al. All-Optical Magnetic Recording with Circularly Polarized Light. *Phys. Rev. Lett.* 99, 047601 (4 2007).

[2] J. P. van der Ziel, P. S. Pershan, and L. D. Malmstrom. Optically-Induced Magnetization Resulting from the Inverse Faraday Effect. *Phys. Rev. Lett.* 15, 190–193 (5 1965).

[3] A. R. Khorsand, M. Savoini, A. Kirilyuk, et al. Role of Magnetic Circular Dichroism in All-Optical Magnetic Recording. *Phys. Rev. Lett.* 108, 127205 (12 2012).

[4] Dmitri K Gramotnev and Sergey I Bozhevolnyi. Plasmonics beyond the diffraction limit. *Nat. Photonics* 4, 83–91 (2010).

[5] Todd Van Mechelen and Zubin Jacob. Universal spin-momentum locking of evanescent waves. *Optica* 3, 118–126 (2016).

Spin-wave dynamics in curved magnets

Gyandeep Pradhan[1,*], Vincent Vlaminck[2], Yves Henry[1], Riccardo Hertel[1], Jérôme Robert[1], and Matthieu Bailleul[1]

[1]*Institut de Physique et Chimie des Matériaux de Strasbourg,France*
[2]*Microwave Department, IMT Atlantique, Brest, France*
*gyandeep.pradhan@ipcms.unistra.fr

Spin waves or magnons, have captivated researchers in the realm of condensed matter physics due to their significant contributions to the dynamics of magnetic materials. They have potential applications in areas like spintronics, magnonic logic, and memory devices,magnonic waveguides, sensors, and spin wave computing. In recent investigations, researchers have directed their attention toward exploring spin waves in reduced dimensions including thin films, nanotubes, and 2D materials [1]. Within this context, a novel area of interest lies in the study of spin waves within curved magnetic structures [2].

Curved 3D magnetic systems have shown distinct static and dynamic properties with respect to their counterpart thin films. Theoretical studies have shown that the interplay between the surface curvature and magnetic charges results in a symmetry breaking which may lead to the emergence of anisotropies and magneto chiral interactions[3]. Such interactions could lead to various effects such as curvature-induced spin wave non-reciprocity effect in ferromagnetic materials predicted for nanotubes and curved magnetic thin shells, in a magnetic vortex state (VS) [4, 5]. In this communication, we report about the fabrication and characterization of ferromagnetic nanoscale half-pipe structures suitable for the observation of this effect.

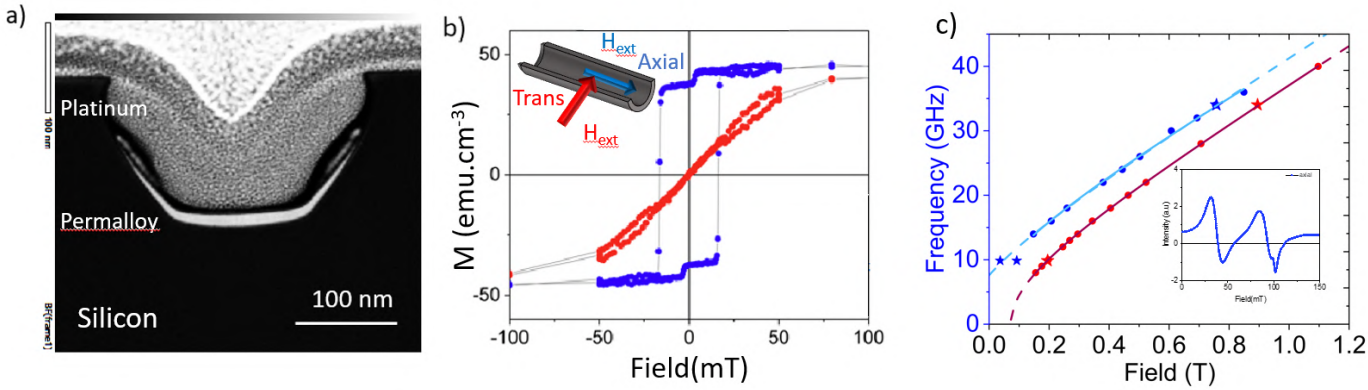

Figure 1: a) TEM imaging of cross-sectional view of a magnetic half pipe on a silicon susbtrate. b) SQUID measurements of an array of Permalloy half pipes c) Dependence of ferromagnetic resonance frequency as a function of applied field in both axial and transverse configuration(see sketch in panel b). Circles: coplanar waveguide FMR, stars: cavity FMR, inset: cavity FMR spectrum at 9 GHz in transverse configuration.

The fabrication process of the curved magnetic half-pipe structures involved several steps. We began by using e-beam lithography to pattern 100 nm wide lines on silicon substrates. These pre-patterned substrates were then subjected to reactive ion etching using SF_6 gas[6], resulting in the formation of grooves of diameter 300 nm and height of 250 nm. To create the desired half-pipe structures, a layer of Permalloy ($Ni_{80}Fe_{20}$) with a thickness of 20 nm was deposited onto the pre-patterned substrate using a sputtering technique. This deposition process resulted in the formation of the half-pipe structures, as depicted in Fig. 1 (a). The half pipe has a central part of width 120 nm and two rotated side branches. The stack in Fig. 1 (a) is Titanium(5 nm)/Permalloy(12 nm)/Ti(5 nm) and filled with Platinum on the top for preparation of the TEM grid.

SQUID magnetometry measurements revealed an easy direction of magnetization aligned along the length of the half-pipe structures, and a semi-hard direction of magnetization oriented transverse to the half-pipe, as shown in the inset of Fig. 1 (b). The magnetization dynamics in the permalloy half-pipe were investigated by broad band ferromagnetic resonance(FMR) in a flip chip coplanar geometry. The dependence of the FMR frequency for the applied field for both axial and transverse configurations as shown in Figure 1 (c) shows a magnetic uniaxial anisotropy of 75 mT along the half-pipe. Complementary measurements using the cavity FMR technique(X band and Q band) reveal extra peaks (inset of Fig. 1 (c)), which we attribute to the strongly inhomogenous magnetic landscape developing under the field.

Acknowledgments

This work is supported by ANR-FWF project Magfunc ANR 20-CE91-005.

References

[1] Anjan Barman et al. The 2021 Magnonics Roadmap. *Journal of Physics: Condensed Matter* 33, 413001 (2021).

[2] Robert Streubel, Florian Kronast, Peter Fischer, et al. Retrieving spin textures on curved magnetic thin films with full-field soft X-ray microscopies. *Nature Communications* 6 (2015).

[3] Denis D Sheka, Volodymyr P Kravchuk, and Yuri Gaididei. Curvature effects in statics and dynamics of low dimensional magnets. *Journal of Physics A: Mathematical and Theoretical* 48, 125202 (2015).

[4] Jorge A. Otálora, Ming Yan, Helmut Schultheiss, Riccardo Hertel, and Attila Kákay. Curvature-Induced Asymmetric Spin-Wave Dispersion. *Phys. Rev. Lett.* 117, 227203 (22 2016).

[5] L. Körber, R. Verba, Jorge A. Otálora, et al. Curvilinear spin-wave dynamics beyond the thin-shell approximation: Magnetic nanotubes as a case study. *Phys. Rev. B* 106, 014405 (1 2022).

[6] Parashara Panduranga, Aly Abdou, Zhong Ren, Rasmus H. Pedersen, and Maziar P. Nezhad. Isotropic silicon etch characteristics in a purely inductively coupled SF_6 plasma. *Journal of Vacuum Science & Technology B* 37, 061206 (2019).

Interplay between diffusion and magnon-drag thermopower in iron-based nanowire networks

Tristan da Câmara Santa Clara Gomes[1,*], Nicolas Marchal[1], Flavio Abreu Araujo[1], and Luc Piraux[1]

[1]*Institute of Condensed Matter and Nanosciences, Université catholique de Louvain, Louvain-la-Neuve, Belgium*

*tristan.dacamara@uclouvain.be

Ferromagnetic transition metals and their alloys exhibit large thermooelectric power S compared to other metals. For instance, the Seebeck coefficient of Ni and Co are found to be respectively -20 and -30 $\mu V/K$. In contrast large positive thermopower of $+15$ $\mu V/K$ is observed in bulk Fe. Moreover, due to their large electrical conductivity σ, they can exhibit very large power factors $\mathrm{PF} = S^2\sigma$, which is the physical parameter that relates to the output power density of a thermoelectric material, with the largest room temperature PF found for bulk Co [1]. The large thermopower of the transition metals and alloys arises from contribution of the diffusion thermopower S_d because of the pronounced structure of the d-band and the high energy derivative of the density of states at the Fermi level, large diffusion thermopowers are observed [2], and significant potential contribution from magnon-drag thermopower S_MD. Despite several experimental and theoretical work carried out on different materials, it is still difficult to obtain experimental evidence for the existence of magnon-drag effects, due to the complex separation of thermoelectric power into its different components. In pioneering work, Blatt et al. [3] measured the thermopower in iron over a wide temperature range and concluded that in Fe, magnon-drag plays a dominant role. Here, we report the measurements on the thermoelectric power of 45 nm diameter interconnected nanowire networks consisting of pure Fe, dilute FeCu and FeCr alloys and Fe/Cu multilayers. The interconnected nanowire networks (as presented in Fig. 1) are obtained by direct electrodeposition in flexible polymer template with cylindrical crossed nanopores from a sputtered gold cathode [1, 4], which can be locally removed to form an electrode pattern as shown in Fig. 1(a).

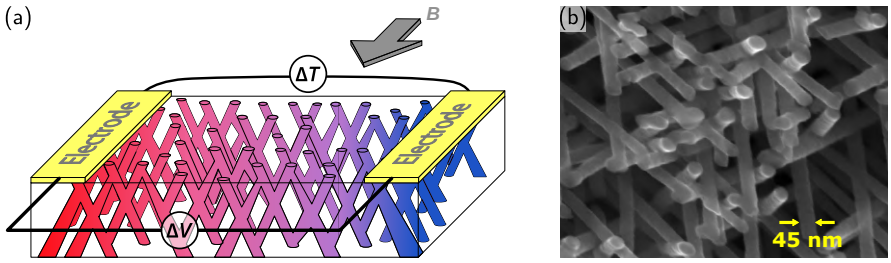

Figure 1: (a) Device configuration for measurement of the (magneto-)thermopower in crossed nanowire network; the magnetic field B is along the in-plane direction of the nanowire film. (b) SEM image of the self-supported interconnected Fe nanowires showing a nanowire network with a 45 nm diameter and a 20% packing density.

Fig. 2(a) shows the temperature evolution of the thermopower of Fe, FeCu and Fe/Cu multilayer nanowire networks. The values obtained for Fe are very close to those found in bulk Fe at all temperatures studied. The introduction of Cu impurities in Fe leads to a reduction of the total measured thermopower which becomes negative for $Fe_{90}Cu_{10}$ nanowires (~ -7 μV/K at 300 K). A slope $\alpha \sim -0.05$ μV/K^2 can be extract from the linear S_d contribution from all these data, which corresponds well to the value extracted from previously reported measurements in bulk Fe, FeCo and FePt alloys (see Fig. 2(b)). This indicates that only S_MD is affected by the introduction of Cu, Co and Pt impurities. Subtracting the linear S_d contribution from the data, S_MD has been estimated, as reported in Fig. 2(c). For pure Fe, we estimated $S_\mathrm{d} \approx -15$ μV/K from our data, which is largely supplanted by the estimated $S_\mathrm{MD} \approx +30$ μV/K [4]. Fig. 2(a) also shows that the measured thermopower for Fe/Cu multilayer is negative and varies almost linearly with temperature, reaching about -11 μV/K at 300 K. This indicates a dominant contribution of charge carrier diffusion to the thermopower, as previously found in other magnetic multilayers, and a cancellation of the magnon-drag effect, leading to this large and negative value, which is slightly smaller than $S_\mathrm{d} \approx -15$ μV/K due to the contribution of the small positive thermopower of the Cu layers. The magneto-resistance (MR) and magneto-thermopower (MTP) effects have been measured on Fe/Cu multilayer nanowires (see Fig. 3(a)) showing larger MTP effect compared to MR. From these measurements, we can extract the linear Gorter-Nordheim relation between $\Delta S(H) = S(H) - S_{H=0}$ vs. $\Delta G = 1/R(H) - 1/R_{H=0}$ (see Fig. 3(b)), which is characteristic of a dominant diffusion thermopower. Finally, the spin-dependent Seebeck coefficient $S_\uparrow - S_\downarrow$ in Fe has been directly extracted from the data in Fig 3(a) and reaches about -7.6 μV/K at ambient temperature (see Fig. 3(c)) [4].

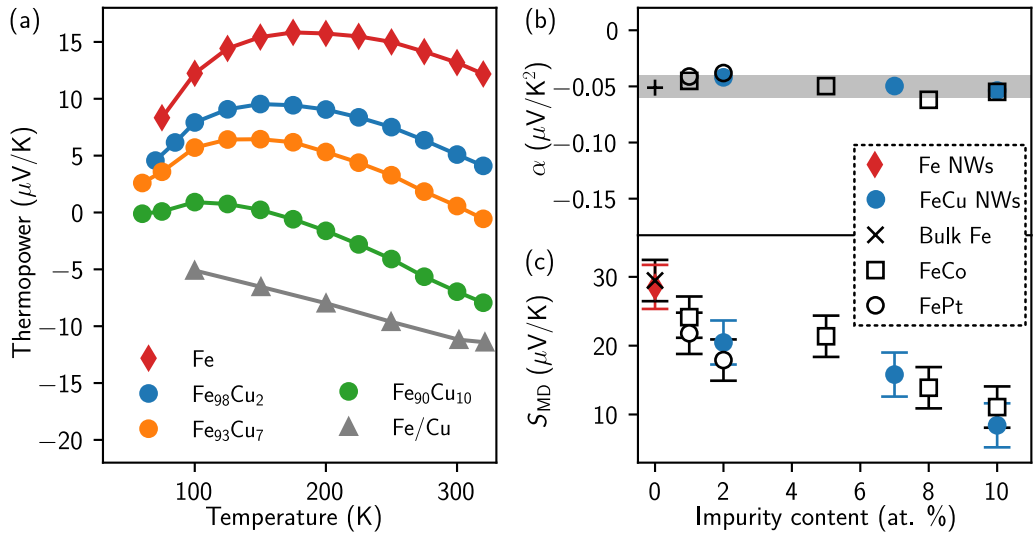

Figure 2: (a) Temperature dependence of the thermopower S of 45 nm diameter nanowire networks made of pure Fe, Fe-rich FeCu alloys and Fe(7 nm)/Cu(10 nm) multilayer. (b-c) Estimated values of the slope α of the linear S_d contribution (b) and estimated room temperature values of S_{md} (c) for bulk Fe and dilute Fe-based alloys: Fe and FeCu nanowires (present work), FeCo [5] and FePt [3].

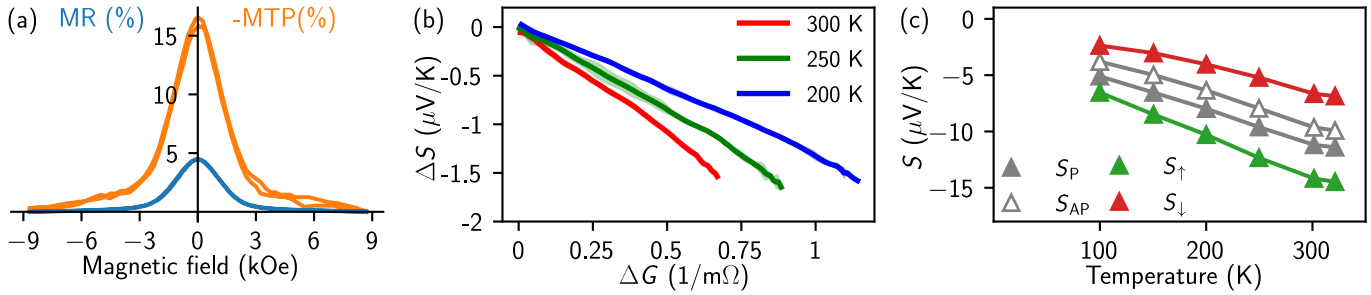

Figure 3: (a) Room-temperature magnetoresistance (in blue) and magneto-Seebeck (in orange) curves for a Fe/Cu multilayer nanowire network. (b) Linear variation of $\Delta S(H)$ vs. ΔG at different temperatures, illustrating the Gorter-Nordheim characteristics. (c) Temperature variation of the measured Seebeck coefficients at zero and saturating magnetic fields, S_{AP} and S_P, along with the calculated spin-dependent Seebeck coefficients $S_\uparrow$ and $S_\downarrow$.

References

[1] Tristan da Câmara Santa Clara Gomes, Nicolas Marchal, Flavio Abreu Araujo, and Luc Piraux. Flexible thermoelectric films based on interconnected magnetic nanowire networks. *Journal of Physics D: Applied Physics* 55, 223001 (2022).

[2] Frank J. Blatt, Peter A. Schroeder, Carl L. Foiles, and Denis Greig. *Thermoelectric Power of Metals*. Springer, Boston, MA, 1976.

[3] F. J. Blatt, D. J. Flood, V. Rowe, P. A. Schroeder, and J. E. Cox. Magnon-Drag Thermopower in Iron. *Phys. Rev. Lett.* 18, 395–396 (11 1967).

[4] Nicolas Marchal, Tristan da Câmara Santa Clara Gomes, Flavio Abreu Araujo, and Luc Piraux. Interplay between diffusion and magnon-drag thermopower in pure iron and dilute iron alloy nanowire networks. *Scientific Reports* 13, 9280 (2023).

[5] Y. Zheng, El. J. Weiss, N. Antolin, W. Windl, and J. P. Heremans. Magnon drag effect in Fe-Co alloys. *Journal of Applied Physics* 126, 125107 (2019).

Spin dynamics in $NdCo_x$/Al/YIG trilayer systems

David S. Schmool[1, *], Daniel Markó[1, 2], Ibtissem Benguettat-El Mokhtari[1], Luis Manuel Álvarez-Prado[3, 4], Javier Díaz[3, 4], Carlos Quirós[3, 4], Irene Lucas[5, 6], Pilar Cavero[7], Soraya Sangiao[5, 6], and Luis Morellón[5, 6]

[1]*Université Paris-Saclay, UVSQ, CNRS, GEMaC, 78000 Versailles, France*
[2]*Silicon Austria Labs GmbH, Europastr. 12, 9523 Villach, Austria*
[3]*Departamento de Física, Facultad de Ciencias, Universidad de Oviedo, C/ Federico García Lorca n∘ 18, 33007 Oviedo, Spain*
[4]*Centro de Investigación en Nanomateriales y Nanotecnología (CINN), CSIC-Universidad de Oviedo, 33940 El Entrego, Spain*
[5]*Departamento de Física, Universidad de Zaragoza, Pedro Cabruna 12, 50009 Zaragoza, Spain*
[6]*Instituto de Ciencia de Aragón (INA), Universidad de Zaragoza, Mariano Esquillor Edificio I+D, 50018, Zaragoza, Spain*
[7]*Centro Universitario de la Defensa, Academia General Militar, 50090 Zaragoza, Spain*
david.schmool@uvsq.fr

Spin dynamics in the form of broadband VNA - FMR provides a convenient and highly-sensitive measurement of the magnetic properties and the magnetic behaviour of low dimensional magnetic systems. In this work, we present a detailed study of multilayer systems consisting of a hard magnetic NdCo x film (with x = 7.5 and 9) coupled to a soft thin magnetic film via an intervening Al film of 5 nm. The principal aim of this study is to determine the effect of the magnetic coupling between the hard and soft layers. The hard magnetic NdCo layer has perpendicular anisotropy, which results in a periodic magnetic stripe domain structure at magnetic fields below the saturation field.

In previous work, we have studied the above system using permalloy as the soft layer [1], where we observe hysteretic behaviour in the soft magnetic layer which derives from the properties of the NdCo film, while the FMR signal from this layer (NdCo) is not directly observed in the spectra [2, 3], as shown in Fig. 1 for the sample with $NdCo_{7.5}$ (65 nm)/Al (5 nm)/Py (10 nm). We note that the samples are saturated in the positive (negative) direction before measurements in the descending (ascending) field measurement.

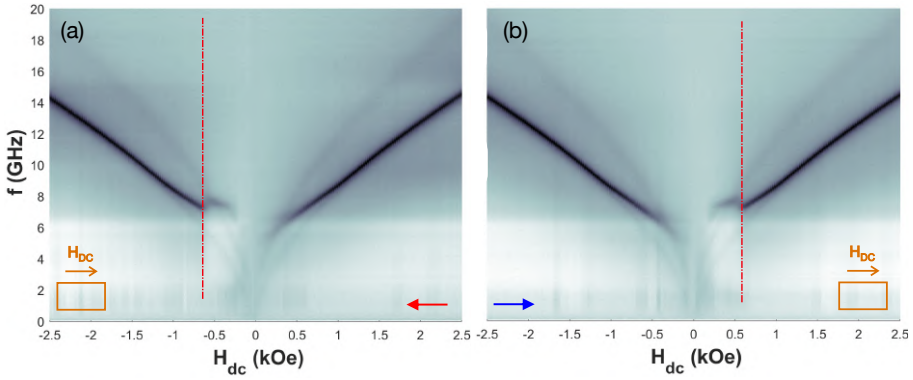

Figure 1: Frequency – field characteristics for the NdCo7.5 (65 nm)/Al (5 nm)/Py (10 nm) sample for the (a) descending and (b) ascending field branches.

These spectra show an intense, and reasonably sharp, resonance line that derives from the Py layer. The behaviour is asymmetric and arises from the interaction of the Py layer with the NdCo film, being intimately related to the stripe domain structure of the latter [4] and thus gives rise to the observed magnetic hysteresis. Comparison with magnetometry measurement also show a correspondence with critical and coercive fields [2, 3]. In the samples where the Py layer is replaced with a 12 nm YIG film, there are a number of additional features that can be observed. Due to growth requirements, the YIG layer is deposited before the NdCo film, while for the Py samples, the NdCo layer is deposited first. What is interesting to note are the broad dark regions in these measurements which arise from the NdCo films. For the sample with $NdCo_9$, the out-of-plane anisotropy is fairly weak and we can observe the in-plane components of the magnetocrystalline anisotropy. These are indicated in Fig. 2 (a) (i) and (iii) for the easy and hard axes, respectively. The blue lines denote the NdCo signal, while the red line corresponds to that for the YIG layer. While YIG spectra are practically identical for the two in-plane directions measured, the NdCo resonance lines are different. This shows an in-plane anisotropy component for the $NdCo_9$, with an anisotropy field of $H_K \simeq 0.2$ kOe, that conforms to the zero-field resonance of $f_0 = \gamma H_K / 2\pi \simeq 5$ GHz.

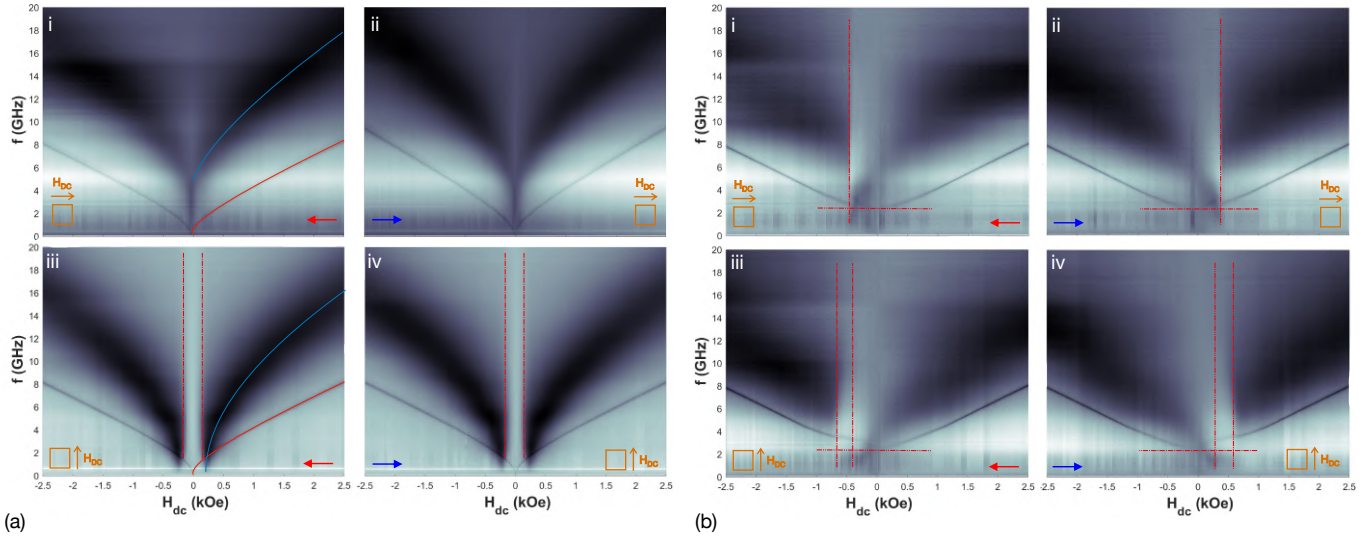

Figure 2: Frequency - field characteristics for the (a) YIG (12 nm)/Al (5 nm)/NdCo9 (65 nm) sample and (b) YIG (12 nm)/Al (5 nm)/$NdCo_{7.5}$ (65 nm) sample. The descending (ascending) field branches are indicated by red (blue) arrows and the easy (top - i and ii) and hard (bottom - iii and iv) are also shown. The red lines mark the YIG signal, while the blue that for the NdCo.

We now consider the YIG (12 nm)/Al (5 nm)/$NdCo_{7.5}$ (65 nm) sample, whose spectra are shown in Fig. 2(b). Here the NdCo out-of-plane anisotropy is stronger and the low-field behaviour is much changed with respect to that of the $x = 9$ sample. Firstly, there appears to be little or no significant in-plane anisotropy in the NdCo layer. Secondly, the low-field switching is now asymmetric and shows that the hysteresis in the FMR arises from here and is imprinted in the YIG film. Indeed this latter shows very similar hysteretic behaviour to that in the Py samples shown earlier. The switching in the NdCo, on passing through the origin, makes a very abrupt change, as indicated by the red vertical dashed line, Fig. 2(b) i and ii). This can now be seen directly as causing the jump in the soft layer (YIG) resonance line and unequivocally demonstrates the origin of the FMR hysteresis in this layer.

Acknowledgments

D.S.S. acknowledges financial support from the Institut de Physique of the CNRS for experimental equipment. This study has been supported by Spanish MICIN under grant PID2019-104604RB/AEI/10.13039/501100011033 and by Asturias FICYT under grant AYUD/2021/51185 with the support of FEDER funds.

References

[1] Krzysztof Szulc, Silvia Tacchi, Aurelio Hierro-Rodríguez, et al. Reconfigurable Magnonic Crystals Based on Imprinted Magnetization Textures in Hard and Soft Dipolar-Coupled Bilayers. *ACS Nano* 9, 14168–14177 (2022).

[2] Daniel Markó, Fernando Valdés-Bango, Carlos Quirós, et al. Tunable ferromagnetic resonance in coupled trilayers with crossed in-plane and perpendicular magnetic anisotropies. *Applied Physics Letters* 115, 082401 (2019).

[3] David S. Schmool, Daniel Markó, Ko-Wei Lin, et al. Ferromagnetic Resonance Studies in Magnetic Nanosystems. *Magnetochemistry* 7, 126 (2021).

[4] David S. Schmool, Daniel Markó, Aurelio Hierro-Rodríguez, et al. Ferromagnetic Resonance Hysteresis in NdCo/Al/Py trilayers. *In preparation* (2023).

Physics-informed neural networks for nutating anti-ferromagnetic moments

Pascal Thibaudeau[1,*], Matthieu Carreau[2], and Stam Nicolis[3]

[1]*CEA, DAM, Le Ripault, BP 16, F-37260, Monts, France*
[2]*Télécom Paris, Institut Polytechnique de Paris, Palaiseau, F-91120, France*
[3]*Institut Denis Poisson, Université de Tours, Université d'Orléans, CNRS (UMR7013), Parc de Grandmont, Tours, F-37200, France*
*pascal.thibaudeau@cea.fr

With the rapid development of miniaturized devices in spintronics, the dynamics of nanomagnets is of both theoretical and practical interest. The equations of motion for a magnetic moment, embedded in a medium, that describe the average magnetization, are differential equations, that contain time derivatives on both sides and cannot be–in general–recast in a form that is useful for usual numerical methods. Physics-Informed Neural Networks (PINNs) provide the framework for solving differential equations, without imposing a particular format. They are, thus, ideally suited for solving the equations for a dampened (parametrized by λ) and inertial magnetic moment (parametrized by τ) [1, 2], as given by

$$\dot{\boldsymbol{M}} = \boldsymbol{M} \times \left(\boldsymbol{\Omega} + \lambda \dot{\boldsymbol{M}} + \ddot{\boldsymbol{M}}\right)$$

where t/τ becomes a rescaled time and $\boldsymbol{\Omega} \equiv \tau \boldsymbol{\omega}$ is a constant precession axis. We have benchmarked the performance of feedforward neural networks in accomplishing such tasks and discuss advantages and shortcomings. We have also adapted this approach to the case of more than one sub-lattices, making it possible to address the modeling of ultrafast switching of both ferrimagnets and antiferromagnets [3].

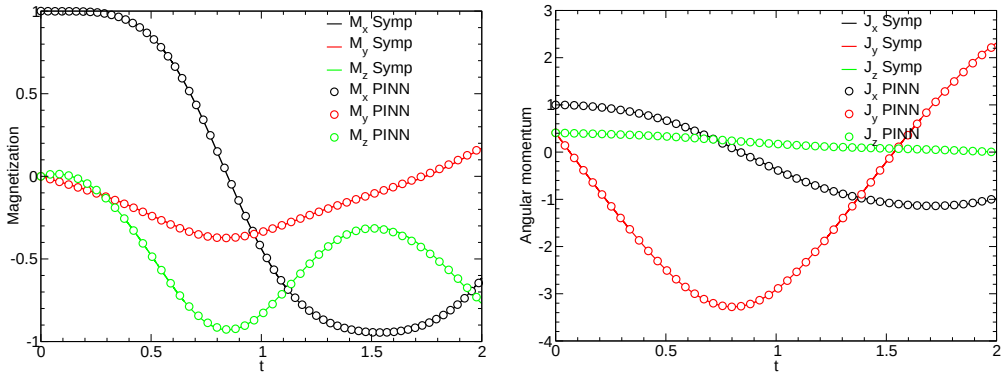

Figure 1: Magnetization $\boldsymbol{M}$ and angular momentum $\boldsymbol{J}$ dynamics predicted by symplectic integration and PINNs.

Acknowledgments

The Federation CaSciModOT (Calcul Scientifique et la Modélisation à Orléans et Tours) is acknowledged for its financial support.

References

[1] I. Makhfudz, E. Olive, and S. Nicolis. Nutation Wave as a Platform for Ultrafast Spin Dynamics in Ferromagnets. *Appl. Phys. Lett.* 117, 132403 (2020). arXiv: 1910.11897.

[2] Pascal Thibaudeau and Stam Nicolis. Emerging Magnetic Nutation. *Eur. Phys. J. B* 94, 196 (2021). arXiv: 2103.04787.

[3] Théophile Chirac, Jean-Yves Chauleau, Pascal Thibaudeau, Olena Gomonay, and Michel Viret. Ultrafast Antiferromagnetic Switching in NiO Induced by Spin Transfer Torques. *Phys. Rev. B* 102, 134415 (2020). arXiv: 2004.09822.

Émission unidirectionnelle d'onde de spin par effet Tcherenkov

Gauthier Philippe[1, *], Jarosław W. Kłos[1], and Mathieu Moalic[1]

[1]*Département de physique des Nanostructures, ISQI, Faculté de Physique, Adam Mickiewicz University, Poznań, Pologne*
*gauphi@st.amu.edu.pl

L'effet Tcherenkov est un phénomène existant pour tous types d'ondes. Il peut être observé lorsque la source d'une onde poursuit un mouvement à une vitesse supérieur à la vitesse de propagation de l'onde.

En 2013, Ming Yan et al [1] ont démontré, à l'aide de simulations micro magnétique, l'existence d'un effet Tcherenkov pour les ondes de spin générées par une impulsion de champ magnétique en mouvement.

Les auteurs ont aussi démontré que pour des systèmes ferromagnétiques 2D et 3D le front d'onde prend la forme un cône.

Dans nos travaux, nous avons reproduit les résultats obtenus par M. Yang en utilisant le logiciel de simulation micro magnétique MuMax3. Nous avons aussi étudié le cas d'une paire de sources qui garde une distance constante et se déplaçant à la même vitesse.

Pour certaines distances et vitesses, nous avons observé des interférences destructives de nos ondes de spin devant ou derrière nos sources. Dans ces situations, le système se comporte comme une antenne unidirectionnelle d'onde de spin, pouvant généré des ondes de spin à différentes fréquences uniquement devant ou derrière nos sources. L'un des principaux défis pour réaliser des observations expérimentales de l'effet Tcherenkov pour les ondes de spin est de créer une source pouvant se déplacer à une vitesse de l'ordre du km/s. L'une des idées possibles serait d'utiliser le champ magnétique d'un vortex au sein d'un supraconducteur [2] (Abrikosov lattices), qui pourrait se déplacer au sein d'une couche supraconductrice placer au-dessus de la couche ferromagnétique.

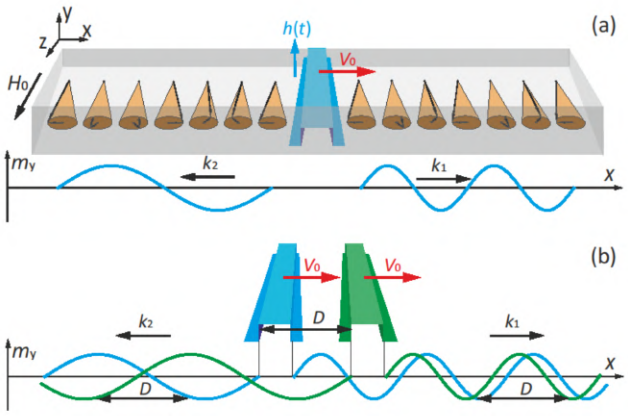

Figure 1: a) impulsion magnétique, b) paire d'impulsions

Remerciement

Les auteurs remercient le centre national des sciences de Pologne pour son soutien sous le projet:
No: 2021/43/I/ST3/00550.

References

[1] Ming Yan, Attila Kákay, Christian Andreas, and Riccardo Hertel. Spin-Cherenkov effect and magnonic Mach cones. *Phys. Rev. B* 88, 220412 (22 2013).

[2] E H Brandt. The flux-line lattice in superconductors. *Reports on Progress in Physics* 58, 1465–1594 (1995).

Poster 2.15, November 15th, 10h50–13h00

Inversion of the polarity of angular velocity inside a precessing magnet

Giovanni Olivetti[1,*], Thierry Valet[1], Grégoire De Loubens[2], Kei Yamamoto[3], Yoshichika Otani[4,5], Benjamin Pigeau[6], and Olivier Klein[1]

[1]*Université Grenoble Alpes, CEA, CNRS, Grenoble INP, Spintec, 38054 Grenoble, France*
[2]*SPEC, CEA, CNRS, Université Paris-Saclay, 91191 Gif-sur-Yvette, France*
[3]*Advanced Science Research Center, Japan Atomic Energy Agency, Tokai 319-1195, Japan*
[4]*RIKEN Center for Emergent Matter Science (CEMS), Wako 351-0198, Japan*
[5]*Department of Basic Science, The University of Tokyo, Tokyo 152-8902, Japan*
[6]*Université Grenoble Alpes, CNRS, Institut Néel, 38054 Grenoble, France*
*giovanni.olivetti@neel.cnrs.fr

Recent progress in magneto-acoustic effect have demonstrated the benefits of using circularly polarized vector fields to excite the magnetization dynamics [1–3]. In this case, a discrimination occurs depending on the sense of gyration and it is often assumed that the proper polarity of angular velocity is uniquely set by the direction of equilibrium magnetization and the sign of the gyromagnetic ratio.

Using an axisymmetric eigen-solver (developed by Thierry Valet), we have found numerically that the above statement is in general not true and the angular velocity can spatially change its sign relative to the magnetization vector. It emerges in finite size object due to self-demagnetizing effect, where a spin-wave minimizes its magnetostatic energy by inverting its sense of gyration. This leads to the spatial segregation of the magnetization dynamics in different regions with opposite angular velocity.

As an example we compare in Fig.1 the dynamics of two Walker modes propagating either clockwise or counterclockwise along the edge of a normally magnetized disk. For each eigen-value, ω_0, the eigen-solver associates two eigen-vectors $\mathbf{m}_{0^\circ}$ and $\mathbf{m}_{90^\circ}$, respectively the phase and the quadrature, which allows to reconstruct the time evolution of the dynamical magnetization $\mathbf{m} = \mathbf{m}_{0^\circ} \cdot \cos(\omega_0 t) - \mathbf{m}_{90^\circ} \cdot \sin(\omega_0 t)$. Using the colormap shown in the legend, we plot the spatial variation of the angle between $\mathbf{m}_{0^\circ}$ and $\mathbf{m}_{90^\circ}$ for two indices $\ell = \pm 8$. Here a change of color indicates a change in the direction of rotation.

The implications of our findings are relevant to the conservation of total angular momentum inside a magnetic system.

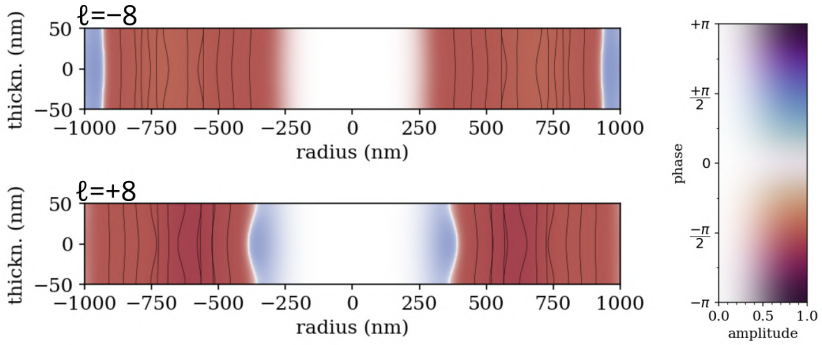

Figure 1: Comparison of the dynamics of two Walker modes with azimuthal indices $\ell = \pm 8$ propagating along the edge of disk. The figure is a view along a sagittal section. The colormap shows the angle between $\mathbf{m}_{0^\circ}$ and $\mathbf{m}_{90^\circ}$ respectively the phase and quadrature eigen-vectors.

References

[1] Mingran Xu, Kei Yamamoto, Jorge Puebla, et al. Nonreciprocal surface acoustic wave propagation via magneto-rotation coupling. *Science Advances* 6 (2020).

[2] K. An, A. N. Litvinenko, R. Kohno, et al. Coherent long-range transfer of angular momentum between magnon Kittel modes by phonons. *Physical Review B* 101 (2020).

[3] K. An, R. Kohno, A. N. Litvinenko, et al. Bright and Dark States of Two Distant Macrospins Strongly Coupled by Phonons. *Physical Review X* 12 (2022).

Micromagnetic simulations of magnon nonlinear interactions in YIG disk magnetic vortex

Sali Salama[1,2,*], Maryam Massouras[1], Abdelmadjid Anane[2], and Jean-Paul Adam[1]

[1]*Centre de Nanosciences et de Nanotechnologies, CNRS, Université Paris-Saclay, Palaiseau, 91120, France.*
[2]*Unité Mixte de Physique ,CNRS, Thales, Université Paris Saclay, Palaiseau, 91767, France*
sali.salama@universite-paris-saclay.fr

Magnons that describe the Eigen excitations of a magnetic system possess unique properties that make them suitable for carrying, processing, and storing information. For instance, they exhibit nonlinear interactions when excited at high amplitudes. These nonlinear interactions can be used to perform nonconventional computing which aims at reducing the energy consumption in data processing. This study presents micromagnetic simulations to understand magnon nonlinear interactions in Yttrium iron garnet (YIG) disks with a vortex state. We obtain the dispersion relation which is essential in understanding the linear and the nonlinear phenomena. Then we move from linear to the nonlinear regime, focusing on three magnon splitting and coupling with the core gyration. We use MuMax3, a software that utilizes finite difference discretization of space, to perform the micromagnetic simulations. It calculates the magnetization dynamics in both space and time. The micromagnetic parameters used in the simulations are: saturation magnetization $M_s = 140 \times 10^3 A/m$, damping constant $\alpha = 10^{-3}$, exchange stiffness constant $A_{ex} = 3.7 \times 10^{-12} J/m$ and first order cubic anisotropy constant $K_{c1} = -464\ J.m^{-3}$. Due to cubic anisotropy, the static out-of-plane magnetization outside the vortex core will not exhibit uniformity. Instead, it will display a distinct three-fold symmetry.

The disk used in this study has a thickness of 65 nm and a diameter of 500 nm. The rotational symmetry of the disk leads to the formation of radial eigenmodes with mode number n and azimuthal eigenmodes with mode number m[1]. To obtain the dispersion relation, we excite the disk in the r.f. range using a cardinal sine function perpendicular to the disk plane with specific spatial symmetry, a Bessel function to excite a given radial mode, and a cosine function to excite azimuthal mode. Fig.1 shows the obtained dispersion relation with the mode spatial profiles [2]. It shows a splitting of the azimuthal number 1 due to the hybridization with the core gyration. The mode at 2.019 GHz exhibits azimuthal number 3

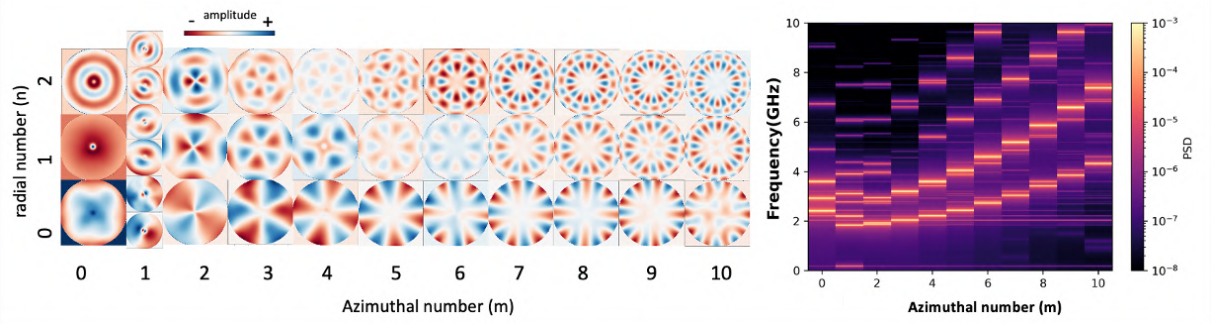

Figure 1: The dispersion relation for 500nm YIG disk with the mode spatial profiles

and radial number 0 and can be excited despite the symmetry of the excitation due to the cubic anisotropy.

Applying a 0.01 mT rf magnetic field amplitude yields a linear response, as indicated by the diagonal line in Figure 2a. Increasing the rf field to 0.1 mT produces some bands of nonlinear interactions. At an excitation frequency of 2.92 GHz, corresponding to radial mode number $n = 1$ and azimuthal mode $m = 0$ in Figure 1, we observe four magnon modes equally distributed around f_{exc}, with a frequency spacing of 170 MHz (δf). The in-plane component of the magnetization exhibits a gyration with a frequency of 170 MHz starting after 200ns, the same as the modes distributed around f_{exc}, which indicates coupling to the gyration frequency. Exciting the disk with 2mT rf magnetic field amplitude results in different processes of nonlinear interactions. The vertical bands below 3GHz are coming from coupling with the core gyration. However the nonlinear interactions above 4GHz are coming from 3 magnon scattering except the process at 4.02GHz where we have two kinds of nonlinear interactions. Initially, three magnon scattering occurs at 1.824GHz and 2.194GHz, followed by gyration motion that begins 400ns later. Additionally, the secondary modes arising from three magnon scattering couple to this gyration, as demonstrated by the evolution of the mode population over time in Fig.3 so the gyration is like a relaxation channel for these modes. These two modes coming from three magnon scattering have the same radial and azimuthal numbers as the selection rule of having different radial numbers is relaxed due to the hybridization with the core gyration [3]. Another two modes appear at the same time as the gyration motion, the mode which has 3 fold symmetry and a mode with azimuthal 2 and radial 0. The effect of having two processes, three magnon scattering followed by coupling with the gyration motion is coming from the anisotropy because removing the anisotropy will suppress the gyration motion, and we will have just three magnon scattering processes.

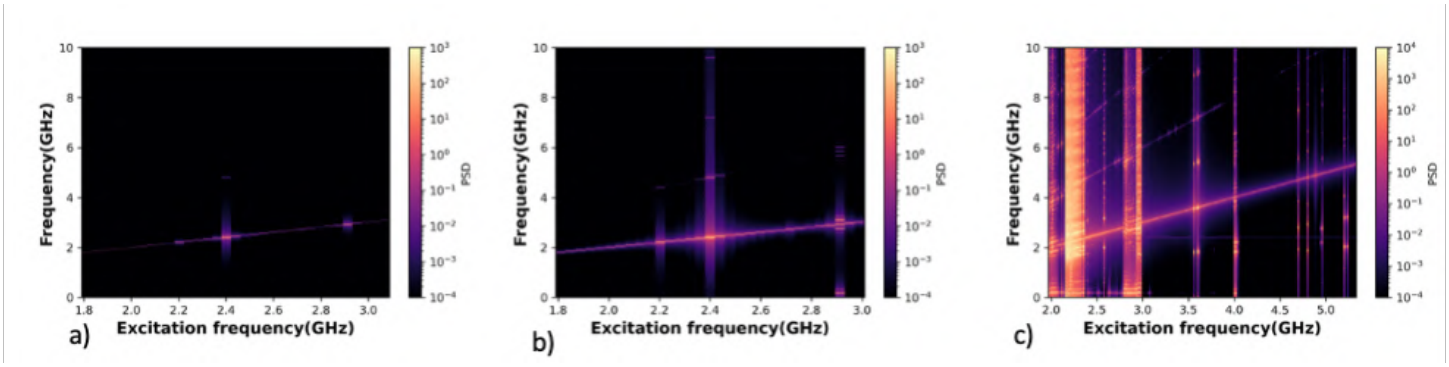

Figure 2: The power spectral density map for 500nm YIG disk with 65nm thickness a)the linear response at 0.01mT rf magnetic field amplitude b)the nonlinear response at 0.1mT c)2mT

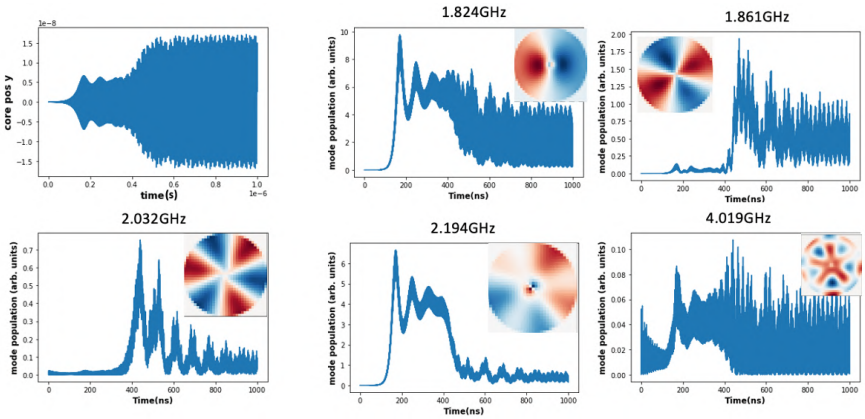

Figure 3: The evolution of the mode populations and the spatial profiles for the gyration motion and the secondary modes of three magnon scattering when the disk is excited with 2mT and 4.02GHz

Acknowledgments

This work was supported by the French National Research Agency (ANR) [under a public grant overseen as part of the Investissements d'Avenir program (Labex NanoSaclay, reference: ANR-10- LABX-0035), SPICY, and a research contract No. ANR-20-CE24-0012 (MARIN)] and by the European Commission under FET-Open Grant No. 899646 (K-NET).

References

[1] K Schultheiss, R Verba, F Wehrmann, et al. Excitation of whispering gallery magnons in a magnetic vortex. *Physical review letters* 122, 097202 (2019).

[2] Lukas Körber. "Theory and Simulation on Nonlinear Spin-Wave Dynamics in Magnetic Vortices". MA thesis. TECHNISCHE UNIVERSITÄT DRESDEN, 2019.

[3] Roman Verba, Lukas Körber, Katrin Schultheiss, et al. Theory of Three-Magnon Interaction in a Vortex-State Magnetic Nanodot. *Physical Review B* 103, 014413 (2021).

Poster 2.17, November 15th, 10h50–13h00

Spin-wave near-field diffraction model for in-plane magnetized films

Vincent Vlaminck[1,2,*], Loic Temdie[1,2], Vincent Castel[1,2], Matthias Benjamin Jungfleisch[3], Yves Henry[4], Daniel Stoeffler[4], and Matthieu Bailleul[4]

[1]*IMT Atlantique, Dpt. MO, Technopole Brest-Iroise CS83818, 29238 Brest Cedex 03, France*
[2]*Lab-STICC/NSF (UMR 6285), CNRS, Technopole Brest-Iroise CS83818, 29238 Brest Cedex 03, France*
[3]*University of Delaware, Dept. of Physics and Astronomy, Newark, Delaware, USA*
[4]*Université de Strasbourg, CNRS, Institut de Physique et Chimie des Matériaux de Strasbourg, UMR 7504, F-67000 Strasbourg, France*
*vincent.vlaminck@imt-atlantique.fr

Mastering spin waves interference at the sub-micron scale is central for the development of wave-based computing applications such as reservoir computing [1], holographic memory [2], or spectral analysis [3]. The complexity of spin dynamics, inherently due to its dependence to numerous parameters, and also to the intricacy of magnon-magnon interactions, requires heavy computational methods, which can limit the scope of study. In this context, we developed an efficient tool to study the near-field diffraction (NFD) patterns of spin wave in homogeneous out-of-plane magnetized thin films for arbitrary distribution of excitation field [4]. In this communication, we extend our NFD model to in-plane magnetized films, taking into account the coupling between higher order standing spin-wave modes in order to recover the thickness dependence of the interference patterns. We show in particular how caustic beams can be directly emitted from a sharply constricted stripline (see Fig. 1). This model allows to explore efficiently magnon beamforming over the wide range of parameters such as field, frequency, magnetic properties, shape and scale of antennas.

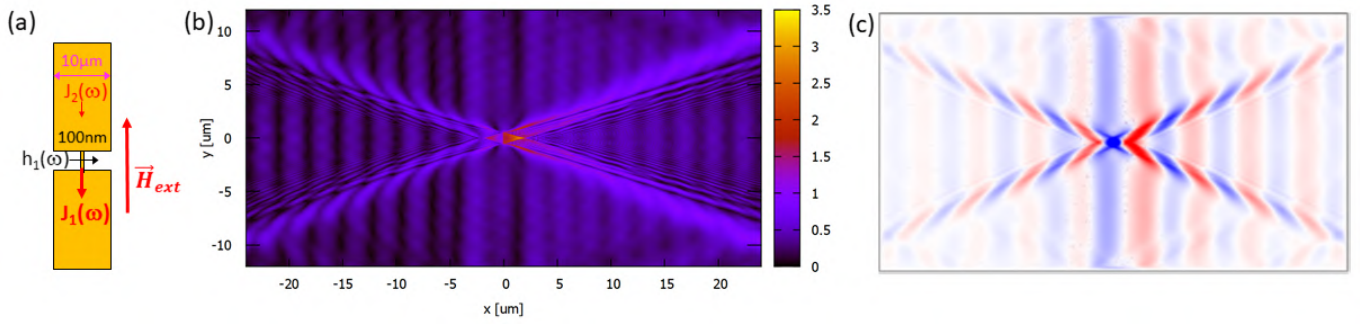

Figure 1: (**a**) Sketch of a constricted stripline. (**b**) NFD and (**c**) MuMax3 micromagnetic simulations of the spin wave amplitude m_x in a 25 nm thick CoFeB film resulting from a 100 nm-wide and 1 μm long constriction as sketched in (**a**) at f=13 GHz, and for a external static field $\mu_0 H_{ext}$=100mT applied along y (color palette units in mT).

Acknowledgments

This work was supported by the French ANR project "*MagFunc*", the Département du Finistère through the project "*SOSMAG*", and the FACE Foundation & French Embassy through the project "*Magnon Interferometry*".

References

[1] A. Papp, G. Csaba, and W. Porod. Characterization of nonlinear spin-wave interference by reservoir-computing metrics. *Applied Physics Letters* 119, 112403 (2021).

[2] Alexander Khitun. Parallel database search and prime factorization with magnonic holographic memory devices. *Journal of Applied Physics* 118, 243905 (2015).

[3] Ádám Papp, Wolfgang Porod, Árpád I. Csurgay, and György Csaba. Nanoscale spectrum analyzer based on spin-wave interference. *Scientific Reports* 7 (2017).

[4] V. Vlaminck, L. Temdie, V. Castel, et al. Spin wave diffraction model for perpendicularly magnetized films. *Journal of Applied Physics* 133, 053903 (2023).

Time-resolved Noncommutativity of Parametric Excitations in YIG disks

Maryam Massouras[1,*], Massimiliano d'Aquino[2], Salvatore Pierna[2], Claudio Serpico[2], Jean-Paul Adam[1], György Csaba[3], and Joo-Von Kim[1]

[1]*Centre de Nanosciences et de Nanotechnologies, CNRS, Université Paris-Saclay, Palaiseau, France*
[2]*Università degli Studi di Napoli Federico II, Naples, Italy*
[3]*Pázmány Péter Catholic University, Budapest, Hungary*
*maryam.massouras@c2n.upsaclay.fr

Parametric pumping is an efficient way to populate single modes in magnetic microstructures. For information processing, it is essential to examine the influence and interactions between modes. We examine this phenomenon with the simulated excitations of 1-μm diameter YIG disks at 300 K, whereby we investigate the transient mode population dynamics computed with the MuMax3 code [1] by projecting the magnetization dynamics onto precomputed eigenmode profiles [2] [Fig. 1.b)]. The figure highlights the main features for two modes, $k = 8, 11$, with frequencies of $f_8 = 2.813$ GHz and $f_{11} = 2.885$ GHz. Fig. 1.c) shows the evolution of the mode populations when the system is excited at $f_A = 2f_8$ and $f_B = 2f_{11}$ driven at $b_{rf\,8} = 0.90$ mT and $b_{rf\,11} = 1.05$ mT (supercriticality at 1.5) separately. The time-resolved populations show that modes $k = 8$ and $k = 11$ populations dominate along with satellite modes $k = 14, 5$ for the former and $k = 17, 7$ for the latter. When these driving frequencies are toggled using the sequences in Fig. 1.d), we see from the mode spectrogram that the order of the frequency toggle has a strong bearing on the overall dynamics: we observe mode inhibition by the first excitation. However this noncommutativity differs depending on the excited modes: commutativity, mode suppression, satellite modes suppression are also observed. Such rich nonlinear behavior is indeed very promising for information processing.

Acknowledgments

This work is supported by the Horizon2020 Framework Programme of the European Commission under contract number 899646 (k-Net).

References

[1] Arne Vansteenkiste, Jonathan Leliaert, Mykola Dvornik, et al. The design and verification of MuMax3. *AIP advances* 4, 107133 (2014).

[2] Massimiliano d'Aquino, Claudio Serpico, Giovanni Miano, and Carlo Forestiere. A novel formulation for the numerical computation of magnetization modes in complex micromagnetic systems. *Journal of Computational Physics* 228, 6130–6149 (2009).

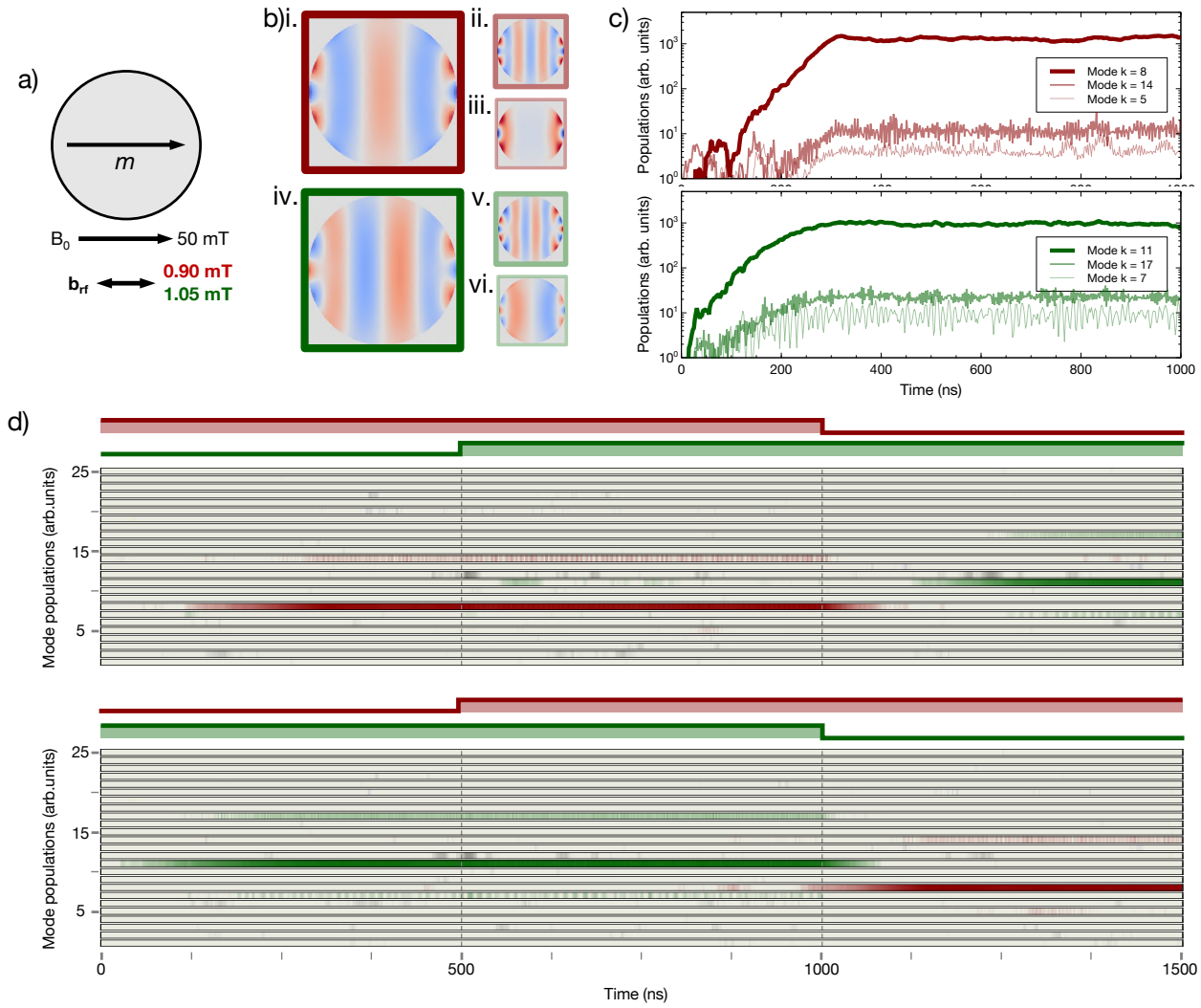

Figure 1: a) Geometry. b) Eigenmode profiles i. $k = 8$; ii. $k = 14$; iii. $k = 5$; iv. $k = 11$; v. $k = 17$ and vi. $k = 7$. c) Mode population versus time under a driving frequency of $f_A = 2 \times 2.813$ GHz (top) and $f_B = 2 \times 2.885$ GHz (bottom). d) Populations of the first 25 modes under the pulse sequences f_A, $f_A + f_B$, f_B (top) and f_B, $f_B + f_A$, f_A (bottom), where the duration of each pulse is 500 ns.

Rashba Edelstein Effect enhancement induced by insertion of a light metallic layer

Nicolas Sebe[1,*], S. Krishnia[1], Y. Sassi[1], F. Ajejas[1], N. Reyren[1], S. Collin[1], T. Denneulin[2], A. Kovács[2], R. E. Dunin-Borkowski[2], A. Fert[1], J.-M. George[1], V. Cros[1], and H. Jaffrès[1]

[1]*Unité Mixte de physique CNRS-Thales, Palaiseau, France*
[2]*Ernst Ruska-Centre for Microscopy and Spectroscopy with Electrons (ER-C 1) and Peter Grünberg Institut (PGI-5),Forschungszentrum Jülich GmbH, 52425 Jülich, Germany*
*nicolas.sebe@cnrs-thales.fr

Spin-orbit interaction (SOI) at metallic interfaces with broken inversion symmetry [1] has been recently the centre of spintronic research because it enables fast and efficient magnetisation dynamics for spin-based memory (e.g. SOT-MRAM), skyrmion and neuromorphic devices. Indeed, the dynamics of magnetisation in spintronics devices is mainly controlled by the efficient spin-orbit torques (SOT) exerted by the generated out-of-equilibrium transverse angular momentum like played by the spin currents. Two main mechanisms i.e. (a) spin Hall effect (SHE) in heavy metals such as Pt, Ta and (b) spin or orbital Rashba effect (REE) at interfaces may thus contribute leading to a damping-like (DL) and a field-like (FL) torque [2]. More recently, the occurrence of Rashba effects and orbital Hall in systems integrating light elements were also shown to generate torque or to enhance the already existing SOT in well engineered stack and heterostructures [3, 4].

In order to tackle these fundamental issues and provide some routes for improvement of SOT-based devices, we demonstrate here how the insertion of a light metal element interface profoundly affects with a strong benefit both the nature of spin-orbit torque and its efficiency in terms of damping-like and field-like effective fields acting on a very adjacent thin Co layer. We will more focus on the case of Pt/Co/Al/Pt systems with variable thicknesses integrating a top Co/Al interface [5]. We show how the insertion of a Co/Al interface leads to a huge enhancement, by about one order of magnitude, of the FL torque upon the increase of the Al thickness up to 3 nm. By varying the Al and the bottom Pt thicknesses, we undoubtedly demonstrate the occurrence of a Rashba interaction in Co/Al that we discuss in terms of spin vs. orbital Rashba interactions. On the other hand, from the variation of the torque vs. the Co thickness at the very low thickness limit (t_{Co} varying from 0.55 to 1.4 nm) (see Fig. 1), we extract the main parameters governing the transverse spin-dissipation related to spin-precession and spin-decoherence and discuss the ensemble of those phenomena that we correlate to the respective spin-Hall magnetoresistance (SMR) and anomalous Hall effect (AHE) response.

Starting from such discovery of large Rashba effect the Co/Al interface in these series, we have presently investigated the SOT properties of CoFeB/Al, Co/CoFeB/Al and CoFeB/Co/Al systems. Such systems are more adapted to MRAM technologies because CoFeB presents less damping and less coercivity than Co. The measurements have been performed in the 2nd harmonic voltage method in both DL and FL configurations as well as both angular and field sweep geometries.

The resulting FL and DL SOT properties vs. thickness, anisotropy and magnetic domain configuration will be largely discussed. We will give the main trends for each systems.

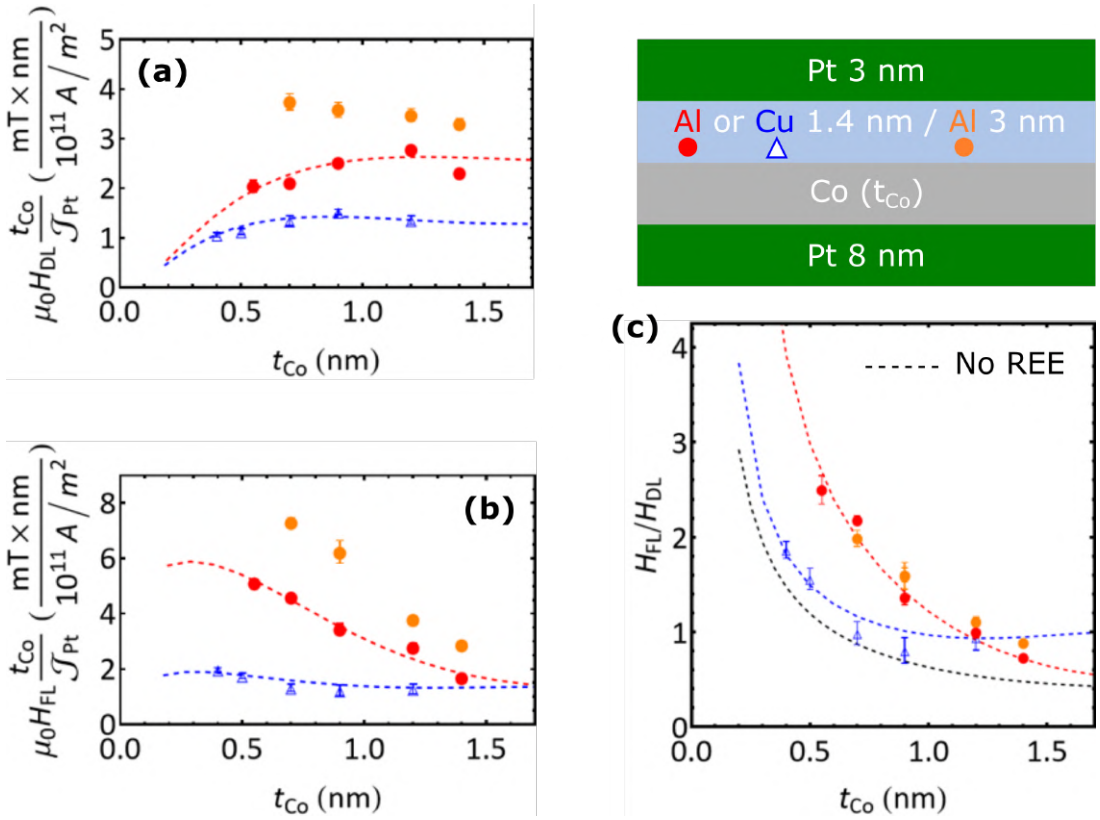

Figure 1: Co layer thickness dependence of **(a)** DL-SOT field and **(b)** FL-SOT fields multiplied by Co thickness for $10^{11}A/m^2$ current density in Pt in Pt8|Co(t_{Co})|Al1.4|Pt3 (red circles), Pt8|Co(t_{Co})|Cu1.4|Pt3 (blue triangles) and Pt8|Co(t_{Co})|Al3|Pt3 (orange circles) samples **(c)** $\zeta = H_{FL}/H_{DL}$ as a function of t_{Co}. The dashed lines are fits with the theoretical model.

Acknowledgement

This work has been supported by the ANR-20-CE30-0022 “ORION”. N. Sebe benefits from a France 2030 government grant managed by the ANR (ANR-22-PEPR-Electronique-EMCOM).

References

[1] Anjan Soumyanarayanan, Nicolas Reyren, Albert Fert, and Christos Panagopoulos. Emergent phenomena induced by spin–orbit coupling at surfaces and interfaces. *Nature* 539, 509–517 (2016).

[2] Aurelien Manchon, Jakub Železnỳ, Ioan M Miron, et al. Current-induced spin-orbit torques in ferromagnetic and antiferromagnetic systems. *Reviews of Modern Physics* 91, 035004 (2019).

[3] Junyeon Kim, Dongwook Go, Hanshen Tsai, et al. Nontrivial torque generation by orbital angular momentum injection in ferromagnetic-metal/Cu/Al 2 O 3 trilayers. *Physical Review B* 103, L020407 (2021).

[4] Shilei Ding, Andrew Ross, Dongwook Go, et al. Harnessing orbital-to-spin conversion of interfacial orbital currents for efficient spin-orbit torques. *Physical review letters* 125, 177201 (2020).

[5] S. Krishnia, Y. Sassi, F. Ajejas, et al. *Large interfacial Rashba interaction and giant spin-orbit torques in atomically thin metallic heterostructures*. 2022. arXiv: 2205.08486 [cond-mat.mes-hall].

Core dynamics of a spin-torque vortex oscillator with non-uniform in-plane polarizer

L. Kokkinos [1,*] and J.-V. Kim[1]

[1]*Centre des Nanosciences et Nanothecnhologies, CNRS, Université Paris-Saclay, 91120, Palaiseau, France*
**loukas.kokkinos@universite-paris-saclay.fr*

Spin torque nano-oscillators (STNOs) are devices that exhibit several interesting properties, such as wide frequency range, that could be very interesting for technological applications, in high-frequency communications and RF detection just to name a few. These devices also appear to be good candidates for non-conventional computing, and artificial neural networks, owing to the very interesting non-linear dynamical regimes they present [1, 2].

One of the most commonly studied types of STNOs are Spin-Torque Vortex Oscillators (STVOs). These structures often consist of a stacking of a ferromagnetic free layer in a vortex magnetization, a non-magnetic (or insulator) spacer layer, and a pinned ferromagnetic layer. Several studies have shown that when applying a current through those devices, the vortex core can exhibit self-sustained gyrotropic motion. The gyration regimes have been shown to vary with the magnetic configuration of the pinned layer. For instance, the magnetization component perpendicular to the film plane governs the existence of steady-state gyration.

In this work, we study the effect of a non-uniform polarizer on the dynamics of the vortex core in a magnetic tunnel junction (MTJ) STVO. This work consists of a numerical investigation, using the open source micromagnetic simulator MuMax3 [3]. The studied STVO is based on the geometry shown in Ref. [2], which comprises a circular magnetic tunnel junction with a free ferromagnetic layer of 300 nm in diameter and 7 nm in thickness. The fixed layer's magnetization consists of a non-uniform, almost circular, in-plane configuration, obtained as a ground state under the effect of an Oersted-Ampere field. A schematic of the STVO geometry, along with the profile of the magnetization in both the free and the fixed magnetic layers are given in Figure 1.

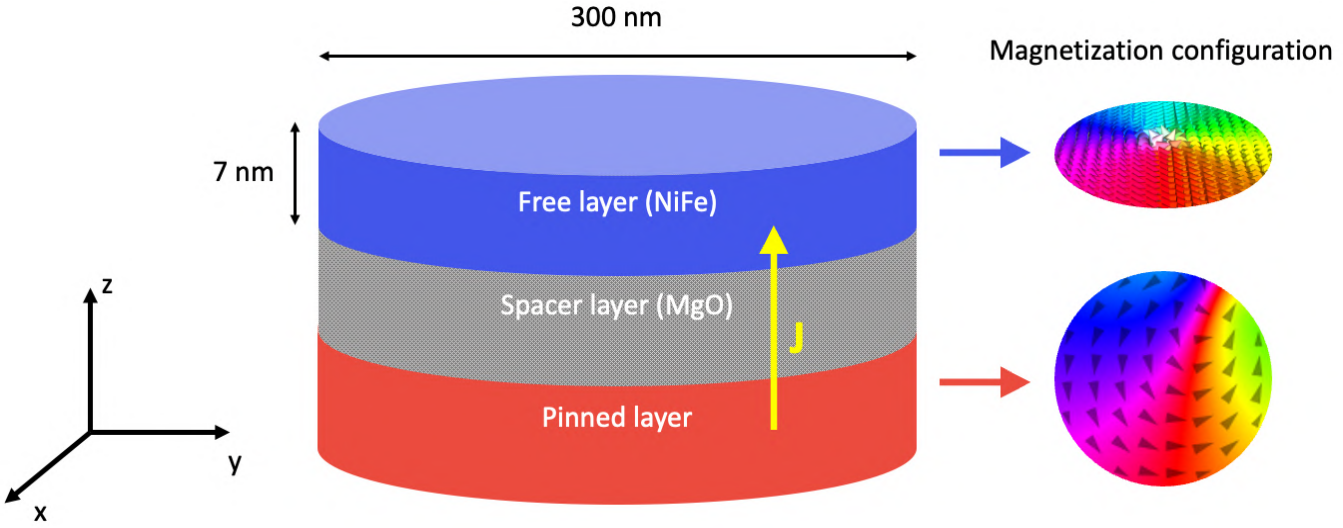

Figure 1: *Schematic of the simulated STVO, where J indicates the applied current flow. The magnetic configuration in both the fixed and the pinned layers is also depicted.*

In addition to the exchange and dipolar interactions, we account for contributions from current induced Oersted-Ampere field, along with the damping- and field-like Slonczewski spin-transfer torques [4] in the equations of motion. This last contribution is controlled by the secondary Slonczewski spin-transfer torque parameter ϵ' in MuMax3.

Our simulations suggest that the introduction of (circular) non-uniformity in the in-plane magnetized polarizer favors the core dynamics in the free layer. This is illustrated by the power spectral density (PSD) maps in Figures 2a and 2d, which show the evolution of the gyration frequency of our core in respect to the applied current I, for two different values of the field-like torque parameter $\epsilon' = \{-0.2; 0.1\}$. These maps were obtained by running simulations for each current value, and computing the FFT of the in-plane magnetization component to get their respective frequency spectra.

Both these cases present a clear pure gyrotropic motion for low currents up to approximately 11mA for $\epsilon' = 0.1$ and 12 mA for $\epsilon' = -0.2$. At higher current values, the system exhibits non-linear dynamics in both cases. In the case of $\epsilon' = 0.1$ (Fig. 2a), 11 mA represents a threshold above which we no longer observe oscillations, but instead a pinning of the vortex core. When $\epsilon' = -0.2$ (Fig. 2d), above the threshold of 12 mA, more gyration frequencies start to appear for the same current value. We were able to attribute this to core reversal dynamics through the analysis of our results. At very high currents ($\geq$ 16 mA), both cases exhibit an unstable and possibly chaotic state. Some of the core trajectories are shown in Figures 2b , 2c, 2e and 2f to better visualize those oscillation regimes.

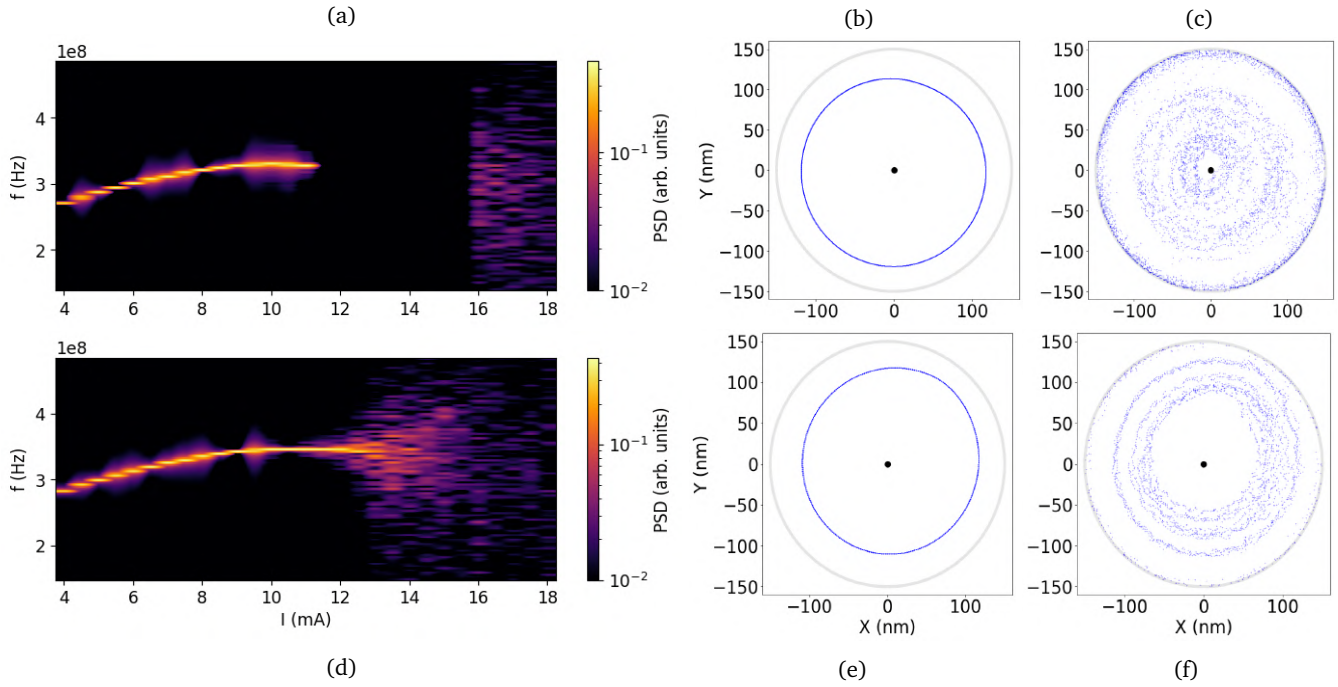

Figure 2: *(a) and (d) show the color map of the power spectral density (PSD) as a function of applied current for* $\epsilon' = 0.1$ *and* $\epsilon' = -0.2$*, respectively.(b),(c) Core trajectory for* $\epsilon' = 0.1$ *and* $I = 8$ *and 16 mA, respectively. (e),(f) Core trajectory for* $\epsilon' = -0.2$ *and* $I = 8$ *and 13.5 mA, respectively.*

References

[1] M.-W. Yoo, D. Rontani, J. Létang, et al. Pattern generation and symbolic dynamics in a nanocontact vortex oscillator. *Nature Communications* 11, 601 (2020).

[2] S. Wittrock, P. Talatchian, Miguel Romera, et al. Beyond the gyrotropic motion: Dynamic C-state in vortex spin torque oscillators. *Applied Physics Letters* 118 (2021).

[3] A. Vansteenkiste, J. Leliaert, M. Dvornik, et al. The design and verification of MuMax3. *AIP Advances* 4 (2014).

[4] J.C. Slonczewski. Current-driven excitation of magnetic multilayers. *Journal of Magnetism and Magnetic Materials* 159, L1–L7 (1996).

Complex dynamics in mutually coupled spin torque vortex oscillators

Katia Ho[1,*], Steffen Wittrock[1,2], Salvatore Perna[3], Roberta Dutra[4], Ricardo Ferreira[5], Claudio Serpico[3], Paolo Bortolotti[1], Romain Lebrun[1], and Vincent Cros[1]

[1]*Unité Mixte de Physique CNRS, Thales, Université Paris-Saclay, 91767, Palaiseau, France*
[2]*Helmholtz-Zentrum Berlin fur Materialien und Energie GmbH, Hahn-Meitner-Platz 1, 14109 Berlin, Germany*
[3]*Department of Electrical Engineering and ICT, University of Naples Federico II, 80125 Naples, Italy*
[4]*Centro Brasileiro de Pesquisas Fésicas (CBPF), Rua Dr. Xavier Sigaud 150, Rio de Janeiro 22290-180, Brazil*
[5]*International Iberian Nanotechnology Laboratory (INL), 471531 Braga, Portugal*
katia.ho@cnrs-thales.fr

Spin torque nano-oscillators are spintronic devices in which radiofrequency magnetization oscillations can be generated through spin-transfer effects. Due to their nonlinearity, these devices display interesting properties such as spectral purity, frequency stability, and high tunability, opening up possibilities from wireless telecommunication to neuromorphic computing [1].

In this study, we will focus on vortex-based spin-torque nano-oscillators (STVO) and study the response of mutually coupled STVOs. To couple them, we use the RF current emitted by one STVO, which is first amplified and then sent through the antenna located above the second STVO and vice versa. The resulting external RF field hence mediates the coupling between the two STVOs.

Using this approach, beyond the expected improvement of their RF properties, i.e., power emission and spectral purity [2], we have recently shown that strong coupling can lead to new phenomena beyond synchronization, such as amplitude death, mode branching, and non-trivial states associated with exceptional points (EPs) [3]. EPs, defined as singularities of non-Hermitian problems, can indeed emerge from such systems. Combining experimental results (Fig. 1) and theoretical modeling (Fig. 2), we succeed in demonstrating that the presence of mode branching (Fig. 1) can be connected to the coalescence of the system complex eigenvalues, i.e., the existence of an EP, in a specific current range.

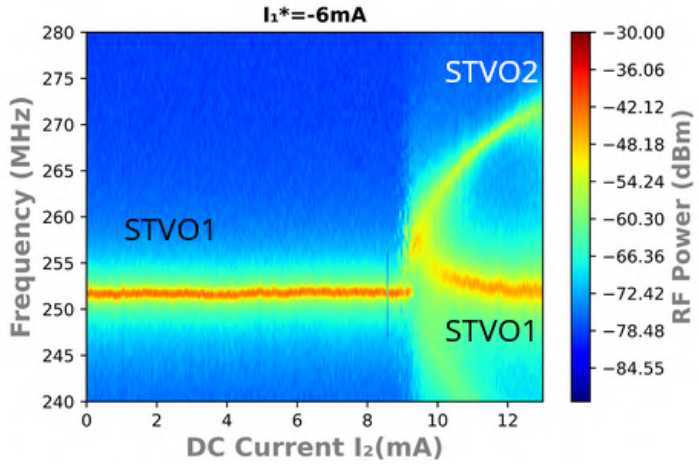

Figure 1: Oscillation frequency spectra of the coupled STVOs versus STVO2 current $I_{DC,2}$ and fixed $I_{DC,1}$. An EP is observed at (I_1^*, I_2) = (-6,9.45) mA.

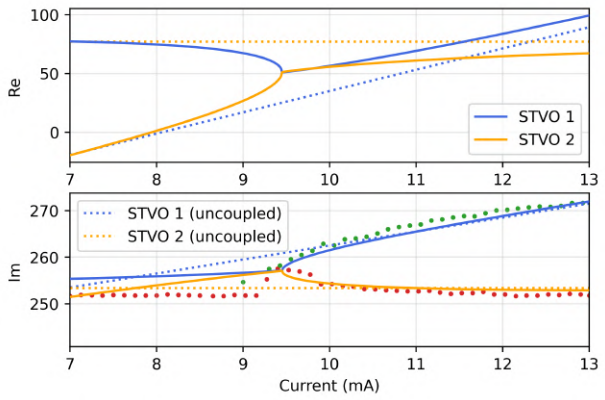

Figure 2: Corresponding complex eigenvalues versus STVO2 current $I_{DC,2}$. Eigenvalues are in dashed (uncoupled) and solid (coupled) lines. Raw data points are represented by dotted lines.

The next step is to investigate, both in frequency and time domain, how these EPs' existence is sensitive to the individual properties of each STVO and the path used to approach this EP state [4]. For instance, we also observe a dependence on the coupling strength, which may be another key for the EP's control. As depicted in Fig. 3 for three different gain

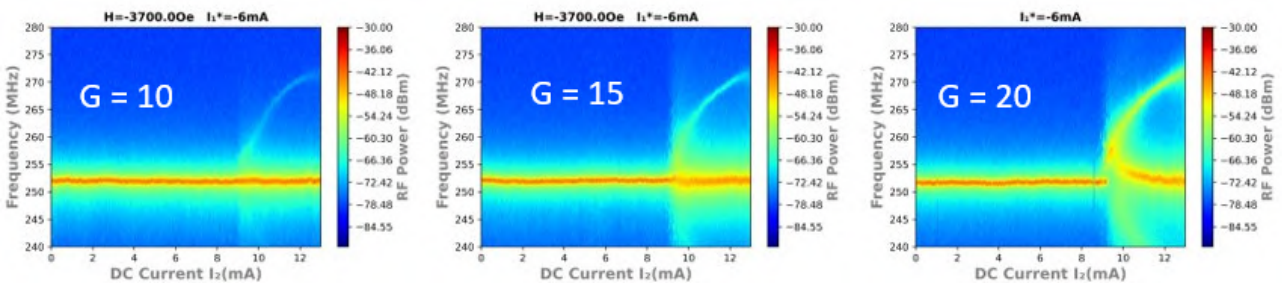

Figure 3: Oscillation frequency spectra of the coupled STVOs versus STVO2 current $I_{DC,2}$ and fixed at I_1^* = -6 mA for different gain amplitude of 10, 15 and 20 dBm.

amplitudes from +10 to +20 dBm, we relate the appearance of branching to the strengthened interaction between the coupled oscillators.

We believe that this study opens spintronic devices to the field of non-Hermitian Hamiltonian physics, already observed in several variable loss/gain systems in photonics and electronics [5]. By proving the engineering of EPs for high sensitivity mode control, the objective will be to show the potential of this technique in magnetic sensor-type systems.

Acknowledgments

This work was supported by a government grant managed by the ANR as a part of the France 2030 investment plan from PEPR SPIN ANR-22-EXSP SPINCOM.

References

[1] N. Locatelli, V. Cros, and J. Grollier. Spin-torque building blocks. *Nature Materials* 13, 11–20 (2013).

[2] R. Lebrun, S. Tsunegi, P. Bortolotti, et al. Mutual synchronization of spin torque nano-oscillators through a long-range and tunable electrical coupling scheme. *Nature Communications* 8 (2017).

[3] Steffen Wittrock, Salvatore Perna, Romain Lebrun, et al. *Non-hermiticity in spintronics: oscillation death in coupled spintronic nano-oscillators through emerging exceptional points*. 2023. arXiv: 2108.04804 [cond-mat.mes-hall].

[4] C. Dembowski, H.-D. Gräf, H. L. Harney, et al. Experimental Observation of the Topological Structure of Exceptional Points. *Physical Review Letters* 86, 787–790 (2001).

[5] Jan Wiersig. Review of exceptional point-based sensors. *Photonics Research* 8, 1457 (2020).

Current-controlled periodic polarity reversal in a spin-torque vortex oscillator

Chloé Chopin[1,*], Simon de Wergifosse[1], Anatole Moureaux[1], and Flavio Abreu Araujo[1]

[1]*Institute of Condensed Matter and Nanosciences, UCLouvain, Louvain-la-Neuve, Belgium*
chloe.chopin@uclouvain.be

A magnetic vortex is a topologically protected texture leading to nonlinear dynamics. These two features confer a high interest to devices like spin-torque vortex oscillators (STVOs). A magnetic vortex is characterized by its chirality which describes its curling in-plane magnetization, and its polarity that defines the orientation of the out-of-plane magnetization in the vortex core. Periodical reversal of the vortex polarity triggered by different external magnetic field excitations, in-plane ac current [1] or dc current flowing through a nanocontact in a spin-valve [2] were reported. It can lead to a confinement regime in which the trajectory of the vortex core remains bounded within two orbits s_{min} and s_{max}. However, to the best of our knowledge, it was not shown for a MTJ-based STVO excited by an out-of-plane dc current.

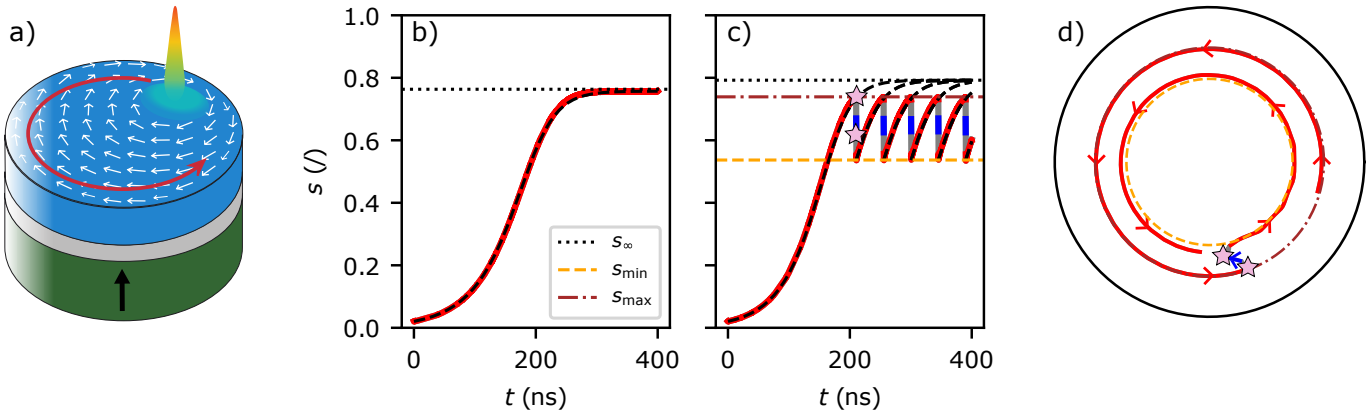

Figure 1: a) STVO with the polarizer in green, insulator in gray and the free layer with a magnetic vortex as a ground state in blue. b) Evolution of the reduced vortex core position $s(t)$ in the steady-state regime saturating at s_∞. The dashed line is the fit using Eq. 1. c) Evolution of $s(t)$ in the confinement regime. The trajectory is plotted in red (resp. blue) for a positive (resp. negative) polarity. The black dashed line is the estimation of $s(t)$ using Eq. 1 and s_∞. Pink stars indicate polarity reversals. d) Trajectory of the vortex core inside the magnetic dot while in the confinement regime. The vortex core motion is represented by arrows. When the polarity is negative, the gyration sense is reversed.

A magnetic dot made of permalloy with a radius R of 500 nm and a thickness h of 9 nm is studied by micromagnetic simulations using mumax^3 [3] (see Fig. 1a)). A spin-polarized current perpendicular to the plane is injected to trigger the vortex core motion due to spin-transfer torque. The evolution of the reduced vortex core position $s(t)$ in the auto-oscillating regime is fitted with the following equation [4] as seen in Fig. 1b):

$$s(t) = \frac{s_0}{\sqrt{\left(1 + \frac{s_0^2}{\alpha/\beta}\right) e^{-2\alpha t} - \frac{s_0^2}{\alpha/\beta}}} \tag{1}$$

with s_0 the initial reduced vortex core position, α and β two values that depends on the input current density J_{dc}. These values can be fitted linearly by $\alpha(J_{\text{dc}}) = a_J \cdot J_{\text{dc}} + a$ and $\beta(J_{\text{dc}}) = b_J \cdot J_{\text{dc}} + b$. The steady-state orbit can then be predicted by $s_\infty(J_{\text{dc}}) = \sqrt{-\alpha(J_{\text{dc}})/\beta(J_{\text{dc}})}$ as seen in Fig. 2a). In addition, $s_\infty(J_{\text{dc}})$ and $\alpha(J_{\text{dc}})$ are used to predict $s(t)$ in the confinement regime as in Fig. 1c). Indeed, fitting the confinement regime with Eq. 1 gives poor results. So, the evolution of $s(t)$ in the confinement regime is predicted instead. Finally, in both the auto-oscillating and resonant regimes, the evolution of $s(t)$ can be analytically modeled using this method.

Depending on the input current density J_{dc}, three regimes arise. The resonant and steady-state regimes are well-known and correspond to the regimes when the vortex core relaxes to its equilibrium position ($s = 0$) and where it reaches a stable orbit ($s = s_\infty$). The third regime is the confinement regime where the vortex core is confined between two orbits s_{min} and s_{max} due to a double reversal process. First, the vortex polarity is reversed through the process of creation and annihilation

of a vortex-anti-vortex pair [1] with the emission of spin-waves [5]. As the velocity of the vortex core increases, it undergoes a deformation with the development of a dip with an opposite magnetization. At the critical velocity [6], the dip amplitude is the same as the one of the vortex core and the vortex polarity is reversed. The vortex is then in the resonant regime and relaxes towards its equilibrium position as seen in Fig. 1d). Then, the vortex experiences a second polarity reversal as a new dip reaches the same amplitude of the vortex core and spin-waves are once again generated. At the end of this second reversal, the vortex core is at s_{min} and in the auto-oscillating regime again. This double reversal happens periodically, leading to a sustained confinement regime that can be described by three parameters: s_{min}, s_{max} and the frequency f_{conf} at which the double reversals occur.

The orbits s_{min} and s_{max} decrease [2] with the amplitude of J_{dc} while f_{conf} increases as seen in Fig. 2. Thus, the frequency of spin-waves generation can be controlled with J_{dc}. Furthermore, the vortex chirality has a huge impact on the vortex dynamics. Indeed, the confinement regime is only seen for a negative chirality as for a positive chirality, the vortex core is expelled from the magnetic dot before it reaches its critical velocity.

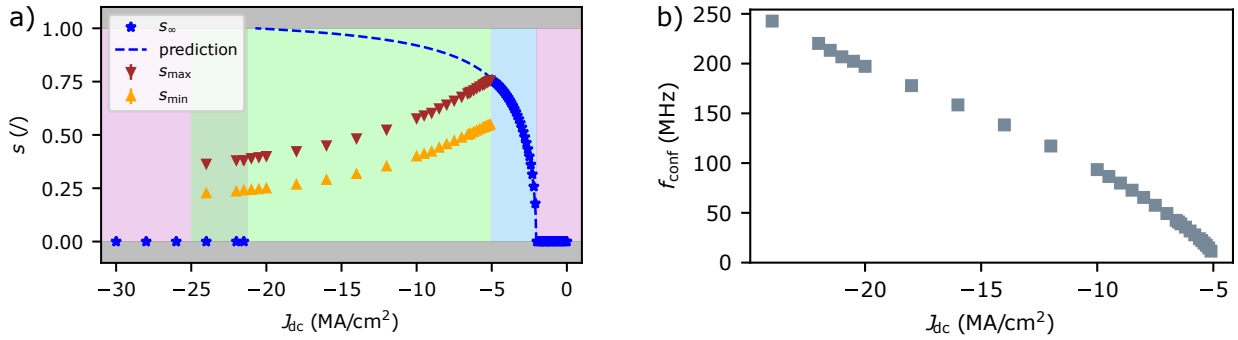

Figure 2: a) Evolution of s_∞, s_{max} and s_{min} with J_{dc}. The dashed blue line is the prediction of s_∞ using $\alpha(J_{\text{dc}})$ and $\beta(J_{\text{dc}})$ that is injected in Eq. 1 to model $s(t)$. The resonant, steady-state and confinement regimes are symbolized by pink, blue and green backgrounds respectively. b) Evolution of f_{conf} with J_{dc}.

The confinement regime presents a nonlinear and periodical dynamics that can be interesting for neuromorphic computing with STVO as the vortex core remains in a transient regime and never reaches saturation. The dynamics of the vortex core is piece-wise analytically described in the confinement regime, this is a first step towards its complete modeling. In addition, the emergence of the confinement regime depends on the vortex chirality and J_{dc} as well as s_{min}, s_{max} and f_{conf}. Thus, J_{dc} can be used to tune the confinement regime properties.

References

[1] K. Yamada, S. Kasai, Y. Nakatani, et al. Electrical switching of the vortex core in a magnetic disk. *Nature Materials* 6, 270–273 (2007).

[2] S. Petit-Watelot, J.V. Kim, A. Ruotolo, et al. Commensurability and chaos in magnetic vortex oscillations. *Nature Physics* 8, 682–687 (2012).

[3] A. Vansteenkiste, J. Leliaert, M. Dvornik, et al. The design and verification of MuMax3. *AIP Advances* 4, 107133 (2014).

[4] A. Moureaux, S. de Wergifosse, C. Chopin, J. Weber, and F. Abreu Araujo. Neuromorphic spintronics accelerated by an unconventional data-driven Thiele equation approach (2023).

[5] R. Hertel and C. M. Schneider. Exchange Explosions: Magnetization Dynamics during Vortex-Antivortex Annihilation. *Physical Review Letters* 97 (2006).

[6] K.S. Lee, S.K. Kim, Y.S. Yu, et al. Universal Criterion and Phase Diagram for Switching a Magnetic Vortex Core in Soft Magnetic Nanodots. *Physical Review Letters* 101 (2008).

Controlling interfacial spin-orbit related effects with light element interface

Sachin Krishnia[1,*], Nicolas Sebe[1], Tristan Da Camara Santa Clara Gomes[1], Yanis Sassi[1], Luis Moreno Vicente-Arche[1], Sophie Collin[1], Thibaud Denneulin[2], András Kovács[2], Rafal E. Dunin-Borkowski[2], Philippe Ohresser[3], Nicolas Jaouen[3], Jean-Marie George[1], André Thiaville[4], Albert Fert[1], Henri Jaffrès[1], Nicolas Reyren[1], and Vincent Cros[1]

[1]*Unité Mixte de Physique, CNRS, Thales, Université Paris-Saclay, 91767, Palaiseau, France*
[2]*Ernst Ruska-Centre for Microscopy and Spectroscopy with Electrons (ER-C 1) and Peter Grünberg Institut (PGI-5), Forschungszentrum Jülich GmbH, 52425 Jülich, Germany*
[3]*Synchrotron SOLEIL, L'Orme des Merisiers, 91190, Saint Aubin, France*
[4]*Laboratoire de Physique des Solides, Université Paris-Saclay, CNRS, Orsay 91405, France*
*sachinbudana@gmail.com

In the last decade, intensive efforts have been made to stabilize chiral spin textures, such as magnetic skyrmions, and their current-induced dynamics by harvesting interfacial spin-orbit coupling effects for fast and energy-efficient spin-based memory, sensor and neuromorphic devices. The stabilization of skyrmions is a consequence of energy competition between several effects, notably the interfacial perpendicular magnetic anisotropy (PMA) and chiral Dzyaloshinskii–Moriya interaction (DMI). A typical structure of the multilayers of interest is composed of a heavy material (e.g. Pt, Ta, W), which serves as a source of spin-orbit coupling, a magnetic material (e.g. Co, Fe) and a lighter element (e.g. Ru, Al, Cu) in which chiral domain walls or skyrmions can be stabilized [1]. Another consequence of spin-orbit coupling is the charge-spin interconversion either via the spin Hall effect in the bulk of heavy metals (Pt, Ta, W) or the Rashba Edelstein effect (REE) at inversion asymmetric interfaces, notably at interfaces with oxydes. However, the role of light element interface on interfacial anisotropy, DMI and charge-to-spin conversion mechanisms has been overlooked so far and needs substantial attention.

In this study, we have investigated how the interfacial anisotropy, spin-orbit torques and DMI evolve with a light element interface in our model system: Pt|Co|Al [2]. So far, these properties have been considered to be influenced by the heavy-metal/ferromagnet interface only. We have experimentally measured the occurrence of an unexpected strong REE in terms of dominating field-like torque in all metallic Pt|Co|Al systems with perpendicular magnetic anisotropy. However and historically, it was considered that optimal oxidation of the Co|Al interface is necessary to obtain PMA [3]. The PMA in Pt|Co|AlOx is considered to be promoted by the hybridization of *d*-orbitals of Co with *p*-orbitals of oxygen at the Co|AlOx interface. Manchon *et al.* found that in the absence of oxygen atoms at Co|AlOx interface, the Co magnetization goes in-plane.

Our objective has been to perform a systematic study of the SOC effects in Ta(5)|Pt(8)|Co(0.9)|Al(t_{Al}) system (thickness indicated in nm) by varying the Al thickness from 0.1 nm to 3 nm without any capping layer. Our x-ray photoelectron spectroscopy (XPS) and x-ray absorption spectroscopy (XAS) results reveal that for $t_{Al} = 0.7$ nm, the Co remains unoxidized, whereas the Al is fully oxidized, establishing perfect conditions to achieve PMA. For this condition, the anisotropy field of Co is found to be 1.2 T, which decreases with Al thickness and the easy axis goes in-plane, as expected. However, the anisotropy of Co strikingly goes from in-plane to out-of-plane as the Al thickness exceeds t_{Al} =1.6 nm (Fig.1a). At such thicknesses, transmission electron microscopy (TEM) and other characterization tools suggest that the Co|Al interface is uniformly unoxidized. The strength of PMA further increases with Al thickness and the effective anisotropy field saturates to 1.8 T, a much higher value than the anisotropy of Pt|Co|AlOx. Additionally, we also have quantified the DMI using Brillouin Light Spectroscopy (BLS). The evolution of effective DMI (D_{eff}) as a function of Al thickness is displayed in (Fig.1b). The DMI follows $1/t_{Al}$ dependence in the measured range before saturating at t_{Al} =2 nm.

As Al is a light element with negligible spin-orbital coupling, its strong impact on interfacial mechanisms suggests the modification in the density of states at the Co|Al interface. We have recorded XAS spectra to probe the electronic states of the Co *d*-band. As shown in Fig. 2, the XAS spectra show clear and strong Al thickness dependence of their intensity. The L_3 absorption peak intensity decreases with Al thickness *i.e.* with increasing metallic Al content. The variation in XAS intensity and shape reflects the change in electron population at the Fermi level or the density of states of Co due to the metallic Al interface for thicker Al. Our results demonstrate the orbital hybridization and electronic charge redistribution at the Co|Al interface and establish a correlation with the DMI. As a consequence, the DMI decreases monotonically with the Al thickness and saturates for 2 nm thick Al. Additionally, the charge-to-spin conversion mechanisms and resultant spin-orbit torques in this system will be discussed in detail.

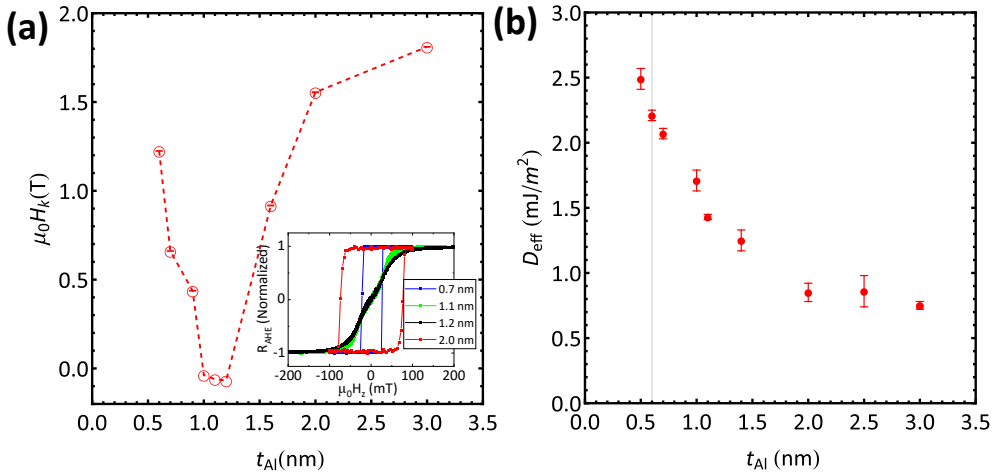

Figure 1: (a) Al layer thickness dependence of out-of-plane magnetic anisotropy in Ta(5)|Pt(8)|Co(0.9)|Al(t_{Al}) series of samples. Inset shows the normalized anomalous Hall effect loops as a function of out-of-plane magnetic field for four different Al thicknesses. (b) The effective DMI constant as a function of Al thickness.

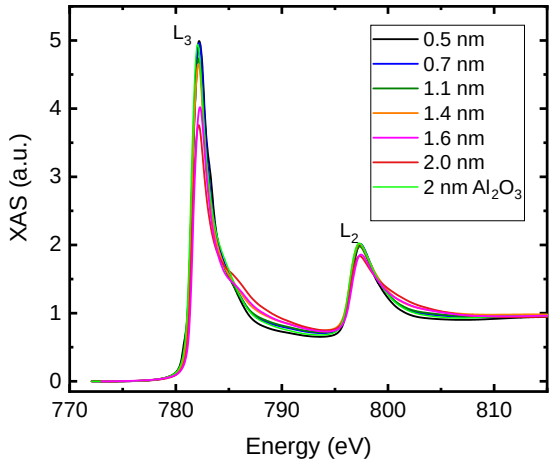

Figure 2: Average XAS spectra in Ta(5)|Pt(8)|Co(0.9)|Al(t_{Al}) series of samples for various Al thicknesses. The change in the XAS intensity indicates the distinct density of states with metallic Al and AlOx interfaces. .

Acknowledgments

This work has been supported by the ANR-20-CE30-0022 “ORION”. N. Sebe benefits from a France 2030 government grant managed by the ANR (ANR-22-PEPR-Electronique-EMCOM).

References

[1] Albert Fert, Nicolas Reyren, and Vincent Cros. Magnetic skyrmions: advances in physics and potential applications. *Nature Reviews Materials* 2, 17031 (2017).

[2] S. Krishnia, Y. Sassi, F. Ajejas, et al. *Large interfacial Rashba interaction and giant spin-orbit torques in atomically thin metallic heterostructures*. 2022. eprint: arXiv:2205.08486.

[3] A. Manchon, C. Ducruet, L. Lombard, et al. Analysis of oxygen induced anisotropy crossover in Pt/Co/MOx trilayers. *Journal of Applied Physics* 104 (2008).

Spin-orbit torque measurements on multilayers stacks

Greis Cipi[1,*], Sujit Panigrahy[1], and Stanislas Rohart[1]

[1]*Laboratoire de Physique des Solides, Université Paris Saclay, CNRS, Orsay, France*
*greis.cipi@universite-paris-saclay.fr

Magnetic skyrmions are topologically protected chiral spin textures evidenced in materials characterized by broken inversion symmetry. Their interests relies on the possibility to develop innovating spintronic devices and applications [1], as they can be moved in nanotracks using electrical currents, which opens perspectives for information processing, and alternatives to traditional CMOS electronics [2]. In the perspective to provide an efficient integration in spintronic applications, it is necessary to investigate their dynamics. A powerful tool we have to manipulate the magnetic textures whenever we are dealing with a system characterized by a large spin-orbit coupling at the interface, is the spin-orbit torque (SOT) [3].

Among the magnetic materials, synthetic antiferromagnets (SAFs) are quite promising for the development of skyrmions. As a matter of fact, thanks to the antiferromagnetic coupling of the two layers, it is possible to stabilize a coupled pair of skyrmions that can be moved when excited by spin-orbit torque [4]. Due to their topological properties, their motion is affected by a gyroptropic force, which deflects the skyrmion away from the current induced applied force. Such gyrotropic deflection vanishes by exploiting the antiferromagnetic coupling in SAFs: the skyrmions in the two layers are characterized by opposite topological numbers, thus the gyrotropic forces point towards opposite directions compensating each other. The coupled skyrmions therefore behave like a solitonic particle, whose motion follows the current direction [4, 5]. In Co-based multilayers, where the antiferromagnetic coupling is guaranteed by a Pt/Ir spacer, it was possible to observe coupled skyrmions following linear trajectories and reaching velocities up to 250 m/s [6]. These results need a quantitative understanding and an analysis of the current induced torque is required. Thus, this study proposes to characterize the torque on each of the two magnetic layer, that compose the SAF of interest, independently by exploiting harmonic Hall voltage measurements [7, 8].

The original SAF of interest is composed of Ta(3)/Pt(5.4)/Co(1)/Ir(0.8)/Pt(0.7)/Co(1)/Ta(4.5), where the thicknesses are given in nm. In such a stack, the Pt/Co interfaces are characterized by a large spin-orbit coupling which provides a large DMI, necessary to stabilize skyrmions. In addition, the thick Pt and Ta layers allow a charge to spin current conversion leading to a polarized spin accumulation at the interface, through the Rashba or spin Hall effects (SHE), which induces a torque on the adjacent magnetic layer. More in detail, this torque can be described as an additional induced effective field $\Delta\vec{H}$, which can be split into two terms, namely the *damping-like* term ΔH_{DL} and the *field-like* one ΔH_{FL}. The former is proportional to the vector product $\hat{m} \times \hat{p}$, where $\hat{m}$ is the magnetization direction of the magnetic layer and $\hat{p}$ is the spin direction of the electron entering the magnetic layer through Rashba or SHE, whereas the latter is simply proportional to $\hat{p}$. The Ir/Pt spacer, instead, guarantees the antiferromagnetic coupling of the two Co layers as its thickness is thin enough enough to allow the RKKY interaction, to be tuned for an antiferromagnetic coupling (0.5 T). To perform the analysis on the SOTs independently on each layer, two sets of samples were growth by MBE, namely the *bottom layer* and *top layer*. The former reproduces the SAF composition without the top Co layer, whereas in the latter, the bottom Co layer is missing. To improve the magnetic properties of the top Co layer that are degraded at the Co/Ta interface, we also test Co/X/Ta interfaces with X=Ir, Cu and Al.

The magnitude of the SOT investigated uses the second harmonic generation, using the anomalous Hall effect. The sample is patterned into Hall crosses where a low frequency ($\omega \approx 10$ Hz) current is applied. The Hall voltage, related to the out-of-plane component, contains several frequencies. The ω component contains information on the static properties (namely anisotropy field), and the 2ω component contains information on the SOT. We observe an efficient SOT torque for both layers, with identical signs, as shown in Fig. 1. Considering that at the bottom (top) layer the Pt (Ta) SOT-source layer is placed below (on top of) the Co, this evidenced that the charge to spin conversion in Pt and Ta have opposite signs. From this analysis it was possible to evaluate the efficiency of the charge to spin current conversion θ_{SH}, which was found to be equal to 0.27 for the two cases discussed (see Fig. 1(c)).

Acknowledgments

This work was supported by the French National Research Agency (ANR) [under contract ANR-17-CE24-0025 (topsky) and a public grant overseen as part of the “Investissements d’Avenir” program (Labex NanoSaclay, reference: ANR-10-LABX-0035), SPICY and through the PEPR Spin (Chirex project).

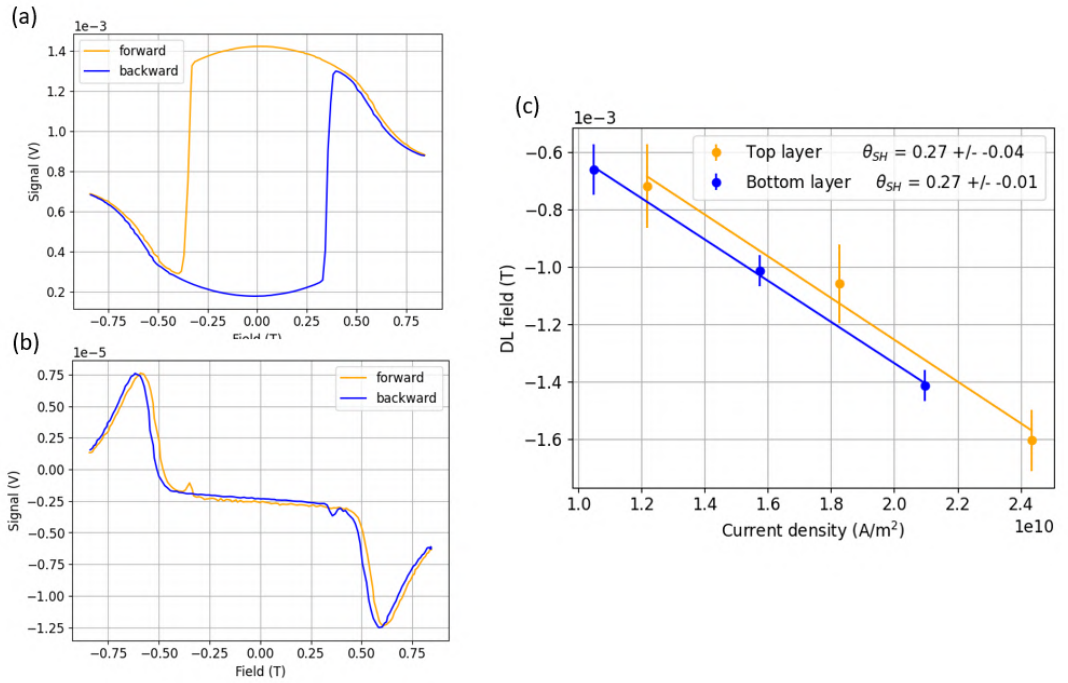

Figure 1: In (a) the hysteresis loop for the *top layer* Co/Ir/Ta acquired from the first harmonic signal of the Hall Voltage measurements: in this case it can be noted a magnetic anisotropy field of 0.66 T. In (b) the second harmonic signal in the damping-like configuration performed again on the Co/Ir/Ta *top layer*. In (c) the behaviour of the damping-like field ΔH_{DL} for the Co/Ir/Ta *top layer*, in orange, and the *bottom layer*, in blue, with respect to the current density: assuming that the current induced field arise from the spin Hall effect, it was possible to evaluate the spin Hall angle θ_{SH}, describing the efficiency of the charge to spin current conversion. In both the cases showed, it was obtained $\theta_{SH} = 0.27$.

References

[1] A. Fert, V. Cros., and J. Sampaio. Skyrmions on the track. *Nature Nanotechology* 8, 152–156 (2013).

[2] Giovanni Finocchio, Felix Büttner, Riccardo Tomasello, Mario Carpentieri, and Mathias Kläui. Magnetic skyrmions: from fundamental to applications. *J. Phys. D: Appl. Phys.* 49, 423001 (2016).

[3] André Thiaville, Stanislas Rohart, Émilie Jué, Vincent Cros, and Albert Fert. Dynamics of Dzyaloshinskii domain walls in ultrathin magnetic films. *EPL (Europhys. Lett.)* 100, 57002 (2012).

[4] Xichao Zhang, Yan Zhou, and Motohiko Ezawa. Magnetic bilayer-skyrmions without skyrmion Hall effect. *Nature Communications* 7, 10293 (2016).

[5] Sujit Panigrahy, Sougata Mallick, João Sampaio, and Stanislas Rohart. Skyrmion inertia in synthetic antiferromagnets. *Phys. Rev. B* 106, 144405 (2022).

[6] Sujit Panigrahy, Sougata Mallick, João Sampaio, André Thiaville, and Stanislas Rohart. Nucleation and motion of synthetic antiferromagnetic skyrmions at zero field. *Colloque Louis Néel 2023* (2023).

[7] Masamitsu Hayashi, Junyeon Kim, Michihiko Yamanouchi, and Hideo Ohno. Quantitative characterization of the spin-orbit torque using harmonic Hall voltage measurements. *Phys. Rev. B* 89, 144425 (14 2014).

[8] Sachin Krishnia, Eloi Haltz, Léo Berges, et al. Spin-Orbit Coupling in Single-Layer Ferrimagnets: Direct Observation of Spin-Orbit Torques and Chiral Spin Textures. *Phys. Rev. Appl.* 16, 024040 (2 2021).

Poster 2.25, November 15th, 10h50–13h00

Spin-orbit torque magnetic tunnel junction characterization at cryogenic temperatures

K. S. Senapati[1,*], A. Fassatoui[1], G. Gaudin[1], S. Couet[2], and K. Garello[1]

[1]*Univ. Grenoble Alpes, CEA, CNRS, Spintec, 38000 Grenoble, France*
[2]*imec, Kapeldreef 75, 3001 Leuven, Belgium*
**kintali.senapati@cea.fr*

The concern of high power consumption for computing is pushing the embedded memory technology to go non-volatile data storage. Hence, magnetoresistive RAM (MRAM) is currently being actively investigated owing to its less static power consumption, unparalleled speed, scalability and endurance compared to conventional volatile memories (SRAM and DRAM). It uses spin degree of freedom along with charge of electrons to read and write a memory device which is primarily based on magnetic tunnel junction (MTJ). Reading mechanism for an MTJ is operated by using the tunnel magnetoresistance (TMR) effect. Spin transfer torque MRAM and toggle MRAM are already under production whereas spin orbit torque (SOT) MRAM is under research stage along with other candidates. SOT-MRAM has an advantage over others with respect to its faster and high endurance writing methods [1]. The SOT writing mechanism is mediated by spin hall effect and Rashba-Edelstein effect creating two torques: dampinglike and fieldlike.

So far most of the research on SOT-MRAM is concentrated at room temperature whereas the low temperature regime is relatively unexplored which could open up its capabilities for cryogenic computing and data storage [2]. We are currently investigating switching of SOT-MTJ, using W as SOT material [1], at cryogenic temperatures. Firstly, we will report on the RH characteristics of SOT-MTJ as a function of temperature, down to 10K, for different critical dimensions (50 to 100nm MTJ diameter). We already observe almost linear dependence of coercivity and TMR variations with lowering of temperature as shown in Fig 1(centre), which is reported by other studies [3] as well.

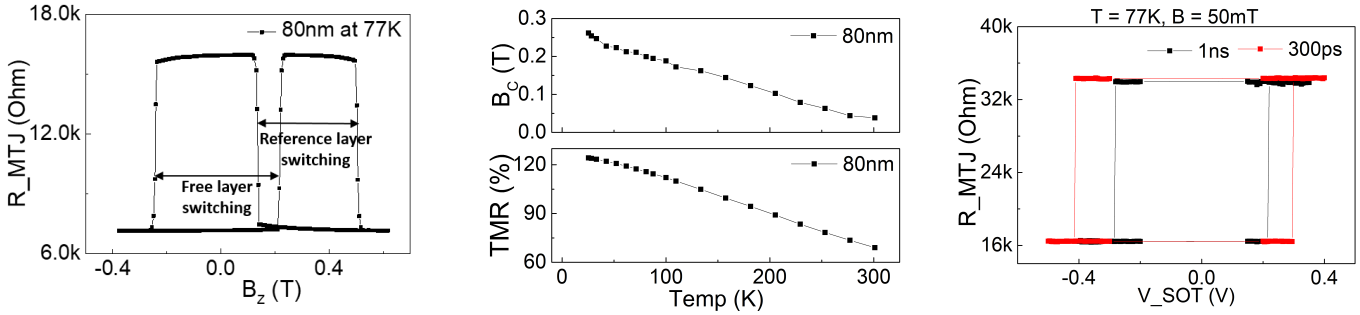

Figure 1: Left: Resistance vs perpendicular field measurement of a 80nm SOT-MTJ device at 77K. Centre: Coercivity and TMR characterisation of a 80nm SOT-MTJ device as a function of low temperature. Right: Electrical switching of a 60nm SOT-MTJ device at 77K using pulses of frequency 1ns and 300ps.

In second part, we will present temperature dependence of switching parameters like critical switching current, write error rate and spin hall angle obtained from SOT-switching probability measurements [4]. We show in Fig. 1(right) preliminary measurements of SOT-induced switching at 77K temperature for a 60nm device at 1ns and 300ps.

This study will allow establishing a benchmark of SOT-MTJ properties and figures of merit against other technologies envisioned for cryogenic devices, and to identify pathway toward using SOT physics and devices for low temperature applications.

Acknowledgments

We thank Laurent Vila and Aurélie Kandazoglou for cryogenic setup access and experimental support.

References

[1] Kévin Garello, Kevin Garello Yasin, Sebastien Couet, et al. SOT-MRAM 300MM Integration for Low Power and Ultrafast Embedded Memories. *2018 IEEE Symposium on VLSI Circuits*, 81–82 (2018).

[2] Minh Hai Nguyen, Guilhem J. Ribeill, Martin V. Gustafsson, et al. Cryogenic Memory Architecture Integrating Spin Hall Effect based Magnetic Memory and Superconductive Cryotron Devices. *Scientific Reports* 10 (2020). arXiv: 1907.00942.

[3] Lili Lang, Yujie Jiang, Fei Lu, et al. A low temperature functioning CoFeB/MgO-based perpendicular magnetic tunnel junction for cryogenic nonvolatile random access memory. *Applied Physics Letters* 116, 022409 (2020).

[4] Viola Krizakova, Manu Perumkunnil, Sébastien Couet, Pietro Gambardella, and Kevin Garello. Spin-orbit torque switching of magnetic tunnel junctions for memory applications. *Journal of Magnetism and Magnetic Materials* 562, 169692 (2022).

Engineering of spin-orbit torque devices for improved writing

M. Biagi[1,*], J. Faure-Vincent[1], A. Fassatoui[1], R. Sousa[1], and K. Garello[1]

[1]*Grenoble INP, SPINTEC, CEA, 38000 Grenoble, France*
marco.biagi@cea.fr

There is considerable interest in electrically controlling nano-magnets (spintronics) in order to develop non-volatile magnetic memories (MRAM) [1]. Indeed, the microelectronics industry is facing major challenges related to the volatility of CMOS cache memory elements (usually SRAM and eDRAM), and MRAMs are among the most credible low power and fast enough candidates to compete with SRAM and replace them at cache level. Most advanced MRAM devices are magnetic tunnel junctions (MTJ) that are operated by spin transfer torque (STT) effect for the write and tunnel magnetoresistance (TMR) effect for the read. Nowadays, commercial products using this technology for micro-controller and eFlash replacement start appearing on market. Meanwhile, Spin-orbit torques (SOT) have emerged as a credible next-generation mechanism for MRAM technology that allows for faster and more efficient magnetization writing [1]. SOT are typically generated in heavy metal non-magnetic materials such as W, Pt or Ta [1]. It relies on spin-orbit coupling effects for converting charge currents into spin currents, which are then transferred to an adjacent ferromagnetic layer, e.g. the free layer (FL) of an MTJ (Fig.1a). The proof of concept of SOT-MRAM was rapidly confirmed [2] and is now in the phase of R&D industrial developments [3].

While some important roadblocks have been overcome, such as the realization of a deterministic switching without magnetic field, and the development materials with giant SOT efficiency [1], other important technology requirements that must be met are poorly addressed so far: the device manufacturing yield must be close to 100%, and the write error rate has to be less than $1x10^6$. Yield is challenging to achieve due to the SOT-MRAM fabrication approach: the typical integration of SOT-MRAM is based on a particular configuration of the MTJ stack configuration called "top-pinned". The storage layer FL is located at the bottom of the MTJ (Fig.1a), in contact with the SOT layer. The etching of the MTJ pillar must therefore precisely stop on the SOT metal, which penalizes the manufacturing yield by nano-shorts due to metal re-deposition on the tunnel barrier sidewalls, as well as the density. On the other hand, write error rate (WER) is poorly reported, but shown to be impacted by SOT field like term [4].

To address these issues, we propose engineering the SOT/FL interface as shown in Fig.1b. The addition of a spacer layer between the FL and the SOT track can provide several advantages in the fabrication process, by improving the fabrication yield, expanding the margin of error during the etching of the pillar, but also enabling a control of Γ_{FL}/Γ_{AD} torque ratio. This would path the way towards the integration of giant SOT efficiency material such as topological insulators (TI), whose implementation in real devices in hindered by the strong intermixing with the FL. In addition, the spacer layer could modulate the field-like component of the SOT, that is responsible for writing errors, optimizing the performances of the devices.

To screen the suitable materials for the spacer layer, we implemented an automated measurement method on prober. It is based on the loop shift method (HLS) [5] that allows to characterize the SOT efficiency components (damping-like ξ_{DL}), and the Dzyaloshinskii-Moriya interaction (DMI) effective field in hall bars (HB) (Fig.1c): Interfacial DMI is known to stabilize homochiral Néel domain wall (DW), and the interaction between the SOT and the DW moments give rise to an effective field along z (axis reference in Fig.1c) that translate into a shift of the hysteresis loop, and is proportional to the injected current and the SOT efficiency $H^z_{eff} \propto \xi J_e$. Measuring the loop shift as a function of the current bias and in-plane field H_x, is possible to extract ξ_{DL} as the saturation value i.e. when H_x overcome H_{DMI} (Fig.2a). We first verified the accuracy of the estimation of H_{DMI} via current-induced DW motion: plotting the DW velocity as function of the in-plane field, when $B_x = H_{DMI}$ the DW is reoriented into Bloch-type, and the DL torque acting on the DW moment will be zero, giving zero velocity (Fig.2b).

In this poster, we will present the implementation of the HLS method on prober, and we will show that it is possible to extend it to the quantification of field-like term ξ_{FL}. These results will be compared to to alternative measurement techniques such as second harmonic method [6] and domain wall motion studies.

These studies will open the possibility to efficiently study promising solutions for high-efficiency SOT-MRAM.

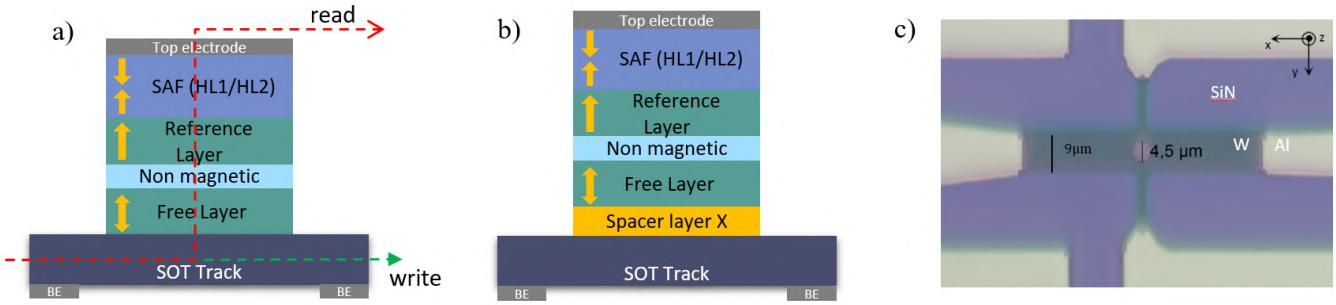

Figure 1: a) Top-pinned SOT-MRAM MTJ, b) proposed layout with addition of spacer layer X, c) optical microscope image of fabricated W/CoFeB/MgO/CoFeB/Ta HB with dot etched at the cross-point. The etching is stopped at the SOT track, and the dot is encapsulated in silicon nitrite to prevent oxidation.

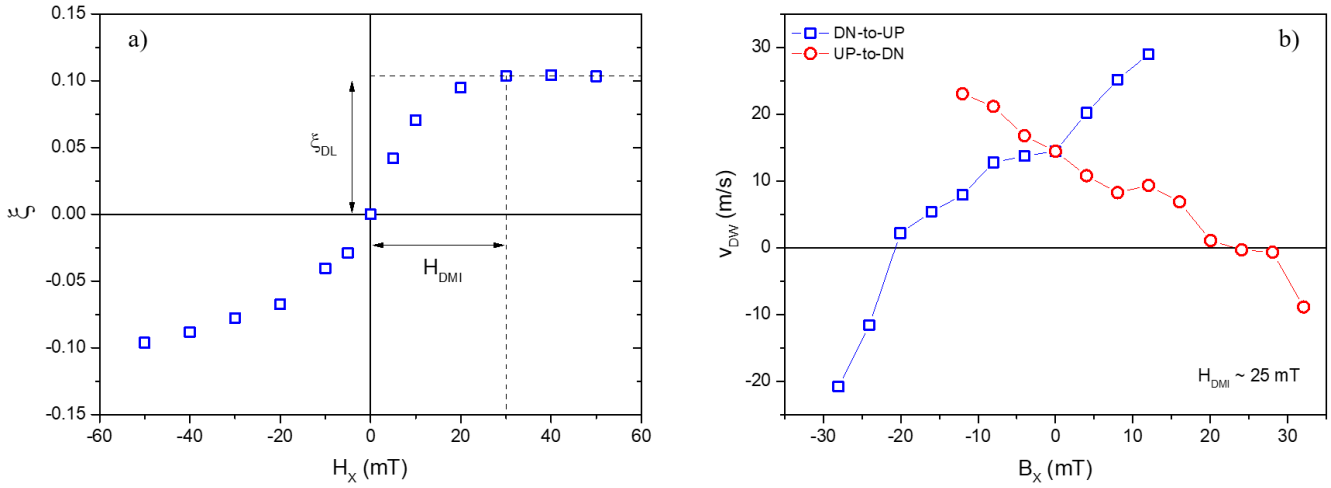

Figure 2: a) Efficiency as a function of the applied in-plane field, for a sample W(2.55)/CoFeB(1)/MgO(1.25)/ /CoFeB(0.5)/Ta(3) patterned into HB with dot of diameter 4.5 μm. b) Domain wall speed for down-to-up and up-to-down transitions as function of the applied in-plane field for a sample W(2.9)/CoFeB(1)/ /MgO(1.25)/CoFeB(0.5)/Ta(3). Layers thickness is expressed in nm between parentheses.

References

[1] Viola Krizakova, Manu Perumkunnil, Sébastien Couet, Pietro Gambardella, and Kevin Garello. Spin-orbit torque switching of magnetic tunnel junctions for memory applications. *Journal of Magnetism and Magnetic Materials* 562, 169692 (2022).

[2] Murat Cubukcu, Olivier Boulle, Marc Drouard, et al. Spin-orbit torque magnetization switching of a three-terminal perpendicular magnetic tunnel junction. *Applied Physics Letters* 104, 042406 (2014).

[3] K. Garello, F. Yasin, S. Couet, et al. "SOT-MRAM 300MM Integration for Low Power and Ultrafast Embedded Memories". *2018 IEEE Symposium on VLSI Circuits*. IEEE, 2018.

[4] Viola Krizakova, Marco Hoffmann, Vaishnavi Kateel, et al. Tailoring the Switching Efficiency of Magnetic Tunnel Junctions by the Fieldlike Spin-Orbit Torque. *Physical Review Applied* 10, 44070 (2022).

[5] Chi-Feng Pai, Maxwell Mann, Aik Jun Tan, and Geoffrey S. D. Beach. Determination of spin torque efficiencies in heterostructures with perpendicular magnetic anisotropy. *Physical Review B* 93 (2016).

[6] Kevin Garello, Ioan Mihai Miron, Can Onur Avci, et al. Symmetry and magnitude of spin–orbit torques in ferromagnetic heterostructures. *Nature Nanotechnology* 8, 587–593 (2013).

Poster 2.27, November 15th, 10h50–13h00

Spintronic encoding of quantum information onto individual atoms within solid-state junctions

Mathieu Lamblin[1,*], Kostantine Katcko[1], Etienne Urbain[1], Franck Ngassam[1], Lalit Kandpal[1], Bhavishya Chowrira[1], Filip Schleicher[1], Ufuk Halisdemir[1], Di Wang[3], Torsten Scherer[3], Damien Mertz[1], Daniel Lacour[2], Sebastien Geiskopf[2], Michel Hehn[2], and Martin Bowen[1,*]

[1]*Institut de Physique et Chimie des Matériaux de Strasbourg, UMR 7504 CNRS, Université de Strasbourg, 23 Rue du Lœss, BP 43, 67034 Strasbourg, France*
[2]*Institut Jean Lamour UMR 7198 CNRS Université de Lorraine BP 70239, Vandœuvre les Nancy 54506, France*
[3]*Institute of Nanotechnology, Karlsruhe Institute of Technology, Hermann-von-Helmholtz Platz 1, 76344 Eggenstein-Leopoldshafen, Germany*
mathieu.lamblin@ipcms.unistra.fr, bowen@unistra.fr

An electrical current that flows across individual atoms or molecules can generate exotic quantum-based behavior, from memristive effects to Coulomb blockade [1] and the promotion of quantum excited states [2]. These fundamental effects typically appear one at a time in model junctions built using atomic tip or lateral techniques. So far, however, a viable industrial pathway for such devices has been lacking.

We first present experiments on vertical magnetic molecular nanojunctions [3]. The electrically excited quantum state of the spin chain formed by Co phthalocyanine molecules coupled to a ferromagnetic electrode constitutes a distinct magnetic unit endowed with a coercive field. This generates a specific steady-state magnetoresistance trace that is tied to the spin-flip conductance channel, and is opposite in sign to the ground state magnetoresistance term, as expected from spin excitation transition rules. The experimental 5.9 meV thermal energy barrier between the ground and excited spin states is confirmed by density functional theory, in line with macrospin phenomenological modeling of magnetotransport results.

We have also studied 'industrializable' magnetic tunnel junctions with a MgO barrier containing C atoms [4]. We demonstrate that the effective nanotransport path [5] due to the resulting localized paramagnetic [6] states involves individual C atoms. Their discrete energy levels promote Coulomb blockade effects that can be reproducibly shifted in energy by charging events on neighboring C atoms. The tunnel coupling between these transport and environmental carbon atoms promotes quantum interference effects. Spin-polarized transport induces spin accumulation that lifts the spin degeneracy of the unpaired C electron in MgO. This leads to a voltage shift in Coulomb peaks and quantum interference effects between the datasets in the MTJ's P and AP magnetic states. Spin accumulation also accounts for the huge enhancement of the spintronic performance when a Coulomb peak is memristively controlled.

References

[1] Pascal Gehring, Jos M. Thijssen, and Herre S. J. van der Zant. Single-molecule quantum-transport phenomena in break junctions. *Nature Reviews Physics* 1, 381–396 (2019).

[2] Andreas J. Heinrich, William D. Oliver, Lieven M. K. Vandersypen, et al. Quantum-coherent nanoscience. *Nature Nanotechnology* 16, 1318–1329 (2021).

[3] Kostantine Katcko, Etienne Urbain, Franck Ngassam, et al. Encoding Information on the Excited State of a Molecular Spin Chain. *Advanced Functional Materials* 31, 2009467 (2021).

[4] Mathieu Lamblin et al. Encoding Information onto the Charge and Spin State of a Paramagnetic Atom Using MgO Tunnelling Spintronics. *In Preparation* (2023).

[5] Michał Studniarek, Ufuk Halisdemir, Filip Schleicher, et al. Probing a Device's Active Atoms. *Advanced Materials* 29, 1606578 (2017).

[6] K. Katcko, E. Urbain, B. Taudul, et al. Spin-driven electrical power generation at room temperature. *Communications Physics* 2 (2019).

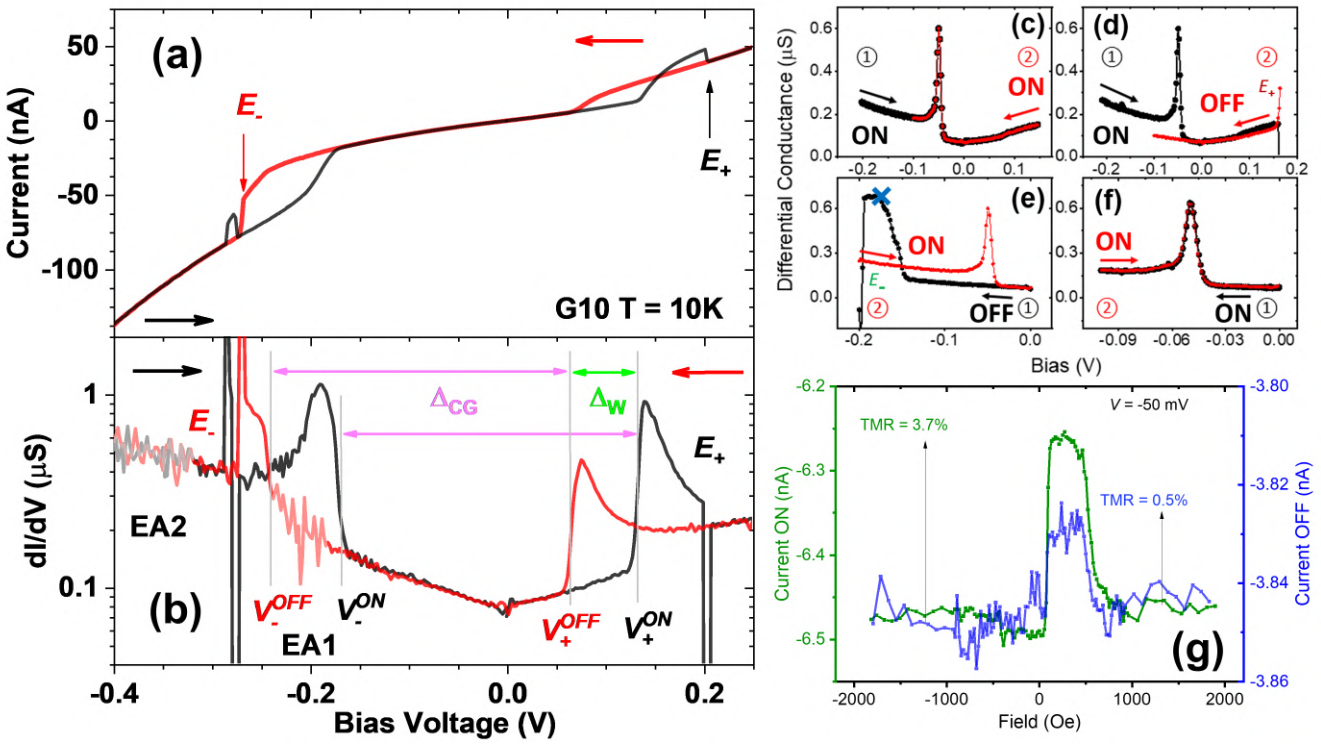

Figure 1: **Memristive Coulomb blockade at the atomic level.** (a) IV and (b) differential conductance $\mathrm{d}I/\mathrm{d}V$ data at $T = 10$ K on junction G10. The E_+ and E_- writing events cause a shift $\Delta_W = 73$ mV in the otherwise constant energy gap $\Delta_{CG} = 310$ mV between conductance peaks. Transport noise due to interference with an environmental atom are shown using semi-transparent datapoints (c-f) $\mathrm{d}I/\mathrm{d}V$ data upon sweeping bias to test the interplay between the presence of the Coulomb blockade peak and the writing events E_- and E_+. The black data labeled 1 code for the initial branch state of the junction, then the sweep direction is inverted and the return branch is represented in red and labeled 2. [4]

Ultrafast counterintuitive magnetization reversal in ferromagnetic spin valves

Junta Igarashi[1,*], Wei Zhang[1,2,3], Quentin Remy[1,4], Eva Díaz[1], Jun Xiao Lin[1], Julius Hohlfeld[1], Michel Hehn[1,5], Stéphane Mangin[1,4,5], Jon Gorchon[1], and Grégory Malinowski[1]

[1]*Université de Lorraine, CNRS, IJL, F-54000 Nancy, France*
[2]*2Anhui High Reliability Chips Engineering Laboratory, Hefei Innovation Research Institute, Beihang University, Hefei 230013,China*
[3]*MIIT Key Laboratory of Spintronics, School of Integrated Circuit Science and Engineering, Beihang University, Beijing 100191, China*
[4]*Cavendish Laboratory, University of Cambridge, Cambridge, UK*
[5]*Center for Science and Innovation in Spintronics, Tohoku University, 2-1-1 Katahira, Aoba-ku, Sendai 980-8577 Japan*
*junta.igarashi@univ-lorraine.fr

The manipulation of magnetic materials without the use of magnetic fields is of great fundamental and technical interest. The discovery of spin-transfer torque (STT) [1, 2] allowed us to control the magnetization direction electrically in magnetic devices within nanoseconds, which paved the way for non-volatile applications such as spin-transfer-torque magnetoresistive random access memory. However, the threshold current (or energy consumption) for magnetization reversal rapidly increases below ten picoseconds [3]. This is because spin-angular-momentum-transfer has to overcome the energy barrier for magnetization reversal while the pulse current is applied. Current-induced STT switching below a few hundred picoseconds while maintaining enough retention property is still challenging as long as the magnitude of magnetization remains the same. Ultra-short optical pulses can directly manipulate the magnitude of magnetization at sub-picoseconds time scales [4]. When ultrafast demagnetization occurs, angular momentum conservation implies that the angular momentum will either dissipate locally into the lattice [5–7] or will be transferred in the form of a spin current to another part of the sample [8–11]. In a multilayered structure such as spin valves, spin currents generated by laser excitation result in different demagnetization times within less than a picosecond depending on its magnetic configuration: demagnetization is faster for an initially antiparallel (AP) configuration [8]. However, magnetization reversal in ferromagnetic spin valves by a single femtosecond laser pulse has not been achieved. Magnetization reversal starting from the AP state can still be expected as an extension of the previous study [8]. In contrast, it has yet to be discovered if it is theoretically feasible for ultrafast magnetization reversal starting from parallel (P) configuration.

Here we demonstrate an optically induced sub-picosecond magnetization reversal in archetypical rare-earth-free spin valves of [Pt/Co]/Cu/[Co/Pt] that are used for current-induced STT switching [12, 13]. Surprisingly, we observe magnetization reversal starting from the P state, which is unprecedented and counterintuitive in ultrafast magnetism [13]. We also reveal that the mechanism behind this phenomenon could be understood in the analogy of current-induced STT switching [13, 14].

Acknowledgments

The authors thank E. E. Fullerton, B. Koopmans, S. Petit-Watelot, N. Bergeard, S. Iihama, and H. Arisawa for fruitful discussion and S. Suire for upgrades to the setup used in part of the studies. This work is supported by the ANR-20-CE09-0013 UFO, the Institute Carnot ICEEL for the project “CAPMAT” and FASTNESS, the Région Grand Est, the Metropole Grand Nancy, for the Chaire PLUS by the impact project LUE-N4S, part of the French PIA project “Lorraine Université d’Excellence” reference ANR-15-IDEX-04-LUE, the “FEDERFSE Lorraine et Massif Vosges 2014-2020”, a European Union Program, the European Union’s Horizon 2020 research and innovation program COMRAD under the Marie Skłodowska-Curie grant agreement No 861300, the Academy of Finland (Grant No. 316857), the ANR project ANR-20-CE24-0003 SPOTZ, the Sakura Program, the JSPS Bilateral Program, the Tohoku University-Université de Lorraine Matching Funds, and CSIS cooperative research project in Tohoku University. This article is based upon work from COST Action CA17123 MAGNETOFON, supported by COST (European Cooperation in Science and Technology). J.I. acknowledges support from JSPS Overseas Research Fellowships. W.Z. gratefully acknowledges the National Natural Science Foundation of China (Grants No. 12104030), China Postdoctoral Science Foundation (Grants No.2022M710320) and China Scholarship Council. All fundings were shared equally among all authors.

References

[1] J.C. Slonczewski. Current-driven excitation of magnetic multilayers. *Journal of Magnetism and Magnetic Materials* 159, L1–L7 (1996).

[2] L. Berger. Emission of spin waves by a magnetic multilayer traversed by a current. *Physical Review B* 54, 9353–9358 (1996).

[3] D. Bedau, H. Liu, J.-J. Bouzaglou, et al. Ultrafast spin-transfer switching in spin valve nanopillars with perpendicular anisotropy. *Applied Physics Letters* 96, 022514 (2010).

[4] E. Beaurepaire, J.-C. Merle, A. Daunois, and J.-Y. Bigot. Ultrafast Spin Dynamics in Ferromagnetic Nickel. *Physical Review Letters* 76, 4250–4253 (1996).

[5] B. Koopmans, G. Malinowski, F. Dalla Longa, et al. Explaining the paradoxical diversity of ultrafast laser-induced demagnetization. *Nature Materials* 9, 259–265 (2009).

[6] C. Dornes, Y. Acremann, M. Savoini, et al. The ultrafast Einstein–de Haas effect. *Nature* 565, 209–212 (2019).

[7] S. R. Tauchert, M. Volkov, D. Ehberger, et al. Polarized phonons carry angular momentum in ultrafast demagnetization. *Nature* 602, 73–77 (2022).

[8] G. Malinowski, F. Dalla Longa, J. H. H. Rietjens, et al. Control of speed and efficiency of ultrafast demagnetization by direct transfer of spin angular momentum. *Nature Physics* 4, 855–858 (2008).

[9] Dennis Rudolf, Chan La-O-Vorakiat, Marco Battiato, et al. Ultrafast magnetization enhancement in metallic multilayers driven by superdiffusive spin current. *Nature Communications* 3 (2012).

[10] Gyung-Min Choi, Byoung-Chul Min, Kyung-Jin Lee, and David G. Cahill. Spin current generated by thermally driven ultrafast demagnetization. *Nature Communications* 5 (2014).

[11] A. J. Schellekens, K. C. Kuiper, R.R.J.C. de Wit, and B Koopmans. Ultrafast spin-transfer torque driven by femtosecond pulsed-laser excitation. *Nature Communications* 5 (2014).

[12] S. Mangin, D. Ravelosona, J. A. Katine, et al. Current-induced magnetization reversal in nanopillars with perpendicular anisotropy. *Nature Materials* 5, 210–215 (2006).

[13] Junta Igarashi, Wei Zhang, Quentin Remy, et al. Optically induced ultrafast magnetization switching in ferromagnetic spin valves. *Nature Materials* 22, 725–730 (2023).

[14] Quentin Remy. Ultrafast magnetization reversal in ferromagnetic spin valves: An s—d model perspective. *Phys. Rev. B* 107, 174431 (2023).

Poster 2.29, November 15th, 10h50–13h00

Caractérisation électrique de barrières tunnel de MgO dopées carbone

S. Geiskopf [1,*], D. Lacour[1], M. Bowen[2], and M. Hehn[1]

[1]*Institut Jean Lamour UMR7198, Nancy, France*
[2]*Institut de physique et de chimie des matériaux de Strasbourg UMR 7504, Strasbourg, France*
sebastien.geiskopf@univ-lorraine.fr

Dans sa plus simple expression une jonction tunnel magnétique est composée de deux couches ferromagnétiques (les électrodes) séparées par une fine couche isolante : la barrière tunnel. Le courant tunnel circulant perpendiculairement au plan des couches mesuré après application d'une différence de potentiel entre les deux électrodes ferromagnétiques est fortement dépend de l'orientation relative des aimantations des électrodes : c'est l'effet tunnel polarisé en spin.

Depuis plusieurs années nous nous intéressons à l'impact de la présence d'états électroniques localisés dans la bande interdite de l'isolant constituant la barrière. Nous avons pu montrer par exemple l'impact qu'ont les lacunes d'oxygène sur le transport tunnel polarisé en spin [1].

Dans ce poster nous présenterons nos plus récent résultats concernant le transport tunnel polarisé en spin au sein de jonctions tunnel dont la barrière est constituée une couche de 2.5nm de MgO dopée en carbone. En plus des caractéristiques usuellement utilisées pour qualifier les jonctions tunnels magnétiques des mesures d'IETS pour inelastic tunneling spectroscopy, (voir dérivées secondes sur la figure) seront utilisées pour compléter notre analyse.

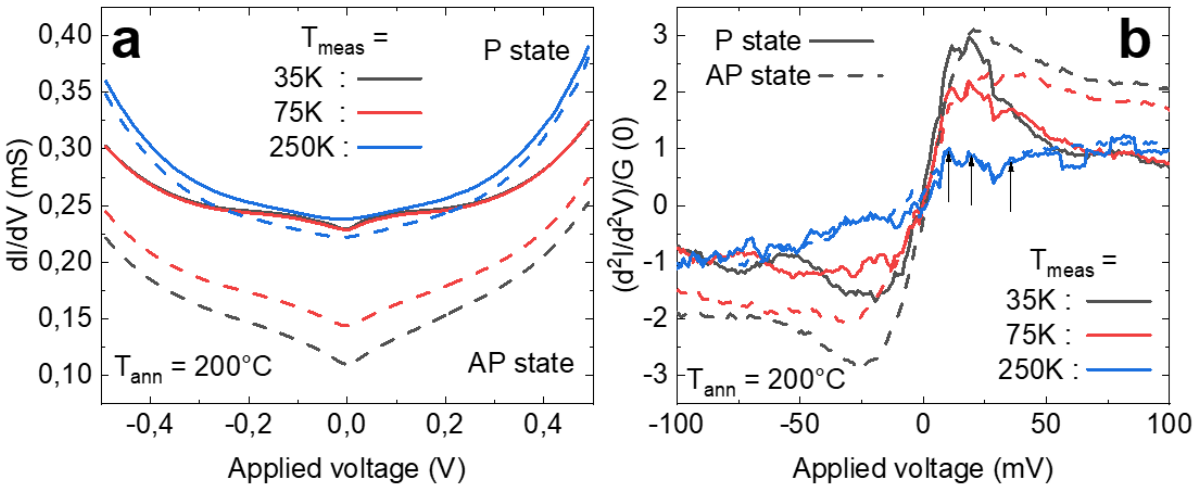

Figure 1: a. Conductances et b. IETSs mesurées d'une JTM dont la barrière est dopée carbone dans les configugrations parallèle (P) et antiprallèle (AP) des aimantations à différentes températures.

[1] F. Schleicher et al., Nat. Com. 5, 4547 (2014)

Acknowledgments

Nous remercions l'ANR SpinElec pour avoir contribuée en partie à cette étude.

Effects of self-torque in rare earth-transition metal alloy on the magnetization switching by spin-orbit torque

Po-Wei Lee[1,*], Chang-Chang Huang[1], Chih-Huang Lai[1], and Stéphane Mangin[2]

[1]*Dept. Materials Science & Engineering, National Tsing Hua University, Hsinchu, Taiwan*
[2]*Institut Jean Lamour, CNRS UMR 7198, Université de Lorraine, F-54011 Nancy, France*
powei.lee@univ-lorraine.fr

We investigated the spin-orbit torque (SOT) switching of the single CoTb layer with or without the heavy metals (Pt and W) in different thickness to identify the self-torque effects generated in the CoTb layer. The generation of self-torque heavily depends on the thickness of CoTb. The SOT switching was not observed for a single CoTb layer with 3 nm in thickness, suggesting self-torque may be quite weak in a very thin film. A deterministic SOT switching can be obtained for a single 9 nm CoTb layer. The amplitude of the self-torque generated in CoTb is comparable to the Pt/Co case with the same switching polarity as the Pt/Co one. When 3 nm CoTb was deposited on Pt or W underlayer, the J_c is smaller in W/CoTb than that of Pt/CoTb, which can be attributable to a high spin Hall angle of W and negligible self-torque of CoTb. On the other hand, when the CoTb is increased to 9 nm, the J_c of W/CoTb is significantly increased and becomes higher than that of Pt/CoTb. The enhanced J_c of W/CoTb may result from the opposite sign of spin orbit torque generated in W and CoTb. Since the self-torque generated in 9 nm CoTb becomes substantial, the competition of spin orbit torque between W and CoTb occurs, leading to a high J_c. We define the switching efficiency

$$\eta = \frac{\sqrt{2H_k^2 - H_x^2}}{J_c} \times M_s t \tag{1}$$

based on the macrospin model [1], in which H_k and H_x are anisotropy field and applied magnetic field along the x direction. The variations of η with the layer structure is shown in Table 2. The addition of SOT from Pt and self-torque from CoTb leads to enhanced switching efficiency when the thickness of CoTb is increased. On the other hand, the competition of SOT from W and self-torque in TbCo of W/CoTb devices was revealed by increasing the thickness of CoTb. We further confirm this interplay by reversing the stack order, that is, CoTb/W, in which the efficiency is substantially enhanced.

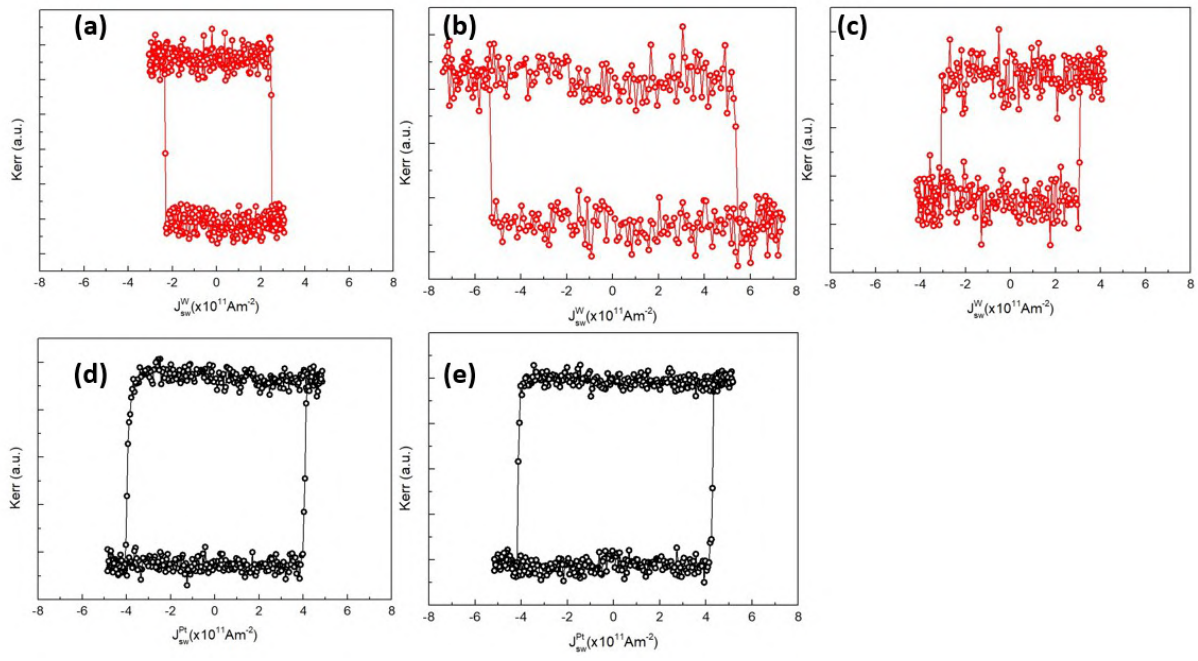

Figure 1: SOT switching curves for (a) W/CoTb 3 nm (b) W/CoTb 9 nm, (c) CoTb 9 nm/W, (d) Pt/CoTb 3 nm, and (e) Pt/CoTb 9 nm.

Layer Structure	Pt/Co/AlOx	Pt/CoTb 3nm	Pt/CoTb 9nm	W/CoTb 3nm	W/CoTb 9nm	CoTb 9nm/W
SOT switching efficiency ($x10^{-14}$emuOe/Acm^2)	1.54	2.55	5.67	4.44	3.96	6.82

Figure 2: SOT switching efficiency for various layer structures.

References

[1] Tomohiro Taniguchi, Seiji Mitani, and Masamitsu Hayashi. Critical current destabilizing perpendicular magnetization by the spin Hall effect. *Physical Review B* 92, 024428 (2015).

Poster 2.31, November 15th, 10h50–13h00

Dynamic properties of large ferromagnetic granular systems

J. Mordret[1,*], G. Delhaye[1], B. Lépine[1], Y. Patat[1], J-C. Le Breton[1], S. Tricot[1], and P. Schieffer[1]

[1]*Univ Rennes, CNRS, IPR (Institut de Physique de Rennes) - UMR 6251, F-35000, Rennes, France*
**julien.mordret@univ-rennes.fr*

Nanometer-sized constrictions in ferromagnetic nanostructures are of great interest due to their unique properties and potential applications in nanomagnetism and spintronics [1]. By confining magnetic domains to very small regions, these structures allow to explore the fundamental properties of magnetism and even to control magnetic configurations at the atomic scale which can be used for developing new technologies.

Our study focuses on the magnetization reversal within an atomic constriction that separates magnetic nanostructures of the same material in the shape of mounds, discs and Wulff polyhedrons at the nanoscale (see Fig. 1). We used atomistic magnetic simulations for modeling our systems. Our calculations show that the domain wall is almost entirely confined within the atomic-sized constriction in agreement with conclusions drawn from an analytical model [2].

We also found that the domain wall extension is primarily determined by the geometric properties of the islands-constriction system rather than intrinsic material properties like magnetocrystalline anisotropy, exchange coupling, or material saturation magnetization.

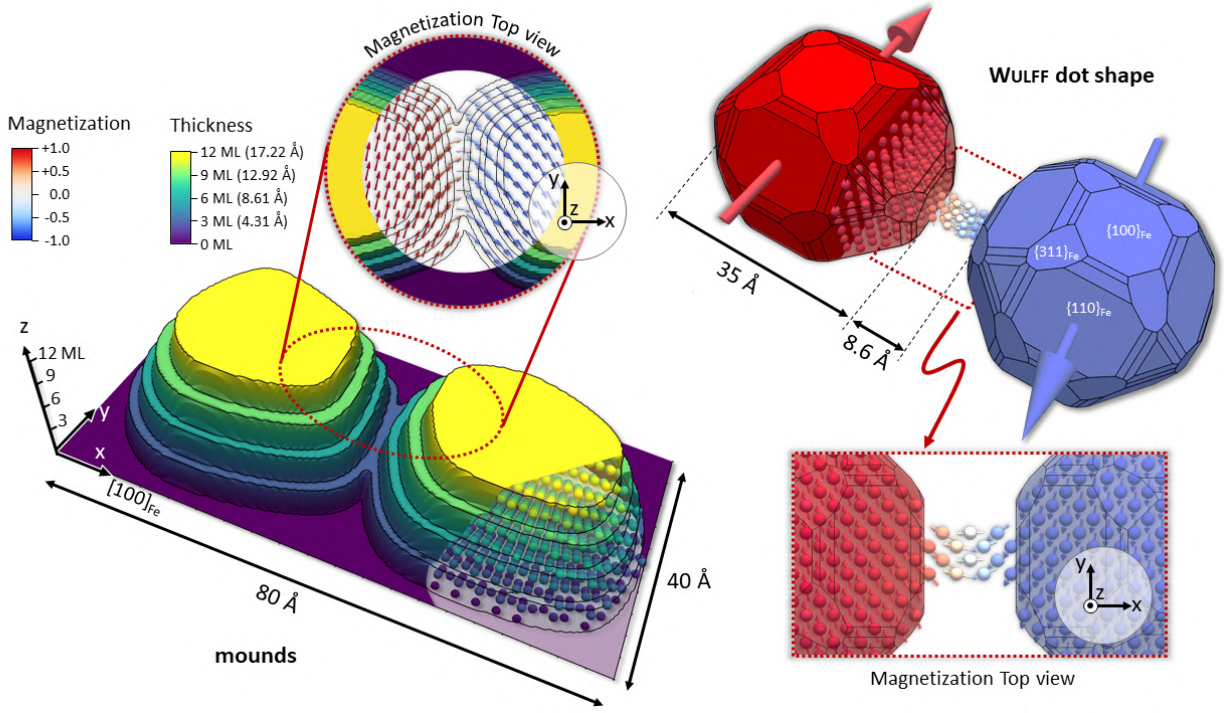

Figure 1: Atomic magnetic moment orientations for two nanoscale dots connected by an atomic constriction. On the left-hand side, dots are shaped like mounds as could be the result of the Ehrlich-Schwoebel effect on the growth [3], whereas on right-hand side, dot shape is the result of a simple Wulff construction. Both illustrations corresponds to granular ultrathin films with a low scale roughness as observed for many metal/oxide or metal/semiconductor surfaces. Dots magnetization is constrained 180° apart by pining the moments of few atoms on the outer edges but almost all the magnetization rotation take place inside the constriction.

We demonstrate that magnetic interactions between nanometric islands connected by an atomic bridge can be approximated by two macrospins coupled by an effective Heisenberg exchange interaction for which we assessed the strength as a function of the geometric parameters of the atomic constriction.

This result allowed us to successfully model the magnetic properties of large ferromagnetic island assemblies whose individual magnetic properties such as magnetization and shape anisotropy can be specified.

A key aspect to the correct treatment of such systems is the ability to accurately take into account the effect of the demagnetizing field on these heterogeneous layers. We specifically designed a code to efficiently calculate dynamical properties of these systems. Our study revealed that the low-scale roughness of ultra-thin epitaxial films strongly modify the magnetization dynamic in a sub-micrometer systems. These findings are of significant importance for the future design and development of high-performance devices based on magnetic systems at the nanoscale.

References

[1] C. Reichhardt, C. J. O. Reichhardt, and M. V. Milo ševi ć. Statics and dynamics of skyrmions interacting with disorder and nanostructures. *Rev. Mod. Phys.* 94, 035005 (3 2022).

[2] P. Bruno. Geometrically Constrained Magnetic Wall. *Phys. Rev. Lett.* 83, 2425–2428 (12 1999).

[3] Joseph A. Stroscio, D. T. Pierce, M. D. Stiles, A. Zangwill, and L. M. Sander. Coarsening of Unstable Surface Features during Fe(001) Homoepitaxy. *Phys. Rev. Lett.* 75, 4246–4249 (23 1995).

Magnetoresistance for current limiting devices

Jérémy Létang[1,*], Luiz Enger[1], Stefan Dan Costea[2], Stefano Lumetti[1], Perla Malagò[1], Jürgen Kosel[1], and Michael Ortner[1]

[1]*Silicon Austria Labs GmbH, Europastraße 12, 9524 Villach, Austria*
[2]*Eaton European Innovation Center, Bořivojova 2380, 252 63, Roztoky u Prahy, Czech Republic*
**jeremy.letang@silicon-austria.com*

State-of-the-art fault current limiters are based on active components or inductors, and are large and expensive devices. Here, we propose a new passive and miniaturized magnetoresistance-based system [1] strongly reducing device size and cost. The extraordinary magnetoresistance (EMR) effect was chosen as it exhibits the largest resistance ratio among the known magnetoresistive (MR) phenomena, reaching values up to 10^7 % [2].

Many works have studied EMR in high-mobility materials (like semiconductors [3], graphene [4] and heterostructures [5]) mainly for magnetic field sensing [2, 5]. For current limiter applications, only 2-terminal geometries are applicable. Through 2D finite element simulations (COMSOL), we have studied several geometry and material parameter combinations to understand if and how EMR-based current limiters can be realized. For instance, we have designed different planar shapes and sizes for the electrodes (such as van der Pauw disk [3], multibranch geometry [2], bar type geometry [5] or stripes). For 2-terminal systems, our simulations show that the EMR ratio reaches its largest value in simple sandwich designs, that maximize the resistance variation between current paths where the electrons cross the metal-semiconductor interface tangentially and normally, respectively. Comparing the EMR ratio values reported in the literature [2, 3, 5] with those resulting from our simulations, we suppose that the higher EMR values displayed by 4-terminal systems arise from a combination of Hall and EMR effects. 2-terminal systems, where the Hall effect is absent, exhibit instead lower EMR ratios.

Simulations show that EMR saturates with lateral extension of such 2-terminal systems. This EMR saturation varies as a function of electron mobility and out-of-plane magnetic field according to the following empirical relation: EMR = $19.1(\mu B)^2$. This is in agreement with previous works [3]. It shows that it is possible to reach high EMR values of about 2000 % at a magnetic field of 1 T when the semiconductor materials mobility is around 10^5 cm2/(Vs). Such values are very promising for current limiter components. This behavior can also be found with a simple 2-channel model which describes 2-terminal systems, where electrons follow the least resistive path. It fits to the simulation data and gives EMR = 8480l/(0.29+l), with l being the lateral extension of our system.

In summary, this work investigates a new passive and compact current limiter device concept based on the EMR effect. With proper mobility and good interfaces, an EMR ratio as high as 2000% can be achieved in a 2-terminal system, which could make this technology suitable to replace state-of-the-art fault current limiter components

References

[1] Petr KOPEJTKO. “Current controlling element based on saturation of a magnetic circuit”. 2022.

[2] T. H. Hewett and F. V. Kusmartsev. Geometrically enhanced extraordinary magnetoresistance in semiconductor-metal hybrids. *Physical Review B* 82, 212404 (2010).

[3] S. A. Solin, Tineke Thio, D. R. Hines, and J. J. Heremans. Enhanced Room-Temperature Geometric Magnetoresistance in Inhomogeneous Narrow-Gap Semiconductors. *Science* (2000).

[4] Simone Pisana, Patrick M. Braganca, Ernesto E. Marinero, and Bruce A. Gurney. Tunable Nanoscale Graphene Magnetometers. *Nano Letters* 10, 341–346 (2010).

[5] Jian Sun and Jürgen Kosel. Extraordinary Magnetoresistance in Semiconductor/Metal Hybrids: A Review. *Materials* 6, 500–516 (2013).

Power efficiency of anomalous-Hall transducer: the case of GdCo

Daniel Lacour[1], Michel Hehn[1], Min Xu[1], and Jean-Eric Wegrowe[2,*]

[1]*Institut Jean Lamour UMR 7198 CNRS, Université de Lorraine, Vandoeuvre les Nancy France*
[2]*Laboratoire des Solides Irradiés, Ecole polytechnique, CNRS, CEA, Université Paris-Saclay, F 91128 PALAISEAU, France*
*jean-eric.wegrowe@polytechnique.edu

The search for low power consumption electronic devices is one of the main motivation for spintronics. Indeed, the spins attached to the charge carriers allow a direct manipulation of the magnetization states. Accordingly, the power used is that of the spin degrees-of-freedom, and not directly the Joule power. Yet the transport of the spin attached to the charge carriers follows the thermodynamic rules that determines Joule dissipation. In the case of Hall effect (HE), anomalous Hall effect (AHE), or spin-Hall effect (SHE), the Joule dissipation is minimized due to the presence of an effective magnetic field that breaks the time-invariance symmetry at the microscopic scale[1] . The transport of electric carriers is then described by a typical “Hall-like" term that appears in the Ohm’s law[2,3,4,5].

It is well-known that the force associated with a magnetic field - typically the Lorentz force for the HE - cannot produce mechanical work in vacuum. More generally, due to the Onsager reciprocity relations, it is often assumed that the Hall-current produced by Hall-like effects is *dissipationless* [6,7,8]. But it is not necessarily the case: typically, the power associated with the Hall voltage in a perfect Hall bar is indeed null, but the power associated with a perfect Corbino disk dissipates [4,5]. The dissipation of the anomalous Hall current is the object of the present study.

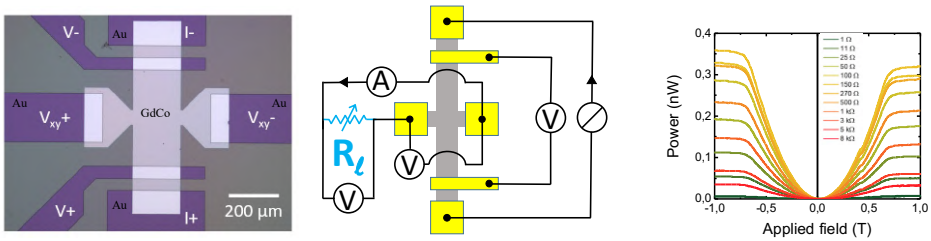

Figure 1: Left: Photo of the device. Center: Sketch of the Hall bar with the load circuit. Right: Power $P = V_{xy}I_{xy}$ measured as a function of the perpendicular magnetic field for different values of the load resistance.

We have measured the dissipation of the anomalous-Hall current injected into a lateral load circuit. The anomalous-Hall current is generated by a $Co_{75}Gd_{25}$ ferrimagnetic Hall bar and injected into lateral contacts lithographied at the two edges (see Figure 1). The current, the voltage and the power injected in the lateral circuit are studied as a function of the magnetization states, the load resistance, and the temperature. The maximum power consumption is of the order of the square of anomalous-Hall angle. A sharp maximum is observed, which corresponds to the condition of resistance matching. The observations are in agreement with recent predictions based on a non-equilibrium variational approach [2].

Indeed, the predicted expression of the Power efficiency is given by the expression [2] :

$$\frac{P(R_l)}{P_0} = \theta_{AH}^2 \frac{\frac{\rho_{AH}}{\alpha R_l}}{\left(1+\frac{\rho_{AH}}{\alpha R_l}\right)^2} \tag{1}$$

where $P_0 = V_{xx}I_{xx} = 80\,\mu W$ is the constant input power injected into the GdCo layer and $\rho_{AH} = 1.3\,10^{-2}\ \mu\Omega.m.T^{-1}$ is the anomalous Hall conductivity per Tesla deduced from the anomalous Hall voltage V_{xy}^0, the longitudinal current I_{xx} and the geometrical parameters of the Hall bar defined in Fig.1(left). The anomalous Hall angle per Tesla of the $Co_{75}Gd_{25}$ layer is $\theta_{AH} = 6\ 10^{-3}\ T^{-1}$. The parameter α is an unknown geometrical parameter that allows the known load resistance R_l to be converted into the load conductivity. The parameter α is deduced from an independent fit.

The result of the study can be summarized in the figure below that represents the power efficiency injected in the load circuit as a function of the load resistance R_l:

Note the sharp maximum for $\alpha = 1$: this is the expression of the “maximum power transfer theorem” (resistance matching). The maximum transfer is very small: of the order of $\theta_{AH}^2 \sim 10^{-5}$. The excellent correspondance between the theoretical predictions and the experimental verification is a strong indication of the validity of the variational method developed in reference [2]. Beyond, these results suggest the validity of the description of the spin-Hall effect proposed in reference [3], for which - in contrast to the present study - the power dissipation due to the spin degrees-of-freedom plays a major role. The application to Spin-Orbit Torque (or charge-to-spin current conversion devices) will be discussed.

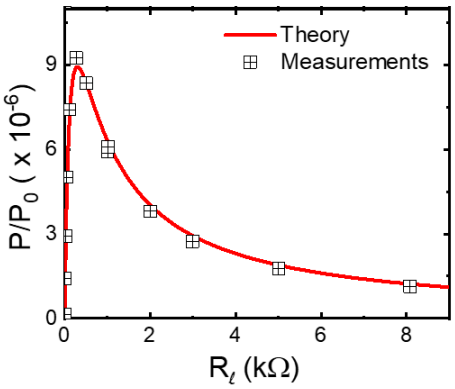

Figure 2: Power-efficiency of the transducer as a function of the load resistance. The squares are measured points and the line is calculated form Eq.(1) (reference [2])

Acknowledgments

The authors would like to thank the *Orion program* (Investissement d'Avenir France 2030).

Poster 2.34, November 15th, 10h50–13h00

Modelling of spin-orbitronics effects at interfaces

Poonam Kumari[1,*], Alexander Smogunov[1], and Cyrille Barreteau[1]

[1]*SPEC, CEA Saclay, Gif-sur-Yvette Cedex, 91191 France*
poonam.kumari@cea.fr

Spin-orbitronics, which is based on the use of orbital angular momentum as an information carrier, has gained significant attention in the recent past. In the structures which lack inversion symmetry, a formation of orbital angular momentum (OAM) in the bloch wave functions which is independent of spin orbit coupling (SOC) has been predicted and is considered to be a more generic effect implying that the orbital moment of the electron is the main driving force behind the Rashba effect rather than its spin [1]. This OAM mediated Rashba effect is called Orbital Rashba effect (ORE), and has been studied in different systems like metal surface [2], oxide surfaces [3], two dimensional (2D) materials[4].

In this work, we aim at exploring and predicting, this phenomena at various interfaces, via modelling tools which includes Density Functional Theory (DFT), Wannier functions, tight-binding based electronic structure calculations as well as transport within the Non-equilibrium Green functions (NEGF) formalism, using different codes (Quantum ESPRESSO [5], WANNIER90[6], Quantum ATK [7]). We have modelled a number of surfaces like oxidized Cu films, GaAs-Fe surface, 2D materials such as MoS_2 Nanoribbons and Lateral heterostructures (LH) composed of NbS_2 and WSe_2 shown in Figure 1. In these materials due to significant hybridization at the surface/interface there is an emergence of prominent ORE. We have calculated the chiral orbital texture in the momentum space in these materials. Our results will encourage further experimental investigations.

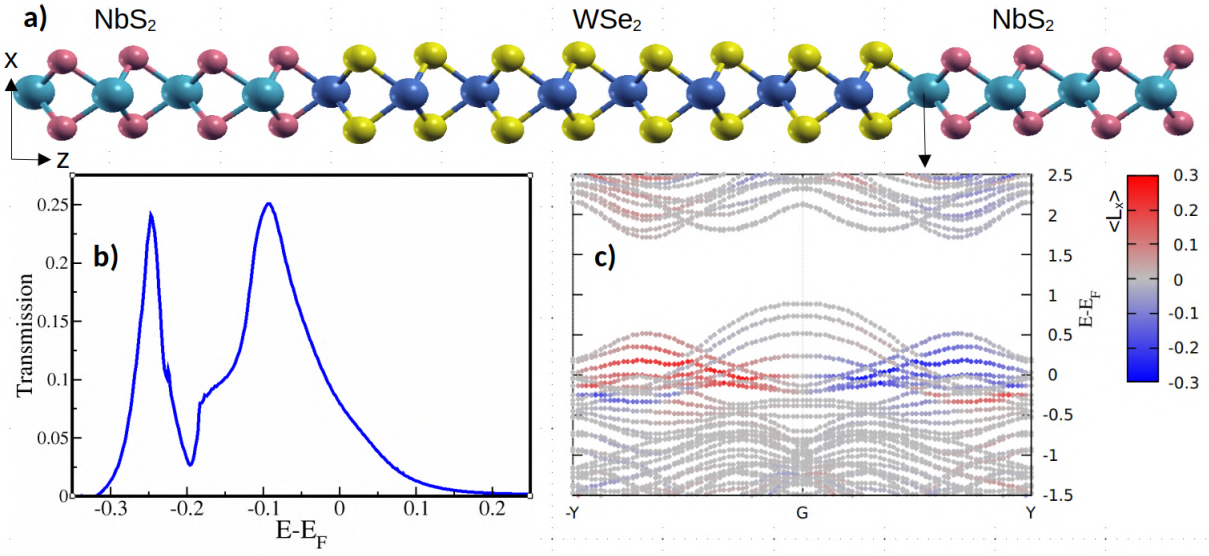

Figure 1: Shows 2D NbS_2/WSe_2 Lateral Heterostructure: a) structre, b) transmission profile, c) bandstrcuture, where the color indicates the OAM expectation value of each state projected onto the surface Nb atom.

Acknowledgments

The authors thank the ORION (Orbitronics in non-centrosymmetric structures) project for the financial support.

References

[1] Seung Ryong Park, Choong H. Kim, Jaejun Yu, Jung Hoon Han, and Changyoung Kim. Orbital-Angular-Momentum Based Origin of Rashba-Type Surface Band Splitting. *Phys. Rev. Lett.* 107, 156803 (15 2011).

[2] Beomyoung Kim, Choong H. Kim, Panjin Kim, et al. Spin and orbital angular momentum structure of Cu(111) and Au(111) surface states. *Phys. Rev. B* 85, 195402 (19 2012).

[3] Dongwook Go, Daegeun Jo, Tenghua Gao, et al. Orbital Rashba effect in a surface-oxidized Cu film. *Phys. Rev. B* 103, L121113 (12 2021).

[4] Luis M. Canonico, Tarik P. Cysne, Alejandro Molina-Sanchez, R. B. Muniz, and Tatiana G. Rappoport. Orbital Hall insulating phase in transition metal dichalcogenide monolayers. *Phys. Rev. B* 101, 161409 (16 2020).

[5] Paolo Giannozzi, Stefano Baroni, Nicola Bonini, et al. QUANTUM ESPRESSO: a modular and open-source software project for quantum simulations of materials. *Journal of Physics: Condensed Matter* 21, 395502 (2009).

[6] Arash A. Mostofi, Jonathan R. Yates, Young-Su Lee, et al. wannier90: A tool for obtaining maximally-localised Wannier functions. *Computer Physics Communications* 178, 685–699 (2008).

[7] Søren Smidstrup, Troels Markussen, Pieter Vancraeyveld, et al. QuantumATK: An integrated platform of electronic and atomic-scale modelling tools. *J. Phys: Condens. Matter* 32, 015901 (2020).

Poster 2.35, November 15th, 10h50–13h00

Insulator-to-metal transition in $NiFe_2O_4$ ultra-thin films

Kedar Sharma[1], Lionel Calmels[1], and Rémi Arras[1,*]

[1]*CEMES, CNRS, Université de Toulouse, France*
*remi.arras@cemes.fr

Spinel ferrites are attractive for a large variety of applications, in particular in the fields of electronics and spintronics [1], to develop memories based on extrinsic multiferroics [2] or resistive-switching mechanisms [3]. In addition to their good magnetic properties, a noticeable interest in ferrites comes from their chemical composition which includes two very abundant and non-toxic elements, i.e. iron and oxygen. To improve the performances of ferrite-based devices, a good control of their electronic and magnetic properties is nonetheless mandatory, which can only be reached with a good understanding of the intricate coupling between their atomic structure and these properties.

$NiFe_2O_4$ is a versatile ferrimagnetic insulator, with a high Curie temperature. We performed first-principles calculations to investigate how its electronic and magnetic properties can vary in (001) thin films, due to the increased contribution of surfaces and/or interfaces with a ferroelectric material. We will discuss about the possible electronic reconstructions which could arise because of the polar character of this oxide. We will also see how the stability of structural defects can be modified in thin films, as their occurrence can drastically affect the magnetic and conductive properties [4–6].

Acknowledgments

This study has been supported through the ANR Grant ANR-19-CE09-0036. This work was granted access to the HPC resources of CALMIP (Allocation No. 2021-2023/P1229).

References

[1] A. Hirohata, H. Sukegawa, H. Yanagihara, et al. Roadmap for emerging materials for spintronic device applications. *IEEE Trans. Magn.* 51, 1 (2015).

[2] N. Jedrecy, T. Aghavnian, J.-B. Moussy, et al. Cross-Correlation between Strain, Ferroelectricity, and Ferromagnetism in Epitaxial Multiferroic $CoFe_2O_4/BaTiO_3$ Heterostructures. *ACS Appl. Mater. Interfaces* 10, 28003 (2018).

[3] W. Hu, Ni Qin, G. Wu, et al. Opportunity of Spinel Ferrite Materials in Nonvolatile Memory Device Applications Based on Their Resistive Switching Performances. *J. Am. Chem. Soc.* 134, 14658 (2012).

[4] U. Lüders, M. Bibes, J.-F. Bobo, et al. Enhanced magnetic moment and conductive behavior in $NiFe_2O_4$ spinel ultrathin films. *Phys. Rev. B* 71, 134419 (2005).

[5] K. Sharma, L. Calmels, D. Li, A. Barbier, and R. Arras. Influence of the cation distribution, atomic substitution, and atomic vacancies on the physical properties of $CoFe_2O_4$ and $NiFe_2O_4$ spinel ferrites. *Phys. Rev. Mater.* 6, 124402 (2022).

[6] Y. Nonaka, Y. K. Wakabayashi, G. Shibata, et al. Origin of magnetically dead layers in spinel ferrites MFe_2O_4 grown on Al_2O_3: Effects of postdeposition annealing studied by XMCD. *Phys. Rev. Mater.* 7, 044413 (2023).

Poster 2.36, November 15th, 10h50–13h00

Spin pumping in LSMO/YBCO heterostructures

H. Hassan[1,*], S. J. Carreira[1], J. Santamaría[2], M. Anane[1], and J. E. Villegas[1]

[1]*Unité Mixte de Physique, CNRS, Thales, Université Paris-Saclay, 91767, Palaiseau, France*
[2]*GFMC, Dept. Fisica de Materiales, Facultad de Fisica, Universidad Complutense, 28040 Madrid, Spain*
**hadi.hassan@cnrs-thales.fr*

Superconductivity and magnetism are often seen as antagonistic effects, and joining them can seem counter intuitive at first. However spin-pumping in s-wave superconductors has shown to be a successful method to study the coexistence between non-equilibrium spin polarized currents and the superconducting condensate [1].

In the present work, we use wideband ferromagnetic resonance (FMR) to study spin-pumping in epitaxial bilayers of $La_{0.7}Sr_{0.3}MnO_3$ (LSMO), a half metal, and $YBa_2Cu_3O_{7-d}$ (YBCO), a d-wave superconductor. The interface between these layers depends on the crystallographic orientation of the $NdGaO_3$ (NGO) substrates : $(110)_0$ and $(100)_0$ (Fig. 1a-b), subsequently giving access to different pumping channels for the spin currents.

We evaluated the spin conductance at the LSMO/YBCO interface by analyzing the magnetization dynamics in LSMO. We found that the Gilbert damping shows an upturn followed by a drop as the heterostructures are cooled across the normal-superconducting transition when the ab-plane of the YBCO is parallel to the interface (grown on NGO $(110)_0$) (Fig. 1c), and a drop followed by an upturn when the ab-plane is tilted 45° with respect to the interface (grown on NGO $(100)_0$) (Fig. 1d). The latter case is reminiscent to the phenomena we recently reported for d-wave superconductors, where the opening of the superconducting gap reduces the spin injection efficiency and leads to a drop in the damping, followed by an upturn due to spin resolved Andreev bound states [2]. However, the upturn observed in the damping for samples grown on NGO $(110)_0$ reflects an increment in the spin injection efficiency which could be ascribed to long range spin pumping mediated by spin triplets. This possibility is supported by the generation of spin triplets in c-axis oriented LSMO/YBCO interfaces [3]. These findings put in evidence the anisotropic character of the superconducting gap in YBCO and the potential of this interface in the field of superconducting spintronics.

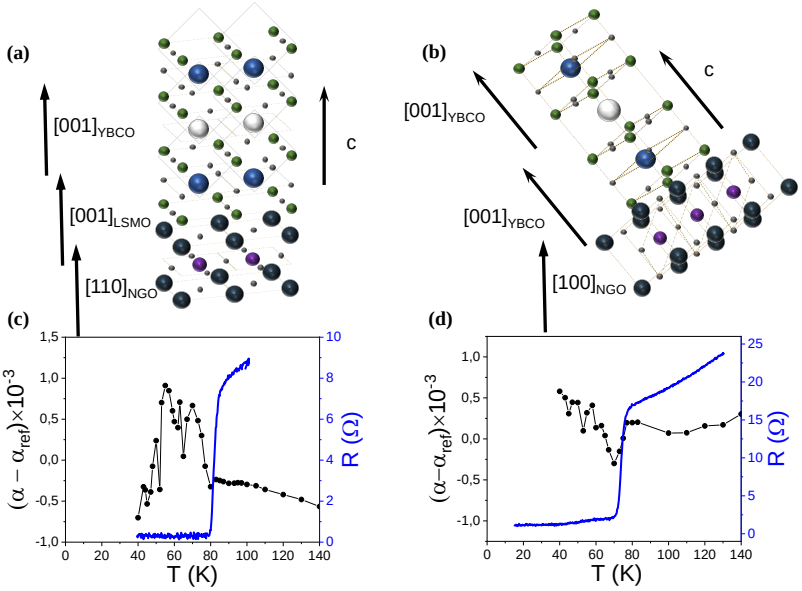

Figure 1: Scheme of the crystalline structure of the LSMO/YBCO interface for (a) NGO (110) and (b) NGO (100). (c-d) show the Damping (left axis in black) and Resistance (right axis in blue) vs Temperature for (c) YBCO/LSMO//NGO(110) and (d) YBCO/LSMO//NGO(100).

Acknowledgments

Work supported by French ANR grant “SUPERFAST”, COST action “SUPERQUMAP” and EU H2020 Marie Curie Actions Nº 890964 “SUPERMAGNONICS”.

References

[1] Yunyan Yao, Qi Song, Yota Takamura, et al. Probe of spin dynamics in superconducting NbN thin films via spin pumping. *Physical Review B* 97 (2018).

[2] S. J. Carreira, D. Sanchez-Manzano, M.-W. Yoo, et al. Spin pumping in d-wave superconductor-ferromagnet hybrids. *Physical Review B* 104 (2021).

[3] D. Sanchez-Manzano, S. Mesoraca, F. A. Cuellar, et al. Extremely long-range, high-temperature Josephson coupling across a half-metallic ferromagnet. *Nature Materials* 21, 188–194 (2021).

Enhancing the output signal of a MagnetoElectric Spin-Orbit logic device

Charles-Élie Fillion[1,*], Erlaitz Gomez-Castrillo[1], Julien Bréhin[1], Witold Skowronski[2], Luis E. Hueso[1,3], and Fèlix Casanova[1,3]

[1]*CIC nanoGUNE, 20018 Donostia-San Sebastián, Basque Country, Spain*
[2]*Institute of Technology, AGH University of Science and Technology, 30-059 Kraków, Poland*
[3]*IKERBASQUE, Basque Foundation for Science, 48009 Bilbao, Basque Country, Spain*
*ce.fillion@nanogune.eu

The MagnetoElectic Spin-Orbit (MESO) logic has emerged as one of the best candidates to complement standard CMOS transistors technology [1]. It enables information to be written, stored and read electrically in a non-volatile way, leading to low power consumption for next-generation spintronic logic devices [2]. In a MESO device, two logic states are determined by the magnetization direction of a nanostructured ferromagnetic layer (green layer in Fig. 1a). The MESO device is composed of two modules: one to write the logic state (ME writing module) by controlling the magnetization direction using the MagnetoElectric coupling and the other to read it (SO reading module) through spin-to-charge conversion in a material with high spin-orbit coupling [3, 4], also called spin-orbit material (SOM). In this work, we focus on the SO module, in which the magnetic state readout is possible using the inverse spin Hall effect (iSHE). More precisely, a spin polarized current is created by flowing a charge current through the ferromagnet. Due to the iSHE, this spin polarized current is converted to a transverse voltage V_{iSHE} that will carry the information about the magnetization in the ferromagnet (see Fig. 1a,b). The voltage difference between the two magnetization direction is called the output signal, ΔV_{iSHE}, or ΔR_{iSHE} if normalized to the injected current (see Fig. 1c). Reaching a large output signal ΔR_{iSHE} is a requirement for the MESO concept to work, as it will allow to switch the next writing module of the MESO device, opening the way to highly energy efficient devices.

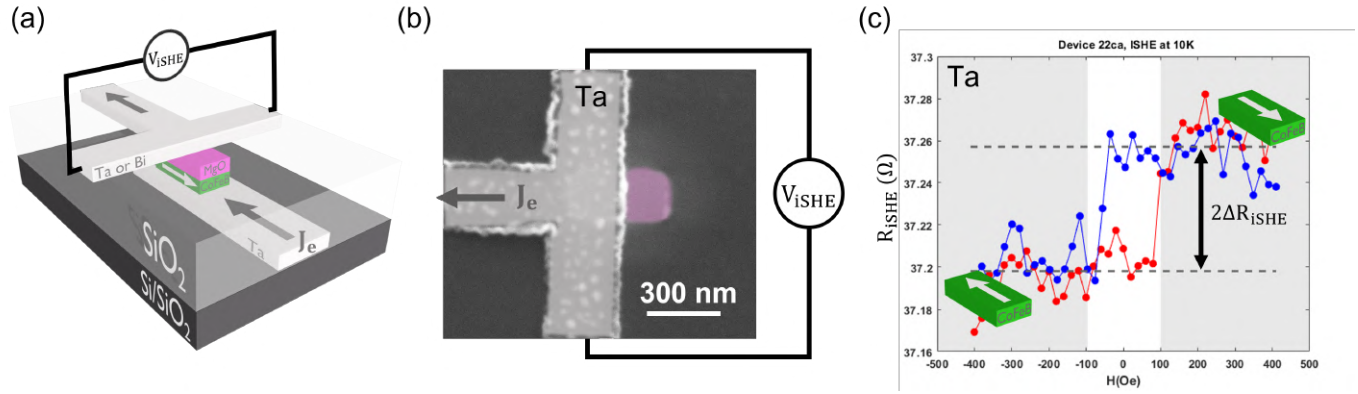

Figure 1: (a) Sketch of the T-shape reading module of the MESO device. A current flows along the bottom Ta electrode, gets spin-polarized by passing through the CoFeB layer, and is converted back into a transverse charge current, whose sign depends on the magnetization direction of the nanostructured CoFeB (white arrow). (b) Magnetic state readout using the iSHE: Transverse resistance from V_{iSHE} as a function of the magnetic field. The two magnetization directions are indicated, and the red color (resp. blue) corresponds to the forward field sweep (resp. backward).

Here, we present two techniques to improve the output signal of the SO module, for which we have designed, patterned and fabricated test devices in a T-shape geometry (see Fig. 1a,b). On the one hand, we are exploring SOM with high resistivity and spin-orbit coupling, such as Ta, Bi or BiSb, expected to enhance the spin-to-charge conversion efficiency [5]. However, increasing the resistivity of the SOM brings additional problems such as electrical and spin conductivity mismatch, reducing the spin injection efficiency [6]. Thus, on the other hand, we explore the addition of a crystalline MgO tunnel barrier between the ferromagnet and the SOM (purple layer in Fig. 1a,b), solving both of these issues at the same time and improving the spin injection [6]. Our first working devices allow a clear readout of the magnetic state, as shown in Fig. 1c, which we expect to be highly improved by our ongoing optimization of the material properties, device geometry and fabrication process.

Acknowledgments

This work is supported by Intel Corporation through the “FEINMAN 2.0” Intel Science Technology Center and by the Spanish MICINN (Project No. PID2021-122511OB-I00 and Maria de Maeztu Units of Excellence Programme No. CEX2020-001038-M). E.G.-C. thanks the Basque Government for a Ph.D. fellowship. W.S. acknowledges grant No. PPN/BEK/2020/1/00118/DEC/1 from Polish National Agency for Academic Exchange."

References

[1] Sasikanth Manipatruni, Dmitri E. Nikonov, and Ian A. Young. Beyond CMOS computing with spin and polarization. *Nature Physics* 14, 338–343 (2018).

[2] Sasikanth Manipatruni, Dmitri E. Nikonov, Chia-Ching Lin, et al. Scalable energy-efficient magnetoelectric spin–orbit logic. *Nature* 565, 35–42 (2019).

[3] Diogo C. Vaz, Chia-Ching Lin, John Plombon, et al. “Functional Demonstration of a Fully Integrated Magneto-Electric Spin-Orbit Device”. *2021 IEEE International Electron Devices Meeting (IEDM)*. San Francisco, CA, USA: IEEE, 2021, 32.4.1–32.4.4.

[4] Van Tuong Pham, Inge Groen, Sasikanth Manipatruni, et al. Spin–orbit magnetic state readout in scaled ferromagnetic/heavy metal nanostructures. *Nature Electronics* 3, 309–315 (2020).

[5] Zhendong Chi, Guanxiong Qu, Yong-Chang Lau, et al. Spin Hall effect driven by the spin magnetic moment current in Dirac materials. *Phys. Rev. B* 105, 214419 (2022).

[6] A. Fert and H. Jaffrès. Conditions for efficient spin injection from a ferromagnetic metal into a semiconductor. *Physical Review B* 64, 184420 (2001).

Ferroelectric Nonlinear Hall Effect in GeTe

Théo Frottier[1,*], Salvatore Teresi[1], Williams Savero-Torres[1], Michael Wissmann[1], Aurélie Kandazoglou[1], Paolo Sgarro[1], Maxime Culot[1], Filip Osana[1], Boris Croes[2], Jean-Philippe Attané[1], Frédéric Leroy[2], Aurélien Manchon[2], Louis Hutin[3], Fabien Cheynis[2], and Laurent Vila[1]

[1]*Université Grenoble Alpes / CEA / IRIG / SPINTEC, Grenoble, France*
[3]*Université Grenoble Alpes / CEA / LETI, Grenoble, France*
[2]*Aix Marseille Université / CNRS / CINAM / AMUTECH, Marseille, France*
**theo.frottier@cea.fr*

In condensed matter physics, Hall effects correspond to the appearance of non-diagonal terms in the conductivity tensor. From the ordinary Hall effect to the quantum anomalous Hall effect, the discoveries of the various Hall effects have always been the source of profound insight in the physics of condensed matter transport. A new member of the Hall family, recently predicted theoretically [1] and measured [2], is the Nonlinear Anomalous Hall Effect (NLAHE).

The main characteristic of this new effect is that, unlike the ordinary Hall effect or the anomalous Hall effect, the relationship between the applied current and the transverse electric field is nonlinear. It does not require any symmetry breaking by a magnetic field, like for the ordinary Hall effect, or by a magnetization, like in the case of the anomalous Hall effect. In other words, the NLAHE does not require -and must not have- time reversal symmetry breaking. Instead, a spatial symmetry breaking is required, which can be found in non-centro-symmetric systems.

Ferroelectric materials, which possess a remanant electric polarization, are a particular class of non-centro-symmetric materials. The sign of NLAHE has been predicted [3] to depend on the sign of the ferroelectric polarization, however this non-volatile Ferroelectric control of the NLAHE (FENLHE) has not been demonstrated clearly yet.

Germanium Telluride (GeTe) is a room temperature semi-conducting ferroelectric, whose non-centro-symmetry should lead to a substantial NLAHE. High quality GeTe [111] stacks were grown by molecular beam epitaxy. We then patterned Hall bars by electronic beam lithography, and measured their transport properties.

The nonlinearity can be probed using lock-in techniques, as it leads to the appearance of second harmonic signals. We show that we have in-plane NLAHE in GeTe [111] (see Fig. 1). We also used an Atomic Force Microscopy (AFM) setup with a conductive tip to apply electric fields locally. We demonstrate the remnant control of the sign of the NLAHE (see Fig. 2), after applying electrical fields with a conductive AFM tip. This result is to our knowledge the first demonstration of the non-volatile control of the NLAHE by the ferroelectric polarization.

References

[1] Inti Sodemann and Liang Fu. Quantum nonlinear Hall effect induced by Berry curvature dipole in time-reversal invariant materials. *Physical review letters* 115, 216806 (2015).

[2] Kaifei Kang, Tingxin Li, Egon Sohn, Jie Shan, and Kin Fai Mak. Nonlinear anomalous Hall effect in few-layer WTe2. *Nature materials* 18, 324–328 (2019).

[3] Hua Wang and Xiaofeng Qian. Ferroelectric nonlinear anomalous Hall effect in few-layer WTe2. *npj Computational Materials* 5, 119 (2019).

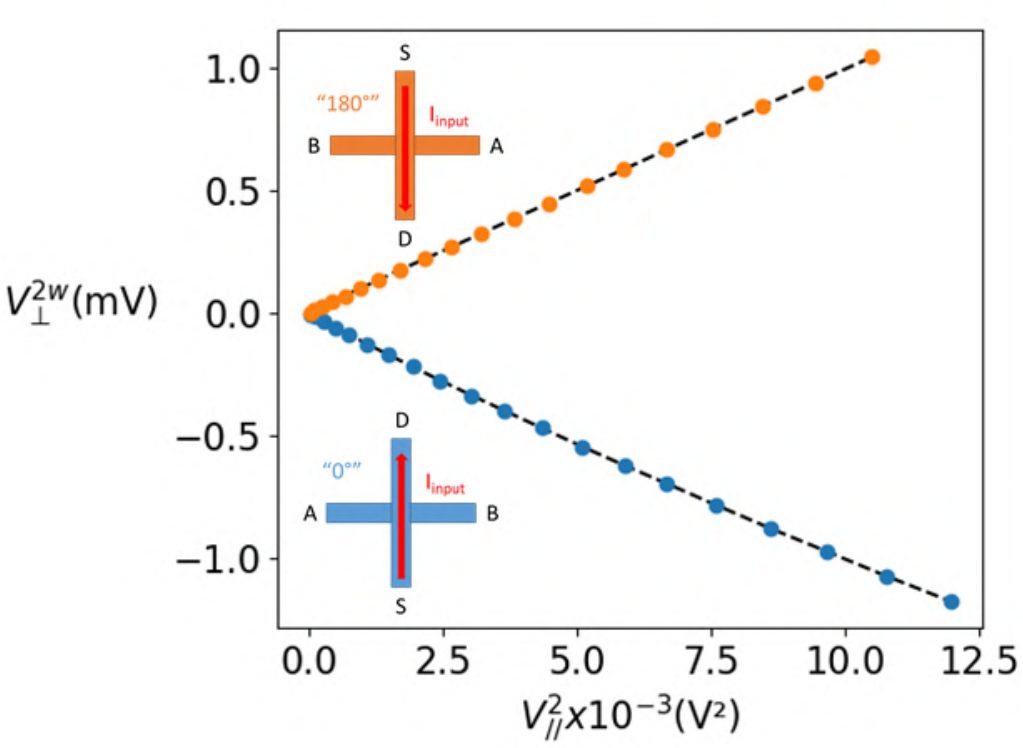

Figure 1: In-plane measurements of the NLAHE in two opposite directions. In absence of any non-linearity in the Hall contributions, the second harmonic $V_{\perp}^{2\omega}$ signal is expected to be 0. The presence of a non-zero signal indicates the presence of a non-linear contribution. The signal varies, as expected for the NLAHE, quadratically with the applied longitudinal field. The change of sign of the signal for a 180° rotation of the setup is the guarantee that the signal is not due to heating effects, which could also be responsible for a non-linear contribution.

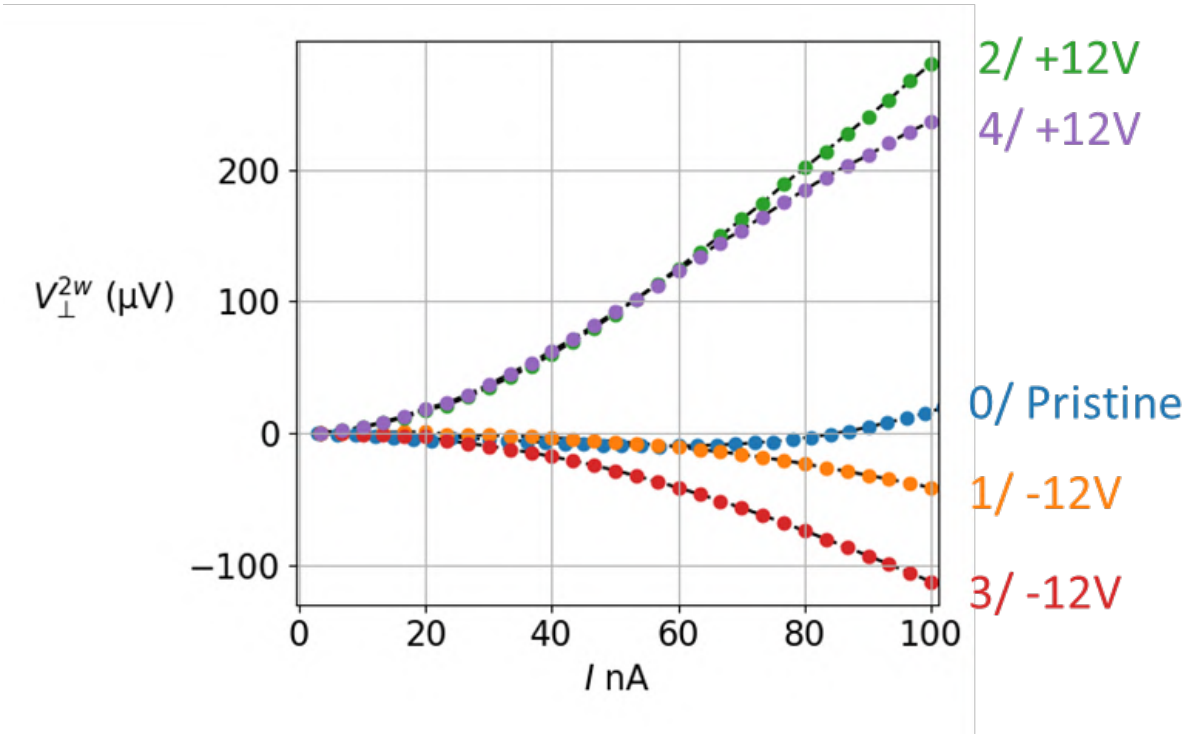

Figure 2: NLAHE measurements after having applied different electrical fields with the conductive tip of an AFM. The colored labels indicate the order of the measurement and the amplitude of the voltage applied with the tip before the measurement.

Poster 2.39, November 15th, 10h50–13h00

Finite size effect on the Hall response of altermagnetic Mn_5Si_3

Javier Rial[1, 2, *], Miina Leiviska[1], Helena Reichlova[3,4], Ismaïla Kounta[5], Antonin Bad'ura[4,6], Sebastian Beckert[3], Rafael Lopes Seeger[1], Isabelle Joumard[1], Florian Disdier[1], Gilles Gaudin[1], Dominik Kriegner[3,4], Eva Schmoranzerova[6], Libor Smejkal[4,7], Jairo Sinova[4,7], Tomas Jungwirth[4,8], Sebastian T. B. Goennenwein[3,9], Lisa Michez[5], and Vincent Baltz[1]

[1] *Univ. Grenoble Alpes, CNRS, CEA, Grenoble INP, Spintec, Grenoble, France*
[2] *Univ. Autonoma de Madrid, Madrid, Spain*
[3] *IFM, Technische Universität Dresden, Dresden, Germany*
[4] *Institute of Physics, Czech Academy of Sciences, Czech Republic*
[5] *Aix Marseille Univ, CNRS, CINaM, Marseille, France*
[6] *Faculty of Mathematics and Physics, Charles University, Prague, Czech Republic*
[7] *Institut fur Physik, Johannes Gutenberg Universität Mainz, Germany*
[8] *School of Physics and Astronomy, University of Nottingham, Nottingham, United Kingdom*
[9] *Universitat Konstanz, Fachbereich Physik, Konstanz, Germany*
[10] *Institute of Physics, Czech Academy of Sciences, Czech Republic*
**javier.rialrodriguez@cea.fr*

Epitaxial thin film of Mn_5Si_3 [1, 2] is a candidate to the recently predicted class of magnetic materials called 'alter'magnet [3], and more specifically to the anisotropic d-wave magnetic phases that features an unconventional combination of strong time reversal symmetry breaking responses and a vanishing net magnetization. The Mn_5Si_3 compound displays a large spontaneous anomalous Hall (AHE) response of a few $S \cdot cm^{-1}$ below its Néel temperature of about 200 K, to which adds a topological-like (THE-like) signal below about 90 K, wherein some twisting of the magnetic moments is expected to occur, as opposed to a collinear arrangement above [1, 2]. What is the anisotropic response of the AHE signal and what is the exact origin of the THE-like signal are some questions which are still pending and that we will present here. To address the first point, measurements were taken for a current and/or an external magnetic field applied along several crystallographic directions. For the second point a systematic study of the finite size effects was performed so as to understand whether the THE-like signal is the result of an actual topological effect related to the electrons picking up a Berry phase on interaction with the non-collinear spin structure of Mn_5Si_3 below 90 K or whether it is the bare summation of several AHE signals of opposite sign, in an inhomogeneous médium [4].

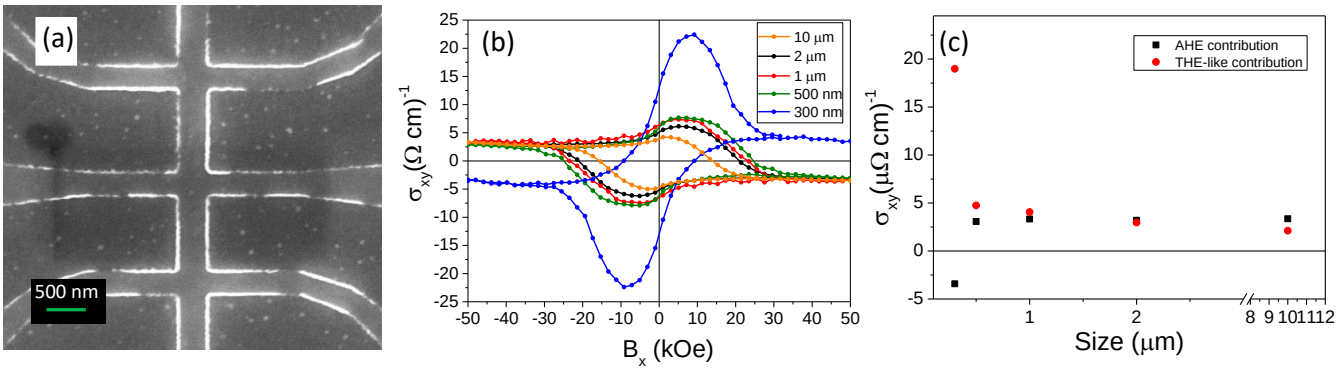

Figure 1: (a) SEM image of around 300 nm Mn_5Si_3 Hall Bar. (b) Hall conductivity of Mn_5Si_3 Hall bars of several lateral sizes, measured at 90 K. (c) Lateral size dependence of the spontaneous anomalous (AHE) and topological-like (THE-like) contributions to the Hall conductivity.

Acknowledgments

This work was supported by the French national research agency (ANR) and the Deutsche Forschungsgemeinschaft (DFG) (Project MATHEEIAS- Grant No. ANR-20-CE92-0049-01 / DFG-445976410). JR acknowledges MINECO for the Margaritas Salas (MS) program (2022-2024).

References

[1] Ismaïla Kounta, Helena Reichlova, Dominik Kriegner, et al. Competitive actions of MnSi in the epitaxial growth of Mn_5Si_3 thin films on Si(111). *Physical Review Materials* 7 (2023).

[2] Helena Reichlová, Rafael Lopes Seeger, Rafael González-Hernández, et al. *Macroscopic time reversal symmetry breaking by staggered spin-momentum interaction*. 2020.

[3] Libor Šmejkal, Jairo Sinova, and Tomas Jungwirth. Emerging Research Landscape of Altermagnetism. *Physical Review X* 12 (2022).

[4] A. Gerber. Interpretation of experimental evidence of the topological Hall effect. *Physical Review B* 98 (2018).

Poster 2.40, November 15th, 10h50–13h00

Spin wave properties of CoFeB multilayers grown on piezoelectric substrates

Rafel Lopes Seeger[1,2,*], Florian Millo[2], Asma Mouhoub[2], Laura Thevenard[3], Grégoire de Loubens[1], Aurélie Solignac[1], and Thibaut Devolder[2]

[1]*SPEC, CEA, CNRS, Université Paris-Saclay, 91191 Gif-sur-Yvette, France*
[2]*Université Paris-Saclay, CNRS, Centre de Nanosciences et de Nanotechnologies, 91120 Palaiseau, France*
[3]*Institut des Nanosciences de Paris, Sorbonne Université, CNRS, UMR 7588, 4 place Jussieu, F-75005 Paris, France*
*rafaelseeger@gmail.com

The elastic coupling between a magnetic film and the substrate is desired in SAW-FMR devices [1–3] and in magnetoacoustics [4] when one harness the interaction between a surface acoustic wave (SAW) hosted by a piezoelectric substrate and the ferromagnetic resonance (FMR) of the magnetic film. We study CoFeB single films grown on various crystalline orientations of $LiNbO_3$ substrates and on oxidized silicon [5]. We identify the annealing conditions that are appropriate to induce or suppress in-plane uniaxial anisotropy. Anisotropy fields can be increased by annealing up to 11 mT when using substrates with anisotropic surfaces. They can be decreased to below 1 mT when using isotropic surfaces. In the first case, the increase in anisotropy originates from the biaxial strain in the film caused by the anisotropic thermal contraction of the substrate when back at room temperature after strain relaxation during annealing. In the second case, anisotropy is progressively removed by applying successive orthogonal fields that are assumed to progressively suppress any chemical ordering within the magnetic film. The method can be applied to CoFeB/Ru/CoFeB synthetic antiferromagnets (SAFs) but the tuning of the anisotropy comes with a decrease of the interlayer exchange coupling and a drastic change of the exchange stiffness. Particularly, vanishing anisotropy is required for resonant coupling between the SAW and the spin waves in SAFs [6].

We have also combined broadband FMR and FMR microscopy techniques to study spin waves properties in the magnetic films grown on $LiNbO_3$ substrates. We were particularly interested on the coupling between the acoustic media and the magnetic films. In order to better understand to what extent this coupling may occur in SAF structures, we analytically studied the magneto-elastic and magneto-rotation torques associated to a travelling acoustical wave and we estimated the power that the SAW can transfer to the SAF spin waves. Finally, this formalism was applied to various surface acoustical waves, such as the Rayleigh wave of a semi-infinite Z-$LiNbO_3$ substrate and the guided Rayleigh wave of thin Z-$LiNbO_3$ film on a sapphire substrate.

Acknowledgments

This work was supported by a public grant overseen by the French National Research Agency (ANR) as part of the "Investissements d'Avenir" program (Labex NanoSaclay, reference: ANR-10-LABX-0035, project SPICY). R. L. S and F. M. acknowledge the French National Research Agency (ANR) under Contract No. ANR-20-CE24-0025 (MAXSAW).

References

[1] M. Weiler, L. Dreher, C. Heeg, et al. Elastically Driven Ferromagnetic Resonance in Nickel Thin Films. *Phys. Rev. Lett.* 106, 117601 (2011).

[2] P. Kuszewski, J.-Y. Duquesne, L. Becerra, et al. Optical Probing of Rayleigh Wave Driven Magnetoacoustic Resonance. *Phys. Rev. Appl.* 10, 034036 (2018).

[3] Pauline Rovillain, Jean Yves Duquesne, Louis Christienne, et al. Impact of Spin-Wave Dispersion on Surface-Acoustic-Wave Velocity. *Physical Review Applied* 18 (2022).

[4] M. Küß, M. Albrecht, and M. Weiler. Chiral Magnetoacoustics. *Front. Phys.* 10 (2022).

[5] Rafael Lopes Seeger, Florian Millo, Asma Mouhoub, et al. Inducing or suppressing the anisotropy in multilayers based on CoFeB. *Phys. Rev. Mater.* 7, 054409 (2023).

[6] Roman Verba, Vasil Tiberkevich, and Andrei Slavin. Wide-band nonreciprocity of surface acoustic waves induced by magnetoelastic coupling with a synthetic antiferromagnet. *Physical Review Applied* 12 (2019).

On the metamagnetic phase transition in B2-FeRh nanocrystals

V. Dupuis[1,*], G. Herrera[1], J. Moreau[1], A. Tamion[1], L. Bardotti[1], D. Le Roy[1], F. Tournus[1], O. Boisron[1], S. Gonzalez[2], I.C. Infante[2], M. Bugnet[3], P. Schoeffmann[4], P. Ohresser[4], E. Otero[4], and F. Wilhelm[5]

[1]*Institut Lumière Matière, CNRS UMR 5306, Univ. Lyon 1, F-69622 Villeurbanne*
[2]*Institut des Nanotechnologies de Lyon, CNRS UMR 5270, ECL INSA, F-69621 Villeurbanne*
[3]*MATEIS, CNRS UMR 5510, Univ. Lyon 1, INSA Lyon, F-69621 Villeurbanne*
[4]*Synchrotron SOLEIL, L'Orme de Merisiers, Saint Aubin, BP 48, F-91192 Gif-sur-Yvette*
[5]*European Synchrotron Radiation Facility, BP 220, F-38043 Grenoble*
veronique.dupuis@univ-lyon1.fr

Near equiatomic composition, FeRh bulk alloys in the CsCl-type (B2) chemically ordered phase present a metamagnetic transition from the antiferromagnetic (AFM) state at low temperature to the ferromagnetic state (FM) above a critical temperature T_t of 370 K, accompanied by a 1% volume expansion. Despite the high material cost, the competition near room temperature between both magnetic orders of FeRh holds great potential applications including magnetocaloric refrigeration, ultrafast spintronics, antiferromagnetic spintronics, and recording data. Although the magnetic properties of FeRh nanostructures have been extensively studied over the last 25 years, the mechanism behind the AFM to FM transition is still widely debated and not well understood [1].

Beyond previous studies on monocrystalline FeRh films [2, 3], here we propose to explore metamagnetic phase transition in an original 150 nm-thick nanogranular film, made of FeRh clusters preformed in the gas phase using the Low Energy Cluster Beam Deposition (LECBD) technique, which is subsequently UHV annealed at high temperature to reach the B2 phase. The global thermal magnetization measured by SQUID reveal the same linear behavior for transition temperature versus applied magnetic field, as in the bulk. But conversely to the bulk, the presence of a broad and asymmetric metamagnetic transition with residual magnetization below T_t reveal a non negligible sample proportion that remains in the FM state at low temperature. The same magnetic behavior has been obtained at the Rh L edge from XMCD measurements on ID12-ESRF, which evidence strong nanoalloy effects in FeRh nanograins but also probably dipolar interactions between grains that counteract FM/AFM transition in the cooling mode. We have related the co-existence of both magnetic orders at low temperature to a triggering size between smaller grains still FM at surface/interface regions and larger AFM grains at the center of the film as observed from Scanning Transmission Electron Microscopy (STEM-HAADF) in cross-section. (see Fig. 1)

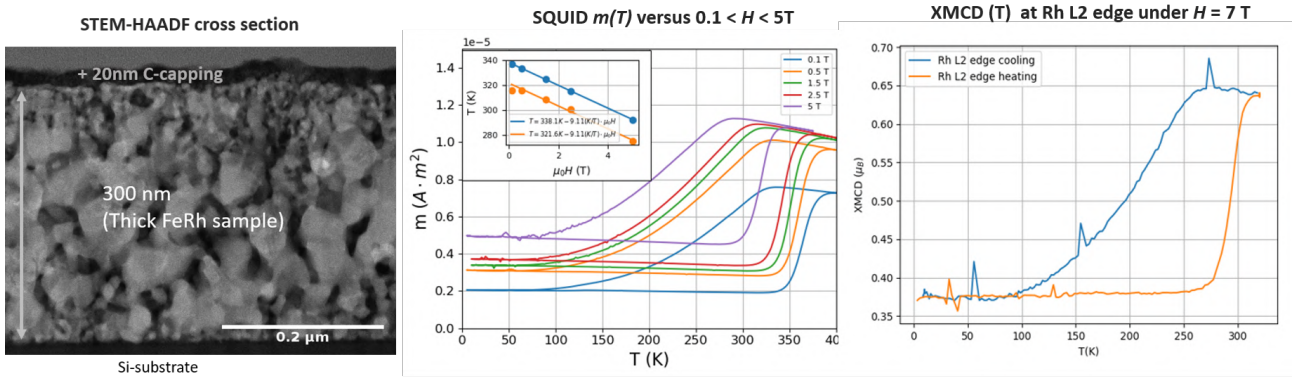

Figure 1: STEM-HAADF on thick film after annealing (left), Thermal global SQUID magnetization with both linear minimum and maximum transition temperatures as function of applied field in insert (center) and XMCD evolution at Rh L2 edge measured in cooling down and heating up mode under 7 Tesla (right) on ID12-ESRF

Moreover, we prepared well-defined samples made of B2 FeRh NPs diluted in amorphous carbon matrix by mass-selected LECBD to avoid coalescence upon annealing. We put in evidence the persistence of FM order down to very low-temperature in the 2-10 nm diameter range [4, 5]. This anomalous magnetic order has been ascribed to finite size effects due to structural intrinsic relaxation at nanoscale. The objective of VOLtage Control of NANOmagnet ANR projet (2020-24) is to study hybrid multiferroïc nanostructures (0D/2D) in order to control magnetic order under external stimuli as strain or voltage in the previously paper of Cherify et al. on thin FeRh films [3]. In the case of bimetallic nanoclusters deposited on perovskite oxide substrate, a strong interplay between surface chemical reactivity, configuration, morphology and magnetic state is expected

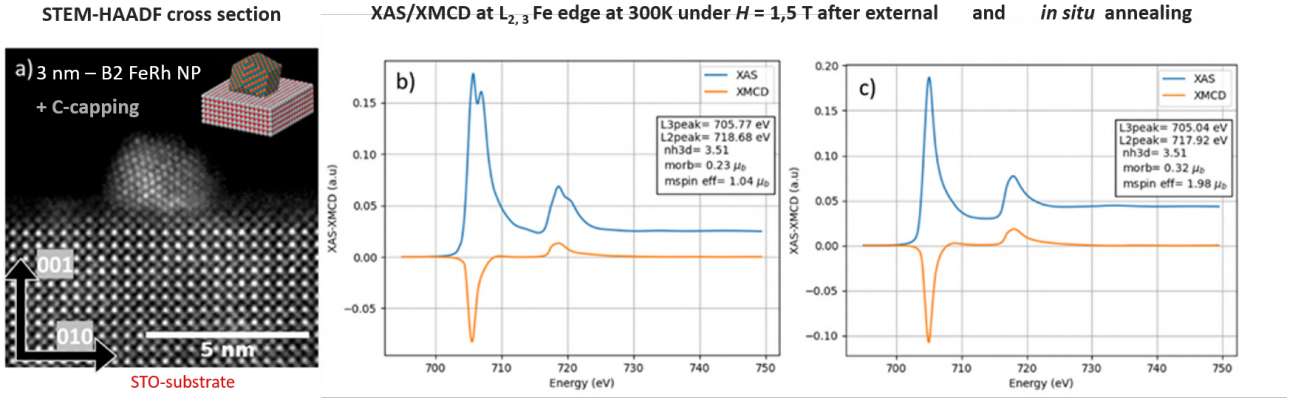

Figure 2: Epitaxy observed from STEM-HAADF on 3nm NP of B2 FeRh [011]/STO[020] with carbon capping. b) XAS/XMCD signal at Fe $L_{2,3}$ edge after external or c) in situ annealing 3h at 700°C in UHV chamber at DEIMOS-SOLEIL

to be exacerbated. So we also present experimental results obtained on mass-selected FeRh NPs with 3 nm and 7 nm in diameter deposited on TiO_3 based substrate with Carbon capping and subsequently UHV annealed at 700°C. (see Fig. 2)

Using synchrotron radiation, we have observed the chemical ordering of FeRh nanoparticles into the B2 crystalline phase upon annealing from grazing incidence X-ray diffraction (GIXRD), which is also accompanied by a Fe (resp. Rh induced) magnetic moment evolution visible from X-ray magnetic circular dichroism (XMCD) measurements at Fe (resp. Rh) L edge at DEIMOS-SOLEIL (resp. ID12-ESRF). Despite their random deposition, the orientation dependence of X-ray diffraction B2 FeRh peaks indicates that particles are finally adopting preferential orientations on $SrTiO_3$ (STO (001)) substrate. In addition to the usual epitaxy relationship met for thin films, a novel orientation is observed (corresponding to a 45° in-plane rotation), as well as other favourable coincidences for particles on STO (001) observed from STEM-HAADF in cross section (see Fig.2a). At the same time, surface sensitive XMCD measurements at Fe L edge reveal that NPs assemblies on STO, systematically appear to be (partially) oxidized after transfer in air while FeRh nanoparticles can be reduced thanks to in situ vacuum annealing (see Fig.2b). Concerning magnetic behavior, as for previous FeRh NPs embedded in carbon matrix [4, 5], no metamagnetic phase transition has been observed in this NPs size-range from XMCD measurements neither at Fe nore at Rh L edges. We can conclude that the triggering size is not enough altered by the presence of strain from STO monocrystal substrate to induce AF order in so small nanocristallites.

Acknowledgments

This work is part of the PhD thesis of G. Herrera with financial support of VOLCONANO ANR-19-CE09-0023.

References

[1] L H Lewis, C H Marrows, and S Langridge. Coupled magnetic, structural, and electronic phase transitions in FeRh. *Journal of Physics D: Applied Physics* 49, 323002 (2016).

[2] Jiangwei Cao, Nguyen T. Nam, Sho Inoue, et al. Magnetization behaviors for FeRh single crystal thin films. *Journal of Applied Physics* 103, 07F501 (2008). eprint: https://doi.org/10.1063/1.2828812.

[3] R. O. Cherifi, V. Ivanovskaya, L. C. Phillips, et al. Electric-field control of magnetic order above room temperature. *Nature Materials* 13, 345–351 (2014).

[4] A. Hillion, A. Cavallin, S. Vlaic, et al. Low Temperature Ferromagnetism in Chemically Ordered FeRh Nanocrystals. *Phys. Rev. Lett.* 110, 087207 (8 2013).

[5] Herrera, Guillermo, Robert, Anthony, Dupuis, Veronique, et al. Chemical and magnetic order in mass-selected large FeRh nanomagnets embedded in a carbon matrix. *Eur. Phys. J. Appl. Phys.* 97, 32 (2022).

Poster 2.42, November 15th, 10h50–13h00

Nanocomposites Photostrictifs-Magnétostrictifs en Épitaxie Verticale

C. Rodríguez[1,*], M. Hennes[1], D. Demaille[1], Y. Zheng[1], D. Hrabovsky[2], and F. Vidal[1]

[1]*Institut des NanoSciences de Paris, 4 place Jussieu, 75005 Paris, France*
[2]*Plateforme de Mesures Physiques à Basse Température, 4 place Jussieu, 75005 Paris, France*
*cortez@insp.jussieu.fr

Constitués de réseaux de piliers nanométriques incorporés perpendiculairement *dans* un film mince, les nanocomposites verticalement alignés (VAN) présentent une sensibilité accrue aux effets d'interface et un fort couplage de réseau avec la matrice environnante. En exploitant l'épitaxie et le grand rapport interface/volume présent dans cette architecture, nous étudions l'interaction de deux effets physiques faisant intervenir des contraintes mécaniques : la photostriction et la magnétostriction.

Le système modèle est composé de piliers de $CoFe_2O_4$ (CFO) au sein d'une matrice de $SrRuO_3$ (SRO). Le premier de ces matériaux présente une forte magnétostriction $\left(\sim -590 \times 10^{-6}\right)$ [1], tandis que le second présente une dilatation photoinduite (non thermique) de l'ordre de $\sim 1\%$ à saturation [2], avec un temps de réponse en dessous de la nanoseconde [3]. Ainsi, un couplage efficace dans ce VAN conduirait à une évolution des propriétés magnétiques *des piliers* sous excitation optique *de la matrice*, à des échelles de temps potentiellement ultrarapides.

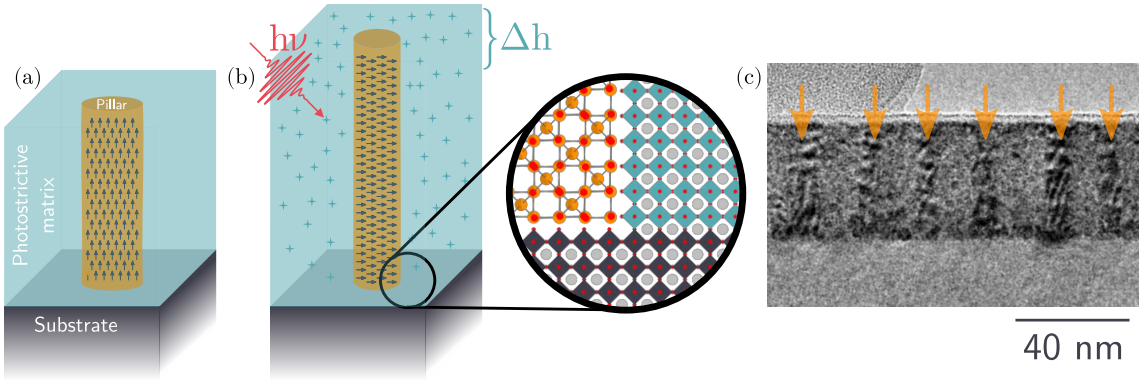

Figure 1: Schéma d'un nanofil dans un VAN sous compression (a) et tension (b) selon son axe de révolution. La tension est produite par la déformation photoinduite de la matrice. Coupe transverse d'un VAN vue par microscopie électronique à transmission (c), des flèches oranges indiquent les endroits où se trouvent les nanofils.

Bien que des effets induits par la lumière dans ces systèmes aient été mis en évidence [4], une compréhension détaillée des processus physiques sous-jacents, ainsi qu'une description quantitative des échelles de temps pertinentes pour la déformation photoinduite et le contrôle de l'aimantation font actuellement défaut. Cependant, ces informations sont d'une importance cruciale pour le développement de dispositifs hybrides ultrarapides, où des impulsions optiques de l'ordre de la femtoseconde pourraient être utilisées pour manipuler l'état d'aimantation de structures magnétiques nanométriques.

Dans le cadre de futures études résolues en temps, nous présentons une investigation systématique des paramètres de dépôt sur la nanoarchitecture finale et sur les propriétés magnétiques résultantes, ainsi que leur optimisation pour de futures recherches en femtomagnétisme. Tous les échantillons ont été fabriqués par ablation laser pulsé dans des conditions de croissance optimisées pour l'épitaxie sur des substrats de $SrTiO_3$. En utilisant la diffraction des rayons X et la microscopie électronique en transmission, nous montrons que les nanopiliers obtenus ont un diamètre d'environ 5 à 10 nm avec une hauteur de l'ordre de l'épaisseur de la couche mince. D'autre part, nous montrons que les nanofils sont soumis à une contrainte épitaxiale compressive dans la direction perpendiculaire au plan, ce qui stabilise une aimantation perpendiculaire.

Remerciements

Nous remercions l'Agence Nationale de la Recherche, contrat No. ANR-21-CE09-0042, pour leur soutien financier.

References

[1] R. M. Bozorth. Anisotropy and Magnetostriction of Some Ferrites. *Physical Review* 99, 1788–1798 (1955).

[2] Tzu-Chiao Wei, Hsin-Ping Wang, Heng-Jui Liu, et al. Photostriction of Strontium Ruthenate. *Nature Communications* 8, 15018 (24, 2017).

[3] Kang Wang, Bingbing Zhang, Weimei Xie, et al. Coupling Among Carriers and Phonons in Femtosecond Laser Pulses Excited SrRuO3: A Promising Candidate for Optomechanical and Optoelectronic Applications. *ACS Applied Nano Materials* 2, 3882–3888 (28, 2019).

[4] Heng-Jui Liu, Long-Yi Chen, Qing He, et al. Epitaxial Photostriction–Magnetostriction Coupled Self-Assembled Nanostructures. *ACS Nano* 6, 6952–6959 (2012).

Magnetization dynamics affected by phonon pumping

Richard Schlitz[1,2,*], Luise Siegl[2], Takuma Sato[4], Weichao Yu[3], Gerrit E. W. Bauer[4], Hans Huebl[5], and Sebastian T. B. Goennenwein[2]

[1]*Department of Materials, ETH Zürich, 8093 Zürich, Switzerland*
[2]*Department of Physics, University of Konstanz, 78457 Konstanz, Germany*
[3]*State Key Laboratory of Surface Physics and Institute for Nanoelectronic Devices and Quantum Computing, Fudan University, Shanghai 200433, China*
[4]*AIMR and CSRN, Tohoku University, Sendai 980-8577, Japan*
[5]*Walther-Meißner-Institut, Bayerische Akademie der Wissenschaften, 85748 Garching, Germany*
*richard.schlitz@mat.ethz.ch

Combining phonons with ultralow attenuation with the tunability of magnetic excitations outlines a promising path for improving magnon-based applications [1, 2]. However, to optimally merge phononics and magnonics, a full understanding of the magnon-phonon coupling needs to be established in order to engineer the coupling strength. In 2018, Streib et al. predicted that in heterostructures of a magnetic insulator and a nonmagnetic insulator an additional contribution to the magnetic damping arises from the emission of phonons into the nonmagnetic substrate, proportional to the magnon-phonon coupling strength within the magnetic insulator [3].

I will present evidence for the pumping of phonons in high-resolution ferromagnetic resonance investigations of yttrium iron garnet (YIG) on gadolinium gallium garnet (GGG) substrates, showing that these two effects are reliant on the same physical mechanism [4]. Characterizing the ferromagnetic resonance in a wide frequency range, we can observe both, the high cooperativity regime, where magnons and phonons hybridize into magnon-polarons [5], and the incoherent regime, where the pumped phonons constitute a dissipative flow of energy away from the magnetic system, verifying the predictions by Streib et al.. Additionally, we confirm that the magnon-phonon coupling can be straightforwardly understood by considering the overlap integral of the magnon and phonon amplitude profile across the film thickness [6].

References

[1] Yi Li, Chenbo Zhao, Wei Zhang, Axel Hoffmann, and Valentyn Novosad. Advances in coherent coupling between magnons and acoustic phonons. *APL Materials* 9, 060902 (2021).

[2] D. A. Bozhko, V. I. Vasyuchka, A. V. Chumak, and A. A. Serga. Magnon-phonon interactions in magnon spintronics (Review article). *Low Temperature Physics* 46, 383–399 (2020).

[3] Simon Streib, Hedyeh Keshtgar, and Gerrit E. W. Bauer. Damping of Magnetization Dynamics by Phonon Pumping. *Physical Review Letters* 121, 027202 (2018).

[4] Richard Schlitz, Luise Siegl, Takuma Sato, et al. Magnetization dynamics affected by phonon pumping. *Physical Review B* 106, 014407 (2022).

[5] K. An, A. N. Litvinenko, R. Kohno, et al. Coherent long-range transfer of angular momentum between magnon Kittel modes by phonons. *Physical Review B* 101, 060407(R) (2020).

[6] A. Litvinenko, R. Khymyn, V. Tyberkevych, et al. Tunable Magnetoacoustic Oscillator with Low Phase Noise. *Physical Review Applied* 15, 034057 (2021).

Investigation of ultrafast magneto-acoustic interactions in ferromagnetic cobalt/nickel multilayers

Valentin Cherruault[1,*], Corentin Pfaff[2], Thomas Hauet[2], Karine Dumesnil[2], Jon Gorchon[2], Abdelmadjid Anane[3], Stephane Andrieu[2], and Thomas Pezeril[1,4,*]

[1]*Institut de physique de Rennes, UMR CNRS 6251, Rennes, France*
[2]*Institut Jean Lamour, UMR CNRS 7198, Nancy, France*
[3]*Unité Mixte de Physique, CNRS / Thales, Palaiseau, France*
[4]*Department of Chemistry, Massachusetts Institute of Technology, Cambridge, MA USA*
*valentin.cherruault@univ-rennes.fr,
thomas.pezeril@univ-rennes.fr

Understanding the role of the lattice degrees of freedom in the magnetization state of ferromagnetic materials at ultrafast timescales is crucial for the development of new energy-efficient technological applications merging spintronics and high frequency ultrasounds. In the present study, we use femtosecond lasers to pump and probe epitaxial ferromagnetic superlattices $[Co_x/Ni_3]$ stacked as follows: $11\bar{2}0$ sapphire substrate / V (5 nm) / Au (20 nm) / Ni (3) / $[Co_x/Ni_3]$ ×5 / MgO (100 nm). Each nickel layer is three atoms thick while the cobalt layers have a variable height x from one to three atoms. Interfacial anisotropy in such superlattice creates perpendicular magnetic anisotropy [1, 2]. The ultrashort laser pump pulse partially demagnetizes the sample [3] and generates as well ultrashort acoustic waves in the vanadium metallic layer through ultrafast electronic heating [4]. These two concomitant effects enable us to investigate the remagnetization process upon demagnetization and the influence of the lattice deformation on the magnetization state. These two contributions to the magnetization state perturbation can be disentangled in time thanks to the gold layer that delays the acoustic wave generated in vanadium and injected in the magnetic layer, from the instantaneous partial laser demagnetization. With out-of-plane magnetization orientation, the acoustic pulses do not create any magnetic torque and act as a non-thermal magnetic stimuli. The absence of magnetic torque is sustained by the absence of magnetic precession in the results. The perturbation of the sample magnetization is optically probed by polar MOKE (magneto-optic Kerr effect) measurements. MOKE measurements of the probe light polarization provide immediate information on the magnetization variation at femtosecond timescale.

We experimentally observe a large transient MOKE modification of the probe polarization that corresponds to the time-of-flight of the picosecond acoustic pulse excited in vanadium and traversing the $[Co_x/Ni_3]$ superlattice. We experimentally reveal that this MOKE signal that does not depend on the magnetic state of the sample drastically depends on the in-plane sample orientation. These experimental results are assigned to complex interplay between ultrafast acousto-optic, ultrafast magneto-acoustic and ultrafast magneto-optic interactions that render the investigation of the direct coupling between spins and the lattice intricate. To our knowledge, this MOKE response is not compatible with classical magnetostriction, and points towards a linear magnetoelastic coupling, commonly known as piezomagnetism. This hint of piezomagnetism in a multilayered ferromagnetic material opens the door to a new way of controlling magnetism via ultrafast stresses, and should trigger new studies seeking a better understanding and further enhancement of this effect. Our findings are modeled analytically and numerically for a better understanding of the complexity of these fundamental interactions and to shine light on under-explored pathways for ultrafast spin-logic manipulation based on ultrafast acoustic waves.

References

[1] S. Girod et al. Strong perpendicular magnetic anisotropy in Ni/Co(111) single crystal superlattices. *Appl. Phys. Lett.* 94, 1–3 (2009).

[2] S. Andrieu et al. Co/Ni multilayers for spintronics: high spin-polarization and tunable magnetic anisotropy. *Phys. Rev. Mat.* 2 (2018).

[3] B. Koopmans et al. Explaining the paradoxical diversity of ultrafast laser-induced demagnetization. *Nature materials* 9, 259–265 (2009).

[4] C. Thomsen, H. T. Grahn, H. J. Maris, and J. Tauc. Surface generation and detection of phonons by picosecond light pulses. *Phys. Rev. B* 34, 4129–4138 (1986).

Spin waves propagation in an FeN guide induced by the excitation of an inserted Fe pad

Igor Ngouagnia[1,*], Louis Christienne[2], Jean-Yves Duquesne[2], Pauline Rovillain[2], Massimiliano Marangolo[2], Abdelmadjid Anane[3], Yves Henry[1], and Daniel Stoeffler[1]

[1]*IPCMS, Université de Strasbourg, CNRS, Strasbourg, France*
[2]*INSP, Sorbonne Université, CNRS, Paris, France*
[3]*Unité Mixte De Physique, CNRS, Thales, Université Paris-Saclay, Palaiseau, France*
*igor.ngouagnia@ipcms.unistra.fr

During the last decade, a number of basic building blocks of the magnonic paradigm have been experimentally demonstrated such as the magnon-transistor [1], the spin-torque-induced amplification of spin waves (SWs) [2] and the magnonic diode [3]. However, up to now, those building blocks intrinsically consume much more energy per logic-gate than their CMOS counterparts as they still rely on Ampere fields for signal transduction and amplification. An innovative approach based on elastic strain can be used to overcome this issue, allowing an energy efficient and large scale integration of voltage controlled magnonic circuits. Indeed, taking advantage of the resonant MagnetoElastic Coupling (MEC), Surface Acoustic Waves (SAWs) can be used to excite Ferromagnetic Resonance (FMR) of Fe films epitaxially grown on top of a piezoelectric substrate, even at low frequencies (≤ 1 GHz) [4].

The goal of this study is therefore to use SAW and resonant MEC to trigger magnetization precession in a small Fe pad (few hundreds of nm long), in order to excite a propagating SW in a waveguide connected to the pad (see Fig. 1(a)). Thus, the traditional inductive antennas found in magnonic devices are replaced here by SAW-induced SW emission. To prevent the waveguide from being affected by the travelling SAW, one uses an original approach consisting in slightly modifying the SWs spectrum by implanting N-atoms in the pristine Fe structure. Such implantation indeed leads to a high level of tunability of the Fe film magnetic anisotropy, allowing the desired control of the SW dispersion [5].

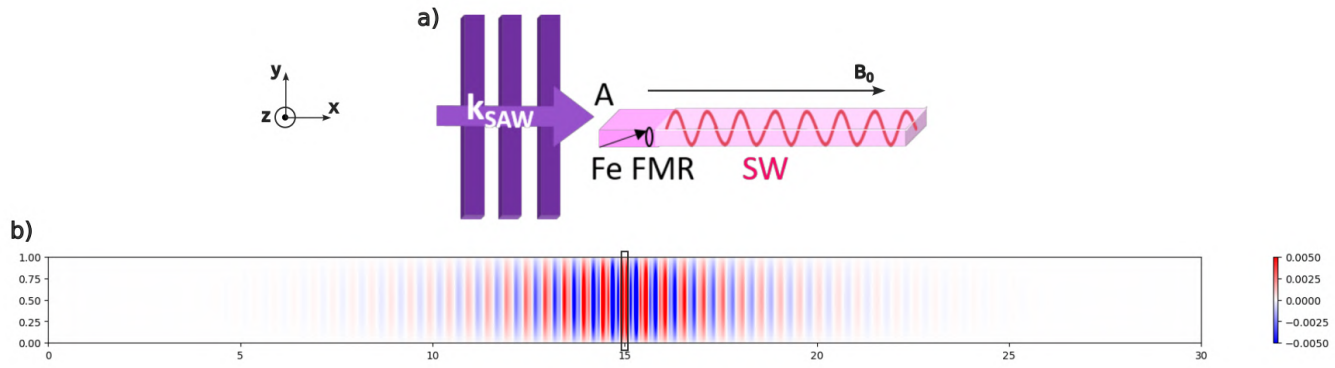

Figure 1: (a) Sketch of a simple SW emitter with an Fe pad inserted in an FeN waveguide. Propagation of SWs in the waveguide thanks to the resonant excitation of magnetization precession in the Fe pad by SAWs. An external magnetic field B_0 is applied along the SAW propagation direction (the x-axis). (b) Snapshot of the dynamic transverse component m_y of the magnetization in the mid-plane along z, obtained from micromagnetic simulation using Mumax3. The waveguide is $L_x = 30\,\mu$m long, $L_y = 1\,\mu$m large and $L_z = 53$ nm thick. The location of the $L_{Fe} = 200$ nm long Fe pad at the centre of the waveguide is shown in the figure. The pad is excited out-of resonance at a frequency of 4 GHz with an homogeneous pumping field of 0.1 mT for $B_0 = 30$ mT.

Fig. 2(a) shows the simulated resonance spectrum of a 200 nm and 400 nm long pad at the centre of the FeN waveguide, for a static field $B_0 = 30$ mT along the x-axis. The dispersion curve of the corresponding waveguide is shown in Fig. 2(b). The resonance modes of the 200 nm pad indicated by the red dashed lines are below or at the minimum frequency of the waveguide dispersion curve $f_{min} \approx 3$ GHz. Thus, by exciting the pad at these frequencies with a small uniform rf field, there is no propagation of spin waves within the waveguide. Two solutions can be used to overcome this issue. The first approach is to vary the size of the pad, which can result in resonant modes in the pad above f_{min}, as shown in the case of the 400 nm long pad with a resonance mode around 4 GHz. The second approach is to excite the 200 nm pad out-of-resonance at a frequency higher than f_{min}. Fig. 1(b) shows a simulation result when using this approach where the 200 nm pad has been excited at 4 GHz. In this case, it is possible to excite and propagate spin waves over distances larger than 5 µm. All these simulation results were obtained by exciting the pad with a magnetic field, but the ultimate goal is to mimic in Mumax3 the real experimental excitation with the SAW.

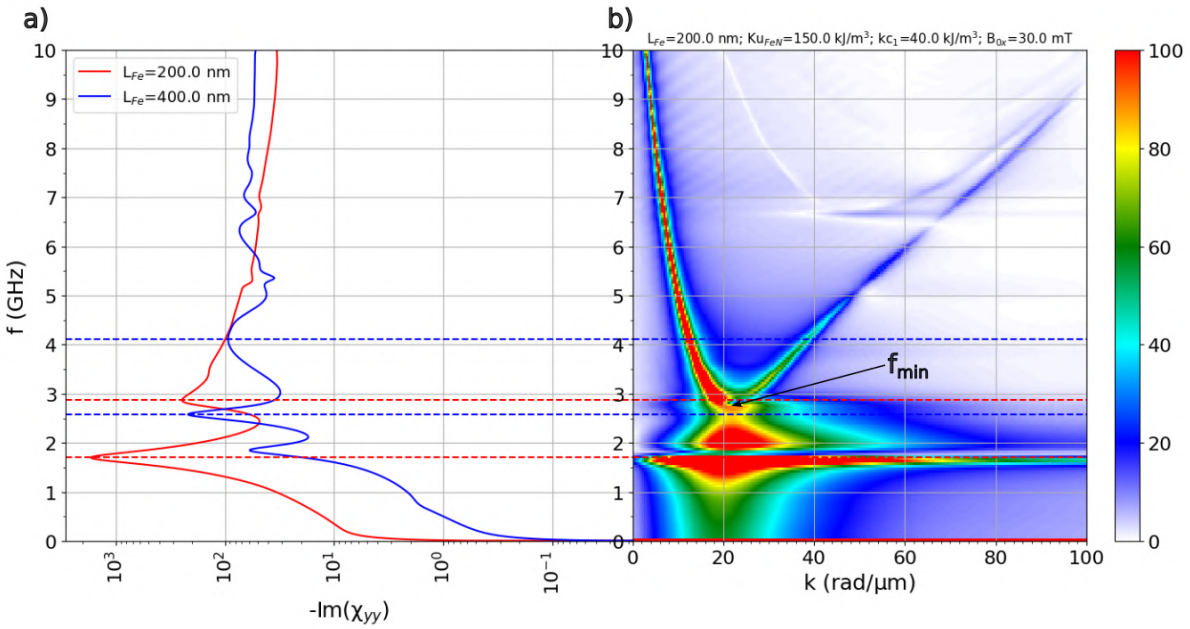

Figure 2: (a) Resonance spectra of two Fe pads of lengths 200 and 400 nm, located at the centre of the waveguide. (b) Dispersion curve of the waveguide of Fig. 1(b) with the 200nm long pad at its centre. The high intensity around $f \approx 1.8$ GHz and $k \approx 22$ rad/µm corresponds to the Fe pad resonance. The red and blue dashed lines correspond respectively to the frequencies of the resonance modes of the 200 and 400 nm long pads. The values of the uniaxial and cubic anisotropy constants of the FeN guide are given and are different from those of the Fe pad $Ku_{Fe} = 100\,\mathrm{kJ/m^3}$ and $Kc_{1_{Fe}} = 49.6\,\mathrm{kJ/m^3}$

.

Acknowledgments

The authors acknowledge support from the Agence Nationale de la Recherche Grant No. ANR-22-CE24-0015 SACOUMAD.

References

[1] Andrii V. Chumak, Alexander A. Serga, and Burkard Hillebrands. Magnon transistor for all-magnon data processing. *Nature Communications* 5 (2014).

[2] M. Evelt, V. E. Demidov, V. Bessonov, et al. High-efficiency control of spin-wave propagation in ultra-thin yttrium iron garnet by the spin-orbit torque. *Applied Physics Letters* 108, 172406 (2016).

[3] Matías Grassi, Moritz Geilen, Damien Louis, et al. Slow-Wave-Based Nanomagnonic Diode. *Phys. Rev. Appl.* 14, 024047 (2 2020).

[4] J.-Y. Duquesne, P. Rovillain, C. Hepburn, et al. Surface-Acoustic-Wave Induced Ferromagnetic Resonance in Fe Thin Films and Magnetic Field Sensing. *Phys. Rev. Appl.* 12, 024042 (2 2019).

[5] T. Amarouche, L.-C. Garnier, M. Marangolo, et al. Influence of ion implantation parameters on the perpendicular magnetic anisotropy of Fe-N thin films with stripe domains. *Journal of Applied Physics* 121, 243903 (2017).

Effets de courbure et de déformation mécanique sur la distribution de l'aimantation de nano-objets

M. Khelif[1,*], N. Challab[1], S. Chiroli[1], D. Faurie[1], F. Zighem[1], and M. Haboussi[1]

[1]*LSPM-CNRS UPR3407,Université Sorbonne Paris Nord, Villetaneuse, France*
maya.khelif1@univ-paris13.fr

Après avoir fait l'objet de nombreuses études fondamentales et donné lieu à de multiples applications au cours du siècle passé (notamment dans les années 60-70), les effets magnéto-mécaniques connaissent un réel regain d'intérêt ces dernières années, en raison de leur implication dans de nouvelles thématiques phares du nanomagnétisme telles que la « straintronique-magnétique ». Dans cette thématique, des déformations élastiques (statiques) imposées au système permettent de contrôler certaines propriétés magnétiques de celui-ci. L'influence de ces effets magnétoélastiques est aussi très étudiée dans les dispositifs magnétiques flexibles, généralement composés d'un système magnétique déposé sur un substrat polymère, dont les applications vont d'objets de la vie quotidienne aux dispositifs microélectroniques.

Par ailleurs, de nombreuses études théoriques et numériques récentes ont montré que des objets magnétiques fortement courbés pouvaient donner naissance à des textures magnétiques complexes. Ces effets suscitent un fort enthousiasme dans la communauté du magnétisme. Une question centrale des nouvelles recherches qui en résultent, est comment les caractéristiques géométriques telles que la courbure, l'épaisseur, ou bien matérielles comme la qualité de l'interface, ou plus généralement la déformation mécanique et son hétérogénéité impactent voire contrôlent-elles les changements des propriétés magnétiques des systèmes étudiés ainsi que les nouveaux phénomènes (magnétiques) qu'elles génèrent. A l'heure actuelle, seuls les effets géométriques sont généralement pris en compte dans les modélisations théoriques et numériques d'objets magnétiques courbés. Pourtant, de tels systèmes sont nécessairement soumis à des déformations mécaniques dans la réalité, entraînant des effets magnétiques (magnéto-mécaniques) additionnels qui viennent se rajouter aux purs effets dus à la géométrie initiale.

Nous avons développé un outil de simulations numériques sous COMSOL Multiphysics® permettant de mettre en évidence les effets de courbure sur le magnétisme des objets étudiés en présence ou en absence de déformation mécanique. Cet outil est basé sur la résolution des équations de la mécanique du solide couplées à celles du micromagnétisme (équation de Landau-Lifshitz-Gilbert) dans un cadre non linéaire. Des résultats numériques seront présentés pour montrer la capacité prédictive de l'outil numérique développé.

Propriétés magnéto-mécaniques de couches minces sur substrats flexibles mesurées par MOKE *in situ*

Hatem Ben Mahmoud[1,*], Damien Faurie[1], Pierre-Olivier Renault[2], and Fatih Zighem[1]

[1]*LSPM-CNRS, Université Sorbonne Paris Nord, France*
[2]*Pprime Institute, CNRS-Université de Poitiers, France*
hatem.benmahmoud@sorbonne-paris-nord.fr

Ces dernières années, la recherche dans le domaine de l'électronique extensible et flexible a gagné en importance, notamment dans le domaine des systèmes magnétiques fabriqués sur des substrats flexibles [1]. Ces systèmes subissent diverses déformations pendant leur utilisation quotidienne. Dans ce contexte, l'un des principaux défis est de comprendre l'effet de l'endommagement sur ces systèmes lors de déformations importantes et d'établir la relation entre les phénomènes mécaniques et le comportement magnétique, en exploitant le couplage magnéto-élastique [2]. Pour étudier ces phénomènes, nous avons développé deux nouveaux dispositifs expérimentaux qui combinent un magnétomètre à effet Kerr magnéto-optique (MOKE) et une machine de traction uniaxiale, ainsi qu'un autre dispositif avec une machine de traction biaxiale couplée à la diffraction des rayons X (XRD). Ces dispositifs permettent de suivre l'évolution des propriétés magnétiques des films minces et des nanostructures en réponse aux contraintes appliquées, jusqu'à une déformation d'environ 10%. L'objectif est de provoquer des phénomènes mécaniques irréversibles tels que la plasticité et la formation de fissures, afin de différencier les effets potentiels de la magnétostatique et de la magnétoélasticité.

Nous avons étudié des films minces magnétiques présentant différents coefficients de magnétostriction, y compris un film mince avec une magnétostriction nulle. Parmi ces films, nous avons examiné le cobalt ($\lambda = -14\ 10^{-6}$), le $Ni_{78}Fe_{22}$ ($\lambda = +1.5\ 10^{-6}$) et le $Ni_{80}Fe_{20}$ ($\lambda \approx 0$), qui ont été déposés sur une couche de tungstène de différentes épaisseurs, puis sur un substrat en Kapton (50µm).

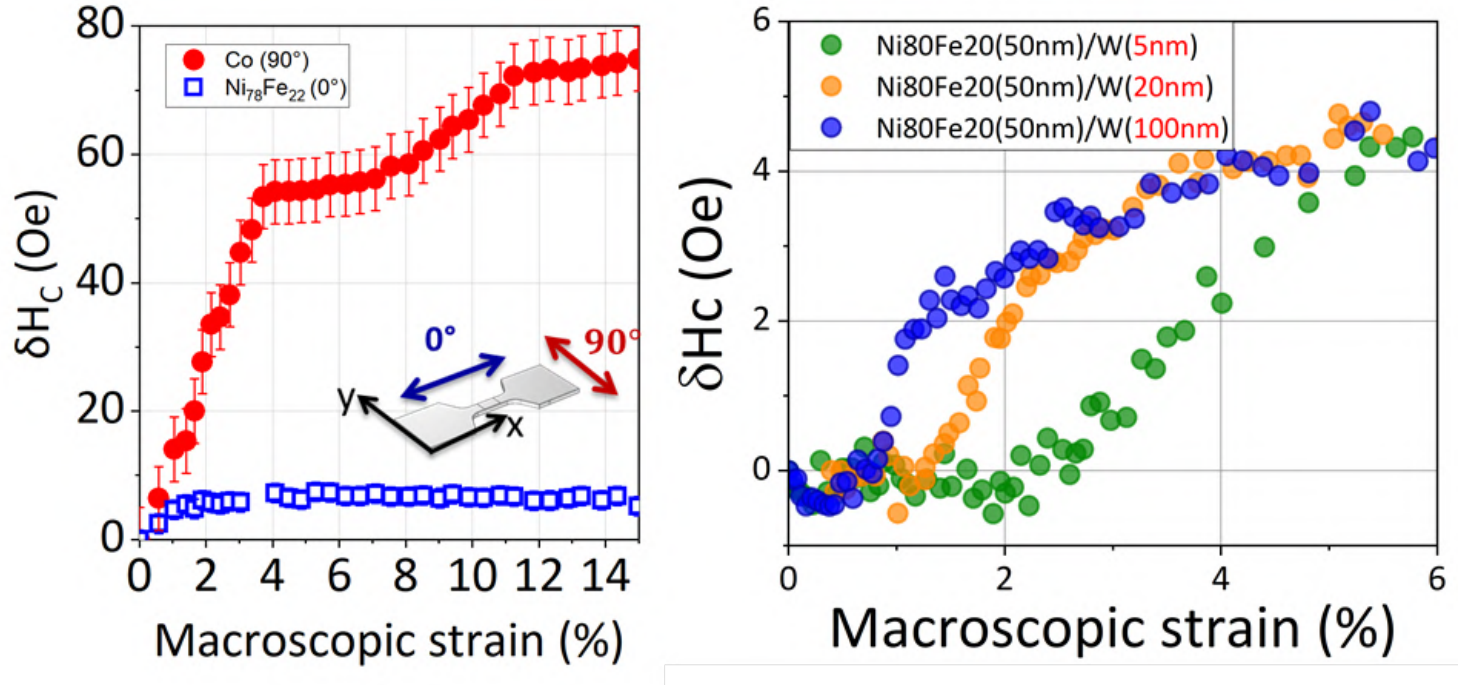

Figure 1: (a) La variation du champ coercitif (H_c) en fonction de la déformation appliquée pour le cobalt (Co) et le $Ni_{78}Fe_{22}$ d'épaisseur 50 nm déposée sur Kapton (127 µm) en essai uniaxial (b) la variation du champ coercitif (H_c) en fonction de la contrainte appliquée pour le $Ni_{80}Fe_{20}$ (50nm)/W avec différentes épaisseurs déposée sur kapton(50µm) en essai biaxial.

La figure 1-a présente la variation du champ coercitif (H_c) en fonction de la déformation appliquée pour le cobalt (Co) et le $Ni_{78}Fe_{22}$ (50 nm) en essai uniaxial. Pour le Co, H_c varie linéairement avec la déformation dans le domaine élastique (0-3.7%). À partir de 3.7%, le phénomène de fissuration multiple entraîne une évolution non linéaire de H_C. En ce qui concerne le $Ni_{78}Fe_{22}$, l'évolution globale de H_C est nettement plus faible dans le régime élastique et de fissuration multiple (8 Oe au lieu de 80 Oe pour le film de Co). Cela indique que le développement des fissures joue un rôle mineur dans le

comportement magnétique des films faiblement magnétostrictifs. La figure 1-b présente la variation du champ coercitif (H_c) en fonction de la contrainte appliquée pour le $Ni_{80}Fe_{20}$ (50nm) avec différentes épaisseurs de W en essai biaxial. Cette évolution dépend de l'effet de l'épaisseur de W. Plus l'épaisseur est grande, plus la fissuration se produit tôt et les fragments sont de taille importante [3]. Ceci est corrélé à la taille des fragments observée ex situ.

Nous présenterons le développement instrumental du dispositif (machine de traction couplée au magnétomètre) ainsi que les mécanismes sous-jacents aux propriétés mesurées pour différents systèmes.

References

[1] M Melzer, D Makarov, and O G Schmidt. A review on stretchable magnetic field sensorics. *Journal of Physics D: Applied Physics* 53, 083002 (2019).

[2] F Zighem and D Faurie. A review on nanostructured thin films on flexible substrates: links between strains and magnetic properties. *Journal of Physics: Condensed Matter* 33, 233002 (2021).

[3] Oleksandr Glushko, Marlene Mühlbacher, Christoph Gammer, et al. Exceptional fracture resistance of ultrathin metallic glass films due to an intrinsic size effect. *Scientific Reports* 9 (2019).

Generation of circulating cavity magnon polaritons in a compact geometry resonator

Guillaume Bourcin[1, 2], Jeremy Bourhill[3], Maxime Ardisson[1, 2, 4], David Spenato[5], David Dekadjevi[5], Jean-Philippe Jay[5], Alain Fessant[5], Isabella Boventer[4], Romain Lebrun[4], Vincent Vlaminck[1,2], and Vincent Castel[1,2]

[1]*IMT Atlantique, Technopole Brest-Iroise, CS 83818, Brest Cedex 3 29238, France*
[2]*Lab-STICC, NSF (UMR 6285), CNRS, Technopole Brest-Iroise, CS 83818, Brest Cedex 3 29238, France*
[3]*Quantum Technologies and Dark Matter Research Lab, Department of Physics, University of Western Australia, 35 Stirling Highway, Crawley, Western Australia 6009, Australia*
[4]*Thales Research and Technologies, Palaiseau, France*
[5]*Laboratoire d'optique et de magnétisme OPTIMAG, Brest, France*
*vincent.castel@imt-atlantique.fr

We have recently demonstrated the generation of circularly polarised unidirectional cavity magnon polaritons in a torus cavity [1]. This was achieved by the observation of a three-mode interaction picture when the magnetic resonance of a 1.8 mm YIG sphere and a cavity resonance were tuned coincident in frequency and the sphere is positioned at precise radial locations. The confirmation of predicted results [2] demonstrates the feasibility of a proposed multiple sphere setup, in which the magnets are placed along the same radial line and will coherently couple to one another, generating a high-power unidirectional photon beam with high coherence and narrow bandwidth.

To test these hypotheses, we recently designed and fabricated a compact torus cavity using SIW technology as shown in Fig.1. SIW stands for substrate integrated waveguide, which means that by increasing the dielectric permittivity of the medium carrying the electromagnetic waves, it is possible to reduce the size of the devices. Note that the multiple sphere configuration was not possible in the cavity from [1] due to its external diameter (60 mm). The reduction of the SIW cavity to an external diameter of 36 mm will permit to apply a uniform magnetic across the entire system. The frequency mode of interest is the second azimuthal harmonic of the TE mode of the cavity, resonating at 10.8 GHz, same as [2]. Here, we will present frequency-domain simulations and room temperature measurements of two- and three-port devices for a single and multiple YIG sphere setup.

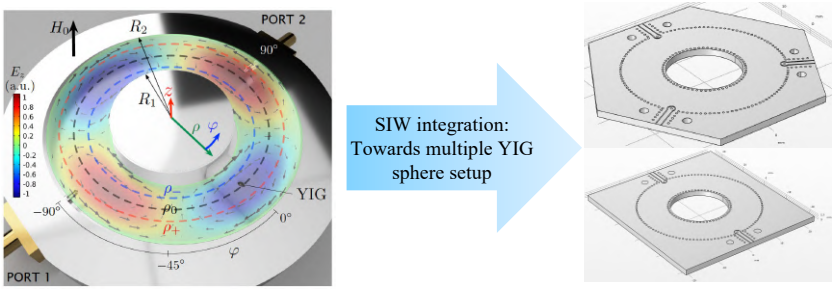

Figure 1: Compact torus cavity in SIW technology

Acknowledgments

This work is part of the research program supported by the CPER Project SpaceTechDroneTech, by Brest Métropole, and the ANR project ICARUS (ANR-22-CE24-0008-03).

References

[1] Jeremy Bourhill, Weichao Yu, Vincent Vlaminck, et al. Generation of Circulating Cavity Magnon Polaritons. *Phys. Rev. Appl.* 19, 014030 (1 2023).

[2] Weichao Yu, Tao Yu, and Gerrit E. W. Bauer. Circulating cavity magnon polaritons. *Phys. Rev. B* 102, 064416 (6 2020).

Spincavitronics System: Engineering Level Attraction in Multimode System

Guillaume Bourcin[1, 2, *], Jeremy Bourhill[3], Maxime Ardisson[1, 2, 4], Isabella Boventer[4], Romain Lebrun[4], Vincent Vlaminck[1, 2], and Vincent Castel[1, 2]

[1]*IMT Atlantique, Technopole Brest-Iroise, CS 83818, Brest Cedex 3 29238, France*
[2]*Lab-STICC, NSF (UMR 6285), CNRS, Technopole Brest-Iroise, CS 83818, Brest Cedex 3 29238, France*
[3]*Quantum Technologies and Dark Matter Research Lab, Department of Physics, University of Western Australia, 35 Stirling Highway, Crawley, Western Australia 6009, Australia*
[4]*Thales Research and Technologies, Palaiseau, France*
guillaume.bourcin@imt-atlantique.fr

Level attraction for photon-magnon coupling in the magnonic system has been observed experimentally very recently [1]. This type of coupling has various potential applications, such as backscattering isolation, non-reciprocal wave propagation and unidirectional signal amplification [2]. The nature of this coupling is different from that of coherent coupling leading to level repulsion. A different approach is therefore required to observe it. Among the systems known to generate level attraction are dissipative coupled systems [3] and two-tone driving [4]. These two systems are the most recent experiments to observe level attraction. The first system is called "open cavity" and involves travelling waves, while the second involves two phase-shifted drives for each oscillator (being the magnon and the photon). Here, we present a multimode system, which is a "closed" system involving level attraction [5]. The aim of this study is to identify the parameters that enable the transition from level repulsion to level attraction, so as to design and optimize cavities for all types of use.

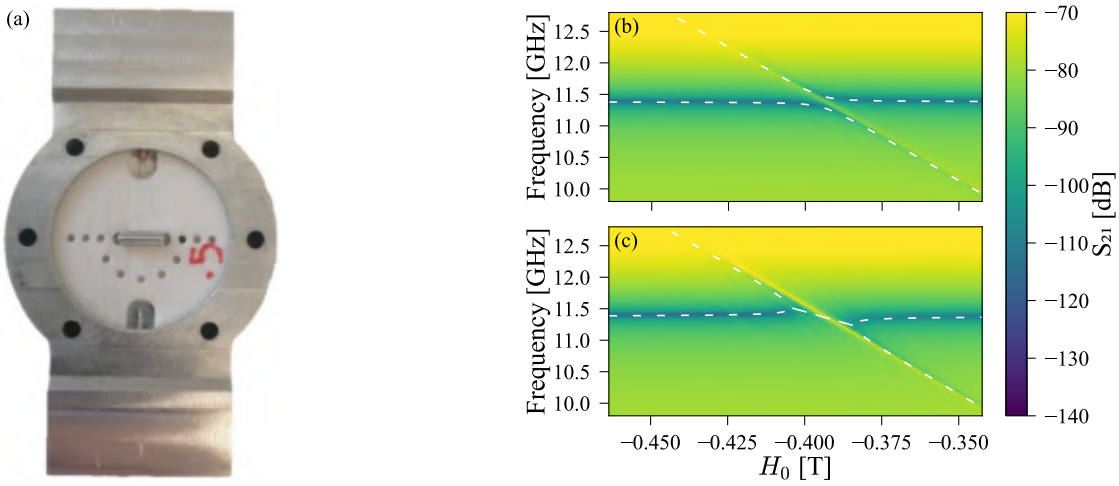

Figure 1: 3D printed cavity in (a); and measurements at RT of the transmission spectra of levels repulsion and attraction vs the frequency and the applied static magnetic field H_0 in (b) and (c), respectively.

The hybrid system presented here consists of a double re-entrant cavity and a commercial YIG single crystal sphere of 1 mm in diameter (see Fig.1 (a)). A dielectric with a permittivity of 10 is placed between the two posts allowing to generate an antiresonance in the S_{21} parameter. The transmission probe must be placed at the antiresonance to observe level attraction. Depending on the position of the YIG sphere in the cavity, repulsion or attraction of the levels can be observed as shown in Fig.1 (b) and (c), respectively.

Acknowledgments

This work is part of the research program supported by the CPER Project SpaceTechDroneTech, by Brest Métropole, and the ANR project ICARUS (ANR-22-CE24-0008-03).

References

[1] M. Harder, Y. Yang, B. M. Yao, et al. Level Attraction Due to Dissipative Magnon-Photon Coupling. *Physical Review Letters* 121, 137203 (2018).

[2] Yi-Pu Wang and Can-Ming Hu. Dissipative couplings in cavity magnonics. *Journal of Applied Physics* 127, 130901 (2020).

[3] Bimu Yao, Tao Yu, Xiang Zhang, et al. The microscopic origin of magnon-photon level attraction by traveling waves: Theory and experiment. *Physical Review B* 100, 214426 (2019).

[4] Isabella Boventer, Christine Dörflinger, Tim Wolz, et al. Control of the coupling strength and linewidth of a cavity magnon-polariton. *Physical Review Research* 2, 013154 (2020).

[5] J W Rao, C H Yu, Y T Zhao, et al. Level attraction and level repulsion of magnon coupled with a cavity anti-resonance. *New Journal of Physics* 21, 065001 (2019).

Poster 2.50, November 15th, 10h50–13h00

Spincavitronics System: Approaching Deep-Strong Coupling

Guillaume Bourcin[1, 2, *], Jeremy Bourhill[3], Vincent Vlaminck[1, 2], and Vincent Castel[1, 2]

[1]*IMT Atlantique, Technopole Brest-Iroise, CS 83818, Brest Cedex 3 29238, France*
[2]*Lab-STICC, NSF (UMR 6285), CNRS, Technopole Brest-Iroise, CS 83818, Brest Cedex 3 29238, France*
[3]*Quantum Technologies and Dark Matter Research Lab, Department of Physics, University of Western Australia, 35 Stirling Highway, Crawley, Western Australia 6009, Australia*
*guillaume.bourcin@imt-atlantique.fr

Over the last decade, quantum systems offering new computational and sensing capabilities have emerged [1]. One of these promising hybrid systems involves the interaction between photons and magnons. This interaction is quantitatively known by the strength coupling g and furthermore by its ratio with the cavity frequency g/ω. It exists three different domains of this ratio: the Strong Coupling (SC) for $g/\omega < 0.1$; the Ultra-Strong Coupling (USC) for $0.1 < g/\omega < 1$; and the Deep-Strong Coupling (DSC) for $g/\omega > 1$. One of the objectives of this last decade is to achieve the USC, and to approach the DSC [2]. Here, we present a tuneable hybrid system which makes possible experimental observation of a coupling regime from USC to DSC at room temperature (RT).

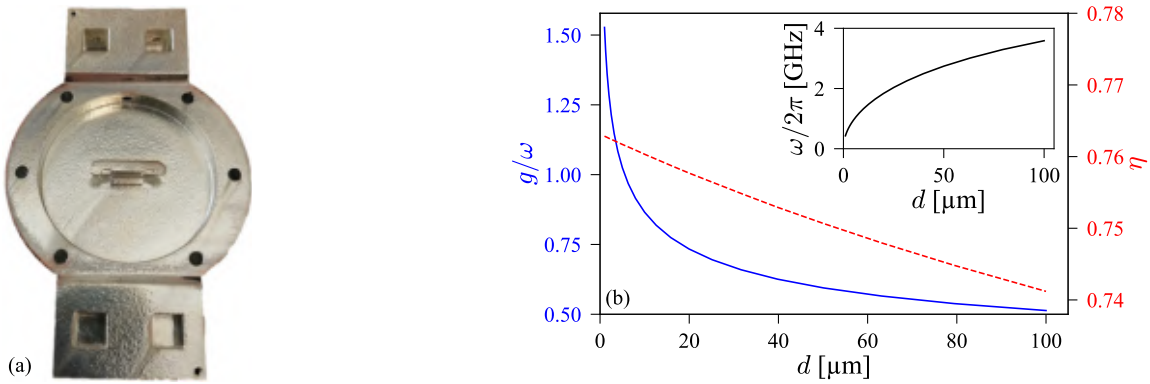

Figure 1: 3D printed cavity in (a); and the evolution of the ratio g/ω and the filling factor η vs the gap d in (b). Inset: Evolution of the cavity frequency vs d.

The hybrid system presented here is made of a double re-entrant cavity and a commercial single crystal of YIG (see Fig.1 (a)). This cavity has two different low-frequency modes. The magnetic field of the lower mode is not focused inside the YIG and is therefore not useful for the study. On the other hand, the magnetic field of the upper mode is almost totally focused inside the YIG. This allows us to recently demonstrate the experimental observation of a coupling regime from SC to USC [3].

Two new features have been added to this new device in order to observe DSC. First, to approach the DSC, a plate at the top of one of the posts reduces ω for a fixed distance d between the top of the post and the cavity. Second, we were able to filter out the low-frequency photon mode completely. This is useful for avoiding overlap between the hybrid modes and the lower photonic mode. It is also possible to adjust the g/ω ratio by decreasing d, which will decrease ω without changing g, achieving DSC for $d = 3$ μm as shown in Fig.1 (b).

Acknowledgments

This work is part of the research program supported by the CPER Project SpaceTechDroneTech, by Brest Métropole, and the ANR project ICARUS (ANR-22-CE24-0008-03).

References

[1] Dany Lachance-Quirion, Yutaka Tabuchi, Arnaud Gloppe, Koji Usami, and Yasunobu Nakamura. Hybrid quantum systems based on magnonics. *Applied Physics Express* 12, 070101 (2019).

[2] I.A. Golovchanskiy, N.N. Abramov, V.S. Stolyarov, et al. Approaching Deep-Strong On-Chip Photon-To-Magnon Coupling. *Physical Review Applied* 16, 034029 (2021).

[3] Guillaume Bourcin, Jeremy Bourhill, Vincent Vlaminck, and Vincent Castel. Strong to ultrastrong coherent coupling measurements in a YIG/cavity system at room temperature. *Physical Review B* 107, 214423 (2023).

Poster 2.51, November 15th, 10h50–13h00

The coupling phase in microwave cavity magnonics

Alan Gardin[1,2,3,*], Jeremy Bourhill[2,4], Vincent Vlaminck[2,3], Christian Person[2,3], Christophe Fumeaux[5], Giuseppe Tettamanzi[1,6], and Vincent Castel[2,3]

[1]*School of Physics, The University of Adelaide, Adelaide SA 5005, Australia*
[2]*IMT Atlantique, Technopole Brest-Iroise, CS 83818, 29238 Brest Cedex 3, France*
[3]*Lab-STICC (UMR 6285), CNRS, Technopole Brest-Iroise, CS 83818, 29238 Brest Cedex 3, France*
[4]*ARC Centre of Excellence for Engineered Quantum Systems and ARC Centre of Excellence for Dark Matter Particle Physics, , Department of Physics, University of Western Australia, 35 Stirling Highway, Crawley, Western Australia 6009, Australia*
[5]*School of Electrical and Electronic Engineering, The University of Adelaide, Adelaide SA 5005, Australia*
[6]*School of Chemical Engineering and Advanced Materials, The University of Adelaide, Adelaide SA 5005, Australia*
*alan.gardin@imt-atlantique.fr

The coherent interaction between microwave photons and magnons is well understood and originates from the Zeeman coupling between spins and a magnetic field [1, 2]. In the language of second-quantisation, the magnon/photon interaction Hamiltonian in the rotating wave approximation can be written [3, 4]

$$H_I = \hbar g(e^{i\varphi} c m^\dagger + e^{-i\varphi} c^\dagger m), \tag{1}$$

where c (m) are the annihilation operator for the cavity (magnon) mode. Interestingly, the coupling phase factor φ can usually be neglected in the standard configurations considered in cavity magnonics, as described in Fig. 1.

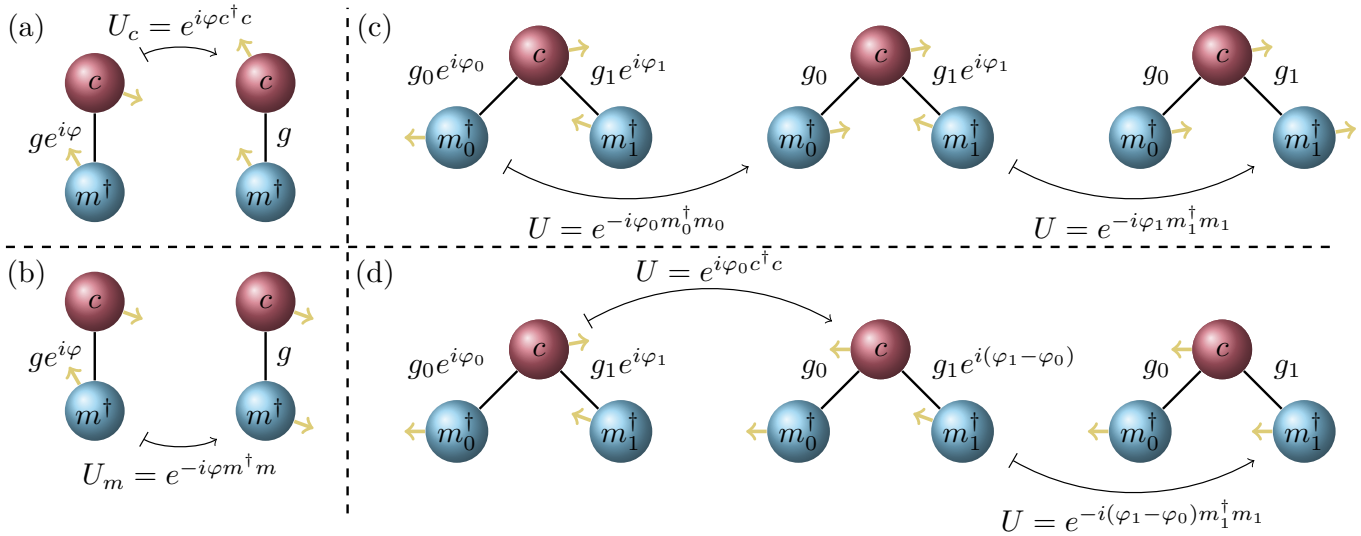

Figure 1: In systems that are not loop-coupled, the coupling phase can be neglected. In (a) and (b) we illustrate how the coupling phase φ can be eliminated for a simple magnon/photon system. In (c) and (d), we consider two magnon modes coupling to a single cavity mode, and again the coupling phases can be ignored.

However, if two magnon modes simultaneously couple with two cavity resonances (see Fig. 2), this phase cannot be ignored and changes the physics of the system. We consider two such systems, each differing by the sign of one of the magnon/photon coupling strengths. This simple difference, originating from the various coupling phases in the system, is shown to preserve, or destroy, two potential applications of hybrid photon/magnon systems, namely dark mode memories [5] and cavity-mediated coupling [6]. The observable consequences of the coupling phase in this system is akin to the manifestation of a discrete Pancharatnam–Berry phase [7], which is a signature of a synthetic gauge field.

Acknowledgments

We acknowledge financial support from Thales Australia and Thales Research and Technology. This work is part of the research program supported by the European Union through the European Regional Development Fund (ERDF), the Ministry of Higher Education and Research, the Brittany region through the CPER SpaceTechDroneTech, and the ANR project ICARUS (22-CE24-0008-01).

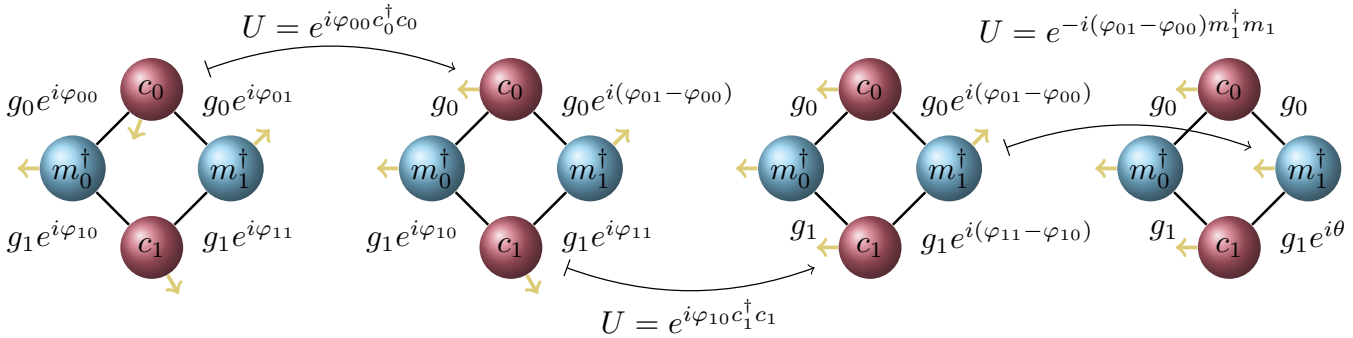

Figure 2: If two magnon modes both simultaneously couple to two cavity modes, the system is loop-coupled. In loop-coupled systems, the coupling phases cannot be ignored and parametrise the physics.

References

[1] Jeremy Bourhill, Vincent Castel, Alexandre Manchec, and Gwendal Cochet. Universal characterization of cavity–magnon polariton coupling strength verified in modifiable microwave cavity. *Journal of Applied Physics* 128, 073904 (2020).

[2] Babak Zare Rameshti, Silvia Viola Kusminskiy, James A. Haigh, et al. Cavity magnonics. *Physics Reports* 979, 1–61 (2022).

[3] Alan Gardin, Jeremy Bourhill, Vincent Vlaminck, et al. Manifestation of the Coupling Phase in Microwave Cavity Magnonics. *Physical Review Applied* 19 (2023).

[4] Graeme Flower, Maxim Goryachev, Jeremy Bourhill, and Michael E Tobar. Experimental implementations of cavity-magnon systems: from ultra strong coupling to applications in precision measurement. *New Journal of Physics* 21, 095004 (2019).

[5] Xufeng Zhang, Chang-Ling Zou, Na Zhu, et al. Magnon dark modes and gradient memory. *Nature Communications* 6 (2015).

[6] Vahram L. Grigoryan and Ke Xia. Cavity-mediated dissipative spin-spin coupling. *Physical Review B* 100 (2019).

[7] Raffaele Resta. Manifestations of Berry's phase in molecules and condensed matter. *Journal of Physics: Condensed Matter* 12, R107–R143 (2000).

Cavity-FMR studies of LPE epitaxial YIG films

Hervé Hurdequint[1,*], Grégoire de Loubens[1], and Jamal Ben Youssef[2]

[1]*SPEC, CEA, CNRS, Université Paris-Saclay, Gif-sur-Yvette, France*
[2]*LabSTICC, CNRS, Université de Bretagne Occidentale, Brest, France*
**herve.hurdequint@universite-paris-saclay.fr*

The recent progress in the elaboration of very thin epitaxial YIG films has brought a renewed interest for exploiting the resonance properties of such films. We highlight below basic results we have obtained in our cavity-FMR studies at X-band (9.725 GHz) on the 3 films whose characteristics are given below. These films correspond to (111) oriented YIG layers deposited by LPE [1] on GGG substrates. We have: F1[YIG58], F2[YIG44], F3[YIG15], with thicknesses in nm. We performed a detailed study of the angular variation of the resonance spectrum (angle θ_H of the dc field with the film normal). A basic observation in these YIG films is that the resonance spectrum corresponds indeed to the superposition of individual resonances (arising from different parts of the film, weakly coupled by the dipolar interactions). We summarize below the results obtained for the main characteristics (lineshape, field for resonance H_{res}, linewidth ΔH) of the principal resonance (central peak of absorption).

Angular variation of H_{res}: results and analysis. In perpendicular (PER) geometry, the resonance condition [2, 3] reads $(\omega/\gamma) = H_{PER} - H_{eff}$, where $H_{eff} = H_i - 2/3H_{an}$, $H_i = 4\pi M - H_A$ designates the total uniaxial anisotropy with $H_A = 2K/M$ (spin-orbit origin) and $H_{an} = 2K_1/M$ is the YIG cubic anisotropy. Taking the measured value for 4πM and the bulk value for H_{an} (- 87 Oe), we get for the 3 virgin YIG films : F1 : $H_i = 1.657$ kOe, hence $(-H_A) = 37$ Oe (easy plane); F2: $H_i = 1.572$ kOe, hence $H_A = 48$ Oe (easy axis); F3: $H_i = 1.570$ kOe, hence $H_A = 130$ Oe (easy axis). One observes thus that the uniaxial perpendicular anisotropy changes sign versus the YIG thickness.

Angular variation of the linewidth ΔH: results and analysis. The linewidth of the principal resonance is the sum of two different contributions: $\Delta H = \Delta + \Delta H_{inh}$. The first one Δ corresponds to the *relaxation* rate of the magnetization vector (related to the intrinsic damping parameter α). The second one is an inhomogeneous width corresponding to a distribution ΔH_{res}. The basic observation (as illustrated on the Figure 1 which displays the angular variation of the peak-to-peak linewidth ΔH_{AB} for F2) is that the linewidth is characterized by a sharp *minimum* for a *specific* orientation θ_H, where it reduces to the intrinsic width Δ. This behavior is well accounted for theoretically [2] and the present work where the theoretical framework will be explicitly described. The inhomogeneous contribution ΔH_{inh}, induced by a distribution $P(H_i)$ [of characteristic width ΔH_i] has been discussed. We highlight basic results derived from the analysis.

Intrinsic damping parameter α for the 3 films: F1[YIG58], F2[YIG44], F3[YIG15]. We get: for F1, $\Delta H_{min} = 1.23$ Oe at $\theta_H \sim 45$ deg corresponding to $\alpha(\text{F1}) = 2.5 \times 10^{-4}$; for F2, $\Delta H_{min} = 1.13$ Oe at $\theta_H \sim 31$ deg leading to $\alpha(\text{F2}) = 2 \times 10^{-4}$; for F3, $\Delta H_{min} = 2.56$ Oe at $\theta_H \sim 36$ deg leading to $\alpha(\text{F3}) = 5.2 \times 10^{-4}$. In summary, the very low values of the damping parameter α found for these LPE very thin epitaxial YIG films illustrate their high quality. The inhomogeneous width observed in PER geometry provides a good estimation of the width ΔH_i of the distribution $P(H_i)$. For F1, we find $\Delta H_i = 2.05$ Oe corresponding to a remarkable low value (1.25×10^{-3}) of the relative inhomogeneity ($\Delta H_i/H_i$) extended to the mm size film.

References

[1] N. Beaulieu, N. Kervarec, N. Thiery, et al. Temperature Dependence of Magnetic Properties of a Ultrathin Yttrium-Iron Garnet Film Grown by Liquid Phase Epitaxy: Effect of a Pt Overlayer. *IEEE Magnetics Letters* 9, 1–5 (2018).

[2] Hervé Hurdequint. FMR studies of ultrathin permalloy layers sandwiched by Al_2O_3. *Journal of Magnetism and Magnetic Materials* 242-245, 521–524 (2002).

[3] Hiroshi Makino and Yasuharu Hidaka. Determination of magnetic anisotropy constants for bubble garnet epitaxial films using field orientation dependence in ferromagnetic resonances. *Mat. Res. Bull.* 16, 957–966 (1981).

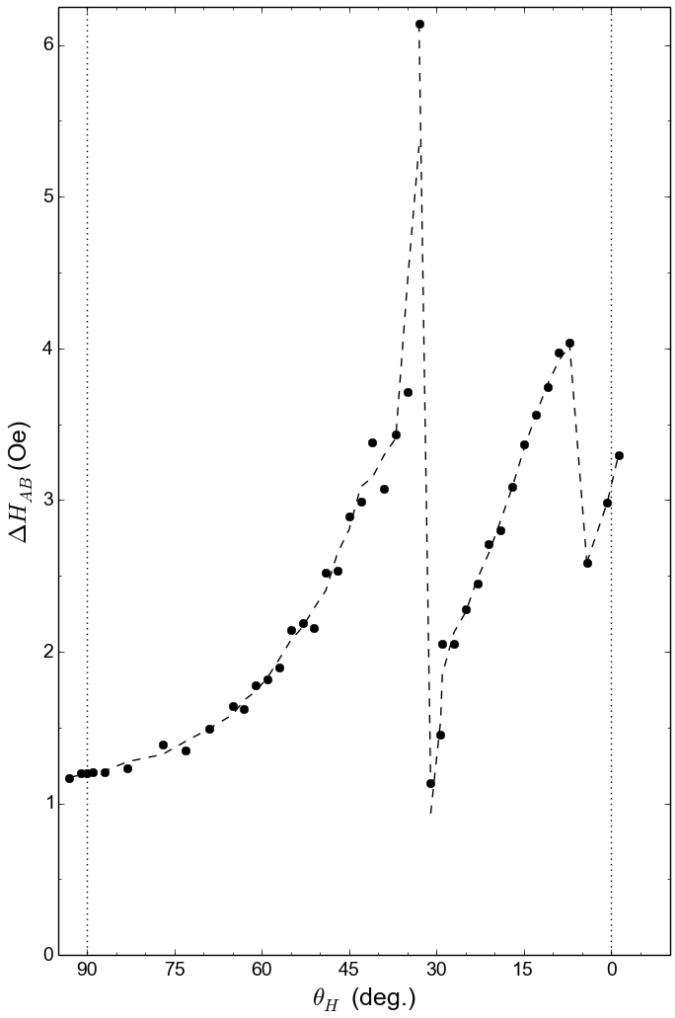

Figure 1: Angular variation of the peak-to-peak linewidth ΔH_{AB} for F2.

Observation of Antiferromagnetic Cavity Magnon Polariton in Cr_2O_3

Maxime Ardisson[1,*], Vincent Castel[1], Romain Lebrun[2], and Isabella Boventer[2]

[1]*IMT Atlantique, Technopole Brest-Iroise, CS 83818, 29238 Brest Cedex 3, France*
[2]*Unité Mixte de Physique CNRS, Thales, Université Paris-Saclay, Palaiseau 91767, France*
*maxime.ardisson@imt-atlantique.fr

Over the last decade, cavity magnonics has attracted a lot of attention. The study of the associated quasi- particle of cavity magnonics, cavity magnon polaritons (CMP), which refer to strongly coupled magnon-photon system, offers new possibilities of sensing and quantum information processing [1, 2] as well as a new interesting platform for disruptive RF applications. Cavity magnonics generally operates with standard ferromagnetic materials like YIG due to its ultra-low magnetic damping. Recent studies have focused on two directions: (i) reaching magnon-photon regime in the quantum regime and (ii) in identifying new approaches to tune the coupling between magnon and photons from dissipative to conservative [3]. Antiferromagnetic materials (AFM) have until now been barely studies in the field of cavity magnonics for two main reasons: their sub-THz and THz frequencies are not easily accessible in standard ferromagnetic resonance measurements, and the dissipation rates of antiferromagnetic excitations are generally large. On the other hand, this higher operating frequency offers the possibility to be less sensitive to temperature fluctuations when operating at low temperature, and the variety of antiferromagnetic modes potentially offers the possibility to achieve bright and dark mode coupling in the same system.

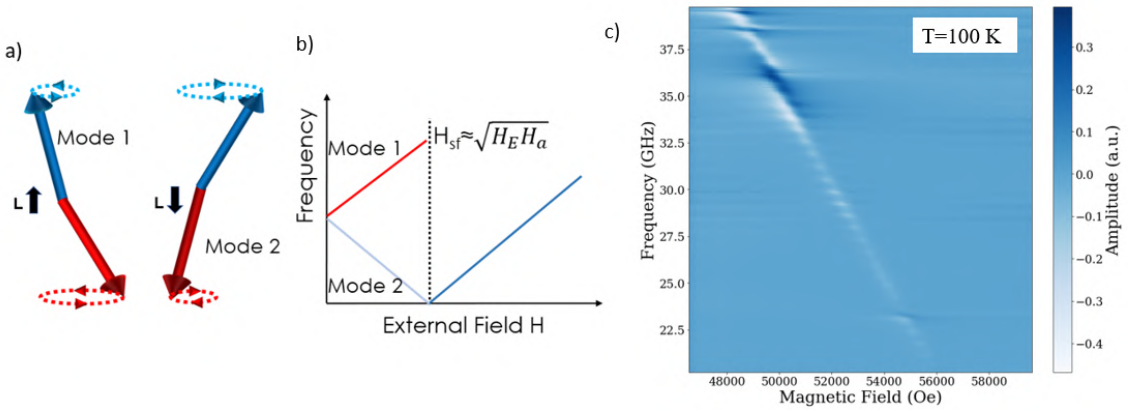

Figure 1: a) Sketch of the orientation of the two circularly polarized modes with different handedness for an easy-axis AFM. b) describes the dependency of ω according to the external field, around the spin flop field HSF with HE and HA the exchange and anisotropy fields respectively. In c) is displayed an exemplary result of the magnon photon coupling in the easy axis AFM Cr_2O_3. The avoided level crossing at 36 GHz is due to the coupling of cavity photon with magnons from the low frequency mode.

Recently, it has been demonstrated that low damping AFMs like iron oxide offer the possibility to reach a strong coupling regime between cavity photons and antiferromagnetic magnons [4, 5]. Here, we propose to extend this approach to another uniaxial antiferromagnet with a low magnetic damping as Cr_2O_3. Cr_2O_3 is an easy axis AFM, displaying two energetically degenerate magnon branches that are left and right-handed circularly polarized. We first investigated the magnon photon coupling in Cr_2O_3 using the left-handed mode shown as Mode 2 in Fig. 1a). Exemplarily, Fig. 1c) shows a measurement at 100 K of which evidences the possibility to also achieve a strong coupling with the left-handed mode of Cr_2O_3, here with a cavity mode around 36 GHZ. Our goal is then to extend this study to the right-handed mode of Cr_2O_3 and demonstrate the possibility to switch on/off the coupling with AFM modes depending on the polarization of the excitation.

Acknowledgments

This work is part of the research program supported by the ANR project ICARUS (ANR-22-CE24-0008-03).

References

[1] Dany Lachance-Quirion, Yutaka Tabuchi, Arnaud Gloppe, Koji Usami, and Yasunobu Nakamura. Hybrid quantum systems based on magnonics. *Applied Physics Express* 12, 070101 (2019).

[2] Babak Zare Rameshti, Silvia Viola Kusminskiy, James A. Haigh, et al. Cavity magnonics. *Physics Reports* 979, 1–61 (2022).

[3] Yutaka Tabuchi, Seiichiro Ishino, Toyofumi Ishikawa, et al. Hybridizing Ferromagnetic Magnons and Microwave Photons in the Quantum Limit. *Physical Review Letters* 113 (2014).

[4] I. Boventer, H. T. Simensen, B. Brekke, et al. Antiferromagnetic Cavity Magnon Polaritons in Collinear and Canted Phases of Hematite. *Physical Review Applied* 19 (2023).

[5] Y. Xiao, X. H. Yan, L. H. Bai, et al. Magnon photon coupling for magnetization antiparallel to the magnetic field. *Physical Review B* 103 (2021).

Poster 2.54, November 15th, 10h50–13h00

THz generation dependence of Co_xFe_{1-x} alloy composition

Harjinder Singh[1, *], Jude C. Stewart[1], Víctor H. Ortiz[2], Ramya Mohan[2], Richard B. Wilson[2], Gregory Malinowski[1], and Jon Gorchon[1]

[1]*Université de Lorraine, CNRS, IJL, F-54000 Nancy, France*
[2]*Department of Mechanical Engineering and Materials Science and Engineering Program, University of California, Riverside, California 92521, USA*
*singh.harjinder9@etu.univ-lorraine.fr

Spintronics-based THz emitters that are driven by spin-to-charge conversion are considered excellent sources of THz radiation owing to their large bandwidth, simple fabrication process, and low power operation compared to standard THz sources. In general, a spintronics-based THz emitter is composed of a ferromagnetic layer (FM) adjacent to a non-magnetic layer (NM). Upon being excited with a femtosecond laser pulse, a thermal gradient is created, which generates hot electrons that will induce a spin current in the FM. The induced spin current flows to adjacent NM material creating a charge current due to the inverse spin Hall effect (ISHE). This results in the THz emission from the NM material [1, 2].

Here, we demonstrate the effect of Co_xFe_{1-x} alloy composition on the THz emission. With this, we are trying to probe the underlying mechanism for magnetization dynamics in the fs time scale with the change in alloy composition. We found that the THz signal has a monotonic decrease with the increase in *x i.e.*, Co concentration. This change in amplitude could be due to the different Curie temperatures (T_c) corresponding to different compositions of Co_xFe_{1-x}. Pratzer *et al.* shows a similar dependence for T_c with the Co concentration in CoFe alloy[3]. Along with this, the results of ultrafast magnetization dynamics will be discussed in this poster.

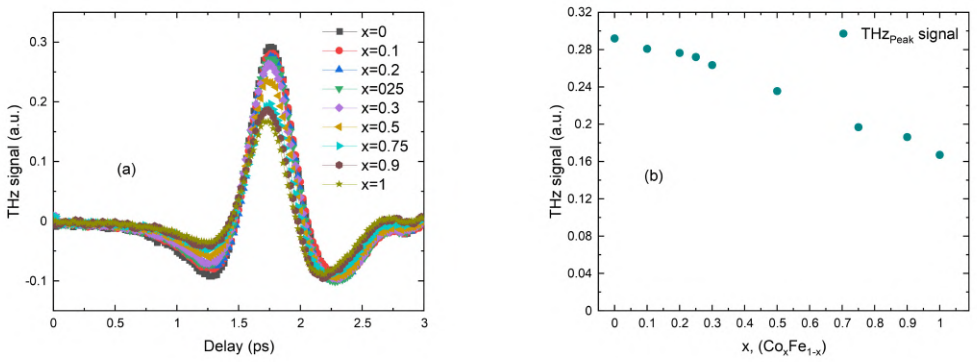

Figure 1: THz signal obtained for the stack Ta(2 nm)/Co_xFe_{1-x}(2 nm)/Pt(2 nm) alloy (a) THz pulses obtained for different Co concentration. (b) THz peak amplitude variation as a function of Co concentration.

Acknowledgments

The author(s) would like to thank the ORION program for its contribution to the funding of Master's research internship. This work has benefited from a government grant managed by the Agence Nationale de la Recherche with the reference ANR-20-SFRI-0009.

References

[1] T. Seifert, S. Jaiswal, U. Martens, et al. Efficient metallic spintronic emitters of ultrabroadband terahertz radiation. *Nature Photonics* 10, 483–488 (2016).

[2] Jon Gorchon, Stéphane Mangin, Michel Hehn, and Gregory Malinowski. Is terahertz emission a good probe of the spin current attenuation length? *Applied Physics Letters* 121, 012402 (2022).

[3] M. Pratzer and H. J. Elmers. Structural and Magnetic Properties of Co-Fe Binary Alloy Monolayers on W(110). *Physical Review Letters* 90, 077201 (2003).

Poster 2.55, November 15th, 10h50–13h00

Inverse Rashba-Edelstein effect in CoFeB/MgO magnetic bilayers revealed with THz emission spectroscopy

Artem Levchuk[1, 2, *], Vincent Juvé[1], Tadele Otomalo[1], Aurelie Solignac[2], Gwennaëlle Vaudel[1], Jean-Yves Chauleau[2], Pascal Ruello[1], and Michel Viret[2]

[1]*Institut des Molécules et Matériaux du Mans, UMR 6283 CNRS, Le Mans Université, Le Mans, France*
[2]*CEA Saclay, DRF/IRAMIS/SPEC, UMR 3680 CEA-CNRS, Gif-sur-Yvette, France*
*artem.levchuk@cea.fr

Spintronics is the thriving field of research to control the electron spin degree of freedom for potential applications in computing, storage and memory, and fundamental science. Spintronic devices are promising for lower power consumption, higher information density, and non-volatility compared to conventional electronics. However, to utilize the electron spin to its fullest potential, the question about efficient generation, detection, transport, and inter-conversion of the electron's intrinsic angular momentum has to be answered. Over the last three decades, the scientific community has mastered spin control in the static regime (DC)[1]. The breakthrough in transient and ultrafast spintronics can be attributed to the detection of the terahertz (THz) radiation emitted as a consequence of an ultrafast demagnetization[2] and ultrashort spin-current burst injection from a ferromagnet into a metallic layer[3]. In such a Ferromagnet/Metal heterostructure, the THz emission is mediated via the Inverse Spin-Hall effect (ISHE). Recently, it has been demonstrated that the time-varying charge current can be generated via spin injection at a Rashba-split interface[4–6] (IREE) or via a hot-carrier gradient established in the magnetic heterostructures[7] (through anomalous Hall or Nernst effects, for example).

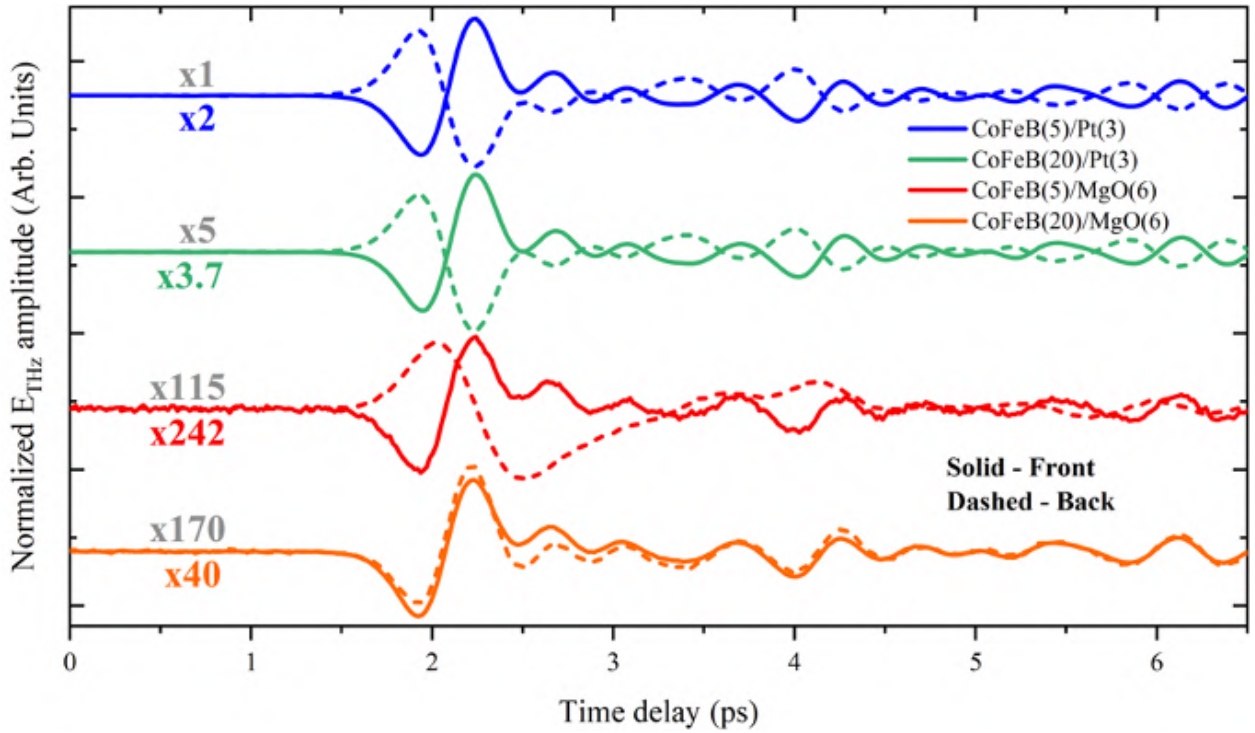

Figure 1: Normalized THz emission measured from the CoFeB(5 nm)/Pt(3 nm), CoFeB(20 nm)/Pt(3 nm), CoFeB(5 nm)/MgO(6 nm), and CoFeB (20 nm)/MgO(6 nm) hybrid nanostructures. The solid lines show the signal obtained when the pump pulse impinges on the capping Pt/MgO layer and the dashed curves are measured when excited from the side of the substrate. If any, the change in the THz polarity between the two sample orientations (solid vs. dashed) is directly associated with a reversal of the in-plane charge current related to a reversal of the relevant light-induced spin-polarized current.

In this work, we use 165 femtosecond, 805 nm laser pulses to generate the ultrafast spin-current bursts in 5 and 20 nm thick ferromagnet CoFeB. This net spin current can then be converted into a transient in-plane charge current within the ferromagnet itself (AHE or ANE), through the injection into the Rashba states established at the CoFeB/MgO interface[6]

(IREE) or injection into the 3 nm thick Pt layer (ISHE) deposited onto the CoFeB. The ultrafast spin-to-charge conversion mediated by the Hall or Rashba conversion subsequently leads to a charge current burst and free-space emission of broadband THz electromagnetic radiation. Employing THz-Time Domain spectroscopy, we have recorded the THz radiation emitted from a set of CoFeB/MgO and CoFeB/Pt bilayers due to the spin-to-charge conversion at the sub-picosecond timescale. Specifically, we address the symmetry of the spin-to-charge conversion inside the bulk of the ferromagnet and inside the heavy-metal Pt or at the CoFeB/MgO Rashba interface. For fixed experimental conditions, Figure 1 shows that the sample reversal and excitation from the capping Pt or MgO layers (solid lines) compared to the pumping from the substrate side (dashed lines) leads to the complete reversal of the direction of the injected spin-polarized current and reversal of the polarity of the emitted THz. On the other hand, the symmetric THz emission from CoFeB (20 nm)/MgO (6 nm) strongly suggests that the generation of the transient charge current and subsequent THz emission is driven by the spin-orbit coupling within the 20 nm thick CoFeB ferromagnetic film (i.e., bulk contribution such as AHE). Conducting a comparative analysis of experiments on CoFeB/Pt and CoFeB/MgO bilayers, we have identified that in the CoFeB (5 nm)/MgO (6 nm) bilayer, the THz emission is mainly driven by spin-injection and subsequent spin-to-charge conversion at the Rashba-split interface along with a significant contribution of bulk effects. This is associated with a strong decrease in the total emission intensity for the IREE system. We suggest that this is due to the spread in the energy of the emitted spin carriers and their relative inefficiency to fill the "optimized" Rashba split electron band structure close to the Fermi level[6]. This latter effect has been addressed by changing the pump pulse photon energy. Doing so, we demonstrate the tunability of the Inverse Rashba-Edelstein spintronic emitter, opening new perspectives for ultrafast spintronics.

References

[1] Igor Žutić, Jaroslav Fabian, and S. Das Sarma. Spintronics: Fundamentals and applications. *Reviews of Modern Physics* 76, 323–410 (2004).

[2] E. Beaurepaire, G. M. Turner, S. M. Harrel, et al. Coherent terahertz emission from ferromagnetic films excited by femtosecond laser pulses. *Applied Physics Letters* 84, 3465–3467 (2004).

[3] T. Kampfrath, M. Battiato, P. Maldonado, et al. Terahertz spin current pulses controlled by magnetic heterostructures. *Nature Nanotechnology* 8, 256–260 (2013).

[4] T. J. Huisman, R. V. Mikhaylovskiy, J. D. Costa, et al. Femtosecond control of electric currents in metallic ferromagnetic heterostructures. *Nature Nanotechnology* 11, 455–458 (2016).

[5] Matthias B. Jungfleisch, Qi Zhang, Wei Zhang, et al. Control of Terahertz Emission by Ultrafast Spin-Charge Current Conversion at Rashba Interfaces. *Physical Review Letters* 120, 207207 (2018).

[6] Olivier Rousseau, Cosimo Gorini, Fatima Ibrahim, et al. Spin-charge conversion in ferromagnetic Rashba states. *Physical Review B* 104, 134438 (2021).

[7] Qi Zhang, Ziyan Luo, Hong Li, et al. Terahertz Emission from Anomalous Hall Effect in a Single-Layer Ferromagnet. *Physical Review Applied* 12, 054027 (2019).

Poster 2.56, November 15th, 10h50–13h00

All-optical Helicity-Independent Switching State Diagram in Gd-Fe-Co Alloys

Boyu Zhang[1,*], Jiaqi Wei[1], Michel Hehn[2], Gregory Malinowski[2], Weisheng Zhao[1], and Stéphane Mangin[2]

[1]*Fert Beijing Institute, MIIT Key Laboratory of Spintronics, School of Integrated Circuit Science and Engineering, Beihang University, China*

[2]*Institut Jean Lamour, UMR CNRS 7198, Université de Lorraine, France*

*boyu.zhang@buaa.edu.cn

Ultrafast magnetization switching induced by a single femtosecond laser pulse, under no applied magnetic field has attracted a lot of attention in the last 10 years because of its high potential for low-energy and ultrafast memory applications. Single-pulse helicity-independent switching has mostly been demonstrated for Gd-based materials. It is now necessary to optimize the pulse duration and the energy needed to switch a Gd-Fe-Co magnet depending on the alloy thickness and composition.

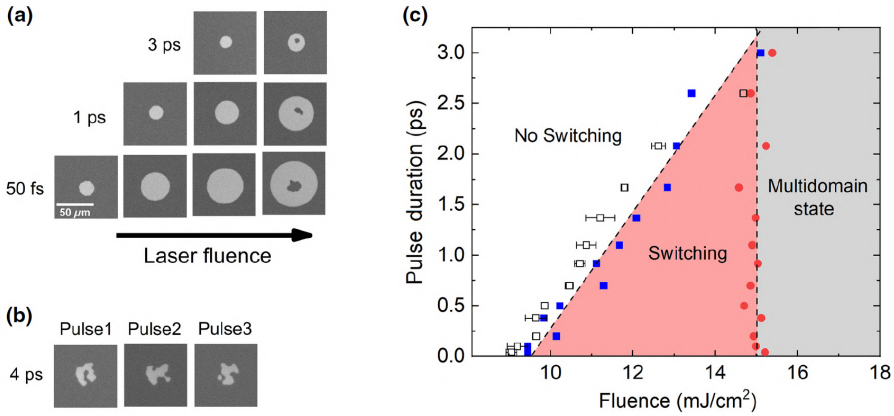

Figure 1: Magneto-optical images and all-optical helicity-independent switching (AO HIS) state diagram for a 20-nm $Gd_{24}(FeCo)_{76}$ film. (a) Magneto-optical images of $Gd_{24}(FeCo)_{76}$ after exposure to a single linearly polarized laser pulse with a pulse duration of 50 fs, 1 ps, and 3 ps, and with various fluences ranging from 9.5 to 15 mJ/cm^2. (b) Magneto-optical images of $Gd_{24}(FeCo)_{76}$ after exposure to a single linearly polarized laser pulse with a pulse duration of 4 ps and a fluence of 17 mJ/cm^2. (c) AO HIS state diagram: switching fluence F_{switch} (open black square and full blue square) and multidomain fluence F_{multi} (full red dot) as a function of the pulse duration for a single linearly polarized laser pulse. The blue full squares represent the switching fluences F_{switch} recorded when the diameter of switched area reaches around 10 μm. The open squares are the fitting results obtained via the method proposed by Liu *et al.* [1]. The spatial FWMH of laser beam is around 70 μm.

Here we experimentally report state diagrams showing the magnetic state obtained after one single pulse depending on the laser pulse duration and fluence for various Gd-Fe-Co thin films with different compositions and thicknesses (Fig. 1). We demonstrate that these state diagrams share similar characteristics: the fluence window for switching narrows for longer pulse duration and for the considered pulse-duration range the critical fluence for single-pulse switching increases linearly as a function of the pulse duration while the critical fluence required for creating a multidomain state remains almost constant. Calculations based on the atomistic spin model qualitatively reproduce the experimental state diagrams and their evolution. By studying the effect of the composition and the thickness on the state diagram, we demonstrate that the best energy efficiency and the longest pulse duration for switching are obtained for composition around the magnetic compensation[2].

Acknowledgments

This work is supported by the ANR-15-CE24-0009 UMAMI and the ANR-20-CE09-0013, by the Institute Carnot ICEEL for the project “Optic-switch” and Matelas, by the Région Grand Est, by the Metropole Grand Nancy, by the impact project LUE-N4S, part of the French PIA project “Lorraine Université d’Excellence,”reference ANR-15-IDEX-04-LUE, and by the “FEDERFSE Lorraine et Massif Vosges 2014-2020,” a European Union Program. The authors gratefully acknowledge the National Natural Science Foundation of China (Grant No. 61627813), the Program of Introducing Talents of Discipline to Universities (Grant No. B16001) and the Beijing Municipal Science and Technology Project (Grant No. Z201100004220002).

References

[1] J. M. Liu. Simple technique for measurements of pulsed Gaussian-beam spot sizes. *Optics Letters* 7, 196 (1982).

[2] J. Wei, B. Zhang, M. Hehn, et al. All-optical Helicity-Independent Switching State Diagram in Gd-Fe-Co Alloys. *Physical Review Applied* 15, 054065 (2021).

Manipulating exchange bias with a single femtosecond laser pulse

Boyu Zhang[1, *], Gregory Malinowski[2], Zongxia Guo[1, 2], Wei Zhang[1], Hangtian Wang[1, 2], Pierre Vallobra[1], Stéphane Mangin[2], Weisheng Zhao[1], and Michel Hehn[2]

[1]*Fert Beijing Institute, MIIT Key Laboratory of Spintronics, School of Integrated Circuit Science and Engineering, Beihang University, China*
[2]*Institut Jean Lamour, UMR CNRS 7198, Université de Lorraine, France*
*boyu.zhang@buaa.edu.cn

Ultrafast manipulation of magnetic order has challenged our understanding the fundamental and dynamic properties of magnetic materials. So far single shot magnetic switching has been limited to ferrimagnetic alloys and multilayers [1]. Whether a similar scenario can be observed in antiferromagnets remains unknown. In ferromagnetic (FM)/antiferromagnetic (AFM) bilayers, exchange bias arises from the interfacial exchange coupling between the two layers and results in a field shift (H_e) of the FM layer hysteresis loop. Exchange bias phenomena have found widespread use in fundamental scientific research and a large variety of spintronic devices, including sensors and magnetic random-access memory (MRAM) [2]. Many studies have already focused on the possibility to manipulate the exchange bias effect using thermal annealing with or without applied magnetic field and spin polarized current [3, 4]. Here we demonstrate the possibility to manipulate the exchange bias (change of the sign and amplitude of H_e) with a single femtosecond laser pulse in perpendicular to film plane magnetized IrMn/CoGd bilayers, as shown in Fig. 1. We have studied the influence of the laser fluence and the number of pulses for various IrMn thicknesses to determine the fastest and the most energy-efficient way to set the exchange bias field. Our results establish a method to set the exchange bias in a bilayer system that has potential application for ultrafast and energy-efficient spintronic devices.

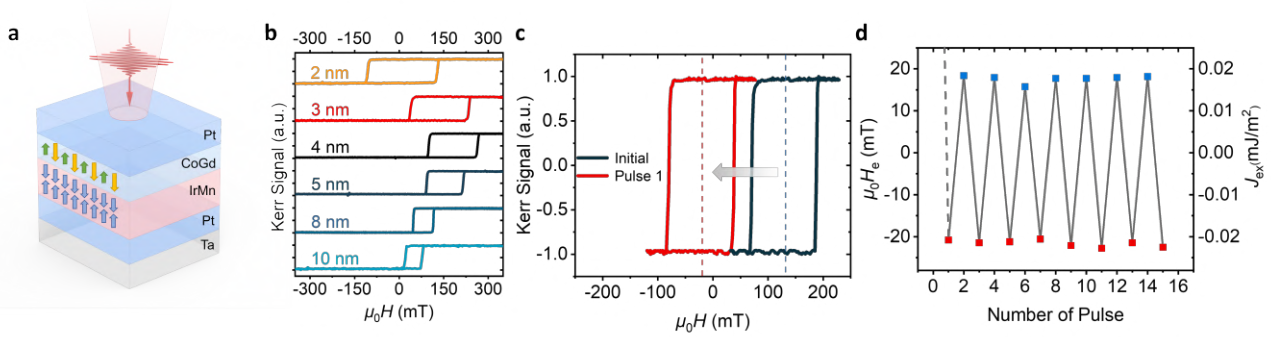

Figure 1: (a), Sketch of the IrMn/CoGd bilayer. (b), Hysteresis loops obtained on the annealed stacks for IrMn thickness from 2 to 10 nm measured by MOKE. (c), Hysteresis loop of IrMn(5)/CoGd(4) before and after exposure to a single linearly polarized laser pulse with a pulse duration of 40 fs and a fluence of 17 mJ/cm^2 (d), Modulation of the exchange bias field as a function of the number of pulses with a pulse duration of 40 fs and a laser fluence of 17 mJ/cm^2.

Acknowledgments

This work is supported by the ANR-15-CE24-0009 UMAMI and the ANR-20-CE09-0013, by the Institute Carnot ICEEL for the project "Optic-switch" and Matelas, by the Région Grand Est, by the Metropole Grand Nancy, by the impact project LUE-N4S, part of the French PIA project "Lorraine Université d'Excellence," reference ANR-15-IDEX-04-LUE, and by the "FEDERFSE Lorraine et Massif Vosges 2014-2020," a European Union Program. The authors gratefully acknowledge the National Natural Science Foundation of China (Grant No. 12104031, 12104030, 61627813), the Program of Introducing Talents of Discipline to Universities (Grant No. B16001), the Beijing Municipal Science and Technology Project (Grant No. Z201100004220002), China Postdoctoral Science Foundation (Grants No.2022M710320) and China Scholarship Council.

References

[1] I. Radu, K. Vahaplar, C. Stamm, et al. Transient ferromagnetic-like state mediating ultrafast reversal of antiferromagnetically coupled spins. *Nature* 472, 205–208 (2011).

[2] J. Nogués and I.K. Schuller. Exchange bias. *Journal of Magnetism and Magnetic Materials* 192, 203–232 (1999).

[3] I.L. Prejbeanu, M. Kerekes, R.C. Sousa, et al. Thermally assisted MRAM. *Journal of Physics: Condensed Matter* 19, 165218 (2007).

[4] P. Lin, B. Yang, M. Tsai, et al. Manipulating exchange bias by spin-orbit torque. *Nature Materials* 18, 335–341 (2019).

Poster 2.58, November 15th, 10h50–13h00

Ultrafast magnetization dynamics in nanostructured thin layers

Juliette Dubois[1,*], Boris Vodungbo[1], Marcel Hennes[2], Guillaume Lambert[3], Emmanuelle Jal[1], Renaud Delaunay[1], and Franck Vidal[2]

[1]*Sorbonne Université, CNRS, Laboratoire de Chimie Physique - Matière et Rayonnement, LCPMR, F-75005 Paris, France*

[2]*Sorbonne Université, CNRS, Institut des nanosciences de Paris, INSP, F-75005*

[3]*Laboratoire d'Optique Appliquee, ENSTA ParisTech, CNRS, Ecole Polytechnique, Institut Polytechnique de Paris, 828 Bd des Marechaux, 91702 Palaiseau, France*

juliette.dubois.loa@ensta-paris.fr

Controlling magnetization without using magnetic fields is a technology-driven strong motivation in the quest for new electronic devices allowing for fast control with low energy consumption. In that regard, hybrid materials coupling heavy metals and lighter 3d transition metals have been developed for current assisted magnetization switching, while electric-field control would make use of multiferroic materials [1]. However, the fastest control can be achieved using light: indeed all-optical switching has emerged recently as a powerful technique to drive the magnetization of thin films [2].

We are trying to adopt such an all-optical strategy to drive the magnetization state of magnetostrictive nanowires grown inside a photostrictive matrix [3]. In this type of sample, the magnetic anisotropy of the nanowires could be controlled by an optical trigger wich will modify the strain in the matrix. This approach could allow to finely tune the magnetic properties for applications.

Since the hybrid samples of nanowires embedded in a photostrictive matrix are still being optimized at the Institut des Nanosciences de Paris, in my first year of PhD I focused on the study of the magnetization dynamics of thin films made with the same material as the nanowires: a nickel rich (> 80 %) cobalt-nickel alloy. The femtosecond magnetization dynamics has already been studied in several ferromagnetic alloys and multilayers systems such as iron-nickel or cobalt-platinum. These systems typically show ultrafast demagnetization as discovered by Beaurepaire et al. in pure nickel in 1996 [4] but there have been contradictory results concerning possible different demagnetization time or delays in the onset of the demagnetization of the different elements composing the system [5], [6]. Ultrafast demagnetization has not been studied so far with element selectivity in cobalt-nickel alloys and we hope that our report will contribute to the development of a unified picture of this phenomenon in alloys.

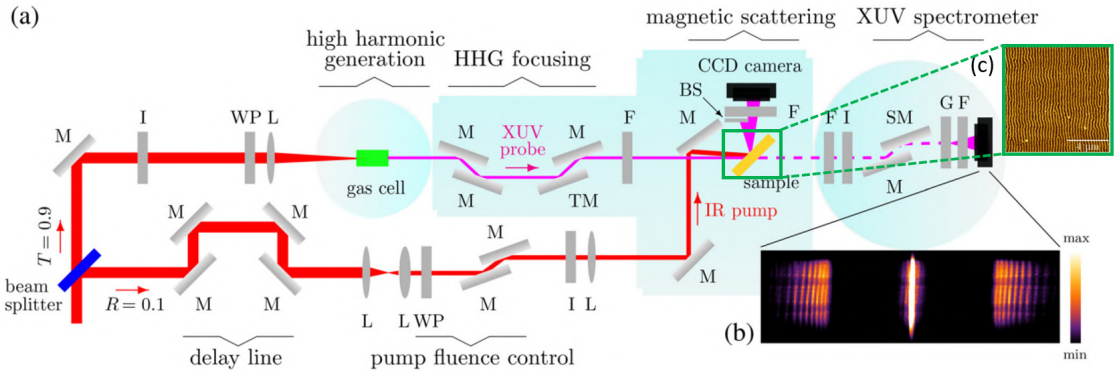

Figure 1: Pump-probe time resolved XUV resonant magnetic scattering setup (a) Details of the experiment. M : flat mirror, TP : toroidal mirror, SM : spherical mirror, I : iris, L: lens, WP : half wave plate, BS : neam stop, F : Al filter, G : grating. The pressure in the HHG chamber (light blue) is kept below $10\times^4$ mbar. (b) Spectrometer CCD snapshot. (c) MFM image of the Co15Ni85 sample showing the stripe domains with a periodicity of 260 nm.

To study the magnetization dynamics in our samples, we are pumping them out of equilibrium using 30 fs, 2.5 mJ and 800 nm infrared (IR) pulses from a 5 kHz Ti:Sapphire laser (Coherent laser Elite duo). Only a small fraction of the pulses is used for the pump, the main part is focused into a gas cell to generate high harmonics (see experimental setup on figure 1). As a reminder, high harmonics generation (HHG) is a non-linear phenomenon which allows one to get from a ω frequency laser a radiation at ωq frequencies, with q the harmonic orders [7]. Therefore, HHG constitute a XUV source that allows us to probe the magnetization state of the sample with chemical selectivity by accessing the absorption M edges of cobalt and nickel between 55 and 70 eV.

The sample we have studied is a 100 nm thick cobalt-nickel film grown on a silicon substrate. Because of the magnetostriction of this alloy, a weak perpendicular magnetic anisotropy exists inside the thin layer. Therefore, above a threshold thickness (several tens of nanometer here), a magnetic structure consisting of alternating nanometric magnetic domains with out of plane components of opposite directions will appear. We can align these domains by applying a magnetic field in the plane of the film: the magnetic domains will tend to align in the direction of the magnetic field (figure 1 (c)). This structure will act as a diffraction grating for photon energies in resonance with the M absorption edges of cobalt (around 60 eV) and nickel (around 67 eV) [8].

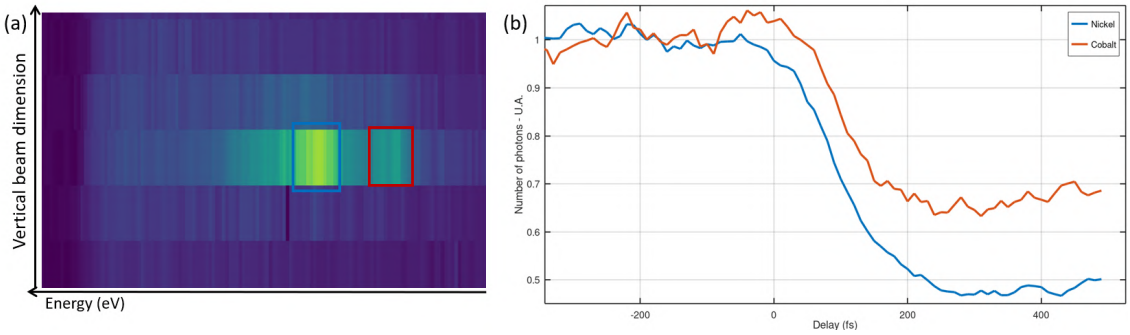

Figure 2: Preliminary result (a) Magnetic scattering on the CCD camera - Blue box : nickel scattering spot, Red box : cobalt scattering spot, (b) Magnetization variations of CoNi sample depending on the delay - the curves correspond to the intensity integrations on the zones showed on the left image.

When we send the HHG beam onto the sample, we can then observe a reflected scattering pattern on a CCD camera (see figure 2(a)). There are two main spots on this pattern corresponding to nickel (higher intensity) and cobalt (lower intensity). By following the intensity of these spots as a function of the time delay between the pump and the probe, we can reconstruct the magnetization dynamics of cobalt and nickel simultaneously (see figure 2(b)). The preliminary results indicate that there is a delay of about 20 to 30 fs between the onset of demagnetization of cobalt and nickel and that the cobalt demagnetizes less than nickel (see figure 2(b)). The data analysis is still ongoing and this observation remains to be ascertained. Moreover, we plan to study other film compositions and we have to confront our results to models which have been developed to explain the ultrafast demagnetization in nickel-iron and cobalt-platinum systems [5], [6].

References

[1] Ying-Hao Chu, Lane W. Martin, Mikel B. Holcomb, et al. Electric-field control of local ferromagnetism using a magnetoelectric multiferroic. *Nature Materials* 7, 478–482 (2008).

[2] C. D. Stanciu, F. Hansteen, A. V. Kimel, et al. All-Optical Magnetic Recording with Circularly Polarized Light. *Physical Review Letters* 99 (2007).

[3] F. Vidal, Y. Zheng, J. Milano, et al. Nanowires formation and the origin of ferromagnetism in a diluted magnetic oxide. *Applied Physics Letters* 95, 152510 (2009).

[4] E. Beaurepaire, J.-C. Merle, A. Daunois, and J.-Y. Bigot. Ultrafast Spin Dynamics in Ferromagnetic Nickel. *Physical Review Letters* 76, 4250–4253 (1996).

[5] M. Hennes, G. Lambert, V. Chardonnet, et al. Element-selective analysis of ultrafast demagnetization in Co/Pt multilayers exhibiting large perpendicular magnetic anisotropy. *Applied Physics Letters* 120, 072408 (2022).

[6] Marcel Hennes, Benedikt Rösner, Valentin Chardonnet, et al. Time-Resolved XUV Absorption Spectroscopy and Magnetic Circular Dichroism at the Ni M2, 3-Edges. *Applied Sciences* 11, 325 (2020).

[7] G. Lambert, B. Vodungbo, J. Gautier, et al. Towards enabling femtosecond helicity-dependent spectroscopy with high-harmonic sources. *Nature Communications* 6 (2015).

[8] Boris Vodungbo, Bharati Tudu, Jonathan Perron, et al. Indirect excitation of ultrafast demagnetization. *Scientific Reports* 6 (2016).

Co-Tb alloy thin films: from static magnetic properties to laser-induced ultrafast demagnetization and domain wall broadening

M. Hennes[1,*], A. Merhe[2], A. Ahlawat[2], X. Liu[2], D. Weder[3], C. von Korff Schmising[3], M. Schneider[3], C. M. Günther[4], B. Mahieu[5], G. Malinowski[6], M. Hehn[6], D. Lacour[6], F. Capotondi[7], E. Pedersoli[7], I. P. Nikolov[7], V. Chardonnet[2], C. Rodríguez[1], D. Demaille[1], Y. Zheng[1], F. Vidal[1], J. Lüning[8], E. Jal[2], and B. Vodungbo[2]

[1]*Sorbonne Université, CNRS, Institut des NanoSciences de Paris, INSP, 75005 Paris, France*
[2]*Sorbonne Université, CNRS, Laboratoire de Chimie Physique – Matière et Rayonnement, LCPMR, 75005 Paris, France*
[3]*Max Born Institut für Nichtlineare Optik und Kurzzeitspektroskopie, 12489 Berlin, Germany*
[4]*Institut für Optik und Atomare Physik, Technische Universität Berlin, 10623 Berlin, Germany*
[5]*Laboratoire d'Optique Appliquée, ENSTA ParisTech, CNRS, Ecole Polytechnique, Université Paris-Saclay, 91762 Palaiseau Cedex, France*
[6]*Institut Jean Lamour, CNRS, Université de Lorraine, 54000 Nancy, France*
[7]*FERMI, Elettra-Sincrotrone Trieste, 34149 Basovizza, Trieste, Italy*
[8]*Helmholtz-Zentrum Berlin für Materialien und Energie GmbH, 14109 Berlin, Germany*
*marcel.hennes@sorbonne-universite.fr

Magnetic thin films with perpendicular anisotropy can exhibit nanoscale domain patterns which provide an ideal testbed to analyse ultrafast spatial changes of spin textures induced by femtosecond laser pulses. While a variety of experiments has been performed on ferromagnetic alloys and multilayers [1], unraveling for example the importance of superdiffusive spin transport [2], less data are available on ferrimagnetic alloys.

In this work, we start by presenting an analysis of static magnetic properties in sputter-deposited ferrimagnetic Co-Tb thin films. By combining MFM, MOKE and SQUID/VSM measurements with micromagnetic simulations, we provide a systematic description of the impact of film thickness, concentration, and temperature on anisotropy and the resulting magnetic domain structure. We then proceed by showing time-resolved resonant magnetic x-ray scattering experiments performed at the Co $M_{2,3}$ and Tb O_1 edge used to study laser-induced demagnetization effects in a $Co_{88}Tb_{12}$ alloy exhibiting regular magnetic stripe domains.

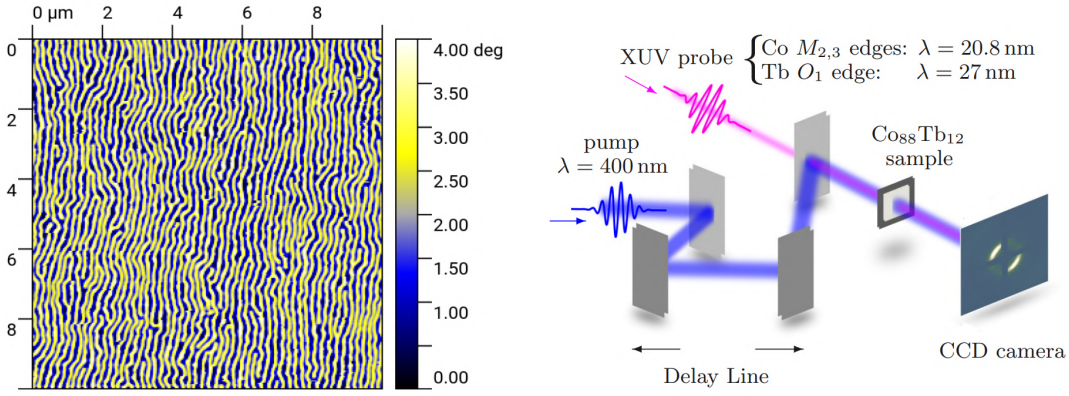

Figure 1: (a) Magnetic domain structure in a $Co_{92}Tb_8$ thin film (50 nm thickness) evidenced with magnetic force microscopy (MFM). (b) Schematic of the pump-probe XRMS setup used in the present study.

In these thin films, we evidence an ultrafast decrease of magnetization on sub-ps timescales in the Co as well as in the Tb sublattice, and we provide a quantitative description of the demagnetization behavior. Combining the femtosecond temporal with nanometer spatial resolution of our pump-probe experiments, we show that on ultrashort timescales (<1 ps), no detectable change in domain size and domain wall size occurs [3, 4]. However, we evidence a broadening of the domain walls which sets in after several ps and which we attribute to a decrease of the uniaxial anisotropy due to energy transfer to the lattice. Our static temperature-dependent magnetometry measurements corroborate this interpretation [5].

Acknowledgments

The authors are grateful for financial support received from the CNRS-MOMENTUM, the UMAMI ANR-15-CE24-0009, the CNRS-PICS, Emergence-Sorbonne Université and Emergence-INP programs, and thank the scientific and technical teams of the FERMI user facility for the help provided during the experiment. The authors also acknowledge the staff of the MPBT (physical properties - low temperature) platform of Sorbonne Université for their support.

References

[1] Boris Vodungbo, Julien Gautier, Guillaume Lambert, et al. Laser-induced ultrafast demagnetization in the presence of a nanoscale magnetic domain network. *Nature Communications* 3, 999 (2012).

[2] B. Pfau, S. Schaffert, L. Müller, et al. Ultrafast optical demagnetization manipulates nanoscale spin structure in domain walls. *Nature Communications* 3, 1100 (2012).

[3] Dmitriy Zusin, Ezio Iacocca, Loïc Le Guyader, et al. Ultrafast perturbation of magnetic domains by optical pumping in a ferromagnetic multilayer. *Phys. Rev. B* 106, 144422 (14 2022).

[4] Rahul Jangid, Nanna Zhou Hagström, Meera Madhavi, et al. *Evidence of extreme domain wall speeds under ultrafast optical excitation*. 2023. arXiv: 2303.16131 [cond-mat.mes-hall].

[5] M. Hennes, A. Merhe, X. Liu, et al. Laser-induced ultrafast demagnetization and perpendicular magnetic anisotropy reduction in a $Co_{88}Tb_{12}$ thin film with stripe domains. *Phys. Rev. B* 102, 174437 (17 2020).

Electronic structure drives the game: subpicosecond magnetic phase transition in FeRh,

Federico Pressacco[1], Davide Sangalli[2], Vojtěch Uhlíř[3], Matteo Gatti[4], and Fausto Sirotti[5,*]

[1]*The Hamburg Centre for Ultrafast Imaging, Hamburg University, Hamburg, Germany*
[2]*European Theoretical Spectroscopy Facility (ETSF),(FLASHit), Monterotondo, Italy*
[3]*CEITEC BUT, Brno University of Technology, Brno, Czech Republic*
[4]*European Theoretical Spectroscopy Facitlity (ETSF), LSI, IP Paris, Palaiseau France*
[5]*Laboratoire de Physique de la Matiére Condensée, CNRS - IP Paris, Palaiseau, France*
**Fausto.Sirotti@polytechnique.edu*

Abstract

Magnetism is intrinsically linked to the concept of phase transition: ferromagnetic order can be destroyed simply by increasing temperature. In some cases, temperature favours a change in magnetic order. Metallic FeRh undergoes a first-order meta-magnetic phase transition from antiferromagnetic to ferromagnetic order at 360 K. It couples structural, magnetic and electronic order parameters. We show that, from the point of view of electronic structure, the phase transition triggered by ultrafast laser pulses is complete in 300 fs. Well before the structural and magnetic parameters stabilise.

The magnetic order is extracted from the specific characteristics of the electronic structure: the ferromagnetic phase has a minority spin band crossing the Fermi level. With synchrotron radiation experiments and ab initio calculations we have identified the fingerprint of the FM phase in FeRh, it consist of a narrow peak in the electronic density of states, located about 150 meV below the Fermi energy E. [1] [2] We used state of the art momentum microscope (HEXTOF) end station) to perform pump-probe experiments at the monochromatized PG2 beamline of the FLASH free electron laser using near-infrared (800nm, 1.55 eV) pulses of 90 fs coupled with 130 fs soft X-ray pulses with a photon energy of 123.5 eV. We measured electron energy distribution curves (EDC) as a function of the delay between the optical pump and X-ray probe pulses. [3]The relaxation of electrons toward the Fermi energy and the subsequent changes in the electron density near the Fermi level at different time delays are well identified from the differential matrix, presented in Fig: 1 a.

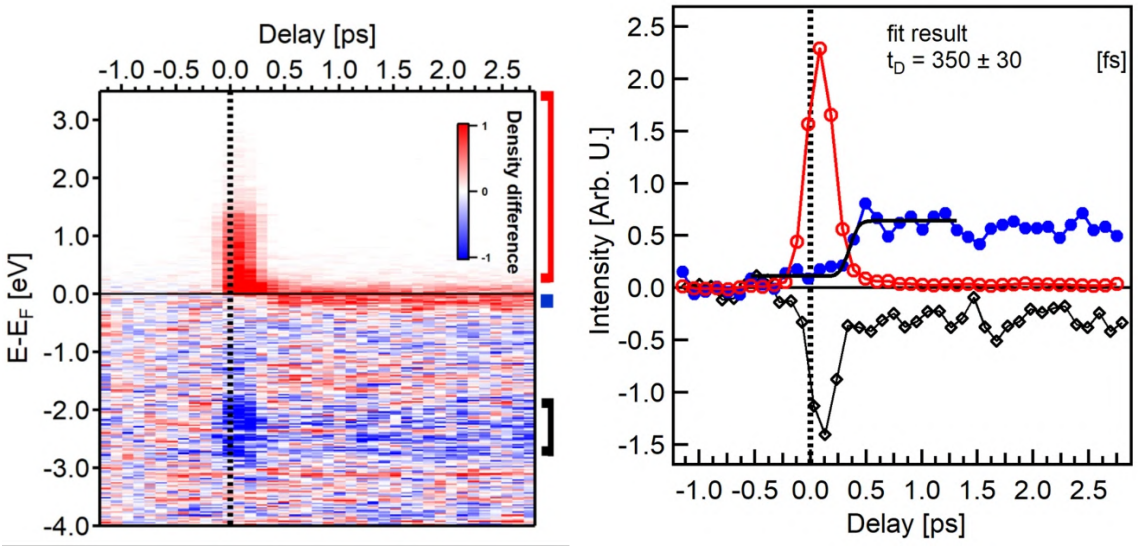

Figure 1: a) Energy and delay dependent differential matrix of the photoemission signal. The average of the spectra measured before the pump (between - 1 ps and -0.5 ps) is subtracted from each spectrum. The laser induced increase in the electronic density close to the Fermi level is observed at positive time delays. The red, blue and black bars on the right hand side mark the representative integration regions for tracking the electronic dynamics. b) Temporal evolution of the electronic density in the three regions marked in a)

We selected three energy ranges marked by the red, blue and black bars placed on the right-hand side of Fig: 1 b. The first (red) identifies the total number of electrons injected into the unoccupied states upon photoexcitation. The second (blue) monitors the formation of the Fe-minority peak across the phase transition, and the third (black) follows the modification of deeper bands. The time evolution of the integrated signals in each range is shown in Fig. 1b. The The energetic distribution of band structure is independent of spin alignment along a particular direction.

The injection of electrons into the unoccupied states takes place near zero delay and then rapidly decays (red empty circles), the process being finished by about 500 fs. The data represented by black diamonds in Fig. 1b nearly mirror the population of the unoccupied levels up to 300 fs, with a fast depletion and recovery. The curve stabilises thereafter at a finite value, implying permanent modifications of the deeper bands after 300 fs, already, during which the Fe minority peak is still shifting toward its final position at 150 meV below EF. The intensity at the position of the Fe-minority peak starts to grow as early as the laser excitation (filled blue circles), due to both the modification of the electronic structure and the Fermi level smearing. It is only about 300 fs after the excitation that the electronic density corresponding to the minority band peak displays a sharp increase, associated with a persistent band structure modification. So far this established the fastest timescale related to the meta-magnetic phase transition in FeRh.

Time-dependent density functional theory calculations of the electronic structure of FeRh [3] are used to interpret the laser-induced dynamics near the zero-time delay. In particular, they suggest that a significant charge and spin transfer from the Fe atoms toward the Rh ones, together with intra-atomic electron redistributions, are the ultimate origin of the phase transition. The overall very good agreement between theory and experiment indicates that the changes in the band structure are as important as changes in the electron population for describing ultrafast dynamics of phase transitions.

Our findings supported by theoretical calculations demonstrate that the microscopic manifestation of this magnetic first order phase transition resides in particular features of the electronic structure. During the ultrafast laser pumping, hot electron excitation triggers a significant charge and spin redistribution, resulting in the establishment of the FM phase.

References

[1] F. Pressacco, V. Uhlír, M. Gatti, et al. Stable room-temperature ferromagnetic phase at the FeRh (100) surface. *Scientific Reports* 6, 22383 (2016).

[2] F. Pressacco, V. Uhlíř, M. Gatti, et al. Laser induced phase transition in epitaxial FeRh layers studied by pump-probe valence band photoemission. *Struct. Dyn.* 5, 034501 (2018).

[3] F. Pressacco, D. Sangalli, V. Uhlíř, et al. Subpicosecond metamagnetic phase transition in FeRh driven by non-equilibrium electron dynamics. *Nature Communications* 12, 5088 (2021).

Dynamics of vortex state generation in laser demagnetized permalloy packman dots

Anda E. Stanciu[1, *], Mauro Fanciulli[2, 3], Thierry Ruchon[2], Maurizio Sacchi[4, 5], Bernard Dieny[1], and Liliana D. Buda-Prejbeanu1[1]

[1]*1 Univ. Grenoble Alpes, CEA, CNRS, Grenoble INP, SPINTEC, 38000 Grenoble, France*
[2]*Université Paris-Saclay, CEA, CNRS, LIDYL, 91191 Gif-sur-Yvette, France*
[3]*Laboratoire de Physique des Matériaux et Surfaces, CY Cergy Paris Université, France*
[4]*Sorbonne Université, CNRS, Institut des NanoSciences de Paris, INSP, 75005 Paris, France*
[5]*Synchrotron SOLEIL, L'Orme des Merisiers, Saint-Aubin, B. P. 48, 91192 Gif-sur-Yvette, France*
**anda-elena.stanciu@cea.fr*

Magnetic Helicoidal Dichroism (MHD) was predicted using classical electromagnetic theory in analogy with Magnetic Circular Dichroism (MCD) as a phenomenon observed with beams carrying Orbital Angular Momentum (OAM) instead of Spin Angular Momentum (SAM) [1]. MHD appears as a consequence of the interference of OAM carrying light modes that are populated after the interaction with a magnetic topology. Upon interaction of an OAM carrying beam (of topological charge l) with a magnetic topology, the intensity of the outgoing beam is determined by a redistribution into $l + n$ modes, where n represents all the azimuthal decomposition coefficients of the magnetic structure symmetry. An application of MHD is using it as a probing tool based on its capability to give information about the magnetization distribution in the sample [2].

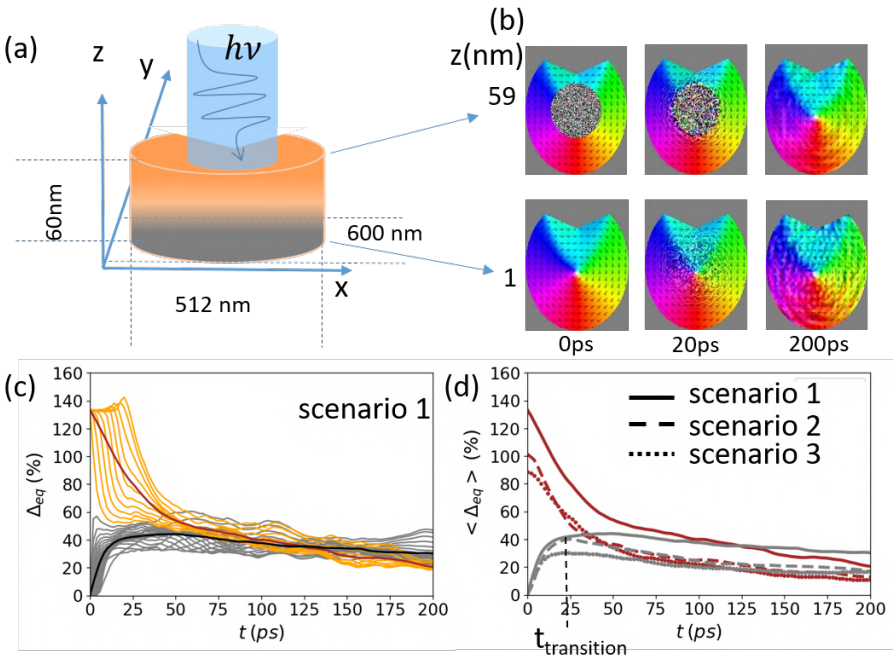

Figure 1: (a) Schematics of the simulated Py dot. (b) In-plane magnetization distribution at bottom surface of the dot ($z = 1nm$) and top surface respectively ($z = 59nm$) for different time values; The color code is linked to the in-plane polar angle of the magnetization vector. (c) Time evolution of the vortex structure deformation at different z position going gradually from the top to the bottom surface. Δ_{eq} is defined as the difference between the time evolving micromagnetic configuration and the vortex equilibrium configuration: Color code: orange - demagnetized regions affected by the laser; gray - regions unexposed to the laser. The corresponding deformation average curves by regions are brown and black for the top (heated) and bottom (initially unaffected) parts of the dots respectively. (d) Deformation average curves for the 3 scenarios mentioned in the text.

Very promising experiments have recently been carried out on magnetic vortices, which are magnetization structures whose symmetry makes it possible to observe MHD, since only two coefficients of the decomposition (corresponding to $n = 1$) are non-zero [1] . Particular systems that allows the stabilization of a magnetic vortex are permalloy (Py) dots with a triangular indent (packman shape) in which the magnetic vortex is centered in the middle of the dot [2] . Since the laser

penetration depth is of the order of $20nm$, the bottom structure of the packman is considered as unaffected by the pump laser pulse. We carried out systematic micromagnetic simulations [3] of the mechanism of reconstruction of the vortex structure after the action of the pump laser beam, which heats the permalloy and demagnetizes it.

The size, shape and material parameters of the packman sample were selected to ensure that the vortex state corresponds to the ground state of the system at remanence. Several scenarios of demagnetization were considered depending on the laser beam features (e.g. diameter, attenuation length, see Fig. 1 (a)) . The size of the laser beam was chosen either smaller (scenario 1) or larger (scenario 2) than the sample surface. The penetration of the laser through the sample thickness was also varied (scenario 3) affecting thus the volume of the sample that was demagnetized.

The simulations have shown that the structure of the micromagnetic configuration evolves in a two-stage mechanism. Firstly, due to the demagnetization of the top $20nm$ of the packman dot, the initially unaffected bottom part of the dot gets strongly disturbed due to the exchange interactions with the demagnetized top part (Fig. 1 (b): $t = 20ps$, $z = 1nm$). This is a fast process which takes place in about $25ps$. A maximum of deformation of the structure is then observed followed by a second stage involving spin-wave propagation over the entire volume of the sample corresponding to a much slower process longer than $200ps$ (Fig.1b: $t = 200ps$, $z = 1nm$ and $z = 59nm$). These characteristic times of the magnetic vortex recovery remain to be confirmed by future MHD experiments.

Acknowledgments

The financial support through the project HELIMAG (ANR-21-CE30-0037) is acknowledged.

References

[1] M. Fanciulli, M. Breseau D.and Vimal, M. Luttmannn, M Sacchi, and T. Ruchon. Electromagnetic Theory of Helicoidal Dichroism in Reflection from Magnetic Structures. *PHYSICAL REVIEW A* 103, 1–22 (2021).

[2] M. Fanciulli, M. Pancaldi, E. Pedersoli, et al. Observation of Magnetic Helicoidal Dichroism with Extreme Ultraviolet Light Vortices. *PHYSICAL REVIEW LETTERS* 128, 1–7 (2022).

[3] A. Vansteenkiste, J. Leliaert, M. Dvornik, et al. The Design and Verification of MuMax3. *AIP Advances* 4, 1–22 (2014).

Poster 2.62, November 15th, 10h50–13h00

Ultrafast pure spin current transport through antiferromagnetic insulators

Sanjay René[1,*], Artem Levchuk[1], Zixin Li[1], Pauline Dufour[2], Amr Abdelsamie[2], Aurélie Solignac[1], Jean-Baptiste Moussy[1], Stéphane Fusil[2], Vincent Garcia[2], Michel Viret[1], and Jean-Yves Chauleau[1]

[1]*SPEC UMR 3680 CEA-CNRS, Univ Paris Saclay, CEA Saclay Orme des merisiers, 91191 Gif-sur-Yvette*
[2]*Unité Mixte de Physique CNRS/Thalès UMR 137, Univ Paris Saclay, 91767 Palaiseau*
Sanjay.rene@cea.fr

The ever-growing demand for data consumption pushes new information technologies to process larger volumes of data at a faster rate and lower energy cost. For ultrafast information handling, spin currents which are the vector of spin information, can be generated, propagated and detected on the sub-picosecond timescale and at nano-sizes [1]. Therefore, the research field of ultrafast spintronics stands for a major player to tackle these challenges. Among the large variety of magnetic textures, antiferromagnets, where each neighboring spins is antiparallelly aligned, present several interesting features: "magnonic-type" spin currents can be propagated in antiferromagnetic insulators [2] even over considerable distances in insulating single crystals [3]; and antiferromagnets exhibit peculiar dynamic properties since their magnetic resonances [4] directly lie in the THz range (see for example [5]). Therefore antiferromagnetic insulators could be appealing candidates to propagate and manipulate magnonic spin currents and spin information at THz frequencies. This concept has been clearly evidenced in the DC and GHz regime (see for example [3]), but opened questions remain regarding antiferromagnetic spin current transport properties at picosecond timescales, i.e. when spin currents coherently match the specific antiferromagnetic THz resonance. This is the main objective of the present work in which we aim at studying the transfer of spin angular momentum to antiferromagnetic insulators at picosecond and sub-picosecond timescales. Our experimental approach consists in evaluating the effect of an adjacent AF layer on the ultrafast demagnetization of a ferromagnet/antiferromagnet bilayer by performing time-resolved magneto-optical measurements (Tr-MOKE). (Fig 1). This technique, based on femtosecond laser pulses, is a standard pump/probe approach allowing to track the ultrafast dynamics of a ferromagnetic layer [6]. In this presentation, we will show experimental evidence for ultrafast spin current transfer in two prototypical high frequency antiferromagnetic insulators, namely NiO and BiFeO3, both with resonant frequencies in the THz range. BiFeO3 is also known as the archetypal room temperature multiferroic whose advantages in controlling its spin textures will be discussed. Importantly, ferromagnetic resonance (FMR) measurements performed on the same systems allow us to compare the GHz and THz regimes.

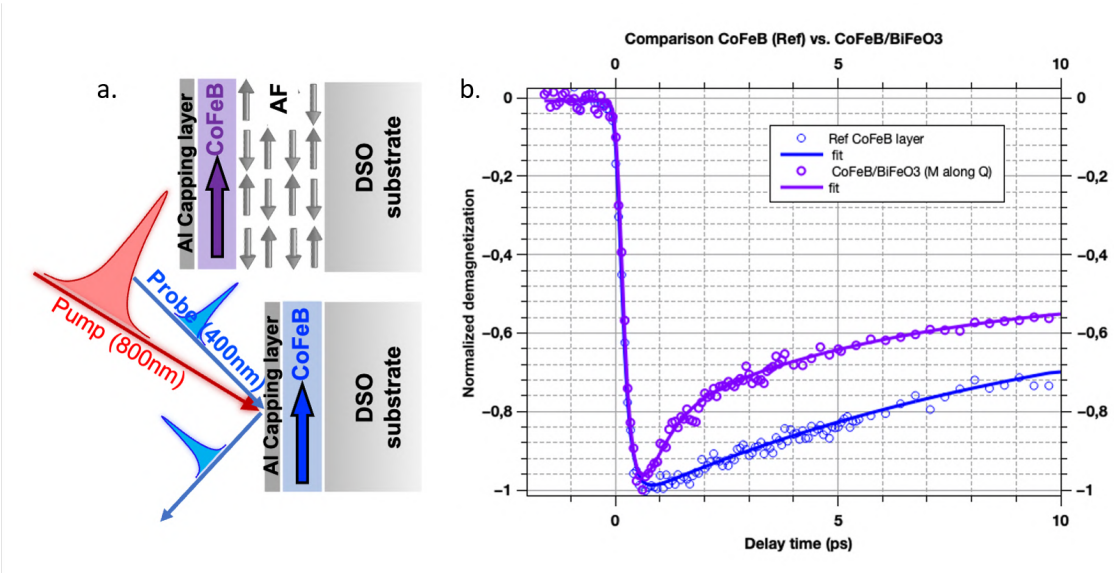

Figure 1: a. Ultrafast time-resolved magneto-optics. b. Ultrafast demagnetization curves for a single layer of CoFeB and a bilayer of CoFeB/BFO.

References

[1] Grégory Malinowski, Nicolas Bergeard, Michel Hehn, and Stéphane Mangin. Hot-electron transport and ultrafast magnetization dynamics in magnetic multilayers and nanostructures following femtosecond laser pulse excitation. *The European Physical Journal B* 91 (2018).

[2] Christian Hahn, Grégoire de Loubens, Vladimir V. Naletov, et al. Conduction of spin currents through insulating antiferromagnetic oxides. *EPL (Europhysics Letters)* 108, 57005 (2014).

[3] R. Lebrun, A. Ross, S. A. Bender, et al. Tunable long-distance spin transport in a crystalline antiferromagnetic iron oxide. *Nature* 561, 222–225 (2018).

[4] F. Keffer and C. Kittel. Theory of Antiferromagnetic Resonance. *Physical Review* 85, 329–337 (1952).

[5] Tobias Kampfrath, Alexander Sell, Gregor Klatt, et al. Coherent terahertz control of antiferromagnetic spin waves. *Nature Photonics* 5, 31–34 (2010).

[6] Jean-Yves Bigot. Femtosecond magneto-optical processes in metals. *Comptes Rendus de l'Académie des Sciences - Series IV - Physics* 2, 1483–1504 (2001).

Thursday November 16th

Session 5: Spin-charge conversion and THz emission 08h30 – 10h30 *Chair: Nicolas Bergeard*				
08h30 – 08h50	**Salvatore Teresi**	SPINTEC	Room temperature spin-charge inter conversion in sputtered GeTe nanodevices	page 273
08h50 – 09h10	**Aurélie Kandazoglou**	SPINTEC	Spin-charge interconversion in oxides for low-power memory and logic devices	page 275
09h10 – 09h30	**José Solano**	IPCMS	Determination of the degree of spin-polarization of the electron current in the half-metal Co_2MnSi	page 277
09h30 – 09h50	**Sylvain Massabeau**	UMR CNRS/Thales	Terahertz time-domain spectroscopy platform for spin-to-charge conversion study of spintronic emitters: application on $PtSe_2/Bi_2Se_3$ TMD/TI structures	page 279
09h50 – 10h10	**Matthias Riepp**	IPCMS DESY	THz-Induced Spin Dynamics in Nanoscale Multi-Domain State with Perpendicular Magnetic Anisotropy	page 281
10h10 – 10h30	**Martin Mičica**	LPENS	Atomic-layer controlled THz Spintronic emission from Two dimensional $PtSe_2$/ferromagnet heterostructures	page 283

Room temperature spin-charge interconversion in sputtered GeTe nanodevices

S. Teresi[1,*], M. Cosset-Cheneau[1], T. Frottier[1], W. Savero-Torres[1], M. Wissmann[1], M. Culot[1], F. Osana[1], A. Kandazoglou[1], P. Sgarro[1], J. Paterson[2], A. Oysel Mestre[2], F. Hippert[3], F. Leroy[4], B. Croes[4], M. Bibes[5], A. Manchon[4], A. Marty[1], J. P. Attané[1], F. Cheynis[4], G. Prenat[1], L. Hutin[2], P. Noé[2], and L. Vila[1]

[1]*Université Grenoble Alpes / CEA / IRIG / SPINTEC, Grenoble, France*
[2]*Université Grenoble Alpes / CEA / LETI, Grenoble, France*
[3]*Université Grenoble Alpes / CNRS / Grenoble INP / LMGP, Grenoble, France*
[4]*Aix Marseille Université / CNRS / CINAM / AMUTECH, Marseille, France*
[5]*Unité Mixte de Physique CNRS/Thalès, Université Paris-Saclay, Palaiseau, France*
**salvatore.teresi@cea.fr*

Spin-charge interconversion (StC) driven by spin-orbit (SO) phenomena has opened new avenues for designing spin-logic architectures with low-power consumption. Recently, Intel has proposed a device called MESO [1] (Magneto-Electric Spin-Orbit) predicted to have switching energies at the attoJoules scale (aJ/bit computing), orders of magnitude smaller than that of current non-volatile technologies. This new concept has the power to challenge or complete the CMOS technology in the next decade while still being a suitable option for new logic paradigms like in-memory computing. The writing process requires magnetization reversal, while the reading component relies on the StC signal resulting from SO phenomena.

Recent studies in spintronics have led to the discovery of spin-charge interconversion phenomena in ferroelectric materials. The possibility to control the spin-charge interconversion by switching the material ferroelectric state [2],[3] allowed us to propose the FerroElectric Spin Orbit device [3]. Its biggest advantage with respect to the MESO device is the possibility to avoid the necessity of multiferroic switching to change the StC output signal of the device. Its overall simplicity make FESO a valid alternative to MESO as a Beyond-CMOS spin-logic based devices.

In this context, the large-scale fabrication of such devices is a foreseeable challenge. Furthermore it is difficult to develop functional nanodevices whose spin transport properties are similar to those of the unpatterned layers. Engineering the ferromagnet (FM) thickness and the interlayer between the FM and the SHA material are found to be fundamental to optimize the signal and improve the yield. Here, we discuss the potential of sputtered GeTe as a spin-orbit material for FESO devices. GeTe is a ferroelectric semiconductor, whose spin-charge conversion depends on the ferroelectric polarisation state [2]. We study the transport properties of sputtered GeTe, and then demonstrate the spin-charge interconversion in GeTe-based nanodevices at room temperature (see Fig. 1).

We also study the potential for MESO devices of a parent compound, Sb_2Te_3, a toplogical insulator whose surface states can be used to perform spin-charge conversion. In conclusion, we will also discuss the advantages of our design for geometrical downscaling (Fig. 1 (d)).

Acknowledgments

This project received funding from the European Union's Horizon 2020 research and innovation program under the Marie Skłodowska-Curie Grant Agreement No. 955671. We also acknowledge support of the Institut Universitaire de France, of the French Research Agency (ANR) as part of the project CONTRABASS (ANR-20-CE24-0023), and of the Plateforme Technologique Amont (PTA) for technical support.

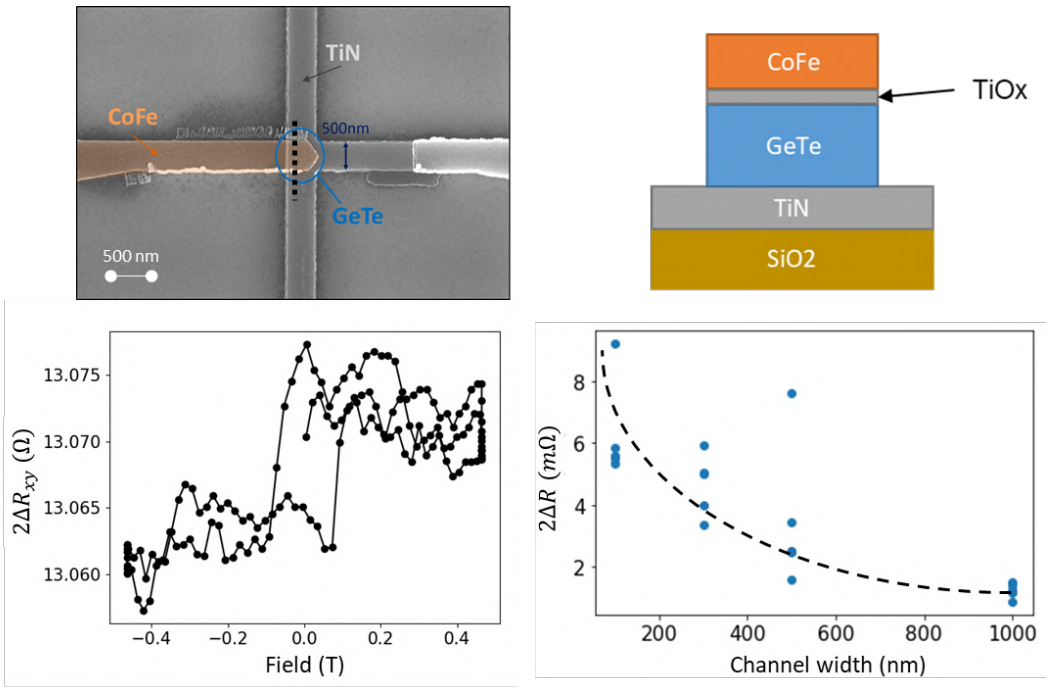

Figure 1: (a) Scanning electron microscopy of a nanofabricated GeTe device. (b) Cross section of the different layers composing the devices (along the black dotted line of (a)). (c) Charge-to-spin interconversion signal. Geometrical scaling of the interconversion signal with the channel width.

References

[1] Sasikanth Manipatruni, Dmitri E. Nikonov, Chia-Ching Lin, et al. Scalable energy-efficient magnetoelectric spin–orbit logic. *Nature* 565, 35–42 (2018).

[2] Sara Varotto, Luca Nessi, Stefano Cecchi, et al. Room-temperature ferroelectric switching of spin-to-charge conversion in germanium telluride. *Nature Electronics* 4, 740–747 (2021).

[3] Paul Noël, Felix Trier, Luis M. Vicente Arche, et al. Non-volatile electric control of spin–charge conversion in a SrTiO3 Rashba system. *Nature* 580, 483–486 (2020).

Spin-charge interconversion in oxides for low-power memory and logic devices

Aurélie Kandazoglou[1, *], Maxen Cosset-Cheneau[1], Paolo Sgarro[1], Williams Savero-Torres[1], Salvatore Teresi[1], Théo Frottier[1], Maxime Culot[1], Stéphane Auffret[1], Manuel Bibes[2], Jean-Philippe Attané[1], and Laurent Vila[1]

[1]*Université Grenoble Alpes, CEA, CNRS, SPINTEC, 38000 Grenoble, France*
[2]*Unité Mixte de Physique, CNRS, Thales, Université Paris-Saclay, Palaiseau, France*
*aurelie.kandazoglou@cea.fr

In order to develop new low-power technologies, the current-induced detection of a magnetic state has drawn an increasing attention towards spin-orbitronics. This research and development field in indeed at the origin of new concepts such as the Magneto-Electric Spin-Orbit (MESO) technology proposed by Intel, relying on magneto-electric switching and spin-charge interconversion in a spin-orbit coupling material. MESO is a non-volatile logic/computing technology, meaning that the information storage does not require a continuous voltage application and can be embedded directly in the computing element. Consequently, it could allow an in-memory computing device operating in the atto-joule range.

In parallel of these developments, we have recently proposed the Ferro-Electric Spin-Orbit (FESO) device [1], which is based on the control of the spin-orbit properties by ferroelectricity. The FESO device relies on spin injection, spin-to-charge conversion and a non-volatile mechanism such as ferroelectricity or charge-trapping. Its main advantage compared to the MESO technology proposed by Intel is that it does not require a complex magneto-electric switching.

In order to have a switchable spin-charge interconversion, it is primordial to choose a spin-orbit coupling material. Recently, oxide 2D electron gases (2DEG) have emerged as promising orbitronics systems, which benefit from an efficient spin-charge interconversion through the Rashba-Edelstein effects. We have demonstrated an enhancement of the spin-to-charge conversion efficiency by two orders of magnitude in $SrTiO_3$-based 2DEG compared to conventional heavy metals [2], along with a non-volatile ferroelectric control of the spin-to-charge conversion detected using spin-pumping experiments [1] and the non-volatile electric-control of spin-orbit torques (charge-to-spin conversion) detected using the Second Harmonic Hall method [3]. While demonstrating the non-volatile electric-control of the spin-to-charge and charge-to-spin conversions has required two different patterned devices using different techniques, the FESO device relies on a fully electrical signal detection, making possible to measure electrically both the spin-to-charge and charge-to-spin conversions on the same device.

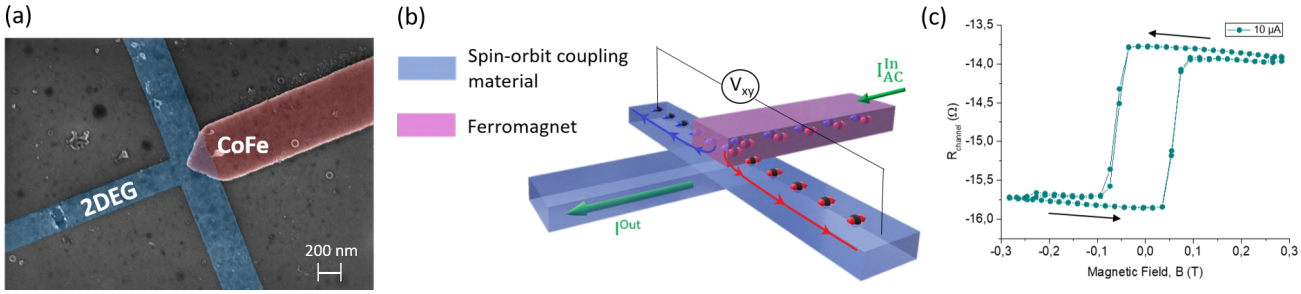

Figure 1: (a) Scanning electron microscope image of the oxide-based FESO device. (b) Measurement principle scheme of the FESO device, in which a spin-polarized current is injected from the top ferromagnetic layer towards the spin-orbit coupling material, in order to generate a transverse voltage. (c) Spin-to-charge conversion signal at 10 K, applying a 10 µA AC current at 67 Hz.

Here, we demonstrate the reading functionality of an oxide-based FESO device. The T-shaped part (in blue on Fig.1) is composed of a 500 µm thick $SrTiO_3$ substrate, on which a Ta layer is deposited to create a 2DEG at the $SrTiO_3$/Ta interface. The spin-orbit coupling properties of the 2DEG enable to consider it as a Rashba interface, which enables the spin-charge interconversion. The ferromagnetic injection layer (in pink on Fig.1) is a CoFe layer. The AC charge current injected in the ferromagnetic layer gets spin-polarized. This leads to a spin accumulation at the CoFe/2DEG interface, and thus to the injection of a spin current in the 2DEG. Adding a tunnel barrier, usually a MgO layer in between the ferromagnet and the 2DEG, favors the spin injection and then the spin-to-charge conversion in the 2DEG. The produced charge current is

detected through the voltage measurement V_{xy}.

Magneto-transport measurements enabled to obtain a reproducible strong spin-to-charge conversion. The signal indeed shows a hysteresis behavior, with an amplitude up to 2 Ω. In addition, the reverse charge-to-spin conversion measurement also revealed the same signal amplitude, which demonstrates an equivalent efficiency for both spin-charge conversions in this oxide-FESO device. Moreover, the study of the temperature dependence of the signal amplitude highlights the decreasing spin-to-charge conversion when increasing the temperature. This is mainly due to the decreasing conduction of the 2DEG which is responsible for the conversion. We also evidence the contribution of side effects such as the planar Hall effect and the anomalous Hall effect studying the shape of the measured signal. Their respective contributions are determined thanks to an angular dependence of the signal for the planar Hall effect, and to simulations for the anomalous Hall effect. On top of that, we demonstrate the electric-control of the spin-charge interconversion, whose origin in this system appears to be charge trapping.

In conclusion, we present a new kind of spintronic device, the Ferro-Electric Spin-Orbit (FESO) device, based on an oxide 2DEG. We demonstrate that the spin-to-charge interconversion due to the spin-orbit coupling can be directly measured and electrically controlled. This constitutes a step towards the development of a non-volatile spintronics, in which the information can be controlled by a ferroelectric state, thus resulting in a drastic reduction of the power consumption of non-volatile spintronic logic devices.

Acknowledgments

This work has received support from Institut Universitaire de France, from the French Research Agency (ANR) as part of the project CONTRABASS (ANR-20-CE24-0023), from the Marie Sklodowska–Curie H2020-MSCA-ITN-2020 SPEAR grant agreement 955671 project and from the ERC Advanced Grant No. 833973 "FRESCO". The authors would also like to thank the Plateforme Technologique Amont (PTA) for technical support.

References

[1] Paul Noël, Felix Trier, Luis M. Vicente Arche, et al. Non-volatile electric control of spin–charge conversion in a SrTiO3 Rashba system. *Nature* 580, 483–486 (2020).

[2] Diogo C. Vaz, Paul Noël, Annika Johansson, et al. Mapping spin–charge conversion to the band structure in a topological oxide two-dimensional electron gas. *Nat. Mater.* 18, 1187–1193 (2019).

[3] Cécile Grezes, Aurélie Kandazoglou, Maxen Cosset-Cheneau, et al. Non-volatile electric control of spin-orbit torques in an oxide two-dimensional electron gas. *Nat Commun* 14, 2590 (5, 2023).

Determination of the degree of spin-polarization of the electron current in the half-metal Co_2MnSi

J. Solano[1,*], A. Friedel[2,3], P. Pirro[3], S. Petit-Watelot[2], S. Andrieu[2], and M. Bailleul[1]

[1]*Institut de Physique et Chimie des Matériaux de Strasbourg, CNRS-Université de Strasbourg, 67034 Strasbourg, France*

[2]*Institut Jean Lamour, UMR CNRS 7198, Université de Lorraine, Nancy 54500, France.*

[3]*Fachbereich Physik and Landesforschungszentrum OPTIMAS, Technische Universitat Kaiserslautern, Germany*

jose.solano@ipcms.unistra.fr

In the spintronics community there is a constant search for materials that can sustain the propagation of spin information with low losses. Although magnetic insulators posses the record of lowest magnetic precession damping, their small magnetization and inability to host electron currents reduce their potential uses in spintronic devices. Therefore, there is a technological and fundamental interest in novel metallic ferromagnets where electrons can be used to carry spin without major precession losses. Half metals are materials that combine the best of both worlds: they have conduction electrons with a single spin orientation at the Fermi level (100% spin-polarized density of states) that reduces drastically the electron-magnon scattering and consequently the magnetic losses. A textbook example of these type of materials is the Heusler compound Co_2MnSi that has been shown to have a very low Gilbert damping factor α between 1×10^{-3} to 5×10^{-4} and an almost entirely spin-polarized density of states at the Fermi energy[1, 2]. In this study, we look further into the quasi-bulk transport properties of this material by measuring for the first time the degree of spin-polarization of the electron current $P = (\rho_\downarrow - \rho_\uparrow)/(\rho_\downarrow + \rho_\uparrow)$ by spin-wave Doppler shift[3].

The platform of our investigation are epitaxial $Co_2MnSi(20\,nm)/MgO(8\,nm)/Ti(4\,nm)$ films grown by molecular beam epitaxy on (001) MgO substrates. We characterized the magnetic properties of the films by broadband ferromagnetic resonance from which we confirm a low Gilbert damping factor of $\alpha = 1.0 \times 10^{-3}$ for perpendicularly magnetized films and $\alpha = 1.3 \times 10^{-3}$ for in-plane magnetized films. Additionally, this technique[4] allows us to determine the effective magnetization, cubic anisotropy and exchange stiffness constants.

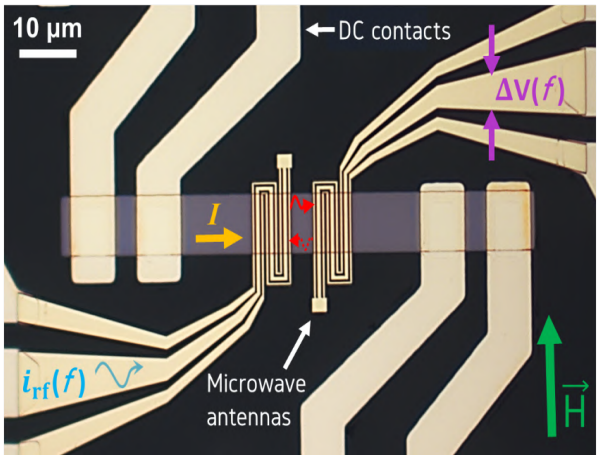

Figure 1: Spin wave Doppler shift device with a $MgO/Co_2MnSi/MgO/Ti$ strip

For the spin-wave Doppler shift measurements, the films are patterned into 15 µm-wide strips that serve as guides for electron conduction and spin wave propagation. An electrical current is injected and a voltage measured by 4 patterned DC-contacts, while nanofabricated microwave antennas allow us to perform spin wave spectroscopy (see Fig. 1). We measure the mutual inductance between the two antennas [Fig. 2 (a)] and determine the spin wave frequency shift produced by the applied electron current [inset of Fig. 2 (a)].

As expected from the adiabatic spin transfer torque (STT) process[5], we observe that the Doppler shift $\delta f_{Doppler} = (|\delta_{k>0}| + |\delta_{k<0}|)/4$ increases linearly with the applied electrical current. From the corresponding slope, we extract the degree of spin-polarization of the current $P = 1.0 \pm 0.1$ (see Fig. 2 (b)). This confirms that majority electrons are the charge carriers of the electrical current in Co_2MnSi. This agrees with the theoretical 100% spin-polarized density of states, and the energy gap observed by spin-resolved photoemission for the minority band[1, 2]. In addition to the characterization of the adiabatic process, we also estimate the non-adiabatic STT parameter β [5] from the variation of the magnitude of mutual inductance with applied current.

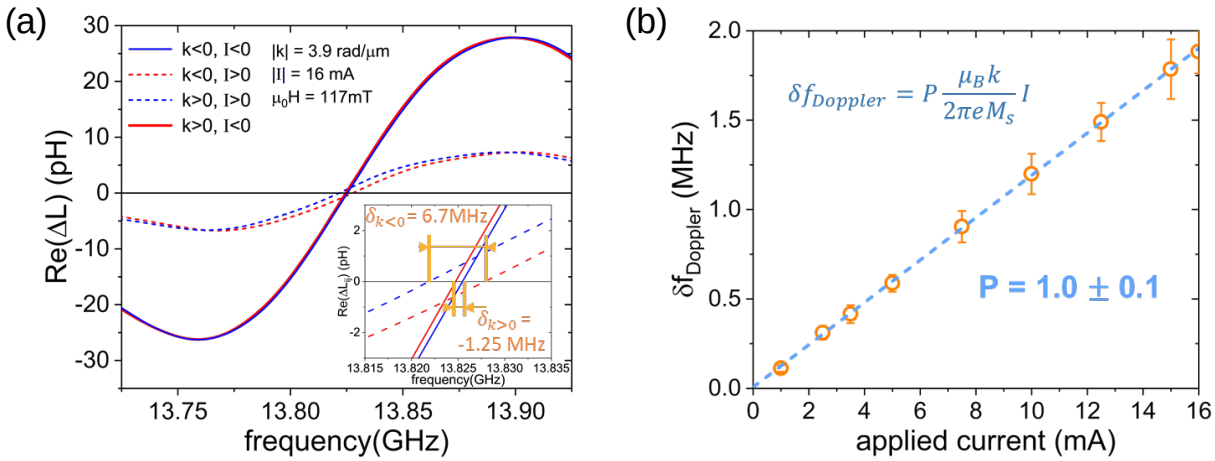

Figure 2: (a) Real component of the mutual inductance signal between antennas produced by the propagation of spin waves under an electrical current of 16 mA, (b) Spin wave Doppler frequency shift vs. applied electron current.

Acknowledgments

We acknowledge financial support from Agence Nationale de la Recherche (France) under Contract No. ANR-20-CE24-0012 (MARIN), and to the Interdisciplinary Thematic Institute QMat, as part of the ITI 2021- 2028 program of the University of Strasbourg, CNRS 9 and Inserm, IdEx Unistra (ANR 10 IDEX 0002). We also acknowledge the technical support of Romain Bernard, Sabine Siegwald and Hicham Majjad in the STnano platform, and of Marc Lenertz in the X-ray diffraction platform of IPCMS.

References

[1] Stéphane Andrieu, Amina Neggache, Thomas Hauet, et al. Direct evidence for minority spin gap in the Co2MnSi Heusler compound. *Physical Review B* 93, 094417 (2016).

[2] C. Guillemard, S. Petit-Watelot, L. Pasquier, et al. Ultralow Magnetic Damping in Co2Mn -Based Heusler Compounds: Promising Materials for Spintronics. *Physical Review Applied* 11, 064009 (2019).

[3] Vincent Vlaminck and Matthieu Bailleul. Current-induced spin-wave Doppler shift. *Science (New York, N.Y.)* 322, 410–413 (2008).

[4] J. Solano, O. Gladii, P. Kuntz, et al. Spin-wave study of magnetic perpendicular surface anisotropy in single crystalline MgO/Fe/MgO films. *Physical Review Materials* 6, 124409 (2022).

[5] Matthieu Bailleul and Jean-Yves Chauleau. “Spin Wave Confinement: Propagating Waves, Second Edition”. Ed. by Sergej O. Demokritov. Second edition. Pan Stanford Publishing, 2017. Chap. Current-Induced Spin Wave Doppler Shift.

Terahertz time-domain spectroscopy platform for spin-to-charge conversion study of spintronic emitters: application on $PtSe_2/Bi_2Se_3$ TMD/TI structures

Sylvain Massabeau[1,*], Martin Mičica[3], Khasan Abdukayumov[4], Romain Lebrun[1,2], Sukhdeep Dhillon[3], Matthieu Jamet[4], Jean-Marie George[1], and Henri Jaffrès[1]

[1]*Unité Mixte de Physique, CNRS, Thales, Université Paris-Saclay, F-91767 Palaiseau, France*
[1,2]*Thales Research and Technology TRT, Palaiseau, France*
[3]*Laboratoire de Physique de l'Ecole Normale Supérieure LPENS, Paris, France*
[4]*Université Grenoble Alpes, CEA, Grenoble INP, IRIG-Spintec, Grenoble, France*
*sylvain.massabeau@cnrs-thales.fr

Standard spintronic terahertz emitters (STE) typically consist of nanometer thick ferromagnetic (FM)/heavy metal (HM) junctions. While excited by a femtosecond near-infrared laser, an out-of-equilibrium spin current is generated in the former [1], that is converted to a transient charge-current in the latter, defining a spin-to-charge conversion (SCC). This current then gives rise to a linearly polarized Terahertz (THz) pulse, where the polarization can be easily controlled by a small applied magnetic field. Owing to the gap-less and broadband THz field emitted by such ultrathin materials, STE have raised considerable interest [2] as novel source for THz spectroscopy as well as an exciting platform to study the SCC mechanisms via THz time-domain spectroscopy (TDS).

In standard FM/HM STE, the SCC is mainly driven by a bulk mechanism - the inverse spin Hall effect (ISHE) - occuring in the HM due to its large spin-orbit coupling. Additionally, at the interfaces where a strong Rashba effect is observed, an incoming spin current may be converted in charge current via an interfacial mechanism, the inverse Rashba-Edelstein effect (IREE). Consequently, the stronger the Rashba effect is, higher is the SCC, and so the THz emission.

Motivated by recent theoretical works [3] showing large Rashba splitting at transition metal dichalcogenide/toplogical insulator interfaces made of $PtSe_2/Bi_2Se_3$, as well as recent experimental works showing an increase of THz emission via IREE in these heterostructures [4], we propose to experimentally study the SCC efficiency of such systems using THz-TDS.

Our three samples under investigation have the following structure : Al/Co/$PtSe_2$(xML)/Bi_2Se_3(yQL) on a sapphire substrate (ML: monolayer, QL: quintuple layer), with (x=0,y=2) considered as the reference, and two other samples with 2ML of $PtSe_2$, with y=2 and y=10 respectively. In all experiments, the STE are excited on Co face by a Yb-doped solid state femtosecond laser coupled to an optical parametric amplifier, delivering 80 fs pulses centered at the desired wavelength, and the emitted THz pulses are detected using electro-sampling with a THz-TDS system in transmission configuration. Owing to our widely tunable laser setup, we performed THz emission measurements using pump central wavelengths of 670, 780 and 940 nm.

The pump beam polarization is fixed and linear, we apply a small and fixed in-plane magnetic field (+B $\sim$ 40 mT) and we measure the THz emission while rotating the sample over the pump beam axis. In order to separate the magnetic/non-magnetic contributions $S_{mag}/S_{non-mag}$ from the THz time traces S_{+B}, we perform the same measurements with a reversed magnetic field (-B) and compute the following quantities:

$$S_{mag} = \frac{S_{+B} - S_{-B}}{2} \quad \text{and} \quad S_{non-mag} = \frac{S_{+B} + S_{-B}}{2} \tag{1}$$

The peak-to-peak values of each S_{mag} and $S_{non-mag}$ time traces for each angle are then reported on a polar plot.

For the magnetic contribution (see Fig. 1), we observe an isotropic emission for all samples, as expected from the linear response theory (1st order of perturbation). The addition of $PtSe_2$(2ML) in the structure leads to a decrease of the THz emission, which might originates from a pure optical absorption. However, by increasing the thickness of Bi_2Se_3, the emission is increased, even larger than the reference. The enhancement of the magnetic contribution to the THz emission thus might originate from the existence of a large Rashba splitting at the $PtSe_2$(2ML)/Bi_2Se_3(10QL) interface or from a SCC via ISHE in the bulk Bi_2Se_3 as both mechanisms coexist [5].

We now turn on the non-magnetic contribution to the THz emission, as shown in Fig. 2. We note that only the sample with $PtSe_2$ and the thicker layers of Bi_2Se_3 exhibit a significant THz signal. The emission pattern is anisotropic, showing two 3-fold symmetries, which may originate either from the dichalcogenide or from the insulating layers (rectification effects or shift currents). Interestingly, if we compare the magnetic and non-magnetic contributions for this specific sample (right figures in Fig. 1 and Fig. 2), we see that the THz emission amplitudes have opposite variations with respect to the excitation wavelength. This evolution is in agreement with literature for the magnetic contribution. For the non-magnetic contribution, it could originate from the formation of a Schottky barrier at the $PtSe_2$(2ML)/Bi_2Se_3(10QL) interface, which would impose specific electron transmission conditions at the interface, depending on the energy gap of $PtSe_2$.

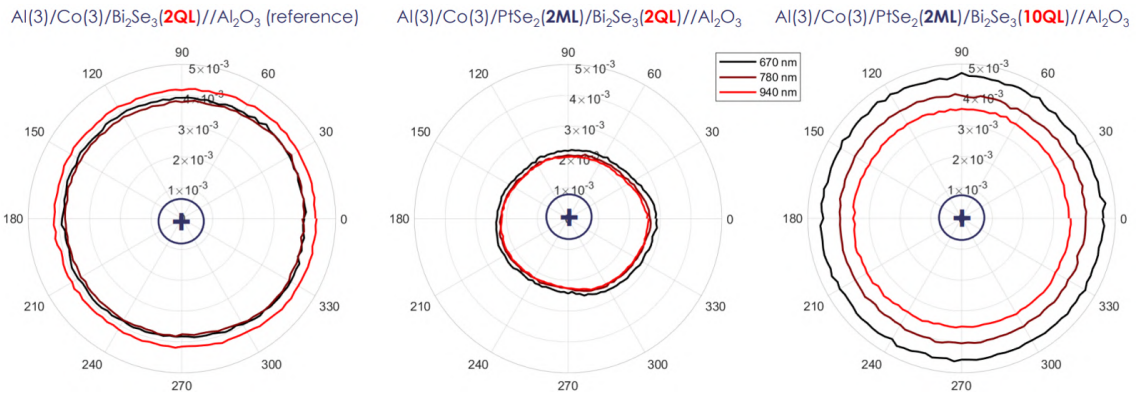

Figure 1: Magnetic contribution to THz emission in our samples of interest, extracted using Eq. 1, for various excitation wavelengths. The signs indicate the phase of the THz temporal traces. The numbers in parenthesis indicates the thickness of the Al and Co layers in nm.

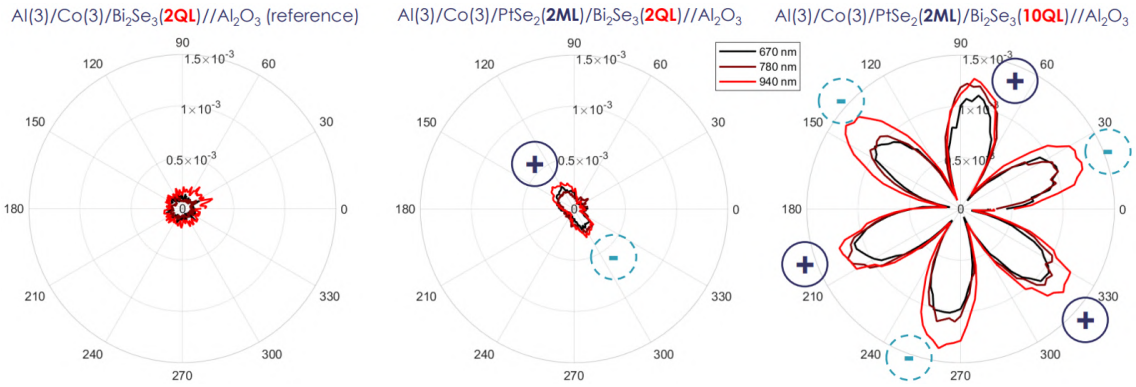

Figure 2: Non-magnetic contribution to THz emission in our samples of interest, extracted using Eq. 1, for various excitation wavelengths. The signs indicate the phase of the THz temporal traces, which changes depending on the sample angle. The numbers in parenthesis indicates the thickness of the Al and Co layers in nm.

In conclusion, we have performed THz-TDS on spintronic emitters made of transition metal dichalcogenide/ topological insulator layers, showing complex THz emission patterns and interactions with the pump energy. In order to conclude on the main mechanisms involved in the THz emission, we are currently investigating a fourth system made of Bi_2Se_3(10QL) without $PtSe_2$. Additionally, one could use the near-infrared idler pump from our system (0.5 - 1.03 eV) to pump the emitters below the $PtSe_2$(2ML) gap (0.65 - 0.85 eV) in order to better understand its role in the non-magnetic THz emission process.

Acknowledgments

This work was supported by the French Agence Nationale de la Recherche under the program ESR/EquipEx+ (Grant No. ANR-21-ESRE-0025).

References

[1] T. Seifert, S. Jaiswal, U. Martens, et al. Efficient metallic spintronic emitters of ultrabroadband terahertz radiation. *Nature Photonics* 10, 483–488 (2016).

[2] Evangelos Th. Papaioannou and René Beigang. THz spintronic emitters: a review on achievements and future challenges. *Nanophotonics* 10, 1243–1257 (2021).

[3] Shahid Sattar and J. Andreas Larsson. Tunable Electronic Properties and Large Rashba Splittings Found in Few-Layer Bi $_2$ Se $_3$ /PtSe $_2$ Van der Waals Heterostructures. *ACS Applied Electronic Materials* 2, 3585–3592 (2020).

[4] K. Abdukayumov, M. Mičica, F. Ibrahim, et al. Atomic-layer controlled THz Spintronic emission from Epitaxially grown Two dimensional PtSe$_2$/ferromagnet heterostructures (2023).

[5] Anand Nivedan and Sunil Kumar. Excitation wavelength-dependent ultrafast THz emission from surface and bulk of three-dimensional topological insulators. *Journal of Physics D: Applied Physics* 56, 255101 (2023).

THz-Induced Spin Dynamics in Nanoscale Multi-Domain State with Perpendicular Magnetic Anisotropy

M. Riepp[1, 2, *], A. Philippi-Kobs[3], L. Müller[2], R. Frömter[4], W. Roseker[2], R. Rysov[2], K. Bagschik[2], S. Bajt[5], R. Pan[2], T. Golz[2], N. Stojanovic[6], and G. Grübel[2]

[1]*Université de Strasbourg, CNRS, Institut de Physique et Chimie des Matériaux de Strasbourg (IPCMS), UMR 7504, 67000 Strasbourg, France*
[2]*Deutsches Elektronen-Synchrotron DESY, Notkestraße 85, 22607 Hamburg, Germany*
[3]*Institut für Experimentelle und Angewandte Physik, Christian-Albrechts-Universität zu Kiel, Leibnitzstraße 19, 24098 Kiel, Germany*
[4]*Institute of Physics, Johannes Gutenberg-Universität Mainz, Staudinger Weg 7, 55128 Mainz, Germany*
[5]*The Hamburg Centre for Ultrafast Imaging, Luruper Chaussee 149, 22761 Hamburg, Germany*
[6]*Institute for Optical Sensor Systems, Deutsches Zentrum für Luft- und Raumfahrt, Rutherfordstraße 2, 12489 Berlin, Germany*
*matthias.riepp@ipcms.unistra.fr

The possibility of manipulating magnetic states on pico- down to femtosecond time scales by ultrashort light pulses opens promising new ways for energy efficient spintronics and high-density data recording applications. Scientific breakthroughs over the past 25 years include the discovery of ultrafast *laser-induced demagnetization* [1] and *all-optical switching* of the magnetization [2]. Both mechanisms rely on the excitation of the magnetic material with a femtosecond optical laser, i. e., the generation of a highly non-equilibrium hot electron distribution with an energy of a few 1 eV, and the consecutive transfer of energy to spin and phonon degrees of freedom. Hence, such *on-off* and *toggle* switching of the magnetization can be understood as pure thermal phenomena involving incoherent spin dynamics. The manipulation of spins in a coherent way, as observed, e. g., in [3], has become possible through the availability of highly intense light pulses in the THz spectral range (≈ 0.1–10 THz), both at linear accelerators like LCLS or FLASH [4, 5] and in the laboratory [6], reaching peak electric and magnetic field amplitudes in the range of a few 1 GV m^{-1} and 1 T, respectively. With a photon energy of only a few 1–10 meV, THz radiation allows to directly access numerous low-energy excitations, such as lattice vibrations and coherent spin precessions.

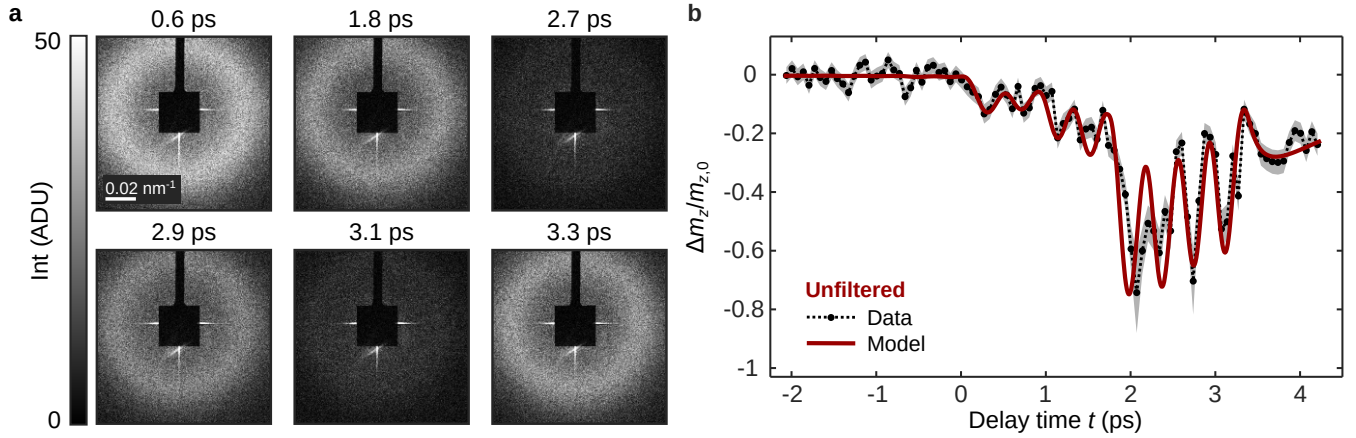

Figure 1: **a** Scattering images $I_m(\mathbf{q})$ for selected delay times t obtained by TR-XRMS from the magnetic multi-domain state of a Co/Pt thin film at the BL3 instrument of FLASH. **b** Ultrafast response of the magnetization $\Delta m_z(t)/m_{z,0}$ to polychromatic THz excitation. The data is modeled as a convolution of incoherent ultrafast demagnetization and coherent spin precession.

We report on the ultrafast response of a magnetic multi-domain state upon polychromatic THz excitation employing time-resolved XUV resonant magnetic scattering (TR-XRMS) at the free-electron laser FLASH. Scattering images from the Co/Pt thin film with perpendicular magnetic anisotropy (PMA) and nanoscale magnetic domains are shown in Fig. 1 **a** for selected pump–probe delay times t. We observe an ultrafast de- and re-magnetization within only 1 ps, when blocking high-energy components of the THz spectrum with a longpass filter, and a step-like demagnetization over ≈ 2 ps with a precessional recovery, when using the full THz spectrum (see Fig. 1 **b**). We develop a unified model which is capable of

describing both responses via the convolution of incoherent ultrafast demagnetization and coherent spin precession in the presence of PMA. For the case of using the filtered THz spectrum, at any time, the magnetic anisotropy energy is much larger than the thermal energy so that the precessional spin dynamics are strongly damped. Only for the case of using the unfiltered THz spectrum, the high-energy electronic excitations result in a substantial phonon excitation and thus a noticable transient reduction of PMA. Analysis of the temporal evolution of the lateral domain configuration via the position of the first-order magnetic scattering ring reveals that the domain state remains largely unperturbed throughout these ultrafast dynamics. Our results shed new light on the coherent response of spins to intense THz radiation in ferromagnetic Co/Pt thin films with PMA and nanoscale magnetic multi-domain state.

Acknowledgments

We would like to thank the team at FLASH for their great support, E. Jal, B. Vodungbo, M. Hennes, N. Bergeard and C. Boeglin for fruitful discussions and acknowledge funding by the Deutsche Forschungsgemeinschaft (DFG, German Research Foundation) – SFB-925 – project 170620586.

References

[1] E. Beaurepaire, J.-C. Merle, A. Daunois, and J.-Y. Bigot. Ultrafast Spin Dynamics in Ferromagnetic Nickel. *Physical Review Letters* 76, 4250–4253 (1996).

[2] C. D. Stanciu, F. Hansteen, A. V. Kimel, et al. All-Optical Magnetic Recording with Circularly Polarized Light. *Physical Review Letters* 99 (2007).

[3] Mostafa Shalaby, Andreas Donges, Karel Carva, et al. Coherent and incoherent ultrafast magnetization dynamics in 3d ferromagnets driven by extreme terahertz fields. *Physical Review B* 98 (2018).

[4] Ziran Wu, Alan S. Fisher, John Goodfellow, et al. Intense terahertz pulses from SLAC electron beams using coherent transition radiation. *Review of Scientific Instruments* 84 (2013).

[5] Rui Pan, Ekaterina Zapolnova, Torsten Golz, et al. Photon diagnostics at the FLASH THz beamline. *Journal of Synchrotron Radiation* 26, 700–707 (2019).

[6] Peter Salén, Martina Basini, Stefano Bonetti, et al. Matter manipulation with extreme terahertz light: Progress in the enabling THz technology. *Physics Reports* 836-837, 1–74 (2019).

Atomic-layer controlled THz Spintronic emission from Two dimensional $PtSe_2$/ferromagnet heterostructures

M. Mičica[1,*], K. Abdukayumov[2], F. Ibrahim[3], C. Vergnaud[3], A. Marty[3], J.-Y. Veuillen[4], P. Mallet[4], I. Gomes de Moraes[3], D. Dosenovic[5], A. Ouerghi[6], V. Rendard[7], F. Mesple[7], F. Bonell[3], H. Okuno[5], M. Chshiev[3], J.-M. George[8], H. Jaffres[8], S. Dhillon[1], and M. Jamet[2]

[1]*Laboratoire de Physique de l'Ecole Normale Supérieure, ENS, Université PSL, CNRS, Sorbonne Université, Université de Paris, Paris, France*
[2]*Univ. Grenoble Alpes, CEA, CNRS, Grenoble INP, IRIG-Spintec, 38000 Grenoble, France*
[3]*Univ. Grenoble Alpes, CEA, CNRS, Grenoble INP, IRIG-Spintec, 17 avenue des Martyrs, 38054 Grenoble CEDEX 9, France*
[4]*Université Grenoble Alpes, CNRS, Grenoble INP, Institut NEEL, 38000 Grenoble, France*
[5]*Université Grenoble Alpes, CEA, IRIG-MEM, 38000 Grenoble, France*
[6]*Université Paris-Saclay, CNRS, Centre de Nanosciences et de Nanotechnologies, 91120, Palaiseau, France*
[7]*Université Grenoble Alpes, CEA, CNRS, IRIG-PHELIQS, 38000 Grenoble, France*
[8]*Unité Mixte de Physique, CNRS, Thales, Université Paris-Saclay, F-91767 Palaiseau, France*
*martin.micica@phys.ens.fr

Abstract - Spintronic emitters have become an important THz photonic source with broadband THz emission and the ability to magnetically control the emitted polarization through ultrafast spin-to-charge conversion (SCC). This work has recently driven investigations of two-dimensional (2D) materials for new types of spintronic THz sources. One such 2D material is the transition-metal dichalcogenide $PtSe_2$. Here we present THz spintronic sources based on high quality epitaxially grown CoFeB/$PtSe_2$/graphene heterostructures, with $PtSe_2$ thicknesses ranging from 1 to 15 monolayers. The unique thickness dependent electronic structure of $PtSe_2$ permits to demonstrate the different origins of the THz emission - from the inverse Rashba-Edelstein effect in monolayer PtSe2 to the inverse spin Hall effect for multilayers. This unique bandstructure flexibility makes $PtSe_2$ an ideal candidate as a THz spintronic 2D material and to further study and explore the underlying mechanisms and engineering of ultrafast SCC.

During the past two decades, two-dimensional (2D) materials have raised tremendous interest in the scientific community for the unique and specific properties as a result of their reduced dimensionality and van der Waals character. In particular, when isolated to one monolayer (ML), transition metal dichalcogenides (TMD) 1H-MX_2 (with M=Mo, W and X=S, Se) become direct bandgap semiconductors with remarkable optical properties [1]. Platinum diselenide ($PtSe_2$) is a very recent TMD that shows several key properties like air stability, high carrier mobility and high photoelectrical response in the near-infrared range [2]. Moreover, it exhibits a layer-dependent bandgap: one monolayer of $PtSe_2$ is a 1.9 eV bandgap semiconductor while layers greater than 3 ML it becomes semi-metallic [3]. Finally, the strong spin-orbit coupling of $PtSe_2$ makes it an excellent candidate to study spin-to-charge conversion (SCC) in van der Waals materials. In this respect, it constitutes a unique system to observe the transition from inverse Rashba-Edelstein effect (IREE) in the semiconducting phase to inverse spin Hall effect (ISHE) in the semi-metallic phase. Terahertz (THz) emission spectroscopy in this respect has become a powerful and established tool to probe SCC [4]. The associated devices are then known as spintronic THz emitters and were first demonstrated with metallic ferromagnetic (Co, Fe...)/nonmagnetic (Pt, W...) thin films. They present several advantages compared to other THz sources such as broadband THz emission, high efficiency and easy control of radiation parameters. To date, very few 2D materials have been incorporated in THz spintronic emitters and they all exhibit the 1H crystal symmetry, which is not favorable to convert in-plane polarized spins into charge currents.

In this work [5], we have grown single crystalline mono and multilayers of 1T-$PtSe_2$ on graphene, followed by amorphous CoFeB, with atomically sharp interfaces. We used a full set of characterization tools to demonstrate the structural and chemical preservation of $PtSe_2$ after CoFeB deposition. SCC was then studied on these advanced 2D samples using THz emission spectroscopy as a function of $PtSe_2$ thickness (from 1 to 15 ML), that showed the generation of efficient THz electric fields. This THz emission is shown to arise from the 1T crystal structure and large spin-orbit coupling of $PtSe_2$. The measured peak electric field as a function of number $PtSe_2$ are shown in Figure 1. The THz electric field clearly shows a two-step dependence with $PtSe_2$ thickness, which we interpret as the transition from the IREE in the semiconducting regime to the ISHE in the semimetallic regime (around 3 to 4 MLs). As shown by ab initio calculations in figure 1b that takes into account the different SCC mechanisms, the IREE arises from the large Rashba spin splitting at the $PtSe_2$/graphene interface by the combination of large spin-orbit coupling and electron transfer from graphene to $PtSe_2$, generating an interface electric field. By fitting the thickness dependence, we can extract the out-of-plane spin diffusion length in $PtSe_2$ to be 2-3 nm and find that SCC by IREE at the PtSe2/Gr interface is twice as efficient than that of ISHE in bulk $PtSe_2$. This is summarized

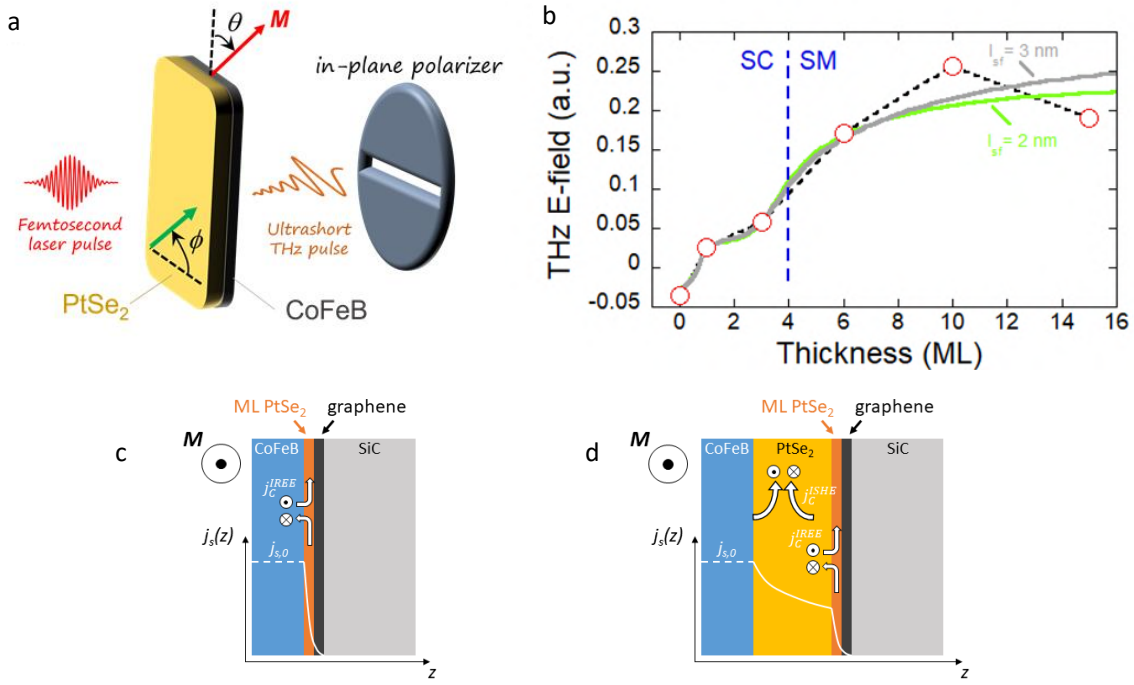

Figure 1: a) Optical excitation of CoFeB/$PtSe_2$/graphene junctions for THz generation. b) Normalized peak THz field obtained from samples with different number of $PtSe_2$ layers. Transition from semiconductor (SC) to semimetal (SM) can be estimated around 4 monolayers. c) and d) Illustration of the spin-to-charge conversion in CoFeB/$PtSe_2$/graphene samples. In the sample with 1 monolayer $PtSe_2$ a) the contribution is due to IREE and thick $PtSe_2$ sample b) where both ISHE and IREE are presented. White curve: profile of js(z). js(0) is the effective spin current injected in $PtSe_2$ from optically pumped CoFeB.

in Figure c) and d) where IREE takes place in the $PtSe_2$ monolayer in contact with graphene and ISHE in the semimetallic bulk $PtSe_2$ respectively.

To summarize, owing its unique thickness dependent electronic structure, $PtSe_2$-ferromagnetic heterostructures have shown THz emission and has enabled to observe the transition from IREE to ISHE in a single 2D material system. This opens up novel applications of these structures to THz spintronics. For example, by further adjusting the Fermi level position by gating the semiconductor material, it will be possible to modulate and dramatically enhance the SCC efficiency, and achieve electronically controlled spintronic THz emission.

References

[1] Kin Fai Mak, Changgu Lee, James Hone, Jie Shan, and Tony F. Heinz. Atomically Thin MoS_2: A New Direct-Gap Semiconductor. *Phys. Rev. Lett.* 105, 136805 (13 2010).

[2] Frédéric Bonell, Alain Marty, Céline Vergnaud, et al. High carrier mobility in single-crystal PtSe2 grown by molecular beam epitaxy on ZnO(0001). *2D Materials* 9, 015015 (2021).

[3] Banglin Cao, Zimeng Ye, Lei Yang, Li Gou, and Zegao Wang. Recent progress in Van der Waals 2D PtSe2. *Nanotechnology* 32, 412001 (2021).

[4] T. Seifert, S. Jaiswal, U. Martens, et al. Efficient metallic spintronic emitters of ultrabroadband terahertz radiation. *Nature Photonics* 10, 483–488 (2016).

[5] K. Abdukayumov, M. Mičica, F. Ibrahim, et al. Atomic-layer controlled THz Spintronic emission from Epitaxially grown Two dimensional $PtSe_2$/ferromagnet heterostructures (2023). arXiv: 2305.06895.

Session 6: Chiral and topological magnetic textures
11h00 – 13h00
Chair: Stanislas Rohart and Aurore Finco

11h00 – 11h20	**Alban Simonnot**	SPEC	Modelling magnetic walls in NiO	page 286
11h20 – 11h40	**Arthur Chaudron**	UMR CNRS/Thales	Tailoring Topological Polar Nanotextures in Multiferroic $BiFeO_3$ Thin Films	page 287
11h40 – 12h00	**Anaïs Fondet**	CEMES	Towards room temperature nanoscale skyrmions in ferromagnetic metallic superlattices	page 289
12h00 – 12h20	**Sujit Panigrahy**	LPS	Nucleation and motion of synthetic antiferromagnetic skyrmions at zero field	page 291
12h20 – 12h40	**Capucine Gueneau**	SPINTEC	Control of Domain Wall Chirality in a Double Wedge System	page 293
12h40 – 13h00	**Ping Che**	UMR CNRS/Thales	Observations of bubble resonances in a magnetic insulator via time-resolved scanning transmission X-ray microscopy	page 295

Modelling magnetic walls in NiO

Alban Simonnot[1,2 *], Frédéric Miserque[1], Jean-Baptiste Moussy[2], Michel Viret[2], Jean-Yves Chauleau[2], and Alain Chartier[1]

[1]*Université Paris-Saclay, CEA, Service de recherche en Corrosion et Comportement des Matériaux, 91191 Gif Sur Yvette, France*
[2]*Université Paris-Saclay, CEA/CNRS, Service de physique de l'état condensé, 91191 Gif sur Yvette, France*
**alban.simonnot@cea.fr*

NiO is a text-book example of an antiferromagnetic oxide that could be part of spintronic devices. It has a complex magnetic structure, in which four possible T domains (favorite magnetization staggering direction) with 3 possible S orientations each (favorite orientations of spin) may stabilize, making a total of 12 possible configurations or 12 so called TS domains. Transition zones - i.e. domain walls (DWs) - between TS domains may occur in NiO. They usually exhibit complicated spin configurations which drastically influence the magnetic properties. These DWs may also turn out to be detrimental for the use of NiO - or any antiferromagnetic compound - in spintronic devices. In fact, some experimental and theoretical studies have been dedicated to DWs in NiO [1], but a complete description at the atomic scale is still missing.

In the present work, we provide insights on a large variety of domain walls (DWs) in NiO at the atomic scale and try to establish links with experimental observations. We employ for that purpose an Heisenberg description of spin interactions in NiO on a rigid lattice as implemented in Vampire [2], an Atomic Spin Dynamic (ASD) software, for which superexchange interactions and anisotropic constants were carefully optimized in order to reproduce the magnetic structure and the Néel temperature.

For each domain wall simulated, we analyse in detail the spin profile and we calculate both X-ray Magnetic Linear Dichroism-PhotoEmission Electron Microscope (XMLD-PEEM) and Nitrogen Vacancies Magnetometry (NVM) images from which we deduce their widths (when possible).

We observe in our simulations that spins have to go through the direction common to both circumscribing T domains when they transit throughout DWs. Indeed, their detailed configurations in DWs are driven by both bordering T domains. However, we show that for any surface corresponding to one T domain of the walls, DWs do have enough ferrimagnetic character so that widths can be seen and measured with NVM technique. Conversely, XMLD-PEEM images always exhibit significant changes of intensity whatever the surface plane and the DW type. It therefore reveals easy to determine the width of all DWs with this technique.

We also find that the calculated DWs widths show a $\sqrt{1/K_2}$ dependence in good agreement with theory [3]. The extrapolated widths of DWs using experimental anisotropic constants correspond nicely to experimental observations [1]. Moreover, some widths observed in experiments can be re-interpreted and even unequivocally related to specific DWs.

References

[1] Kuniaki Arai, Taichi Okuda, Arata Tanaka, et al. Three-dimensional spin orientation in antiferromagnetic domain walls of NiO studied by x-ray magnetic linear dichroism photoemission electron microscopy. *Physical Review B* 85, 104418 (2012).

[2] R. F. L. Evans, W. J. Fan, P. Chureemart, et al. Atomistic spin model simulations of magnetic nanomaterials. *Journal of Physics: Condensed Matter* 26, 103202 (2014).

[3] C. Mitsumata and A. Sakuma. Generalized Model of Antiferromagnetic Domain Wall. *IEEE Transactions on Magnetics* 47, 3501–3504 (2011).

Tailoring Topological Polar Nanotextures in Multiferroic $BiFeO_3$ Thin Films

A. Chaudron[1,*], A. Finco[2], V. Jacques[2], M. Viret[3], J. Chauleau[3], Z. Li[3], A. Abdelsamie[1], P. Dufour[1], S. Collin[1], K. Bouzehouane[1], S. Fusil[1], and V. Garcia[1]

[1]*Unité Mixte de Physique CNRS, Thales, Université Paris-Saclay, Palaiseau, France*
[2]*L2C, Université de Montpellier, CNRS, Montpellier, France*
[3]*SPEC, CEA, CNRS, Université Paris-Saclay, Gif-sur-Yvette, France*
*arthur.chaudron@cnrs-thales.fr

Bismuth Ferrite ($BiFeO_3$) exhibits both a ferroelectric and antiferromagnetic behavior at room temperature, placing itself at the forefront of research on multiferroic materials. In the rhombohedral phase, its ferroelectric polarization lies along the diagonals of the unit cell, while its antiferromagnetic order has been shown to depend on the applied strain.

Thus, in epitaxially strained thin films, $BiFeO_3$ can display bulk-like (type-1) spin cycloids, exotic (type-2) spin cycloids, or a G-type antiferromagnetic order. Because of the magnetoelectric coupling, both ferroic orders of $BiFeO_3$ are coupled together, yielding a one-to-one correspondence between the ferroelectric polarization direction and the propagation direction of the spin cycloid in thin films [1].

In this context, I will present the consequences of this magnetoelectric coupling on topological polar nanotextures designed on epitaxial $BiFeO_3$ thin films. It will be shown that stable multiferroic topological structures can be induced electrically, with antiferromagnetic domain wall patterns precisely following that of their ferroelectric counterparts.

Such textures are written through the interaction of a conductive AFM tip with either a bottom or top electrode created via electronic beam lithography [2], and their characterization is performed by vector piezoresponse force microscopy (PFM) and scanning NV-center magnetometry.

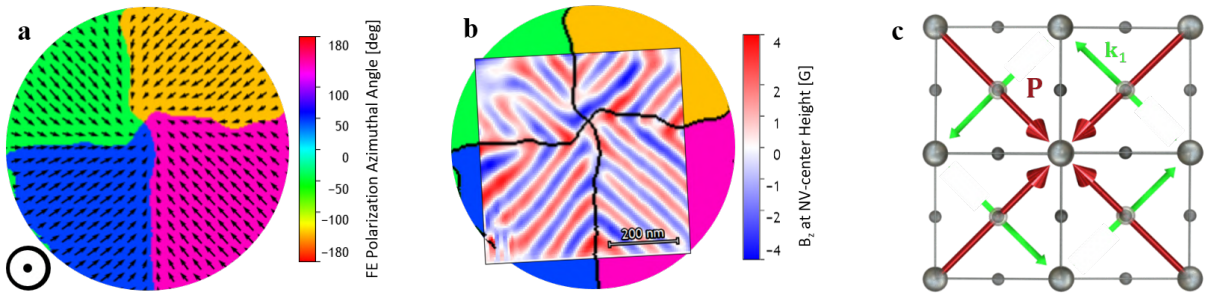

Figure 1: Magnetoelectric coupling in a ferroelectric center-convergent state under compressive strain. **a**, PFM vector map and underlying ferroelectric texture. **b**, Overlap with magnetic field measured by NV-center magnetometry. **c**, Schematics of ferroelectric polarization and coupled spin cycloid propagation directions in all four quadrants.

Among the textures stabilized under compressively strained thin films, the four-quadrant center-divergent and center-convergent ferroelectric textures all display a chiral in-plane rotation of the spin cycloid propagation direction around the center, while it remains perpendicular to the ferroelectric polarization (see Fig. 1).

When the films are grown under slight tensile strain, the same ferroelectric textures yield a unique and uniform in-plane spin cycloid propagation direction on all quadrants.

Finally, and quite exotically, those same ferroelectric textures on films grown under larger tensile strain exhibit a one-to-one correspondence between the canted G-type antiferromagnetic moment direction and the ferroelectric polarization, as illustrated in Fig. 2.

In all cases, those multiferroic topological polar textures, resulting from electrical writing, contrast with the as-grown state patterns of the thin films, thus paving the way for potential applications in high-density multiferroic topological memories for instance.

Acknowledgments

The authors thank support from the French Agence Nationale de la Recherche (ANR) through the TATOO (ANR-21-CE09-0033) project. This project has received funding from the European Union's Horizon 2020 research and innovation programme under grant agreement No 964931 (TSAR).

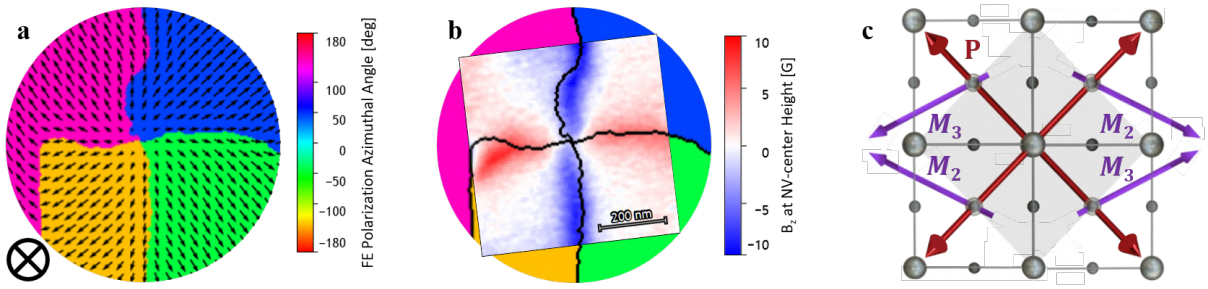

Figure 2: Magnetoelectric coupling in a ferroelectric center-divergent state under tensile strain. **a**, PFM vector map and underlying ferroelectric texture. **b**, Overlap with magnetic field measured by NV-center magnetometry. **c**, Schematics of ferroelectric polarization and coupled G-type magnetization directions in all four quadrants.

References

[1] A. Haykal, J. Fischer, W. Akhtar, et al. Antiferromagnetic textures in BiFeO3 controlled by strain and electric field. *Nature Communications* 11, 1704 (2020).

[2] Wenda Yang, Guo Tian, Hua Fan, et al. Nonvolatile Ferroelectric-Domain-Wall Memory Embedded in a Complex Topological Domain Structure. *Advanced Materials*, 2107711 (2022).

Towards room temperature nanoscale skyrmions in ferromagnetic metallic superlattices

Anaïs Fondet[1,*], Thomas Blon[2], Sebastien Weber[1], Cyrill B. Muratov[3,4], Anne Bernard-Mantel[1], and Christophe Gatel[1]

[1]*CEMES-CNRS, Toulouse, France*
[2]*LPCNO, Toulouse, France*
[3]*Departimento di Matematica, Universitá di Pisa, L. Bruno Pontecorvo, 5, 56127 Pisa, Italy*
[4]*Department of Mathematical Sciences, New Jersey Institute of Technology, Newark, NJ 07102, USA*
*anais.fondet@cemes.fr

Magnetic skyrmions, which consist of local swirls of spins, are a prime example of topologically nontrivial spin textures. Nanoscale isolated skyrmions exist at low temperature in bulk chiral materials, while in thin films and multilayers, room temperature (RT) stable skyrmions exhibit intermediate sizes ranging between 50 nm to a few μm. Ferromagnetic metallic superlattices are materials which are promising for the development of RT nanoscale skyrmions due to the high tunability of their properties. There exist a large number of experimental studies reporting the observation of stripe domains and skyrmion bubbles in metallic multilayers, for example Pt/Fe/Ir[1] and Ta/Co/Pt[2]. It is well understood that these skyrmions and stripes are created by a combined action of the stray field effect and the Dzyaloshinskii-Moria interaction (DMI)[3]. These non-collinear spin structures can also be easily simulated numericaly[2]. However, in a system with a high number of degree of freedom, the quest remains open regarding how to optimize the parameters to obtain the most compact and stable skyrmion and the development of adequate analytical tools could lead to breakthrough and transform this quest from a random walk to a guided tour.

We focused our investigations on a classical $[Pt/Co/Ta]_n$ metallic superlattices system, n being the number of repetition of the tri-layer. Samples are fabricated by magnetron sputtering at LPCNO. In this system, RT skyrmionic bubbles as small as 50 nm have been observed when the Co thickness was tuned close to the spin reorientation transition[2]. In our study, we work with Pt/Co/Ta trilayers with a fixed Co thickness of 0.8 nm and we tune the thickness of the total system by varying the number of repetitions n. This allows us to tune selectively the effect of the stray field while keeping roughly constant the system intrinsic parameters (magneto-crystalline anisotropy, saturation magnetisation, DMI). Spatially resolved magnetic measurements are performed using magneto-optic techniques and TEM methods - in particular Lorentz microscopy (LTEM) and Electron Holography (EH) for nanoscale studies (see figure 1). We were able to image the magnetic micro-structures of $[Pt/Co/Ta]_n$ multilayers with various different number of repetition. We studied the sample without applied field, but also with in-situ applied field (using LTEM), in order to study the formation of magnetic skyrmions by applied magnetic field, the stripe-skyrmion transition, and the presence of skyrmion lattice or isolated skyrmions in certain samples (see figure 1 (b)). We could correlate magnetic contrast observation with applied field to magnetic hysteresis obtained from VSM measurements. We also studied the influence of the temperature on the stripe pattern and on the formation of skyrmions. We will present an experimental study of the stripe domain structures and skyrmions as a function of the multilayer total thickness.

In complement with the experimental observations, we used a combination of micromagnetic simulations based on Mumax3 and analytical modeling to analyze the variations of the stripes periods. The very good agreement between the simulation and the analytical model (see figure 1(a)) allows us to demonstrate that the stray field effect becomes fully non-local in the intermediate thickness regime under study. We obtained an analytical formula for the stripe period which enables us to predict the minimum stripe width (and consequently the minimum skyrmion size) that can be observed in this experimental system, with the associated magnetic parameters that have to be modified in order to obtain them. The micromagnetic simulations also confirm that there is a negligible z dependence of the spin structure and that the Néel rotation is preserved due to the predominance of the DMI over the stray field effects. This is in agreement with the Lorentz TEM observations that do not display any contrast for the stripe and skyrmions without tilting the sample, which is a sign of a Néel rotation. We will present complementary studies where the temperature and applied magnetic field are used to promote the nucleation and tune the skyrmions sizes and densities.

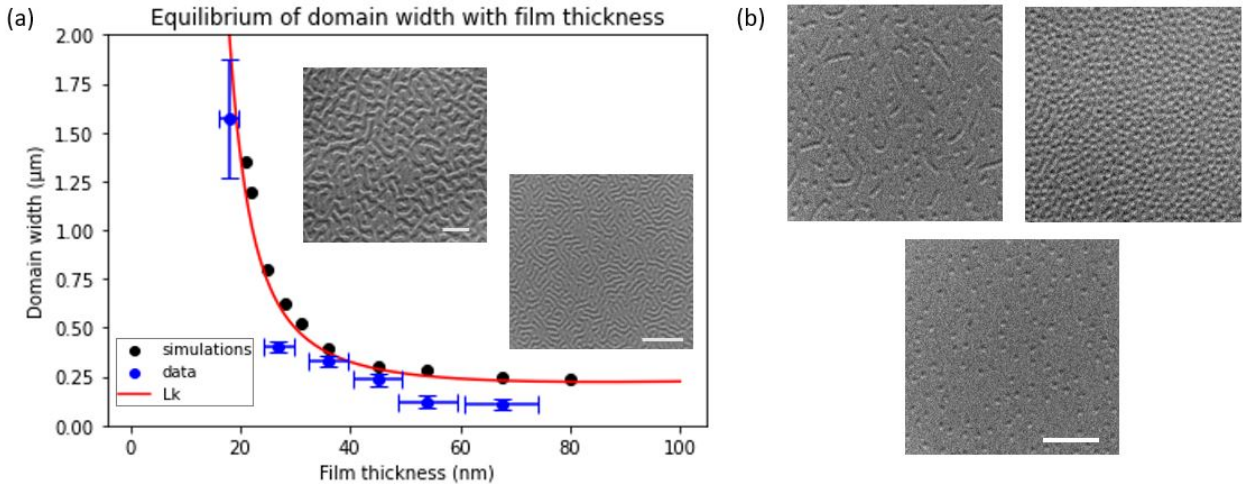

Figure 1: (a) Study of the stripe domain width as a function of the multilayer thickness in $[Pt/Co/Ta]_n$ multilayers. Insets: LTEM observation of stripe domains at zero applied field for two different numbers of repetition n (b) Skyrmions observed by LTEM under different applied magnetic fields, and 30° tilt of sample, presenting mixed stripe-skyrmion, skyrmion lattice and isolated skyrmions magnetic configurations. Scale bars are 2µm long.

References

[1] C Moreau-Luchaire, C Moutafis, N Reyren, et al. Additive interfacial chiral interaction in multilayers for stabilization of small individual skyrmions at room temperature. *Nat Nano* 11, 444–448 (2016).

[2] Lei Wang, Chen Liu, Nasir Mehmood, et al. Construction of a Room-Temperature Pt/Co/Ta Multilayer Film with Ultrahigh-Density Skyrmions for Memory Application. *ACS Appl. Mater. Interfaces* 11, 12098–12104 (2019).

[3] Anne Bernand-Mantel, Lorenzo Camosi, Alexis Wartelle, et al. The skyrmion-bubble transition in a ferromagnetic thin film. *SciPost Phys.* 4, 27 (2018).

Nucleation and motion of synthetic antiferromagnetic skyrmions at zero field

Sujit Panigrahy[1,*], Sougata Mallick[1], João Sampaio[1], André Thiaville[1], and Stanislas Rohart[1]

[1]*Université Paris-Saclay, CNRS, Laboratoire de Physique des Solides, Orsay, France*
Sujit.panigrahy@universite-paris-saclay.fr

Nano-scale size, nontrivial topology and particle-like motion are some of the characteristics of magnetic skyrmions that make them attractive for next-generation nanoscale information storage devices [1]. Significant advances have been made in the recent past to understand the underlying mechanisms to stabilize and move these particle-like excitations in ferromagnetic thin films [2]. These advancements have allowed researchers to routinely stabilize and move skyrmions at room temperature. However, there are several challenges that are yet to be overcome if skyrmions are to be used in functional devices. Arguably, the most important of these challenges is to overcome the skyrmion Hall effect (SkHe) [3], which is an intrinsic property of skyrmions in ferromagnets owing to their non-trivial topology. Due to this property, skyrmions deflect from a straight trajectory along the applied current direction and deviate towards the edge of the device where they can be annihilated causing loss of information. It also limits the velocity of skyrmions in the race-track [4]. To circumvent this problem, synthetic antiferromagnets (SAF) can be designed, where due to opposite topology of skyrmions in two ferromagnetic sublayers, the composite skyrmion is predicted to move along the current direction without any SkHe [5]. Another challenge is to eliminate the use of magnetic field for stabilizing skyrmions, which increases the complexity of devices. It is even more important in the case of SAF, as they are insensitive to magnetic field. We have proposed and experimentally verified a methodology to nucleate and move skyrmions in ferromagnets at zero magnetic field by engineering the effective anisotropy [6]. This acts as a guideline towards stabilising zero field skyrmions in SAF.

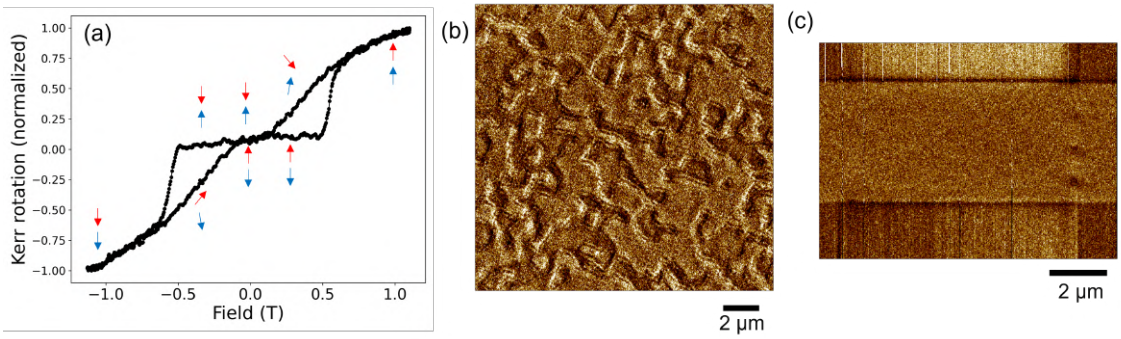

Figure 1: Hysteresis loop of a balanced SAF with out-of-plane field. The sketched arrows indicate the macrospin alignment of the top (red) and bottom (blue) Co layer (a). MFM image of the as-grown state (b), and zero field state after saturation (c).

In this study we show nucleation and motion of SAF skyrmions in a Co based multilayer at room temperature and zero external magnetic field. To stabilize these textures, we explore a multilayer of [Pt(5nm) /Co(t_b) /Ir(0.6nm)/ Pt(0.8nm)/ Co(t_t) / Ta(5nm)]. Here, the two Co layers are antiferromagnetically coupled through an Ir/Pt spacer with an exchange field of about 0.5 T. To ensure the same sign of Dzyaloshinskii-Moriya interaction (DMI) in both layers, each Co layer has asymmetric interfaces with a Pt layer beneath it. To promote efficient current induced motion, Co layers are in contact with thick layers which act as spin current sources. Since the positions of the thick layers (below for bottom and above for top Co) are different, two layers with opposite spin Hall effect (Pt and Ta in our case) are required to drive skyrmions. It is to be noted that the top and bottom Co layers have different interfaces. The bottom Co layer exhibits out-of-plane (OOP) anisotropy, while the top Co layer has in-plane (IP) anisotropy. Hysteresis behaviour of an optimised sample (keeping the zero field state homogeneous yet reducing its stability as much as possible) is shown in Fig. 1 (a). Through magnetic force microscopy (MFM) imaging, it is verified that the as grown state is textured (Fig. 1 (b)). These two properties combined make this sample ideal to study nucleation and dynamics of skyrmions at zero field.

After optimization of sample properties, we study their current-induced propagation in micrometric tracks. To maintain homogeneity of current lines, we choose flat contact pads on top of the magnetic track. Due to naturally occurring small inhomogeneities at the contact, we see specific nucleation points in the sample. Simultaneous nucleation and motion of skyrmions with radius varying from 50-400 nm were observed (Fig. 2 (a-c)) along with nucleation of some larger domains close to the edge of the track (neglected during analysis). Fig. 2 (d) and (e) show skyrmion velocity and skyrmion Hall angle (SkHA) as a function of current density. These skyrmions could move up to 300 m/s for the largest current density

of 8×10^{11} A/m^2. On the other hand, a mean SkHA of less than 3 degrees is observed for all the applied current densities. This confirms the predictions of large velocity and vanishingly small SkHA for SAF skyrmions. In a unbalanced situation (30% uncompensated SAF; bottom layer dominating), we observed a SKHA of around 30 degrees. The deflection direction reverses by reversing the magnetization polarity. This proves the topological nature of these textures. Further, due to the presence of two sublayers with a finite interlayer coupling and different interfacial properties, the SAF layer has a rich magnetization dynamics. We explore this by detecting the spectra of inelastic light scattering by magnons (Brillouin light scattering).

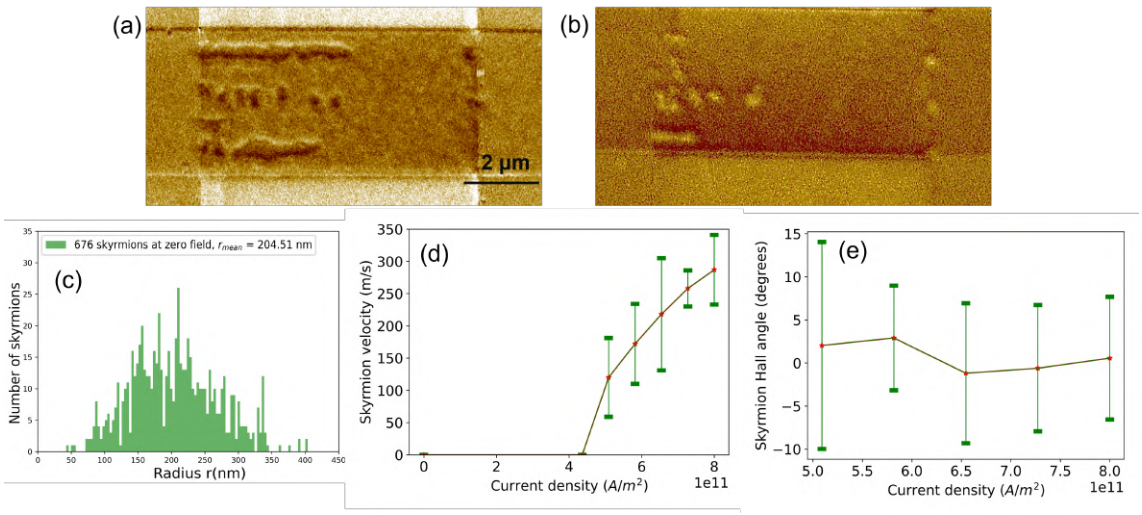

Figure 2: Skyrmion nucleation from homogeneous state after sending ten 7.3×10^{11} A/m^2, 4 ns pulses (a,b). Saturation magnetic field direction has been changed between (a) and (b) without noticeable changes in skyrmion motion contrary to ferromagnets. Nucleated skyrmion radius distribution (c). Skyrmion velocity (d) and SKHA (e) as a function of current density.

Acknowledgements

This work was supported by the French National Research Agency (ANR) [under contract ANR-17-CE24-0025 (TOPSKY) and a public grant overseen as part of the "Investissements d'Avenir" program (Labex NanoSaclay, reference: ANR-10-LABX-0035), SPICY].).

References

[1] Albert Fert, Vincent Cros, and João Sampaio. Skyrmions on the track. *Nature Nanotechnology* 8, 152–156 (2013).

[2] Olivier Boulle, Jan Vogel, Hongxin Yang, et al. Room-temperature chiral magnetic skyrmions in ultrathin magnetic nanostructures. *Nature Nanotechnology* 11, 449–454 (2016).

[3] Wanjun Jiang, Xichao Zhang, Guoqiang Yu, et al. Direct observation of the skyrmion Hall effect. *Nature Physics* 13, 162–169 (2016).

[4] Roméo Juge, Soong-Geun Je, Dayane de Souza Chaves, et al. Current-Driven Skyrmion Dynamics and Drive-Dependent Skyrmion Hall Effect in an Ultrathin Film. *Physical Review Applied* 12 (2019).

[5] Xichao Zhang, Yan Zhou, and Motohiko Ezawa. Magnetic bilayer-skyrmions without skyrmion Hall effect. *Nature Communications* 7 (2016).

[6] Sougata Mallick, Sujit Panigrahy, Gajanan Pradhan, and Stanislas Rohart. Current-Induced Nucleation and Motion of Skyrmions in Zero Magnetic Field. *Physical Review Applied* 18 (2022).

Control of Domain Wall Chirality in a Double Wedge System

Capucine Gueneau[1,*], Johanna Fischer[1], Charles-Elie Fillion[1], Fatima Ibrahim[1], Raj Kumar[1], Libor Vojacek[1], Stefania Pizzini[2], Laurent Ranno[2], Djoudi Ourdani[3], Mohamed Belmeguenai[3], Yves Roussigné[3], Salim-Mourad Chérif [3], Stéphane Auffret[1], Isabelle Joumard[1], Olivier Boulle[1], Gilles Gaudin[1], Mairbek Chshiev[1,4], Liliana D. Buda-Prejbeanu[1], Claire Baraduc[1], and Hélène Béa[1,4]

[1]*Univ. Grenoble Alpes, CNRS, CEA, SPINTEC, Grenoble, France*
[2]*Univ. Grenoble Alpes, CNRS, Institut NEEL, Grenoble, France*
[3]*Laboratoire des Sciences des Procédés et des Matériaux (LSPM), Villetaneuse, France*
[4]*Institut Universitaire de France (IUF), France*
*capucine.gueneau@cea.fr

In ultrathin Heavy Metal/Ferromagnet/Metal Oxide (HM/FM/MOx) heterostructures with Perpendicular Magnetic Anisotropy (PMA), interfacial Dzyaloshinskii-Moriya Interaction (DMI) generally plays an important role in the stabilization of Néel domain walls with a given sense of rotation, also called chirality [1],[2]. The sign of the DMI coefficient D determines the chirality of DWs (Fig. 1a). This antisymmetric exchange interaction arises from the combination of spin-orbit coupling and structural inversion asymmetry at HM/FM and FM/MOx interfaces. A fine tuning of interfaces allows a control of the DMI strength. In regions with small DMI amplitude, we previously observed that a gate voltage can tune DMI sign and dynamically invert domain wall chirality [3]. Hence low DMI samples are promising for the versatile and dymanic control of unique skyrmions.

In a previous study [4], we showed that the chirality of DWs and the DMI sign in a sputtered Ta/FeCoB/TaOx trilayer may be inverted by tuning the FeCoB thickness and FeCoB/TaOx interface oxidation state. We first used a quantitative measurement of the coefficient D by Brillouin Light Scattering (BLS). Additionnaly, in the regions where DMI is too small to be measured, we used qualitative study of DMI sign using the Current Induced Motion (CIM) of DWs [5] observed under polar Magneto-Optical Kerr Effect microscopy. The CIM technique is based on the Spin Hall Effect, which involves the application of an electric current to generate a transverse spin current in the Heavy Metal (HM) layer. As a result, a spin accumulation occurs at the HM/FM interface, which polarization is determined by the Spin Hall Angle of the HM. At the interface between the HM and FM layers, the angular momentum of the accumulated spins is transferred to those within the FM layer. This transfer leads to the generation of a Spin-Orbit Torque, which induces the motion of the domain wall (DW). The Damping-Like component of this torque depends on both the direction of magnetization and the spin accumulation. This implies that the motion will be in opposite directions depending on the chirality of the magnetic texture: Clockwise (CW) (resp. Counter Clock-Wise (CCW)) DW moves along (resp. against) the current when using a HM with a negative spin Hall angle like Ta.

In order to better understand the material dependence and the underlying mechanisms of the DMI sign variation, we present here a systematic study of the influence on DMI sign of FeCoB thickness and FeCoB/TaOx oxidation state. For this purpose, the FeCoB layer is deposited with a thickness gradient perpendicular to a second gradient of Ta that is subsequently oxidized, leading to an oxidation gradient of the FeCoB/TaOx interface (Fig. 1b). Both gradients influence the anisotropy in our sample leading to different regions with In-Plane (IP) anisotropy, PMA and Paramagnetic regime. The previously observed changes in DMI sign have been found at the transition between paramagnetic regime and PMA as well as between PMA and IP anisotropy [4]. In our double wedge sample, chirality has been extracted over the whole PMA region by direct observation of DW motion (see Fig. 2a). Our observation of the DMI sign transition (red dotted line in Fig. 2a) reveals a stair-like evolution, indicating the importance of the layer coverage percentage.

In order to clarify this phenomenon we performed *ab initio* calculations. They reveal a change in the sign of the DMI energy at the interface between Fe and Ta as a function of the oxidation of the Ta interfacial layer (see Fig. 2b). This observation holds regardless of the disorder in the oxygen atoms at the interface as we can see in Fig. 2b for different configurations shown in its insets.. Similarly, when examining the DMI sign relative to the thickness of Fe for different oxidation state at the interface, *ab initio* calculations exhibit good agreement with

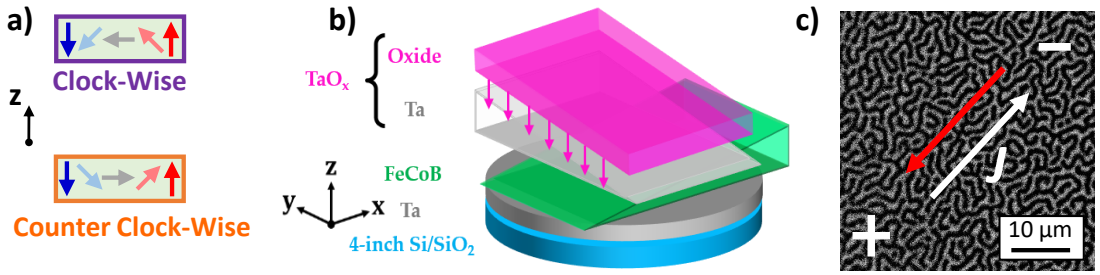

Figure 1: a) Representation of a Clock-Wise CW (Top) and Counter Clock-Wise CCW (Bottom) Néel domain wall. b) Schematic representation of our double wedge sample. c) Differential MOKE image of CCW DW. A microbonded wire is used to send current. The current direction J and the DW motion are represented by a white and a red arrow respectively.

our experimental results. Finally, with the such calculations we are able to untangle the mechanisms of the DMI sign change as a function of both oxidation state and ferromagnetic thickness. These findings may help to design future devices with a controlled value and sign of DMI in order to optimize domain wall mobility [4].

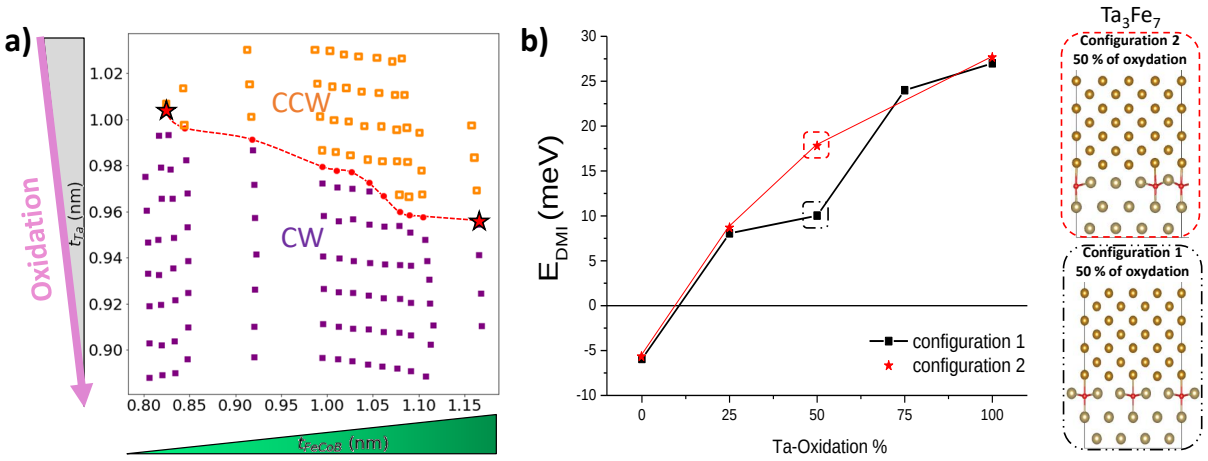

Figure 2: a) Map of the DW chirality in the PMA region with respect to FeCoB thickness (t_{FeCoB}) and oxidation state (t_{Ta}). Regions with CW (resp. CCW) DWs are represented with full purple squares (resp. empty orange squares) and DMI sign crossover is represented by red circles. The dashed line is a guide to the eye. The two stars correspond to DMI sign inversion observed in [4] b) *Ab initio* calculated DMI energy (in meV) as a function of the interfacial Ta layer oxydation (in %), for two different configurations of the oxygen atomes representing 50 % of oxydation: corresponding to an ordered interface (configuration 1, bottom) or more disordered interface (configuration 2, top).

Acknowledgments

This work has been supported by ANR-19-CE24-0019 project ADMIS.

References

[1] I. Dzyaloshinsky. A thermodynamic theory of "weak" ferromagnetism of antiferromagnetics. *Journal of Physics and Chemistry of Solids* 4, 241–255 (1958).

[2] T. Moriya. Anisotropic Superexchange Interaction and Weak Ferromagnetism. *Physical Review* 120, 91–98 (1960).

[3] C.E. Fillion et al. Gate-controlled skyrmion and domain wall chirality. *Nature Communications* 13, 5257 (2022).

[4] R. Kumar et al. Control of Skyrmion Chirality in Ta/FeCoB/TaOx Trilayers by TaOx Oxidation and FeCoB Thickness. *Physical Review Applied* 19, 024064 (2023).

[5] S. Emori et al. Current-driven dynamics of chiral ferromagnetic domain walls. *Nature Materials* 12, 611–616 (2013).

Observations of bubble resonances in a magnetic insulator via time-resolved scanning transmission X-ray microscopy

Ping Che[1,*], Diane Gouéré[1], Sebastian Wintz[2,3], Aya El Kanj[1], Andrea Mucchietto[4], Dirk Grundler[4,5], Gisela Schütz[2], Romain Lebrun[1], Vincent Cros[1], and Abdelmadjid Anane[1]

[1]*Unité Mixte de Physique, CNRS/Thales, Université Paris-Saclay, 91767 Palaiseau, France*
[2]*Max Planck Institute for Intelligent Systems, 70569 Stuttgart, Germany*
[3]*Helmholtz-Zentrum Berlin für Materialien und Energie GmbH, 14109 Berlin, Germany*
[4]*Laboratory of Nanoscale Magnetic Materials and Magnonics, Institute of Materials (IMX), École Polytechnique Fédérale de Lausanne (EPFL), Lausanne, Switzerland*
[5]*Institute of Electrical and Micro Engineering (IEM), École Polytechnique Fédérale de Lausanne (EPFL), Lausanne, Switzerland*
*ping.che@cnrs-thales.fr

Magnetic bubbles and bubble lattices are of great importance for investigations in magnonics because of their non-trivial magnon band structures [1, 2] and skew scattering predicted between spin waves and magnetic bubbles [3, 4]. Understanding their resonance and scattering processes with spin waves are fundamental to bubble-based devices. Magnetic bubbles, e.g. skyrmions, are found in multiple material systems, such as bulk chiral magnets and ultra-thin multilayers consisting of ferromagnetic layers and normal metal layers with strong spin-orbit coupling. However, those systems host bubbles and skyrmions either typically at cryogenic temperature or the damping parameters are significantly increased.

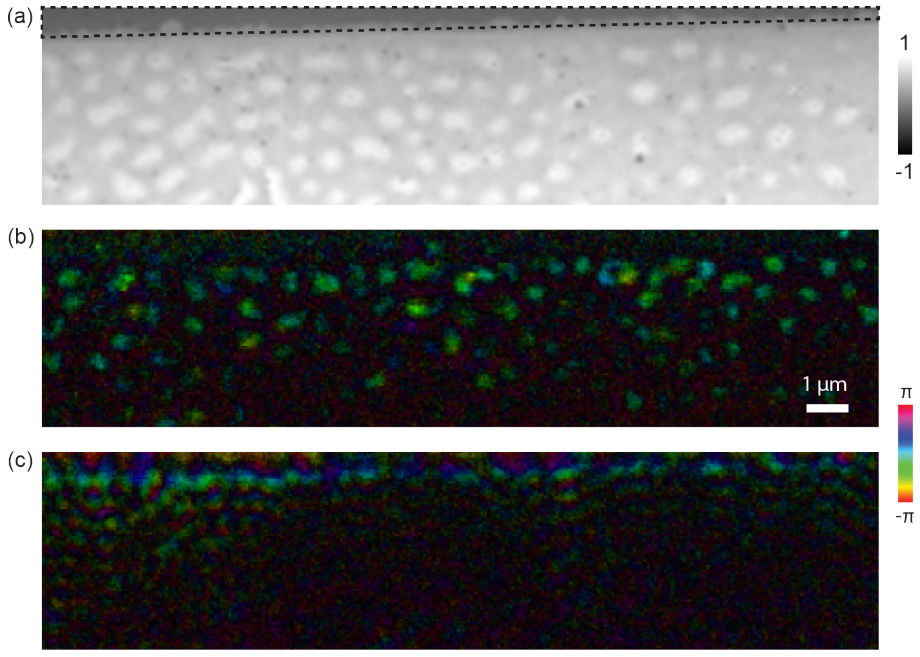

Figure 1: (a) Static X-ray transmission image of bubble and lattices in Bi-doped YIG film. The black dotted frame marks the edge of the antenna. White and black colors represent the X-ray transmission signal. (b and c) Phase distribution of bubble dynamics at 70 MHz and 360 MHz, respectively.

In this work, magnetic bubbles down to 250 nm-diameter in low-damping 20 nm-thick Bi-doped YIG [5] were stabilized by controlling the anisotropy (see Fig. 1(a)). We utilize the Maxymus time-resolved scanning transmission X-ray microscope (STXM) at Bessy II [6] to image the spin dynamic behavior of the bubbles using the x-ray at the L3 edge of Fe (709 eV). Below 100 MHz, multiple types of magnetic bubble resonance were observed, as shown in Fig. 1(b), depending on the shape of the bubbles. Above 100 MHz, spin waves excited from the antenna propagate through the area of resonating magnetic bubbles and interact with them. The phase image in Fig. 1(c) clearly indicates the wavefront in the region of the bubbles and bubble lattices. Isolated bubble resonances were also observed at different applied fields. Our observations offers insight into the manipulation of magnetic bubbles using spin waves and pave the way for bubble-based magnonic device designs.

Acknowledgments

We acknowledge financial support from the Horizon 2020 Framework Program of the European Commission under FET-Open grant agreement no.899646 (k-NET) and from SNSF via grant 197360.

References

[1] M. Garst, J. Waizner, and D. Grundler. Collective spin excitations of helices and magnetic skyrmions Review and perspectives of magnonics. *J. Phys. D. Appl. Phys.* 50 (2017).

[2] T. Weber, D. M. Fobes, J. Waizner, et al. Topological magnon band structure of emergent Landau levels in a skyrmion lattice. *Science* 375, 1025–1030 (2022).

[3] C. Schütte and M. Garst. Magnon-skyrmion scattering in chiral magnets. *Phys. Rev. B* 90, 094423 (2014).

[4] Junichi Iwasaki, Aron J. Beekman, and Naoto Nagaosa. Theory of magnon-skyrmion scattering in chiral magnets. *Phys. Rev. B* 89, 064412 (2014).

[5] Diane Gouéré, Hugo Merbouche, Aya El Kanj, et al. Temperature-independent ferromagnetic resonance shift in Bi-doped YIG garnets through magnetic anisotropy tuning. *Physical Review Materials* 6, 114402 (11 2022).

[6] Volker Sluka, Tobias Schneider, Rodolfo A. Gallardo, et al. Emission and propagation of 1D and 2D spin waves with nanoscale wavelengths in anisotropic spin textures. *Nat. Nanotechnol.* 14, 328–333 (2019).

Index of authors

Sponsors


LABORATOIRE
CHARLES COULOMB
MONTPELLIER


L'AVENIR DEPUIS 1220
UNIVERSITÉ DE
MONTPELLIER


CAYLAR
INSTRUMENTATION SCIENTIFIQUE


neyco
HEF® PHOTONICS


CIQTEK


nami
the quantum wave


ZABRE


Zurich
Instruments


anr


FRANCE
2030
PROGRAMME
DE RECHERCHE
SPINTRONIQUE